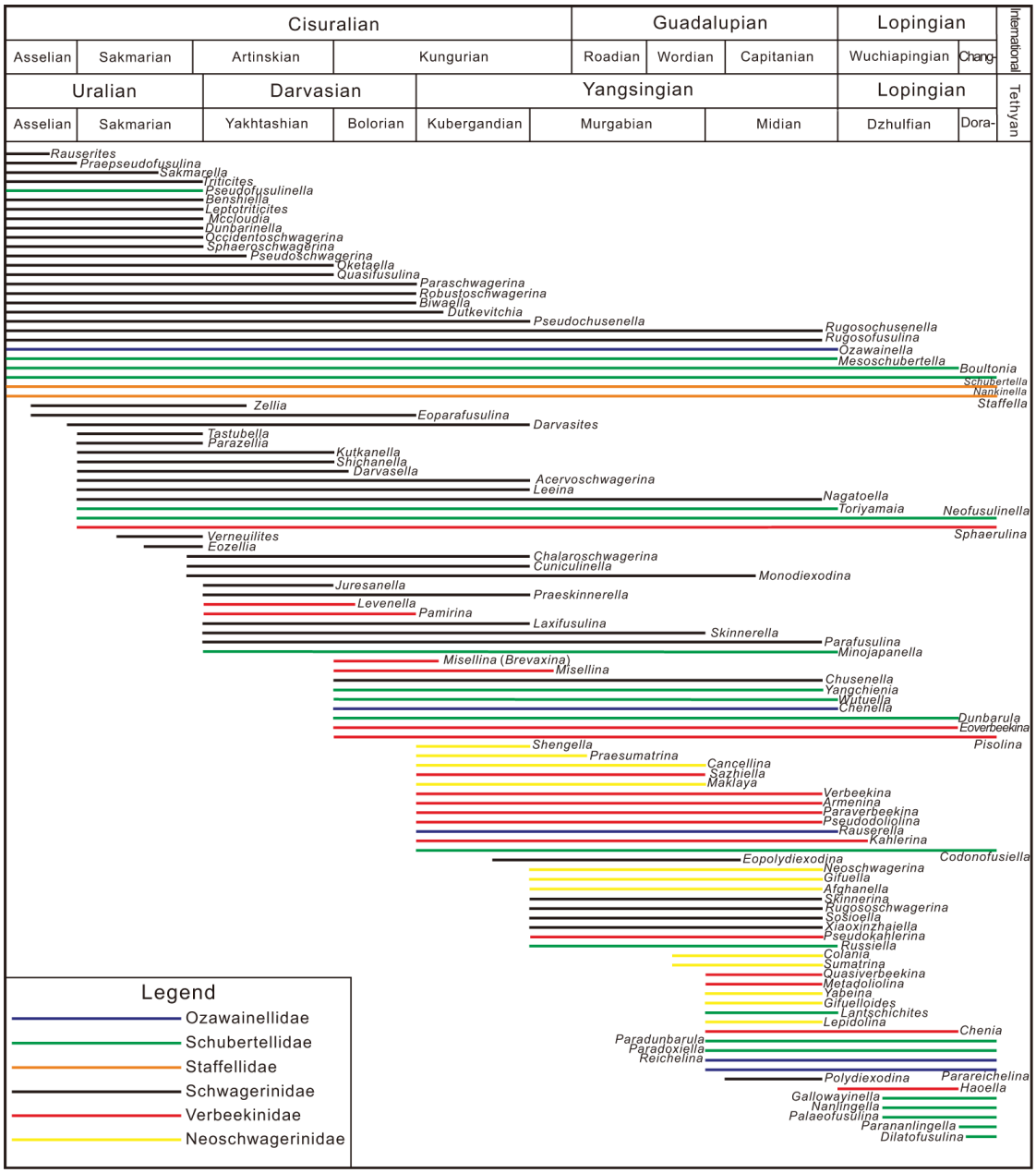

Fig. 1. Rough ranges of the main Permian fusuline genera. The taxonomy of the fusulines mainly follows Sheng *et al.* (1988).

(Ota & Isozaki 2006). The schubertellids experienced a new diversification during the late Dzhulfian that gave rise to *Gallowayinella*, *Nanlingella* and *Palaeofusulina.* Unfortunately, all fusulines died out at the end of Permian due to the severe mass extinction event (Jin *et al.* 2000; Shen *et al.* 2011). Overall, the history of fusulines during the Permian witnessed a process of origination, diversification and extinction. Most importantly, these evolution and extinction events have provided a solid basis for the biostratigraphic subdivisions.

Biostratigraphy of Permian fusulines

Fusulines are considered to have lived in warm and shallow-marine environments, which explained their wide distribution in tropical and subtropical

regions during the Permian (Ross 1982; Vachard *et al.* 2010). However, because of geographical barriers and climatic gradients, the fusulines showed distinct palaeobiogeographical provinces (Ross 1967; Ozawa 1987; Kobayashi 1997*a*, 1999). Six broad palaeogeographical regions were recognized based on previous palaeobiogeographical studies (Ozawa 1987; Kobayashi 1997*a*) (Fig. 2). The most conspicuous palaeobiogeographical boundary was drawn between the Tethyan region and the North American Craton region because the vast Pangaea supercontinent hampered the faunal communications between these two regions. As a result, the fusuline fauna on each side of the supercontinent could not be correlated, especially in terms of middle and late Permian fusulines (Kobayashi 1997*a*, 1999). In order to facilitate the correlations of fusuline biostratigraphy between different regions, detailed descriptions of fusuline biostratigraphy from every block/region are provided here.

Eastern Tethyan region

The Eastern Tethyan region is centred on South China Block (Ozawa 1987). It consists of the South China Block, the Indochina Block, the North China Block, the Tarim Block, the North Qiangtang–Qamdo Block, seamounts within the Palaeotethys Ocean, Darvaz, north Afghanistan and southern Fergana, and the Urals and the Russian Platform (Fig. 3).

South China Block. The South China Block was located at equatorial regions during the Late Palaeozoic (Metcalfe 2013). This huge block has preserved a complete biostratigraphic zonation ranging from the Early Carboniferous to latest Permian (Sheng 1963; Xiao *et al.* 1986; L.X. Zhang *et al.* 1988; Sheng & Jin 1994).

The earliest Permian fusulines are marked by the appearance of pseudoschwagerinids in the Maping or Chuanshan Formation in South China, which differ from the underlying *Triticites*-bearing fusuline assemblages (e.g. Lin *et al.* 1979; Xiao *et al.* 1986; L.X. Zhang *et al.* 1988; Shi *et al.* 2009; Li *et al.* 2010). The Zisongian fusulines can be subdivided into two fusuline zones: the lower *Pseudoschwagerina uddeni* Zone (or *Pseudoschwagerina uddeni–P. texana* Zone) and the upper *Sphaeroschwagerina* Range Zone (Xiao *et al.* 1986; L.X. Zhang *et al.* 1988) (for the full species names see Appendix A). The lower *Pseudoschwagerina uddeni* Zone contains many species of *Pseudoschwagerina* and *Eoparafusulina.* The upper *Sphaeroschwagerina* Range Zone in the Houchang section in Guizhou Province is composed of three

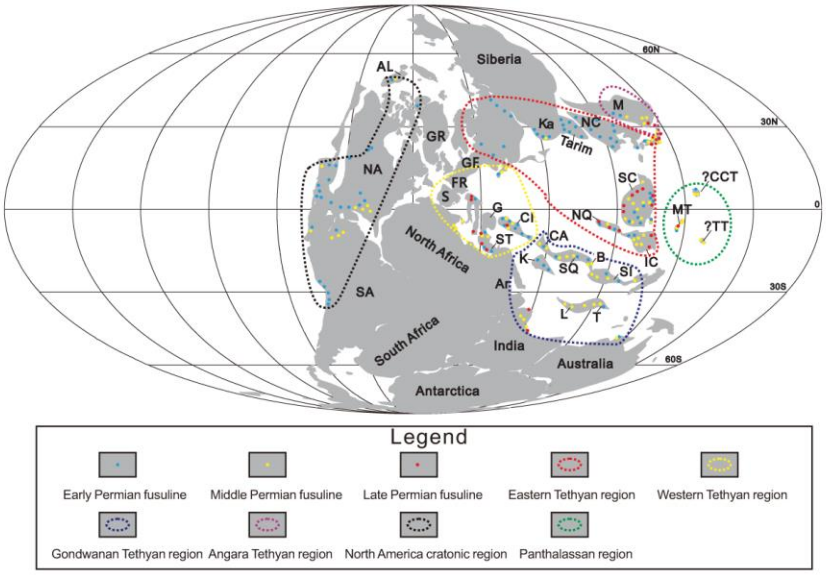

Fig. 2. Sketch map showing the distribution of fusulines during the Late Permian and the main palaeobiogeographical regions. The base map is modified from Scotese (2001). Abbreviations of tectonic blocks/regions are as follows, in alphabetical order: AL, Alaska; AR, Arabia Plate; B, Baoshan Block; CA, Central Afghanistan; CCT, Cache Creek Terrane in Canada; CI, Central Iran; FR, France; G, Greece; GE, Germany; GR, Greenland; IC, Indochina Block; K, Karakorum; Ka, Kazakhstan; L, Lhasa Block; M, Mongolia; MT, Mino Terrane in Japan; NA, North America; NC, North China; NQ, North Qiangtang Block; S, Spain; SA, South America; SC, South China; SI, Sibumasu Block; SQ, South Qiangtang Block; ST, Southern Turkey; T, Tengchong Block; TT, Torlesse Terrane in New Zealand.

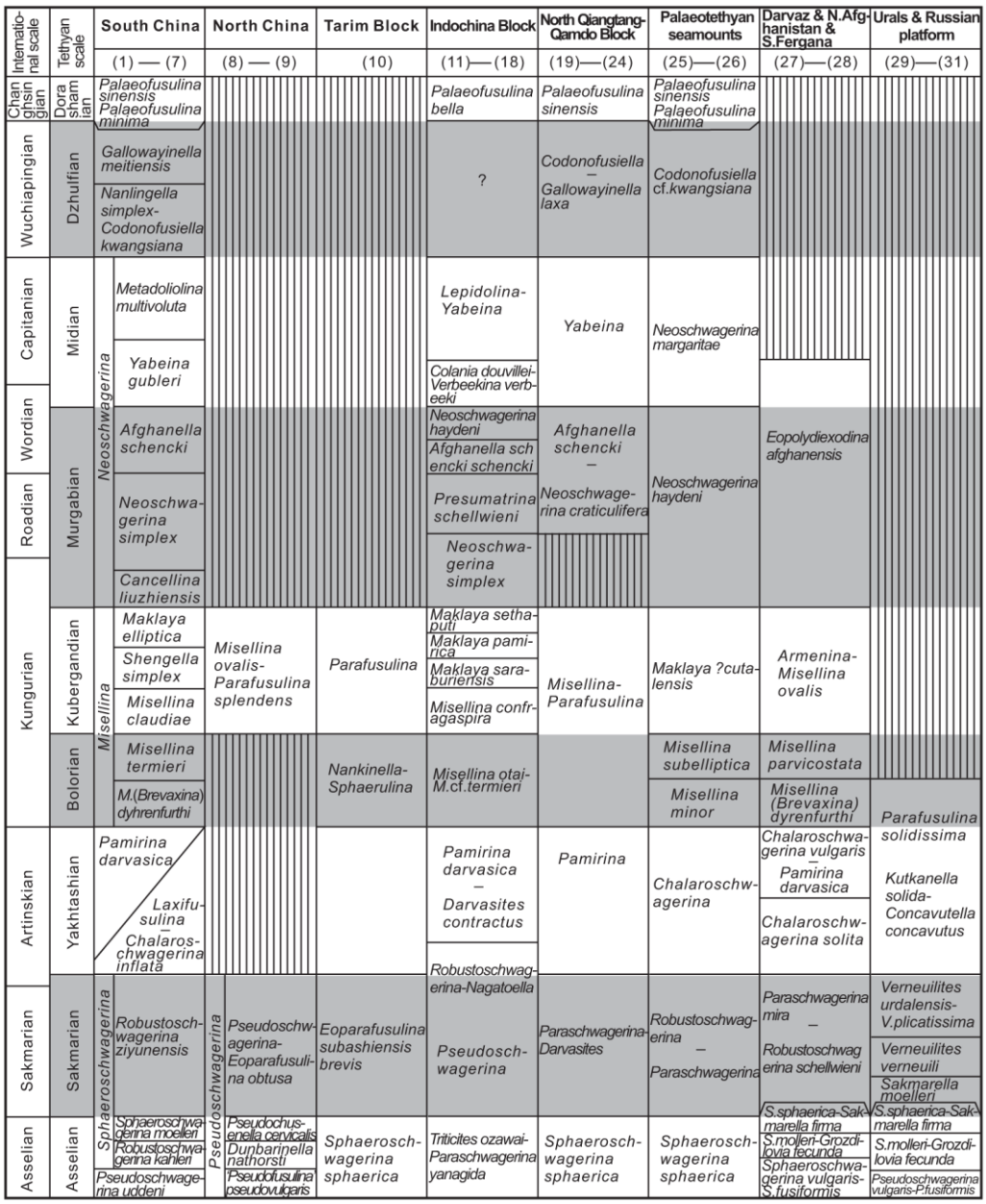

Fig. 3. Schematic framework of Permian fusuline biozones in the Eastern Tethyan region. The references are: (1) Xiao *et al.* (1986); (2) Z.H. Zhang *et al.* (1988); (3) Xu *et al.* (1986); (4) Sheng (1963); (5) Rui *et al.* (1984); (6) Sheng & Jin (1994); (7) Sheng & Zhang (1958); (8) Zhang (1983); (9) Xia (1981); (10) Zheng & Lin (1991); (11) Igo (1972); (12) Toriyama *et al.* (1965); (13) Dawson (1993); (14) Igo *et al.* (1993); (15) Toriyama *et al.* (1974); (16) Toriyama & Kanmera (1979); (17) Fontaine *et al.* (2002); (18) Ingavat *et al.* (1980); (19) Zhang *et al.* (2016); (20) Sichuan Regional Geological Survey & Nanjing Institute of Geology & Palaeontology (1982); (21) Liu (1993); (22) Niu *et al.* (2006); (23) Niu *et al.* (2010); (24) Zhao *et al.* (2006); (25) Ueno *et al.* (2003); (26) Ueno & Tsutsumi (2009); (27) Leven *et al.* (1992); (28) Leven (1997); (29) Rauzer-Chernousova (1965); (30) Forke (2002); (31) Chuvashov *et al.* (1990).

subzones: the *Robustoschwagerina kahleri* Subzone, the *Sphaeroschwagerina moelleri* Subzone and the *Robustoschwagerina ziyunensis* Subzone, in ascending order (Xiao *et al.* 1986). The *Robustoschwagerina kahleri* and *Sphaeroschwagerina moelleri* subzones show a stepwise increase of

subglobular to globular pseudoschwagerinids, such as *Sphaeroschwagerina*, *Zellia* and *Robustoschwagerina*. In contrast, the *Robustoschwagerina ziyunensis* Subzone was dominated by large *Robustoschwagerina* species and abundant *Eoparafusulina* species (Xiao *et al.* 1986). The fusulines in the Zisongian Stage can be broadly correlated with those from the Maping Stage, in which the fusulines were divided into three zones, respectively: the *Pseudoschwagerina morsei–Robustoschwagerina xiaodushanica* Zone, the *Pseudoschwagerina parabeedei–Sphaeroschwagerina sphaerica* Zone and the *Pseudoschwagerina robusta–Zellia chengkungensis* Zone (Zhou *et al.* 1987).

The overlying fusuline assemblage is characterized by the appearance of *Pamirina* species synchronously in various areas in South China, such as the Zhengan area in Shanxi Province (Ding *et al.* 1989), the Longlin area in Guangxi Province (Huang & Zeng 1984) and the Ziyun area in Guizhou Province (Xiao *et al.* 1986). Xiao *et al.* (1986) established the *Pamirina darvasica* Zone, which was assigned to the Longlin Stage according to the Permian timescale of South China (Jin *et al.* 1999). The contemporaneous fusuline assemblages in outer shelf or slope environments, however, are often dominated by schwagerinids such as *Chalaroschwagerina* and *Laxifusulina*, which were recognized as the *Laxifusulina–Chalaroschwagerina inflata* Zone (Xu *et al.* 1986). Also, in the restricted platform environment, the fusulines are dominated by the *Pseudoendothyra* assemblage (Wu & Yang 1998).

The evolutionary trend, from *Pamirina* via *Misellina* (*Brevaxina*) to *Misellina*, has been reported in the Chihsia Formation and Houziguan limestone (Xu *et al.* 1986). The *Misellina* Range Zone established by Xiao *et al.* (1986) includes five subzones, respectively: the *Misellina* (*Brevaxina*) *dyhrenfurthi* Subzone, the *Misellina termieri* Subzone, the *M. claudiae* Subzone, the *Shengella simplex* Subzone and the *Maklaya elliptica* Subzone, in ascending order. These five subzones recorded a clear evolutionary progress of the following aspects: (1) the appearance of numerous parachomata in *Misellina* (*Brevaxina*); (2) the increase in size of *Misellina*; (3) the appearance of axial septula in *Shengella* and *Maklaya* subsequently. It should be noted, however, that in some places the underlying two subzones are often replaced by many schwagerinids, such as *Darvasites*, *Pseudochusenella*, *Praeskinnerella* and *Nagatoella*, which was named as the *Darvasites* Zone or *Pseudochusenella cushmani* Zone (originally the *Schwagerina cushmani* Zone) (Zhou 1982). The *Miselline claudiae* Subzone was widely distributed in the Chihsia Formation of South China (Wang 1978; Xiao *et al.* 1986; Ding *et al.* 1989). The *Shengella simplex* and *Maklaya elliptica* subzones also bear species of *Pseudodoliolina*, *Eoverbeekina* and *Neofusulinella*.

The overlying fusuline assemblage is dominated by neoschwagerinids, which were ascribed to the *Neoschwagerina* Zone (Xiao *et al.* 1986). This zone comprises the *Cancellina liuzhiensis* Subzone, the *Neoschwagerina simplex* Subzone, the *Afghanella schencki* Subzone, the *Yabeina gubleri* Subzone and the *Metadoliolina multivoluta* Subzone, in ascending order (Xiao *et al.* 1986). The *Cancellina liuzhiensis* Subzone is dominated by species of *Cancellina* and other genera, such as *Praesumatrina*, *Paraverbeekina*, *Pseudodoliolina*, *Verbeekina* and sporadic primitive *Neoschwagerina.* This subzone may correspond to the upper part of the *Cancellina* Subzone of Sheng (1963) or the *Praesumatrina neoschwagerinoides–Parafusulina multiseptata* Zone in the upper part of the Chihsia Formation in Tonglu in Zhejiang (Wang & Tang 1986). The *Neoschwagerina simplex* and *Afghanella schencki* subzones are dominated by diverse species of *Neoschwagerina*, *Afghanella*, *Verbeekina*, *Neofusulinella* and *Parafusulina*. The appearance of *Yabeina* marks the lower boundary of the *Yabeina gubleri* Subzone, which includes the species of *Yabeina*, *Neoschwagerina*, *Verbeekina*, *Chusenella*, *Sumatrina* and *Codonofusiella* (Xiao *et al.* 1986). The uppermost subzone in the *Neoschwagerina* Zone is the *Metadoliolina multivoluta* Zone, which is characterized by advanced species of *Metadoliolina*. However, with the demise of large-shelled neoschwagerinids in the uppermost part of this subzone, the fusuline assemblage is dominated by small schubertellids such as *Codonofusiella*, *Lantschichites* and *Dunbarula.* This subzone roughly corresponds to the upper part of the *Yabeina* Zone of Sheng (1963). The fusulines from this zone were also documented from the Yanqiao Formation in eastern South China (Sheng & Wang 1962).

The Late Permian fusuline assemblages were divided into four zones: the *Nanlingella simplex–Codonofusiella kwangsiana* Zone, the *Gallowayinella meitienensis* Zone, the *Palaeofusulina minima* Zone and the *Palaeofusulina sinensis* Zone, in ascending order (Sheng & Jin 1994). The *Nanlingella simplex–Codonofusiella kwangsiana* Zone is dominated by species of *Codonofusiella*, *Nankinella*, *Reichelina* and primitive *Nanlingella* (Rui *et al.* 1984). The decrease in *Codonofusiella* and the appearance of *Gallowayinella* is the feature of the *Gallowayinella meitienensis* Zone. The appearance of primitive *Palaeofusulina*, *Palaeofusulina minima*, marks the lower boundary of the *Palaeofusulina* Zone. Also, primitive *Palaeofusulina* occurred in both zones. The uppermost part of the fusuline zone is the *Palaeofusulina sinensis* Zone, which is widespread in the upper part of the Changxing Formation or Longdongchuan Formation in

South China (Sheng & Zhang 1958; Sheng 1963; Sun 1979). The former two zones are generally ascribed to Wuchiapingian/Dzhulfian, whereas the latter two are Changhsingian/Dorashamian in age (Wang *et al.* 1997; Jin *et al.* 2003; Leven 2004). However, the discovery of the *Palaeofusulina* assemblage at the base of the Heshan Formation in the Penglaitan section indicates an age of early Wuchiapingian (Wang & Jin 2006); further detailed taxonomic study is needed in the future.

North China Block. The North China Block has been a stable block since the beginning of the Palaeozoic (Shi 2006). This block underwent long-term erosion from the Late Ordovician, up until transgression took place during the Late Carboniferous (e.g. Wang *et al.* 1992). Fusulines were found in several limestone beds within the Taiyuan Formation in this block (Zhang 1983; Zhang *et al.* 1989; Jiang *et al.* 2001). They were often represented in the *Pseudoschwagerina* Zone (Zhang 1983; Zhang & Xia 1985; Zhang *et al.* 1989; Jiang *et al.* 2001) or *Sphaeroschwagerina* Zone (Song *et al.* 2014). The *Pseudoschwagerina* Zone in the Taiyuan Formation of the Xishan section near Taiyuan city was divided into four subzones, respectively: the '*Pseudofusulina*' *pseudovulgaris* Subzone, the *Dunbarinella nathorsti–Dunbarinella nathorsti laxa* Subzone, the *Pseudochusenella cervicalis* Subzone and the *Pseudoschwagerina texana–Eoparafusulina obtusa* Subzone, in ascending order (Zhang 1983), with the uppermost subzone being most probably of Sakmarian age (Zhang 1990).

Post-Sakmarian fusulines were not reported from the mainland of North China because of the retreat of seawater. However, in the northern margin of the North China Block, the Sanmianjing Formation in the Kangbao area of Hebei Province yields many fusulines referable to the *Misellina ovalis–Parafusulina splendens* assemblage (Xia 1981). Common fusulines in this assemblage comprise *Misellina ovalis*, *M. claudiae*, *Parafusulina splendens*, *P. yabei* and *Chusenella sinensis* (Sheng 1962; Xia 1981). This assemblage indicates a Kubergandian age.

Tarim Block. Shallow-water carbonates with diverse marine faunas prevailed in the Tarim Block during the Late Carboniferous and early Permian. The appearance of *Pseudoschwagerina* or *Sphaeroschwagerina* in the lower part of the Kangkeling Formation in the Keping area, in the lower part of the Xiaohaizi Formation in the Bachu area and in the middle part of the Tahaqi Formation in the SW Tarim Block marks the beginning of the Permian (Zhang 1963; Zheng & Lin 1991; Zhu 1997; Wang *et al.* 2011*b*). The Permian succession in the Subashi area near Keping City was subdivided into the following fusuline zones: the *Sphaeroschwagerina sphaerica* Zone, the *Eoparafusulina subashiensis brevis* Zone, the *Nankinella–Sphaerulina* Zone and the *Parafusulina splendens* Zone, in ascending order (Zheng & Lin 1991).

The lowermost *Sphaeroschwagerina sphaerica* Zone comprises species of *Sphaeroschwagerina*, *Pseudoschwagerina*, *Triticites*, *Paraschwagerina*, *Zellia*, *Quasifusulina*, *Schubertella* and *Eoparafusulina*, and is coeval with the *Pseudoschwagerina parasphaerica* Subzone in the Keping area (Zhang 1963), the *Praepseudofusulina–Sphaeroschwagerina* Zone in the Wuzunbulake area (Wang *et al.* 2011*b*), and the *Sphaeroschwagerina vulgaris* and *S. karnica* zones in the Paojianggou area (Zhu 1997). The age of the *Sphaeroschwagerina sphaerica* Zone is Asselian.

The *Eoparafusulina subashiensis brevis* Zone overlies the *Sphaeroschwagerina sphaerica* Zone. In this zone, many *Eoparafusulina* species have taken over the pseudoschwagerinids of the underlying zone (Zheng & Lin 1991). This *Eoparafusulina*-dominated assemblage was also documented in the Wuzunbulake, Bachu and Paojianggou areas (Zheng & Lin 1991; Zhu 1997; Wang *et al.* 2011*b*). The age of this assemblage is most likely to be Sakmarian.

The Balikelike Formation in the Subashi section records the youngest fusuline assemblage in the Tarim Block (Zheng & Lin 1991). This assemblage comprises species of *Chalaroschwagerina*, *Sphaerulina*, *Darvasites*, *Nankinella* and *Pisolina* in the lower part of the formation, and species of *Parafusulina* in the upper part. They were ascribed to the *Nankinella–Sphaerulina* and *Parafusulina* zones, respectively (Zheng & Lin 1991). The ages of these zones are most probably Bolorian and Kubergandian, respectively (Zheng & Lin 1991). Other areas in the Tarim Block deposited terrestrial sediments without any marine faunas during the middle and late Permian.

Indochina Block. The Indochina Block is bounded by the Song Ma Suture Zone in Vietnam and the Jinghong–Nan–Uttaradit–Sra Kaeo sutures in western Yunnan and central Thailand (Metcalfe 2013). This block was situated in the tropical zone of low latitude (Metcalfe 2013), which accounts for the flourishing Permian fusulines.

The Asselian fusulines are grouped into the *Triticites ozawai–Paraschwagerina yanagidai* assemblage in the Phetchabun area of central Thailand (Igo 1972) and the *Sphaeroschwagerina sphaerica–Rugosofusulina extensa* assemblage in the Terbat Formation of eastern Malaysia (Sakamoto & Ishibashi 2002). The *Triticites ozawai–Paraschwagerina yanagidai* assemblage was once considered

to be of latest Gzhelian age (Igo *et al.* 1993). Since the typical Permian species *Pseudoschwagerina toriyamai* was also reported from the highest level of this zone (Igo 1972), the stratigraphic age of this zone should be at least partially Asselian.

A younger fusuline assemblage was reported from the limestones in the Noankowtok area of Thailand. It is represented by many species of *Pseudoschwagerina*, such as *P. sphaerica*, *P.* cf. *muongthensis rossica* and *P. turbida*, which indicates an age of Sakmarian according to Toriyama *et al.* (1965). A further younger fusuline fauna, composed of species of sporadic *Robustoschwagerina*, *Nagatoella* and *Toriyamaia* in the Saraburi area, was named as the *Robustoschwagerina–Nagatoella* assemblage of latest Sakmarian–earliest Yakhtashian age (Dawson 1993). The Yakhtashian fusulines were reported from the Changwat Loei area of NE Thailand (Igo *et al.* 1993). The fusulines of this age are mainly represented by *Pamirina darvasica*, *Darvasites contractus*, *Pseudoreichelina darvasica* and *Nankinella* ?*loiensis* (Igo *et al.* 1993).

The succeeding zones were established based on the evolution of neoschwagerinids, which are well exposed in the Khao Phrong Phrab and the Khao Khao areas of Sara Buri, central Thailand (Toriyama *et al.* 1974; Toriyama & Kanmera 1979; Ingavat *et al.* 1980). The lowermost zone was named the *Misellina otai–Misellina* cf. *termieri* Zone from the Khao Phrong Phrab area (Toriyama *et al.* 1974). Fusulines of this zone may also occur in the Wang Saphung area of northern Thailand, which comprise *Misellina termieri* and *Pravitoschwagerina thailandensis* (Toriyama 1982), indicating an age of Kubergandian according to Leven (2004). Kubergandian fusulines in the Phrong Phrab area were subdivided into the *Misellina confragaspira* Zone, the *Maklaya saraburiensis* Zone, the *M. pamirica* Zone and the *M. sethaputi* Zone, in ascending order (Toriyama *et al.* 1974). In these zones, species of *Maklaya*, *Pseudodoliolina*, *Neofusulinella*, '*Pseudofusulina*', *Parafusulina*, *Chusenella* and *Neothailandina* were reported (Toriyama *et al.* 1974). Fusulines documented from the limestones in the NE of Salavan, southern Laos are equivalent to the *Misellina confragaspira* Zone (Fontaine *et al.* 1999). The succeeding fusuline zone is the *Neoschwagerina simplex* Zone, which is characterized by the appearance of many primitive species of *Neoschwagerina* such as *Neoschwagerina simplex*, *N. schuberti* and *N. tenuis* (Toriyama *et al.* 1974; Toriyama 1975), which indicate a Murgabian age. The upper part of this zone, however, is transformed to the *Afghanella megaspherica–Neoschwagerina* cf. *kueichowensis* Zone in the Khao Khao area (Toriyama & Kanmera 1979). The overlying *Afghanella pesuliensis–Pseudodoliolina pseudolepida* Zone was considered to be contemporaneous with the *Praesumatrina schellwieni* Zone in the Khao Phrong Phrab area (Toriyama & Kanmera 1979). The succeeding fusulines in the Khao Khao area were subdivided into the *Afghanella schencki schencki* Zone and the *Neoschwagerina haydeni* Zone, which are dominated by species of *Neoschwagerina*, *Afghanella*, *Verbeekina*, *Chusenella* and *Pseudodoliolina*, but devoid of any *Yabeina* or *Lepidolina* species (Toriyama & Kanmera 1979). Thus, these two fusuline zones are most probably of late Murgabian age. In comparision, fusuline fossils of both zones are not preserved in the adjacent Khao Phrong Phrab area.

The next younger zone was named the *Colania douvillei–Verbeekina verbeeki* Zone by Ingavat *et al.* (1980). The fusulines in this zone are dominated by *Colania douvillei*, *Sumatrina annae*, *Verbeekina verbeeki*, *Schubertella simplex*, and a few species of *Reichelina* and *Rauserella* in the Khao Imot area (Ozawa 1970). Horizons 3 and 4 from the Khao Tham Yai limestone in the Khao Tham Yai area, northern Thailand consist of *Colania douvillei*, *Verbeekina verbeeki*, *Sumatrina* sp. and *Codonofusiella* sp., which are equivalent to the *Colania douvillei–Verbeekina verbeeki* Zone (Fontaine *et al.* 2002). The youngest middle Permian fusuline zone is the *Lepidolina multiseptata* Zone, which is widely distributed in the Indochina Block. The fusulines from this zone include species of *Lepidolina*, *Yabeina*, *Metadoliolina*, *Chusenella*, *Verbeekina*, *Reichelina*, *Russiella*, *Rauserella*, *Kahlerina* and *Dunbarula* (Ingavat *et al.* 1980). This zone has been widely documented in Thailand (Fontaine *et al.* 2002), Cambodia (Gubler 1935; Nguyen 1986) and East Malaysia (Igo 1966).

Dzhulfian fusulines have not yet been reported from the Indochina Block. Dorashamian fusulines, however, have been widely reported in this block. They were grouped into the *Palaeofusulina bella* Zone by Ingavat *et al.* (1980). The fusulines from this zone comprise *Palaeofusulina bella*, *P. sinensis*, *P. fusiformis*, *P. laxa*, *Codonofusiella kwangsiana*, *Gallowayinella guidingensis*, *Reichelina changhsingensis* and *R. cribroseptata*, and have been documented in northern Thailand, southern Cambodia and eastern Malaysia (e.g. Aw *et al.* 1977; Ueno & Sakagami 1991; Fontaine *et al.* 2013).

North Qiangtang–Qamdo Block. The North Qiangtang–Qamdo Block is sandwiched between the Jinshajiang Suture Zone in the north and the Longmu Co–Shuanghu Suture Zone in the south (Zhang *et al.* 2013*a*). This block was located in low-latitude areas during the Permian (Metcalfe 2013; Zhang *et al.* 2013*a*).

The earliest Permian fusulines in this block can be grouped into the *Sphaeroschwagerina sphaerica*

Zone, which was distributed in the Raggyorcaka Lake and Tanggula areas of northern Tibet, and in the Machala area in eastern Tibet (Sichuan Regional Geological Survey & Nanjing Institute of Geology and Palaeontology 1982; Liu 1993; Zhang *et al.* 2016). The fusulines in this zone comprise *Sphaeroschwagerina sphaerica*, *Sphaeroschwagerina parasphaerica*, *Pseudoschwagerina* sp. and *Montiparus tobensis*. The age of this zone is clearly Asselian (Zhang *et al.* 2016). The Sakmarian fusulines can only been recognized in eastern Tibet, where they consist of diverse species of *Paraschwagerina*, *Darvasites* and *Leeina* (Sichuan Regional Geological Survey & Nanjing Institute of Geology and Palaeontology 1982). These fossils are grouped as the *Paraschwagerina–Darvasites* assemblage here. The overlying fusuline assemblage in the North Qiangtang–Qamdo Block is represented by the Yakhtashian *Pamirina* Zone in the Tanggula area that includes *Pamirina pulchra* and *P. nobilis* (Liu 1993). Bolorian and Kubergandian fusulines are not easily differentiated in several areas in this block (Liu 1993; Niu *et al.* 2006). They are composed of *Sphaerulina hunanica*, *Nankinella orbicularia*, *Wutuella wutuensis*, *Misellina claudiae*, *Parafusulina yunanica* and *P. splendens*, which were ascribed to the *Misellina–*'*Schwagerina*' assemblage (Niu *et al.* 2006). Since species of '*Schwagerina*' are not well developed in this assemblage, it is renamed here as the *Misellina–Parafusulina* assemblage.

The equivalent of the *Neoschwagerina simplex* Zone in this block is dominated by clastic rocks lacking fusulines. The overlying strata were dominated by limestones named as the Jiushidaoban Formation in the Tanggula area of northern Tibet and the Jiaoga Formation in the Qamdo area in eastern Tibet (Liu 1993; Niu *et al.* 2010). Abundant fusuline fossils were found in these limestones, including *Neoschwagerina craticulifera*, *N. douvillei*, *Sumatrina annae*, *S. longissima* and *Afghanella schencki*. They were grouped into the *Afghanella schencki–Neoschwagerina craticulifera* assemblage (Niu *et al.* 2010), indicating an age of late Murgabian. A younger fusuline assemblage occurs in the upper part of the Jiushidaoban Formation and the Suojia Formation. It contains *Yabeina gubleri*, *Sumatrina annae* and *Chusenella schwagerinaeformis*, and was named as the *Yabeina* Zone (Liu 1993).

The late Permian strata, characterized by paralic facies in the lower part and limestones in the upper part, are distributed widely in the North Qiangtang–Qamdo Block (Sichuan Regional Geological Survey & Nanjing Institute of Geology and Palaeontology 1982). Two assemblages, the *Codonofusiella–Gallowayinella laxa* assemblage and the *Palaeofusulina sinensis* Zone, in ascending order, were established in the Labuchari Formation (Zhao *et al.* 2006), and refer to Dzhulfian and Dorashamian ages, respectively.

Seamounts within the Palaeotethys Ocean. Along the Changning–Menglian Suture Zone in western Yunnan, China and the Inthanon Zone in Thailand, a series of limestones developed that have been recognized to be seamounts located within the Palaeotethys Ocean (Ueno & Igo 1997; Ueno *et al.* 2003; Ueno & Tsutsumi 2009). The fusuline successions, ranging from Serpukhovian to latest Permian, were recorded in the Yutangzhai area of western Yunnan (Ueno *et al.* 2003; Ueno & Tsutsumi 2009). Early Permian fusulines are represented by *Sphaeroschwagerina sphaerica* and *Rugosofusulina latispiralis* in so-called Ytz 5, which indicates a late Asselian age (Ueno *et al.* 2003). The overlying fusuline assemblages Ytz 6 and Ytz 7 are dominated by *Robustoschwagerina–Paraschwagerina* and *Chalaroschwagerina* faunas, indicating Sakmarian and Yakhtashian ages, respectively (Ueno *et al.* 2003). Although the genera *Levenella* and *Pamirina* were not found, their descendent genera *Misellina–Maklaya–Neoschwagerina* lineage was well recorded in the limestones, indicating a Bolorian–Murgabian age (Ueno *et al.* 2003). The Midian fusuline assemblage consists only of *Neoschwagerina margaritae*, *N.* sp. and *Verbeekina verbeeki*, and lacks many of the other genera common in Tethys regions, such as *Yabeina*, *Lepidolina* and schwagerinid species (Ueno *et al.* 2003).

Late Permian fusulines were discovered in the Shifodong section. They were subdivided into three biozones: the *Codonofusiella* cf. *C. kwangsiana* Zone, the *Palaeofusulina minima* Zone and the *Palaeofusulina sinensis* Zone, in ascending order (Ueno & Tsutsumi 2009). The *Codonofusiella* cf. *C. kwangsiana* Zone is Dzhulfian in age as evidenced by the absence of either neoschwagerinids or *Palaeofusulina* species, whereas the latter two zones are Dorashamian in age because of the dominance of *Palaeofusulina* species (Ueno & Tsutsumi 2009).

Darvaz, north Afghanistan and southern Fergana. Darvaz, north Afghanistan and southern Fergana were located at the southern margin of Eurasia during Late Palaeozoic time (Angiolini *et al.* 2016). The fusulines reported from these blocks show a continuous succession from Late Carboniferous to the early Permian (e.g. Bensh 1972; Leven & Scherbovich 1978; Leven *et al.* 1992; Leven 1997). The middle Permian fusulines, however, were mainly reported from north Afghanistan (Leven 1997).

Asselian fusulines were grouped into three zones in Darvaz (Leven *et al.* 1992). They are the *Sphaeroschwagerina vulgaris–Sphaeroschwagerina fusiformis* Zone, the *Sphaeroschwagerina*

moelleri–Grozdilovia fecunda Zone and the *Sphaeroschwagerina sphaerica–Sakmarella firma* Zones, in ascending order (Leven *et al.* 1992). These zones contain species of *Sphaeroschwagerina*, *Pseudoschwagerina*, *Rugosofusulina*, *Rugosochusenella*, *Dunbarinella*, *Quasifusulina*, *Grozdilovia*, *Sakmarella* and *Dutkevitchia* (Leven & Scherbovich 1978; Leven *et al.* 1992). The overlying zone was named as the *Paraschwagerina mira–Robustoschwagerina schellwieni* Zone of Sakmarian age (Leven *et al.* 1992). This zone is marked by the appearance of some new elements such as *Robustoschwagerina*, *Biwaella*, *Darvasites* and *Zellia*. During the Yakhtashian, the fusulines were grouped into the lower *Chalaroschwagerina solita* Zone and the upper *Chalaroschwagerina vulgaris–Pamirina darvasica* Zone (Leven *et al.* 1992). These two zones are typified by the occurrence of *Chalaroaschwagerina*, *Pamirina* and *Misellina* (*Brevaxina*). With the evolution of *Misellina* (*Brevaxina*) and *Misellina*, the *Misellina* (*Brevaxina*) *dyhrenfurthi* and *Misellina* (*Misellina*) *parvicostata* zones are established that indicate a Bolorian age, and the *Armenina–Misellina* (*Misellina*) *ovalis* Zone with additional Schwagerinidae genera such as *Skinnerella* and *Parafusulina* in the Kubergandian (Leven *et al.* 1992).

Murgabian and Midian fusulines are well documented in north Afghanistan (Ciry & Amiot 1965; Lys & Lapparent 1971; Vachard 1980; Leven 1997; Colpaert *et al.* 2015). They were assigned to the *Eopolydiexodina afghanensis* Zone because of its wide distribution of *Eopolydiexodina afghanensis* (Thompson 1946; Amiot *et al.* 1965). The associated genera include *Afghanella*, *Neoschwagerina*, *Verbeekina*, *Minojapanella*, *Sumatrina*, *Parafusulina* and *Codonofusiella* (Lys & Lapparent 1971).

The Urals and the Russian Platform. Late Carboniferous and Early Permian fusulines are widely distributed in the vast Russian Platform and Ural Mountains (e.g. Rauzer-Chernousova 1965; Mikhailova 1974; Alksne & Isakova 1980; Chuvashov *et al.* 1990; Davydov 1990*b*; Davydov *et al.* 1997).

The Asselian in the southern Urals was once considered to contain two zones, respectively, the lower *Sphaeroschwagerina moelleri–Grozdilovia fecunda* Zone and the upper *Sphaeroschwagerina sphaerica–Sakmarella firma* Zone (Rauzer-Chernousova 1965; Chuvashov *et al.* 1990). However, in the Pechora area of the northern Urals, the *Pseudoschwagerina vulgaris–Pseudoschwagerina fusiformis* Zone occurred below the first appearance of the *Sphaeroschwagerina* species (Mikhailova 1974; Papulov 1986; Chuvashov *et al.* 1990). Overall, Asselian fusulines in the Russian Platform and Urals are characterized by various species of *Pseudoschwagerina* and *Sphaeroschwagerina*, associated with *Grozdilovia*, *Sakmarella*, *Triticites*, *Daixina*, *Rugosofusulina* and *Jigulites*.

Sakmarian fusulines dominated by diverse pseudofusulinid species are mainly distributed in the southern Urals. The lower Sakmarian Tastubian horizon bears two zones, the *Sakmarella moelleri* Zone and the *Verneuilites verneuili* Zone, in ascending order (Rauzer-Chernousova 1965). These two zones are dominated exclusively by abundant pseudofusulinids and rare *Paraschwagerina* species. The upper Sakmarian Sterlitamaklan horizon is also dominated by pseudofusulinid species that have been grouped into the *Verneuilites urdalensis–Verneuilites plicatissima* Zone (Forke 2002).

The Yakhtashian fusulines are characterized by the *Kutkanella solida–Concavutella concavutus* Zone (Forke 2002). The pseudofusulinids in these faunas are hard to correlate with contemporaneous faunas in South China. The post-Yakhtashian fusulines in the Urals have diminished greatly, with only sporadic *Parafusulina solidissima* found in Bolorian strata in the Kungur area (Chuvashov *et al.* 1990).

Western Tethyan region

The Western Tethyan region was located at the western terminus of the Tethyan Ocean during the Permian. It covers Iran, Turkey, the Italian island of Sicily, Greece, Tunisia and the Carnic Alps (Fig. 4). According to Kobayashi (1997*a*), the Western Tethyan region differs from the Eastern Tethyan region in the absence of *Lepidolina* species during the middle Permian.

Iran. During the middle and late Permian, the main part of Iran (except for the Zagros Mountains) rifted away from the Gondwanan margin (Gaetani *et al.* 2009). These blocks included the Alborz Block in northern Iran, the Yazd and Tabas blocks in central Iran, and the Sanandaj-Sirjan Block in SW Iran (Leven & Gorgij 2011*a*).

Asselian fusulines were widely reported from the Emarat Formation in the Alborz Mountains (Gaetani *et al.* 2009), the Zaladou Formation in the Yazd Block and the Tabas Block (Leven & Taheri 2003; Leven & Gorgij 2006), and the Vazhnan Formation in the Sanandaj-Sirjan Block (Baghbani 1993; Leven & Gorgij 2011*b*). The fusuline genera in this stage include *Pseudoschwagerina*, *Sphaeroschwagerina*, *Praepseudofusulina*, *Ruzhenzevites* and *Anderssonites*. They were ascribed to the *Pseudoschwagerina–Praepseudofusulina* assemblage in the lower part and the *Sphaeroschwagerina–Eoparafusulina* assemblage in the upper part (Gaetani

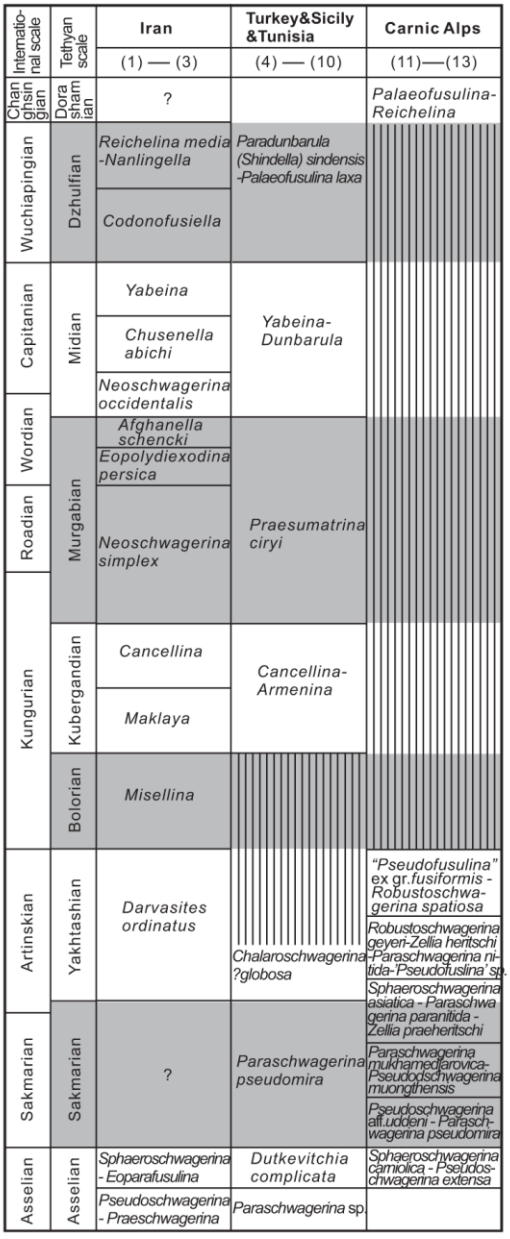

Fig. 4. Schematic framework of Permian fusuline biozones in the Western Tethyan region. References are: (1) Gaetani *et al.* (2009); (2) Kobayashi & Ishii (2003); (3) Baghbani (1993); (4) Kobayashi & Altiner (2008); (5) Vachard *et al.* (2001); (6) Vachard & Moix (2013); (7) Kobayashi & Altiner (2011); (8) Skinner & Wilde (1966); (9) Skinner & Wilde (1967); (10) Vachard *et al.* (2003); (11) Forke (2002); (12) Noe (1988); (13) Pasini (1985).

et al. 2009). These two assemblages are broadly comparable with the *Pseudoschwagerina*–'*Pseudofusulina*' Zone of Baghbani (1993).

Sakmarian fusulines are not reported from the Iranian blocks, except for the Kahmard Block which is included in the Gondwana Tethyan region in this paper. Yakhtashian fusulines were documented from an isolated limestone succession in the Abadeh area (Kobayashi & Ishii 2003). The fusulines were named as the *Darvasites ordinatus* Zone, which comprises *Darvasites ordinatus*, *Chalaroschwagerina* cf. *mengi*, *Leeina fusiformis* and *Pamirina* (*Levenella*) *leveni* (Kobayashi & Ishii 2003).

A younger fusuline fauna was reported by Leven & Gorgij (2008). It consists of *Skinnerella*, *Paraleeina* and *Misellina* in the lower part and *Kubergandella*, *Chusenella*, *Misellina* and *Armenina* in the upper part, suggesting a Bolorian–Kubergandian age (Leven & Gorgij 2008). These fusulines are equivalent to the *Misellina*, *Maklaya* and *Cancellina* zones of Baghbani (1993). Murgabian fusulines were grouped into the *Neoschwagerina simplex* Zone in the lower part and the *Eopolydiexodina persica* (or *Eopolydiexodina douglasi*) Zone in the upper part (Baghbani 1993; Kobayashi & Ishii 2003). The latter zone can be traced across several Peri-Gondwanan blocks and the southern Eurasia margin (Ueno 2003; Colpaert *et al.* 2015). The *Eopolydiexodina persica* Zone is overlain by the *Afghanella schencki* Zone of late Murgabian age (Kobayashi & Ishii 2003). This zone is dominated by many neoschwagerinids, such as *Afghanella*, *Sumatrina*, *Verbeekina* and *Pseudodoliolina* (Kobayashi & Ishii 2003). The overlying fusulines in the Abadeh area were grouped into the *Neoschwagerina occidentalis* Zone and *Chusenella abichi* Zone (Kobayashi & Ishii 2003). Common genera in these zones include *Neoschwagerina*, *Kahlerina*, *Wutuella*, *Sumatrina*, *Dunbarula* and *Chenella*, indicating a Midian age. Late Midian fusulines were reported from the upper part of the Abadeh Formation (Baghbani 1993). They are composed of *Yabeina*, *Metadoliolina*, *Reichelina*, *Kahlerina*, *Chusenella* and *Sichotenella*, and were assigned to the *Yabeina* Zone by Baghbani (1993).

Late Permian fusulines were divided into two zones: the lower *Codonofusiella* Zone and the upper *Reichelina media*–*Nanlingella* Zone (Baghbani 1993). Both zones were ascribed to a Dzhulfian age (Taraz *et al.* 1981; Baghbani 1993). The Dorashamian fusulines were not developed in the Abadeh area because the topmost part of the Hambast Formation was probably not suitable to accommodate fusulines but was favourable for ammonoids and conodonts (Taraz *et al.* 1981; Shen & Mei 2010).

Turkey, Sicily and Tunisia. The Tauride Block of southern Turkey, the Italian island of Sicily and southern Tunisia were located at the western

terminus of the Palaeotethys Ocean (Şengör *et al.* 1984). The allochthonous Aladag unit in Turkey preserved a good carbonate sequence recording Early and Middle Permian fusulines (Kobayashi & Altiner 2008; Okuyucu 2008). The earliest Permian fusulines were represented by *Pseudoschwagerina robusta*, *Quasifusulina minina*, *Paraschwagerina* sp. and *Dutkevitchia complicata*, which were grouped into the lower *Paraschwagerina* sp. Zone and the upper *Dutkevitchia complicata* Zone (Kobayashi & Altiner 2008). The Sakmarian fusuline zone was named as the *Paraschwagerina pseudomira* Zone. It differs from the underlying zone in containing species of *Robustoschwagerina*, *Darvasites* and *Zellia* (Kobayashi & Altiner 2008; Okuyucu 2008). A slightly younger fusuline assemblage was reported from the Permian limestone boulders in the Lercara Formation in Sicily (Vachard *et al.* 2001). It is composed of *Chalaroschwagerina*? *globosa*, *Robustoschwagerina* cf. *schellwieni* and *Minojapanella*? sp., suggesting an early Yakhtashian age (Vachard *et al.* 2001).

The Bolorian fusulines are scarce in this region. The Kubergandian fusulines were found in the allochthonous limestones that constain *Cancellina*, *Armenina*, *Pseudodoliolina* and *Nankinella* (Vachard & Moix 2013). Murgabian fusulines contain *Praesumatrina ciryi*, *Verbeekina erki*, *Dunbarula protomathieui* and *Rauserella* ?sp. (Kobayashi & Altiner 2011). Midian fusulines were widely distributed in the island of Sicily and the Djebel Tebaga area of Tunisia (Skinner & Wilde 1966, 1967; Ghazzay *et al.* 2015). They were represented by *Yabeina*, *Dunbarula*, *Neoschwagerina*, *Yangchienia*, *Chusenella*, *Lantschichites*, *Rauserella* and *Kahlerina* (Skinner & Wilde 1966, 1967; Ghazzay *et al.* 2015). A similar assemblage was also found in the Ankara area of Turkey (Skinner 1969). This assemblage is referable to the *Yabeina–Dunbarula* assemblage here. By contrast, in eastern Turkey, the equivalent fusulines were named as the *Chusenella* Zone, which contains more species of *Chusenella* (Köylüoglu & Altiner 1989).

Late Permian fusulines were documented from southern Greece and southern Turkey (Lys & Marcoux 1978; Unal *et al.* 2003; Vachard *et al.* 2003). The fusulines were dominated by *Paradunbarula* (*Shindella*) *shindensis*, *Sphaerulina zisonzhengensis*, *Codonofusiella paradoxica*, *Palaeofusulina laxa*, *Reichelina cribroseptata* and *R.* sp. (Lys & Marcoux 1978; Unal *et al.* 2003; Vachard *et al.* 2003). They were named as the *Paradunbarula* (*Shindella*) *shindensis–Palaeofusulina laxa* Zone here.

The Carnic Alps. Permian fusulines occurred from the lower part of the Grenzland Formation, and contain the species of *Sphaeroschwagerina*, *Pseudoschwagerina*, *Paraschwagerina*, *Rugosofusulina* and *Triticites*. They were grouped in the *Sphaeroschwagerina carniolica–Pseudoschwagerina extensa* Zone and the *Pseudoschwagerina* aff. *uddeni–Paraschwagerina pseudomira* Zone (Forke 2002). According to Davydov *et al.* (2013), the age of the former zone is late Asselian, whereas that of the latter zone is Sakmarian. The overlying *Paraschwagerina mukhamedjarovica–Pseudoschwagerina muongthensis* Zone and *Sphaeroschwagerina asiatica–Paraschwagerina paranitida–Zellia praeheritschi* Zone in the upper part of the Grenzland Formation are different from the underlying two zones in the occurrence of *Zellia* and *Darvasites* (Forke 2002). The fusulines from the Upper '*Pseudoschwagerina*' limestone were ascribed to the *Robustoschwagerina geyeri–Zellia heritschi–Paraschwagerina nitida–*'*Pseudofusulina*' sp. Zone (Forke 2002). Similarly, the fusuline biostratigraphy from the equivalent Zweikofel Formation was divided into the *Sakmarella fluegeli–Zellia colanii* Zone, the *Sakmarella lubenbachensis–Robustoschwagerina nucleolata* Zone, the *Leeina pseudodivulgata–Chalaroschwagerina incomparabilis* Zone and the *Chalaroschwagerina solita floccose–Perigondwania forkii* Zone, in ascending order (Davydov *et al.* 2013). The age of these zones was considered to be Yakhtashian (Davydov *et al.* 2013). The fusulines in the overlying Trogkofel limestones bear *Biwaella* and *Robustoschwagerina*, which were grouped into the Yakhtashian *Leeina* ex gr. *fusiformis–Robustoschwagerina spatiosa* Zone (Forke 2002).

Middle Permian fusulines are unclear in the Carnic Alps. However, late Permian deposits developed well there. They are represented by the Bellerophon Formation and the lower Tesero Member of the Werfen Formation, representing the major second-rank transgressive–regressive cycles (Loriga *et al.* 1986). Fusulines were found in the upper part of the Bellerophon Formation and the lower part of the Werfen Formation (Loriga *et al.* 1986; Noe 1988). They consist of *Staffella* sp., *Nankinella quasihunanensis* and *Reichelina cribroseptata* of Dorashamian age (Pasini 1985; Noe 1988).

Gondwanan Tethyan region

The Gondwanan Tethyan region refers to both blocks derived from the northern Gondwanan margin during the early Permian and those areas in the Gondwana margin, such as southern Afghanistan, Central Pamir, South Pamir, Karakorum, the South Qiangtang and Lhasa blocks in northern Tibet, the Baoshan and Tengchong blocks in western Yunnan, the Sibumasu Block in SE Asia, the exotic limestone blocks within the Indus–YarlungTsangpo Suture Zone in southern Tibet, and

the northern Gondwanan margin (Fig. 5). Because of the influence of Late Palaeozoic glaciation, there was no record of earliest Permian fusulines until the demise of glaciation from the latest Sakmarian.

South Afghanistan–Central and South Pamirs–Karakorum. The areas extended from the Kahmard Block of eastern Iran to Karakorum, through south Afghanistan, the Central Pamir Block and the

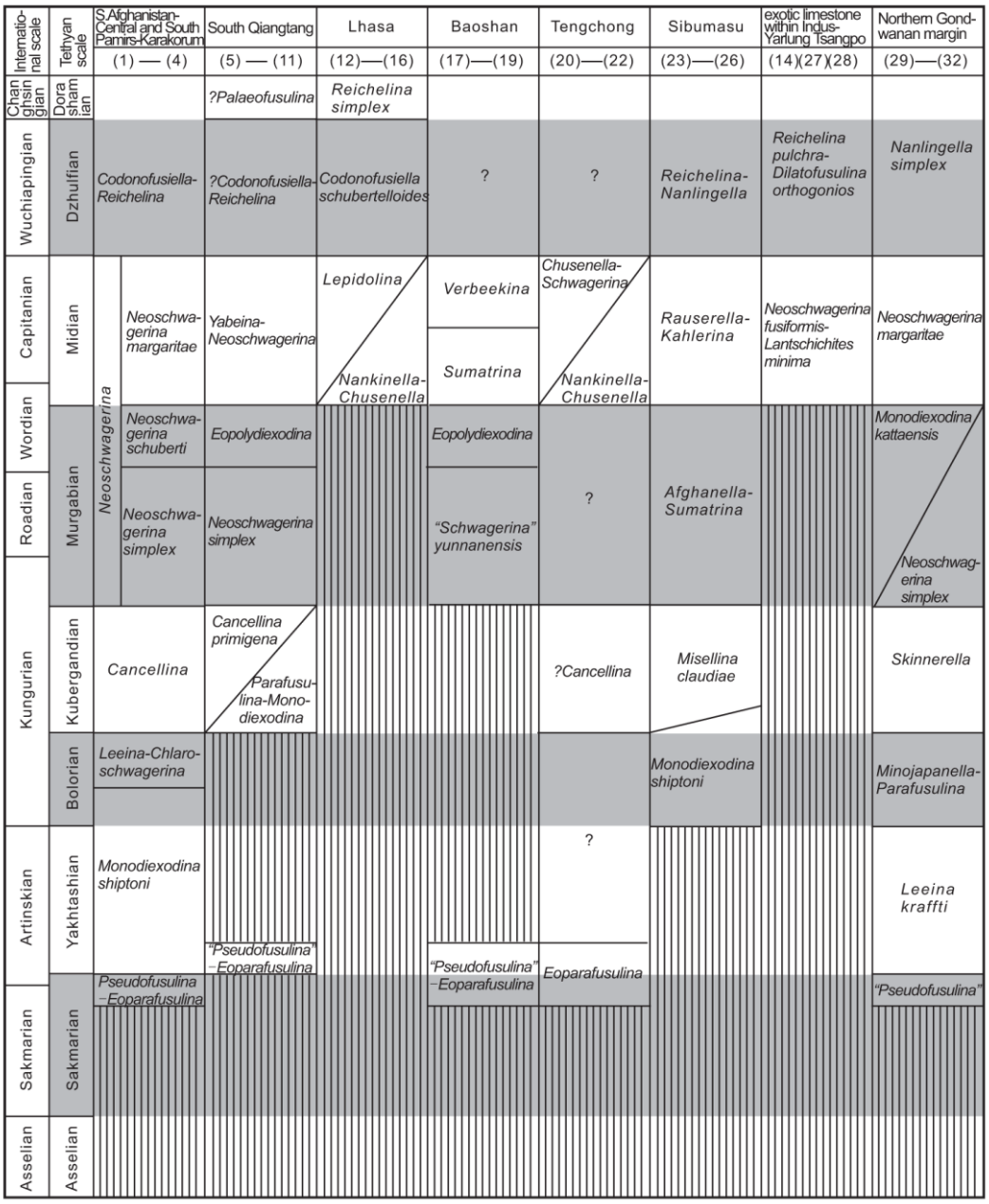

Fig. 5. Schematic framework of Permian fusuline biozones in the Gondwanan Tethyan region. References are: (1) Leven (1993); (2) Gaetani & Leven (2014); (3) Leven (1967); (4) Lys & Lapparent (1971); (5) Zhang *et al.* (2013*b*); (6) Nie & Song (1983*a*); (7) Nie & Song (1983*b*); (8) Zhang *et al.* (2012*a*); (9) Zhang (1991); (10) Cheng *et al.* (2005); (11) Wu & Lan (1990); (12) Zhang *et al.* (2010); (13) Zhu (1982*b*); (14) Wang *et al.* (1981); (15) Zhang Y.J. *et al.* (2014); (16) Chen *et al.* (1999); (17) Shi *et al.* (2011); (18) Huang *et al.* (2009); (19) Huang *et al.* (2015*b*); (20) Fan (1993); (21) Shi *et al.* (2017); (22) Shi *et al.* (2008); (23) Ingavat & Douglass (1981); (24) Ueno *et al.* (2015); (25) Ueno (2003); (26) Fontaine & Suteethorn (1988); (27) Zhang *et al.* (2009); (28) Wang *et al.* (2010); (29) Angiolini *et al.* (2006); (30) Hauser *et al.* (2000); (31) Vachard *et al.* (2002); (32) Pakistan–Japanese Working Group (1985).

South Pamir Block represent a huge continental slice rifting from the Gondwanan margin during the early Permian (Stampfli & Borel 2002; Davydov & Arefifard 2007; Leven *et al.* 2011; Angiolini *et al.* 2015).

The earliest fusuline record in these blocks is represented by the Kalaktash fusuline assemblage preserved in Central Pamir (Leven 1993), the eastern Hindu Kush (Gaetani & Leven 1993; Leven 2010), southern Afghanistan (Leven 1997) and the Kahmard Block of Iran (Davydov & Arefifard 2007; Leven *et al.* 2011; Leven & Gorgij 2013). This fauna is dominated by the '*Pseudofusulina*'–*Eoparafusulina* assemblage that consists of many special species such as '*Pseudofusulina*' *pamirensis*, '*Pseudofusulina*' *karapetovi karapetovi*, *Eoparafusulina pamirensis*, *E. regina* and *Neodutkevitchia insignis*. They were associated with some pseudoschwagerinids, such as *Robustoschwagerina psharti*, *Zellia nunosei* and *Sphaeroschwagerina zhongzanica*, in the Dangikalon Formation in Central Pamir (Leven 1993). The age of this assemblage in these blocks is considered to be late Sakmarian (Leven 1993).

A slightly younger fusuline zone was named as the *Monodiexodina shiptoni* Zone (Gaetani & Leven 2014). This zone was reported from the eastern Karakorum and eastern Hindu Kush (Leven 2010; Gaetani & Leven 2014). The associated fusulines in the eastern Hindu Kush include *Minojapanella*, *Darvasites* and *Chalaroschwagerina* (Leven 2010). The age of this assemblage is most probably Yakhtashian or early Bolorian (Leven 1967; Gaetani & Leven 2014). The *Monodiexodina shiptoni* Zone was succeeded by the *Leeina*–*Chalaroschwagerina* assemblage in the Shaksgam Valley of Karakorum, with its age being most likely Bolorian (Gaetani & Leven 2014). However, the equivalent assemblage in SE Pamir contains many species of *Misellina* and *Parafusulina* (Leven 1967). Kubergandian fusulines are widely distributed in South Pamir and Karakorum, where they were named as the *Cancellina* Zone (Leven 1967) or the *Cancellina*–*Pseudodoliolina*–*Parafusulina* assemblage (Gaetani & Leven 2014). The *Cancellina* Zone bears diverse genera such as *Cancellina*, *Parafusulina*, *Pseudodoliolina*, *Neofusulinella*, *Misellina*, *Armenina* and *Yangchienia* (Leven 1967). The succeeding fusuline zone developed in South Pamir is the *Neoschwagerina* Zone, which comprises *Neoschwagerina simplex*, *N. schuberti* and *N. margaritae* subzones, in ascending order (Leven 1967). These zones were well correlated with those from southern Afghanistan (Lys & Lapparent 1971). The ages of these zones range from Murgabian to Midian in light of the evolution of neoschwagerinids.

The late Permian fusuline fauna was documented in the Karabelesskaya Formation from SE Pamir (Leven 1967). It contains *Sphaerulina zisongzhengensis*, *Nankinella* sp., *Reichelina pulchra*, *Codonofusiella* sp. and *Paradunbarula pamirica*, which indicates a Dzhulfian–Dorashamian age.

South Qiangtang Block. The South Qiangtang Block was part of the Gondwanan continent before its departure from Gondwana during the Artinskian (Zhang *et al.* 2012*a*). Consequently, the fusulines did not appear until the demise of glaciation in this block: that is, since the Artinskian (Nie & Song 1983*a*; Zhang *et al.* 2013*b*). The earliest fusuline fauna in the South Qiangtang Block is represented by diverse fusulines in the Qudi Formation (Nie & Song 1983*b*; Zhang *et al.* 2013*b*). These fusulines are dominated by '*Pseudofusulina*' or *Eoparafusulina* elements of the typical Kalaktash fusuline fauna similar to those found in other Peri-Gondwanan blocks (Leven 1993). However, it should be noted that the Kalaktash fusuline elements such as '*Pseudofusulina*' *pamirensis*, *Neodutkevitchia insignis* and *N. tumidiscula* found in the central Qiangtang Block were associated with *Chalaroschwagerina vulgaris* and *C. globosa*, which indicate a Yakhtashian age (Zhang *et al.* 2013*b*).

The succeeding fusuline fauna in the South Qiangtang Block is dominated by *Parafusulina*–*Monodiexodina* fauna in the Tunglonggongba Formation in the Duoma area of the western Qiangtang Block (Nie & Song 1983*b*) or the lower part of the Lugu Formation (or Cainaha Formation) (Zhang 1991; Y.C. Zhang *et al.* 2014). Its equivalent fauna found in the central Qiangtang Basin is composed of *Cancellina primigena*, *Neofusulinella giraudi*, *Nankinella orbicularia* and *Chusenella schwagerinaeformis*, which can be roughly ascribed to the *Cancellina primigena* Zone of Kubergandian age (Zhang *et al.* 2012*b*). The succeeding fusuline fauna was represented by the *Neoschwagerina simplex* Zone of Murgabian age in the lower part of the Xianqian Formation (Zhang 1991) or the middle part of the Lugu Formation (unpublished data). The overlying fusuline assemblage in the Xianqian Formation is dominated by *Dunbarula*, *Yangchienia*, *Parafusulina* and *Chusenella* (Zhang 1991). The equivalent fusuline fauna in the Lugu Formation is dominated by *Eopolydiexodina* species (Cheng *et al.* 2005; Colpaert *et al.* 2015). The Longge Formation in the Duoma area yields a younger fusuline fauna comprising *Yabeina*, *Neoschwagerina*, *Verbeekina*, *Colania* and *Kahlerina*, and can be assigned to the *Yabeina*–*Neoschwagerina* assemblage of Midian (Liang *et al.* 1983; Nie & Song 1983*c*).

As far as the late Permian fusulines are concerned, Wu & Lan (1990) reported *Codonofusiella* and *Reichelina* from the Rehepan Formation and

Palaeofusulina from the Qinshuihe Formation in the west of the South Qiangtang Block. However, these fusulines have never been described nor illustrated. Thus, the validity of these assemblages needs to be confirmed in the future.

Lhasa Block. The Lhasa Block is bounded by the Yarlung Tsangpo Suture Zone to the south and the Bangong–Nujiang Suture Zone to the north. Because of the influence of glacio-marine deposits on the northern Gondwanan margin, the faunas in the Largar, Angjie formations and the lower part of the Xiala Formation are represented by cool-water biota, such as solitary corals, cool-water brachiopods and the conodont *Vjalovognathus*, but are devoid of any fusulines (Zhang *et al.* 2010, 2013*a*; Yuan *et al.* 2016). The fusulines occur in the middle part of the Xiala Formation or the Luobadui Formation (Zhu 1982*b*; Zhang *et al.* 2010). In the Xainza area, the fusulines in the Xiala Formation are dominated by diverse *Chusenella* and *Nankinella*, and, thus, were named as the *Nankinella–Chusenella* assemblage (Zhu 1982*a*; Zhang *et al.* 2010). Associated fusulines include *Staffella*, *Schwagerina*, *Armenina*, *Rugosochusenella*, *Neoschwagerina* and *Verbeekina* (Zhu 1982*a*; Zhang *et al.* 1985, 2010; Wang & Zhou 1986; Huang *et al.* 2007). The equivalent fusuline assemblage in the Luobadui Formation in the Lhunzhub area, however, is dominated by *Lepidolina* (originally described as *Yabeina*) (Wang *et al.* 1981; Zhu 1982*b*). Coexisting fusulines include *Dunbarula*, *Neoschwagerina*, *Verbeekina* and *Chusenella* (Wang *et al.* 1981; Zhu 1982*b*). The compositional difference between different regions in the Lhasa Block was considered to be the result of different palaeoenvironments (Zhang *et al.* 2010).

The distribution of late Permian fusulines in the Lhasa Block is restricted compared with that of middle Permian fusulines. According to limited reports in the Xainza area, the Dzhulfian fusulines are composed of *Codonofusiella schubertelloides* and *Reichelina* sp. (Y.J. Zhang *et al.* 2014). The advent of *Colaniella parva* in the top of the Xiala Formation indicates a possible Dorashamian age (unpublished data). The fusulines in this interval are dominated by *Reichelina changhsingensis* and *Codonofusiella* sp. The equivalent sequence in the Tsochen area in the Lhasa Block also bears *Reichelina simplex* according to Chen *et al.* (1999).

Baoshan Block. The Baoshan Block is bounded by the Lancangjiang Fault, the Kejie Fault and the Nandinghe Fault on the east, and by the Nujiang Fault on the west (Jin 2002). Similar to the South Qiangtang and Lhasa blocks, the lowermost Permian in this block is dominated by glacio-marine diamictites and pebbly mudstone, namely the Dingjiazhai Formation (Jin 2002; Jin *et al.* 2011). The earliest fusulines occurred in the uppermost part of the Dingjiazhai Formation, which are dominated by the *Eoparafusulina–*'*Pseudofusulina*' assemblage (Ueno 2003; Shi *et al.* 2011). This fauna indicates a Sakmarian–early Yakhtashian age and resembles contemporaneous assemblages in other peri-Gondwanan regions such as Central Pamir and Karakorum (Ueno *et al.* 2002; Shi *et al.* 2011).

The younger fusuline fauna was documented from the lower part the Shazipo Formation. These fusulines were well studied in the Xiaoxinzhai section and Bawei section in the southern Baoshan Block (Huang *et al.* 2009, 2015*a*, 2017). In the Xiaoxinzhai section, the fusulines constitute four zones, the '*Schwagerina*' *yunnanensis* Zone, the *Eopolydiexodina* Zone, the *Sumatrina* Zone and the *Verbeekina* Zone, in ascending order, with the former two zones belonging to the Murgabian and latter two zones belonging to the Midian (Huang *et al.* 2009, 2015*a*). The fusulines in the '*Schwagerina*' *yunnanensis* Zone are composed of schwagerinids, such as *Chusenella*, '*Schwagerina*'and *Parafusulina*, and some verbeekinids, such as *Pseudodoliolina* and *Verbeekina* (Huang *et al.* 2009). The *Eopolydiexodina* Zone can be distinguished from the underlying '*Schwagerina*' *yunnanensis* Zone by the dominance of *Eopolydiexodina* and other genera such as *Xiaoxinzhaiella* and *Neofusulinella* (Huang *et al.* 2009). According to Huang *et al.* (2015*b*), the neoschwagerinids and verbeekinids took over the schwagerinids in the overlying two zones. In the Bawei section, however, the fusulines are typified by the *Yangchienia–Nankinella* assemblage in the lower Shazipo Formation, and *Chusenella–Rugosofusulina* assemblage in the upper Shazipo Formation (Huang *et al.* 2015*b*, 2017). The compositional difference between the Bawei and Xiaoxinzhai sections is considered to be the result of different depositional environments (Huang *et al.* 2015*b*).

Tengchong Block. The Tengchong Block is situated to the west of the Baoshan Block (Jin 2002). The fusulines from this block have received limited study (Fan 1993; Shi *et al.* 2008, 2017). The earliest fusuline record in this block is characterized by the dominance of *Eoparafusulina* in the lower part of the Dadongchang Formation, which could be correlated with the Kalatkash fauna in the peri-Gondwanan regions (Shi *et al.* 2008). Fan (1993) reported the occurrence of *Cancellina* fauna in the upper part of the Guanyingshan Formation (equivalent to lower part of the Dadongchang Formation). However, this fauna was not found in later research (Shi *et al.* 2017). Middle Permian fusulines in the middle part of the Dadongchang Formation are

typified by the dominance of the *Nankinella–Chusenella* assemblage, and those in the Yanpozi Formation in the southern Tengchong are dominated by *Chusenella–Schwagerina* according to Shi *et al.* (2017). These two assemblages are quite similar to those found in the Xainza area of the Lhasa Block.

Sibumasu Block. The Sibumasu Block proposed by Metcalfe (1984) includes the Baoshan and Tengchong blocks in western Yunnan, China, Shan State in eastern Myanmar, western Thailand, Peninsular Thailand, western Malaya and Sumatra. As the latest research has indicated that the Baoshan and Tengchong blocks may have not adjoined with the Shan State of eastern Myanmar during the Late Palaeozoic (Zhang *et al.* 2013*a*; Xie *et al.* 2016), the Sibumasu Block cited in this paper does not include the Baoshan and Tengchong blocks in western Yunnan.

The Sibumasu Block, like other Peri-Gondwanan blocks, was dominated by glacio-marine deposits during the earliest Permian (Metcalfe 2013). The earliest fusuline fauna is represented by the antitropical *Monodiexodina shiptoni* fauna in western Thailand (Ingavat & Douglass 1981). Its age was considered to be Bolorian or early Kubergandian (Ueno 2006). However, a nearly contemporaneous assemblage from the Tarn To Formation in the Yala area, southernmost Peninsular Thailand and the Kinta Valley in Malaysia yields abundant Tethyan fusulines ascribed to the *Misellina claudiae* Zone and *Leeina kraffti* Zone, in ascending order (Ishii 1966; Ueno *et al.* 2015). The appearance of these Tethyan elements was explained to be the result of a spike in warming in the Sibumasu Block (Ueno *et al.* 2015).

The middle Permian fusulines have a lower diversity. They are scattered in the Ratburi limestone in western Thailand and the Plateau limestone group in the Shan Plateau in eastern Myanmar. In some places, such as the Sakangyi area in eastern Myanmar and the Doi Pha Daeng area in eastern Thailand, the fusulines are composed of *Neoschwagerina*, *Afghanella* and *Sumatrina* (Fontaine & Suteethorn 1988; Zaw *et al.* 2011). Other genera in the Ratburi limestone include *Rauserella*, *Kahlerina*, *Minojapanella*, *Yangchienia*, *Eopolydiexodina*, *Rugososchwagerina*, *Chusenella* and *Nankinella* (Ueno 2003). *Eopolydiexodina* is a characteristic genus in the Sibumasu Block, which is closely linked to many other Peri-Gondwanan blocks (Ueno 2003).

The late Permian fusulines are more limited in the Sibumasu Block, and were reported from western Thailand. They contain a few genera such as *Reichelina*, *Nanlingella*, *Codonofusiella*, *Staffella* and *Nankinella* (Fontaine & Suteethorn 1988; Ueno 2003).

Exotic limestone blocks within the Indus–Yarlung Tsangpo Suture Zone. Some isolated blocks, scattered in the mélange of the Indus–Yarlung Tsangpo Suture Zone in southern Tibet, are known as the exotic limestone blocks (Shen *et al.* 2003). These limestones yield abundant fusulines ranging from Midian to latest Changhsingian in age (Lys *et al.* 1980; Wang *et al.* 1981, 2010; Wang & Ueno 2009; Zhang *et al.* 2009; Zhang 2010). Middle Permian fusulines were reported from the Xilanta Formation in the Gyanyima limestone block (Zhang *et al.* 2009; Zhang 2010) and the Lasaila limestone block in Zhongba County (Wang *et al.* 1981). All these fusulines bear similarities with South China, such as the presence of *Neoschwagerina*, *Verbeekina*, *Chusenella*, *Codonofusiella*, *Yangchienia* and *Lantschichites* (Wang *et al.* 1981; Zhang *et al.* 2009). However, some characteristic middle Permian fusulines have not yet been reported in these exotic limestone blocks, such as *Afghanella*, *Sumatrina*, *Yabeina* and *Lepidolina.* These fusulines are grouped into the *Neoschwagerina fusiformis–Lantschichites minima* assemblage.

Late Permian fusulines in these exotic limestone blocks were widely documented (Lys *et al.* 1980; Wang & Ueno 2009; Wang *et al.* 2010). The exact age of these fusulines is not easily determined due to a lack of *Palaeofusulina*, but they can be broadly ascribed to late Dzhulfian–Dorashamian. The fusulines in these blocks are dominated by *Reichelina*, *Parareichelina*, *Codonofusiella*, *Dilatofusulina* and *Nankinella* (Lys *et al.* 1980; Wang *et al.* 1981, 2010), and were grouped into the *Reichelina pulchra–Dilatofusulina orthogonios* assemblage by Wang *et al.* (2010).

Northern Gondwanan margin. The fusulines occurred in the Gondwanan margin such as Oman, Timor and Salt Range of Pakistan with gradual demise of the early Permian glaciation. In the margin of the Arabian plate, the earliest record of fusulines is represented by some '*Pseudofusulina*' species including '*P*'. *inobservabilis*, '*P*'. ex gr. *karapetovi karapetovi*, '*P*'. aff. *karapetovi tezakensis* and '*P*'. *licis* (Angiolini *et al.* 2006). Those fusulines indicate a late Sakmarian age, and represent the typical Kalaktash fusuline fauna reported from the Central Pamir (Leven 1993). The Yakhtashian and Bolorian fusulines were reported from the Aseelah units, which were originally deposited on the carbonate platform in the northern Arabian plate (Hauser *et al.* 2000). The Yakhtashian fusuline fauna consists of *Leeina kraffti*, *Schubertella* cf. *simplex* and *Minojapanella* cf. *elongata*, whereas Bolorian fusuline yields *Minojapanella* cf. *elongata*, *M.* cf. *parva* and *Skinnerella* ex gr. *japonica* (Hauser *et al.* 2000). The Yakhtashian and Bolorian fusulines were also documented from the Bua-bai

limestone in Timor, where the fusulines consist of sporadic species of *Monodiexodina wanneri*, *Praeskinnerella* sp. and *Nankinella* sp. (Haig *et al.* 2017).

The succeeding fusuline assemblage in Oman is represented by *Skinnerella visseri* and *S. arabica* in the Qarari unit of the Batain group, indicating a Kubergandian age (Leven & Heward 2013). The Murgabian and Midian fusulines were reported from the Aseelah unit. They were represented by *Neoschwagerina simplex* in the lower and many advanced neoschwagerinids such as *Neoschwagerina margaritae*, *N. occidentalis* and *Colania douvillei* in the upper (Hauser *et al.* 2000; Vachard *et al.* 2002). The Murgabian fusulines also occurred in the Salt Range of Pakistan, where they were represented by only *Monodiexodina kattaensis* and *Codonofusiella laxa* (Douglass 1970). In Timor, the only Midian fusuline is represented by *Lantschichites weberi* from the Maubisse group (Schubert 1915; Thompson 1949).

The Lopingian fusulines were not reported from Oman, but sporadically occurred in the upper part of the Wargal Formation in the Salt Range, Pakistan. They comprise mainly *Nanlingella simplex*, *Reichelina* sp., and *Codonofusiella* aff. *schubertelloides* referable to the *Nanlingella simplex* Zone (Pakistan–Japanese Working Group 1985).

Angara Tethyan region

Angara Tethyan region refers to the blocks to the north of North China, which were located at relatively high latitude areas in the Northern Hemisphere (Ozawa 1987). It includes the Southern Kitakami and Hida terranes in northern Japan, Southern Primorye in eastern Russia and the Inner Mongolia area in northern China (Fig. 6). The blocks in this region are characterized by the occurrence of the antitropical genus *Monodiexodina* during the middle Permian.

Southern Kitakami Terrane. The Southern Kitakami Terrane, different from those pre-Cretaceous accretionary terranes in Japan, was always in a position proximal to the China continents during the Permian (Tazawa 1991; Kobayashi 1999). The earliest Permian sequence in the Southern Kitakami Terrane is represented by the Sakamotozawa Formation, which rests unconformably above the Upper Carboniferous strata (Kanmera & Mikami 1965). This formation was subdivided into four units, respectively the Sa and Sb members in the lower subformation and the Sc and Sd subformation in the upper subformation (Mikami 1965). Kanmera & Mikami (1965) established the *Zellia nunosei* and *Eoparafusulina langsonensis* zones in the Sb member of the Sakamotozawa Formation. These two zones consist of diverse fusuline species such as *Zellia nunosei*, *Eoparafusulina langsonensis*, *Nipponitella explicata* and *Quasifusulina tenuissima* (Kanmera & Mikami 1965). The fusulines contained in the Sa member include *Eoparafusulina* aff. *perplexa*, *Nipponitella explicata* and *Quasifusulina*? sp., which were considered to be similar to the fusuline elements in the overlying Sb member (Ueno *et al.* 2007). In the basal part of the Sakamotozawa in the Kamiyasse area of Kesennuma, however, the fusulines are composed of *Dutkevitchia*? *hindukushiensis*, *Shichanella* cf. *callosa*, *Pseudochusenella* ex gr. *cushmani*, *Nipponitella* sp. and *Eoparafusulina* sp. (Ueno *et al.* 2011). Thus, the fusulines in the Sa and Sb members in the Sakamotozawa Formation indicate a Sakmarian age (Watanabe 1991; Ueno *et al.* 2011). In the Sc and Sd members of the Sakamotozawa Formation, Kanmera & Mikami (1965) established the *Chalaroschwagerina vulgaris*, *Leeina fusiformis* and *Shichanella callosa* zones, respectively. Watanabe (1991) assigned a Yakhtashian age for these three zones. However, the upper part of the Sakamotozawa Formation contains elements of *Misellina* (Choi 1972; Ueno *et al.* 2009). So, the *Leeina fusiformis* and *Shichanella amgibua* zones in the Sd member of the Sakamotozawa Formation were considered to be Bolorian in age in terms of the presence of '*Pseudofusulina*' *dzamantalensis*, *Darvasites minatoi* and *Kubergandella*? sp. (Ueno *et al.* 2009).

Besides the Sakamotozawa Formation, the Midian fusulines were widely reported from the Southern Kitakami Terrane (Choi 1970, 1973; Kobayashi *et al.* 2009). They can be grouped into four zones, the *Sumatrina annae* Zone, the *Monodiexodina sutchanica* Zone, the *Parafusulina motoyoshi* Zone and the *Lepidolina shiraiwensis* Zone, in ascending order (Shiino *et al.* 2008; Kobayashi *et al.* 2009). The species *Sumatrina annae* was found in the Hoso-o Formation accompanying with *Pseudodoliolina pseudolepida* (Shiino *et al.* 2008). At the bottom of the overlying Kamiyasse Formation or equivalent beds in the Southern Kitakami Terrane, *Monodiexodina sutchanica* is highly concentrated (Ehiro & Misaki 2004; Kobayashi *et al.* 2009). The overlying fusuline elements consist of *Parafusulina motoyoshiensis*, *P. oyensis*, *Chusenella pseudocrassa*, *C. sinensis*, which were ascribed to the *Parafusulina motoyoshiensis* Zone (Kobayashi *et al.* 2009). The *Lepidolina shiraiwensis* fauna occurs in the upper part of the Kamiyasse Formation, which may correspond to the *Lepidolina multiseptata* Zone of Choi (1973). The fusulines in this zone include *Lepidolina shiraiwensis*, *L. multiseptata*, *Verbeekina verbeeki*, *Chusenella andersoni* and *Codonofusiella* sp. (Kobayashi *et al.* 2009).

The Late Permian fusulines are represented by scarce species such as *Nanlingella* cf. *meridionalis*,

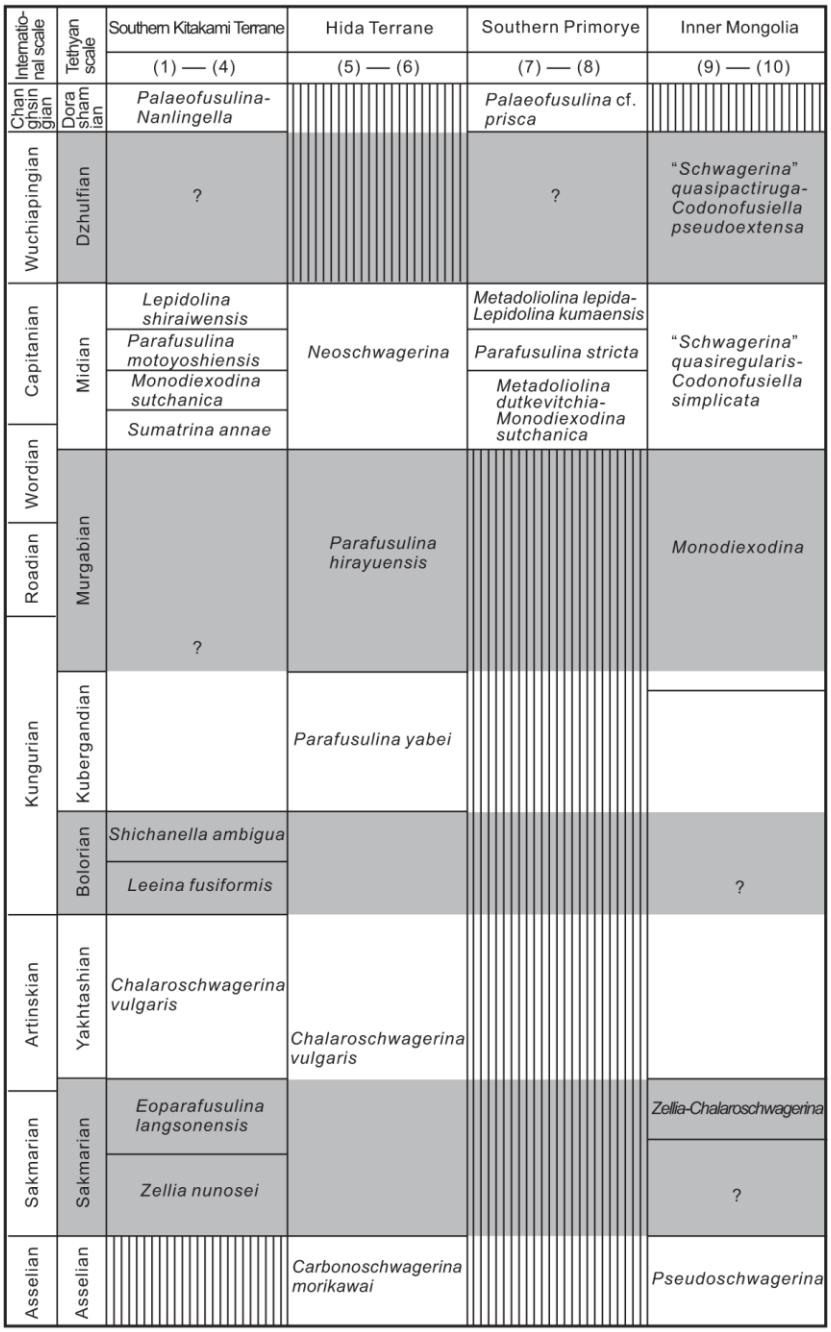

Fig. 6. Schematic framework of Permian fusuline biozones in the Angara Tethyan region. References are: (1) Kanmera & Mikami (1965); (2) Ueno *et al.* (2009); (3) Kobayashi *et al.* (2009); (4) Kobayashi (2002); (5) Igo (1957); (6) Igo (1959); (7) Kotlyar *et al.* (2006); (8) Ueno *et al.* (2005); (9) Sheng (1958); (10) Xia (1981).

Palaeofusulina sp., *Reichelina changhsingensis* and *Nankinella* sp. in the upper part of the Toyoma Formation (Kobayashi 2002). These fusulines overall indicate a Dorashamian age.

Hida Terrane. Like the South Kitakami Terrane, the Hida Terrane is located in the inner zone of Japan. The lowermost Permian fusulines are characterized by the *Carbonoschwagerina morikawai* Zone in the upper part of the Mizuyagadani Formation. There are species of *Carbonoschwagerina*, *Quasifusulina*, *Triticites* and *Rugosofusulina* (Igo 1957; Niikawa 1978). The overlying zone was documented in the lower part of the Hirayu Group, where the

Pseudoschwagerina Zone was covered by the *Chalaroschwagerina vulgaris* Zone (Igo 1959). This zone may range up to Bolorian because of the presence of *Misellina minor*. The succeeding zone is represented by the *Parafusulina yabei* Zone and the *Parafusulina hirayuensis* Zone, in ascending order (Igo 1959). The latter zone may range into Murgabian as evidenced by the dominance of typical *Parafusulina* and *Pseudodoliolina* (Igo 1959). The uppermost part of the Hirayu Group yields scarce *Neoschwagerina margaritae* and '*Schwagerina*' sp. that were grouped into the *Neoschwagerina* Zone (Igo 1959). This zone is probably Midian in age.

Southern Primorye. Southern Primorye area in Russia was composed of many terranes such as Voznesensk, Nakhimovsk and Okrainsk terranes (Kotlyar *et al.* 2006). The lower Permian strata in South Primorye are composed of terrestrial sediment with diverse plant fossils. The occurrence of fusulines starts as late as Midian (Kotlyar *et al.* 2006). Overall, the fusulines found in the Chandalaz Formation were grouped into three zones, respectively the *Metadoliolina dutkevitchi–Monodiexodina sutchanica* Zone, the *Parafusulina stricta* Zone and the *Metadoliolina lepida–Lepidolina kumaensis* Zone, in ascending order (Ueno *et al.* 2005; Kotlyar *et al.* 2006). The *Metadoliolina dutkevitchi–Monodiexodina sutchanica* Zone contains *Metadoliolina*, *Monodiexodina*, *Minojapanella*, *Lantschichites*, *Codonofusiella*, *Pseudofusulina*, *Parafusulina* and *Reichelina* (Sosnina 1981; Ueno *et al.* 2005; Kotlyar *et al.* 2006). The overlying *Parafusulina stricta* Zone is characterized by the appearance of *Lepidolina multiseptata* and rare *Yabeina* (Kotlyar *et al.* 2006). The *Metadoliolina lepida–Lepidolina kumaensis* Zone occurs in the upper part of the Chandalaz Formation, and is much more diverse than the underlying two zones. The common genera found in this zone include *Metadoliolina*, *Lepidolina*, *Sichotenella*, *Rauserella*, *Reichelina*, *Parareichelina*, *Minojapanella*, *Lantschichites*, *Codonofusiella*, *Chusenella*, *Parafusulina*, *Kahlerina* and *Pseudokahlerina* (Sosnina 1981; Kotlyar *et al.* 2006).

Late Permian fusulines were discovered in the Yastrebovka or equivalent formations in Southern Primorye (Sosnina 1981; Kotlyar *et al.* 2006). The fusulines consist of *Palaeofusulina* cf. *prisca*, *Shindella* sp., *Sphaerulina zisongzhengensis*, *Reichelina ulachensis* and *R. chorensis* (Sosnina 1981; Vuks & Chediya 1986; Kotlyar *et al.* 2006). Their age is Dorashamian in terms of abundant *Colaniella parva* in this assemblage (Kotlyar *et al.* 2006).

Inner Mongolia. Abundant fusulines were reported from the central part of Inner Mongolia of China, which tectonically belongs to the southern margin of the Altaid Belt (Shen *et al.* 2006). The Permian sequence is dominated by siliciclastic rocks and limestones beds (e.g. Han 1975; Xia 1981). The fusulines were found discretely in limestone beds. The lowermost zone is the *Pseudoschwagerina* Zone characterized by species of *Pseudoschwagerina*, *Triticites*, *Quasifusulina* and '*Schwagerina*'. It is of Asselian age and was reported in the Baiyunebo area (Sheng 1958; Han 1975). A younger fusuline fauna occurred in the Sonid right banner area yields *Eoparafusulina*, *Zellia*, *Chalaroschwagerina* and *Nipponitella*. This fauna probably suggests a late Sakmarian age. The overlying fusuline zone was named as the *Monodiexodina* Zone, which comprises *Monodiexodina*, *Parafusulina*, *Laxifusulina*, *Pseudodoliolina*, *Yangchienia* and *Armenina* (Xia 1981). Its age is broadly assigned to late Kubergandian to Murgabian. The upper two zones, respectively the '*Schwagerina*' *quasiregularis–Codonofusiella simplicata* Zone in the upper part of the Zhesi Formation and the '*Schwagerina*' *quasipactiruga–Codonofusiella pseudoextensa* Zone in the Yihewusu Formation, indicate a Murgabian to Midian age (Xia 1981). It is noteworthy that no neoschwagerinids have ever been reported in these two zones.

Panthalassan region

During the Permian, many seamounts developed in the Panthalassa Ocean. Those seamounts collapsed when they were amalgamated with continents surrounding the Panthalassan Ocean. So, the fusulines belonging to Panthalassan Province were dispersed in many allochthonous terranes in Japan, Canada, and New Zealand (Fig. 7).

Akiyoshi Terrane. The Akiyoshi Terrane in the Inner Zone of SW Japan represents the oldest accretionary complex in Japan (Ueno 1996). The Omi limestone in the south of Niigata Prefecture may represent the NE extremity of the Akiyoshi Terrane (Ueno & Nakazawa 1993). The Akiyoshi limestone in the Akiyoshidai area preserves a complete carbonate succession ranging from Early Carboniferous to middle Permian in the Panthalassa Ocean (Ueno 1996). The biostratigraphic schemes of Ota (1997) and Ueno (1996) are adopted in this paper.

The Permian starts from the appearance of *Pseudoschwagerina muongthensis*, which is associated with *Schubertella kingi*, '*Schwagerina*' *primigena* and '*S*'. *okafujii*. They were grouped in the *Pseudoschwagerina muongthensis* Zone (Ota 1997). This zone corresponds to the *Triticites simplex* Subzone of Toriyama (1954) because this subzone is also dominated by species of *Pseudoschwagerina* and *Triticites*. Its age is most likely to be Asselian. The overlying fusulines include

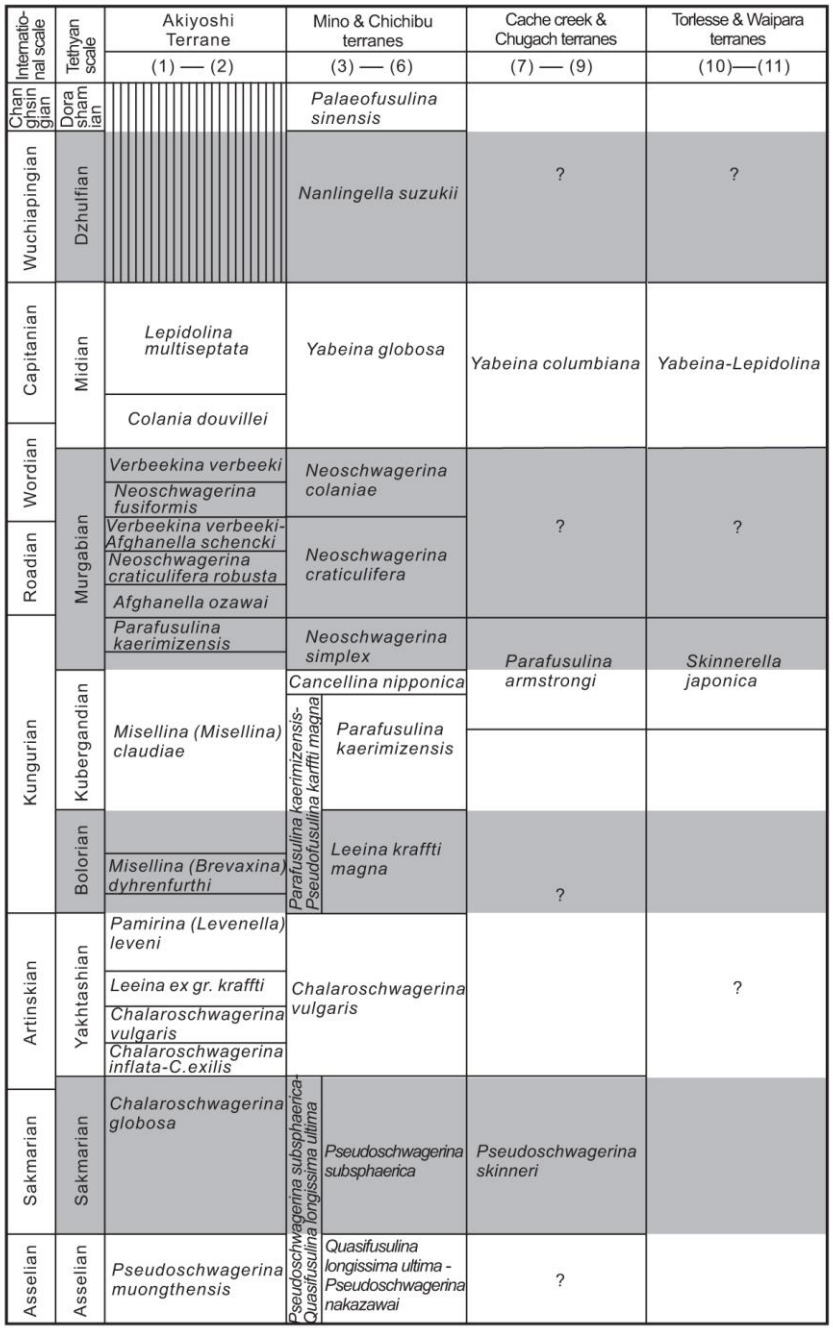

Fig. 7. Schematic framework of Permian fusuline biozones in the Panthalassan region. References are: (1) Ota (1997); (2) Ueno (1996); (3) Nogami (1961); (4) Kobayashi (2011); (5) Ota & Isozaki (2006); (6) Kobayashi (1997*b*); (7) Sada & Danner (1992); (8) Thompson & Verville (1950); (9) Rui & Nassichuk (1996); (10) Leven & Grant-Mackie (1997); (11) Vachard & Ferriere (1991).

Chalaroschwagerina globosa and *Paraschwagerina* sp., which was ascribed to the *Chalaroschwagerina globosa* Zone.

The overlying fusulines were named as the *Chalaroschwagerina inflata–Chalaroschwagerina exilis* Zone with newly appeared species of *Biwaella* and *Mesoschubertella* (Ueno 1996). The succeeding fusulines were grouped into the *Chalaroschwagerina vulgaris* and *Leeina* ex gr. *kraffti* zones, which comprise mostly *Chalaroschwagerina*, pseudofusulinid species and some small taxa such as *Pseudoendothyra* and *Schubertella* (Ueno 1996). The

above-mentioned three zones were assigned to the lower Yakhtashian (Ueno 1996). The overlying fusulines are dominated by small forms such as *Pamirina* (*Levenella*), *Minojapanella*, *Pseudoreichelina*, *Staffella* and *Pseudoendothyra*, which were named as the *Pamirina* (*Levenella*) *leveni* Zone. Because the species *Misellina* (*Brevaxina*) *nipponica* occurs in the upper part of this zone, the age of the *Pamirina* (*Levenella*) *leveni* Zone is clearly late Yakhtashian–lower Bolorian (Ueno 1996). The appearance of *Misellina* (*Brevaxina*) *dyhrenfurthi otai* marks a new zone in which primitive *Misellina* elements also occurred (Ueno 1996). The overlying zone was named as the *Misellina claudiae* Zone by Ueno (1996). It should be noted, however, that the *Misellina claudiae* Zone used here is different from those adopted widely in South China because many neoschwagerinids occurred in this zone in the Akiyoshi limestone such as *Maklaya pamirica* and *Neoschwagerina simplex* (Ueno 1996). The presence of the species *Neoschwagerina simplex* indicates a Murgabian age for the upper part of this zone.

The *Misellina claudiae* Zone is succeeded by the *Parafusulina kaerimizensis* Zone. In the latter zone, many schwagerinids occurred, including *Parafusulina kaerimizensis*, *P. lutugini* and *Chusenella alpina* (Ueno 1996). Above this zone, *Afghanella*, *Neoschwagerina*, *Verbeekina* and *Pseudodoliolina* appeared successively. They were assigned into the *Afghanella ozawai*, *Neoschwagerina craticulifera robusta*, *Verbeekina verbeeki–Afghanella schencki*, *Neoschwagerina fusiformis* and *Verbeekina verbeeki* zones, in ascending order (Ueno 1996).

The following fusuline zones include the *Colania douvillei* Zone and the *Lepidolina multiseptata* Zone, in ascending order (Ueno 1996). Common genera in these zones are *Verbeekina*, *Sumatrina*, *Kahlerina* and *Pseudokahlerina* (Ueno 1996). These two zones overall indicate a Midian age.

Mino and Chichibu terranes. Many seamounts developed in the Panthalassa Ocean during the Permian, and were later accreted to mainland Japan during the Jurassic–Early Cretaceous (Kobayashi 1999, 2011; Ueno *et al.* 2006). These seamounts were preserved as blocks of various sizes in the mélange, which were roughly included into the Mino Terrane or the Chichibu Terrane. The biostratigraphy of these limestone blocks has been thoroughly studied (e.g. Honjo 1959; Zaw 1999; Kobayashi 2011, 2012).

Among all the limestone blocks studied, the Akasaka limestone preserved a good record of fusuline zonations (e.g. Ozawa 1927; Zaw 1999). However, fusulines older than Kubergandian have not been discovered in the Akasaka limestone. These older fusulines have been reported from the Itsukaichi-Ome area of west Tokyo and the Atetsu Plateau (Nogami 1961; Kobayashi 2005). The early Permian fusulines were classified into the *Pseudoschwagerina subsphaerica–Quasifusulina longissima ultima*, *Chalaroschwagerina vulgaris* and *Parafusulina kaerimizensis–Leeina kraffti magna* zones, in ascending order (Nogami 1961). The former zone consists of the lower *Quasifusulina longissima ultima–Pseudoschwagerina nakazawai* Subzone and the upper *Pseudoschwagerina subsphaerica* Subzone, respectively, most probably indicating an Asselian–Sakmarian age. The overlying *Chalaroschwagerina vulgaris* Zone is composed of *C. vulgaris* and *C. globosa* of Yakhtashian age. The *Parafusulina kaerimizensis–Leeina kraffti magna* Zone also comprises the lower *Leeina kraffti magna* Subzone and the upper *Parafusulina kaeimizensis* Subzone (Nogami 1961). The latter subzone was considered to be equivalent to the *Parafusulina nakamigawai* Zone in the lower part of the Akasaka limestone, which indicates a Kubergandian age (Kobayashi 2011).

The overlying zone in the Akasaka limestone is the *Cancellina nipponica* Zone. It consists of *Cancellina*, *Codonofusiella*, *Neofusulinella*, *Toriyamaia* and *Pseudoreichelina* (Kobayashi 2011). The Murgabian fusulines in the Akasaka limestone were grouped into three zones according to the evolution of *Neoschwagerina*; they are the *Neoschwagerina simplex* Zone, the *N. craticulifera* Zone and the *N. colaniae* Zone from lower to upper. It is noticeable that *Gifuella* was found in both the *Neoschwagerina craticulifera* and *N. colaniae* zones, however, this genus was not found in the Akiyoshi Terrane. The appearance of *Yabeina* species above the *Neoschwagerina colaniae* Zone marks the beginning of the Midian age. It was ascribed to the *Yabeina globosa* Zone, which is identical to the *Yabeina igoi* Zone of Zaw (1999).

Many large fusulines went extinct across the Guadalupian–Lopingian boundary (Ota & Isozaki 2006). Thus, the remaining fusulines in the Dzhulfian were grouped into the *Nanlingella suzukii* Zone, which comprises small taxa such as *Nanlingella*, *Codonofusiella* and *Reichelina* (Ota & Isozaki 2006; Kobayashi 2011). The uppermost Permian fusulines have not been documented from the Akasaka limestone; but they were reported from the Iwai-Kanyo area in west Tokyo (Kobayashi 1997*b*). The fusulines found from the pebbles are referable to the *Palaeofusulina sinensis* Zone (Kobayashi 1997*b*).

Cache Creek and Chugach terranes. Along the western margin of the North American Craton some terranes developed extending from Alaska to central California in the USA. The fusulines are different from those of the North American Craton

faunas in possessing abundant neoschwagerinids. These terranes were roughly ascribed to the Cache Creek Terrane and the Chugach Terrane (Ross 1995; Stevens *et al.* 1997; Johnston & Borel 2007; Kobayashi *et al.* 2007).

The fusulines from these two terranes can be subdivided into three assemblages. The lowest assemblage is characterized by the *Pseudoschwagerina skinneri* fauna, suggesting a Sakmarian age (Sada & Danner 1992). The slightly younger fusulines are dominated by *Parafusulina armstrongi* of late Kubergandian–Murgabian age (Thompson & Verville 1950). The youngest fauna is widely distributed in western Canada and the NW USA (Thompson & Wheeler 1942; Ross 1971; Rui & Nassichuk 1996; Kobayashi *et al.* 2007) or southern margin of Alaska (Stevens *et al.* 1997). These fusulines are named as the *Yabeina columbiana* Zone, which comprises *Yabeina*, *Lepidolina*, *Rauserella*, *Reichelina*, *Codonofusiella* and *Schwagerina*.

Torlesse and Waipara terranes in New Zealand. The Torlesse and Waipara terranes on the eastern margin of New Zealand are different from mainland New Zealand in yielding diverse warm-water Tethyan fusulines (Hornibrook 1951; Vachard & Ferriere 1991; Leven & Grant-Mackie 1997; Leven & Campbell 1998). These fusulines can be grouped into two assemblages. The older assemblage is characterized by the *Skinnerella japonica* assemblage of all *Skinnerella* species, with its age being late Kubergandian–Murgabian (Leven & Campbell 1998). The younger assemblage, however, consists of diverse fusulines such as *Yabeina*, *Reichelina*, *Kahlerina*, *Minojapanella*, *Sichotenella*, *Codonofusiella*, *Rauserella*, *Dunbarula*, *Chusenella*, *Neoschwagerina* and *Lepidolina* (Vachard & Ferrière 1991; Leven & Grant-Mackie 1997). This *Yabeina–Lepidolina* assemblage is Midian in age.

North American Craton region

North America and South America were located at the western margin of Pangaea during the Permian. As the Rheic Ocean closed during the Mississippian, there was little faunal communication between the Palaeotethys and North America (Qiao & Shen 2014). This results in a distinctive bioprovince in North America (Yancey 1975; Kobayashi 1997*a*).

The fusulines are widely distributed in both North and South America. In addition to the USA, some fusulines were also documented from Mexico (e.g. Vachard *et al.* 2000), Guatemala (e.g. Ross 1962), Venezuela (Thompson & Miller 1949), Peru (e.g. Wood *et al.* 2002) and Bolivia (e.g. Dunbar & Newell 1946). Overall, these faunas are broadly correlatable with each other. Thus, the biostratigraphy subdivision scheme of the USA serves as a criterion.

The Lower Permian chronostratigraphy was classified into the Wolfcampian Epoch and the Leonardian Epoch (Ross 1963). The Wolfcampian fusulines were grouped into three zones: the *Triticites–Thompsonites* Zone in the lower part, the *Triticites–Pseudoschwagerina* Zone in the middle and the *Pseudoschwagerina–Eoparafusulina* Zone in the upper part (Ross 1963). The lowest zone, which corresponds to the fusulines in the Bursumian Stage or the Newwellian Stage, contains *Thompsonites*, *Pseudofusulina* and *Leptotriticites*, and these were considered to be the earliest Permian fusulines (Wilde 1990, 2006; Lucas *et al.* 2015). However, because *Pseudoschwagerina* and *Sphaeroschwagerina* are widely considered to be indicators of the Permian, then it is better to place the uppermost part of the Newwellian Stage in the Permian because of the presence of *Pseudoschwagerina* in that interval (Wilde 2006). The succeeding zone is characterized by abundant *Pseudoschwagerina* species in the Middle Wolfcampanian (Nealian Stage) (Ross & Ross 1994). In this regard, the *Pseudoschwagerina uddeni–Occidentoschwagerina* Zone of Wilde (1984) is equivalent to the *Triticites–Pseudoschwagerina* Zone of Ross (1963). The overlying *Pseudoschwagerina–Eoparafusulina* Zone is characterized by the dominance of species of *Pseudoschwagerina*, *Paraschwagerina* and *Eoparafusulina* (Ross 1963).This zone is equivalent to the *Pseudoschwagerina convexa–Eoparafusulina linearis* assemblage of Ross & Ross (2003).

The fusulines of the Leonardian differ greatly from the underlying Wolfcampian fusulines in the appearance of the genus *Parafusulina* (Ross 1963). The lowermost part of the Leonardian faunas was named as the *Praeskinnerella crassitectoria–Praeskinnerella guembeli* Zone, whereas four other zones were subdivided based on the evolution of the *Parafusulina* species. They are the *Parafusulina allisonensis* Zone, the *P. deltoides* Zone, the *P. spissisepta* Zone and the *P. brooksensis–P. vidriensis* Zone, in ascending order (Ross 1960).

The biostratigraphic subdivision of the Guadalupian Series has been studied by many researchers (e.g. Dunbar & Skinner 1937; Wilde & Rudine 2000; Yang & Yancey 2000). The biostratigraphic subdivision scheme of Yang & Yancey (2000) is followed here.

The *Parafusulina bosei* Zone in the lower part of the Road Canyon Formation differs from the underlying Leonardian fusuline fauna in the appearance of genera such as *Rauserella* and *Yangchienia*. From this zone onwards, the biostratigraphic subdivision was based on the evolution of *Parafusulina* from the middle part of the Road Canyon Formation to the upper part of the Word Formation. It was

classified into the *Parafusulina rothi*, *P. trumpyi*, *P. sellardsi* and *P. antimonioensis* zones, in ascending order (Yang & Yancey 2000). The former two zones belong to the Roadian and the latter two are of Wordian age.

The Capitanian Stage is typified by an abundance of the *Polydiexodina* species that was assigned into *Polydiexodina shumardi* Zone in the lower part of the Altuda Formation or Capitan limestone. Some genera, such as *Reichelina* and *Codonofusiella*, occurred from this zone (Yang & Yancey 2000). A spectacular feature during the Capitanian in Texas, USA was the occurrence of *Yabeina texana* in the Guadalupe Mountains (Skinner & Wilde 1955; Nestell & Nestell 2006). With the extinction of large fusulines such as *Yabeina* and *Polydiexodina*, the fusulines in the upper part of the Altuda Formation are dominated by smaller fusulines such as *Reichelina*, *Codonofusiella*, *Paradoxiella*, *Rauserella* and *Lantschichites* (Yang & Yancey 2000; Nestell & Nestell 2006). They were grouped into two zones: the *Reichelina lamarensis* Zone and the *Paraboultonia splendens* Zone, in ascending order (Yang & Yancey 2000). The *Reichelina lamarensis* Zone is equivalent to the *Paradoxiella* and *Reichelina lamarensis* zones of Wilde & Rudine (2000). Accordingly, the *Paraboultonia splendens* Zone of Yang & Yancey (2000) is equal to the *Paraboultonia–Lantschichites* Zone of Wilde & Rudine (2000).

Correlations of different Permian chronostratigraphic scales

Asselian

The Asselian Stage is characterized by the dominance of pseudoschwagerinids with loosely coiled outer volutions, such as *Pseudoschwagerina* and *Sphaeroschwagerina*. The transition of the *Triticites*-dominated assemblage in the Gzhelian of the Late Carboniferous to a *Pseudoschwagerina*- or *Sphaeroschwagerina*-dominated assemblage can be recognized in various regions, such as the Southern Urals (Rauzer-Chernousova 1965), Darvaz (Leven & Scherbovich 1978; Leven *et al.* 1992), South China (Xiao *et al.* 1986; Ding *et al.* 1989), North China (Wang *et al.* 1992), Tarim (Zheng & Lin 1991), Iran (Leven & Taheri 2003) and North America (Ross 1963; Ross & Ross 1994). Consequently, the base of the Asselian on the Tethyan scale corresponds to the base of the Zisongian Stage in South China and the base of the upper part of the Newwellian Stage (lower Wolfcampian) in North America (Fig. 8). In addition to *Pseudoschwagerina* and *Sphaeroschwagerina*, some Gzhelian (latest Carboniferous) genera, such as *Triticites*, *Quasifusulina* and *Rauserites*, can also range up into the Asselian.

Sakmarian

Sakmarian fusuline faunas share a lot of common genera with the underlying Asselian faunas, such as *Pseudoschwagerina*, *Rugosofusulina* and *Paraschwagerina*. That is possibly the reason why both the Asselian and the Sakmarian were grouped into the Zisongian Stage in South China (L.X. Zhang *et al.* 1988; Z.H. Zhang *et al.* 1988; Sheng & Jin 1994). Nevertheless, Sakmarian fusulines are characterized by the flourishing of species of *Eoparafusulina*, *Darvasites* and *Zellia* in the Tethyan region, such as the Carnic Alps (Forke 2002; Davydov *et al.* 2013), the Tarim Block (Zheng & Lin 1991), South China (L.X. Zhang *et al.* 1988; Shi *et al.* 2009), Darvaz (Leven *et al.* 1992) and north Afghanistan (Leven 1997). In North America, diverse species of *Eoparafusulina* and *Paraschwagerina* were documented in the upper part of the Wolfcampian strata such as the Leonox Hills Formation in Texas (Ross 1963), as well as the middle part of the Bird Spring Formation in southern California (Stevens & Stone 2007). Taking into account these similarities, the Sakmarian Stage in the Tethyan region is roughly correlated with the Lenoxian Stage of the upper Wolfcampian (Fig. 8). However, it should be mentioned that the upper part of the Lenoxian may fall within the Yakhtashian Stage of the Tethyan regions because of the presence of the genus *Chalaroschwagerina* (Wilde 1984). Additionally, it should be pointed out that the common Sakmarian fusuline genera, such as *Zellia* and *Darvasites*, in the Tethyan area were not reported in North America.

With regard to the correlations of the Sakmarian of the Tethyan scale with that of the international scale, the sections from the Carnic Alps help to resolve this correlation because of the presence of both fusulines and conodonts (Forke 2002). In those sections, the typical Artinskian conodont *Sweetognathus* aff. *whitei* and *Mesogondolella* cf. *bisseli* coexist with *Zellia*, *Robustoschwagerina* and *Pseudoschwagerina* of the Tethyan Sakmarian age (Forke 2002). Thus, the Tethyan Sakmarian Stage corresponds to the Sakmarian and lowermost Artinskian of the international scale (Fig. 8). The Sakmarian Stage of the Tethyan scale was replaced by the Hermagorian Stage, which is equal to the Sakmarian and the lower part of the Artinskian age of the international scale (Davydov *et al.* 2013)

Yakhtashian. The Yakhtashian fusulines can be differentiated from the underlying Sakmarian fusulines by the apperance of many characteristic genera such as *Chalaroschwagerina*, *Pamirina*

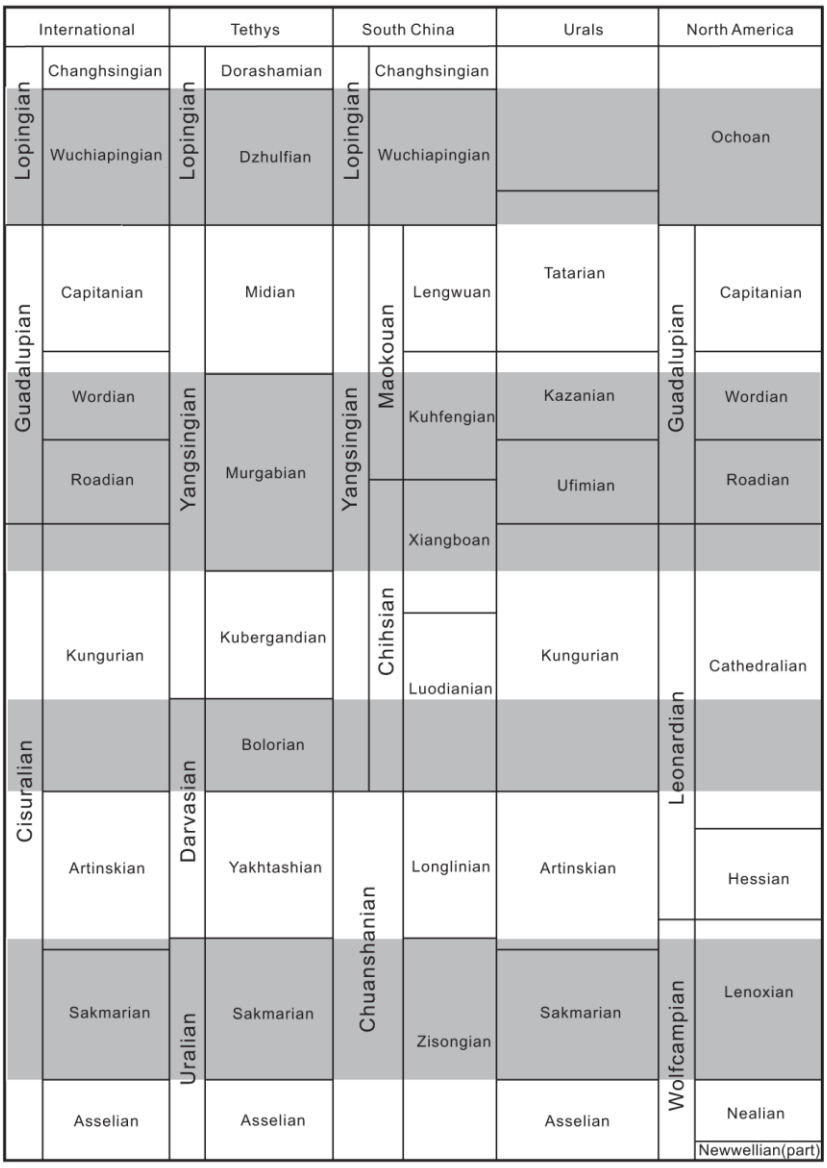

Fig. 8. Correlations of different Permian chronostratigraphic subdivisions between different regions/scales.

(*Levenella*), *Pamirina* (*Pamirina*), *Praeskinnerella*, *Mesoschubertella* and *Toriyamaia*. The base of the Yakhtashian was defined by the occurrence of *Pamirina* (*Levenella*) or *Chalaroschwagerina* (Leven 2004). The *Chalaroschwagerina–Laxifusulina* fauna and the *Pamirina* fauna were considered to be contemporaneous but under a different depositional environment (Xia *et al.* 1986; Xu *et al.* 1986), although it is clear that the first occurrence of *Chalaroschwagerina* was earlier than that of *Pamirina* (*Levenella*) or *Pamirina* (Xu *et al.* 1986; Leven *et al.* 1992; Ueno 1996). The Longlinian Stage in South China is characterized by the *Pamirina–Darvasites* assemblage, which is contemporaneous with the Yakhtashian Stage of the Tethyan scale (Huang *et al.* 1982).

As mentioned earlier, the upper part of the Sakmarian of the Tethyan scale corresponds to the lowermost part of the Artinskian of the international scale. Consequently, the Yakhtashian Stage of the Tethyan scale is Artinskian in age.

Pamirina (*Levenella*) and *Pamirina* (*Pamirina*) have not been documented in America so far. This has hampered a direct correlation of chronostratigraphy between Tethys and North America. However, abundant *Chalaroschwagerina* occurs in the upper part of the Wolfcampian Series (Skinner & Wilde 1965; Magginetti *et al.* 1988; Ross & Ross

1994). In addition, the *Praeskinnerella* species, common in the Yakhtashian in the Tethyan region, are equal to the fusulines from the Hessian Stage of the Leonardian Series in the fusuline evolutionary stage (Ross & Ross 1997). Consequently, the Yakhtashian Stage broadly corresponds to the upper part of the Lenoxian Stage and the Hessian Stage (Leven 2004).

Bolorian

The evolution of *Pamirina* gave rise to *Misellina* (*Brevaxina*) and *Misellina*, which is the basis for the recognition of the base of the Bolorian Stage of the Tethyan scale (Leven 2004) or the Luodianian Stage of the South China scale (Sheng & Jin 1994). Common genera that prevailed in the Bolorian Stage include *Misellina* (*Brevaxina*), primitive *Misellina*, *Chalaroschwagerina*, *Darvasites*, *Leeina* and *Praeskinnerella* (Leven 2004). In correlation, the Luodianian of South China contains the *Misellina* (*Brevaxina*) *dyhrenfurthi*, *Misellina termieri*, *M. claudiae* and *Shengella simplex* zones, in ascending order (Xiao *et al.* 1986; Sheng & Jin 1994), which is longer than the Bolorian Stage. Consequently, the Bolorian Stage corresponds to the lower part of the Luodianian Stage in South China (Fig. 8).

The Bolorian of the Tethyan scale is hardly correlatable with the American scale owing to the lack of *Misellina* (*Brevaxina*) and *Misellina* in North America. In terms of the conodonts and ammonoids, the Bolorian Stage corresponds to part of the Cathedralian Stage of the American scale (Jin *et al.* 1997; Leven 2004).

Kubergandian

The Kubergandian Stage is typified by advanced forms of *Misellina*, such as *Misellina ovalis* and *M. claudiae*, and primitive neoschwagerinids, such as *Cancellina* successively (Leven 2004). Common genera found in the Kubergandian Stage include *Misellina*, *Armenina*, *Pseudodoliolina*, *Yangchienia*, *Maklaya*, *Cancellina*, *Nankinella*, *Neofusulinella*, *Pisolina*, *Sphaerulina* and *Parafusulina*. The Xiangboan Stage in South China contains two zones, the *Cancellina liuzhiensis* and the *Neoschwagerina simplex* zones, based on the sections from the Houchang area (Xiao *et al.* 1986). Consequently, the Kubergandian corresponds to the upper part of the Luodianian Stage and the lower part of the Xiangboan Stage.

The correlation of the Kubergandian Stage with the international scale has been a contentious issue (Leven 2004; Leven & Gorgij 2011*a*; Wang *et al.* 2011*a*; Angiolini *et al.* 2015). This stage was originally correlated with the Roadian Stage (Jin *et al.* 1997); however, the latest study of the strata in both South China and Japan confirmed that the conodont *Mesogondolella siciliensis–Sweetognathus guizhouensis* coexists with *Neoschwagerina simplex* of typical Murgabian species (Henderson & Mei 2003; Shen *et al.* 2013). These facts indicate that the Kubergandian Stage falls within the Kungurian Stage of the international scale. However, the Kubergandian Stage was correlated to the lower Roadian by Davydov *et al.* (2013) and to the upper Kungurian–early Roadian by Angiolini *et al.* (2015). More work is required in the future to verify their precise correlations.

The correlation of the Kubergandian Stage with the American scale is still not easily determined because the fusulines from North America are dominated by *Parafusulina* from the Cathedralian Stage to the Wordian Stage (Wilde 1990; Yang & Yancey 2000; Ross & June 2003). However, some common species such as *Parafusulina bakeri* documented from both South China and North America may indicate that the Kubergandian Stage can be correlated broadly with the upper part of the Cathedralian Stage (Z.H. Zhang *et al.* 1988; Ross & June 2003).

Murgabian. The Murgabian is characterized by the appearance of *Neoschwagerina*, which might be evolved from the *Maklaya* of the underlying Kubergandian Stage (Yang 1985; Leven 2004). In addition, the genus *Cancellina* evolved to *Presumatrina*, *Afghanella* and *Sumatrina* succeedingly during the early Murgabian (Yang 1985). Other genera include *Verbeekina*, *Armenina*, *Cancellina*, *Yangchienia*, *Chusenella* and *Parafusulina*, which are similar to the underlying Kubergandian Stage. However, the schwagerinid genus *Eopolydiexodina* developed well in bi-temperate regions in the Tethyan region during the Murgabian (Ueno 2003).

The Guadalupian Series of North America was adopted as the candidate Middle Permian chronostratigraphy in the international scale. However, a direct correlation between the Middle Permian Tethyan scale and the North American (international) scale is difficult because the Guadalupian Series in North America is dominated by abundant schwagerinids, such as *Parafusulina* and *Polydiexodina*, whereas in the Tethys it is dominated by abundant neoschwagerinids. However, conodonts and ammonites play important roles in this correlation. As mentioned previously, *Neoschwagerina simplex*, an index species of the base Murgabian, was found to coexist with Kungurian conodonts (Henderson & Mei 2003; Shen *et al.* 2013). Consequently, the lowermost Murgabian may be correlated with the upper part of the Kungurian of the international scale. With regard to the upper boundary of the Murgabian, both conodonts and ammonites proved that it falls within the Wordian Stage (e.g. Rui & Nassichuk 1996; Henderson & Mei

2003). However, this assignment was challenged by Angiolini *et al.* (2015), who claimed that the uppermost Murgabian fusulines coexist with Capitanian conodonts. Such a discrepancy requires more work in the future.

As previously stated, *Neoschwagerina simplex* occurred in the upper part of the Xiangboan Stage (Xiao *et al.* 1986). Thus, the lower part of the Murgabian is correlatable with the upper part of the Xiangboan Stage. Upwards, the Xiangboan Stage in China was succeeded by the Khufengian Stage (Sheng & Jin 1994). The Kuhfengian Stage was originated from the Kuhfeng Formation, which is characterized by ammonoids, conodonts, brachiopods and radiolarians (Sheng & Jin 1994). The equivalent strata in the Houchang section in the Guizhou Province bear two zones: the *Neoschwagerina craticulifera* Zone and the *N. margaritae* Zone (Xiao *et al.* 1986; L.X. Zhang *et al.* 1988). Because the *Neoschwagerina margaritae* Zone was regarded as the base Midian Stage (Leven 1996; Ueno *et al.* 2003), the upper boundary of the Murgabian Stage thus falls within the upper part of the Kuhfengian Stage. In conclusion, the Murgabian of the Tethyan scale corresponds to the upper Xiangboan Stage and the lower Kuhfeng Stage of South China (Fig. 8).

Midian. The base of the Midian Stage is characterized by the occurrence of the genus *Yabeina* (Leven 2004). This genus represents the most advanced forms of neoschwagerinids. In the Akasaka limestone of Japan, *Yabeina* occurs in the *Neoschwagerina margaritae* Zone (Zaw 1999). In South China, *Yabeina* first occurs in the upper part of the Houziguan limestone (Xiao *et al.* 1986). In addition, *Yabeina* or *Lepidolina* occur widely in Western Tethyan regions (e.g. Skinner & Wilde 1967), the Gondwanan Tethyan area (Zhu 1982*b*) and Panthalassan regions (e.g. Zaw 1999; Kobayashi *et al.* 2007; Kobayashi 2011). Common genera of the Midian Stage include *Yabeina*, *Lepidolina*, *Metadoliolina*, *Dunbarula*, *Kahlerina*, *Lantschichites*, *Reichelina*, *Codonofusiella* and *Paradoxiella*.

As mentioned above, the lower boundary of the Midian Stage corresponds to the upper Wordian of the international scale or the upper Kuhfeng Stage of the South China scale based on the evidence of coexisting conodonts and ammonoids (e.g. Rui & Nassichuk 1996; Henderson & Mei 2003). Thus, the middle and upper part of the Midian Stage is equal to the Lengwuan Stage of South China and the Capitanian Stage of the North American (international) scale because both the Lengwuan Stage and the Capitanian Stage possess *Yabeina*, *Reichelina*, *Kahlerina* and *Codonofusiella* typical of the Tethyan Midian Stage.

The upper boundary of the Midian Stage correlates well with the upper boundary of the Capitanian Stage or the Lengwuan Stage because this boundary marks the greatest mass extinction event for fusulines, especially for those schwagerinids and neoschwagerinids (Jin *et al.* 1994; Yang *et al.* 2004). A more detailed study has proved that the loss of schwagerinids and neoschwagerinds takes place prior to the Guadalupian–Lopingian boundary (Ota & Isozaki 2006; Groves & Wang 2013). This biostratigraphic information was well documented from both the Panthalassan region and the North American region, where many smaller fusulines, such as *Reichelina*, *Codonofusiella*, *Paradoxiella*, occurred in the latest Midian and latest Capitanian stages (Wilde & Rudine 2000; Yang & Yancey 2000; Nestell & Nestell 2006; Ota & Isozaki 2006).

Dzhulfian

Because of the extinction of the neoschwagerinids and schwagerinids during the latest Midian, the remaining fusulines in the Dzhulfian of the late Permian have reduced greatly in diversity. The most dominant genera during the Dzhulfian Stage are *Codonofusiella*, *Nankinella* and *Reichelina* (Sheng 1963; Rui 1979). In the meantime, the genera, such as *Gallowayinella*, *Tewoella*, *Paradunbarula* and *Palaeofusulina*, started to diversify (Leven 2004).

The stratotypes for the Wuchiapingian and Changhsingian stages are from South China (Jin *et al.* 2006*a*, *b*). The base of the Changhsingian Stage was defined by the first occurrence of *Clarkina wangi* (Jin *et al.* 2003). This conodont corresponds to the first occurrence of the fusuline *Palaeofusulina minima* (Jin *et al.* 2003). In addition, *Gallowayinella meitianensis*, underlying the *Palaeofusulina minima* Zone, coexists with *Clarkina orientalis* and *C. liangshanensis* of the upper Wuchiapingian (Wang *et al.* 1997). Consequently, the Dzhulfian Stage of the Tethyan scale is equal to the Wuchiapingian Stage of the South China scale (international scale).

Dorashamian

The Dorashamian Stage is the uppermost stage of the Permian. During this time, the genus *Palaeofusulina* has evolved to the advanced *Palaeofusulina sinensis* assemblage (Sheng & Rui 1984; Sheng & Jin 1994). The associated genera include *Nanlingella*, *Parananlingella*, *Nankinella*, *Sphaerulina*, *Reichelina*, *Staffella* and *Parareichelina* (Leven 2004). As addressed above, the Dorashamian Stage may correspond to the Changhsingian Stage of the South China scale (international scale) (Leven & Gorgij 2011*a*). All these fusulines became extinct by the end of the Dorashamian/Changhsingian because of the onset of the Permian/Triassic mass extinction event (Jin *et al.* 2000; Shen *et al.* 2011).

Summary

Fusulines are a kind of larger benthic foraminifer living in tropical and subtropical environments during the Permian. The rapid evolutionary rate and distinct biostratigraphic subdivision play an important role in global stratigraphic correlation.

Overall, there are several important evolutionary key points that permit the biostratigraphic boundaries to be defined. The advent of *Pseudoschwagerina* or *Sphaeroschwagerina* marks the base of the Asselian Stage. These pseudoschwagerinids gave rise to *Zellia* and *Robustoschwagerina* during the Sakmarian. During the Yakhtashian, *Levenella* and *Pamirina* originated from the Tethyan region and formed the basis of the neoschwagerinids. The following first occurrences of *Misellina (Brevaxina)*, advanced *Misellina*, *Neoschwagerina* and *Yabeina* define the base of the Bolorian, Kubergandian, Murgabian and Midian stages, respectively. Both neoschwagerinids and schwagerinids became extinct by the end of the Midian. The remaining fusulines during the Dzhulfian were small-sized *Codonofusiella* and *Reichelina*, and a few newly formed genera such as *Palaeofusulina* and *Gallowayinella*. *Palaeofusulina*, in particular, has evolved to *Palaeofusulina sinensis*, the index fossil for the Dorashamian/Changhsingian Stage. In summary, the evolutionary milestones of fusulines have formed the basis of fusuline biostratigraphy across the Tethyan region.

By contrast, the evolution of fusulines in the North American Craton region has a different story. The main difference between the Tethyan region and the North American Craton region lies in the faunal compositions from the Leonardian Stage to the Capitanian Stage. The fusulines of North America during this interval are characterized by the dominance of schwagerinids such as *Parafusulina* and *Polydiexodina.* However, *Parafusulina* plays a subordinate role from the Kubergandian to the Midian in the Tethyan region. Therefore, the direct and precise correlation of middle Permian fusuline biostratigraphy between the Tethyan region and the North American Craton region requires further detailed investigation.

We thank Prof. Daniel Vachard and Dr Yukun Shi for their critical reviews, which improved the manuscript greatly. We also thank Prof. Spencer Lucas and Prof. Shuzhong Shen for inviting our paper. This paper is jointly funded by the Strategic Priority Research Programme (B) of the Chinese Academy of Sciences (XDB18000000 and XDB03010102), the National Science Foundation of China (41420104003, 41290260, 41472029 and 41372024), the Ministry of Science and Technology of China (2015FY310100-9), and the Youth Innovation Promotion Association CAS for ZYC (2016282).

References

Alksne, A.E. & Isakova, T.N. 1980. O kompleksakh fuzulinid pogranichnyh otlozhenii Gzheliskogo i Asseliskogo yarusov nekotorykh razrezov yuzhnogo Urala i Russkoi Platformy. *Voprosy Mikropaleontologii*, **23**, 52–62 [in Russian].

Amiot, M., Ciry, R. *et al.* 1965. *Fossils of Karakorum and Chitral*. E.J. Brill, Leiden, The Netherlands.

Angiolini, L., Stephenson, M.H. & Leven, E.J. 2006. Correlation of the Lower Permian surface Saiwan Formation and subsurface Haushi limestone, Central Oman. *Geoarabia*, **11**, 17–38.

Angiolini, L., Zanchi, A. *et al.* 2015. From rift to drift in South Pamir (Tajikistan): Permian evolution of a Cimmerian terrane. *Journal of Asian Earth Sciences*, **102**, 146–169, https://doi.org/10.1016/j.jseaes.2014.08.001

Angiolini, L., Campagna, M. *et al.* 2016. Brachiopods from the Cisuralian–Guadalupian of Darvaz, Tajikistan and implications for Permian stratigraphic correlations. *Palaeoworld*, **25**, 539–568, https://doi.org/10.1016/j.palwor.2016.05.006

Aw, P.C., Ishii, K. & Okimura, Y. 1977. On Palaeofusulina–Colaniella fauna from the Upper Permian of Kelantan, Malaysia. *Transactions and Proceedings of the Palaeontological Society of Japan, New Series*, **1977**, (104), 407–417.

Baghbani, D. 1993. The Permian sequence in the Abadeh region, Central Iran. *In*: *Bibliography of South American Geology: Volume II, Bolivia, Brazil, Chile, Colombia*. Earth Sciences and Resources Institute (ERSI), University of South Carolina, Occasional Publications, 7–22.

Bensh, F.R. 1972. *Stratigrafiya i fuzulinidy verkhnego paleozoya yuzhnoi Fergany*. Akademiya nauk uzbekskoi SSR, institut geologii i geofiziki, Tashkent [in Russian].

Chen, Q.H., Wang, J.P., Wang, S.L. & Wu, K.Y. 1999. Discovery of the Upper Permian series in Cuoqin Basin, Xizang (Tibet) and its geological significance. *Chinese Science Bulletin*, **44**, 1520–1523.

Cheng, L.R., Li, C., Zhang, Y.C. & Wu, S.Z. 2005. The *Polydiexodina* (Fusulinids) fauna from central Qiangtang, Tibet, China. *Acta Micropalaeontologica Sinica*, **22**, 152–162.

Choi, D.R. 1970. Permian fusulinids from Imo, southern Kitakami Mountains, N. E. Japan. *Journal of the Faculty of Science, Hokkaido University, Series 4. Geology and Mineralogy*, **14**, 327–354.

Choi, D.R. 1972. Classification and phylogeny of genus *Misellina* with description of some *Misellina* from the Lower Permian in the Southern Kitakami Mountains, Japan. *Journal of the Faculty of Science, Hokkaido University, Series 4. Geology and Mineralogy*, **15**, 625–645.

Choi, D.R. 1973. Permian Fusulinids from the Setamai-Yahagi district, southern Kitakami Mountains, N.E. Japan. *Journal of the Faculty of Science, Hokkaido University, Series 4, Geology and Mineralogy*, **16**, 1–90.

Chuvashov, B.I., Dupina, G.V., Mizens, G.A. & Chernyh, V.V. 1990. *Opornye razrezy verhnego Karbona i nizhnei Permi zapadnogo sklona urala i priuraliya.*

Akademiya Nauk SSSR. Uraliskoe Otdelenie, Sverdlovsk, Russia [in Russian].

Ciry, R. & Amiot, M. 1965. Sur Quelques Foraminifères Permiens D'Asie Centrale. *In*: Amiot, M., Ciry, R. *et al.* (eds) *Fossils of Karakorum and Chitral*. E.J. Brill, Leiden, 127–133.

Colpaert, C., Monnet, C. & Vachard, D. 2015. Eopolydiexodina (Middle Permian giant fusulinids) from Afghanistan: biometry, morphometry, paleobiogeography, and end-Guadalupian events. *Journal of Asian Earth Sciences*, **102**, 127–145, https://doi.org/10.1016/j.jseaes.2014.10.028

Davydov, V.I. 1990*a*. Clarification of the origin and phylogeny of *Triticites* and of the boundary of the middle and upper Carboniferous. *Paleontological Journal*, **2**, 39–51.

Davydov, V.I. 1990*b*. Zanalinoe Delenie Gzheliskogo yarusa v Donbasse i Preddoneckom protibe po fuzulinidam. *In*: Bogdanova, T.N. & Bugrova, E.M. (eds) *Problemy sovremennoi mikropaleontologii*. 'Nauka' Leningradskoe otdelenie, Leningrad, Russia, 52–63.

Davydov, V.I. 2013. The GSSP at the Aidaralash section is solid and has no alternative. *Permophiles*, **58**, 13–15.

Davydov, V.I. & Arefifard, S. 2007. Permian fusulinid fauna of Peri-Gondwanan affinity from the Kalmard region, east-central Iran and its significance for tectonics and paleogeography. *Palaeontologia Electronica*, **10**, 1–40.

Davydov, V.I. & Arefifard, S. 2013. Middle Permian (Guadalupian) fusulinid taxonomy and biostratigraphy of the mid-latitude Dalan Basin, Zagros, Iran and their applications in paleoclimate dynamics and paleogeography. *GeoArabia*, **18**, 17–62.

Davydov, V.I., Snyder, W.S. & Spinosa, C. 1997. Upper Paleozoic Fusulinacean Biostratigraphy of the Southern Urals. *Permophiles*, **30**, 11–14.

Davydov, V., Krainer, K. & Chernykh, V. 2013. Fusulinid biostratigraphy of the Lower Permian Zweikofel Formation (Rattendorf Group; Carnic Alps, Austria) and Lower Permian Tethyan chronostratigraphy. *Geological Journal*, **48**, 57–100, https://doi.org/10.1002/gj.2433

Dawson, O. 1993. Fusuline foraminiferal biostratigraphy and carbonate facies of the Permian Ratburi Limestone, Saraburi, central Thailand. *Journal of Micropalaeontology*, **12**, 9–33, https://doi.org/10.1144/jm.12.1.9

Ding, P.Z., Jin, T.A. & Sun, X.F. 1989. Carboniferous–Permian boundary of Xikou area of Zhen'an, south Shanxi, east Qinling Range. *Compte Rendu Congrès International de Stratigraphie et de Géologie du Carbonifère*, **2**, 199–206.

Douglass, R.C. 1970. Morphologic study of fusulinids from the Lower Permian of West Pakistan. United States Geological Survey, Professional Papers, **643**, 1–11.

Dunbar, C.O. & Newell, N.D. 1946. Marine Early Permian of the central Andes and its fusuline faunas. Part II. *American Journal of Science*, **244**, 457–491.

Dunbar, C.O. & Skinner, J.W. 1937. Permian Fusulinidae of Texas. *The University of Texas Bulletin*, **3701**, 517–825.

Ehiro, M. & Misaki, A. 2004. Stratigraphic range of the genus *Monodiexodina* (Permian Fusulinoidea): additional data from the Southern Kitakami Massif, Northeast Japan. *Journal of Asian Earth Sciences*, **23**, 483–490.

Fan, J.C. 1993. Bryozoans of Late Carboniferous–early Early Permian in Tengchong area of western Yunnan. *Yunnan Geology*, **12**, 383–406.

Fontaine, H. & Suteethorn, V. 1988. Late Palaeozoic and Mesozoic fossils of West Thailand and their environments. *CCOP Technical Bulletin*, **20**, 1–121.

Fontaine, H., Prinya, P. & Vachard, D. 1999. A microfossil-rich Kubergandian (Lower Middle Permian) limestone of southern Laos. *Proceedings of the International Symposium on Shallow Tethys*, **5**, 170–178.

Fontaine, H., Salyapongse, S., Tien, N.D. & Vachard, D. 2002. The Permian of Khao Tham Yai area in Northeast Thailand. *In*: Mantajit, N. (ed.) *The Symposium on Geology of Thailand: 26–31 August 2002, Bangkok, Thailand*. Department of Mineral Resources, Bangkok, Thailand, 58–76.

Fontaine, H., Hoang, T.T., Kavinate, S., Suteethorn, V. & Vachard, D. 2013. Upper Permian (Late Changhsingian) marine strata in Nan Province, northern Thailand. *Journal of Asian Earth Sciences*, **76**, 115–119, https://doi.org/10.1016/j.jseaes.2013.01.006

Forke, H.C. 2002. Biostratigraphic subdivision and correlation of Uppermost Carboniferous/Lower Permian sediments in the Southern Alps: fusulinoidean and condont faunas from the Carnic Alps (Austria/Italy), Karavanke Mountains (Slovenia), and Southern Urals (Russia). *Facies*, **47**, 201–275.

Gaetani, M. & Leven, E. 1993. Permian stratigraphy and fusulinids from Rosh Gol (Chitral, E Hindu Kush). *Rivista Italiana di Paleontologia e Stratigrafia*, **99**, 307–326.

Gaetani, M. & Leven, E.J. 2014. The Permian succession of the Shaksgam valley, Sinkiang (China). *Italian Journal of Geosciences*, **133**, 45–62, https://doi.org/10.3301/IJG.2013.10

Gaetani, M., Angiolini, L. *et al.* 2009. Pennsylvanian–Early Triassic stratigraphy in the Alborz Mountains (Iran). *In*: Brunet, M.-F., Wilmsen, M. & Granath, J.W. (eds) *South Caspian to Central Iran Basins*. Geological Society, London, Special Publications, **312**, 79–128, https://doi.org/10.1144/SP312.5

Ghazzay, W., Vachard, D. & Razgallah, S. 2015. Revised fusulinid biostratigraphy of the Middle–Late Permian of Jebel Tebaga (Tunisia). *Revue de Micropaleontologie*, **58**, 57–83, https://doi.org/10.1016/j.revmic.2015.04.001

Groves, J.R. & Wang, Y. 2013. Timing and size selectivity of the Guadalupian (Middle Permian) fusulinoidean extinction. *Journal of Paleontology*, **87**, 183–196, https://doi.org/10.1666/12-076R.1

Gubler, J. 1935. Les Fusulinidés Permiens de l'Indochine. *Mémoires de la Société Géologique de France*, **26**, 5–173.

Haig, D.W., Mory, A.J. *et al.* 2017. Late Artinskian–Early Kungurian (Early Permian) warming and maximum marine flooding in the East Gondwana interior rift, Timor and Western Australia, and comparisons

across East Gondwana. *Palaeogeography, Palaeoclimatology, Palaeoecology*, **468**, 88–121, https://doi.org/10.1016/j.palaeo.2016.11.051

Han, J.X. 1975. Late Carboniferous fusulinids from the Amushan area, Wulanchabu district, Inner Mongolia. *Papers of Stratigraphy and Paleontology*, **1**, 132–203.

Hauser, M., Vachard, D., Martini, R., Matter, A., Peters, T. & Zaninetti, L. 2000. The Permian sequence reconstructed from reworked carbonate clasts in the Batain Plain (northeastern Oman). *Comptes Rendus de l'Académie des Sciences, Series IIA – Earth and Planetary Science*, **330**, 273–279.

Henderson, C.M. & Mei, S.L. 2003. Stratigraphic v. environmental significance of Permian serrated conodonts around the Cisuralian–Guadalupian boundary: new evidence from Oman. *Palaeogeography, Palaeoclimatology, Palaeoecology*, **191**, 301–328, https://doi.org/10.1016/S0031-0182(02)00669-7

Honjo, S. 1959. Neoschwagerinids from the Akasaka Limestone (A Paleontological study of the Akasaka Limestone, 1st Report). *Journal of the Faculty of Science, Hokkaido University, Series 4, Geology and Mineralogy*, **10**, 111–162.

Hornibrook, N.B. 1951. Permian fusulinid foraminifera from the North Auckland Peninsula, New Zealand. *Transactions and Proceedings of the Royal Society of New Zealand*, **79**, 319–321.

Huang, H., Jin, X.C. & Yang, X.N. 2007. Middle Permian fusulinids from the Xainza area of the Lhasa Block, Tibet. *Acta Palaeontologica Sinica*, **46**, 62–74 [in Chinese with English abstract].

Huang, H., Jin, X.C., Shi, Y.K. & Yang, X.N. 2009. Middle Permian western Tethyan fusulinids from southern Baoshan block, western Yunnan, China. *Journal of Paleontology*, **83**, 880–896.

Huang, H., Jin, X. & Shi, Y. 2015*a*. A *Verbeekina* assemblage (Permian fusulinid) from the Baoshan Block in western Yunnan, China. *Journal of Paleontology*, **89**, 269–280, https://doi.org/10.1017/jpa.2014.24

Huang, H., Shi, Y. & Jin, X. 2015*b*. Permian fusulinid biostratigraphy of the Baoshan Block in western Yunnan, China with constraints on paleogeography and paleoclimate. *Journal of Asian Earth Sciences*, **104**, 127–144, https://doi.org/10.1016/j.jseaes.2014.10.010

Huang, H., Shi, Y.K. & Jin, X.C. 2017. Permian (Guadalupian) fusulinids of Bawei Section in Baoshan Block, western Yunnan, China: biostratigraphy, facies distribution and paleogeographic discussion. *Palaeoworld*, **26**, 95–114, https://doi.org/10.1016/j.palwor.2016.03.004

Huang, Z.X. & Zeng, X.L. 1984. The early Early Permian (Longlinian stage) fusulinid fauna from Longlin, Guangxi. *Earth Science – Journal of Wuhan College of Geology*, 11–24 [in Chinese with English abstract].

Huang, Z.X., Shi, Y. & Wei, M.C. 1982. A new stratigraphic unit of Permian–Longlinian stage. *Journal of Chengdu College of Geology*, 63–73 [in Chinese with English abstract].

Igo, H. 1957. Fusulinids of Fukuji, southeastern part of the Hida Massif, central Japan. *Science Reports of the Tokyo Kyoiku Daigaku, Section C, Geology, Mineralogy and Geography*, **5**, 153–246.

Igo, H. 1959. Some Permian fusulinids from the Hirayu district, southeastern part of the Hida Massif, central Japan. *Science Reports of the Tokyo Kyoiku Daigaku, Section C, Geology, Mineralogy and Geography*, **6**, 231–254.

Igo, H. 1966. Some Permian fusulinids from Pahang, Malaya. *In*: Kobayashi, T. & Toriyama, R. (eds) *Geology and Palaeontology of Southeast Asia, Volume 13*. University of Tokyo Press, Tokyo, Japan, 30–38.

Igo, H. 1972. Fusulinacean fossils from Thailand. part 6. Fusulinacean fossils from north Thailand. *Geology and Palaeontology of Southeast Asia*, **10**, 63–116.

Igo, H., Ueno, K. & Sashida, K. 1993. Lower Permian Fusulinaceans from Ban Phia, Changwat Loei, Northeastern Thailand. *Transactions and Proceedings of the Palaeontological Society of Japan, New Series*, **169**, 15–43.

Ingavat, R. & Douglass, R.C. 1981. Fusuline fossils from Thailand, part 14. The fusulinid genus *Monodiexodina* from Northwest Thailand. *Geology and Palaeontology of Southeast Asia*, **22**, 23–34.

Ingavat, R., Toriyama, R. & Pitakpaivan, K. 1980. Fusuline zonation and faunal characteristics of the Ratburi limestone in Thailand and its equivalents in Malaysia. *Geology and Palaeontology of Southeast Asia*, **21**, 43–62.

Ishii, K.I. 1966. Preliminary notes of the Permian fusulinids of H. S. Lee Mine No. 8 limestone near Kampar, Perak, Malaya. *Journal of Geoscience, Osaka City University*, **9**, 145.

Jiang, H.C., Wang, M.Z., Zhang, X.Q. & Li, Z.X. 2001. Study on the fusulinida fauna in the Taiyuan Formation from the east area of Jining coalfield, Shandong province. *Acta Palaeontologica Sinica*, **40**, 514–522 [in Chinese with English abstract].

Jin, X.C. 2002. Permo-Carboniferous sequences of Gondwana affinity in southwest China and their paleogeographic implications. *Journal of Asian Earth Sciences*, **20**, 633–646.

Jin, X.C., Huang, H., Shi, Y.K. & Zhan, L.P. 2011. Lithologic boundaries in Permian post-glacial sediments of the Gondwana-affinity regions of China: typical sections, age range and correlation. *Acta Geologica Sinica* (English edn), **85**, 373–386.

Jin, Y.G., Zhang, J. & Shang, Q.H. 1994. Two phases of the end-Permian Mass Extinction. *In*: Embry, A.F., Beauchamp, B. & Glass, D.J. (eds) *Pangea: Global Environments and Resources*. Canadian Society of Petroleum Geologists, Memoirs, **17**, 813–822.

Jin, Y.G., Wardlaw, B.R., Glenister, B.F. & Kotlyar, G.V. 1997. Permian chronostratigraphic subdivisions. *Episodes*, **20**, 6–10.

Jin, Y.G., Shang, Q.H., Wang, X.D., Wang, Y. & Sheng, J.Z. 1999. Chronostratigraphic subdivision and correlation of the Permian in China. *Acta Geologica Sinica*, **73**, 127–138.

Jin, Y.G., Wang, Y., Wang, W., Shang, Q.H., Cao, C.Q. & Erwin, D.H. 2000. Pattern of marine mass extinction near the Permian–Triassic boundary in South China. *Science*, **289**, 432–436.

Jin, Y.G., Henderson, C. *et al.* 2003. Proposal for the Global Stratotype Section and Point (GSSP) for the Wuchiapingian–Changhsingian Stage boundary

(Upper Permian Lopingian Series). *Permophiles*, **43**, 8–23.

Jin, Y.G., Shen, S.Z. *et al.* 2006*a*. The Global Stratotype Section and Point (GSSP) for the boundary between the Capitanian and Wuchiapingian stage (Permian). *Episodes*, **29**, 253–262.

Jin, Y.G., Wang, Y., Henderson, C., Wardlaw, B.R., Shen, S.Z. & Cao, C.Q. 2006*b*. The Global Boundary Stratotype Section and Point (GSSP) for the base of Changhsingian Stage (Upper Permian). *Episodes*, **29**, 175–182.

Johnston, S.T. & Borel, G.D. 2007. The odyssey of the Cache Creek terrane, Canadian Cordillera: implications for accretionary orogens, tectonic setting of Panthalassa, the Pacific superwell, and break-up of Pangea. *Earth and Planetary Science Letters*, **253**, 415–428.

Köylüoglu, M. & Altiner, D. 1989. Micropaléontologie (Foraminifères) et biostratigraphie du Permien supérieur de la région d'Hakkari (SE Turquie). *Revue de Paléobiologie*, **8**, 467–503.

Kanmera, K. & Mikami, T. 1965. Fusuline zonation of the Lower Permian Sakamotozawa Series. *Memories of Faculty of Science, Kyushu University, Series D, Geology*, **16**, 275–320.

Kobayashi, F. 1997*a*. Middle Permian biogeography based on fusulinacean faunas. *In*: Ross, C.A., Ross, J.R.P. & Brenckle, P.L. (eds) *Late Paleozoic Foraminifera: Their Biogeography, Evolution, and Paleoecology; and the Mid-Carboniferous Boundary*. Cushman Foundation for Foraminifera Research, Special Publications, **36**, 73–76.

Kobayashi, F. 1997*b*. Upper Permian foraminifers from the Iwai-Kanyo area, west Tokyo, Japan. *Journal of Foraminiferal Research*, **27**, 186–195, https://doi.org/10.2113/gsjfr.27.3.186

Kobayashi, F. 1999. Tethyan uppermost Permian (Dzhulfian and Dorashamian) foraminiferal faunas and their paleogeographic and tectonic implications. *Palaeogeography, Palaeoclimatology, Palaeoecology*, **150**, 279–307.

Kobayashi, F. 2002. Lithology and foraminiferal fauna of allochthonous limestones (Changhsingian) in the upper part of the Toyoma Formation in the South Kitakami Belt, Northeast Japan. *Paleontological Research*, **6**, 331–342.

Kobayashi, F. 2005. Permian foraminifers from the Itsukaichi-Ome area, west Tokyo, Japan. *Journal of Paleontology*, **79**, 413–432, https://doi.org/10.1666/0022-3360(2005)0792.0.co;2

Kobayashi, F. 2011. Permian fusuline faunas and biostratigraphy of the Akasaka limestone (Japan). *Revue de Paléobiologie*, **30**, 431–574.

Kobayashi, F. 2012. Middle and Late Permian foraminifers from the Chichibu belt, Takachiho area, Kyushu, Japan: implications for faunal events. *Journal of Paleontology*, **86**, 669–687, https://doi.org/10.1666/11-049r.1

Kobayashi, F. & Altiner, D. 2008. Late Carboniferous and Early Permian fusulinoideans in the central Taurides, Turkey: biostratigraphy, faunal composition and comparison. *Journal of Foraminiferal Research*, **38**, 59–73, https://doi.org/10.2113/gsjfr.38.1.59

Kobayashi, F. & Altiner, D. 2011. Discovery of the Lower Murgabian (Middle Permian) based on Neoschwagerinids and Verbeekinids in the Taurides, southern Turkey. *Rivista Italiana di Paleontologia e Stratigrafia*, **117**, 39–50.

Kobayashi, F. & Ishii, K.I. 2003. Paleobiogeographic analysis of Yakhtashian to Midian fusulinacean faunas of the Surmaq formation in the Abadeh region, central Iran. *Journal of Foraminiferal Research*, **33**, 155–165, https://doi.org/10.2113/0330155

Kobayashi, F., Ross, C.A. & Ross, J.R.P. 2007. Age and generic assignment of *Yabeina columbiana* (Guadalupian Fusulinacea) in southern British Columbia. *Journal of Paleontology*, **81**, 238–253, https://doi.org/10.1666/0022-3360(2007)81[238:aagaoy]2.0.co;2

Kobayashi, F., Shiino, Y. & Suzuki, Y. 2009. Middle Permian (Midian) foraminifers of the Kamiyasse Formation in the Southern Kitakami Terrane, NE Japan. *Paleontological Research*, **13**, 79–99, https://doi.org/10.2517/1342-8144-13.1.079

Kotlyar, G.V., Belyansky, G.C., Burago, V.I., Nikitina, A.P., Zakharov, Y.D. & Zhuravlev, A.V. 2006. South Primorye, Far East Russia – A key region for global Permian correlation. *Journal of Asian Earth Sciences*, **26**, 280–293.

Leven, E.J. 1967. Stratigrafiya i fuzulinidy perrmskikh otlozheniy Pamira. *Ademiya Nauk SSSR, Geologicheskiy Institut*, **167**, 1–224 [in Russian].

Leven, E.J. 1993. Early Permian fusulinids from the Central Pamir. *Rivista Italiana di Paleontologia e Stratigrafia*, **99**, 151–198.

Leven, E.J. 1996. The Midian Stage of the Permian and its boundaries. *Stratigraphy and Geological Correlation*, **4**, 540–551.

Leven, E.J. 1997. *Permian Stratigraphy and Fusulinida of Afghanistan with their Paleogeographic and Paleotectonic Implications*. Geological Society of America, Special Papers, **316**.

Leven, E.J. 2004. Fusulinids and Permian scale of the Tethys. *Stratigraphy and Geological Correlation*, **12**, 139–151.

Leven, E.J. 2010. Permian fusulinids of the east Hindu Kush and west Karakorum (Pakistan). *Stratigraphy and Geological Correlation*, **18**, 105–117.

Leven, E.J. & Campbell, H.J. 1998. Middle Permian (Murgabian) fusuline faunas, Torlesse terrane, New Zealand. *New Zealand Journal of Geology and Geophysics*, **41**, 149–156.

Leven, E.J. & Gorgij, M.N. 2006. Upper Carboniferous–Permian stratigraphy and fusulinids from the Anarak region, central Iran. *Russian Journal of Earth Sciences*, **8**, 1–25.

Leven, E.J. & Gorgij, M.N. 2008. Bolorian and Kubergandian stages of the Permian in the Sanandaj-Sirjan zone of Iran. *Stratigraphy and Geological Correlation*, **16**, 455–466, https://doi.org/10.1134/s0869593808050018

Leven, E.J. & Gorgij, M.N. 2011*a*. Fusulinids and stratigraphy of the Carboniferous and Permian in Iran. *Stratigraphy and Geological Correlation*, **19**, 687–776, https://doi.org/10.1134/s0869593811070021

Leven, E.J. & Gorgij, M.N. 2011*b*. First record of Gzhelian and Asselian Fusulinids from the Vazhnan Formation (Sanandaj-Sirjan zone of Iran). *Stratigraphy and Geological Correlation*, **19**, 486–501.

Leven, E.J. & Gorgij, M.N. 2013. Fusulinids from the lower Permian Chili Formation of the Rahdar section, Kalmard block, Central Iran. *Stratigraphy and Geological Correlation*, **21**, 408–420, https://doi.org/10.1134/s0869593813040060

Leven, E.J. & Grant-Mackie, J.A. 1997. Permian fusulinid foraminifera from Wherowhero Point, Orua Bay, Northland, New Zealand. *New Zealand Journal of Geology and Geophysics*, **40**, 473–486.

Leven, E.J. & Heward, A.P. 2013. Fusulinids from isolated Qarari limestone outcrops (Permian), occurring among Jurassic–Cretaceous Batain group (Batain Plain, Eastern Oman). *Rivista Italiana di Paleontologia e Stratigrafia*, **119**, 153–162.

Leven, E.J. & Scherbovich, S.F. 1978. *Fuzulinidy i stratigrafiya assclyskogo yarusa Darvaza*. Izdatel Nauka, Moscow, Russia [in Russian].

Leven, E.J. & Taheri, A. 2003. Carboniferous–Permian stratigraphy and fusulinids of East Iran. Gzhelian and Asselian deposits of the Ozbak-Kuh region. *Rivista Italiana di Paleontologia e Stratigrafia*, **109**, 399–415.

Leven, E.J., Leonova, T.B. & Dmitriev, V.Y. 1992. Permi Darvaz-Zaalayskoy zony Pamira: fuzulinidy, ammonoidei, stratigrafiya. *Rossiyskaya Akademiya Nauk, Trudy Paleontologicheskogo Instituta*, **253**, 1–203 [in Russian].

Leven, E.J., Naugolnykh, S.V. & Gorgij, M.N. 2011. New findings of Permian marine and terrestrial fossils in Central Iran (The Kalmard Block) and their significance for correlation of the Tethyan, Uralian, and west European scales. *Rivista Italiana di Paleontologia e Stratigrafia*, **117**, 355–374.

Li, J.C., Zhang, Z.H., Li, W.S. & Hong, Z.Y. 2010. Fusulinid fauna near the Carboniferous–Permian boundary in Shunchang, Fujian Province. *Geological Science and Technology Information*, **29**, 9–16.

Liang, D.Y., Nie, Z.T., Guo, T.Y., Xu, B.W., Zhang, Y.Z. & Wang, W.P. 1983. Permo-Carboniferous Gondwana–Tethys facies in southern Karakoran Ali, Xizang (Tibet). *Earth Science*, **19**, 9–27 [in Chinese with English abstract].

Lin, J.X., Pan, S.S. & Meng, F.Y. 1979. Late Carboniferous and Early Lower Permian fusulinids from Jiahe, Hunan. *Acta Palaeontologica Sinica*, **18**, 561–571 [in Chinese with English abstract].

Liu, G.C. 1993. Age assignment of Kaixinling Group and Wuli group in the middle Tanggula Mountains. *Qinghai Geology*, **2**, 1–9 [in Chinese with English abstract].

Loriga, C.B., Neri, C., Pasini, M. & Posenato, R. 1986. Marine fossil assemblages from Upper Permian to Lowermost Triassic in the western Dolomites (Italy). *Memorie della Societa Geologica Italiana*, **34**, 5–44.

Lucas, S.G. 2013. Reconsideration of the base of the Permian system. *New Mexico Museum of Natural History and Science Bulletin*, **60**, 230–232.

Lucas, S.G., Krainer, K. & Vachard, D. 2015. The lower Permian Hueco Group, Robledo Mountains, New Mexico (U.S.A.). *New Mexico Museum of Natural History and Science Bulletin*, **65**, 43–95.

Lys, M. & Lapparent, A.F.D. 1971. Foraminifères et microfaciès du Permien de l'Afghanistan central. *Notes et Mémoires sur le Moyen-Orient*, **12**, 49–166.

Lys, M. & Marcoux, J. 1978. Les niveaus du Permien supérieur des Nappes d'Antalya (Taurides occidentales, Turquie). *Comptes Rendus Hebdomadaires des Seances de l'Academie des Sciences*, **286**, 1417–1420.

Lys, M., Colchen, M., Bassoullet, J.P., Marcoux, J. & Mascle, G. 1980. La biozone à *Colaniella parva* du Permien Supérieur et sa microfauna dans le bloc calcaire exotique de Lamayuru, Himalaya du Ladakh. *Revue de Micropaléontologie*, **23**, 76–108.

Magginetti, R.T., Stevens, C.H. & Stone, P. 1988. *Early Permian Fusulinids from the Owens Valley Group, East-Central California*. Geological Society of America, Special Papers, **217**, 1–61.

Metcalfe, I. 1984. Stratigraphy, palaeontology and palaeogeography of the Carboniferous of Southeast Asia. *Mémoires de la Société Géologique de France*, **147**, 107–118.

Metcalfe, I. 2013. Gondwana dispersion and Asian accretion: tectonic and palaeogeographic evolution of eastern Tethys. *Journal of Asian Earth Sciences*, **66**, 1–33, https://doi.org/10.1016/j.jseaes.2012.12.020

Mikami, T. 1965. The type Sakamotozawa Formation. *Journal of Geological Society of Japan*, **71**, 475–493 [in Japanese].

Mikhailova, Z.P. 1974. *fuzulinidy verkhnego karbona pechorskogo priurad'ya*. Akademiya nauk SSSR komi filial institut geologii, Moscow, 1–116 [in Russian].

Nestell, G.P. & Nestell, M.K. 2006. Middle Permian (Late Guadalupian) foraminifers from Dark Canyon, Guadalupe Mountains, New Mexico. *Micropaleontology*, **52**, 1–50.

Nguyen, D.T. 1986. Foraminifera and algae from the Permian of Kampuchea. *CCOP Technical Bulletin*, **18**, 116–137.

Nie, Z.T. & Song, Z.M. 1983*a*. Fusulinids of Lower Permian Qudi Formation from Rutog of Xizang (Tibet), China. *Earth Science – Journal of Wuhan College of Geology*, **19**, 29–42 [in Chinese with English abstract].

Nie, Z.T. & Song, Z.M. 1983*b*. Fusulinids of Lower Permian Tunlonggongba Formation from Rutog of Xizang. *Earth Science – Journal of Wuhan College of Geology*, **19**, 43–55 [in Chinese with English abstract].

Nie, Z.T. & Song, Z.M. 1983*c*. Fusulinids of Lower Permian Maokouian Longge Formation from Rutog, Xizang (Tibet), China. *Earth Science – Journal of Wuhan College of Geology*, **19**, 57–68 [in Chinese with English abstract].

Niikawa, I. 1978. Carboniferous and Permian fusulinids from Fukuji, central Japan. *Journal of the Faculty of Science, Hokkaido University, Series 4. Geology and Mineralogy*, **18**, 533–610.

Niu, Z.J., Duan, Q.F., Wang, J.X., Bai, Y.S., Zeng, B.F., Tu, B. & Bu, J.J. 2006. On the Gadikao Formation in Zhidoi and Zadoi areas, Southern Qinghai. *Journal of Stratigraphy*, **30**, 109–115 [in Chinese with English abstract].

Niu, Z.J., Duan, Q.F., Wang, J.X., He, L.Q. & Bai, Y.S. 2010. Early Permian (Cisuralian) lithostratigraphical succession in volcanic–sedimentary setting from southern Qinghai. *Earth Science – Journal of China University of Geosciences*, **35**, 11–21 [in Chinese with English abstract].

Noe, S. 1988. Foraminiferal ecology and biostratigraphy of the marine Upper Permian and of the

Permian–Triassic boundary in the southern Alps (Bellerophon Formation, Tesero Horizon). *Revue de Paléobiologie*, **S2**, 75–88.

NOGAMI, Y. 1961. Permische Fusuliniden aus dem Atetsu-Plateau Sudwestjapans. Teil 1.Fusulininae und Schwagerininae. *Memoirs of the College of Science, University of Kyoto, Series B*, **27**, 159–225.

OKUYUCU, C. 2008. Biostratigraphy and systematics of late Asselian–early Sakmarian (Early Permian) fusulinids (Foraminifera) from southern Turkey. *Geological Magazine*, **145**, 413–434, https://doi.org/10.1017/s0016756808004482

OTA, A. & ISOZAKI, Y. 2006. Fusuline biotic turnover across the Guadalupian–Lopingian (Middle–Upper Permian) boundary in mid-oceanic carbonate buildups: biostratigraphy of accreted limestone in Japan. *Journal of Asian Earth Sciences*, **26**, 353–368.

OTA, Y. 1997. Middle Carboniferous and Lower Permian fusulinacean biostratigraphy of the Akiyoshi limestone group, Southwest Japan. Part 1. *Bulletin of the Kitakyushu Museum of Natural History*, **16**, 1–97.

OZAWA, T. 1970. Variation and relative growth of *Colania douvillei* (Ozawa) from the Rat Buri limestone. *Geology and Palaeontology of Southeast Asia*, **8**, 19–40.

OZAWA, T. 1987. Permian fusulinacean biogeographical provinces in Asia and their tectonic implications. *In*: TAIRA, A. & TASHIRO, M. (eds) *Historical Biogeography and Plate Tectonic Evolution of Japan and Eastern Asia*. Terra Science Publishing, Tokyo, Japan, 45–63.

OZAWA, Y. 1927. Stratigraphical studies of the Fusulina Limestone of Akasaka, Province of Mino. *Journal of the Faculty of Science, Imperial University of Tokyo, Section 2, Geology, Mineralogy, Geography, Seismology*, **2**, 121–162.

PAKISTAN–JAPANESE WORKING GROUP 1985. Permian and Triassic systems in the Salt Range and Surghar Range, Pakistan. *In*: NAKAZAWA, K. & DICKINS, J.M. (eds) *The Tethys; Her Paleogeography and Paleobiogeography from Paleozoic to Mesozoic*. Tokai University Press, Tokyo, Japan, 221–312.

PAPULOV, G.N. 1986. *Pogranichnye otlozheniya karbona i Permi Urala, Priuraliya i Srednei Azii*. Akademiya nauk SSSR, Uralskii nauchnyi centr, Moscow, 3–151.

PASINI, M. 1985. Biostratigrafia con i foraminiferi del limite formazione di Werfen fra recoaro e la Val Badia (Alpi Meridionali). *Rivista Italiana di Paleontologia e Stratigrafia*, **90**, 481–510.

QIAO, L. & SHEN, S.Z. 2014. Global paleobiogeography of brachiopods during the Mississippian – Response to the global tectonic reconfiguration, ocean circulation, and climate changes. *Gondwana Research*, **26**, 1173–1185, https://doi.org/10.1016/j.gr.2013.09.013

RAUZER-CHERNOUSOVA, D.M. 1965. Foraminifery stratotipicheskogo Razreza sakmarskogo yarusa. *Akademiya nauk SSSR, Geologicheskii Institut*, **135**, 5–79 [in Russian].

ROSS, C.A. 1960. Fusulinids from the Hess Member of the Leonard Formation, Leonard Series (Permian), Glass Mountains, Texas. *Contributions from the Cushman Foundation for Foraminiferal Research*, **11**, 116–133.

ROSS, C.A. 1962. Permian foraminifera from British Honduras. *Palaeontology*, **5**, 297–306.

ROSS, C.A. 1963. *Standard Wolfcampian Series (Permian), Glass Mountains, Texas*. Geological Society of America, Memoirs, **88**.

ROSS, C.A. 1967. Development of Fusulinid (Foraminiferida) fauna realms. *Journal of Paleontology*, **41**, 1341–1354.

ROSS, C.A. 1971. New species of *Schwagerina* and *Yabeina* (Fusulinacea) of Wordian age (Permian) from northwestern British Columbia. *Geological Survey of Canada Bulletin*, **197**, 95–101.

ROSS, C.A. 1982. Paleobiology of fusulinaceans. *Third North American Paleontological Convention Proceedings*, **2**, 441–445.

ROSS, C.A. 1995. Permian fusulinaceans. *In*: SCHOLLE, P.A., PERYT, T.M. & ULMER-SCHOLLE, D.S. (eds) *The Permian of Northern Pangea. Volume 1: Paleogeography, Paleoclimates, Stratigraphy*. Springer, Berlin, 167–185.

ROSS, C.A. & JUNE, J.R.P. 2003. Fusulinid sequence evolution and sequence extinction in Wolfcampian and Leonardian Series (Lower Permian), Glass Mountains, West Texas. *Rivista Italiana di Paleontologia e Stratigrafia*, **109**, 281–306.

ROSS, C.A. & ROSS, J.R.P. 1994. Permian sequence stratigraphy and fossil zonation. *In*: EMBRY, A.F., BEAUCHAMP, B. & GLASS, D.J. (eds) *Pangea: Global Environments and Resources*. Canadian Society of Petroleum Geologists, Memoirs, **17**, 219–231.

ROSS, C.A. & ROSS, J.R.P. 1997. Hessian (Leonardian, Middle Lower Permian) depositional sequences and their Fusulinid Zones, west Texas. *In*: BRENCKLE, P. (ed.) *A Compendium of Upper Devonian–Carboniferous Type Foraminifers from the Former Soviet Union*. Cushman Foundation for Foraminifera Research, Special Publications, **38**, 119–124.

ROSS, C.A. & ROSS, J.R.P. 2003. Sequence evolution and sequence extinction: fusulinid biostratigraphy and species-level recognition of depositional sequences, Lower Permian, Glass Mountains, West Texas, USA. *In*: OLSON, H.C. & LECKIE, R.M. (eds) *Micropaleontologic Proxies for Sea-Level Change and Stratigraphic Discontinuities*. Society of Economic Paleontologists and Mineralogists, Special Publications, **75**, 317–359.

RUI, L. 1979. Upper Permian fusulinids from western Guizhou. *Acta Palaeontologica Sinica*, **18**, 271–297.

RUI, L. & NASSICHUK, W.W. 1996. Upper Permian (Wordian) fusulinaceans from the Cache Creek Terrane, northern British Columbia. *Canadian Journal of Earth Sciences*, **33**, 1022–1036.

RUI, L., ZHAO, J.M., MU, X.N., WANG, K.L. & WANG, Z.H. 1984. Restudy of Wujiaping limestone in Liangshan, Hanzhong, Shanxi Province. *Journal of Stratigraphy*, **8**, 179–193.

SADA, K. & DANNER, W.R. 1992. *Pseudoschwagerina skinneri*, N. sp. from near kamloops in British Columbia, Canada. *Transactions and Proceedings of the Palaeontological Society of Japan, New Series*, **167**, 1259–1263.

SAKAMOTO, T. & ISHIBASHI, T. 2002. Paleontological study of fusulinoidean fossils from the Terbat Formation, Sarawak, East Malaysia. *Memoirs of the Faculty of Science, Kyushu University, Series D, Earth and Planetary Sciences*, **31**, 29–57.

SCHUBERT, R.J. 1915. Die Foraminiferen des Jüngeren Paläozoikums von Timor. *Palaontologien von Timor*, **2**, 49–59.

SCOTESE, C.R. 2001. *Atlas of Earth History, Volume 1, Paleogeography*. PALEOMAP Project, Arlington, TX, USA.

ŞENGÖR, A.M.C., YILMAZ, Y. & SUNGURLU, O. 1984. Tectonics of the Mediterranean Cimmerides: nature and evolution of the western termination of Palaeo-Tethys. *In*: DIXON, J.E. & ROBERTSON, A.H.F. (eds) *The Geological Evolution of the Eastern Mediterranean*. Geological Society, London, Special Publications, **17**, 77–112, https://doi.org/10.1144/gsl.sp.1984.017.01.04

SHEN, S.Z. & MEI, S.L. 2010. Lopingian (Late Permian) high-resolution conodont biostratigraphy in Iran with comparison to South China zonation. *Geological Journal*, **45**, 135–161, https://doi.org/10.1002/gj.1231

SHEN, S.Z., CAO, C.Q., SHI, G.R., WANG, X.D. & MEI, S.L. 2003. Loping (Late Permian) stratigraphy, sedimentation and palaeobiogeography in southern Tibet. *Newsletters on Stratigraphy*, **39**, 157–179.

SHEN, S.Z., ZHANG, H., SHANG, Q.H. & LI, W.Z. 2006. Permian stratigraphy and correlation of Northeast China: a review. *Journal of Asian Earth Sciences*, **26**, 304–326, https://doi.org/10.1016/j.jseaes.2005.07.007

SHEN, S.Z., CROWLEY, J.L. *ET AL.* 2011. Calibrating the end-permian mass extinction. *Science*, **334**, 1367–1372, https://doi.org/10.1126/science.1213454

SHEN, S.Z., YUAN, D.X., HENDERSON, C.M., TAZAWA, J. & ZHANG, Y.C. 2013. Implications of Kungurian (Early Permian) conodonts from Hatahoko, Japan, for correlation between the Tethyan and international timescales. *Micropaleontology*, **58**, 505–522.

SHENG, J.Z. 1958. Some Upper Carboniferous fusulinids from the vicinity of Beiyin Obo, Inner Mongolia. *Acta Palaeontologica Sinica*, **6**, 35–50 [in Chinese with English abstract].

SHENG, J.Z. 1962. Chihsian fusulinids from Kangbao area, Hebei Province. *Acta Palaeontologica Sinica*, **10**, 426–432 [in Chinese with English abstract].

SHENG, J.Z. 1963. Permian fusulinids of Kwangsi, Kueichow and Szechuan. *Palaeontologia Sinica, Series B*, **10**, 1–247 [in Chinese with English abstract].

SHENG, J.Z. & JIN, Y.G. 1994. Correlation of Permian deposits in China. *In*: JIN, Y.G., UTTING, J. & WARDLAW, B.R. (eds) *Permian Stratigraphy, Environments and Resources, Palaeoworld 4*. Nanjing University Press, Nanjing, China, 14–113.

SHENG, J.Z. & RUI, L. 1984. Fusulinaceans from Upper Permian Changhsingian in Mingshan coal field of Leping, Jiangxi. *Acta Micropalaeontologica Sinica*, **1**, 30–46 [in Chinese with English abstract].

SHENG, J.Z. & WANG, Y.H. 1962. The fusulinids of the Maokou stage, southern Kiangsu. *Acta Palaeontologica Sinica*, **10**, 176–190 [in Chinese with English abstract].

SHENG, J.Z. & ZHANG, L.X. 1958. Fusulinids from the type-locality of the Changhsing limestone. *Acta Palaeontologica Sinica*, **6**, 205–214 [in Chinese with English abstract].

SHENG, J.Z., ZHANG, L.X. & WANG, J.H. 1988. *Fusulinids*. Science Press, Beijing, [in Chinese].

SHI, G.R. 2006. The marine Permian of East and Northeast Asia: an overview of biostratigraphy, palaeobiogeography and palaeogeographical implications. *Journal of Asian Earth Sciences*, **26**, 175–206, https://doi.org/10.1016/j.jseaes.2005.11.004

SHI, Y.K., JIN, X.C., HUANG, H. & YANG, X.N. 2008. Permian Fusulinids from the Tengchong Block, Western Yunnan, China. *Journal of Paleontology*, **82**, 118–127.

SHI, Y.K., LIU, J.R., YANG, X.N. & ZHU, L.M. 2009. Fusulinid faunas from the Datangian to Chihsian strata of the Zongdi section in Ziyun county, Guizhou Province. *Acta Micropalaeontologica Sinica*, **26**, 1–30 [in Chinese with English abstract].

SHI, Y.K., HUANG, H., JIN, X.C. & YANG, X.N. 2011. Early Permian fusulinids from the Baoshan Block, Western Yunnan, China and their paleobiogeographic significance. *Journal of Paleontology*, **85**, 489–501, https://doi.org/10.1666/10-039.1

SHI, Y.K., YANG, X.N. & LIU, J.R. 2012. *Early Carboniferous to Early Permian fusulinids from Zongdi Section in Southern Guizhou*. Science Press, Beijing [in Chinese with English abstract].

SHI, Y.K., HUANG, H. & JIN, X.C. 2017. Depauperate fusulinid faunas of the Tengchong block in western Yunnan, China and their paleogeographic and paleoenvironmental indications. *Journal of Paleontology*, **91**, 12–24, https://doi.org/10.1017/jpa.2016.122

SHIINO, Y., SUZUKI, Y. & KOBAYASHI, F. 2008. Middle Permian fusulines from the Hoso-o Formation in Kamiyasse area, southern Kitakami Mountains, Northeast Japan: their biostratigraphic implications. *Journal of Geological Society of Japan*, **114**, 200–205.

SKINNER, J.W. 1969. Permian Foraminifera from Turkey. *The University of Kansas Paleontological Contributions*, **36**, 1–14.

SKINNER, J.W. & WILDE, G.L. 1955. New Fusulinids from the Permian of West Texas. *Journal of Paleontology*, **29**, 927–940.

SKINNER, J.W. & WILDE, G.L. 1965. Permian biostratigraphy and fusulinid faunas of the Shasta lake area, northern California. *The University of Kansas Paleontological Contributions*, 1–98.

SKINNER, J.W. & WILDE, G.L. 1966. Permian fusulinids from Sicily. *The University of Kansas Paleontological Contributions*, **22**, 1–16.

SKINNER, J.W. & WILDE, G.L. 1967. Permian foraminifera from Tunisia. *The University of Kansas Paleontological Contributions*, **30**, 1–22.

SICHUAN REGIONAL GEOLOGICAL SURVEY & NANJING INSTITUTE OF GEOLOGY AND PALAEONTOLOGY 1982. *Stratigraphy and Palaeontology of Western Sichuan and Eastern Tibet, No.1*. Sichuan People's Publishing House, Chengdu, China.

SONG, J.J., SONG, H.B. & HU, B. 2014. Geologic age of the Taiyuan Formation in northwest Henan province: evidences from fusulinids (foraminifera). *Acta Micropalaeontologica Sinica*, **31**, 190–204.

SOSNINA, M.I. 1981. Nekotorye permskie fuzulinidy pal'nego vostoka. *In*: MOBZALEVSKAYA, E.A. & KOLOBOVA, I.M. (eds) *Ezhegodnik vsesouznogo paleontologicheskogo obschestva*. Leningradskoe otdelenie, Leningrad, Russia, 13–34 [in Russian].

STAMPFLI, G.M. & BOREL, G.D. 2002. A plate tectonic model for the Paleozoic and Mesozoic constrained

by dynamic plate boundaries and restored synthetic oceanic isochrons. *Earth and Planetary Science Letters*, **196**, 17–33, https://doi.org/10.1016/s0012-821x(01)00588-x

STEVENS, C.H. & STONE, P. 2007. *The Pennsylvanian–Early Permian Bird Spring Carbonate Shelf, Southeastern California: Fusulinid Biostratigraphy, Paleogeographic Evolution, and Tectonic Implications*. Geological Society of America Special Papers, **429**, https://doi.org/10.1130/2007.2429

STEVENS, C.H., DAVYDOV, V.I. & BRADLEY, D. 1997. Permian Tethyan fusulinina from the Kenai peninsula, Alaska. *Journal of Paleontology*, **71**, 985–994.

SUN, X.F. 1979. Upper Permian fusulinids from Zhen'an of Shanxi and Tewo of Gansu, NW.China. *Acta Palaeontologica Sinica*, **18**, 163–168 [in Chinese with English abstract].

TARAZ, H., GOLSHANI, F. *ET AL.* 1981. The Permian and the Lower Triassic systems in Abadeh region, central Iran. *Memoirs of the Faculty of Science*, **47**, 61–133.

TAZAWA, J. 1991. Middle Permian brachiopod biogeography of Japan and adjacent regions in East Asia. *In*: ISHII, K.I., LIU, X.M., ICHIKAWA, K. & HUANT, B. (eds) *Pre-Jurassic Geology of Inner Mongolia, China*. Matsuya Insatsu, Osaka, Japan, 213–230.

THOMPSON, M.L. 1946. Permian fusulinids from Afghanistan. *Journal of Paleontology*, **20**, 140–157.

THOMPSON, M.L. 1949. The Permian fusulinids of Timor. *Journal of Paleontology*, **23**, 182–192.

THOMPSON, M.L. & MILLER, A.K. 1949. Permian fusulinids and cephalopods from the vicinity of the Maracaibo basin in northern South America. *Journal of Paleontology*, **23**, 1–24.

THOMPSON, M.L. & VERVILLE, G.J. 1950. Cache Creek fusulinids from Kamloops, British Columbia. *Contributions from the Cushman Foundation for Foraminiferal Research*, **1**, 67–70.

THOMPSON, M.L. & WHEELER, H.E. 1942. Permian Fusulinids from British Columbia, Washington and Oregon. *Journal of Paleontology*, **16**, 700–711.

TORIYAMA, R. 1954. Geology of Akiyoshi. *Memories of Faculty of Science, Kyushu University, Series D*, **4**, 39–97.

TORIYAMA, R. 1975. Fusuline fossils from Thailand, Part 9, Permian Fusulines from the Rat Buri limestone in the Khao Phlong Phrab area, Sara Buri, Central Thailand. *Memoirs of the Faculty of Science, Kyushu University, Series D, Geology*, **23**, 1–116.

TORIYAMA, R. 1982. Fusuline fossils from Thailand, part 15. Peculiar spirothecal structure of Schwagerinid from east of Wang Saphung, Changwat Loei Central North Thailand. *Geology and Palaeontology of Southeast Asia*, **23**, 1–7.

TORIYAMA, R. & KANMERA, K. 1979. Fusuline Fossils from Thailand, Part 12. Permian Fusulines from the Ratburi Limestone in the Khao Khao Area, Sara Buri, Central Thailand. *Geology and Palaeontology of Southeast Asia*, **20**, 23–94.

TORIYAMA, R., PITAKPAIV, K. & KANMERA, K. 1965. The Fusulinacean fossils of Thailand. *Memoirs of Faculty of Science, Kyushu University, Series D, Geology*, **17**, 1–69.

TORIYAMA, R., KANMERA, K., KAEWBAIDHOAM, S. & HONGNUSONTHI, A.-n. 1974. Biostratigraphic zonation of the Rat Buri limestone in the Khao Phlong Phrab area, Sara Buri, Central Thailand. *Geology and Palaeontology of Southeast Asia*, **14**, 25–81.

UENO, K. 1992. Verbeekinid and Neoschwagerinid Fusulinaceans from the Akiyoshi limestone group above the Parafusulina kaerimizensis zone, southwest Japan. *Transactions and Proceedings of the Palaeontological Society of Japan, New Series*, **165**, 1040–1069.

UENO, K. 1996. Late Early to Middle Permian fusulinacean biostratigraphy of the Akiyoshi limestone group, southwest Japan, with special reference to the verbeekind and neoschwagerinid fusulinicean biostratigraphy and evolution. *Museo Civico di Rovereto*, **S11**, 77–104.

UENO, K. 2003. The Permian fusulinoidean faunas of the Sibumasu and Baoshan blocks: their implications for the paleogeographic and paleoclimatologic reconstruction of the Cimmerian Continent. *Palaeogeography, Palaeoclimatology, Palaeoecology*, **193**, 1–24, https://doi.org/10.1016/S0031-0182(02)00708-3

UENO, K. 2006. The Permian antitropical fusulinoidean genus *Monodiexodina*: distribution, taxonomy, paleobiogeography and paleoecology. *Journal of Asian Earth Sciences*, **26**, 380–404, https://doi.org/10.1016/j.jseaes.2005.07.003

UENO, K. & IGO, H. 1997. Late Paleozoic foraminifers from the Chiang Dao area, northern Thailand. *Prace Państwowego Instytutu Geologicznego*, **157**, 339–358.

UENO, K. & NAKAZAWA, T. 1993. Carboniferous foraminifers from the lowermost part of the Omi limestone group, Niigata Prefecture, central Japan. *Science Reports of the Institute of Geoscience, University of Tsukuba, Section B: Geological Sciences*, **14**, 1–51.

UENO, K. & SAKAGAMI, S. 1991. Late Permian Fusulinacean fauna of Doi Pha Phlung, North Thailand. *Transactions and Proceedings of Palaeontological Society of Japan, New Series*, **164**, 928–943.

UENO, K. & TSUTSUMI, S. 2009. Lopingian (Late Permian) foraminiferal faunal succession of a Paleo-Tethyan mid-oceanic carbonate buildup: Shifodong Formation in the Changning-Menglian Belt, West Yunnan, Southwest China. *Island Arc*, **18**, 69–93, https://doi.org/10.1111/j.1440-1738.2008.00648.x

UENO, K., MIZUNO, Y., WANG, X.D. & MEI, S.L. 2002. Artinskian conodonts from the Dingjiazhai Formation of the Baoshan Block, West Yunnan, Southwest China. *Journal of Paleontology*, **76**, 741–750.

UENO, K., WANG, Y.J. & WANG, X.D. 2003. Fusulinoidean faunal succession of a Paleo-Tethyan oceanic seamount in the Changning–Menglian Belt, west Yunnan, southwest China: an overview. *The Island Arc*, **12**, 145–161.

UENO, K., SHI, G.R. & SHEN, S.Z. 2005. Fusulinoideans from the early Midian (late Middle Permian) *Metadoliolina dutkevitchi–Monodiexodina sutchanica* zone of the Senkina Shapka section, South Primorye, Far East Russia. *Alcheringa*, **29**, 257–273.

UENO, K., TAZAWA, J.I. & MIYAKE, Y. 2006. Middle Permian fusulinoideans from Hatahoko in the Nyukawa area, Gifu Prefecture, Mono Belt, central Japan. *Science Report of Niigata University (Geology)*, **21**, 47–72.

UENO, K., TAZAWA, J.I. & SHINTANI, T. 2007. Fusuline foraminifera from the basal part of the Sakamotozawa

Formation, south Kitakami Belt, Northeast Japan. *Science Report of Niigata University (Geology)*, **22**, 15–33.

Ueno, K., Shintani, T. & Tazawa, J.I. 2009. Fusuline foraminifera from the upper part of the Sakamotozawa Formation, South Kitakami Belt, Northeast Japan. *Science Report of Niigata University (Geology)*, **24**, 27–61.

Ueno, K., Shintani, T. & Tazawa, J.I. 2011. A fusuline fauna from the basal part of the Sakamotozawa Formation in the Kamiyasse area, South Kitakami Belt, Northeast Japan. *Science Reports of Niigata University (Geology)*, **26**, 23–41.

Ueno, K., Arita, M., Meno, S., Sardsud, A. & Saesaengseerung, D. 2015. An Early Permian fusuline fauna from southernmost Peninsular Thailand: discovery of Early Permian warming spikes in the peri-Gondwanan Sibumasu Block. *Journal of Asian Earth Sciences*, **104**, 185–196, https://doi.org/10.1016/j.jseaes.2014.10.030

Unal, E., Altiner, D., Yilmaz, I.O. & Ozkan-Altiner, S. 2003. Cyclic sedimentation across the Permian–Triassic boundary (Central Taurides, Turkey). *Rivista Italiana di Paleontologia e Stratigrafia*, **109**, 359–376.

Vachard, D. 1980. Téthys et Gondwana au paléozoïque supérieur, les données Afghanes: biostratigraphie, micropaléontologie, paléographie. *Documents et travaux de l'Institut géologique Albert de Lapparent*, **2**, 1–463.

Vachard, D. & Ferriere, J. 1991. An assemblage with *Yabeina* (Fusulinid foraminifera) from the Midian (Upper Permian) of Whangaroa area (Orua Bay, New Zealand). *Revue de Micropaléontologie*, **34**, 201–230.

Vachard, D. & Moix, P. 2013. Kubergandian (Roadian, Middle Permian) of the Lycian and Aladağ Nappes (Southern Turkey). *Geobios*, **46**, 335–356, https://doi.org/10.1016/j.geobios.2013.02.002

Vachard, D., Flores de Dios, A., Buitron, B.E. & Grajales, M. 2000. Biostratigraphie par fusulines des calcaires carboniferes et permiens de San Salvador Patlanoaya (Puebla, Mexique). *Geobios*, **33**, 5–33.

Vachard, D., Martini, R. & Zaninetti, L. 2001. Earliest Artinskian (Early Permian) fusulinids reworked in the Triassic Lercara Formation (NW Sicily). *Journal of Foraminiferal Research*, **31**, 33–47.

Vachard, D., Hauser, M., Martini, R., Zaninetti, L., Matter, A. & Peters, T. 2002. Middle Permian (Midian) foraminiferal assemblages from the Batain Plain (Eastern Oman): their significance to Neotethyan Paleogeography. *Journal of Foraminiferal Research*, **32**, 155–172.

Vachard, D., Zambetakis-Lekkas, A., Skourtsos, E., Martini, R. & Zaninetti, L. 2003. Foraminifera, Algae and Carbonate microproblematica from the Late Wuchiapingian/Dzhulfian (Late Permian) of Peloponnesus (Greece). *Rivista Italiana di Paleontologia e Stratigrafia*, **109**, 339–358.

Vachard, D., Pille, L. & Gaillot, J. 2010. Palaeozoic Foraminifera: systematics, palaeoecology and responses to global changes. *Revue de Micropaleontologie*, **53**, 209–254, https://doi.org/10.1016/j.revmic.2010.10.001

Vuks, G.P. & Chediya, I.O. 1986. Foraminifery ludyanzinskoi svity buhty neizvestiaya (Uzhnoe Primorye) [Lyudianza foraminifera of the Neizvestnaya Bay (South Primorye)]. *In*: Zakharov, Y.D. & Onoprienko, Y.I. (eds) *Korrelyatsiya permo-triasovykh otlozhenij vostoka SSSR [Correlation of Permo-Triassic Sediments of the East USSR]*. DVNC AN SSSR, Vladivostok, Russia, 82–88 [in Russian].

Wang, C.Y., Qin, Z.S., Yun, Y.K., Zhu, X.S., Xu, D.Y. & Chen, G.Y. 1997. Age of *Gallowayinella* and the lower limit of the Changhsingian stage based on conodonts. *Journal of Stratigraphy*, **21**, 100–108 [in Chinese with English abstract].

Wang, J.H. 1978. The boundary and biostratigraphy of the Chihsia Formation in Nanjing area. *Acta Stratigraphic Sinica*, **2**, 67–73 [in Chinese with English abstract].

Wang, J.H. & Tang, Y. 1986. Fusulinids from Chihsia Formation of Lengwu district in Tonglu County, Zhejiang. *Acta Micropalaeontologica Sinica*, **3**, 3–12 [in Chinese with English abstract].

Wang, Y. & Jin, Y.G. 2006. Radiation of the Fusulinoideans between the two phases of the end-Permian mass extinction, South China. *In*: Rong, J.Y., Fang, Z.J., Zhou, Z.H., Zhan, R.B. & Yuan, X.L. (eds) *Originations, Radiations and Biodiversity Changes – Evidences from the Chinese Fossil Record*. Science Press, Beijing, 503–516.

Wang, Y. & Ueno, K. 2009. A new fusulinoidean genus Dilatofusulina from the Lopingian (Upper Permian) of southern Tibet, China. *Journal of Foraminiferal Research*, **39**, 56–65.

Wang, Y., Ueno, K., Zhang, Y.C. & Cao, C.Q. 2010. The Changhsingian foraminiferal fauna of a Neotethyan seamount: the Gyanyima limestone along the Yarlung–Zangbo Suture in southern Tibet, China. *Geological Journal*, **45**, 308–318.

Wang, Y., Wang, J., Chen, J., Wang, W., Shen, S. & Henderson, C.M. 2011*a*. Progress, problems and prospects on the stratigraphy and correlation of the Kungurian Stage, Early Permian (Cisuralian) Series. *Acta Geologica Sinica – English Edition*, **85**, 387–398, https://doi.org/10.1111/j.1755-6724.2011.00407.x

Wang, Y., Wang, W.J., Zhang, Y.C., Qi, Y.P., Wang, X.D. & Liao, Z.T. 2011*b*. Late Carboniferous to Early Permian fusuline assemblages from the Wuzunbulake section, Keping area, Xinjiang. *Acta Palaeontologica Sinica*, **50**, 409–419 [in Chinese with English abstract].

Wang, Y.J. & Zhou, J.P. 1986. New material of fusulinids from Xainza, Xizang. *Bulletin of Nanjing Institute of Geology and Palaeontology, Academia Sinica*, **10**, 141–156 [in Chinese with English abstract].

Wang, Y.J., Sheng, J.Z. & Zhang, L.X. 1981. Fusulinids from Xizang of China. *In*: Nanjing Institute of Geology and Palaeontology (ed.) *Palaeontology of Xizang, Book 3*. Science Press, Beijing, China, 1–80 [in Chinese with English abstract].

Wang, Y.J., Yuan, X.Q. & Geng, G.C. 1992. A new advance of Carboniferous fusulinid study and preliminary exploration of the paleogeography in the Ordos Basin. *Acta Micropalaeontologica Sinica*, **9**, 127–150 [in Chinese with English abstract].

Watanabe, K. 1991. *Fusuline Biostratigraphy of the Upper Carboniferous and Lower Permian of Japan, with Special Reference to the Carbonifeorus–Permian Boundary*. Palaeontological Society of Japan, Special Papers, **32**.

WILDE, G.L. 1984. Systematics and the Carboniferous–Permian boundary. *Comptes Rendus du 9e Congrès International de Stratigraphie et de Géologie du Carbonifère, Washington et Champaign–Urbana 1979*, **2**, 543–558.

WILDE, G.L. 1990. Practical fusulinid zonation: the species concept; with Permian basin emphasis. *West Texas Geological Society, Bulletin*, **29**, 5–34.

WILDE, G.L. 2006. Pennsylvanian-Permian fusulinaceans of the Big Hatchet Mountains, New Mexico. *New Mexico of Natural History and Science Bulletin*, **38**, 1–331.

WILDE, G.L. & RUDINE, S.F. 2000. Late Guadalupian biostratigraphy and Fusulinid faunas, Altuda Formation, Brewster County, Texas. *Smithsonian Contributions to the Earth Sciences*, **32**, 343–371.

WOOD, G.D., GROVES, J.R., WAHLMAN, G.P., BRENCKLE, P.L. & ALEMAN, A.M. 2002. The paleogeographic and biostratigraphic significance of fusulinacean and smaller foraminifers, and palynomorphs from the Copacabana Formation (Pennsylvanian–Permian), Madre de Dios Basin, Peru. *In*: HILLS, L.V., HENDERSON, C.M. & BAMBER, E.W. (eds) *Carboniferous and Permian of the World*. Canadian Society of Petroleum Geologists, Memoirs, **19**, 630–664.

WU, R.Z. & LAN, B.L. 1990. New Late Permian strata from Northwest Tibet. *Journal of Stratigraphy*, **14**, 216–221 [in Chinese].

WU, Z.P. & YANG, X.N. 1998. A study on different fusuinid fauna of the Changme stage, southwest China. *Acta Micropalaeontologica Sinica*, **15**, 37–47.

XIA, G.Y. 1981. Zonation of the Early Permian fusulinid-bearing strata in Inner Mongolia. *In*: *12th Annual Conference of the Palaeontological Society of China, Selected Papers*. Science Press, Beijing, China, 116–126.

XIA, G.Y., LI, J.X., WANG, Y.H. & DONG, W.L. 1986. The fusulinid zones and the boundary of Carboniferous–Permian in Longlin region, Guangxi. *Bulletin of Yichang Institute of Geology and Mineral Resources, CAGS*, **11**, 67–104.

XIAO, W.M., WANG, H.D., ZHANG, L.X. & DONG, W.L. 1986. *Early Permian Stratigraphy and Faunas in Southern Guizhou*. The People's Publishing House of Guizhou, Guiyang, China [in Chinese with English abstract].

XIE, J.C., ZHU, D.C., DONG, G., ZHAO, Z.D., WANG, Q. & MO, X. 2016. Linking the Tengchong Terrane in SW Yunnan with the Lhasa Terrane in southern Tibet through magmatic correlation. *Gondwana Research*, **39**, 217–229, https://doi.org/10.1016/j.gr.2016.02.007

XU, S.Y., XIA, G.Y., YANG, D.L., LI, J.X., LIANG, Z.F., LI, L. & ZHANG, Y.X. 1986. The Carboniferous–Permian boundary in Longlin region, Guangxi. *Bulletin of Yichang Institute of Geology and Mineral Resources, CAGS*, **11**, 1–32.

YANCEY, T.E. 1975. Permian marine biotic provinces in North America. *Journal of Paleontology*, **49**, 758–766.

YANG, X.N. & HAO, Y.C. 1991. A study on ontogeny and evolution of Robustoschwagerinids (Permian Fusulinids). *Acta Palaeotologica Sinica*, **30**, 277–306 [in Chinese with English abstract].

YANG, X.N., LIU, J.R. & SHI, G.J. 2004. Extinction process and patterns of Middle Permian Fusulinaceans in southwest China. *Lethaia*, **37**, 139–147, https://doi.org/10.1080/00241160410005114

YANG, Z.D. 1985. Restudy of fusulinids from the 'Maokou limestone' (Permian) at Datieguan, Langdai Guizhou. *Acta Micropalaeontologica Sinica*, **2**, 307–335 [in Chinese with English abstract].

YANG, Z.D. & YANCEY, T.E. 2000. Fusulinid biostratigraphy and paleontology of the Middle Permian (Guadalupian) strata of the Glass Mountains and Del Norte Mountains, West Texas. *Smithsonian Contributions to the Earth Sciences*, **32**, 185–259.

YUAN, D.X., ZHANG, Y.C. *ET AL.* 2016. Early Permian conodonts from the Xainza area, central Lhasa Block, Tibet, and their palaeobiogeographical and palaeoclimatic implications. *Journal of Systematic Palaeontology*, **14**, 365–383, https://doi.org/10.1080/14772019.2015.1052027

ZAW, W. 1999. Fusuline biostratigraphy and paleontology of the Akasaka Limestone, Gifu prefecture, Japan. *Bulletin of the Kitakyushu Museum of Natural History*, **18**, 1–76.

ZAW, W., AUNG, H.H. & SHWE, K.K. 2011. *Shanita thawtinti*, a new milioloid foraminifer from the Middle Permian of Myanmar. *Micropaleontology*, **57**, 125–138.

ZHANG, L.X. 1963. Late Carboniferous fusulinids from Keping and adjacent regions in Xinjiang. *Acta Palaeontologica Sinica*, **11**, 200–227 [in Chinese with Russian abstract].

ZHANG, L.X. 1991. Early–Middle Permian fusulinids from Ngari, Xizang (Tibet). *In*: SUN, D.L. & XU, J.T. (eds) *Permian Jurassic and Cretaceous Strata and Palaeontology from Rutog Region, Xizang (Tibet)*. Nanjing University Press, Nanjing, China, 42–67 [in Chinese with English abstract].

ZHANG, L.X., RUI, L., WANG, Z.H. & LI, H.Y. 1988. Fusulinids. *In*: ZHANG, L.X., RUI, L. *ET AL.* (eds) *Permian Palaeontology from Southern Guizhou Province*. People's Publishing House of Guizhou, Guiyang, China, 1–123 [in Chinese with English abstract].

ZHANG, L.X., ZHOU, J.P., NIU, B.X. & WANG, H. 1989. Fusulinids from Late Carboniferous Taiyuan Formation in Zibo area, Shandong. *Acta Palaeontologica Sinica*, **28**, 803–818 [in Chinese with English abstract].

ZHANG, Y.C. 2010. Late Middle Permian (Guadalupian) fusuline fauna from the Gyanyima area of Burang County, Tibet, China and its paleobiogeographic implications. *Acta Palaeontologica Sinica*, **49**, 231–250 [in Chinese with English abstract].

ZHANG, Y.C., WANG, Y. & SHEN, S.Z. 2009. Middle Permian (Guadalupian) Fusulines from the Xilanta Formation in the Gyanyima area of Burang County, southwestern Tibet, China. *Micropaleontology*, **55**, 463–486.

ZHANG, Y.C., CHENG, L.R. & SHEN, S.Z. 2010. Late Guadalupian (Middle Permian) fusuline fauna from the Xiala Formation in Xainza County, central Tibet: implication of the rifting time of the Lhasa Block. *Journal of Paleontology*, **84**, 955–973, https://doi.org/10.1666/10-005.1

ZHANG, Y.C., SHEN, S.Z., SHI, G.R., WANG, Y., YUAN, D.X. & ZHANG, Y.J. 2012*a*. Tectonic evolution of the Qiangtang Block, northern Tibet during the Late Cisuralian (Late Early Permian): evidence from

fusuline fossil records. *Palaeogeography, Palaeoclimatology, Palaeoecology*, **350–352**, 139–148, https://doi.org/10.1016/j.palaeo.2012.06.025

Zhang, Y.C., Wang, Y., Zhang, Y.J. & Yuan, D.X. 2012*b*. Kungurian (Late Cisuralian) fusuline fauna from the Cuozheqiangma area, northern Tibet and its palaeobiogeographical implications. *Palaeoworld*, **21**, 139–152, https://doi.org/10.1016/j.palwor.2012.09.001

Zhang, Y.C., Shi, G.R. & Shen, S.Z. 2013*a*. A review of Permian stratigraphy, palaeobiogeography and palaeogeography of the Qinghai–Tibet Plateau. *Gondwana Research*, **24**, 55–76, https://doi.org/10.1016/j.gr.2012.06.010

Zhang, Y.C., Wang, Y., Zhang, Y.J. & Yuan, D.X. 2013*b*. Artinskian (Early Permian) fusuline fauna from the Rongma area in northern Tibet: palaeoclimatic and palaeobiogeographic implications. *Alcheringa: An Australasian Journal of Palaeontology*, **37**, 529–546, https://doi.org/10.1080/03115518.2013.805484

Zhang, Y.C., Shi, G.R., Shen, S.Z. & Yuan, D.X. 2014. Permian Fusuline Fauna from the Lower Part of the Lugu Formation in the Central Qiangtang Block and its Geological Implications. *Acta Geologica Sinica – English Edition*, **88**, 365–379, https://doi.org/10.1111/1755-6724.12202

Zhang, Y.C., Shen, S.Z., Zhai, Q.G., Zhang, Y.J. & Yuan, D.X. 2016. Discovery of a Sphaeroschwagerina fusuline fauna from the Raggyorcaka Lake area, northern Tibet: implications for the origin of the Qiangtang Metamorphic Belt. *Geological Magazine*, **153**, 537–543.

Zhang, Y.J., Zhu, T.X., Yuan, D.X. & Zhang, Y.C. 2014. The discovery of Wuchiapingian fossils of Xiala Formation from Xainza area, Tibet and its significance. *Journal of Stratigraphy*, **38**, 411–418 [in Chinese with English abstract].

Zhang, Z.C. 1983. Biostratigraphy of fusulines in the Upper Carboniferous Taiyuan Formation in Xishan, Taiyuan. *Journal of Stratigraphy*, **7**, 272–278 [in Chinese with English abstract].

Zhang, Z.C. 1990. A restudy of Late Carboniferous fusulinaceans from the western hills of Taiyuan. *Acta Micropalaeontologica Sinica*, **7**, 95–122 [in Chinese with English abstract].

Zhang, Z.C. & Xia, G.Y. 1985. Fusulinid zonation of the Upper Carboniferous Shanxi Formation, southeastern Shanxi. *Regional Geology of China*, **12**, 53–61 [in Chinese with English abstract].

Zhang, Z.G., Chen, J.R. & Yu, H.J. 1985. Early Permian stratigraphy and character of fauna in Xainza district, northern Xizang (Tibet), China. *In*: CGQXP Editorial Committee, Ministry of Geology and Mineral Resources PRC (ed.) *Contribution to the Geology of the Qinhai–Xizang (Tibet) Plateau (16)*. Geological Publishing House, Beijing, China, 117–138 [in Chinese with English abstract].

Zhang, Z.H., Wang, Z.H. & Li, C.Q. 1988. *A Suggestion for Classification of Permian in South Guizhou*. Guizhou People's Publishing House, Guiyang, China [in Chinese with English abstract].

Zhao, B., Duan, L.L. & Chen, H.X. 2006. New data on palaeontology of Late Permian in the Ulanul Hu area, northern Qiangtang Basin, NW China. *Acta Micropalaeontologica Sinica*, **23**, 392–398 [in Chinese with English abstract].

Zheng, Y.T. & Lin, J.X. 1991. Foraminifera and fusulinids. *In*: Southern Xinjiang Petroleum Prospecting Corporation, Xinjiang Petroleum Administration Bureau & Exploration and Development Research Institute, Jianghan Petroleum Administration Bureau (eds) *Sinian to Permian Stratigraphy and Palaeontology of the Tarim Basin, Xinjiang (II), Kalpin–Bachu Region*. The Petroleum Industry Press, Beijing, China, 158–190 [in Chinese with English abstract].

Zhou, T.M., Sheng, J.Z. & Wang, Y.J. 1987. Carboniferous–Permian boundary beds and fusulinid zones at Xiaodushan, Guangnan, eastern Yunnan. *Acta Micropalaeontologica Sinica*, **4**, 123–160 [in Chinese with English abstract].

Zhou, Z.R. 1982. Earliest Permian *Schwagerina cushmani* fusulinid fauna from southeastern Hunan. *Acta Palaeontologica Sinica*, **21**, 225–248 [in Chinese with English abstract].

Zhu, X.F. 1982*a*. Lower Permian fusulinids from Xainza County, Xizang (Tibet). *In*: CGQXP Editorial Committee, Ministry of Geology and Mineral Resources PRC (ed.) *Contribution to the Geology of the Qinhai–Xizang (Tibet) (7)*. Geological Publishing House, Beijing, China, 110–133 [in Chinese with English abstract].

Zhu, X.F. 1982*b*. Lower Permian fusulinids from Lhunzhub County, Xizang (Tibet). *In*: CGQXP Editorial Committee, Ministry of Geology and Mineral Resources PRC (ed.) *Contribution to the Geology of the Qinhai–Xizang (Tibet) (7)*. Geological Publishing House, Beijing, China, 136–148 [in Chinese with English abstract].

Zhu, Z.L. 1997. Carboniferous and Permian fusulinid zonation in southwestern margin of the Tarim basin. *Acta Palaeontologica Sinica*, **36**, 104–115 [in Chinese with English abstract].

Lethaia
AN INTERNATIONAL JOURNAL OF PALAEONTOLOGY AND STRATIGRAPHY

The oryctocephalid trilobite zonation across the Cambrian Series 2-Series 3 boundary at Balang, South China: a reappraisal

YUAN-LONG ZHAO, JIN-LIANG YUAN, JORGE ESTEVE AND JIN PENG

LETHAIA

Zhao Y.-L., Yuan J.-L., Esteve J., Peng J. 2017: The oryctocephalid trilobite zonation across the Cambrian Series 2-Series 3 boundary at Balang, South China: a reappraisal. *Lethaia*, Vol. 50, pp. 400–406.

A systematic revision of the oryctocephalid trilobites provides additional data for the definition of a revised zonation of the Cambrian Series 2-Series 3 boundary at Balang in South China. The zonation offers a new understanding of the biostratigraphical correlation of this debated limit. The biostratigraphical revision was carried out in the Wuliu-Zengjiayan Section and provides the following trilobite zones: (1) *Protorycto-cephalus arcticus*; (2) *Bathynotus kueichouensis—Ovatoryctocara sinensis* Zone (upper part of Cambrian Series 2); and (3) *Oryctocephalus indicus* Zone (base of Cambrian Series 3). This suggests that this section is a suitable candidate GSSP for the base of Cambrian Series 3, Stage 5. The correlation in the Wuliu-Zengjiayan Section suggests that the *P. arcticus* Zone and the *B. kueichouensis—O. sinensis* Zone can be correlated with the *Ovatoryctocara granulata* Zone, while the *O. indicus* Zone is time-equivalent to the *Oryctocephalus reticulatus* Zone in Siberia. The *P. arcticus* Zone and the *B. kuei-chouensis—O. sinensis* Zone can be correlated with the *Eoagnostus roddyi—Arthrico-cephalus chauveaui* Zone and the *Bonnia—Pagetides elegans* Zone in North Greenland, as well as with the upper part of the *Olenellus* Zone, *Nephrolenellus multinodus* Zone in North America. ☐ *Biostratigraphy, China, Greenland, intercontinental correlation, Siberia, trilobites, USA.*

Jorge Esteve ✉ [jorgeves@outlook.es], Departamento de Paleontología, Facultad de CC Geológicas, José Antonio Novais 12, 28040 Madrid, Spain; Yuan-Long Zhao [zhaoyuan-long@126.com], and Jin Peng [gzpengjin@126.com], Resources and Environmental Engineering College, Guizhou University, Guiyang 550025, China; Jin-Liang Yuan [jlyuan@nigpas.ac.cn], Nanjing Institute of Geology and Palaeontology, Chinese Academy of Sciences, Nanjing 210008, China; *manuscript received on 15/01/2016; manuscript accepted on 1/06/2017.*

In recent years, the International Subcommission on Cambrian Stratigraphy (ISCS) has made significant progress towards a decision concerning the base of the provisional Cambrian Stage 5 (Peng *et al.* 2006; Babcock & Peng 2007; Peng & Babcock 2008, 2011; Peng 2009). In 2015, the working group concerned with the Cambrian Stage 5 provided its recommendation on which stratigraphical horizon (of five options) would be used to mark the base of the stage. The base of provisional Stage 5 is likely to be selected at the first appearance datum (FAD) of the oryctocephalid trilobite *Oryctocephalus indicus* (Reed 1910). Oryctocephalids are geographically widely distributed and will have an important role in correlating successions around the base of the Stage 5. The regional lower-middle Cambrian boundary interval and the base of Stage 5 are well exposed in the classic Wuliu-Zengjiayan Section (Peng & Babcock 2001; Sundberg *et al.* 2011; Yuan *et al.* 2011; Zhao *et al.* 2012, 2014, 2015a,b; Wang *et al.* 2014). This has been proposed as a potential GSSP for the base of Stage 5 by Zhao *et al.* (2012; see for further references). The aim of this work was to revise the oryctocephalid trilobite zonation in the Wuliu-Zengjiayan Section and correlate the biozones with sections in other parts of the world.

Revision of the oryctocephalid trilobite zonation in South China

Oryctocephalid trilobites evolved relatively rapidly and are geographically widespread. Hence, they are suitable for biostratigraphy and correlation of Cambrian stages 4 and 5 strata in many parts of the world. The Wuliu-Zengjiayan Section presents good outcrops through the 'Tsinghsutung' Formation (Stage 4) and the Kaili Formation (stages 4 and 5). The trilobite biozonation of this interval is revised and discussed below. The new proposed oryctocephalid trilobite zonation is shown in Figure 1. Selected, biostratigraphically important trilobite species are illustrated in Figure 2.

DOI 10.1111/let.12227

<table>
<tr><th colspan="2"></th><th>South China</th><th>Siberia</th><th>N. Greenland</th><th>N. America</th><th>Australia</th><th colspan="2">Mediterranean area</th></tr>
<tr><th colspan="7"></th><th>Spain</th><th>Morocco</th></tr>
<tr><td rowspan="4">Cambrian Series 3</td><td rowspan="4">Cambrian Stage 5</td><td rowspan="2">Ptychagnostus praecurrens</td><td rowspan="2">Ptychagnostus praecurrens</td><td rowspan="2">Glossopleura</td><td rowspan="2">Ptychagnostus praecurrens</td><td>Pentagnostus shergoldia</td><td>Badulesia tenera</td><td>Badulesia tenera</td></tr>
<tr><td>Ptychagnostus praecurrens</td><td>Eccaparadoxides asturianus</td><td rowspan="2">Kymataspis arenosa</td></tr>
<tr><td>Peronopsis taijiangensis</td><td rowspan="3">Peronopsis recta

Oryctocephalus reticulatus (=O.indicus)</td><td rowspan="2">Oryctocephalus indicus</td><td rowspan="2">Pentagnostus anabarensis</td><td rowspan="2">Eccaparadoxides sdzuyi</td></tr>
<tr><td>Oryctocephalus indicus</td><td>Eokochaspis nodosa</td><td>Acadoparadoxides</td><td rowspan="3">Ornamentaspis frequens

Morocconus notabilis</td></tr>
<tr><td rowspan="4">Cambrian Series 2</td><td rowspan="4">Cambrian Stage 4</td><td rowspan="2">Bathynotus kueichouensis-Ovatoryctocara sinensis</td><td rowspan="2">Ovatoryctocara granulata (Bathynotus) (Paradoxides eopinus)</td><td rowspan="3">Bonnia-Pagetides

Ovatoryctocara granulata</td><td rowspan="2">Nepholenellus multinodosus (Bathynotus)</td><td rowspan="2">Pentagnostus krusei (Bathynotus)</td><td>mureroensis</td></tr>
<tr><td>Protolenus jilocanus</td></tr>
<tr><td>Protoryctocephalus arcticus</td><td>Anabaraspis splendens</td><td>Olenellus</td><td>Xystridura negina</td><td>Protolenus dimarginatus</td><td>Hupeolenus</td></tr>
</table>

Fig. 1. The new oryctocephalid trilobite zonation in South China for the Cambrian Series 2–3 boundary and its international correlation (see text for explanation).

The middle-upper part of the 'Tsinghsutung' Formation has been assigned to the *Protoryctocephalus wuxunensis* Zone (Yuan *et al.* 2002; Yuan & Esteve 2015), while the lowermost part of the Kaili Formation belongs to the *Ovatoryctocara granulata—Bathynotus kueichouensis* Assemblage Zone (Yuan *et al.* 2002; Zhao *et al.* 2007, 2008). These two zones contain trilobites that are crucial for our understanding of the evolution of this trilobite group, and for international correlation, but some problems have been detected. In the Balang area, *P. wuxunensis* has not been recorded from the middle-upper part of the 'Tsinghsutung' Formation, just below the limit with the Kaili Formation. In other areas, however, its FAD generally coincides with that of *Arthricocephalus intermedius*. On the other hand, *Protoryctocephalus arcticus* (Geyer & Peel 2011) appears in large numbers in the middle-upper part of the 'Tsinghsutung' Formation, in the Balang area. *Protoryctocephalus arcticus* was erected by Geyer & Peel (2011), based on many disarticulated specimens from the Henson Gletscher Formation in Peary Land, North Greenland, and about 400 specimens belonging to *P. articus* were collected in the middle-upper part of the 'Tsinghsutung' Formation. The stratigraphical range of the species is between ca. 110 and ca. 272 m from the base of 'Tsinghsutung' Formation in the Songshan Section.

The identification of *O. granulata* has offered many problems. Shanchi Peng (personal com. 2005) was the first to question both the taxonomic basis of this species and its occurrence in South China. Sundberg *et al.* (2011) examined specimens from the lower part of Kaili Formation that they referred to *Ovatoryctocara* cf. *granulata*. One of us (ZYL) has studied material of '*O. granulata*' from the lower part of Kaili Formation, including specimens collected by Sundberg in 2009. Based on taxonomic differences between the type material of *O. granulata* from Siberia, and specimens previously identified as *O. granulata* from the Kaili Formation, Zhao *et al.* (2015a,b) erected the new species *Ovatoryctocara sinensis* for the material from South China. The zone was, accordingly, renamed as the *O. sinensis—B. kueichouensis* Assemblage Zone.

On the basis of extensive material from South China and Siberia, the intraspecific variability of *O. indicus* from Wuliu-Zengjiayan Section and three other sections (Esteve *et al.* 2015, 2017) were examined. The results demonstrate that *O. indicus* is a valid taxon with a very conservative shape among the different populations. Esteve *et al.* (2017) also show that *Oryctocephalus* '*reticulatus*' from the Molodo Section in Siberia is a junior synonym of *O. indicus*, suggesting that the appearance of *O. indicus* in Siberia can be correlated with the *O. indicus* Zone of South China. This taxon seems to demonstrate some geographical differences in sections from South China, but mainly these differences are due to different degrees of preservation (compaction and shearing), although some small morphological differences have been

detected (e.g. eye size). These can be explained by the occurrence of the trilobites in different depositional settings. Preliminary comparisons, using morphometric techniques, between *O. indicus* from Wuliu-Zengjiayan Section and *O. reticulatus* from Molodo River Section, showed minor differences in the shape of the cranidia, though again, both populations likely represent the same taxa (Esteve *et al.* 2017).

In summary, the upper part of Cambrian Series 2 and the lowermost part of Cambrian Series 3 in Balang area can be subdivided into three zones, in ascending order: 1, the *P. arcticus* Zone; 2, the *B. kueichouensis—O. sinensis* Zone (upper part of Cambrian Series 2); and 3, the *O. indicus* Zone (base of Cambrian Series 3).

Intercontinental correlation

The correlation of five other areas on different continents is briefly discussed below (Fig. 1).

Molodo River Section, Siberia

The middle part of Kuonamka Formation in the Molodo River Section embraces the *Ovatoryctocara* and *Kounamkites* zones (Shabanov *et al.* 2008). The biostratigraphically most significant trilobites within the *Ovatoryctocara* Zone are *O. granulata* and *B. kueichouensis*, occurring below the FAD of *Kounamkites* (Shabanov *et al.* 2008; Goryaeva *et al.* 2012; Peng *et al.* 2014). Other biostratigraphically important species from this zone are as follows: *Ovatoryctocara ovata*, *Oryctocephalus frischenfeldi*, *Paradoxides eopinus* among other trilobites (Shabanov *et al.* 2008). Species of *Bathynotus* are important for correlation within the boundary interval (Zhao *et al.* 1990; Peng *et al.* 2009; Webster 2009; Goryaeva *et al.* 2012). Fletcher (2003) noted the importance of *O. granulata* for intercontinental correlation, while Zhao *et al.* (2015a,b), however, questioned the identification of this species from Newfoundland. Nevertheless, from our point of view, *O. granulata* is an excellent guide fossil known from Siberia (Shabanov *et al.* 2008; Naimark *et al.* 2011) and North Greenland (Geyer & Peel 2011). Therefore, we suggest that the zone containing this species in Siberia should be renamed the *O. granulata* Zone. The presence of *B. kueichouensis* in this zone allows us to correlate it with the *B. kueichouensis—O. sinensis* Assemblage Zone from the lower part of the Kaili Formation and with the *P. arcticus* Zone from the middle-upper part of 'Tsinghsutung' Formation in South China.

The *Kounamkites* Zone has yielded the following trilobites, among others: *O.* '*reticulatus*', *Pagetia ferox*, *Peronopsis recta* and *Olenoides aptus*. Several authors, such as Korovnikov (2001) and Zhao *et al.* (2006, 2008, 2012), have suggested that *O.* '*reticulatus*' cannot be differentiated from *O. indicus*. As such, recently, Esteve *et al.* (2017) have considered *O.* '*reticulatus*' as a junior synonym of *O. indicus*. The *Kounamkites* Zone is therefore herein renamed the *O. indicus* (=*O.* '*reticulatus*') Zone, which can be correlated with the *O. indicus* Zone at Balang, Guizhou, South China.

Western North America

Oryctocephalus americanus Sundberg & McCollum 2003 was erected on the basis of disarticulated sclerites from the *Amecephalus arrojosensis* Zone of the Emigrant Formation at Split Mountain and Goldfield Hills, western USA (Sundberg & McCollum 2003). The *A. arrojosensis* Zone lies just below the *O. indicus* Zone (Sundberg & McCollum 2003). *Orytocephalus indicus* differs from *O. americanus* in having only one transglabellar furrow (S1) and two pairs of pygidial marginal spines. However, close examination of the cranidia of *O. americanus* from *A. arrojosensis* Zone (Sundberg & McCollum 2003; pl. 4, figs 1–4) reveals two additional pairs of very shallow transglabellar furrows (S2 and S3). An identical pattern of a shallow tranglabellar furrow is also seen in *O. indicus* from China (see Yuan *et al.* 2002; pl. 18, fig. 4, pl. 20, figs 5, 6, pl. 22, fig. 5), including specimens from the base of the *O. indicus* Zone at the Pingzhai Section in Danzhai County, Guizhou

Fig. 2. A–G, *Oryctocephalus indicus* (Reed 1910) from South China, Siberia, Greenland, the Himalayan region of India and North America; scale bar = 1 mm, except for 2, which is 2 mm. A, dorsal exoskeleton, GTB-26-1-211, Wuliu-Zengjiayan Section of the Kaili Formation, Balang, Jianhe County, Guizhou, China. B, cranidium, HS-72-3, from base of the Tianpeng Formation of Mengzi County, Yunnan Province, China (Luo *et al.* 2009). C, dorsal exoskeleton, with distinct transglabellar furrows in cranidium, from the Kounamkites Zone of the Kuonamka Formation, Molodo River Section, Siberia, previously referred to *Oryctocephalus reticulatus* Lermontova, 1940 by Shabanov *et al.* (2008, pl. 11, fig. 1). D, cranidium from N. Greenland previously referred to *O.* cf. *indicus* by Geyer & Peel (2011, fig. 19A, MGUH 29403 from GGU collection 482335). E, cranidium, from Himalaya of India (see Jell & Hughes 1997; Hughes 2016). F, cranidium, internal mould, USNM 4108055, *Plagiura* Zone, California. G, internal mould of thorax with pygidium, USNM 488757, *Plagiura* Zone, California (see Sundberg & McCollum 1997, figs 9–6, 10). H, *Bathynotus kueichouensis* Lu *in* Wang 1964, dorsal exoskeleton, GTB-6-3-25, Wuliu-Zengjiayan Section of Kaili Formation, Balang, Jianhe County, Guizhou, China; scale bar = 5 mm. I, *Ovatorycara sinensis* Zhao *et al.* 2015a,b, dorsal exoskeleton GTBB1-12-258 Wuliu-Zengjiayan Section of Kaili Formation, Balang, Jianhe County, Guizhou, China; scale bar = 2 mm. J, *Protoryctocephalus arcticus* (Geyer & Peel 2011), dorsal exoskeleton, Q51-2164, Songshan Section, Balang, Guizhou, China; scale bar = 5 mm.

(Zhao *et al.* 2008). We have also observed such an obliteration in 20% of the disarticulated cranidia analysed (n = 135). The number of pygidial marginal spines is highly variable with two and five pairs of pygidial marginal spines of *O. indicus* of the Kaili Formation (Zhao *et al.* 2015a,b). These facts suggest that *O. americanus* can be a junior synonym of *O. indicus*. *Oryctocephalus americanus* (=*O. indicus*)

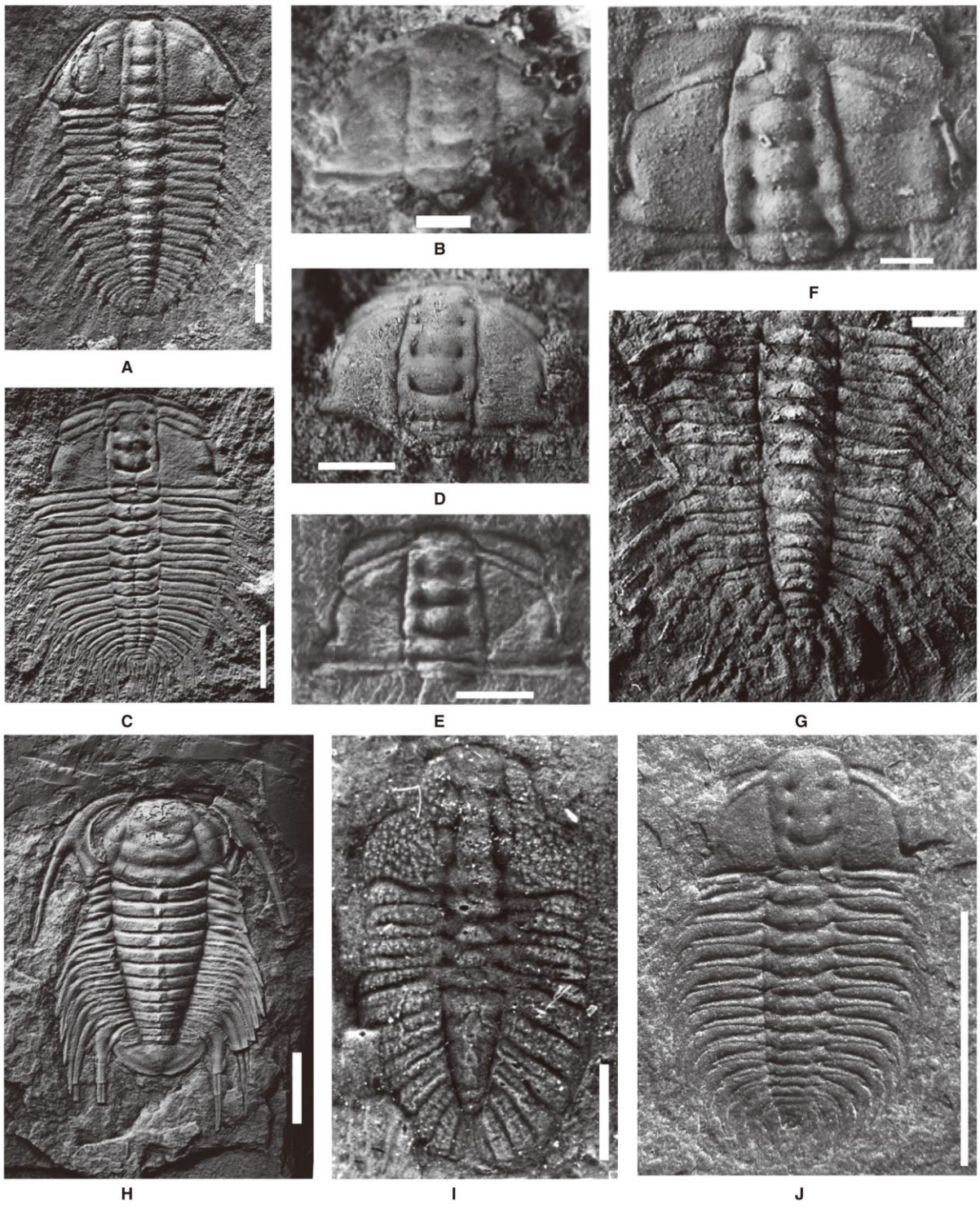

occurs in the *A. arrojosensis* Zone and the FAD is 4 metres above the extinction datum of *Olenellus*. This implies that the boundary between Cambrian Series 2 and Series 3 should be moved down to correlate with the extinction level of *Olenellus*, the current FAD of *O. americanus* (=*O. indicus*) in North America.

North Greenland

Trilobites such as *Pagetides elegans*, *O. granulata* and *P. arcticus* have been described from the upper-middle Henson Gletscher Formation of North Greenland (Geyer & Peel 2011). The trilobite association suggests a correlation with the *Bathynotus kuiechouensis—O. sinensis* Assemblage Zone from the lower part of Kaili Formation and with the *Protoryctocephalus articus* Zone in the middle-upper part of 'Tsinghsutung' Formation.

In Peary Land, North Greenland, *Oryctocephalus* has been recorded from a limestone in the basal Sydpasset Formation. The material has been described as *O.* cf. *indicus* under open nomenclature by Geyer & Peel (2011) due to the lack of pygidia. However, given the variability in the number of segments seen in the pygidia of *O. indicus* from the Kaili Formation, but the conservative cranidium shape from China and Siberia (Esteve *et al.* 2017), the cranidium found in North Greenland could belong to *O. indicus*. If so, a straightforward correlation from Greenland and South China is possible.

Australia

Bathynotus plays an important role in the correlation strata immediately below the FAD of *O. indicus*. The presence of *Bathynotus* in the lower part of the Kaili Formation suggests a correlation with the upper part of Ordain stage containing *Bathynotus* (Kruse *et al.* 2009; Sundberg *et al.* 2016) of Australia (Fig. 1).

Mediterranean area

The Mediterranean area lacks unfortunately cosmopolitan trilobites and correlation needs to be based on other trilobites (see Gozalo *et al.* 2011, 2013). Very few oryctocephalids have been found. Only two species belonging to the genus *Shergoldiella* Geyer 2006 have been reported ?*S. sequei* from Spain (Liñán & Gozalo 1999) and *S. vincenti* from Morocco (Geyer 2006; Zamora *et al.* 2014). These two species are very close related to *O. ovata* (Chernysheva *in* Kryskov *et al.* 1960). According to Naimark *et al.* (2011), the main difference between these two taxa is in the number of segments in the trunk. It is noteworthy that the associated faunas with *O. granulata* in Siberia share some genera or even some species in Morocco, such as *Morocconus notabilis*, *Condylopyge eli*, *Hamatolenus* spp. or *Schistocephalus* (Fletcher 2003). Unfortunately, this does not contribute to improve intercontinental correlation, although it does at least suggest there was a correlation from West Gondwana to other Cambrian continents.

On the other hand, in the Balang area, the combination of cosmopolitan trilobites such as *Olenoides* and *Burlingia* in the *O. indicus* Zone, and *Bathynotus*, *Ovatoryctocara* and *Redlichia* in the *B. kueichouensis—O. sinensis* Assemblage Zone, allows stratigraphical correlation into the Mediterranean area. The base of the Cambrian Stage 5 in the Mediterranean area (e.g. Morocco, Turkey and Portugal) is correlated based on some genus such as *Acadoparadoxides*, *Eccaparadoxides* and *Macannaia* with Siberia and Australia (Gozalo *et al.* 2007), and these two areas can be correlated with that of South China.

Acknowledgements. – This study is supported by grants from the Major State Basic Research Development Program of China (973 Program Nos: 2013CB835002, 2015FY310100), the National Natural Science Foundation of China (40762018, 41362002, 41172005, 41330101) to Zhao and Peng; The Foundation of the Chinese Committee of Stratigraphy, the Foundation of Guizhou Science for Foreign Cooperation (Gscf.G2010-7001) to Zhao, Yuan and Peng. J. Esteve is supported by Juan de la Cierva Grant (FPDI-2013-17337) from MINECO and CGL2013-48877-P from Spanish MINECO. We are grateful to Gian Luigi Pillola (Università di Cagliari, Italy) and one anonymous reviewer for their constructive remarks and suggestions and to Annalisa Ferretti and Peter Doyle for editorial assistance. We also thank Shanchi Peng (Nanjing Institute of Geology and Palaeontology, Chinese Academy of Sciences, Nanjing, China), Loren Babcock (School of Earth Sciences, The Ohio University, USA) and Per Ahlberg (Lund University, Sweden) for their support and help on research of Cambrian Stage 5; we are very grateful to Ronald Parsley (Tulan University) for his comments on the early version of this article.

References

Babcock, L.E. & Peng, S.C. 2007: Cambrian chronostratigraphy: current state and future plans. *Palaeogeography, Palaeoclimatology, Palaeoecology 254*, 62–66.

Esteve, J., Zhao, Y.L., Peng, J. & Sun, H.J. 2015: Ontogeny, morphological variability and taphonomy of *Oryctocephalus indicus* (Reed, 1910) from the Kaili Formation, South China. *2nd International Congress on Stratigraphy, Abstracts,* 99.

Esteve, J., Zhao, Y.L. & Peng, J. 2017: Morphological assessment of the Cambrian trilobites *Oryctocephalus indicus* (Reed 1910) from China and *Oryctocephalus* '*reticulatus*' (Lermontova 1940) from Siberia. *Lethaia 50*, 175–193.

Fletcher, T.P. 2003: *Ovatoryctocara granulata*: the key to a global Cambrian stage boundary and the correlation of the olenellid, redlichiid and paradoxidid realms. *Special Papers in Palaeontology 70*, 73–102.

Geyer, G. 2006: First African oryctocephalid trilobites from the Lower-Middle Cambrian boundary interval. *Palaeoworld 15*, 348–359.

Geyer, G. & Peel, S.J. 2011: The Henson Gletscher Formation of North Greenland and its bearing on the global Cambrian Series 2-Series 3 boundary. *Bulletin of Geosciences 86*, 465–534.

Goryaeva, L.E., Pegel, T.V., Shabanov, Y.Y. & Bushuev, E.V. 2012: New data on stratigraphic range of trilobite *Bathynotus* genus in Cambrian of Siberia platform. *Journal of Guizhou University 29* (Supplement 1), 164.

Gozalo, R., Liñán, E., Dies Álvarez, M.E., Gámez Vintaned, J.A. & Mayoral, E. 2007: The Lower-Middle Cambrian boundary in the Mediterranean subprovince. *In* Linnemann, U., Nance, R.D., Kraft, P. & Zulauf, G. (eds): *The Evolution of the Rheic Ocean: From Avalonian-Cadomian Active Margin to Alleghenian-Variscan Collision*, 359–373. *Geological Society of America Special Paper 423,* 1–630. The Geological Society of America, Inc., Boulder.

Gozalo, R., Bautista, J., Chirivella Martorell, J.B., Esteve, J. & Liñán, E. 2011: Correlation between the base of Drumian Stage and the base of middle Caesaraugustan Stage in the Iberian Chains (NE Spain). *Bulletin of Geosciences 86*, 545–554.

Gozalo, R., Dies Álvarez, M.E., Gámez Vintaned, J.A., Zhuravlev, A., Bauluz, B., Subías, I., Chirivella Martorell, J.B., Mayoral, E., Gursky, H.J., Andrés, J.A. & Liñán, E. 2013: Proposal of a reference section and point for the Cambrian Series 2–3 boundary in the Mediterranean subprovince in Murero (NE Spain) and its intercontinental correlation. *Geological Journal 48*, 142–155.

Hughes, N.C. 2016: The Cambrian palaeontological record of the Indian subcontinent. *Earth Science Reviews 159*, 428–461.

Jell, P.A. & Hughes, N.C. 1997: Himalayan Cambrian trilobites. *Special Papers in Palaeontology 58*, 1–113.

Korovnikov, I.V. 2001: Lower and Middle Cambrian boundary and trilobite from northeast Siberia platform. *Palaeoworld 13*, 270–273.

Kruse, P.D., Jago, J.B. & Laurie, J.R. 2009: Recent developments in Australian Cambrian biostratigraphy. *Journal of Stratigraphy 33*, 35–47.

Kryskov, L.N., Lazarenko, N.P., Ogienko, L.V. & Tchernysheva, N.E. 1960: New early Palaeozoic trilobites of Eastern Siberia and Kazakhstan. *In* Markovsky B.P. (ed.): *New Species of Prehistoric Plants and Invertebrates of the USSR*, *volume 2*, pp. 211–255. VSEGEI, Moscow [in Russian].

Liñán, E. & Gozalo, R. 1999: Nuevos trilobites del Cámbrico inferior de Aragón. *In* Gámez Vintaned, J.A. & Liñán, E. (eds): *25 Años de Paleontología aragonesa. Homenaje al Profesor Leandro Sequeiros*, 255–261. Institución Fernando El Católico, Zaragoza.

Luo, H.L., Hu, S.X., Hou, S.G., Cao, H.G., Zhan, D.Q. & Li, W.H.. 2009: *Cambrian Stratigraphy and Trilobites from Southeastern Yunnan, China*, 250 pp. Yunnan Science and Technology Press, Kunming (in Chinese with English abstract).

Naimark, E., Shabanov, Y.Y. & Korovnikov, I.V. 2011: Cambrian trilobite *Ovatoryctocara* Tchernysheva, 1962 from Siberia. *Bulletin of Geosciences 86*, 405–422.

Peng, S.C. 2009: The newly developed Cambrian biostratigraphic succession and chronostratigraphic scheme for South China. *Chinese Science Bulletin 54*, 4161–4170.

Peng, S.C. & Babcock, L.E. 2001: Cambrian of the Hunan-Guizhou region, South China. *Palaeoworld 13*, 3–51.

Peng, S. & Babcock, L.E. 2008: Cambrian period. In Ogg, J.G., Ogg, G. & Gradstein, F.M. (eds): *Concise Geological Timescale*, pp. 37–46. Cambridge University Press, Cambridge.

Peng, S.C. & Babcock, L.E. 2011: Continuing progress on chronostratigraphic subdivision of the Cambrian System. *Bulletin of Geosciences 86*, 465–534.

Peng, S.C., Babcock, L.E., Geyer, G. & Moczydłowska, M. 2006: Nomenclature of Cambrian epochs and series based on GSSPs – comments on an alternative proposal by Rowland and Hicks. *Episodes 29*, 130–132.

Peng, J., Zhao, Y.L., Yuan, J.L., Yao, L. & Yang, H. 2009: *Bathynotus* – a key trilobite taxon for global stratigraphic boundary correlation between Cambrian Series 2 and Series 3. *Progress in Natural Science 19*, 99–105.

Peng, J., Yuan, J.L., Zhao, Y.L., Sun, H.J., Yang, X.L. & Yang, Y.N. 2014: The trilobite *Bathynotus* from Cambrian Series 2 of China and its implications for global correlation. *GFF 136*, 203–207.

Reed, F.R.C. 1910: The Cambrian fossils of Spiti. *Palaeontologia Indica 15*, 1–70.

Shabanov, Y.Y., Korovnikov, I.V., Pereladov, V.S. & Fefelov, A.F. 2008: The traditional Lower-Middle Cambrian boundary in the Kuonamka Formation of the Molodo River section (the southeastern slope of the Olenek Uplift of the Siberian Platform) proposed as a candidate for GSSP of the lower boundary of the Middle Cambrian and its basal (Molodian) stage, defined by the FAD of *Ovatoryctocara granulata*. In Rozanov, A.Y., Varlamov, A.I., Parkhaev, P.Y., Pak, K.L. (eds): *The Cambrian System of the Siberian Platform, Part 2: North-east of the Siberian Platform*, pp. 8–59. Palaeontological Institute, Moscow.

Sundberg, F.A. & McCollum, L.B. 1997: Oryctocephalids (Corynexochida: Trilobita) of the Lower-Middle Cambrian boundary interval from California and Nevada. *Journal of Paleontology 71*, 1065–1090.

Sundberg, F.A. & McCollum, L.B. 2003: Early and Mid Cambrian trilobites of the outer shelf deposits of Nevada and California. *Palaeontology 42*, 945–986.

Sundberg, F.A., Zhao, Y.L., Yuan, J.L. & Lin, J.P. 2011: Detailed trilobite biostratigraphy across the proposed GSSP for Stage 5 ('Middle Cambrian' boundary) at the Wuliu-Zengjiayan section, Guizhou, China. *Bulletin of Geosciences 86*, 423–464.

Sundberg, F.A., Geyer, G., Krust, P.D., Mccolum, I.B., Peger, T.V., Tylinska, A. & Zhuralev, A. 2016: International correlation of Cambrian Series 2–3, Stage 4–5 boundary interval. *Australasian Palaeontological Memoirs 49*, 83–125.

Wang, Y. (ed.), 1964: *Handbook of Index Fossils of South China*, 173 pp. Science Press, Beijing, 92 pls.

Wang, C.J., Zhao, Y.L., Peng, J., Yang, X.L., Bai, J., Liu, Y. & Chen, T. 2014: Biomarker evidence for biotic and environmental change across the Cambrian Series 2-Series 3 boundary at the Wuliu-Zengjiayan Section, Guizhou, China. *Science China (Earth Sciences) 57*, 2279–2781.

Webster, M. 2009: Systematic revision of the Cambrian trilobite *Bathynotus* Hall, 1860, with documentation of new occurrences in western Laurentia and implications for intercontinental biostratigraphic correlation. *Memoirs of the Association of Australasian Palaeontologists 37*, 369–406.

Yuan, J.L. & Esteve, J. 2015: The earliest species of *Burlingia* Walcott, 1908 (Trilobita) from South China: biostratigraphical and palaeogeographical significance. *Geological Magazine 152*, 358–366.

Yuan, J.L., Zhao, Y.L., Li, Y. & Huang, Y.Z. 2002: *Trilobite Fauna of the Kaili Formation (Uppermost Lower Cambrian-Lower Middle Cambrian) from Southeastern Guizhou, South China*, 422 pp. Shanghai Science and Technology Press, Shanghai (in Chinese with English summary).

Yuan, J.L., Zhu, X.J., Lin, J.P. & Zhu, M.Y. 2011: Tentative correlation of Cambrian Series 2 between South China and other continents. *Bulletin of Geosciences 86*, 397–404.

Zamora, S., Álvaro, J.J., Clausen, S. & Esteve, J. 2014: Open quarry of the Brèche à Micmacca Member crossing the 'telesto level' at Assemame, central Anti-Atlas. *In* Devaere, L., Clausen, S. & Álvaro, J.J. (eds): *Stratigraphic Overview of the Ediacaran and Cambrian from the Anti-Atlas, Morocco*, 72–75. University of Lille I, Lille.

Zhao, Y.L., Huang, Y.Z., Gong, X.Y. & Dai, X.C. 1990: Bathynotus from Kaili Formation (Lower–Middle Cambrian) of Kaili Area, Guizhou. *Acta Palaeontology Sinica 29*, 43–53 (in Chinese with English abstract).

Zhao, Y.L., Yuan, J.L., Peng, S.C., Yang, X.L., Peng, J., Lin, J.P. & Guo, Q.J. 2006: A restudy of *Oryctocephalus indicus* (Reed, 1910). *Progress in Natural Science 11*, 1177–1182.

Zhao, Y.L., Yuan, J.L., Peng, S.C., Babcock, L.E., Peng, J., Lin, J.P., Guo, Q.J. & Wang, Y.X. 2007: New data on the Wuliu-

Zengjiayan section (Balang, South China), GSSP candidate for the base of Cambrian Series 3. *Memoirs of Association of Australasian Palaeontologists 33*, 57–65.

Zhao, Y.L., Yuan, J.L., Peng, S.C., Babcock, L.E., Peng, J., Guo, Q.J., Lin, J.P., Tai, T.S., Yang, R.D. & Wang, Y.X. 2008: A new section of Kaili Formation (Cambrian) and a biostratigraphic study of the boundary interval across the undefined Cambrian Series 2 and Series 3 at Jianshan, Jianhe County, China with a discussion of global correlation based on the first appearance datum of *Oryctocephalus indicus* (Reed, 1910). *Progress in Natural Science 18*, 1549–1556.

Zhao, Y.L., Peng, J., Yuan, J.L., Babcock, L.E., Guo, Q.J., Yin, L.M., Yang, X.L., Tai, S.L., Wang, C.J., Lin, J.P., Gaines, R., Sun, H.J. & Yang, Y.N. 2012: Discussion of candidate stratotypes for GSSP defining the conterminous base of Cambrian provisional Series 3 and Stage 5. *Journal of Guizhou University 29* (Supplement 1), 35–48.

Zhao, Y.L., Yuan, J.L., Guo, Q.J., Peng, J., Yin, L.M., Yang, Y.L., Wang, C.J. & Sun, H.J. 2014: Comments on some important issues concerning the establishment of GSSP for Cambrian Stage 5. *GFF 136*, 333–336.

Zhao, Y.L., Esteve, J., Yuan, J.L., Peng, J. & Sun, H.J. 2015a: Taphonomy and morphologic variation of *Oryctocephalus indicus* from China, Russia and USA. *2nd International Congress on Stratigraphy, Abstracts*, p. 430.

Zhao, Y.L., Yuan, J.L., Guo, Q.J., Peng, J., Yang, X.L. & Esteve, J. 2015b: Restudy of *Ovatoryctocara* Tchernysheva, 1962 from the Kaili Formation, Jianhe County, Guizhou, South China. *Annales de Paléontologie 101*, 193–198.

Global Standard Stratotype-Section and Point (GSSP) for the conterminous base of the Miaolingian Series and Wuliuan Stage (Cambrian) at Balang, Jianhe, Guizhou, China

Article *in* Episodes · June 2019

DOI: 10.18814/epiiugs/2019/019013

CITATIONS
10

READS
912

16 authors, including:

Jin-Liang Yuan
Chinese Academy of Sciences
71 PUBLICATIONS **1,103** CITATIONS
SEE PROFILE

Babcock Loren
The Ohio State University
170 PUBLICATIONS **3,941** CITATIONS
SEE PROFILE

Qingjun Guo
Chinese Academy of Sciences
107 PUBLICATIONS **1,889** CITATIONS
SEE PROFILE

Jin Peng
Huanggang Normal University
80 PUBLICATIONS **1,167** CITATIONS
SEE PROFILE

Article

165

by Yuanlong Zhao[1], Jinliang Yuan[2], Loren E. Babcock[3], Qingjun Guo[4], Jin Peng[1], Leiming Yin[2], Xinglian Yang[1], Shanchi Peng[2,5]*, Chunjiang Wang[6], Robert R. Gaines[7], Jorge Esteve[8], Tongsu Tai[9], Ruidong Yang[1], Yue Wang[1], Haijing Sun[2], and Yuning Yang[1]

Global Standard Stratotype-Section and Point (GSSP) for the conterminous base of the Miaolingian Series and Wuliuan Stage (Cambrian) at Balang, Jianhe, Guizhou, China

[1] College of Resource and Environment Engineering, Guizhou University and Guizhou Research Center for Palaeontology, Guiyang, 550025, China
[2] Nanjing Institute of Geology and Palaeontology, Chinese Academy of Sciences, 39 East Beijing Road, Nanjing 210008, China
[3] School of Earth Sciences, The Ohio State University, 125 South Oval Mall, Columbus, OH 43210, USA
[4] Center for Environmental Remediation, Institute of Geographic Sciences and Natural Resources Research, Chinese Academy of Sciences, Beijing 100101, China
[5] State Key Laboratory of Paleobiology and Stratigraphy, Chinese Academy of Sciences, Nanjing 210008, China; *Corresponding author, *E-mail: scpeng@nigpas.ac.cn*
[6] College of Geosciences & State Key Laboratory of Petroleum Resources and Prospecting, China University of Petroleum, Beijing 102249, China
[7] Geology Department, Pomona College, 185E. Sixth Street, Claremont, CA 91711, USA
[8] Departamento de Paleontolgía, Facultad de CC Geológicas, Universidad Complutense de Madrid, José Antonio Novais 12, 28040, Madrid, Spain
[9] Agency of Kaili Area Protected Fossils, Jianhe, Guizhou 556300, China

(Received: December 17, 2018; Revised accepted: May 20, 2019)

https://doi.org/10.18814/epiiugs/2019/019013

The International Commission on Stratigraphy and the IUGS Executive Committee have recently ratified a Global Standard Stratotype-section and Point (GSSP) defining the conterminous base of the third series and the fifth stage of the Cambrian System. The series and the stage are respectively named the Miaolingian Series and Wuliuan Stage, after the Maioling Mountains in southeastern Guizhou and the Wuliu sidehill, Jianhe County, in eastern Guizhou Province, South China, where the GSSP is located. The GSSP is exposed in a natural outcrop near the Balang Village at a position of 26°44.843'N latitude and 108°24.830'E longitude. It is defined at the base of a silty mudstone layer 52.8 m above the base of the Kaili Formation in the Wuliu-Zengjiayan section, coinciding with the first appearance of the cosmopolitan oryctocephalid trilobite Oryctocephalus indicus *(base of the* O. indicus *Zone). Secondary global markers at or near the base of the series and stage include the peak of a rather large negative carbon isotopic excursion (ROECE excursion), the simultaneous appearance of many acanthomorphic acritarch forms, a transgressive phase of a major eustatic event, and the last appearance of intercontinental polymerid trilobites, either* Bathynotus *or* Ovatoryctocara. *Faunal turnovers close to the base of the Miaolingian Series and Wuliuan Stage have been recognized as being at the base of the* Oryctocephalus indicus *Zone of Amgan Stage in Siberia, the Delamaran Stage in Laurentia, the* Oryctocephalus indicus *Zone in the Indian Himalaya and North Greenland, near the base of the Delamaran Stage in Australia, and within the* Eccaparadocides sdzuyi *Zone in Iberia and the* Ornamentaspis frequens *Zone in Morocco.*

Introduction

The International Subcommission on Cambrian Stratigraphy (ISCS) has recommended a subdivision of the Cambrian System into four series (Peng, 2004, 2006; Babcock et al., 2005; Peng et al., 2006; Babcock and Peng, 2007). Within each series it is expected that two or three stages will be recognized with their boundaries corresponding to horizons that can be precisely correlated with confidence through almost all palaeocontinents. Cambrian boundary positions ratified by the International Union of Geological Sciences (IUGS) and International Commission on Stratigraphy (ICS) (Figs. 1, 2) are: 1, the base of the Terreneuvian Series and Fortunian Stage, which is also the base of Cambrian System, Paleozoic Erathem and Phanerozoic Eonothern, corresponding to the base of *Treptichnus pedum* Zone in Newfoundland (Brasier et al., 1994; Landing, 1994; Gehling et al., 2001; Landing et al., 2007); 2, the base of Drumian Stage corresponding to the base of the *Ptychagnostus atavus* Zone in Utah, USA (Babcock et al., 2007); 3, the base of the Guzhangian Stage corresponding to the base of *Lejopyge laevigata* Zone in Hunan, South China (Peng et al., 2009a); 4, the base of the Furongian Series and Paibian Stage corre-

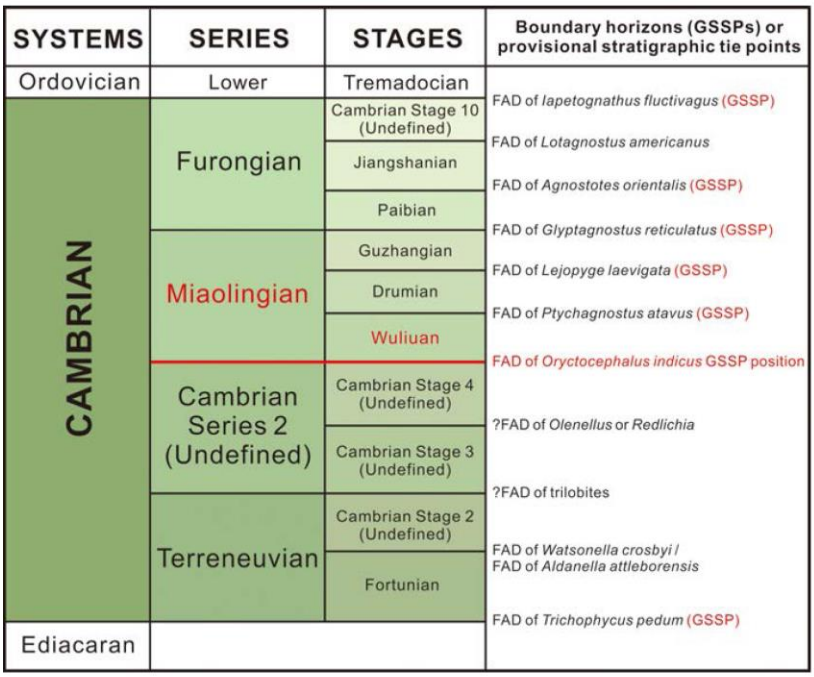

Figure 1. Chart showing working model for global chronostratigraphic subdivision of the Cambrian System, indicating the lower boundary of the newly ratified Miaolingian Series and Wuliuan Stage (modified from Peng et al., 2009a, 2012b).

sponding to the base of *Glyptagnostus reticulatus* Zone in Hunan, South China (Peng et al., 2004a); 5, the base of the Jiangshanian Stage corresponding to the base of the *Agnostotes orientalis* Zone in Zhejiang, Southeast China (Peng et al., 2012a); and 6, the base of Miaolingian Series and Wuliuan Stage, ratified recently, in Southwest China.

The purpose of this paper is to announce ratification of the GSSP for the conterminous base of the Miaolingian Series and the Wuliuan Stage, which coincides with the FAD of the intercontinental oryctocephalid trilobite *Oryctocephalus indicus*. The Miaolingian Series and the Wuliuan Stage are newly named Cambrian chronostratigraphic units, replacing in concept and content the provisional Series 3 and Stage 5 (Figs. 1, 2, 5, 7, 9). The GSSP for the base of the new series and new stage lies within Bed 9 at 52.8 m above the base of the Kaili Formation in the Wuliu-Zengjiayan section that is about 0.5 km North of Balang Village, Jianhe County, eastern Guizhou Province, South China (Figs. 3, 4). This point fulfills all of the geological and biostratigraphic requirements for a GSSP (see Remane et al., 1996). The section is easily accessible, and access for research is unrestricted. It is located within the Jianhe Natural Reserve of Paleontological Fossils and the Miaoling National Geopark, both have been under permanent protection by the government of Guizhou Province since the natural reserve was approved in 2002 and by the Ministry of Land and Mineral Resources of China since the geopark was approved in 2009.

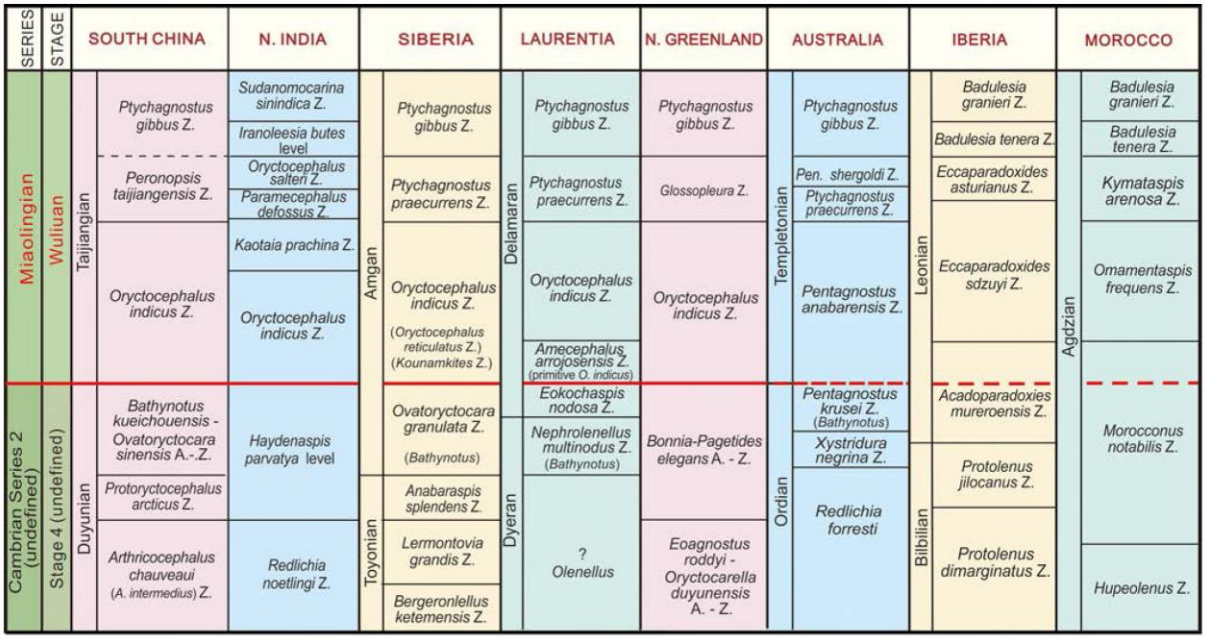

Figure 2. Correlation chart of the interval of Cambrian Stage 4 through Wuliuan Stage (Miaolingian Series). Chart compiled from numerous sources, summarized principally in Yuan and Ng. (2014), Geyer (2015), Zhao et al. (2015, 2017), Hughes (2016), Sundberg et al. (2016), Peng et al. (2017) and Esteve et al. (2017).

Stratigraphic Rank of the Boundary

The Miaolingian Series is the third series of the Cambrian System, and the Wuliuan Stage is the lowermost stage of the Miaolingian Series (Figs. 1, 2). The base of the series and stage defines automatically the top of provisional Cambrian Series 2 and its uppermost stage, the provisional Stage 4, both of which are unnamed yet. The boundary will be a standard series/epoch and stage/age GSSP. The upper boundary of the series is defined by the base of the Furongian Series, and the

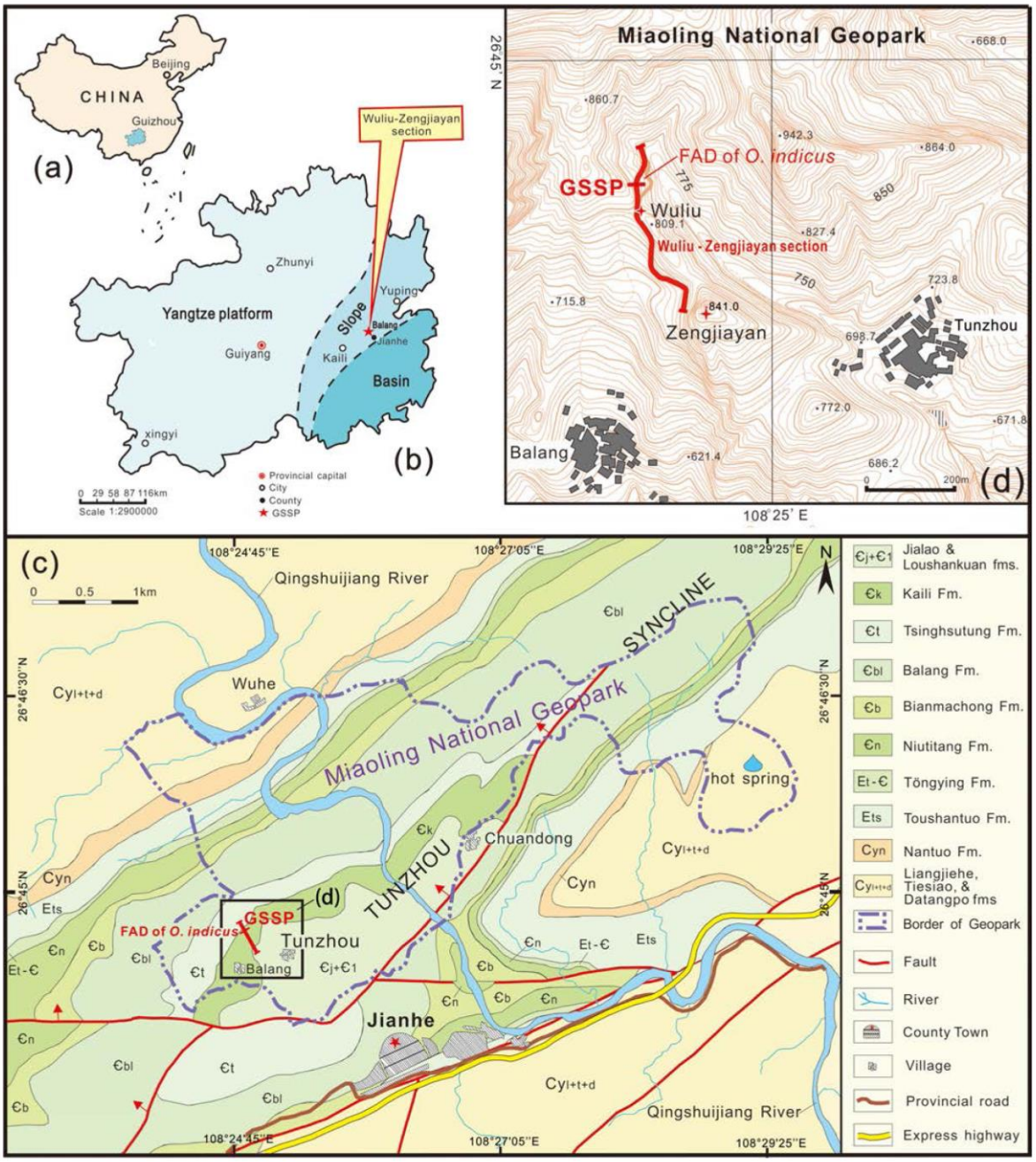

Figure 3. (a) Location of Guizhou in China (outlined blue area); (b) Cambrian palaeogeography of Guizhou with the Wuliu-Zengjiayan GSSP section indicated by a red star; (c) Geological map of the part of eastern Guizhou province, showing the study area and the location of the GSSP section for the Miaolingian Series and Wuliuan Stage (modified from Geological Survey of Guizhou Province, 1966); (d) Topographic map of the Balang and Tunzhou area, indicating location of the Wuliu-Zengjiayan GSSP section with the FAD of* Oryctocephalus indicus *(red line; modified from topographic map G-49-37-55, Dagaowu Sheet, issued by Surveying and Mapping Bureaus of Guizhou and Shaanxi, 1991; 1:10000 sale); the Wuliu-Zengjiayan section is named after the Wuliu sidehill and Zengjiayan hill (indicted by red stars).

upper boundary of the stage is defined by the base of the Drumian Stage of the Miaolingian Series (Fig. 1).

The names Wuliuan and Miaolingian are derived from geographic localities in eastern, where the GSSP is located, and southeastern Guizhou. The name of Wuliuan Stage (and Age) is derived from Wuliu, a side-hill that the Wuliu-Zengjiayan section crosses, and the name Miaolingian Series (and Epoch) is derived from the Miaoling Mountains, which traverse the southeastern part of the Guizhou Province. These mountains are inhabited primarily by the Miao ethnic minority.

Geography and Physical geology of the GSSP

Geographic Location

The Wuliu-Zengjiayan section (Yuan et al., 1997, 1999, 2002; Zhao et al., 2001a, b, 2004, 2007; 2012a, c) is exposed along a hill ridge, which is about 0.5 km northeast of Balang Village, Jianhe County (formerly the village was administered by Taijiang County), Guizhou Province, China (Fig. 3). The studied area lies in the southwest of the Miaoling National Geopark (Fig. 3(c)). The Balang Village is located 2.5 km from the township of Jianhe County, which is easily accessible via the Guiyang-Kaili-Yuping Express Highway. The position of the Wuliu-Zengjiayan section is on topographic map G-49-37-55, Dagaowu Sheet, 1:10000 sale (Fig. 3(d)). The GSSP is exposed near the ridge crest at a position of 26º44.843'N latitude and 108º24.830'E longitude at an elevation of approximately 795 m.

Geological Location

The Cambrian geology of eastern Guizhou, the site of the GSSP section, has been summarized in a number of papers, among which the most notable are the monographs on the Regional Geology of Guizhou Province published by the Guizhou Bureau of Geology and Mineral Resources (1987), and articles by Yin (1987), Yuan et al. (2002), and Zhao et al. (2011).

The Miaoling Mountains in southeastern Guizhou consist of a series of folds and thrust slices resulting from post-Devonian compressional tectonics that affected the area between the Duliujiang and Qingshuijiang river system of eastern Guizhou (Yin, 1987). The Balang area of Jianhe County, eastern Guizhou, is located on the northwestern limb of the Tunzhou Syncline (Fig. 3(c)), which belongs to the Shansui Composite Syncline in the Nanhua fold belt. The lower half of the Cambrian System in this area was deposited on the lower part of the Jiangnan Slope (mostly shale facies), which was located between the Yangtze carbonate platform to the northwest and deeper water facies of the Jiangnan Basin to the southeast (e.g., Yin, 1987; Peng and Babcock, 2001) (Fig. 3(b)). Exposure of Neoproterozoic and Cambrian strata in the Jianhe area is highly favorable. The Precambrian succession there consists of several formations, which, in ascending order, are the Liangjiehe, Tiesiao, Datangpo, Nantuo, Toushantuo (=Doushantuo), and Töngying (=Dengying) formations (the former three units are marked as Cy_{l+t+d} on Fig. 3(c)). The Cambrian succession in this area comprises seven units. In ascending order these are the Niutitang, Bianmachong, Balang, Tsinghsutung, Kaili, Jialao and Loushankuan (=Loushanguan) formations (Fig. 3(c)). Detailed descriptions of these units have been presented in a number of papers (Zhou et al., 1980; Yin, 1987; Pu and Ye, 1991; Zhao et al., 2001a, b). An overview of Cambrian paleogeography, biotic provinces, and geologic history of the region was provided by Peng and Babcock (2001).

The Kaili Formation is exposed widely in eastern and southeastern Guizhou, showing a SW–NE trend across the Danzhai, Taijiang, Jianhe, Zhenyuan and Yuping counties to the Tongren area. The Kaili Formation was deposited in an open-shelf to slope setting (Zhou et al., 1980; Zhang et al., 1996; Zhao et al., 2001a, b; Yuan et al., 2002; Gaines et al., 2011), where it overlies either the Wuxun Formation or the Tsinghsutung Formation and is overlain by the Jialao Formation (Figs. 4(a), 5). The formation is typically about 250 m thick, and straddles the boundary of the provisional Cambrian Series 2 and the Miaolingian Series. The Kaili Formation crops out extensively in the Balang and Chuandong areas (Fig. 3(c)), where it overlies the Tsinghsutung Formation in conformity. The Wuliu-Zengjiayan section contains strata extending from the top part of the Tsinghsutung Formation to the basal part of the Jialao Formation with the GSSP occurring in the lower part of the Kaili Formation. The Kaili Formation contains a total of 47 trilobite genera (subgenera) with 16 genera occurring below the GSSP level, 20 genera above, and 11 genera ranging through the boundary (Zhao et al., 2001a, b; Yuan et al., 2002). Trilobites are commonly articulated and thin shelled, indicating a relatively deep, quiet water sedimentary environment (Zhang et al., 1996; Zhu et al., 1999; Yuan et al., 2002; Gaines et al., 2011).

Location of Level and Specific Point

The boundary interval of the Wuliu-Zengjiayan section consists primarily of silty and calcareous mudstones (Fig. 5) that are abundantly fossiliferous and bear the first appearance datum (FAD) of the widely distributed oryctocephalid trilobite *Oryctocephalus indicus* (Fig. 6(a)–(d)), which is selected as primary marker to define the provisional Stage 5 of Cambrian by the International Subcommission on Cambrian Stratigraphy, at 52.8 m above the base of the Kaili Formation (Zhao et al., 2001a, b). The species *O. indicus* is associated with a large number of trilobites, such as *Pagetia*, *Euarthricocephalus*, *Burlingia* and *Olenoides*. Below GSSP level, the *Bathynotus kueichouensis– Ovatoryctocara sinensis* Assemblage-Zone is recognized (Figs. 4(a), 5, 6), which is characterized by the presence of many trilobites with broad geographic ranges, e.g. *Bathynotus*, *Redlichia*, *Oryctocephalops*, *Ovatoryctocara*, and *Oryctocephalites* (Yuan et al., 1997, 2002; Zhao et al., 2001a, b, 2007, 2012a, c; Sundberg et al., 2011; Fig. 6(e)–(h)).

Stratigraphic Completeness

Detailed bed-by-bed correlation of the Miaolingian strata through eastern Guizhou, coupled with detailed biostratigraphy (Yuan et al., 1997, 1999, 2002; Yin and Yang, 1999; Yang and Yin, 2001; Zhao et al., 2001a, b, 2004, 2005, 2007, 2012a, b, c, 2014, 2015, 2017; Yin et al., 2010; Sundberg et al., 2010, 2011), sedimentology (Zhang et al., 1996; Gaines et al., 2011), carbon isotope chemostratigraphy (Yang et al., 2003; Guo et al., 2005, 2010a, b), sulphur isotope chemostratigraphy (Guo et al., 2014) and biomarkers (Wang et al., 2014) clearly demonstrate the stratigraphic continuity of the basal interval of the Wuliuan

Figure 4. Exposure of the Wuliu-Zengjiayan GSSP for the base of the Wuliuan Stage (coinciding with the FAD of* Oryctocephalus indicus *in the Kaili Formation?near Balang, Jianhe County, Guizhou Province, South China. Strata underlying the Wuliuan GSSP belong to the upper part of undefined Cambrian Stage 4 of provisional Series 2. (a) View of the Wuliu-Zengjiayan section showing three trilobites zones of the Kaili Formation; (b) The boundary interval of the GSSP in Wuli-Zengjiayan section, showing the FAD of* O. indicus *in the lower part of the Kaili Formation; (c) and (d) close-up views of the rectangle areas in (b). (c) Showing the bed numbers in yellow (Bed 9 and 10), the numbers of collecting interval in red on the white marble, and the FAD of O. indicus, which lies at 52.8 m above the Kaili Formation and defines the base of Wuliuan Stage; (d) The "Wuliu Quarry", studied by Sundberg et al. (2011), with identical succession and fossil ranges as the Wuliu-Zengjiayan GSSP section; (e) Partial outcrop of the* O. indicus *Zone, where the rocks yield the Kaili Biota, along with a walk terrace leading to the GSSP site.

Stage (Miaolingian Series) in the Wuliu-Zengjiayan section. Biostratigraphic studies of eastern Guizhou and other countries have revealed a consistent succession of trilobite species and acritarch taxa (e.g., Tchernysheva, 1962; Zhang et al., 1980; Whittington, 1988, 1995; Astashkin et al., 1991; Moczydłowska, 1991; Palmer and Repina, 1993; Jell and Hughes, 1997; Yuan et al., 1997, 2002; Sundberg and McCollum, 1997, 2003; Palmer, 1998; Hughes and Jell, 1999; Yin and Yang, 1999; Sundberg et al., 1999, 2011; Shergold and Whittington, 2000; Yang and Yin, 2001; Korovnikov, 2001, 2006; Zhao et al., 2001a, b, 2004, 2007, 2012a, b, 2014, 2015; Geyer, 2005; Fletcher, 2007; McCollum and Sundberg, 2007; Shabanov et al., 2008; Kruse et al., 2009; Peng et al., 2009b; Yin et al., 2009, 2010; Moczydłowska and Yin, 2012; Hughes, 2016; Singh et al., 2016; Sundberg et al., 2016) as observed in the Wuliu-Zengjiayan section. This section is interpreted to represent continu-

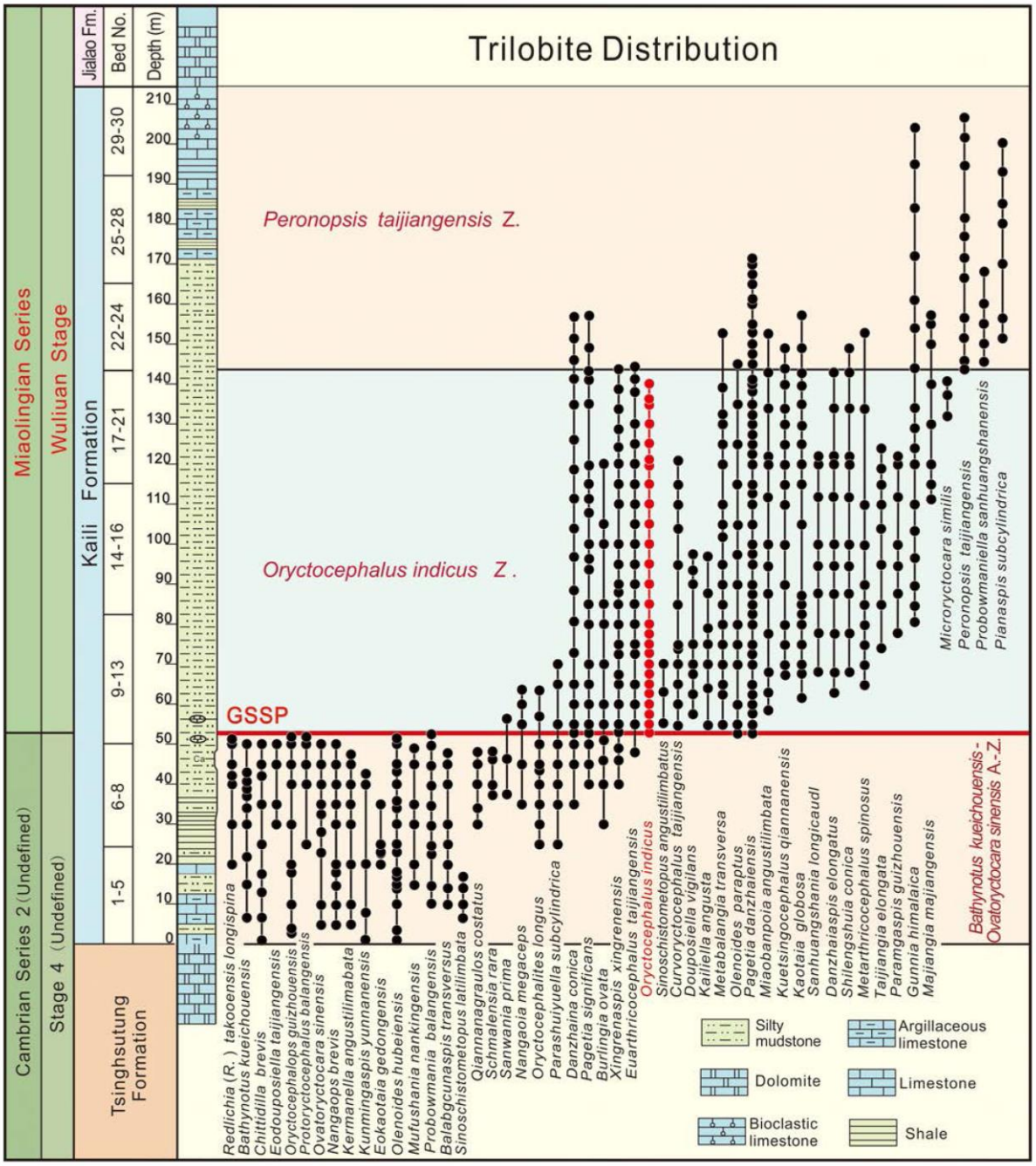

Figure 5. Observed stratigraphic distribution of trilobites in the Wuliu-Zengjiayan section near Balang, Jianhe, Guizhou, South China. The GSSP coincides with the base of the* Oryctocephalus indicus *Zone in this section, lying 52.8 m above the base of the Kaili Formation.

ous deposition of a succession of shales and subordinate lime mudstones across the GSSP boundary interval (Zhang et al., 1996; Yuan et al., 2002; Zhao et al., 2005, 2007, 2012a, c; Sundberg et al., 2010, 2011; Gaines et al., 2011). The section lacks generally syndepositional and tectonic disturbance at the GSSP boundary interval, although small scale folding or minor bedding-plane slippage occurs along some beds and more or less tectonic shearing happened to fossil specimens, which are expected in an inclined succession of fine-clastic strata. Bedding-plane slip surfaces do not appear to have resulted in any loss or repetition of stratigraphic thickness, and event-driven deposition was maintained across the Kaili Formation with no evidence for condensation (Gaines et al., 2011). In addition, the biostratigraphic succession in the section is consistent with numerous reference sections in the region (Zhao et al., 2001a, b, 2007; Fig. 5). Although the section has been affected by mild oxidative weathering, no evidence of significant diagenetic alteration or metamorphism is present.

Thickness and Stratigraphic Extent

The Kaili Formation is 214.2 m thick at the Wuliu-Zengjiayan section (Zhao et al., 2001a, b, 2007, 2012a, c; Yuan et al., 2002). Lithologically, the formation is subdivided into three units: the lower part is composed of thin-bedded limestones with silty mudstone interbeds, with a thickness of 23.7 m (Bed 1–5); the middle part, including the *Oryctocephalus indicus* Zone and the well-known Kaili Biota-bearing interval (Zhao et al., 2005, 2011), is 150.43 m thick (Bed 6–27) and is dominated by silty mudstones, mudstone, calcareous mudstone, and shale layers, containing carbonate lenticles in the lower portion; the upper part, including most of the *Peronopsis taijiangensis* Zone, consists of thin-bedded limestone layers and intercalated shale, grading into grainy limestone and bioclastic limestone with a thickness of 40.07 m (Bed 28–30; Fig. 5).

The GSSP for the base of the Miaolingian Series and the Wuliuan Stage occurs in a succession composed of greenish-grey, internally laminated silty mudstone in the mid-lower part of the Kaili Formation (Figs. 4(b)–(d), 5). The strata below the GSSP belong to the upper part of undefined Cambrian Stage 4 or to the Duyunian Stage in the terminology used for South China.

Provisions for Conservation, Protection, and Accessibility

The exposure containing the GSSP in the Balang area has received permanent protection, due to the geological significance, from the government of Guizhou since 2002, when the Balang area was approved as Jianhe Natural Reserve of Paleontological Fossils. In 2009, this area was included as a part of the Miaoling National Geopark and since then has been managed and protected by both governments of Guizhou Province and Jianhe County.

Access to the outcrop is essentially unrestricted in all seasons. Travel to Guizhou is open to persons of all nationalities, and travel for scientific purposes is always welcomed. Ordinary vehicles can be driven from the Jianhe Township directly to Balang or Tunzhou village in no more than 20 minutes. From either village, the GSSP is easily reached by 20–30 minute walking via paved paths.

Motivation for Selection of the Boundary Level and of the Potential Stratotype Section

Principal Correlation Event (marker) at GSSP Level

The oryctocephalid trilobite *Oryctocephalus indicus* (Reed, 1910) (Fig. 6(a)–(d)) has an intercontinental distribution and its first appearance has been acknowledged as one of the most favorable level for the GSSP defining the base of a global stage (e.g. Jell and Hughes, 1997; Yuan et al., 1997; Hughes and Jell, 1999; Sundberg et al., 1999, 2010, 2011, 2016; Geyer and Shergold, 2000; Korovnikov, 2001, 2006; Peng and Babcock, 2001; Shergold and Geyer, 2001, 2003; Zhao et al., 2001a, b, 2004, 2006, 2007, 2012a, b, c, 2014, 2017; Yuan et al., 2002; Peng, 2003; Sundberg and McCollum, 2003; Babcock et al., 2005, 2014; McCollum and Sundberg, 2005, 2007; Peng et al., 2006, 2012b; Geyer and Peel, 2011; Hughes, 2016; Singh et al., 2016; Esteve et al., 2017; Zhao et al., 2017). Besides South China, the species has been identified from northern India (Indian Himalaya) (Reed, 1910; Jell and Hughes, 1997; Peng et al., 2009b; Hughes, 2016; Singh et al., 2016), western USA (Sundberg and McCollum, 1997, 2003), North Greenland (Geyer and Peel, 2011), North Korea (Saito, 1934), and more possibly from Siberia (Korovnikov, 2001, 2006; Zhao et al., 2006; Fletcher, 2007; Shabanov et al., 2008; Hughes, 2016; Esteve et al., 2017).

Oryctocephalus indicus provides the best and most precise tool for intercontinental correlation in the lower part of Cambrian Series 3 (Zhao et al., 2001a, b, 2012a, b, c, 2014; Yuan et al., 2002; Sundberg et al., 2010, 2011, 2016; Geyer and Peel, 2011; Yuan and Ng, 2014; Hughes, 2016). Some widely distributed trilobites in the *O. indicus* Zone also provide fine tools for intercontinental correlation.

The primitive form of *Oryctocephalus indicus* makes its first appearance in the lower–middle part of the Kaili Formation in the Balang-Chuandong area, Jianhe County, Guizhou Province. Specimens of *O. indicus* with the primitive morphology possess only two pairs of marginal spines on the pygidium. These forms are succeeded and replaced by the advanced morphotype, characterized by three pairs of pygidial marginal spines (Yuan et al., 2002). The advanced form of *O. indicus* occurs in the *O. indicus* Zone of Nevada and California, USA (Sundberg and McCollum, 1997, p. 1075), and the interval of its occurrence can be correlated with the middle–upper part of the *O. indicus* Zone of South China. *Oryictocephalus americanus* from the *Amecephalus arrojosensis* Zone in Nevada, USA (Sundberg and McCollum, 2003), also shows the primitive feature of *O. indicus.* Specimens assigned to *O. americanus* lack connected transglabellar furrows (S2, S3), apparently as a result of taphonomic bias. Sundberg (personal communication, 2008) suggested that it gave rise to the advanced form of *O. indicus* but Zhao et al. (2006, 2007) and Esteve et al. (2017) preferred to regard it as a junior synonym of *O. indicus.* The FAD of *O. indicus* always succeeds the disappearance of *Olenellus* in Laurentia and *Redlichia* in the Indo-Pacific faunal province, allowing precise correlation among these levels in different faunal realms.

Stratigraphically, the first appearance of the primitive form of *Oryctocephalus indicus* at the Wuliu-Zengjiayan section lies 1.2 m above the LAD of the redlichiid trilobite *Bathynotus* and 0.2 m above the LAD of *Redlichia* (Sundberg et al., 2011). In the western United States, the first appearance of *O. indicus* (=*O. americanus*) succeeds

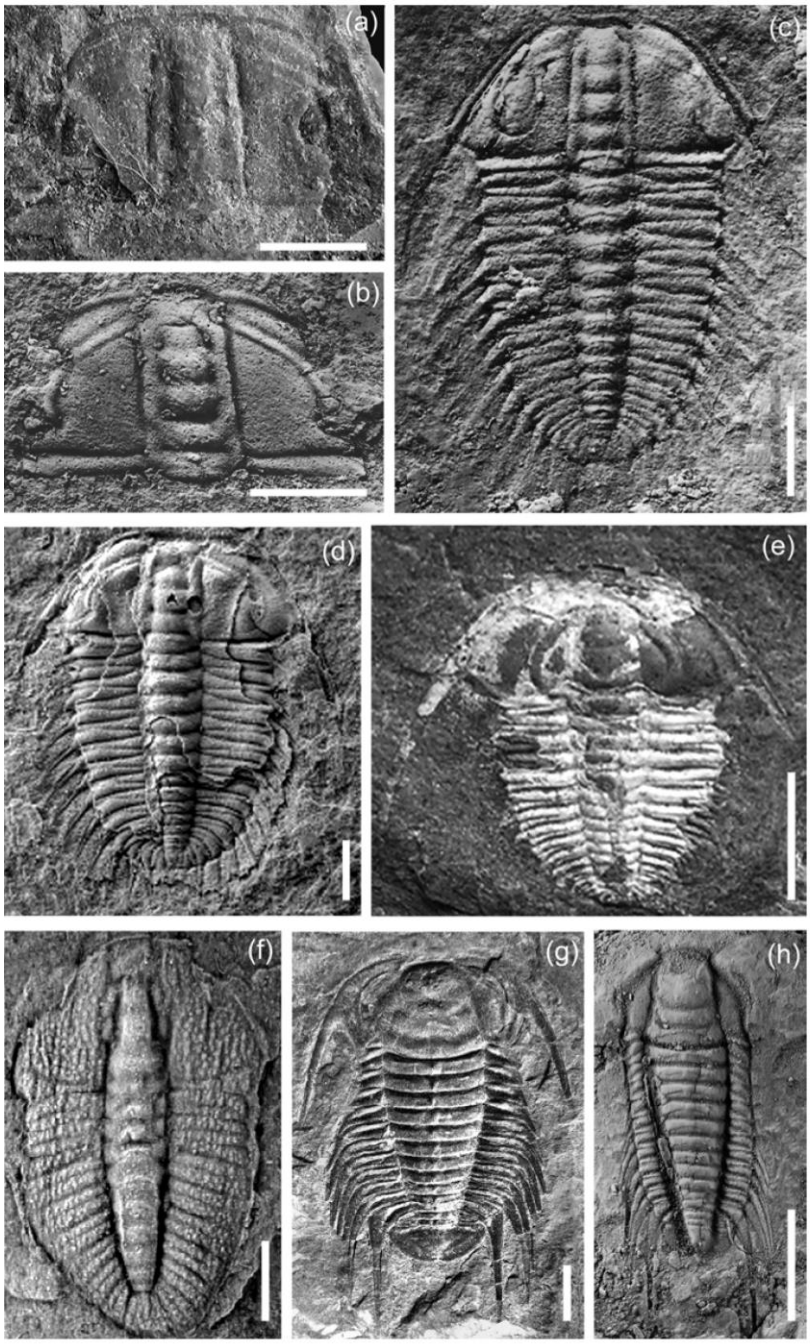

Figure 6. Key trilobite species used for recognition of the base of the Miaolingian Series and Wuliuan Stage. All specimens were collected from the Kaili Formation of the Wuliu-Zengjiayan section; all are dorsal views, collecting horizons are in meters above the base of the formation, (a)–(d)* Oryctocephalus indicus *(Reed, 1910). (a) cranidium, GTBB1-15-19a, 52.8 m (first appearance datum); (b) Cranidium, GTB17-5-119, 120.80 m; (c) Exoskeleton, GTB 20-5-1554, 135.70 m; (d) Exoskeleton, GTB 11-111, 56.70 m; (e)* Redlichia (R.) takooensis longispina *Guo and Zhao, 1998, exoskeleton, GTBB1-3-3, 49.4 m; (f)* Ovatoryctocara sinensis *Zhao, Yuan, Peng, Yang et Esteve, 2015, exoskeleton, GTBFZK-42, 51.8 m; (g)–(h),* Bathynotus kuichouensis *Lu in Wang et al., 1964. (g) Exoskeleton, GTB6-3-25, 25.9 m; (h) Exoskeleton, GTBB1-47-1, 40.6 m. Scale bars = 1 mm for figs. (a)–(b), 2 mm for figs. (c)–(f), 5 mm for figs. (g)–(h).

the disappearance of *Olenellus*. The combination of the FAD of *O. indicus*, the narrow stratigraphic range of *O. indicus,* the stratigraphically abrupt disappearance of redlichiids and olenellid trilobites, and evolutionary advances in oryctocephalids and ptychopariids allows the base of the Wuliuan Stage to be tightly constrained. *Bathynotus*, which occurs at the top of Cambrian Stage 4, is a guide fossil found in the western United States, Siberia, Australia and South China (Webster, 2009; Peng et al., 2014). Its distribution overlaps that of *Olenellus* and *Redlichia*, and this taxon has been treated as the most effective secondary tool for intercontinental correlation.

As discussed previously (Babcock et al., 2004, 2007; Peng et al., 2004b, 2006), the selection of a GSSP in open-shelf to slope deposits, and particularly in one from a low-latitude region such as the South China Platform, is desirable. Slope settings of the Cambrian favored a combination of cosmopolitan trilobites including agnostoids, oryctocephalids and polymerids, such as *Pagetia significans, Euarthricocephalus* and *Curvoryctocephalus* in the *Oryctocephalus indicus* Zone, *Bathynotus*, *Ovatoryctocara* and *Redlichia* in the *Bathynotus kueichouensis–Ovatoryctocara sinensis* Assemblage-Zone, and *Olenoides* and *Burlingia* in that zone and the *Oryctocephalus indicus* Zone as well. This combination of taxa enables a precise stratigraphic correlation into the Siberia, Greenland, and Laurentia (Geyer and Peel, 2011; Sundberg et al., 2016). In addition, based on the important trilobite taxa *Acadoparadoxides*, *Eccaparadoxides* and *Micmacca*, the base of the Wuliuan Stage can be correlated across the Mediterranean region (e.g., Morocco, Turkey and Spain) and also to Siberia and Australia (Liñán et al., 2004, 2008; Gozalo et al., 2007, 2011a, b; Geyer, 2016) although direct correlation of Mediterranean successions to other continents is difficult (Álvaro et al., 2003, 2013; Gozolo et al., 2007; Sundberg et al., 2010, 2016; Geyer and Peel, 2011; Zhao et al., 2012a). However, with the aid of Siberian taxa, the base of the Wuliuan Stage can be correlated, more or less confidently, with that of the Mediterranean region.

Stratotype Section and Point

The stratotype Wuliu-Zengjiayan section consists mainly of the Kaili Formation that rests conformably on the Tsinghsutung Formation and is overlain conformably by the Jia-

lao Formation (Figs. 4(a), 5, 7, 9). Both the Tsinghsutung and Jialao formations are of dolomite facies.

The Kaili Formation in the Wuliu-Zengjiayan section is a mostly monofacial succession of silty mudstone, mudstone, calcareous mudstone and shale with subordinate gray limestone-marlstone in the basal part and limestone in the uppermost parts of the formation (Zhao et al., 2001a, b; Gaines et al., 2011). Soft-sediment deformation, truncation surfaces, and slide surfaces are rare in the section and absent near the GSSP, suggesting deposition on a gentle slope. The interval of the FAD of *O. indicus* is inferred to be a maximum flooding stage of the major eustatic transgression (Zhu et al., 1999; Gaines et al., 2011; Fig. 7).

The Kaili Formation embraces three trilobite zones, including two polymerid zones and one agnostoid zone (Zhao et al., 2012a, c, 2015, 2017; Fig. 5), in ascending order: the *Bathynotus kueichouensis-Ovatoryctocra sinensis* Assemblage-Zone (4.0–52.8 m above the base of the Kaili Formation), the *Oryctcocephalus indicus* Zone (52.8–143.78 m above the base of the Kaili Formation), and the *Peronopsis taijiangensis* Zone (143.78–214.2 m above the base of the Kaili Formation). As mentioned above, the trilobite zonal succession of the Kaili Formation in the Wuliu-Zengjiayan section reveals a complete, tectonically undisturbed, marine succession.

Oryctocephalus indicus makes its first appearance at 52.8 m above the base of the Kaili Formation (Fig. 6(a)), a level defining the base of the Miaolingian Series and Wuliuan Stage (Zhao et al., 2001a, b, 2006, 2007, 2008, 2012a, 2014; Sundberg et al., 2010, 2011). This point in the Wuliu-Zengjiayan section demonstrates a major change in faunal assemblages with the extinction of redlichiids and *Bathynotus* and the appearance of several new ptychoparid taxa, although some oryctocephalid taxa exhibit ranges that cross this horizon (Fig. 5). Current stratigraphic resolution suggests that the FAD of *O. indicus* in

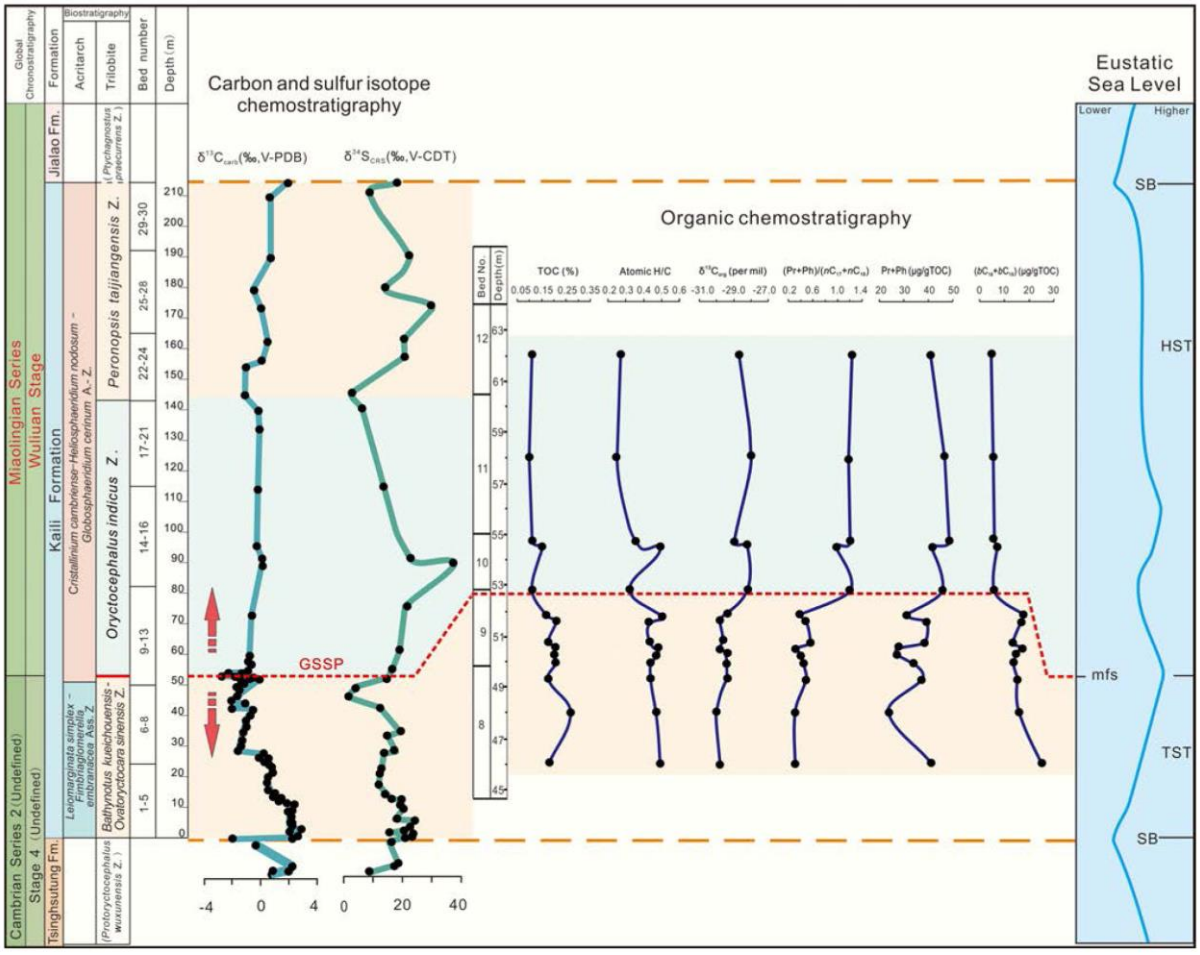

Figure 7. Summary of primary and secondary stratigraphic indicators for the base of the Miaolingian Series and Wuliuan Stage of the Cambrian System. Major stratigraphic tools used to constrain the GSSP of the series and stage are trilobite biostratigraphy (Zhao et al., 2007, 2012, 2015), acritarch biostratigraphy (Yin et al., 2010), carbon and sulfur isotope chemostratigraphy (Guo et al., 2010a, b, 2014), organic chemostratigraphy (Wang et al., 2014) and sequence stratigraphy (Gains et al., 2011). Abbreviations: TOC = total organic carbon content in rocks; atomic H/C = atomic hydrogen/carbon ratio; $d^{13}C_{org}$ data were measured on kerogen samples; Pr = pristane; Ph = phytane; nC_{17}, = normal C_{17}; nC_{18} = normal C_{18}; bC_{18} and bC_{19} = C_{18} and C_{19} midchain monomethyl branched alkanes, respectively, based on m/z 126+140+154+168+196+210+224 mass chromatograms; mfs = maximum flooding surface; SB = sequence boundary; HST = Highstand Systems Tract; TST = Transgressive Systems Tract.

the major Cambrian realms is equivalent in age. In the Wuliu-Zengjiayan section, *O. indicus* ranges across a 90.98 m interval, which is well fossiliferous, especially in its lower portion. The high-resolution data on distributions of trilobite taxa through the stratigraphic interval containing the GSSP in the Wuliu-Zengjiayan section are summarized in Fig. 5. In addition to *O. indicus*, a number of other guide fossils, which have utility for correlation on either an intercontinental or an interregional scale, help to constrain the position of the boundary. The major faunal changes below and above the FAD of *O. indicus* provide excellent data for global correlation of the boundary interval of the Wuliuan Stage. Among the key trilobite levels in the boundary interval, the LADs of *Ovatoryctocara sinensis* (48.8 m above the base of the Kaili Formation, Figs. 5, 6(f)) and *Bathynotus kueichouensis* (48.8 m above the base of the Kaili Formation, Figs. 5, 6(g–h)) can serve as secondary biostratigraphic correlation tools for identifying, with more or less precision, the base of the Miaolingian Series and the Wuliuan Stage (Zhao et al., 2001a, b, 2007, 2012c, 2014; Geyer, 2005; Fletcher, 2007; Peng et al., 2009; Sundberg et al., 2011).

The Wuliu-Zengjiayan section bears exceptionally preserved Burgess-type biota, termed the Kaili Biota. The biota occurs slightly above the FAD of *Oryctocephalus indicus*, containing representatives of at least 11 phyla that include algae, sponges, chancelloriids, cnidarians, "worms", lobopodia, medusiform fossils, brachiopods, molluscs, arthropods, echinoderms and various problematic fossils, of which some of the taxa are non-biomineralizing (Zhao et al., 2005, 2011; Fig. 8). This important biota can serve to constrain the position of the base of the Miaolingian Series and Wuliuan Stage at least in South China.

Besides trilobites and the exceptionally preserved taxa of the Kaili

Figure 8. Some metazoan taxa from the exceptionally preserved Kaili Biota in Balang Area, Jianhe, Guizhou. (a)* Angulosuspongia sinensis *Yang, Babcock et Peng, 2017 attached to* Glyptacrothele bohemica, *GTBM-9-2-1971; (b)* Haplophrentis *cf.* H. carinatus *Matthew, 1899, GTBM-9-3162; (c)* Acrothele *sp., GTBM-9-5365; (d) Palaeoscolecid, gen. et sp. indet., GTBM-9-1b; (e)* Ottoia guizhouensis *Yang, Zhao et Zhang, 2016, GTBM-9-4166; (f) Marrella sp., ventral view, GTBM-9-5-1075; (g)* Naraoia *cf.* N. compacta *Walcott, 1912, showing thin vessels in cephalic area, GTBM-9-3-5098; (h)* Sinoeocrinus lui *Zhao, Huang et Gong, 1994, GTB-9-5-3495; (i) Tuzoia bispinosa Yuan et Zhao, 1999, GM 9-5-1248; (j)* Pararotadiscus guizhouensis *Zhao and Zhu, 1994, GTBJ-13-3-220; (k)* Wiwaxia taijiangensis *Zhao, Qian et Li., 1994, with articulated specimen, GTBM-9-5-8888a. Scale bars equal 5 mm for (a), (b), (e), (g), (i); 10 mm for (h), (j) and 2 mm for others.

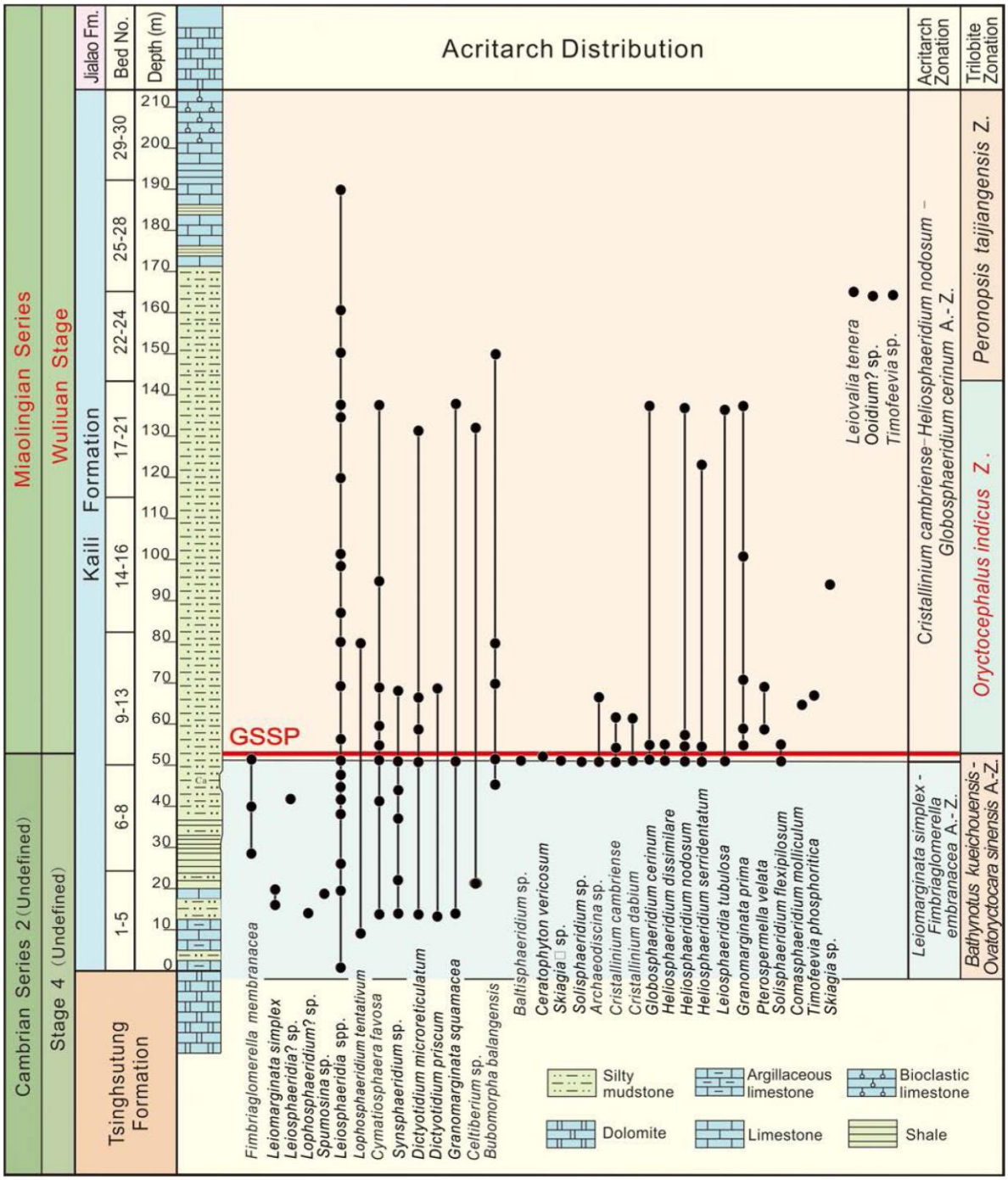

Figure 9. Observed stratigraphic distribution of acritarchs in the Kaili Formation of the Wuliu-Zengjiayan GSSP section (modified from Yin et al., 2010).

Biota, the acritarch assemblage from the Wuliu-Zengjiayan section shows a prominent change close to the FAD of *Oryctocephalus indicus* (Yin and Yang, 1999; Yang and Yin, 2001; Yin et al., 2009, 2010; Figs. 9, 10). The *Leiomarginata simplex-Fimbriaglomerella membranacea* assemblage (0–52 m above the base of the Kaili Formation) below the datum is clearly replaced by the *Cristallinium cambriense-Heliosphaeridium nodosum-Globosphaeridium cerinum* assemblage (52–140 m above the base of the Kaili Formation). This turnover in microfossil assemblages closely corresponds with the major change in trilobite assemblages (Yin and Yang, 1999; Yin et al., 2009). This

result has been confirmed by detailed, bed-by-bed sampling for palynomorphs across a 4 m interval bearing the FAD of *O. indicus* (50.8–54.8 m in Wuliu quarry, Fig. 4(b), (d)) (see Yin et al., 2010). Thus, the acritarch assemblages also help to constrain the base of the Miaolingian Series and Wuliuan Stage, and provide another fossil tool for correlating the boundary interval of South China to those of Baltica and Gondwana, in which the acritarch biostratigraphy has been reported in details (Volkova, 1990; Moczydłowska, 1998, 1999; Palacios, 2015; Moczydłowska and Yin, 2012).

Regional and Global Correlation

The FAD of *Oryctocephalus indicus* in the stratotype Wuliu-Zengjiayan section is one of the most easily recognizable horizons in the Cambrian (see Geyer and Shergold, 2000; Fig. 2). In South China, it is used for defining the base of the regional Wulingian Series and Taijiangian Stage (Peng et al., 2000; Peng and Babcock, 2001). Possible suitability of the FAD of this species for marking a global stage and series boundary has been summarized principally by Shergold and Geyer (2003), and Peng et al. (2004a, b, 2006). Key correlation tools are biostratigraphic ranges of polymerid trilobites, agnostoid trilobites, acritarchs; carbon isotopic ratios; sulfur isotopic ratios; and organic chemostratigraphy; and sequence stratigraphy.

Polymerid Trilobite Biostratigraphy

Two polymerid biozones are recognized in the lower-middle part of the Wuliu-Zengjiayan section (Zhao et al., 2001a, b, 2012a, c, 2015, 2017; Yuan et al., 2002), the lower *Bathynotus kueichouensis-Ovatoryctocara sinensis* Assemblage-Zone and the overlying *Oryctocephalus indicus* Zone (the lowermost zone of the Wuliuan Stage) with their boundary defined by the FAD of *O. indicus* (Figs. 4(a), 5). These two zones have been recognized in a number of sections of the Kaili Formation in eastern Guizhou, for example, the Miaobanpo (Zhao et al., 2001a, b, 2005, 2011), the Jianshan (Zhao et al., 2008), the Fujiachong (Zhao et al., 2012a), the Sanwan (Zhao et al., 2012b) and the Pingzhai (Yuan et al., 2002; Zhao et al., 2012a) sections. The level coinciding with FAD of *O. indicus* may correlate to the base of the Tianpeng Formation of platform facies in Mengzi County of Yunnan Province, South China (Zhao et al., 2014), the base of *Amecephalus arrojosensis* Zone of Emigrant Formation in Great Basin, USA, and occurs in the Parahio Formation, Spiti area, Indian Himalaya (see Singh et al., 2016; Hughes et al., 2018), and the corresponding level in northwestern Korea (Saito, 1934).

Although most of the polymerid trilobites from the biozones are endemic, a few of them provide, more or less, correlation tools of regional or intercontinental scale and allow tielines to be established into some other Cambrian faunal realms. Particularly useful guide fossils are the pandemic forms such as *Oryctocephalus indicus*, *Ovatoryctocara*, *Oryctocephalops*, *Oryctocephalites*, and *Burlingia* (Reed, 1910; Saito, 1934; Lermontova, 1940; Shergold, 1969; Lu et al., 1974; Zhang et al., 1980; Whittington, 1994; Jell and Hughes, 1997; Sundberg and McCollum, 1997, 2003; Yuan et al., 1997, 2002; Zhao et al., 2001a, b, 2006, 2012b, 2014; Sundberg et al., 2011, 2016; Geyer and Peel, 2011; Yuan and Esteve, 2015; Hughes, 2016; Singh et al., 2016; Esteve et al., 2017), the nektobenthic forms such as *Redlichia* and *Bathynotus* (Kobayashi, 1935; Lu, 1950; Lu and Chien, 1964; Öpik, 1970; Zhang et al., 1980; Whittington, 1988; Guo et al., 1999; Shergold and Whittington, 2000; Yuan et al., 2002; Kruse et al., 2004; Peng et al., 2009, 2014; Webster, 2009; Goryaeva et al., 2012; Hughes, 2016; Laurie, 2016), and the benthic trilobite *Olenoides* that has an intercontinental distribution (Yuan et al., 1997, 2002; Wang et al., 2016).

Agnostoid Trilobite Biostratigraphy

A single agnostoid biozone, the *Peronopsis taijiangensis* Zone, is recognized in the upper part of the Wuliu-Zengjiayan section (Yao et al., 2009), replacing the previous *Oryctocephalus orientalis* Zone of Yuan et al. (2002). It lies immediately above the *Oryctocephalus indicus* Zone (Fig. 5), and in eastern Guizhou and western Hunan it is overlain by the agnostoid *Ptychagnostus gibbus* Zone of the Huaqiao Formation (Peng, 2009, 2018). The *Peronopsis taijiangensis* Zone is correlatable with the *Ptychagnotus praecurrens* Zone of Laurentia, where the agnostoid *Ptychagnotus praecurrens* Zone, together with the overlying *Ptychagnotus gibbus* Zone, correlates with the upper half of the polymerid *Oryctocephalus* Zone (Robison and Babcock, 2011; Babcock et al., 2017). *Ptychagnotus praecurrens* is a widespread agnostoid trilobite, known from Sweden (Westergård, 1946; Weidner and Ebbestad, 2014; Ahlberg et al., 2019), England (Rushton, 1966), Russia (Siberia) (Egorova et al., 1976; Naimark, 2008; Shabanov et al.,2008), Australia (Laurie, 2004; Kruse et al., 2009), the USA (Utah and Nevada) (Robison, 1982; McCollum and Sundberg, 2007, Sundberg, 2011), and probably from Kazakhstan (Ergaliev and Ergaliev, 2008).

Although *Ptychagnotus praecurrens* has not been recorded in South China (likely due to facies restriction), strata corresponding to the *P. praecurrens* Zone are apparently present, i.e. the Aoxi Formation in northwestern Hunan, which is composed of grey to light grey, thin- to thick-bedded dolomites but straigraphically is overlain by the *P. gibbus*-bearing Huaqiao Formation (Peng and Robison, 2000). In the Wuliu-Zengjiayan section, the eodiscid trilobite *Pagetia significans* makes its first appearance slightly below the FAD of *O. indicus* (Sundberg et al., 2016; Fig. 5). *Pagetia significans* has been recorded from the Miaolingian strata of Australia (Jell, 1975), North Korea (Kobayashi, 1944), and Indian Himalaya (Jell and Hughes, 1997; Singh et al., 2016).

Acritarch Biostratigraphy

As phytoplanktic microfossils, Cambrian acritarchs are of significance to assist in delineating faunal zones, for indicating changes in the depositional environment, and even defining geological or biological events.

The taxonomic change in organic-walled microfossils (acritarchs) in the Wuliu-Zengjiayan section has been intensively studied (Yin et al., 2010). As discussed above, two acritarch assemblages, the *Leiomarginata simplex-Fimbriaglomerella membranacea* assemblage and the *Cristallinium cambriense-Heliosphaeridium nodosum-Globosphaeridium cerinum* assemblage are recognized below and above the GSSP respectively (Fig. 9). These acritarch assemblage zones are based on continuous sampling of the whole section, and more intensive sampling across a 4 m interval (50.8–54.8 m above the base of the Kaili Formation). Many acanthomorphic acritarch forms, such as *Helios-*

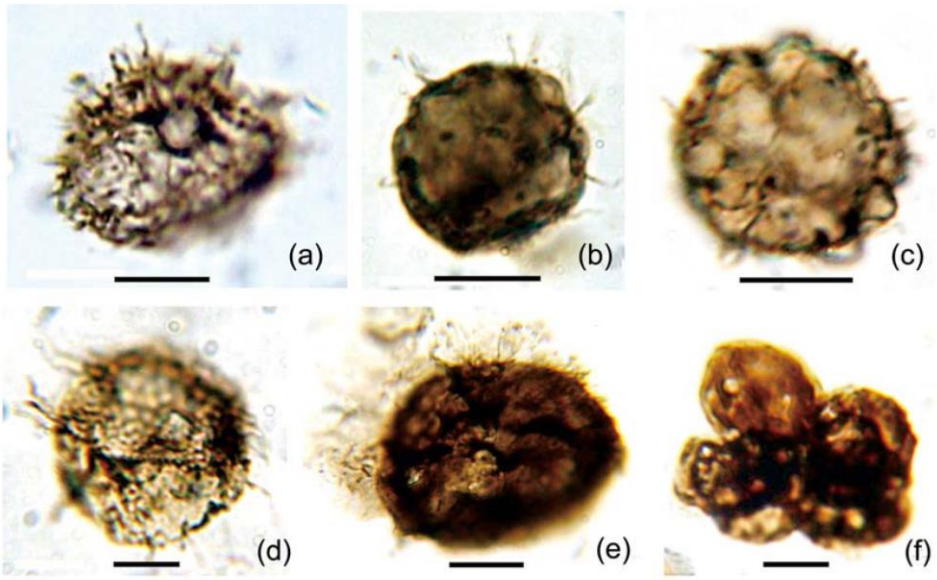

Figure 10. Acritarchs from the Kaili Formation of the Wuliu-Zengjiayan section. Sample numbers are prefixed with either FZX or K. (a)* Heliosphaeridium nodosum *Moczydłowska, 1998, FZX25; (b), (c)* Globosphaeridium cerinum *(Volkova) comb. Moczydłowska, 1991, FZX-25b, FZX24c; (d)* Solisphaeridium flexipilosum *(Slavicova) comb. Moczydłowska, 1998, FZX26; (e)* Comasphaeridium molliculum *Moczydłowska and Vidal, 1988, K69; (f)* Synsphaeridium *sp., K51. All scale bars equal 10 μm.

phaeridium dissimilare, H. nodosum, H. serridentatum, Globosphaeridium cerinum, and *Solisphaeridium flexipilosum* (Fig. 10), exhibit a first appearance at 52.3–52.7 m above the base of the Kaili Formation, which is slightly below the GSSP for the base of Miaolingian Series and Wuliuan Stage.

Heliosphaeridium nodosum, H. dissimilare, H. serridentatum, Globosphaeridium cerinum, *Solisphaeridium frixipilosum* also mark the base of the traditional middle Cambrian in Baltica, and Gondwana (Volkova, 1990; Moczydłowska,1998, 1999; Moczydłowska and Yin, 2012; Palacios, 2015). On the basis of the present record and existing data, it is noted that many species referred to *Heliosphaeridium* range from the provisional Cambrian Series 2 through the Miaolingian Series are even restricted to the Miaolingian Series. Therefore, certain species of *Heliosphaeeridium*, such as *H. dissimilare* and *H. serridentatum*, appear to characterize the Miaolingian Series.

More recently, acritarch assemblages and cryptospore-like microfossils have been obtained from stratigraphic successions spanning the *Oryctocephalus indicus* Zone in the Parahio Valley (Spiti), Indian Himalaya, and the Log Cabin Mine section, eastern Nevada, USA (Yin et al., 2013), showing the obvious change in acritarch taxonomy near the FAD of *Oryctocephalus indicus*. Such a change is significant and indicates an important geobiological event (Yin et al., 2016).

Carbon Isotope Chemostratigraphy

The carbon isotopic composition of carbonate rocks varies between –2.7 and +3.1‰ in the Wuliu-Zengjiayan section (Yang et al., 2003; Guo et al., 2005, 2010a, b). There is a stepwise decline from the base of the Kaili Formation towards the GSSP level, which is marked by peak negative values. Subsequently, there is a long relative stable interval with average seawater values between 0 and 1, and then the formation top (last sample) has a minor positive excursion. The base of the *Oryctocephalus indicus* Zone is marked by a distinctive peak of a rather long negative $\delta^{13}C_{carb}$ excursion with minimum values of –2.7‰ (Fig. 7). Thus, a distinct negative excursion in the carbon isotopic composition occurs from the *Bathynotus kueichouensis–Ovatoryctocara sinensis* Assemblage-Zone through the *O. indicus* Zone. This excursion, near the conterminous base of the Miaolingian Series and Wuliuan Stage, can also be recognized at the Jianshan section nearby (Guo et al., 2010a, b), at other localities on the Yangtze Platform, South China (Zhu et al., 2004), in Siberia (Shabanov et al., 2008), and North America (Montañez et al., 2000; Dilliard et al., 2007).

Sulfur Isotope Chemostratigraphy

The sulfur isotopic composition of sedimentary pyrite displays a similar variation across the provisional Cambrian Series 2 through the Miaolingian Series in the Wuliu-Zengjiayan section (Guo et al., 2014). A shift from $\delta^{34}S_{CRS}$ values around 1.3‰ to more positive values of 19.8‰ through the lower part of Kaili Formation. An excursion towards less ^{34}S enriched values is located slightly below the level of the Cambrian Series 2 to Cambrian Series 3 transition. There are two separate positive excursions in the middle and upper Kaili Formation, and an additional third one occurs at the formation top. The evolution towards more positive $\delta^{34}S$ values could reflect the development of closed system conditions in the early burial environment with respect to sulfate availability in the pore water realm. Comparably ^{34}S enriched pyrite sulfur isotope values and a somewhat similar variation across this stratigraphic transition have been observed in other sections of northwest Spain (Wotte et al., 2012), southern France (Wotte et al., 2012), the

Siberian Platform (Wotte et al., 2011), the USA (Wotte et al., 2011), and Mexico (Loyd et al., 2012).

Organic Chemostratigraphy

Organic geochemical investigations for the boundary interval of the Wuliu-Zengjiayan GSSP section (Bed 8–12) shows that all the geochemical proxies, such as TOC content, $\delta^{13}C_{org}$, atomic H/C value of kerogen, as well as biomarker parameters, co-vary across the section and change rather sharply across the boundary between the provisional Cambrian Series 2 and the Miaolingian Series at the top of Bed 9 (Wang et al., 2014; Fig. 7). For example, the relative abundance of isoprenoid hydrocarbons to *n*-alkanes (or the absolute concentration to TOC) shows an upward increase across the boundary with the $(Pr+Ph)/(nC_{17}+nC_{18})$ values ranging in 0.31–0.56 in the provisional Stage 4 sediments, as compared to 0.98–1.24 in the Wuliuan Stage. The $\delta^{13}C_{org}$ trend is also in accord with the abrupt change in $\delta^{13}C_{carb}$ across the boundary (Guo et al., 2010a, b; Fig. 7).

In general, changes observed are interpreted to reflect primary depositional values, notably variations in the composition of primary productivity and the marine redox condition (Wang et al., 2014). These, in turn, are linked to biological changes (i.e. trilobites and acritarchs respectively; Figs. 5, 6, 9, 10) and a possible regional and global anoxia–extinction event across the transition from the Series 2 to the Miaolingian Series. The extinction of multiple trilobite species at the end of Series 2 is probably related to global anoxia as evidenced by carbon and sulfur isotopes (Guo et al., 2010a, b, 2014; Fig. 7) and organic geochemical result (Wang et al., 2014). Evidently, the organic chemostratigraphic evidences also strongly support to place the base of the Miaolingian Series and Wuliuan Stage at this level.

Sequence Stratigraphy

Sea level changes corresponding to 3rd and 4th order depositional cycles (Fig. 7) caused migration of the adjacent Yangtze carbonate platform, the proximity of which controlled the amount of carbonate sediment delivered to the open-shelf to slope settings upon which the Kaili Formation was deposited. Initial Kaili deposition represents the onset of flooding on the slope. The lower portion of the Kaili Formation has been interpreted to represent a transgressive interval, with maximum flooding in the interval surrounding the GSSP at 52.8 m above the base of the formation (Gaines et al., 2011). The remaining thickness of the middle and upper Kaili Formation is interpreted as a highstand system tract with gradual shallowing and accompanying seaward progradation of the Yangtze carbonate platform, manifested an overall increase in the presence of thin, interbedded carbonates upsection toward the contact with the overlying mixed-siliciclastic carbonate Jialao Formation. The Kaili-Jialao succession has been interpreted to be a complete 3rd order depositional cycle, representing transgression, maximum flooding, and a protracted period of regression accompanied by basin filling (Wang et al., 2006).

Other Regional Reference Sections

For comparative purposes, the Jianshan and Sanwan sections in eastern Guizhou have been studied in detail (Zhao et al., 2008, 2012b). Both sections bear the FAD of *Oryctocephalus indicus* and also fulfill, more or less, the biostratigraphic requirements for a GSSP. Both sections are available with unrestricted access for research purposes. The Sanwan section appears to be a good auxiliary to the Wuliu-Zengjiayan GSSP section if it could receive intensive study in future. The Jianshan section is similar to the Wuliu-Zengjiayan section in litho- and bio-stratigraphic features, but it bears a small tectonic fold within the *O. indicus* Zone (at *ca*. 78.5 m above the base of the Kaili Formation) (Zhao et al., 2008).

Best Estimate of Age for the Base of the Proposed Miaolingian Series and Wuliuan Stage

The age for the base of Miaolingian Series and Wuliuan Stage is estimated at 509.1 ± 0.22 Ma. This age is based on an ash bed in the Upper Comley Sandstone of Shropshire, United Kingdom, which has given a weighted mean $^{206}Pb/^{238}U$ age of 509.02 ± 0.79 Ma on four (of six) single grain fractions (Harvey et al., 2011). This age was newly recalibrated to 509.1 ± 0.62 (with λ errors) by the Isotope Geology Laboratory of Boise State University, USA, as one of the high-resolution radiometric ages of zircon crystals determined by TIMS for the International Commission on Stratigraphy (Peng et al., 2012b; Schmitz, 2012). From immediately overlying beds, trilobites including *Paradoxides harlani* indicate the *P. harlani* Zone of Newfoundland, which is correlatable with the *Oryctocephalus indicus* Zone of South China and Laurentia (Geyer, 2005; Fletcher, 2007), and the base of the traditional 'Middle Cambrian' (St. David's Series) in Shropshire. The base of the traditional Middle Cambrian is estimated to be 510.0 ± 1.0 Ma, an age that is constrained by U-Pb zircon ages from an ash bed in the Hanford Brook Formation, southern New Brunswick (Bowring and Erwin, 1998; Landing et al., 1998). This age was recalibrated as 508.05 ± 2.5 Ma (Peng et al., 2012b; Schmitz, 2012). Although the age of the stratigraphically older New Brunswick ash bed conflicts with the above estimated age for the base of Wuliuan Stage (509.1 ±0.62 Ma), the conflict is easily accommodated within the error ranges for the two dates. Taken together, the two dates give a well-corroborated age for the base of the Miaolingian Series and Wuliuan Stage close to 509 Ma. Montañez et al. (2000) estimated an age of ~509 Ma for the base of the traditional Middle Cambrian of Laurentia, and this estimate is close to the age provided by ICS.

Acknowledgements

We thank the members of the Working Group on Cambrian Stage 5, International Subcommission on Cambrian Stratigraphy (ISCS), and the voting members of ISCS for providing constructive comments and suggestions that improved the original proposal largely. This work was supported in part by grants from the National Natural Science Foundation of China (49060010, 40372023, 41330101), the Ministry of Science and Technology of China (2006CB806401, 2013CB835002, 2015FY310100, 12002CC2600), the National Commission on Stratigraphy of China (95-Special Project-01-1-6, DD20160120-04), the State Key Laboratory on Palaeobiology and Stratigraphy (20191101),

and the Guizhou Bureau of Science and Technology (CGSCFG-2010-7001; Gui. Sci. Tal. [2017] 5788). Zhu Lijun and Yu Meiyi from the Guizhou University and Zhang Zhenghua from the Guizhou Command of Southwest Petroleum are thanked for taking part in earlier studies of the GSSP. We are grateful to Nigel C. Hughes (Riverside) and an anonymous reviewer for their constructive reviews. Special thanks are due to all master students from the College of Resource and Environment Engineering, Guizhou University, and to the local Balang villager Feng Liu and Zhefu Liu for their assistance with the field work. This is a contribution to the IGCP 668 project 'The stratigraphic and magmatic history of Early Paleozoic equatorial Gondwana and its associated evolutionary Dynamics.'

References

Ahlberg, P., Lundberg, F., Erlström, M., Calner, M., Lingskog, A., Dahlqvist, P., and Joachimski, M.M., 2019. Integrated Cambrian biostratigraphy and carbon isotope chemostratigraphy of the Grönhögen-2015 drill core, land, Sweden. Geological Magazine, v. 156(6): pp. 935–949.

Álvaro, J.J., Ahlberg, P., Babcock, L.E., Bordonaro, O.L., Choi, D.K., Cooper, R.A., Ergaliev, G.K., Gapp, I.W., Ghobadi Pour, M., Hughes, N.C., Jago, J.B., Korovnikov, I.V., Laurie, J.R., Lieberman, B.S., Paterson, J.R., Pegel, T.V., Popov, L.E., Rushton, A.W.A., Sukhov, S.S., Tortello, M.F., Zhou, Z.Y., and Żylińska, A., 2013. Global Cambrian trilobite palaeobiogeography assessed using parsimony analysis of endemicity. In: Harper, D.A.T., Servais, T. (Eds.), *Early Palaeozoic biogeography and palaeogeography*. Geological Society of London Memoirs, v. 38, pp. 273–296.

Álvaro, J.J., Elick, O., Geyer, G., Rushton, A.W.A., and Shergold, J.H., 2003. Palaeogeographical controls on the Cambrian trilobite immigration and evolutionary patterns reported in the western Gondwana margin. Palaeogeography, Palaeoclimatology, Palaeoecology, v. 195(1–2), pp. 5–35.

Astashkin, V.A., Pegel, T.V., Shabanov, Y.Y., Sukhov, S.S., Sundukov, V.M., Repina, L.N., Rozanov, A.Y., and Zhuravlev, A.Y., 1991. The Cambrian System on the Siberian Platform correlation chart and explanatory notes. International Union of Geological Science, Publication, v. 27, pp. 1–133.

Babcock, L.E., and Peng, S.C., 2007. Cambrian chronostratigraphy: current state and future plans. Palaeogeography, Palaeoclimatology, Palaeoecology, v. 254, pp. 62–66.

Babcock, L.E., Rees, M.N., Robison, R.A., Langenburg, E.S., and Peng, S.C., 2004. Potential Global Stratotype Section and Point (GSSP) for a Cambrian stage boundary defined by the first appearance of the trilobite *Ptychagnostus atavus*, Drum Mountains, Utah, USA. Geobios, v. 37(2), pp. 149–158.

Babcock, L. E., Peng, S. C., Geyer, G., and Shergold, J. H., 2005. Changing perspectives on Cambrian chronostratigraphy and progress toward subdivision of the Cambrian System. Geoscience Journal, v. 9, pp. 101–106.

Babcock, L.E., Robison, R.A., Rees, M.N., Peng, S.C., and Saltzman, M.R., 2007. The Global boundary Stratotype Section and Point (GSSP) of the Drumian Stage (Cambrian) in the Drum Mountains, Utah, USA. Episodes, v. 30 (2), pp. 85–95.

Babcock, L.E., Peng, S.C., Brett, C. E., Zhu, M.Y., Ahlberg, P., and Bevis, M., 2014. Evidence of global climatic and sea level cycles in the Cambrian, p. 9-11. In: Zhang, R.B. Huang B., 2014. IGCP Project 591 Field Workshop 2014, Extended Summery. Nanjing: Nanjing University Press, Nanjing, pp. 9–11.

Babcock, L.E., Peng, S.C., and Ahlberg, P. 2017: Cambrian trilobite biostratigraphy and its role in developing an integrated history of the Earth system. Lethaia, v. 50, pp. 381–399.

Bowring, S.A., and Erwin, D.H., 1998. A new look at evolutionary rates in deep time: uniting Paleontology and high-precision geochronology. GSA Today, v. 8, pp. 1–8.

Brasier, M.D., Cowie, J., Taylor, M., 1994. Decision on the Precambrian-Cambrian boundary stratotype. Episodes, v. 17(1), pp. 3–8.

Dilliard, K.A., Pope, M.C., Coniglio, M., Hasiotis, S.T., and Lieberman, B.S., 2007. Stable isotope geochemistry of the lower Cambrian Sekwi Formation, Northwest Territories, Canada: implications for ocean chemistry and secular curve generation. Palaeogeography Palaeoclimatology Palaeoecology, v. 256, pp. 174–194.

Egorova, L.I., Shabanov, Y.Y., Rozanov, A.Y., Savitzky, V.E., Tchernysheva, N.E., and Shishskin, B.B., 1976. Elanska and Kuonamka facies stratotypes of the lower boundary of the Middle Cambrian in Siberia. Trudy Sibirskiy Nauchno-issledovat'skiy Institut Geologiy, Geofiziki i Mineral'nogo Syr'ya (SNIIGGIMS), v. 211, pp. 1–168.

Ergaliev, G.Kh., and Ergaliev, F.G., 2008. Middle and Upper Cambrian Agnostida of the Aksai National Geological Reserve, South Kazakhstan (Kyrshabatky River, Malyi Karatau Range). Palaeontological Institute Almaty, Gylym, 359 p.

Esteve, J., Zhao, Y.L., and Peng, J., 2017. Morphological assessment of the Cambrian trilobites *Oryctocephalus indicus* (Reed 1910) from China and *Oryctocephalus* '*reticulatus*' (Lermontova 1940) from Siberia. Lethaia, v. 50, pp. 175–193.

Fletcher, T.P., 2007. The base of Cambrian Series 3: the global significance of key oryctocephalid trilobite ranges in the Kaili Formation of South China. Memoir of Association of Australasian Palaeontologists, v. 33, pp. 29–33.

Gaines, R.R., Mering, J.A. Zhao, Y.L., and Peng, J., 2011. Stratigraphic and microfacies analysis of the Kaili Formation, a candidate GSSP for the Cambrian Series 2–Series 3 boundary. Palaeogeography, Palaeoclimatology, Palaeoecology, v. 311(3–4), pp. 171–183.

Gehling, J.G., Jensen, S., Droser, M.L., Myrow, P.M., and Narbonne, G.M., 2001. Burrowing below the basal Cambrian GSSP, Fortune Head, Newfoundland. Geological Magazine, v, 138(2), pp. 213–218.

Geological Survey of Guizhou Province, 1966. Geological Map of Zhenyuan Sheet, 1:200,000. Guizhou Bureau of Geology, Guiyan.

Geyer, G., 2005. The base of a revised Middle Cambrian: are suitable concepts for a series boundary in reach? Geosciences Journal, v. 9, pp. 81–99.

Geyer, G., 2015. Exotic trilobites from the Lower-Middle Cambrian boundary interval in Morocco and their bearing on the Cambrian Series 3 lower boundary. Paläontologische Zeitschrift, v. 89(4), pp. 749–781.

Geyer, G., 2016. Taxonomy of the '*Micmacca*' group, new Cambrian Chengkouiidae (Trilobita) from Morocco, and their bearing on international correlation. In: Laurie, J.R., Percival, I.G., Jago,J.B., Paterson, J.R., and Brock, G.A. (Eds.), Cambro-Ordovician Studies VI. Australasian Palaeontological Memoir, v. 49, pp. 329–393.

Geyer, G., and Peel, S.J., 2011. The Henson Gletscher Formation of North Greenland and its bearing on the global Cambrian Series 2-Series 3 boundary. Bulletin of Geosciences, v. 86(3), pp. 465–534.

Geyer, G., and Shergold, J., 2000. The quest for internationally recognized divisions of Cambrian time. Episodes, v. 23, pp. 188–195.

Goryaeva, I.E., Pegel, T.V., Shabanov, Y.Y., and Bushuev, E.V., 2012. New data on stratigraphic range of trilobite *Bathynotus* genus in the Cambrian of the Siberian Platform. In: Zhao, Y.L., Zhu, M.Y., Peng, J., Gaines, R.R., and Parsley, R.L. (Eds.), Cryogenian-Ediacaran to Cambrian Stratigraphy and Paleontology of Guizhou, China. *Journal of Guizhou University (Natural Science)*, v. 29 (Supplement 1), p. 64.

Gozalo, R., Liñán, E., Dies Álvarez, M.E., Gámez Vintaned, J.A., and Mayoral, E., 2007. The Lower–Middle Cambrian boundary in the Mediterranean subprovince. In: Linnemann, U., Nance, R.D., Kraft, P., and Zulauf, G. (Eds.), The Evolution of the Rheic Ocean: From Avalonian-Cadomian Active Margin to Alleghenian-Variscan Collision. Geological Society of America Special Paper, v. 423, pp. 359–373.

Gozalo, R., Bautista, J., Chirivella Martorell, J.B., Esteve, J., and Liñán, E., 2011a. Correlation between the base of Drumian Stage and the base of middle Caesaraugustan Stage in the Iberian Chains (NE Spain). Bulletin of Geosciences, v. 86(3), pp. 545–554.

Gozalo, R., Liñán, E., and Chirivella Martorell, J.B., 2011b. The first record of *Dinesus* (Trilobita, Dinesidae) in the Cambrian of the Mediterranean region. Alcheringa, v. 35(1), pp. 1–9.

Guizhou Bureau of Geology and Mineral Resources, 1987. Regional Geology of Guizhou Province. People's Republic of China, Ministry of Geology and Mineral Resources, Geological Memoirs, Series 1, Number 7. Geological Publishing House, Beijing, 698 p.

Guo, Q.J. and Zhao, Y.L., 1998. The Discovery and Significance of Redlichia from the Lower part of Lower –middle Cambrian Kaili Formation. Joural of Guizhou University of Technology, v. 27(1), pp. 51-55.

Guo, Q.J., Zhao, Y.L., and Yuan, J.L., 1999. The restudy of *Redlichia* from the lower part of the Kaili Formation in Kaili area, Guizhou Province. Acta Palaeontologica Sinica, v. 38(Supplement), pp. 157–164.

Guo, Q.J., Strauss, H., Liu, C.Q., Zhao, Y.L., Pi, D.H., Fu, P.Q., Zhu, L.J., and Yang, R.D., 2005. Carbon and oxygen isotopic composition of Lower to Middle Cambrian sediments at Taijiang, Guizhou Province, China. Geological Magazine, v. 142(6), pp. 723–733.

Guo, Q.J., Strauss, H., Liu, C.Q., Zhao, Y.L., Yang, X.L., Peng, J., and Yang, H., 2010a. A negative carbon isotope excursion defines the transition from Cambrian Series 2 to Cambrian Series 3 on the Yangtze Platform, South China. Palaeogeography, Palaeoclimatology, Palaeoecology, v. 285, pp. 143–151.

Guo, Q.J., Strauss, H., Liu, C.Q., Zhao, Y.L., Yang, X.L., Peng, J., and Yang, H., 2010b. Corrigendum to "A negative carbon isotope excursion defines the boundary from Cambrian Series 2 to Cambrian Series 3 on the Yangtze Platform, South China" [*Palaeogeography, Palaeoclimatology, Palaeoecology*, 285, 143–151]. Palaeogeography, Palaeoclimatology, Palaeoecology, v. 288, p. 118.

Guo, Q.J., Strauss, H., Zhao, Y.L, Yang, X.L., Peng, J., Yang, Y.N., and Deng, Y.N., 2014. Reconstructing marine redox conditions for the transition between Cambrian Series 2 and Cambrian Series 3, Kaili area, Yangtze Platform: Evidence from biogenic sulfur and degree of pyritization. Palaeogeography, Palaeoclimatology, Palaeoecology, v. 398(2), pp. 144–153.

Harvey, T.H.P, Williams, M., Condon, D.J., Wilby, P.R., Siveter, D.J., Rushton, A.W.A., Leng, M.J., and Gabbott, S., 2011. A refined chronology for the Cambrian succession of southern Britain. Journal of the Geological Society, London, v. 168, pp. 705–716.

Hughes, N.C., 2016. The Cambrian palaeontological record of the Indian subcontinent. Earth-Science Reviews, v. 159, pp. 428–451.

Hughes, N.C., and Jell, P.A., 1999. The biostratigraphy and biogeography of Himalayan Cambrian trilobites. In: Macfarlane, A., Sorkhabi, and R.B., Quade, J. (Eds.), Himalaya and Tibet: Mountain Roots to Mountain Tops. Geological Society of America Special Paper, v. 328, pp. 109–116.

Hughes, N.C., Myrow, P., Peng, S.C., and Banerjee, D. M., 2018. The Parahio Formation of the Tethyan Himalaya: the type section, thickness, lithostratigraphy and biostratigraphy of the best characterised Cambrian succession in the Indian Subcontinent. Journal of the Palaeontological Society of India, v. 63(1), pp. 1-18.

Jell, P. A., 1975. Australian Middle Cambrian eodiscoids with a review of the superfamily. Palaeontographica Abteilung A, v. 150, pp. 1–97.

Jell, P.A., and Hughes, N.C., 1997. Himalayan Cambrian trilobites. Special Papers in Palaeontology, v. 58, pp. 1–113.

Kobayashi, T., 1935. The Cambro-Ordovician formations and faunas of South Chosen. Palaeontology. Part III. Cambrian faunas of South Chosen with special study on the Cambrian trilobite genera and families. Journal of the Faculty of Science, Imperial University of Tokyo, section 2, v. 4, pp. 49–344.

Kobayashi, T., 1944. On the eodiscids. Journal of the Faculty of Science, Tokyo University, section 2, v. 7, pp. 1–74.

Korovnikov, I.V., 2001. Lower and Middle Cambrian boundary and trilobites from northeast Siberia Platform. Palaeoworld, v. 13, pp. 270–275.

Korovnikov, I.V., 2006. Lower and Middle Cambrian boundary in open shelf facies of Siberian Platform. Palaeoworld, v. 15, pp. 424–430.

Kruse, P.D., Laurie, J.R., and Webby, B.D., 2004. Cambrian geology and palaeontology of the Ord Basin. Memoirs of the Association of Australasian Palaeontologists, v. 30, pp. 1–58.

Kruse, P.D., Jago, J.B., and Laurie, J.R., 2009. Recent developments in Australian Cambrian biostratigraphy. Journal of Stratigraphy, v. 33(1), pp. 35–47.

Landing, E., 1994. Precambrian-Cambrian boundary global stratotype ratified and a new perspective of Cambrian time. Geology, v. 22(2), pp. 179–182.

Landing, E., Bowring, S.A., Davidek, K.L., Westrop, S.R., Geyer, G., and Heldmaier, W., 1998. Duration of the Cambrian: U-Pb ages of the volcanic ashes from Avalon and Gondwana. *Canadian* Journal of Earth Sciences, v. 35, pp. 329–338.

Landing, E, Peng, S, Babcock, L.E. Geyer, G., and Moczydlowska-Vidal, M., 2007. Global standard names for the lowermost Cambrian series and stage. Episodes, v. 30, pp. 287–289.

Laurie, J.R., 2004. Early Middle Cambrian trilobite faunas from NTGS Elkedra 3 corechole southern Georgina Basin, Northern Territory. Cambrian-Ordovician Studies I. Memoir of the Association of Australasian Palaeontologists, v. 30, pp. 221–260.

Laurie, J.R., 2016. Whitehouse's *Redlichia* (Trilobita) specimens from the Georgina Basin, Western Queensland. Australasian Palaeontological Memoirs, v. 49, pp. 75–82.

Lermontova, E.V., 1940. Arthropoda, Class Trilobita. In: Vologdin, A,G. (Ed.), Atlas of the leading forms of the fossil faunas of the U.S.S.R., 1, Cambrian, Gosgeolizdat. Moscow-Leningrad, 112–157.

Liñán, E., Perejón, A., Gonzalo, R., Moreno-Eiris, E., and Oliveira, J.T. de., 2004. The Cambrian System in Iberia. Publicaciones del Instituto Geológico y Minero de España, Series Cuadernos del Museo Geominero, v. 3, pp. 1–63.

Liñán, E., Dies Alvarez, M.E., Gámez Vintaned, J.A., Zhuravlev, A.Yu., Gozalo, R., Bauluz, B., Subias, I., Zamora, S., Chirivella Martorell, J.B., Mayoral, E., Gursky, H.J., Esteve, J., and Andrés, J.A., 2008. Proposed Global Stratotype Section and boundary Point (GSSP) for Cambrian System stage 5 and series 3 in Murero (Spain). In: Voroninoy (Ed.), XIII International Field Conference of the Cambrian Stage Subdivision Working Group. The Siberian Platform, Western Yakutia. Sibirskiy Nauchno-issledovat'skiy Institut Geologiy, Geofiziki i Mineral'nogo Syr'ya (SNIIGGIMS), Novosibirsk, pp. 43–48.

Loyd, S.J., Marenco, P.J., Hagadorn, J.W., Lyons, T.W., Kaufman, A.J., Sourtovar, F., and Corsetti, F.A., 2012. Sustained low marine sulfate concentrations from the Neoproterozoic to the Cambrian: insights from carbonates of northwestern Mexico and eastern California. Earth Planetary Science Letter, v. 339–340(4), pp. 79–94.

Lu, Y.H., 1950. On the genus *Redlichia* with description of its new species. Geological Review, v. 15, pp. 157–169.

Lu, Y.H., and Chien, Y.Y., 1964. Cambrian trilobites. In: Institute of Geology and Palaeontology, Academia Sinica (Ed.), A Handbook of Index Fossils of South China. Science Press, Beijing, pp. 26–39.

Lu, Y.H., Chang (Zhang), W.T., Chien, Y.Y., Chu (Zhu), C.L., Lin, H.L., Zhou, Z.Y., Qian, Y., Zhang, S.G., and Wu, H.J., 1974. Cambrian trilobites. In: Nanjing Institute of Geology and Palaeontology, Academia Sinica (Ed.), Handbook of Stratigraphy and Palaeontology, Southwest China. Science Press, Beijing, pp. 82–107.

Matthew, G.F., 1899, Studies on Cambrian faunas, no. 3: Upper Cambrian fauna of Mt. Stephen, British Columbia. Transactions of the Royal Society of Canada, Series 2, v. 5, pp. 39–66.

McCollum, L.B., and Sundberg, F.A., 2005. The use of *Oryctocephalus indicus* as a "Lower-Middle" Cambrian boundary GSSP: A status report. Acta Micropalaeontological Sinica, v. 22, pp. 113–114.

McCollum, L.B., and Sundberg, F.A., 2007. Cambrian trilobite biozona-

tion of the Laurentian Delamaran Stage in the southern Great Basin, U.S.A.: Implications for global correlations and defining a Series 3 global boundary stratotype. Memoirs of the Association of Australasian Palaeontologists, v. 34, pp. 147–156.

Moczydłowska, M., 1991. Acritach biostratigraphy of Lower Cambrian and the Precambrian-Cambrian boundary in southeastern Poland. Fossils and Strata, v. 29, pp. 1–127.

Moczydłowska, M., 1998. Cambrian acritarchs from upper Silesia, Poland – biochnology and tectonic implications. Fossils and Strata, v. 46, pp. 1–121.

Moczydłowska, M., 1999. The Lower-Middle Cambrian boundary recognized by acritarchs in Baltica and at the margin of Gondwana. Bollettino della Società Paleontologica Italiana, v. 38, pp. 207–225.

Moczydłowska, M., and Vidal,G., 1988. Early Cambrian acritarchs from Scandinavia and Poland. Palynology, v. 12, pp. 1–10.

Moczydłowska, M., and Yin, L.M., 2012. Phytoplanktic microfossils record in the lower Cambrian and their contribution to stage chronostratigraphy. In: Zhao, Y.L., Zhu, M.Y., Peng, J., Gaines, R.R., and Parsley, R.L. (Eds.), Cryogenian-Ediacaran to Cambrian Stratigraphy and Paleontology of Guizhou, China. Journal of Guizhou University (Natural Science), v. 29 (Supplement 1), pp. 49–58.

Montañez, I.P., Osleger, D.A., Banner, J.L., Mack, L.E., and Musgrove, M., 2000. Evolution of the Sr and C isotope composition of Cambrian oceans. GSA Today, v. 10(5), pp. 1–7.

Naimark, E.B., 2008. Morphogenesis in the Genus *Peronopsis* Hawle et Corda, 1847. Paleontological Journal, v. 42(4), pp. 53–64.

Őpik, A.A., 1970. *Redlichia* of the Ordian (Cambrian) of Northern Australia and New South Wales. Bulletin of the Bureau of Mineral Resources of Australia, v. 114, pp. 1–66.

Palacios, T., 2015. Acritarch assemblages from the Oville and Barrios Formations, northern Spain: a pilot proposal of a middle Cambrian (Series 3) acritarch biozonation in northwestern Gondwana. Review of Palaeobotany and Palynology, v. 219(3), pp. 71–105.

Palmer, A.R., 1998. A proposed nomenclature for stages and series for the Cambrian of Laurentia. Canadian Journal of Earth Sciences, v. 35, pp. 323–328.

Palmer, A.R., and Repina, L.N., 1993. Through a glass darkly: taxonomy, phylogeny and biostratigraphy of the Olenellina. The University of Kansas Palaeontological Contribuition, New Series, v. 3, pp. 1–35.

Peng, J., Zhao, Y.L., Yuan, J.L., Yao, L., and Yang, H., 2009. *Bathynotus*: A key trilobite taxon for global stratigraphic boundary correlation between Cambrian Series 2 and Series 3. Progress in Natural Science, v. 19(1), pp. 99–105.

Peng, J., Yuan, J.L. Zhao, Y.L., Sun, H.J., Yang, X.L., and Yang, Y. N., 2014. The trilobite *Bathynotus* from the Cambrian Series 2 of China and its implications for global correlation. GFF, v. 136(1), pp. 203–207.

Peng, S.C., 2003. Chronostratigraphic subdivision of the Cambrian of China. Geologica Acta, v. 1(1), pp. 135–144.

Peng, S.C., 2004. Suggested global subdivision of Cambrian System and two potential GSSPs in Hunan, China for defining Cambrian stages. In: Choi, D.K. (Ed.), Korea 2004, Ninth International Conference of the Cambrian Stage Subdivision Working Group, Abstracts with program. The Paleontological Society of Korea, Taebaek, p. 25.

Peng, S.C., 2006. A new global framework with four series for Cambrian System. Journal of Stratigraphy, v. 30(2), pp. 147–148.

Peng, S.C., 2009. The newly developed Cambrian biostratigraphic succession and chronostratigraphic scheme for South China. *Chinese Science Bulletin* (English Edition), v. 54, pp. 4161-4179.

Peng, S.C., 2018. Cambrian. In: National Committee on Stratigraphy of China (Ed.), Explanation of the Stratigrapgic Chart of China (2014). Geological Press, Beijing, pp. 73-100.

Peng, S.C., and Babcock, L.E., 2001. Cambrian of the Hunan-Guizhou region, South China. Palaeoworld, v. 13, pp. 3–51.

Peng, S.C., and Robison, R.A., 2000. Agnostoid biostratigraphy across the Middle-Upper Cambrian boundary in China. Journal of Paleontology, v. 74, Memoir 53, pp. 1–104.

Peng, S.C., Yuan, J.L, and Zhao, Y.L., 2000. Taijiangian Stage: a new chronostratigraphical unit for the traditional Lower Middle Cambrian in South China. Journal of Stratigraphy, v. 24(1), pp. 53–54.

Peng, S.C., Babcock, L.E., Robison, R.A., Lin, H.L., Rees, M.N., and Saltzman, M.R., 2004a. Global Standard Stratotype-section and Point (GSSP) of the Furongian Series and Paibian Stage (Cambrian). Lethaia, v. 37(4), pp. 365–379.

Peng, S.C., Zhu, X.J., Babcock, L.E., and Wang, H.F., 2004b. Potential Global Stratotype Sections and Points in China for defining Cambrian stages and series. Geobios, v. 37(2), pp. 253–258.

Peng, S.C., Babcock, L.E., Geyer, G., and Moczydłowska, M., 2006. Nomenclature of Cambrian epochs and series based on GSSPs – Comments on an alternative proposal by Rowland and Hicks. Episodes, v. 29(2), pp. 130–132.

Peng, S.C., Babcock, L.E., Zuo, J.X., Lin, H.L., Zhu, X.J., Yang, X.F., Robison, R.A., Qi, Y.P., Bagnoli, G., and Chen, Y.A., 2009a**.** The Global boundary Stratotype Section and Point of the Guzhangian Stage (Cambrian) in the Wuling Mountains, northwestern Hunan, China. Episodes, v. 32(1), pp. 41–55.

Peng, S.C., Hughes, N.C., Heim, N.A., Sell, B. B., Zhu, X.J., Myrow, P.M., and Parcha, S.K., 2009b. Cambrian trilobites from the Parahio and Zanskar Valleys, Indian Himalaya. Lawrence (U.S.A.). Journal of Paleontology, Memoir 71, pp. 1–95**.**

Peng, S.C., Babcock, L E., Zuo, J.X., Lin, H.L., Zhou, C.M., Yang, X.F., Qi, Y.P., Bagnoli, G., Wang, L.W. 2012a. Global Standard Stratotype-section and Point (GSSP) for the base of the Jiangshanian Stage (Cambrian: Furongian) at Duibian, Jiangshan, Zhejiang, Southeast China. Episodes, v. 35(4), pp. 462–477.

Peng, S.C., Babcock, L.E., and Cooper, R.A., 2012b: The Cambrian Period. In: Gradstein, F.M., Ogg, J.G., Schmitz, M.D. and Ogg, G.M. (Eds.), The Geologic Time Scale 2012. Volume 2, Elsevier BV, Amsterdam, pp. 437-488.

Peng, S.C., Babcock, L.E., Zhu, X.J., Lei, Q.P., and Dai, T., 2017. Revision of the oryctocephalid trilobite genera *Arthricocephalus* Bergeron and *Oryctocarella* Tomashpolskaya and Karpinski (Cambrian) from South China and Siberia. Journal of Paleontology, v. 91(5), pp. 933–959

Pu, X.C., and Ye, H.Z., 1991. Cambrian sedimentary facies and palaeogeography framework in southern China. Collected Papers of Lithofacies and Paleogeography, v. 6, pp. 1–16.

Reed, F.A., 1910. The Cambrian fossils of Spiti. Memoirs of Geological Survey of India, Palaeontologia India, v. 15, pp. 1–70.

Remane, J., Bassett, M.G., Cowie, J.W., Gohrbandt, K.H., Lane, H.R., Michelsen, O., and Wang, N.W., 1996. Revised guidelines for the establishment of global chronostratigraphic standards by the International Commission on Stratigraphy (ICS). Episodes, v. 19(3), pp. 77–81.

Robison, R.A., 1982. Some Middle Cambrian agnostoid trilobites from western North America. Journal of Paleontology, v. 56(1), pp. 132–160.

Robison, R.A. and Babcock, L.E., 2011. Systematics, paleobiology, and taphonomy of some exceptionally preserved trilobites from Cambrian Lagerstätten of Utah. Paleontological Contributions, v. 5, pp.1–47.

Rushton, A.W.A., 1966. The Cambrian trilobites from the Purley Shales of Warwickshire. Monograph of Palaeontographical Society of London, v. 120(511), pp. 1–55.

Saito, K., 1934. Older Cambrian trilobite and conchostraca from northwestern Korea. *Japanese* Journal of Geology and Geography, v. 11, pp. 211–237.

Schmitz, M. D., 2012. Radiogenic isotopes geochronology. In: Gradstein, F. M, Ogg, J. G., and Schmith, M. D., and Ogg, G. M. (Eds.), The Geologic Time Scale 2012, Elsevier BV, Amsterdam, pp. 115–126.

Shabanov, Yu.Ya., Korovnikov, I.V., Pereladov, V.S., and Fefelov, A.F., 2008. Excursion 1a. The traditional Lower-Middle Cambrian boundary in the Kuonamka Formation of the Molodo River section (the southeastern slope of the Olenek Uplift of the Siberian Platform) proposed as a candidate for GSSP of the lower boundary of the Middle Cambrian and

its basal (Molodian) stage, defined by the FAD of *Ovatoryctocara granulata*. In: Rozanov, A.Yu, and Varlamoov, A.I. (Eds.), The Cambrian System of the Siberian Platform. Part 2: North-East of the Siberian Platform, XIII International Field Conference of the Cambrian Stage Subdivision Working Group. PIN, RAS, Moscow and Novosibirsk, pp. 8-59.

Shergold, J.H., 1969. Oryctocephalidae (Trilobita: Middle Cambrian) of Australia. *Bulletin of the* Bureau of Mineral Resources of Australia, v. 104, pp. 1–66.

Shergold, J.H., and Geyer, G., 2001. The International Subcommission on Cambrian Stratigraphy: progress report. *A*cta Palaeontoloica Sinica, v. 40, pp. 1–3.

Shergold, J.H. and Geyer, G. 2003. Newsletter 2003. International Subcommission of Cambrian Stratigraphy) International Subcommission on Cambrian Stratigraphy, Würzburg, 12 p.

Shergold, J.H., and Whittington, H.B., 2000. The Cambrian trilobite *Bathynotus* (?Redlichioidea) in the northern Territory, Australia. Alcheringa, v. 24(1–2), pp. 1–10.

Singh, B.P., Virmani, N., Bhargava, O.N., Negia, R.S., Kishore, N., and Gill, A., 2016. Trilobite fauna of basal Cambrian Series 3 (Stage 5) from the Parahio Valley (Spiti), Northwest Himalaya, India and its biostratigraphic significance. Annales de Paléontologie, v. 102(1), pp. 59–67.

Sundberg, F.A., 2011. Delamaran biostratigraphy and lithostratigraphy of southern Nevada. In: Hollingsworth, J.S., Sundberg, F.A. and Foster, J.R. (Eds.), Cambrian stratigraphy and Paleontology of Northern Arizona and Southern Nevada. International Subcommission on Cambrian Stratigraphy. Museum of Northern Arizona Bulletin, v. 67. pp. 174–185.

Sundberg, F.A., and McCollum, L.B., 1997. Oryctocephalids (Corynexochida: Trilobita) of the Lower–Middle Cambrian boundary interval from California and Nevada. Journal of Palaeontology, v. 71(6), pp. 1065–1090.

Sundberg, F.A., and McCollum, L.B., 2003. Early and Middle Cambrian trilobites from the outer-shelf deposits of Nevada and California, USA. Palaeontology, v. 46, pp. 945–986.

Sundberg, F.A., Yuan, J.L., McCollum, L.B., and Zhao, Y.L., 1999. Correlation of Lower-Middle Cambrian boundary of South China and Western United States of America. *Acta Palaeontoloica Sinica,* v. 38 (supplement), pp. 102–107.

Sundberg, F.A., Zhao, Y.L., Yuan, J.L., and Lin, J.P., 2010. Summary of recent quarrying across the proposed GSSP for Stage 5 (Cambrian) at the Wuliu-Zengjiayan section, Guizhou, China. Journal of Stratigraphy, v. 34(2), pp. 289–292.

Sundberg, F.A., Zhao, Y.L., Yuan, J.L., and Lin, J.P., 2011. Detailed trilobite biostratigraphy across the proposed GSSP for Stage 5 ("Middle Cambrian" boundary) at the Wuliu-Zengjiayan section, Guizhou, China. Bulletin of Geosciences, v. 86(3), pp. 423–464.

Sundberg, F.A., Geyer, G., Kruse, P.D., McCollum, L.B., Pegel, T.V., Zylińska, A., and Zhuralev, A.Yu., 2016. International correlation of the Cambrian Series 2–3, Stage 4–5 boundary interval. Memoirs of the Association of Australasian Palaeontologists, v. 49, pp. 83–125.

Tchernysheva, N.Ye., 1962. Cambrian trilobites of the Family Oryctocephalidae. In: Shvedov, N.A. (Ed.), Problems of oil and gas occurrence in the Soviet Arctic, Palaeontology and Biostratigraphy. 3. Trudy Nauchno-Issledovatelskogo Instituta Geologii Arktiki, v. 127, pp. 3-52.

Volkova, N.A., 1990. Middle and Upper Cambrian acritarchs in the East European Platform. Trudy Akademia Nauk SSSR, Geologicheskii Institut, v. 454, pp. 1–116.

Walcott, C.D., 1912. Cambrian geology and paleontology II;Middle Cambrian Branchiopode, Malocrastraca, Trilobita, and Merostomata. Smithsonian Miscellaneous Collections, v. 57, pp. 145–228.

Wang, C.J., Zhao, Y.L., Peng, J., Yang, X.L., Bai, J., Liu, Y., and Chen, T., 2014. Biomarker evidence for biotic and environmental change across the Cambrian Series 2–Series 3 boundary at the Wuliu-Zengjiayan section, Guizhou, China. Science China: Earth Science, v. 57(11), pp. 2781–2790.

Wang, M.K., Zhao, Y.L., Luo, X.C., and Chen, W.Y., 2016. *Olenoides* Meek, 1877 from the "Tsinghsutung Formation" at Balang, Jianhe County, Guizhou Province. Geological Journal of China Universities, v. 22(3), pp. 486–493. (in Chinese with English abstract).

Wang, Y. (Ed.), 1964. Handbook of index fossils of South China. Science Press, Beijing, 173 p.

Wang, Y., Yu, Y.Y., Peng, J., and Wang, P.L., 2006. Discussion on the sequence stratigraphy and sea-level changes of the Kaili Formation at Balang, Jianhe, Guizhou. Journal of Stratigraphy, v. 30(1), pp. 34–42.

Webster, M., 2009. Systematic revision of the Cambrian trilobite *Bathynotus* Hall, 1860, with documentation of new occurrences in western Laurentia and implications for intercontinental biostratigraphic correlation. Memoirs of the Association of Australasian Palaeontologists, v. 37, pp. 369–406.

Weidner, T., and Ebbestad, J.O., 2014. The early Middle Cambrian agnostid *Pentagnostus praecurrens* (Westergård, 1936) from Sweden. Memoirs of the Association of Australasian Palaeontologists, v. 45, pp. 403–419.

Westergård, A.H., 1946. Agnostidea of the Middle Cambrian of Sweden. Sveriges Geologiska Undersökning, Series *C*, v. 477, pp. 1–140.

Whittington, H.B., 1988. Hypostomes and ventral cephalic sutures in Cambrian trilobites. Palaeontology, v. 31(3), pp. 577–609.

Whittington, H.B., 1994. Burlingiids: Small proparian Cambrian trilobites of enigmatic origin. Palaeontology, v. 37, pp. 1–16.

Whittington, H.B., 1995. Oryctocephalid trilobites from the Cambrian of North America. Palaeontology, v. 38, pp. 543–562.

Wotte, T., Strauss, H., and Sundberg, F.A., 2011. Carbon and sulfur isotopes from the Cambrian Series 2–Cambrian Series 3 of Laurentia and Siberia. In: Hollingsworth, J.S., Sundberg, F.A. and Foster, J.R. (Eds.), Cambrian stratigraphy and Paleontology of Northern Arizona and Southern Nevada. International Subcommission on Cambrian Stratigraphy. Museum of Northern Arizona Bulletin, v. 67. pp. 43.

Wotte, T., Strauss, H., Fugmann, A., and Garbe-Schönberg, D., 2012. Paired $\delta^{34}S$ data from carbonate-associated sulfate and chromium-reducible sulfur across the traditional Lower–Middle Cambrian boundary of W-Gondwana. Geochimica et Cosmochimica Acta, v. 85, pp. 228–253.

Yang, R.D., and Yin, L.M., 2001. Acritarch assemblages from the Early–Middle Cambrian Kaili Formation of East Guizhou Province and biostratigraphic implication. Acta Micropalaeontologica Sinica, v. 18, pp. 55–69.

Yang, R.D., Zhu, L.J., and Wang, S.J., 2003. Negative carbon isotopic excursion on the Lower/Middle Cambrian boundary of Kaili Formation, Taijiang County, Guizhou Province, China: Implications for mass extinction and stratigraphic division and correlation. *S*cience in China (Series D), v. 46(9), pp. 872–881.

Yang, X.L., Zhao, Y.L., Babcock, L.E., and Peng, J., 2017. Siliceous spicules in a vauxiid sponge (Demospongia) from the Kaili Biota (Cambrian Stage 5), Guizhou, South China. Scientific Reports, v. 7, 42945, DOI: 10.1038/srep42945.

Yang, Y.N., Zhao, Y.L., and Zhang, X.L., 2016. Fossil priapulid *Ottoia* from the Kaili biota (Cambrian Series 3) of South China. Journal of Systematic Palaeontology, v. 14 (6), pp. 527–543.

Yao, L., Peng, J, Fu, X.P. and Zhao, Y.L., 2009. Ontogenesisof tuzoia bispinosa (arthropoda) from the Middle Cambrian Kaili Biota, Guizhou, China. Acta Palaeontoloica Sinica, v. 48(1), pp. 56–64.

Yin, G.Z., 1987. Cambrian. In: Bureau of Guizhou Geology and Mineral Resources (Ed.), Regional Geology of Guizhou Province. PRC Ministry of Geology and Mineral Resources: Geological Memories series 1, v. 7, Geological Publishing Press, Beijing, pp. 49–96.

Yin, L.M., and Yang, R.D., 1999. Early-Middle Cambrian acritarchs in the Kaili Formation from Taijiang County, Guizhou, China. Acta Palaeontologica Sinica, v. 38 (Supplement), pp. 66–78.

Yin, L.M., Zhao, Y.L., Yang, R.D., and Peng, J., 2010. Acritarchs from the Early–Middle Cambrian Kaili Formation in the Wuliu-Zengjiaya Section, east Guizhou Province, China. Acta Palaeontoloica Sinica, v. 49(2), pp. 164–173.

Yin, L.M., Yang, R.D., Peng, J., and Kong, F.F., 2009. New data regarding acritarch biostratigraphy from the Early–Middle Cambrian Kaili For-

mation in Chuandong, Guizhou Province, China. Progress in Natural Science, v. 19(1), pp. 107–114.

Yin, L.M., Zhao, Y.L., Bian, L.Z., and Peng, J., 2013. Comparison between cryptospores from the Cambrian Log Cabin Member, Pioche Shale, Nevada, USA and similar specimens from the Cambrian Kaili Formation, Guizhou, China. Science China, v. 56(5), pp. 703–709.

Yin, L.M., Wang, C.J., Zhao, Y.L., and Ou, Z.J., 2016. Early-Middle Cambrian palynomorph microfossils and related geochemical events in South China. Journal of Earth Sciences, v. 27(2), pp. 180–186.

Yuan, J.L., and Esteve, J., 2015. The earliest species of *Burlingia* Walcott, 1908 (Trilobta) from South China – biostratigraphical and palaeogeographical significance. Geological Magazine, v. 152(2), pp. 358–366.

Yuan, J.L., and Ng, T.W., 2014. Tentative correlation of the Duyunian (Cambrian Series 2, Stage 4) and the Taijiangian (Cambrian Series 3, Stage 5) between South China and the Mediterranean region. GFF, v. 136(1), pp. 314–319.

Yuan, J.L and Zhao, Y.L., 1999. *Tuzoia* (bivalved arthropods) from the lower- middle Cambrian Kaili Formation of Taijiang, Guizhou. Acta Palaeontologica Sinica. v. 38(Supplement), pp. 88–94

Yuan, J.L., Zhao, Y.L., Wang, Z.Z., Zhou, Z.Y., and Cheng, X.Y., 1997. A preliminary study on Lower-Middle Cambrian boundary and trilobite fauna at Balang, Taijiang, Guizhou, South China. Acta Palaeontologica. Sinica, v. 36(4), pp. 494–524.

Yuan, J.L., Zhao, Y.L., and Guo, Q.J., 1999. On the Kaili Formation. Acta Palaeontologica Sinica, v. 38 (supplement), pp. 15–27.

Yuan, J.L., Zhao, Y.L., Li, Y., and Huang, Y.Z., 2002. Trilobite Fauna of the Kaili Formation (uppermost Lower Cambrian–lower Middle Cambrian) from southeastern Guizhou, South China. Shanghai Science and Technology Press, Shanghai, 423 p.

Zhang, W.T., Lu, Y.H., Zhu, Z.L., Qian, Y.Y., Lin, H.L., Zhou, Z.Y., and Yuan, J.L., 1980. Cambrian trilobite faunas of southwestern China. Palaeontologica Sinica, Series B, 159. Science Press, Beijing, 497 p.

Zhang, Z.H., Shen, J.W., Gong, X.Y., Zhao, Y.L., Mao, J.R., and Yan, C.H., 1996. A preliminary discussion on preservation condition of Kaili Fauna, Middle Cambrian, Taijiang, Guizhou. Acta Palaeontologica Sinica. v. 35(5), pp. 607–622.

Zhao, Y.L. and Zhu, M.Y., 1994. Medusiform fossils of Kaili Fauna from-Taijing, Guizhou. Acta Palaeontology Sinica, v. 33(3), pp. 272–280.

Zhao, Y.L., Huang, Y.Z., and Gong, X.Y., 1994. Echinoderm fossils of Kaili fauna from Taijiang, Guizhou. Acta Palaeontologica Sinica, v. 33(3), pp. 305–324.

Zhao, Y.L., Qian, Y., and Li X.S., 1994. *Wiwaxia* from Early–Middle Cambrian Kaili Formation in Taijiang, Guizhou. Acta Palaeontologica Sinica, v. 33(3), pp. 359–366.

Zhou, Z.Y., Yuan, J.L., Zhang, Z.H., Wu, X.R., and Yin, G.Z., 1980. Division and correlation of Cambrian stratigraphy in Guizhou Province, China. Journal of Stratigraphy, v. 4(4), pp. 273–281.

Zhao, Y.L., Yang, R.D., Yuan, J.L., Zhu, M.Y., Guo, Q.J., Yang, X.L., and Tai, T.S., 2001a. Cambrian stratigraphy at Balang, Guizhou Province, China: Candidate section for a global unnamed series and stratotype section for the Taijiangian Stage. Palaeoworld, v. 13, pp. 189–208.

Zhao, Y.L., Yuan, J.L., and McCollum, L.B., 2001b. A potential GSSP for the Lower and Middle Cambrian boundary near Balang Village, Taijiang County, Guizhou Province, China. Acta Paleontologica Sinica, v. 40, pp. 130–142

Zhao, Y.L., Yuan, J.L., Peng, S.C., Guo, Q.J., Zhu, L.J., Peng, J., and Wang, P.L., 2004. Proposal and prospects for the global Lower-Middle Cambrian boundary. Progress in Natural Science, v. 14(12), pp. 1034–1039.

Zhao, Y.L., Zhu, M.Y., Babcock, L.E., Yuan, J.L., Parsely, R.L., Peng, J., Yang, X.L., and Wang, Y., 2005. Kaili Biota: A taphonomic window on diversification of metazoans from the basal Middle Cambrian: Guizhou, China. Acta Geologica Sinica, v. 79(6), pp. 751–765

Zhao, Y.L., Yuan, J.L., Peng, S.C., Yang, X.L., Peng, J., Lin, J.P., and Guo, Q.J., 2006. A restudy of *Oryctocephalus indicus* (Reed, 1910). Progress in Natural Science, v. 16(11), pp. 1177–1182.

Zhao, Y.L., Yuan, J.L., Peng, S.C., Babcock, L.E., Peng, J., Lin, J.P., Guo, Q.J., and Wang,Y.X., 2007. New data on the Wuliu-Zengjiayan section (Balang, South China), GSSP candidate for the base of Cambrian Series 3. Memoirs of the Association of Australasian Palaeontologists, v. 33, pp. 57–65.

Zhao, Y.L., Yuan, J.L., Peng, S.C., Babcock, L.E., Peng, J., Guo, Q.J., Lin, J.P., Tai, T.S., Yang, R.D., and Wang, Y.X., 2008. A new section of Kaili Formation (Cambrian) and a biostratigraphic study of the boundary interval across the undefined Cambrian Series 2 and Series 3 at Jianshan, Chuandong Village, Jianhe County, China with a discussion of global correlation based on the first appearance datum of *Oryctocephalus indicus* (Reed, 1910). Progress in Natural Science, v. 18, pp. 1549–1556.

Zhao, Y.L., Zhu, M.Y., Babcock, L.E., and Peng, J., (eds.). 2011. The Kaili Biota—Marine organisms from 508 million years ago. Guiyang, Guizhou Science and Technology Press, 247 p.

Zhao, Y.L., Peng, J., Yuan, J.L., Babcock, L.E, Guo, Q.J., Yin, L.M., Yang, X.L., Tai, T.S., Wang, C.J., Lin, J.P., Gaines, R.R, Sun, H.J., and Yang, Y.N., 2012a. Discussion on the Global Standard Stratotype Section and Point (GSSP) for defining the conterminous base of Cambrian provisional Series 3 and Stage 5. In: Zhao, Y.L., Zhu, M.Y., Peng, J., Gaines, R.R., and Parsley, R.L. (Eds.), Cryogenian-Ediacaran to Cambrian Stratigraphy and Paleontology of Guizhou, China. Journal of Guizhou University (Natural Science), v. 29 (Supplement 1), pp. 35-48.

Zhao, Y.L., Yang, Y.N., Peng, J., Yuan, J.L., Sun, H.J., Yan, X., and Zhang, P.X., 2012b. The Kaili Formation and Kaili Biota at the Sanwan Section in Guizhou Province, China and boundary between Cambrian Series 2/Series 3. In: Zhao, Y.L., Zhu, M.Y., Peng, J., Gaines, R.R., and Parsley, R.L. (Eds.), Cryogenian–Ediacaran to Cambrian Stratigraphy and Paleontology of Guizhou, China. Journal of Guizhou University (Natural Science), 29 (Supplement 1), 77–88.

Zhao, Y.L., Peng, J., Yuan, J.L., Guo, Q.J., Tai, T.S., Yin, L.M., Parsley, R.L., Yang, Y.N., Yang, X.L., and Zhang, P.X. 2012c. The Kaili Formation and Kaili Biota at the Wuliu-Zengjiayan Section of Guizhou Province, China and proposed Global Standard Stratotype section and Point (GSSP) of the unnamed Cambrian Series 3, Stage 5. In: Zhao, Y.L., Zhu, M.Y., Peng, J., Gaines, R.R., and Parsley, R.L. (Eds.), Cryogenian-Ediacaran to Cambrian Stratigraphy and Paleontology of Guizhou, China. Journal of Guizhou University (Natural Science), 29(Supplement 1), 108–124.

Zhao, Y.L., Yuan, J.L., Guo, Q.J., Peng, J., Yin, L.M., Yang, X.L., Wang, C.J., and Sun, H.J., 2014. Comments on some important issues concerning the establishment of a GSSP for Cambrian Stage 5. GFF, v. 136(1), pp. 333–336.

Zhao, Y.L., Yuan, J.L., Peng, J., Yang, X.L., and Esteve, J., 2015. Restudy of *Ovatoryctocara* Tchernysheva, 1962 from the Kaili Formation, Jianhe County, Guizhou, South China. Annales de Paléontologie, v. 101(3), pp. 193–198.

Zhao, Y.L., Yuan, J.L., Esteve, J., and Peng, J., 2017. The oryctocephalid trilobite zonation across the Cambrian Series 2–Series 3 boundary at Balang, South China: a reappraisal. Lethaia, v. 50, pp. 400–406.

Zhu, M.Y., Erdtmann, B.D., and Zhao, Y.L., 1999. Taphonomy and paleoecology of the early Middle Cambrian Kaili Lagerstätte in Guizhou, China. Acta Palaeontologica Sinica, v. 38 (Supplement 1), pp. 28–57.

Zhu, M.Y., Zhang, J.M., Li, G.X., and Yang, A.H., 2004. Evolution of C isotopes in the Cambrian of China: implications for Cambrian subdivision and trilobite mass extinctions. Geobios, v. 37(2), pp. 287–301.

Zhao Yuanlong is a Professor at Guizhou Research Center of Palaeontology and College of Resources and Environment Engineering, Guizhou University. He has been working on Cambrian trilobites, chronostratigraphy of Cambrian Series 3 and Stage 5, and early metazoan paleobiology since 1961. As one of primary researchers, he found the Cambrian soft-bodied Kaili Biota with his colleagues. Currently he focuses his research mainly on defining provisional Cambrian Stage 4, and the taxonomy and biostratigraphy of oryctocephalid trilobites.

Jinliang Yuan is a Research Professor at the Nanjing Institute of Geology and Palaeontology, Chinese Academy of Sciences. He has been working on Cambrian biostratigraphy and trilobites, and Devonian, Carboniferous, and Permian trilobites since 1975. Recently he focuses on his research on Cambrian boundaries between Series 2 and the Miaolingian Series in South China and between Miaolingian and Furongian Series in North China, and on biostratigraphy and phylogeny of Cambrian oryctocephalid trilobites.

Loren E. Babcock is a Professor in the School of Earth Sciences at the Ohio State University, Columbus, Ohio, USA. His research interests are centered around trilobite paleobiology, taphonomy, and stratigraphy. In recent years, Babcock has focused attention on development of a global chronostratigraphic subdivision of the Cambrian System. He is currently Chairman of the International Subcommission on Cambrian Stratigraphy from 2012.

Xinglian Yang is a Professor at the Research Center of Palaeontology and College of Resource and Environment Engineering at Guizhou University, Guiyang, Guizhou, China. She has been working on Cambrian Stratigraphy and Palaeontology since 1999. Her research interests are mainly focused on early metazoan paleobiology and Cambrian stratigraphy, especially on the Cambrian sponges and chronostratigraphy of the boundary interval of Cambrian provisional Series 2 and Miaolingian Series in South China.

Journal of Paleontology, page 1 of 10

0022-3360/15/0088-0906
doi: 10.1017/jpa.2018.41

JOURNAL OF PALEONTOLOGY
A PUBLICATION OF THE Paleontological SOCIETY

Paleoecological Significance of Complex Fossil Associations of the Eldonioid *Pararotadiscus guizhouensis* with other Faunal Members of the Kaili Biota (Stage 5, Cambrian, South China)

Yuanlong Zhao,[1] Mingkun Wang,[1] Steven T. LoDuca,[2] Xinglian Yang,[1] Yuning Yang,[1] Yujuan Liu,[1] and Xin Cheng[3]

[1]College of Resource and Environmental Engineering, Guizhou University, Guiyang, Guizhou 550025, China ⟨zhaoyuanlong@126.com⟩, ⟨mkwang1986@163.com⟩, ⟨yangxinglian2002@163.com⟩, ⟨ynyang333@163.com⟩, ⟨liuyujuan0102@163.com⟩
[2]Department of Geography and Geology, Eastern Michigan University, Ypsilanti, Michigan, 48197, USA ⟨sloduca@emich.edu⟩
[3]Institute of Vertebrate Paleontology and Paleoanthropology, China Academy of Sciences, Beijing 100044, China ⟨cheng_xin1982@126.com⟩

Abstract.—The planktonic medusiform taxon *Pararotadiscus guizhouensis* (Zhao and Zhu, 1994) is one of the most abundant components of the Kaili Biota. Many specimens are in direct association with other taxa, including trilobites, brachiopods, hyolithids, echinoderms, and algae, as well as the trace fossil *Gordia*. Four types of interrelationships between *P. guizhouensis* and associated fossils are recognized: symbiosis, co-burial, attachment of benthic taxa on *P. guizhouensis* carcasses, and scavenging of *P. guizhouensis* carcasses. These associations of *P. guizhouensis* within the Kaili Biota are unique among occurrences of medusiform fossils in Burgess Shale-type biotas worldwide and provide important insights concerning ecological complexity in the Kaili Biota and in Cambrian marine communities in general.

Introduction

Many important Cambrian Burgess Shale-type biotas have yielded the problematic medusiform fossils collectively referred to as eldonioids. Described taxa include *Eldonia eumorpha* Sun and Hou, 1987 and *Rotadiscus grandis* Sun and Hou, 1987 from the Chengjiang Biota of Yunnan Province, South China (Sun and Hou, 1987; Chen et al., 1996; Chen and Zhou, 1997; Hou et al., 1999, 2003; Zhu et al., 2002; Chen, 2004; Zhu, 2010); *Eldonia ludwigi* Walcott, 1911 from the Burgess Shale, Spence Shale, and Marjum biotas of western North America (Walcott, 1911; Conway Morris and Robison, 1986, 1988; Briggs et al., 1994; Caron and Jackson, 2008); *Eldonia* sp. from the Sinsk Biota of Siberia (Ivantsov et al., 2005); and *Pararotadiscus guizhouensis* (Zhao and Zhu, 1994) from the Kaili Biota of Guizhou Province, South China (Zhao and Zhu, 1994; Dzik et al., 1997; Zhu et al., 1999; Zhu et al., 2002; Cheng et al., 2009). All of the aforementioned eldonioids are characterized by a disc-shaped body with radial canals and concentric structures, a large alimentary canal, and well-developed tentacles. Specimens are typically preserved as carbonaceous compressions in mudstones, in some cases accompanied by molds of the disc (Gaines et al., 2008). Most researchers have considered eldonioids to have had a planktonic mode of life (Sun and Hou, 1987; Zhao and Zhu, 1994; Zhu et al., 2002; Yang et al., 2007; Chen et al., 1995, 1996; Cheng et al., 2009), although others have interpreted them as benthic (Dzik et al., 1997) or nekto-benthic (Wang et al., 2004, 2009).

Some eldonioids from Burgess Shale-type biotas are preserved with other taxa. For example, the brachiopod *Linguella chengjiangensis* Jin, Hou, and Wang, 1993 and the lobopods *Microdictyon sinicum* Chen, Hou, and Lu, 1989 and *Paucipodia inermis* Chen, Zhou, and Ramsköld, 1995 are found on the discs of *Eldonia eumorpha* in the Chengjiang Biota (Chen and Zhou, 1997). In addition, the hyolithid *Haplophrentis reesei* Conway Morris and Robison, 1988 and the echinoderm *Ctenocystis utahensis* Robison and Sprinkle, 1969 are found on the discs of *Eldonia ludwigi* in the Spence Shale Biota (Conway Morris and Robison, 1986, 1988), and trace fossils are associated with an eldonioid in the Emu Bay Shale of South Australia (Schroeder et al., 2018). Here, we examine the paleoecological significance of taxa associated with specimens of *Pararotadiscus guizhouensis* from the Cambrian Kaili Biota in Guizhou, South China (Zhao and Zhu, 1994; Dzik et al., 1997; Zhu et al., 2002; Cheng et al., 2009).

Research material and preservation

Pararotadiscus guizhouensis is very abundant in the Kaili Biota at the lowermost Cambrian Stage 5 (ca. 509 million year old) and is the only species of medusiform fossil known from the Kaili Formation (Zhao et al., 2011). This organism is found throughout the stratigraphic interval that bears the Kaili Biota, as well as in other horizons in the middle to upper part of the Kaili Formation at the Miaobanpo and the adjacent Wuliu-Zengjiayan (26°44.843' N, 108°24.830' E) sections at Balang village, Jianhe County, Guizhou Province, South China (Figs. 1, 2) (Zhao and Zhu, 1994; Zhu et al., 2002; Cheng et al., 2009; Zhao et al., 2011, 2012). The present study examined 628

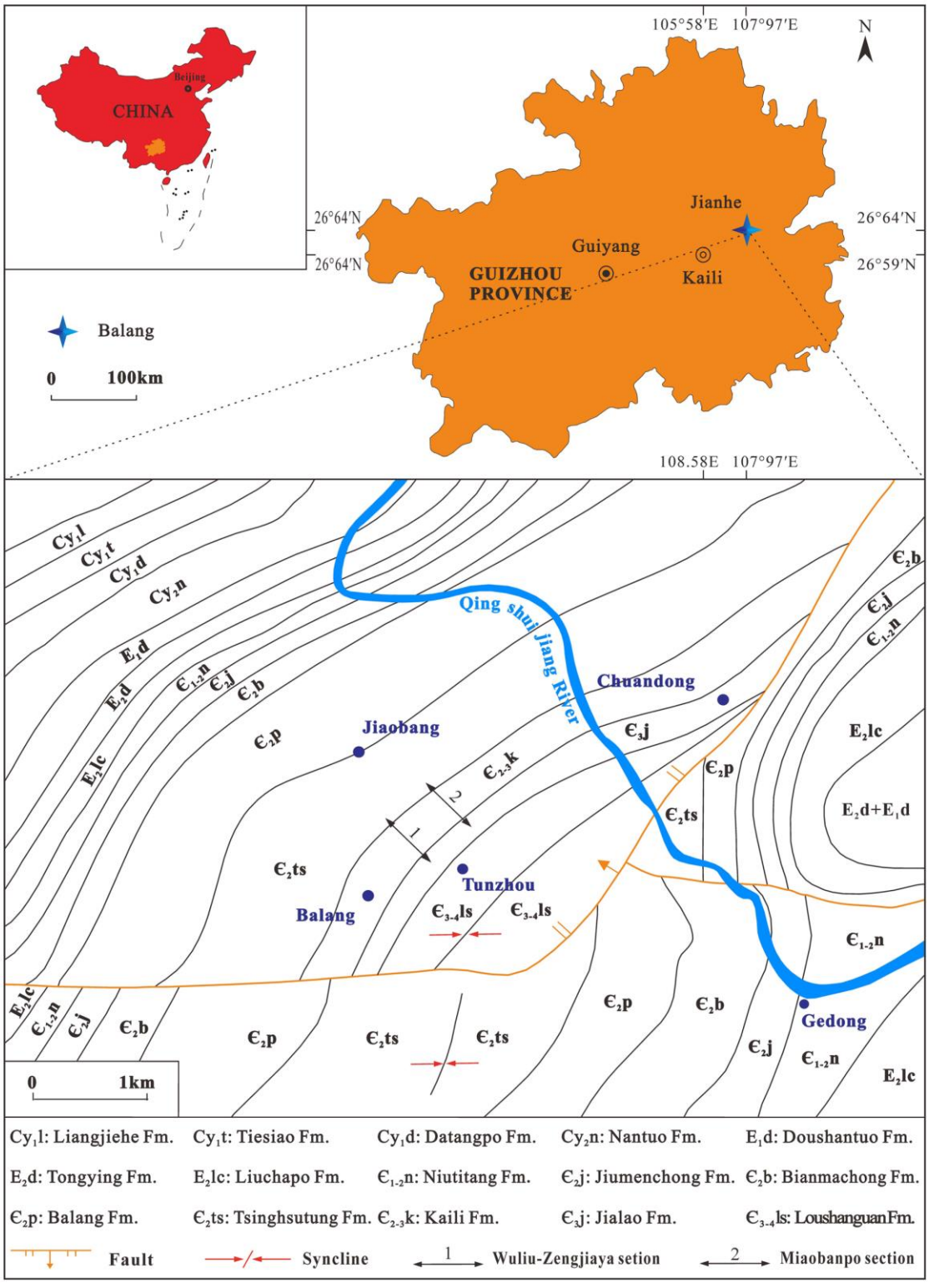

Figure 1. Geological map showing the locations of the Mianbanpo and Wuliu-Zengjiayan sections at Balang, Guizhou Province, China.

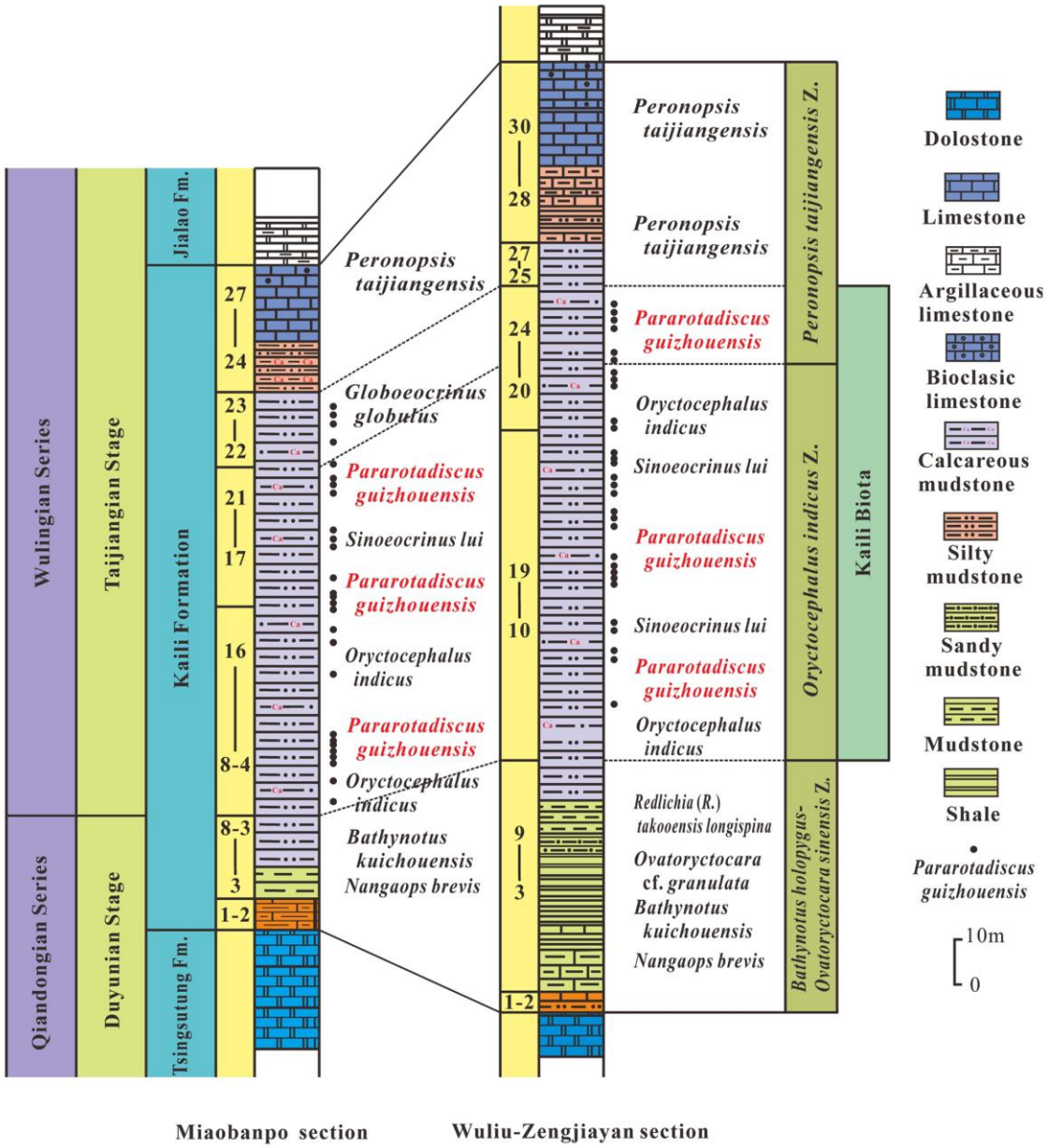

Figure 2. Stratigraphic columns of the Kaili Formation at the Miaobanpo and Zengjiayan sections at Balang, Guizhou Province, China, showing the stratigraphic distribution of *Pararotadiscus guizhouensis*.

specimens (with associated taxa) from the Kaili Formation at the Miaobanpo and Wuliu-Zengjiayan localities. The formation in the study area shows conformable contacts with the overlying Jialao Formation and the underlying Tsinghsutung Formation (Fig. 2).

Almost all specimens of *P. guizhouensis* in the Kaili Biota are preserved as composite molds of the upper and lower portion of the disc, with organic preservation of the alimentary canal evident in many specimens (Zhu et al., 1999, 2002; Gaines et al., 2008; Cheng et al., 2009) (Fig. 3). The disc is divided into four zones from the center to the edge: a central ring, an inner ring, a middle ring, and an outer ring (Zhao and Zhu, 1994) (Fig. 4). Ventral and dorsal portions of the disc are difficult to distinguish from each other. Although numerous specimens exhibit obvious plastic deformation resulting from

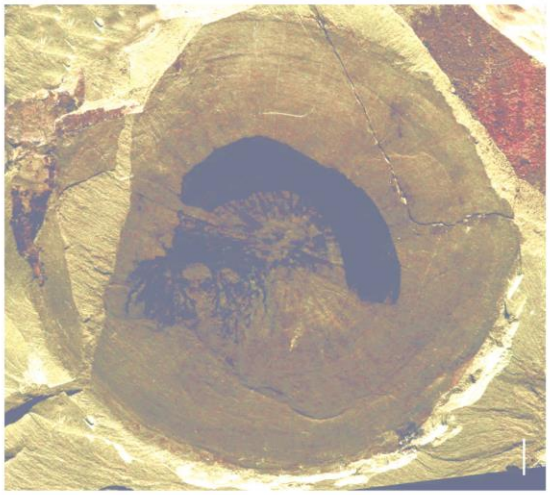

Figure 3. *Pararotadiscus guizhouensis* with alimentary canal and tentacles from the Kaili Biota at the Jinyinshan section, Guizhou Province, China (GTBJ-12-3-22b). Scale bar = 10 mm.

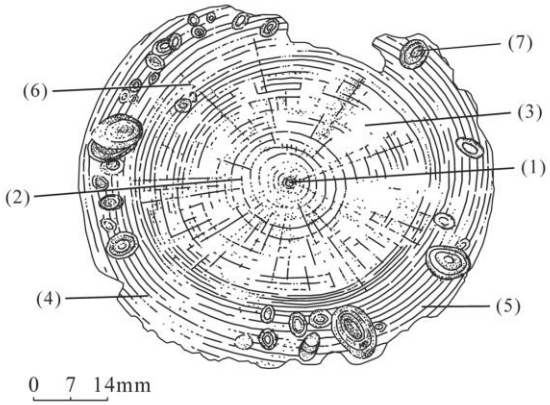

Figure 4. Line drawing of a *Pararotadiscus guizhouensis* specimen showing key features and associated brachiopods (GTB-23-3-103a). Abbreviations as follows: (**1**) central ring; (**2**) inner ring; (**3**) middle ring; (**4**) outer ring; (**5**) concentric ring and ridge; (**6**) radial canal; (**7**) associated brachiopods.

compaction, folding of discs is rare, indicating that the disc of *P. guizhouensis* was probably softer than that of *Rotadiscus grandis* (Zhu et al., 2002). Specimens of *P. guizhouensis* range from 15–155 mm in diameter, with most having a diameter of 40–70 mm; the mean diameter is 55 mm (Zhu et al., 2002).

Repository and institutional abbreviation.—All study specimens are deposited at Guizhou University. Specimen numbers with the GTB prefix are from the Wuliu-Zengjiayan section, and those with the GTBM prefix are from the Miaobanpo section.

Relationships between *Pararotadiscus guizhouensis* and associated taxa

More than 2,500 specimens of *P. guizhouensis* have been collected from the Kaili Biota, of which ~40% are closely associated with other fossils, including trilobites, brachiopods, echinoderms, *Wiwaxia*, algae, and the trace fossil *Gordia marina* (Emmons, 1844). Detailed quantitative data for the 628 specimens with associated taxa examined in the present study are provided in Table 1. Four types of relationships between *P. guizhouensis* and associated fossils are recognized herein: symbiosis, co-burial, attachment of benthic taxa on *P. guizhouensis* carcasses, and scavenging of *P. guizhouensis* carcasses (Table 2). Each relationship is described in detail below.

Table 1. Quantitative data for associations between *Pararotadiscus guizhouensis* and other taxa in the Kaili Biota at Balang village, Guizhou Province, China.

Associated taxa	Number of P. guizhouensis specimens that show association
Complete brachiopods	128
Complete *Pagetia* trilobites	82
Complete juvenile eocrinoids	5
Complete adult eocrinoids	11
Disarticulated trilobites	190
Other fragmentary material	74
Gordia marina traces	138
Total	**628**

Table 2. Four types of relationships between *Pararotadiscus guizhouensis* and associated organisms.

Symbiosis	Benthic fixation	Co-burial	Scavenging
Other living animal taxa with *P. guizhouensis* (commensal)	Other living benthic animal taxa on the carcass of *P. guizhouensis*	Co-burial with *P. guizhouensis* and other taxa	Marine trace *Gordia* made by scavenging the carcass of *P. guizhouensis*, with remains of *P. guizhouensis*

Symbiosis.—Animals including brachiopods, *Pagetia* (trilobite), individual juvenile gogiids, and edrioasteroids (echinoderms) engaged in commensalism and mutualism with *Pararotadiscus guizhouensis*. As noted in a previous study (Zhu et al., 1999), a brachiopod of uncertain affinity, initially interpreted as the bradoriid ostracode *Chuandianella*? *subovata* (Yuan and Huang, 1994), appears to have had a commensal relationship with *P. guizhouensis*. The valves of this small brachiopod are elongate and oval in shape; one end is rounded and appears to be the anterior, the other end is subtriangular (Zhu et al., 1999, pl. 3, fig. D). Commonly, large numbers of these brachiopods are densely distributed on the outer ring of *P. guizhouensis*, each with the long axis oriented perpendicular to the adjacent portion of the rim and the apparent anterior end placed closest to the perimeter (Figs. 4, 5.5, 5.6). This distinctive arrangement suggests that the brachiopods were attached to live specimens of *P. guizhouensis* and benefitted from this relationship by gaining access to currents at a level well above

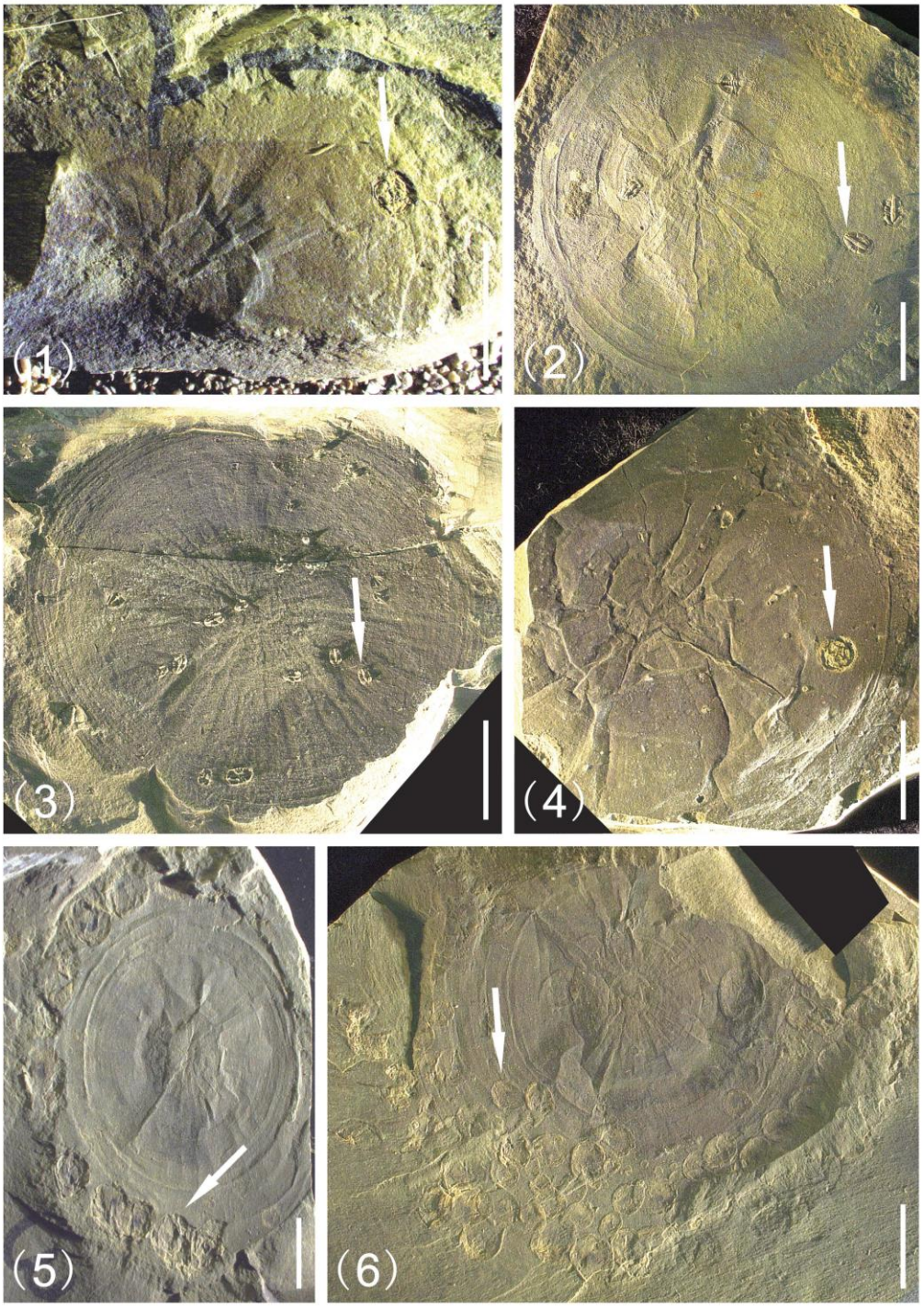

Figure 5. Symbiotic relationships between *Pararotadiscus guizhouensis* and other taxa (indicated by arrows): (**1**) with juvenile *Kailidiscus chinensis* Zhao et al., 2010 (GTBM-17-2908); (**2**) with *Pagetia* (GTBM-9-4-2172b); (**3**) with *Pagetia* (GTBM-8-5-1054);(**4**) with *Pagetia* and *Kailidiscus chinensis* (GTBM-21-576); (**5**) with brachiopods (GTB-21-105); (**6**) with brachiopods (GTB-23-365). Scale bars = 10 mm.

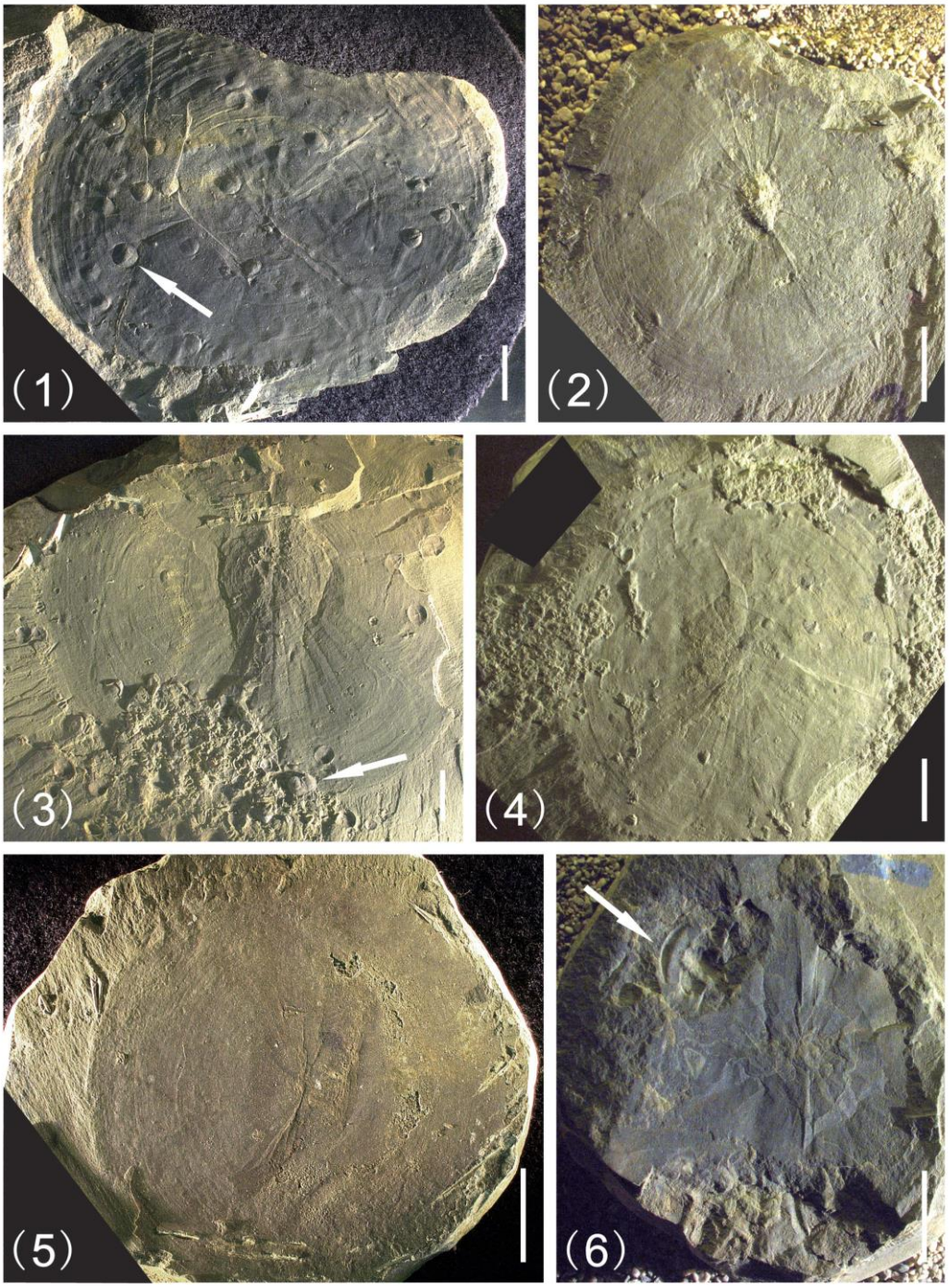

Figure 6. Examples of *Pararotadiscus guizhouensis* with associated taxa (indicated by arrows): (**1**) with dissociated brachiopod valves (GTB-9-3-4207); (**2**) with complete *Sinoeocrinus lui* and *Pagetia* cranidia and pygidia (GTBM-9-3-5004b); (**3**) with dissociated brachiopod valves and cranidia and pygidia of *Pagetia* (GTB-9-4-512); (**4**) with dissociated brachiopod valves and cranidia and pygidia of *Pagetia* (GTBM-9-5-3462); (**5**) with *Haplophrentis* cf. *H. carinatus* (Matthew, 1899) (Mao et al., 1992) and pygidia of *Pagetia* (GTB-9-4-2256); (**6**) with trilobite cranidia (GTBM-17-433). Scale bars = 10 mm.

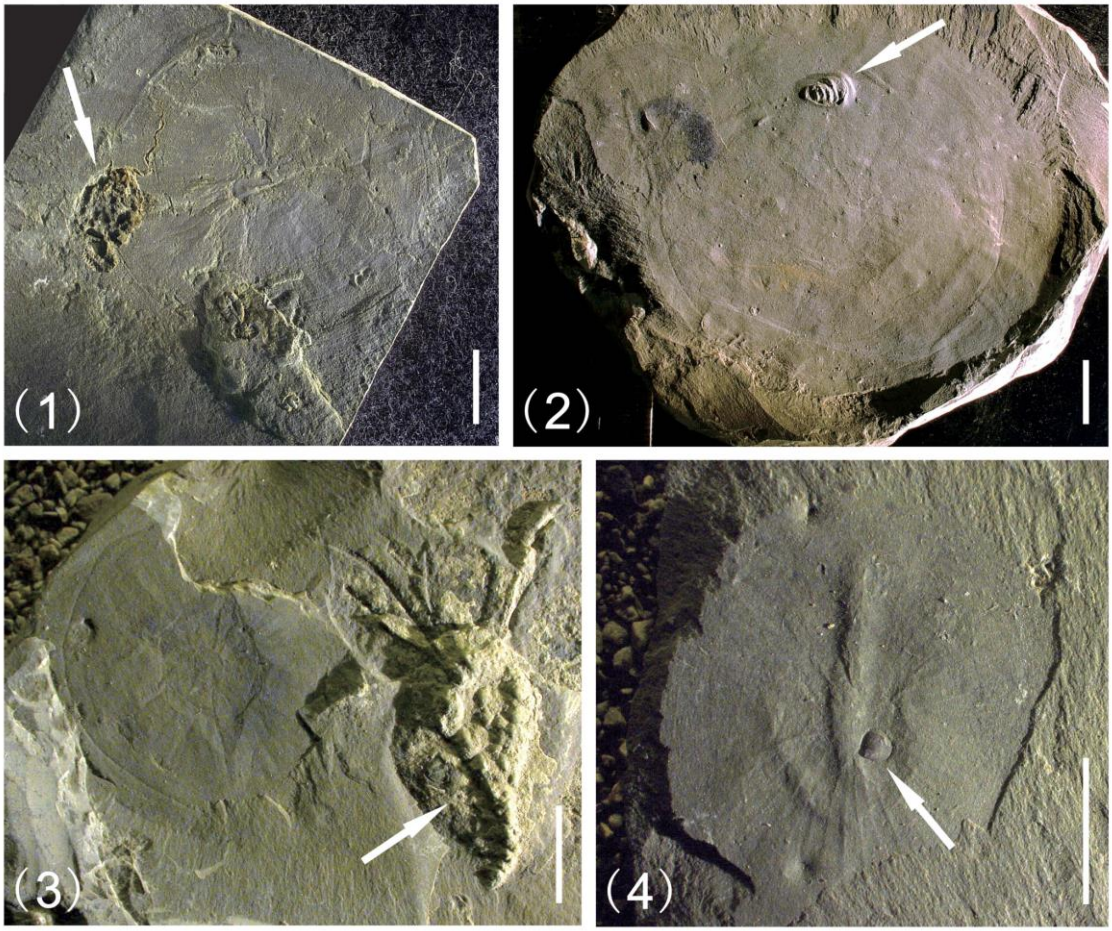

Figure 7. Examples of *Pararotadiscus guizhouensis* with associated taxa (indicated by arrows): (**1**) with *Sinoeocrinus lui* with holdfast (GTBM-10-10122); (**2**) with the monoplacophoran *Oelandiella* cf. *O. accordinononta* Runnegar and Jell, 1976 (GTB-9-5-2884); (**3**) with *Sinoeocrinus lui* with holdfast (GTBM-20-1-32a); (**4**) with brachiopods (GTBM-9-3-2a). Scale bar = 10 mm.

the bottom. Complete specimens of the diminutive trilobite *Pagetia* and juvenile individuals of the echinoderms *Globoeocrinus globouensis* Zhao et al., 2008 and *Kailidiscus chinensis* Y.L. Zhao et al., 2010 are associated with *P. guizhouensis*. They are mainly restricted to the edge and middle ring of the disc (Fig. 5.1–5.4). As with the aforementioned brachiopod specimens, this distribution, together with the planktonic habit of *Pagetia* (Lu et al., 1963; Zhang et al., 1980), suggests that these species, too, had a commensal relationship with *P. guizhouensis*. Notably, brachiopods and lobopods associated with eldonioids in the Chengjiang Biota have also been interpreted to represent a similar type of symbiosis (Chen and Zhou, 1997).

Co-Burial.—On the discs of many specimens of *P. guizhouensis* are found a variety of fragmentary and partial fossils. Examples of this material include cranidia and pygidia of trilobites, disarticulated brachiopod valves, *Wiwaxia* sclerites, echinoderm plates, and algal fragments (Table 1; Fig. 6.1, 6.3–6.6). Among this material, trilobite debris is the most common, fossil brachiopods valves also are commonly preserved on *P. guizhouensis* and account for 24% of the 628 specimens. The fragments and individuals of these taxa settled on the carcasses of *P. guizhouensis* that were lying on the seafloor. The taphonomic characteristics of this material are such that they indicate a post-mortem relationship (i.e., taphocoenoses), whereby remains, including carcass of other organisms, became associated shortly before or during final burial.

Benthic fixation on P. guizhouensis *carcasses*.—Following death, carcasses of *Pararotadiscus guizhouensis* sank to the seabed and lay at the sediment-water interface. Many benthic taxa were attracted by of carcass of *Pararotadiscus guizhouensis*. These included eocrinoids with holdfasts, brachiopods with

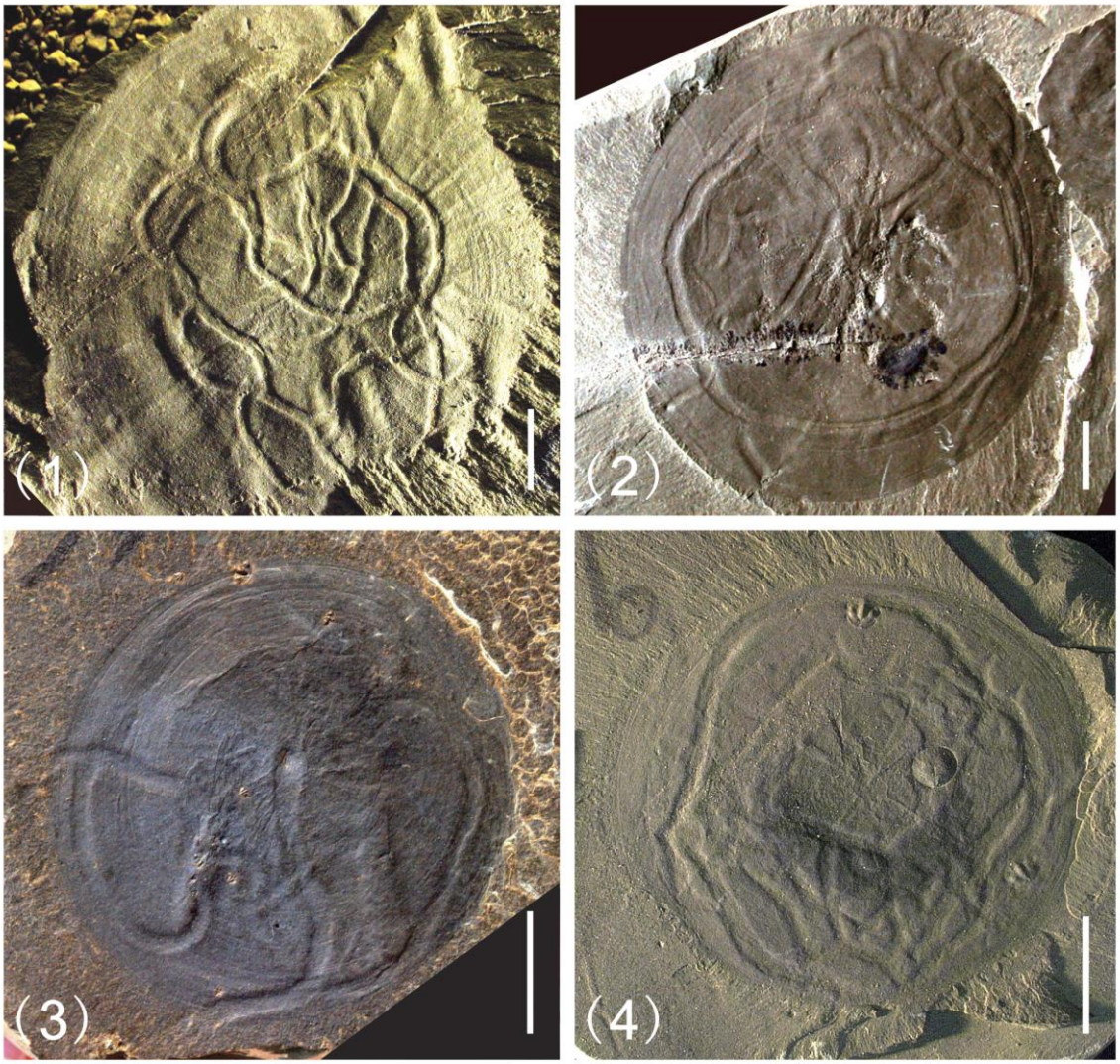

Figure 8. Associations between *Pararotadiscus guizhouensis* and the trace fossil *Helminthoidichnites* sp. (**1**) GTBM-9-4-1934; (**3**) GTBM-9-5-1085; (**4**) GTBM-10-1-7715. Association between *Pararotadiscus guizhouensis* and the trace fossil *Gordia marina* Emmons, 1844; (**2**) GTBM-10-1-9010. Scale bar = 10 mm.

pedicles, monoplacophora, and hyolithids, all of which took up life habits on the disc of *P. guizhouensis* carcasses. After they were buried by sediments, through compaction and lithification, the shells of brachiopods occupied a portion of the disc of *P. guizhouensis* (Figs. 7, 8.1) (Dzik et al., 1997). Some specimens of *P. guizhouensis* show adult specimens of the gogiids *Globoecrinus globulus* Zhao, Parsley, and Peng, 2008 and *Sinoeocrinus lui* Zhao, Huang, and Gong, 1994 attached with holdfasts (Zhao et al., 2008; Yan et al., 2010; F.C. Zhao et al., 2010) (Table 1; Figs. 6.2, 7.1, 7.3). Because these echinoderms are quite large relative to the discs, the surfaces in such cases are interpreted to have been colonized by the eocrinoids after the *P. guizhouensis* specimens died, sank to the seabed, and lay exposed for a time at the sediment-water interface. In this context, carcasses of *P. guizhouensis* formed localized "oases" of relatively hard substrate amid a backdrop of soft mud.

Scavenging of P. guizhouensis *carcasses*.—Some specimens of *P. guizhouensis* show a distinct association with the meandering horizontal ichnofossil *Gordia marina* (Fig. 8), the most common ichnotaxon in the Kaili Biota (Yang, 1993, 1994; Zhu et al., 1999; Wang et al., 2004, 2009; X.G. Zhang et al., 2010). Among the 628 study specimens, 138 (~25%) are preserved in association with *G. marina* (Cheng et al., 2009; Wang et al., 2009)

(Table 1). In most of these cases, *G. marina* traces are largely or entirely confined to the area of the disc, with the highest degree of sinuosity and greatest number of self-crossings at the middle and outer rings (Wang et al., 2004). This distinctive pattern suggests a scavenging relationship between the *G. marina* tracemaker, presumably a worm-like animal (Yang, 1994; Wang et al., 2004), and carcasses of *P. guizhouensis*, thereby forming a distinctive example of thanatocoenosis. No other evidence of scavenging has been detected for specimens of *P. guizhouensis*.

Associations of uncertain paleoecological significance.—In addition to the associations mentioned above, some specimens of *P. guizhouenesis* are associated with individual complete brachiopods with preserved pedicles, monoplacophorans, and hyolithids (Table 1; Fig. 7.2, 7.4). Because the associated specimens are small relative to the discs and do not show a distinctive spatial pattern, it is uncertain whether the associations represent additional examples of symbiosis as opposed to attachment to discs of dead individuals of *Eldonia* on the sea floor.

Discussion

Complex associations between the eldonioid *Pararotadiscus guizhouensis* and other fossils in the Kaili Biota provide an opportunity to gather important additional information about organismal interactions during the Cambrian. Details of these associations, as documented herein, reflect: (1) relationships between living organisms, (2) relationships between living and dead organisms, and (3) juxtaposition that arises purely from mixing during burial. Thus, examples in our study would seem to represent biocoenoses, thanatocoenoses, and taphocoenoses. Notably, the particular examples of symbioses and scavenging behavior documented herein are unique among Cambrian biotas. As such, they contribute to a growing body of evidence that points to a greater degree of ecological complexity among Cambrian marine communities than previously suspected. This view is supported by recent studies that document the attachment of specimens of the linguloid brachiopod *Diandongia* to other animals in the Chengjiang Biota (Z.F. Zhang et al., 2003, 2010) and an ecological association between the brachiopod *Nisusia* and the annelid *Wiwaxia* in the Burgess Shale (Topper et al., 2014, 2017). Further studies of the Kaili Biota hold the promise of yielding additional insights concerning the ecology of the Cambrian biosphere.

Acknowledgments

This study was supported by grants from the Major State Basic Research Development Program of China (2015FY310-100) and the National Natural Science Foundation of China (41330101, 41772021, 41702022, 41662001). We are grateful to M. Zhu and H. Sun (Nanjing Institute of Geology and Palaeontology, Chinese Academy of Science, Nanjing, China), Z. Zhang (Northwestern University), and R. Parsley (Tulane University) for linguistic revision.

References

Briggs, D.E.G., Erwin, D.H., and Collier, F.J., 1994, The Fossils of the Burgess Shale: Washington/London, Smithsonian Institution Press, 238 p.
Caron, J.B., and Jackson, D.A., 2008, Paleoecology of the Greater Phyllopod Bed community, Burgess Shale: Palaeogeography, Palaeoclimatology, Palaeocology, v. 258, p. 222–256.
Chen, J.Y., 2004, The Dawn of Animal World: Nanjing, Jiangsu Science and Technology Press, 366 p. [in Chinese].
Chen, J.Y., and Zhou, G.Q., 1997, Biology of the Chengjiang fauna: Bulletin of the National Museum of Science, v. 10, p. 11–106.
Chen, J.Y., Hou, X.G., and Lu, H.Z., 1989, Early Cambrian netted scale-bearing worm-like sea animal: Acta Palaeontologica Sinica, v. 29, p. 57–71. [in Chinese].
Chen, J.Y., Zhou, G.Q., and Ramsköld, L., 1995, A new Early Cambrian medusiform onychophoran-like animal *Paucipodia* gen. nov. from the Chengjiang fauna, China: Transcations of the Royal Society of Edinburgh, Earth Science, v. 85, p. 275–282.
Chen, J.Y., Zhou, G.Q., Zhu, M.Y., and Ye, G.Y., 1996, The Chengjiang Biota: A Unique Window of the Cambrian Explosion: Taichung, National Museum of Natural Science, 222 p. [in Chinese].
Cheng, X., Fu, X.P., and Zhao, Y.L., 2009, A preliminary study of the medusiform fossils (*Pararotadicus*) associating with brachiopods from the Cambian Kaili Biota, Jianhe, Guizhou: Acta Palaeontologica Sinica, v. 48, p. 672–680. [in Chinese].
Conway Morris, S., and Robison, R.A., 1986, Middle Cambrian priapulids and other soft-bodied fossils from Utah and Spain: University of Kansas Paleontological Contributions, v. 117, p. 1–22.
Conway Morris, S., and Robison, R.A., 1988, More soft-bodied animals and algae from the Middle Cambrian of Utah and British Columbia: University of Kansas Paleontological Contributions, v. 122, p. 1–48.
Dzik, J., Zhao, Y.L., and Zhu, M.Y., 1997, Mode of life of the Middle Cambrian eldonioid lophophorate *Rotadiscus*: Palaeontology, v. 40, p. 385–396.
Emmons, E., 1844, The Taconic System: Based on Observation in New York. Massachusetts, Maine, Vermont, and Rhode Island: Albany, New York, Caroll and Cook, 68 p.
Gaines, R.R., Briggs, D.E.G., and Zhao, Y.L., 2008, Burgess Shale-type deposits share a common mode of fossilization: Geology, v. 36, p. 755–758.
Hou, X.G., Bergström, J., Wang, H.F., Feng, X.H., and Chen, A.L., 1999, The Chengjiang Fauna: Exceptionally Well Preserved Animals from 530 Million Years Ago: Kunming, Yunnan Scientific Technology Press, 191 p. [in Chinese].
Hou, X.G., Aldridge, R.J., Bergstrom, J., Siveter, D.J, Siveter, D.J, and Feng, X. H., 2003, The Cambrian Fossils of Chengjiang, China: The Flowering of Early Animal Life: Malden, Massachusetts, Wiley-Blackwell Publishing, 233 p.
Ivantsov, A.Y., Zhuravlev, A.Y., Leguta, A.V., Krassilov, V.A., Melnikova, L. M., and Ushatinskaya, G.T., 2005, Palaeocology of the Early Cambrian Sinsk biota from the Siberian platform: Palaeogeography, Palaeoclimatology, Palaeoecology, v. 220, p. 69–88.
Jin, Y.G., Hou, X.G., and Wang, H.Y., 1993, Lower Cambrian pediculate lingulids from Yunnan, China: Journal of Paleontology, v. 67, p. 788–798.
Lu, Y.H., Qian, Y.Y., and Zhu, Z.L, 1963, Trilobite: Beijing, Science Press, 231 p. [in Chinese].
Matthew, G.F., 1899, Studies on Cambrian faunas, no. 3: Upper Cambrian fauna of Mt. Stephen, British Columbia: Transactions of the Royal Society of Canada, ser. 2, v. 5, p. 39–66.
Mao, J.R., Zhao, Y.L., Yu, P., and Qian, Y., 1992, Some Middle Cambrian hyolithids from Taijiang, Guizhou: Acta Micropalaeontologica Sinica, v. 9, p. 257–265. [in Chinese with English abstract].
Robison, R.A., and Sprinkle, J., 1969, Ctenocystoidea: new class of primitive echinoderms: Science, v. 166, 3912, p. 1512–1514.
Runnegar, B., and Jell, P.A., 1976, Australian Middle Cambrian molluscs and their bearing on early molluscan evolution: Alcheringa, v. 1, p. 109–138.
Schroeder, N.I., Paterson, J.R., and Brock, G.A., 2018, Eldonioids with associated trace fossils from the lower Cambrian Emu Bay Shale Konservat-Lagerstätte of South Australia: Journal of Paleontology, v. 92, p. 80–86.
Sun, W.G., and Hou, X.G., 1987, Early Cambrian medusae from Chengjiang, Yunnan, China: Acta Palaeontologica Sinica, v. 28, p. 257–271. [in Chinese].
Topper, T.P., Holmer, L.E., and Caron, J.B., 2014, Brachiopods hitching a ride: an early case of commensalism in the middle Cambrian Burgess Shale: Scientific Reports, v. 4, p. 6704.
Topper, T.P., Strotz, L.C., Skovsted, C.B., and Holmer., L.E., 2017, Do brachiopods show substrate-related phenotypic variation? A case study from the Burgess Shale: Palaeontology, v. 60, p. 269–279.
Walcott, C.D., 1911, Middle Cambrian holothurians and Medusae. Cambrian Geology and Palaeontology II: Smithsonian Miscellaneous Collections, v. 57, p. 41–68.
Wang, Y., Zhao, Y.L., Lin, J.P., and Wang, P.L., 2004, Relationship between trace fossils *Gordia* and medusiform fossils *Pararotadiscus* from the Kaili

Biota, Taijiang, Guizhou, and its significance: Geological Review, v. 50, p. 113–119. [in Chinese].

Wang, Y., Lin, J.P., Zhao, Y.L., and Orr, P.J., 2009, Palaeoecology of the trace fossil *Gordia* and its interaction with nonmineralizing taxa from the early Middle Cambrian Kaili Biota, Guizhou Province, South China: Palaeogeography, Palaeoclimatology, Palaeoecology, v. 277, p. 141–148.

Yan, X., Mao, Y.Q., Zhao, Y.L., Peng, J., and Wu, M.Y., 2010, The holdfasts of eocrinoids in Cambrian, Guizhou Province: Acta Palaeontologica Sinica, v. 49, p. 380–388. [in Chinese].

Yang, S.P., 1993, Palaeocology: Beijing, Geological Press, 228 p. [in Chinese].

Yang, S.P., 1994, Trace fossils from Early–Middle Cambrian Kaili Formation of Taijiang, Guizhou: Acta Palaeontologica Sinica, v. 33, p. 250–358. [in Chinese].

Yang, X.L., Zhu, M.Y., Zhao, Y.L., Mao, Y.Q, and Wang, Y.X., 2007, Medusiform fossils from the Middle Cambrian Jialao Formation Jianhe County, Guizhou, China: Acta Palaeontology Sinica, v. 46, p. 232–237. [in Chinese].

Yuan, J.L., and Huang, Y.Z., 1994, Preliminary report nontrilobite arthropods from the Lower-Middle Cambrian Kaili Formation of southeastern Guizhou, South China: Acta Palaeotologica Sinica, v. 33, p. 329–334. [in Chinese].

Zhang, W.T., Lu, Y.H., Zhu, Z.L., Qian, Y.Y., Cin, H.L., Zhou, Z.Y., and Yuan, J.L., 1980, Cambrian trilobite faunas of Southwestern China: Palaeontologica Sinica, Series B, 159, 497 p. [in Chinese].

Zhang, X.G., Bergström, J., Bromley, R.G., and Hou, X,G., 2010, Diminutive trace fossils in the Chengjiang Lagerstätte: Terra Nova, v. 19, p. 407–412.

Zhang, Z.F., Han, J., Zhang, X.L., Liu, J.N., and Shu, D.G., 2003, Pediculate branchiopoda *Diandongia pista* from the Lower Cambrian of south China: Acta Geologica Sinica, v. 77, p. 288–293. [English edition].

Zhang, Z.F., Huang, J., Wang, Y, Emig, C.C., and Shu, D.G., 2010, Epibionts on the lingulate brachiopod *Diangongia* from the early Cambrian Lagerstätte, South China: Proceedings of the Royal Society, v. 277, p. 175–181.

Zhao, F.C., Zhu, M.Y., and Hu, S.X., 2010, Community structure and composition of Cambrian Chengjiang: Science China Earth Science, v. 53, p. 1781–1799.

Zhao, Y.L., and Zhu, M.Y., 1994, Medusiform fossils of Kaili Fauna from Taijiang, Guizhou: Acta Palaeontologica Sinica, v. 33, p. 350–358. [in Chinese].

Zhao, Y.L., Huang, Y.Z., and Gong, X.Y., 1994, Echinoderma fossils of Kaili Fauna from Taijiang, Guizhou: Acta Palaeontological Sinica, v. 33, p. 305–324. [in Chinese with English abstract].

Zhao, Y.L., Parsley, R.L., and Peng, J., 2008, Basal Middle Cambrian short-stalked eocrinoids from the Kaili Biota: Guizhou Province, China: Journal of Paleontology, v. 82, p. 415–422.

Zhao, Y.L., Sumrall, C.D., Parsley, R.L., and Peng, J., 2010, *Kailidiscus*, a new plesiomorphic edrioasteroid from the basal Middle Kaili Biota of Guizhou Province, China: Journal of Paleontology, v. 84, p. 668–680.

Zhao, Y.L, Zhu, M.Y., Babcock, L.E., and Peng, J., 2011, The Kaili Biota: Marine Organisms from 508 Million Years Ago: Guiyang, Guizhou Publishing Group, 251 p. [in Chinese].

Zhao, Y.L., Yang, Y.N., Peng, J., Yuan, J.L., Sun, H.J., Yan, X., and Zhang, P.X., 2012, The Kaili Formation and Kaili Biota at the Sanwan section in Guizhou Province, China and boundary between Cambrian Series 2/ Series 3, *in* Zhao Y.L., Zhu, M.Y., Peng, J., Gaines, R.R., Parsley, R.L., eds., Cryogenian–Ediacaran to Cambrian Stratigraphy and Palaeontology of Guizhou, China. Journal of Guizhou University (Natural Science), (Supplement) 1989, p. 77–88.

Zhu, M.Y., 2010, The origin and Cambrian Explosion of animals: fossil evidences from China: Acta Palaeontological Sinica, v. 49, p. 269–287. [in Chinese with English abstract].

Zhu, M.Y., Erdtmann, B.D., and Zhao, Y.L., 1999, Taphonomy and paleoecology of the early Middle Cambrian Kaili Lagerstatte in Guizhou, China: Acta Palaeomtologica Sinica, v. 38, p. 28–57. [in Chinese].

Zhu, M.Y., Zhao, Y.L., and Chen, J.Y., 2002, Revision of the Cambrian discoidal animals *Stellostomites eumorphus* and *Parardadiscus guizhouensis* from South China: Geobios, v. 35, p. 165–185.

Accepted 9 May 2018

Available online at www.sciencedirect.com

ScienceDirect

Palaeoworld 27 (2018) 423–437

Palaeoworld

www.elsevier.com/locate/palwor

Conodonts of the genus *Lochriea* near the Visean–Serpukhovian boundary (Mississippian) at the Naqing section, Guizhou Province, South China

Yu-Ping Qi [a,*], Tamara I. Nemyrovska [b], Qiu-Lai Wang [a,c], Ke-Yi Hu [d], Xiang-Dong Wang [a], H. Richard Lane [e,1]

[a] *CAS Key Laboratory of Economic Stratigraphy and Palaeogeography, Nanjing Institute of Geology and Palaeontology, and Center for Excellence in Life and Paleoenviroment, Chinese Academy of Sciences, 39 East Beijing Road, Nanjing 210008, China*

[b] *Institute of Geological Sciences, National Academy of Sciences of Ukraine, O. Gonchar Str. 55-b, 01601 Kiev, Ukraine*

[c] *University of Chinese Academy of Sciences, 19A Yuquan Road, Shijingshan District, Beijing 100049, China*

[d] *Centre for Research and Education on Biological Evolution and Environment, Nanjing University, 163 Xianlin Road, Nanjing 210023, China*

[e] *National Science Foundation of USA, Arlington, VA, 22230, USA*

Received 2 January 2018; received in revised form 29 June 2018; accepted 5 September 2018
Available online 11 September 2018

Abstract

The First Appearance Datum (FAD) of the conodont *Lochriea ziegleri* in the lineage *Lochriea nodosa–L. ziegleri* has been considered the most suitable definition and global correlation-level for a revised base of the Serpukhovian Stage. Abundant specimens of *Lochriea* are recorded throughout the Late Visean–early Serpukhovian interval in the Naqing section, South China. Among them, the P1 elements, with wide morphological variability, enable confirmation and refinement of main lineages within the genus. Two lineages are proposed: 1) noded *Lochriea* species, such as *L. mononodosa–L. nodosa–L. ziegleri*, *L. senckenbergica* and *L. multinodosa*, and 2) ridged *Lochriea* species such as *L. monocostata–L. costata–L. cruciformis*. The possibility for their phylogenetic relationships is evaluated in this paper.

Keywords: Lochriea; Lineage; Conodont; Biostratigraphy; Naqing section; South China

1. Introduction

The current global scheme of chronostratigraphic subdivisions of the Carboniferous System was confirmed by the Subcommission for Carboniferous Stratigraphy (SCCS) in late 2003 and ratified by the International Commission of Stratigraphy (ICS) and International Union of Geological Sciences (IUGS) in early 2004 (Heckel, 2004). The Carboniferous now comprises the Mississippian and Pennsylvanian subsystems; a Global Boundary Stratotype Section and Point (GSSP) was selected and ratified for the base of the Pennsylvanian (Lane et al., 1999). The Mississippian comprises the Tournaisian, Visean and Serpukhovian stages. The GSSP for the base of the Carboniferous and thus for the Mississippian and the Tournaisian Stage was ratified (Paproth et al., 1991); however, this boundary is currently under review (Kaiser, 2009; Richards and Task Group, 2009). The GSSP for the base of the Visean was also ratified (Work, 2008). However, the Serpukhovian Stage still doesn't have a GSSP.

The succession constituting the type Visean is exposed in the Namur-Dinant Basin of Belgium, northern France, and southern England. There, the type Visean is represented in a quarry section in Belgium and the contact with the overlying Namurian succession (correlative with the Serpukhovian Stage) is a regional unconformity (Paproth et al., 1983). The Serpukhovian Stage, proposed by Nikitin (1890), was re-introduced into the Russian stratigraphic scheme in 1974 by the Interdepartmental Stratigraphic Committee of the USSR and has become

* Corresponding author at: Nanjing Institute of Geology and Palaeontology, Chinese Academy of Sciences, Nanjing 210008, China.
E-mail addresses: ypqi@nigpas.ac.cn (Y.P. Qi), tamaranemyrovska@gmail.com (T.I. Nemyrovska), qlwang@nigpas.ac.cn (Q.L. Wang), kyhu@nju.edu.cn (K.Y. Hu), xdwang@nigpas.ac.cn (X.D. Wang).
[1] Deceased.

https://doi.org/10.1016/j.palwor.2018.09.001
1871-174X/

widely recognized (Skompski et al., 1995; Gibshman, 2001). The type Serpukhovian was defined in the Moscow Basin and is situated in the Zaborie quarry near the southern margin of the town of Serpukhov. Unfortunately, the lower boundary of the type Serpukhovian is a basin-wide unconformity that resulted from a latest Visean regression and subaerial exposure followed by a Serpukhovian transgression. Deposition of the type Serpukhovian sediments was strongly influenced by major glacial-eustatic sea level changes, which commenced during the late Visean and continued through the Pennsylvanian (Richards and Task Group, 2003; Rygel et al., 2008). Relatively deeper-water, carbonate-slope and basinal sections that may serve as potential candidate sections for a GSSP of the Visean–Serpukhovian (V–S) boundary are known from the Cantabrian Mountains of Spain, the South Urals of Russia, and in southern Guizhou, South China (Richards and Task Group, 2003; Wang and Qi, 2003; Nemyrovska and Samankassou, 2005; Nikolaeva et al., 2005, 2009; Qi and Wang, 2005; Blanco-Ferrera et al., 2009; Qi et al., 2014; Chen et al., 2016).

The Task Group to establish a GSSP close to the existing V–S boundary first assembled in 2002 (Heckel, 2002; Richards and Task Group, 2003). Significant progress toward selecting a basal Serpukhovian GSSP has been achieved since then (Richards and Task Group, 2009, 2014). Before evaluating potential GSSPs, the Task Group had to decide on the biostratigraphical tool (or tools) to precisely identify the boundary. Candidate fossil groups were ammonoids, conodonts, and foraminifers. By 2005, the most-favoured group were the conodonts; in particular, an evolutionary lineage within the genus *Lochriea* was considered to offer the best possibility of providing a tool to identify the boundary (Sevastopulo and Barham, 2014).

The genus *Lochriea* contains eleven species based on the P1 elements including *Lochriea commutata* (Branson and Mehl, 1941), *Lochriea costata* (Pazukhin and Nemirovskaya in Kulagina et al., 1992), *Lochriea cracoviensis* (Belka, 1985), *Lochriea cruciformis* (Clarke, 1960), *Lochriea monocostata* (Pazukhin and Nemirovskaya in Kulagina et al., 1992), *Lochriea mononodosa* (Rhodes et al., 1969), *Lochriea multinodosa* (Wirth, 1967), *Lochriea nodosa* (Bischoff, 1957), *Lochriea saharae* Nemyrovska et al., 2006, *Lochriea senckenbergica* (Nemirovskaya et al., 1994), and *Lochriea ziegleri* (Nemirovskaya et al., 1994). Atakul-özdemir et al. (2012) also assigned *Pseudognathodus homopunctatus* to *Lochriea* on the basis of a cladistic test by using multielement skeletal data of *P. homopunctatus* and the genus *Lochriea*. As *P. homopunctatus* is of less biostratigraphic importance in the V–S boundary interval, its taxonomy will not be discussed in this paper. The diagnoses of the species of *Lochriea* are based on the characters of the P1 elements, and the other elements are shared vicariously by different species (Sevastopulo and Barham, 2014). The multielement composition of *Lochriea commutata*, the type species of this genus, has been confirmed by natural assemblages (Norby, 1976; Varker, 1993; Purnell and Donoghue, 1998). The evolution of the *Lochriea* species has great potential for a stratigraphic application. Morphological trends within the genus *Lochriea* from simple unornamented to complex sculptured forms have been recognized in many sections in Europe and Asia (Nemirovskaya et al., 1994; Skompski et al., 1995; Nemyrovska and Samankassou, 2005; Pazukhin et al., 2009; Qi et al., 2014; Barham et al., 2015). The evolutionary appearance of coarsely ornamented species of *Lochriea* has been regarded to be of great importance for the definition and correlation of the base of the Serpukhovian. Most of the *Lochriea* species are documented in South China sections and the evolutionary relationship among them has been shown by abundant collections (Qi, 2008; Qi et al., 2010, 2014). In addition to the abundant P1 elements of *Lochriea* species, their ramiform elements are common in the South China sections.

The Task Group has concluded that the first evolutionary appearance of the conodont *Lochriea ziegleri* in the lineage *Lochriea nodosa–Lochriea ziegleri* currently presents the best potential for the boundary definition (Richards and Task Group, 2005), although this marker still awaits formal ratification. *Lochriea ziegleri* appeared near the middle of the Brigantian substage in Western Europe, at a level that is correlated to slightly below the base of the type Serpukhovian stage in the Moscow Basin and at a substantially lower horizon than the lower boundary of the Namurian Stage in Western Europe (Sevastopulo and Barham, 2014). When formally adopted, the new basis for defining the V–S boundary will mean that rocks previously regarded as Late Visean in age will become early Serpukhovian. The *L. nodosa–L. ziegleri* lineage is best documented from relatively deep-water sections and has been identified at several sites in Western Europe, Russia, and China (Nemirovskaya et al., 1994; Skompski et al., 1995; Wang and Qi, 2003; Nemyrovska and Samankassou, 2005; Qi and Wang, 2005; Pazukhin et al., 2010; Qi et al., 2010, 2014; Barham et al., 2015). The lineage has not been documented in North America but several relatively long-ranging species including *L. nodosa* (Bischoff, 1957) have been reported there under the genus *Paragnathodus*, a junior synonym of *Lochriea* (Lane and Brenckle, 2005; Groves et al., 2012). Since only one specimen of *L. ziegleri* has been identified from the Barnett Formation at the J. R. Walker Ranch, central Texas, North America (Qi et al., 2010; Richards and Task Group, 2010), correlation of the V–S boundary between Eurasia and North America is difficult.

Carboniferous marine sediments are widely distributed and well-developed in South China, where they form continuous successions of marine carbonates containing conodonts and foraminifers. The Naqing section is the most-studied section across the V–S boundary in South China. Abundant conodonts from the Late Visean to early Serpukhovian deposits of the Naqing section include a large number of elements related to cosmopolitan species of the genera *Gnathodus*, *Lochriea* and *Pseudognathodus*. *Vogelgnathus* and *Mestognathus* are also common. In this section, numerous P1 elements of *Lochriea* species have been found; their evolutionary lineages are quite clear with many transitional forms within each lineage. The First Occurrence Datum (FOD) of *L. ziegleri*, in the evolutionary lineage *L. nodosa–L. ziegleri*, has been moved from

60.60 m (Qi, 2008; Qi et al., 2009), down to 60.38 m (Qi et al., 2010), and then down to 60.10 m now (Qi et al., 2014) above the base of the Naqing section, based on repeated continuous centimeter-scale sampling from 2008 to 2011. There are a number of transitional forms between *L. nodosa* and *L. costata* and between *L. nodosa*, *L. costata* and *L. ziegleri*, as well as between *L. ziegleri* and *L. cruciformis* and *L. senckenbergica*. The aim of this paper is to differentiate and describe the *Lochriea* species and to discuss the *Lochriea* lineages across the V–S boundary in the Naqing section.

In addition, significant Serpukhovian foraminiferal species including *Janishewskina delicata* and *Bradyina* ex gr. *cribrostomata* are found shortly above the V–S boundary as defined by the first appearance of *Lochriea ziegleri* in the Naqing section (Sheng, 2016). Isotopic chemostratigraphy studies show that multiple negative $\delta^{13}C$ excursion (>1‰) can be correlated across the V–S boundary interval in several slope sections including the Naqing, Luokun, and Narao sections in South China (Chen et al., 2016). Moreover, the latest study results on conodonts and ammonoids from the Wenne river bank section in the Rhenish Mountains, Germany indicate that the debut of *L. ziegleri* in this section is at a horizon just 0.5 m below the "*Actinopteria* Shale" and has a position in the ammonoid *Neoglyphioceras suerlandense* Zone, which is contemporary to P2a biozone (*Lusitanoceras granosum*) in British Isles (Wang et al., 2018).

2. Geological setting

During the Mississippian, the southern part of Guizhou belonged to the Dian-Qian-Gui Basin that developed on a passive continental margin of the South China Craton. The Dian-Qian-Gui Basin was bordered to the north and west by the Yangtze oldland, and connected with the Paleotethys Ocean to the south and east (Feng et al., 1999). The paleogeographical architecture in this region was influenced mainly by rifting along NW- and NE-trending fault zones, which led to a complex submarine landscape of small regional basins surrounded by carbonate platforms. In the southern Guizhou region, the Mississippian strata are well-exposed in a suite of outcrops and highway road-cuts, bearing a complex variety of marine facies and fossil assemblages (Qi et al., 2014; Chen et al., 2016). A number of studies on biota, sedimentology, and geochemistry of these sections were carried out in the context of selection of a GSSP for the V–S boundary. The investigated region was generally represented by a carbonate slope setting during this time interval (Chen et al., 2016).

The Naqing section, one of the extraordinarily exposed Carboniferous sections in China, is located near Naqing village (25°15′03.9″N, 106°29′06.9″E) in Luodian County, southern Guizhou Province (Fig. 1), and has been considered an excellent GSSP candidate for the base of several Carboniferous stages, including the Serpukhovian, Moscovian, Kasimovian and Gzhelian (http://www.stratigraphy.org/GSSP/GSSPTable2015-01.pdf). The Late Visean to early Serpukhovian succession in the Naqing section most probably preserves a complete phylogenic lineage of *Lochriea* given the continuous deposition, occurrence of abundant conodonts and relatively high sedimentation rate (ca. 9 m/m.y.) in contrast to condensed sections. The studied interval consists mainly of thin- to medium-bedded, partially siliceous lime mudstone, laminated wacke- to packstone and normal-graded packstone (Chen et al., 2016). Although the frequent occurrence of normal-graded bioclastic wacke- to packstones most likely resulted from turbidity currents or debris flows in a carbonate slope setting, the lack of obvious incision or slump structures suggests no substantial submarine erosion. In total, approximately 11000 well-preserved platform elements of conodonts were extracted from the 32 m thick Late Visean to early Serpukhovian interval, which warrants a high-resolution conodont biostratigraphy and a precise correlation with the global chronostratigraphic scale.

3. Evolutionary changes of *Lochriea* genus and the definition of the V–S boundary

Conodonts of the important Mississippian genera *Gnathodus*, *Pseudognathodus*, *Lochriea*, *Vogelgnathus*, and *Mestognathus* are widely distributed in Visean and Serpukhovian deposits in the Naqing section (Fig. 2). The V–S boundary interval is characterized by abundant specimens of the *Gnathodus bilineatus* and *G. girtyi*, numerous and diverse species of *Lochriea*, abundant *Pseudognathodus homopunctatus*, common *Vogelgnathus campbelli* (Rexroad, 1957) and *V. postcampbelli* (Austin and Husri, 1974), as well as less common *Mestognathus beckmanni* Bischoff, 1957 and *M. bipluti* Higgins, 1961.

The *Gnathodus bilineatus* group dominates in the V–S boundary interval. Numerous and diverse species of *Lochriea* are the next most abundant group and they display the change from simple unornamented platforms to coarsely decorated forms with nodes or ridges. The distinction between species is generally based upon the shape and ornament of the platform (Nemirovskaya et al., 1994; Skompski et al., 1995; Nemyrovska et al., 2006). Nodes or ridges, such as those in *L. ziegleri*, *L. senckenbergica*, *L. cruciformis*, and *L. multinodosa*, distinguish coarsely ornamented species. Species with "weak ornament", including noded and ridged morphotypes together, such as *L. mononodosa* and *L. nodosa* are common, although Pazukhin and Nemirovskaya (in Kulagina et al., 1992) distinguished the ridged species as distinct. Following the method of speciation of *Lochriea* as evaluated above, apart from stratigraphic occurrence alone, the attributes that are important to the evolutionary significance for distinguishing ridged and noded species of *Lochriea* with "weak ornament" are similar to what has been done to the coarsely ornamented species of *Lochriea* (Nemirovskaya et al., 1994). The noded species with weakly developed ornament are considered to give rise to the noded species with a coarse ornament. Thus, *L. mononodosa* could give rise to *L. nodosa* and the latter could give rise to *L. senckenbergica* and *L. multinodosa*. In the same way the ridged species, such as *L. monocostata* could give rise to *L. costata*, which in turn could give rise to *L. cruci-*

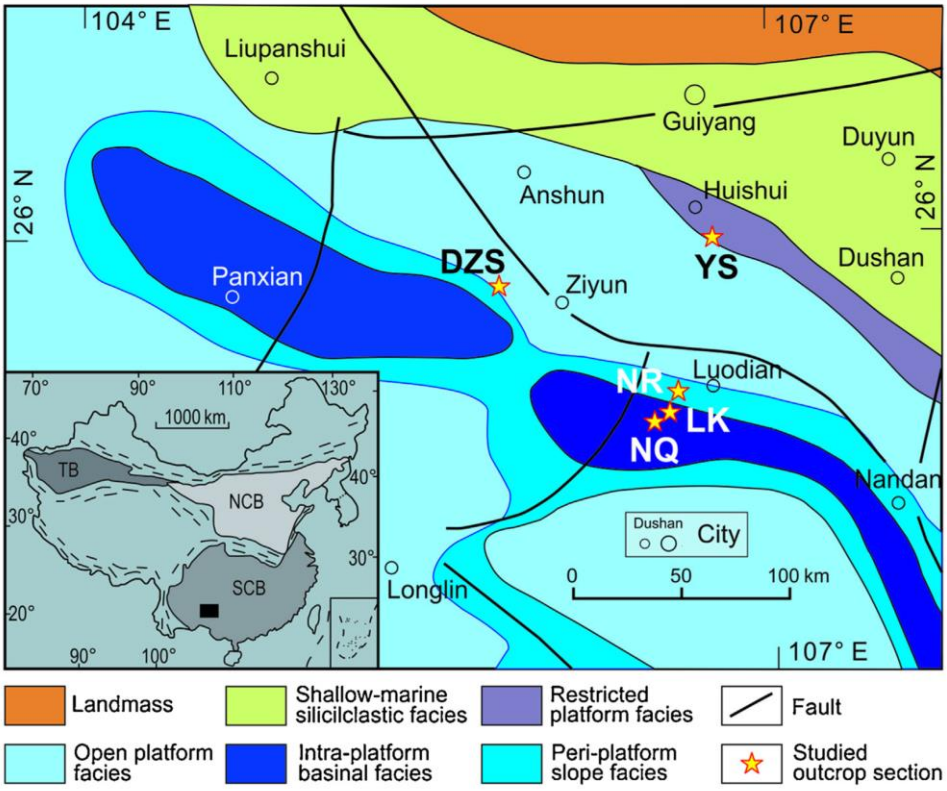

Fig. 1. Location map of the Naqing section (after Chen et al., 2016), NCB = North China Block, SCB = South China Block, TB = Tarim Block. The black square in the map represents the investigated area. Sections: DZS = Dianzishang, LK = Luokun, NQ = Naqing, NR = Narao, YS = Yashui.
[This figure is available in colour online.]

formis. As to *L. ziegleri*, of which the platform is ornamented by thick bars with large nodes on them, it could derive likely from *L. nodosa* (Figs. 3, 4).

L. ziegleri differs from the more simply ornamented *L. nodosa* and *L. costata* by a much coarser and prominent ornament of the platform and the dorsal location of bars or ridges in comparison to more central position of nodes or ridges in *L. nodosa* and *L. costata*. The latter feature distinguishes *L. ziegleri* from the other coarsely ornamented *Lochriea* such as *L. cruciformis* and *L. senckenbergica*. In addition, *L. ziegleri* differs from *L. cruciformis* by having more complicated ridges or bars not connected to the carina. *L. ziegleri* differs from *L. senckenbergica* by having lower ridges or bars decorated by partly fused nodes that are not as prominent and as high as more ventrally located bars in *L. senckenbergica*.

In South China, there are a number of transitional forms between *L. nodosa* and *L. costata* as well as between *L. mononodosa* and *L. monocostata*. This is fertile ground for probable new species among the coarsely ornamented *Lochriea* species. The similar features of *Lochriea* fauna have also been observed in western Ireland (Barham et al., 2015) and in the Rhenish Mountains, Germany (Wang et al., 2018). The evolutionary lineage of *L. nodosa–L. ziegleri* with many transitions in the Naqing section and in many other sections in South China and elsewhere in the world seems to be quite reliable; therefore, it has the greatest potential to be used for the definition of the V–S boundary. Coarsely ornamented *L. ziegleri* is widespread in Eurasia. A well preserved specimen has been found in North America but is not published (Qi et al., 2014). *L. ziegleri* is easily recognizable and more numerous elsewhere than the other coarsely ornamented *Lochriea* species. Its FAD can be well correlated with index foraminifers and ammonoids (Sheng, 2016; Wang et al., 2018). Thus, the FAD of *L. ziegleri* is the current best marker for the base of the global Serpukhovian Stage. So properly it is time to cast a vote for an official boundary marker for the base of the global Serpukhovian Stage by using the FAD of the conodont *L. ziegleri* in the lineage *L. nodosa–L. ziegleri*.

4. Systematic palaeontology

Lochriea Scott, 1942

Type species: *Lochriea montanaensis* Scott, 1942 (M element) = *Spathognathodus commutatus* Branson and Mehl, 1941; Mississippian of North America.

Content of the genus:

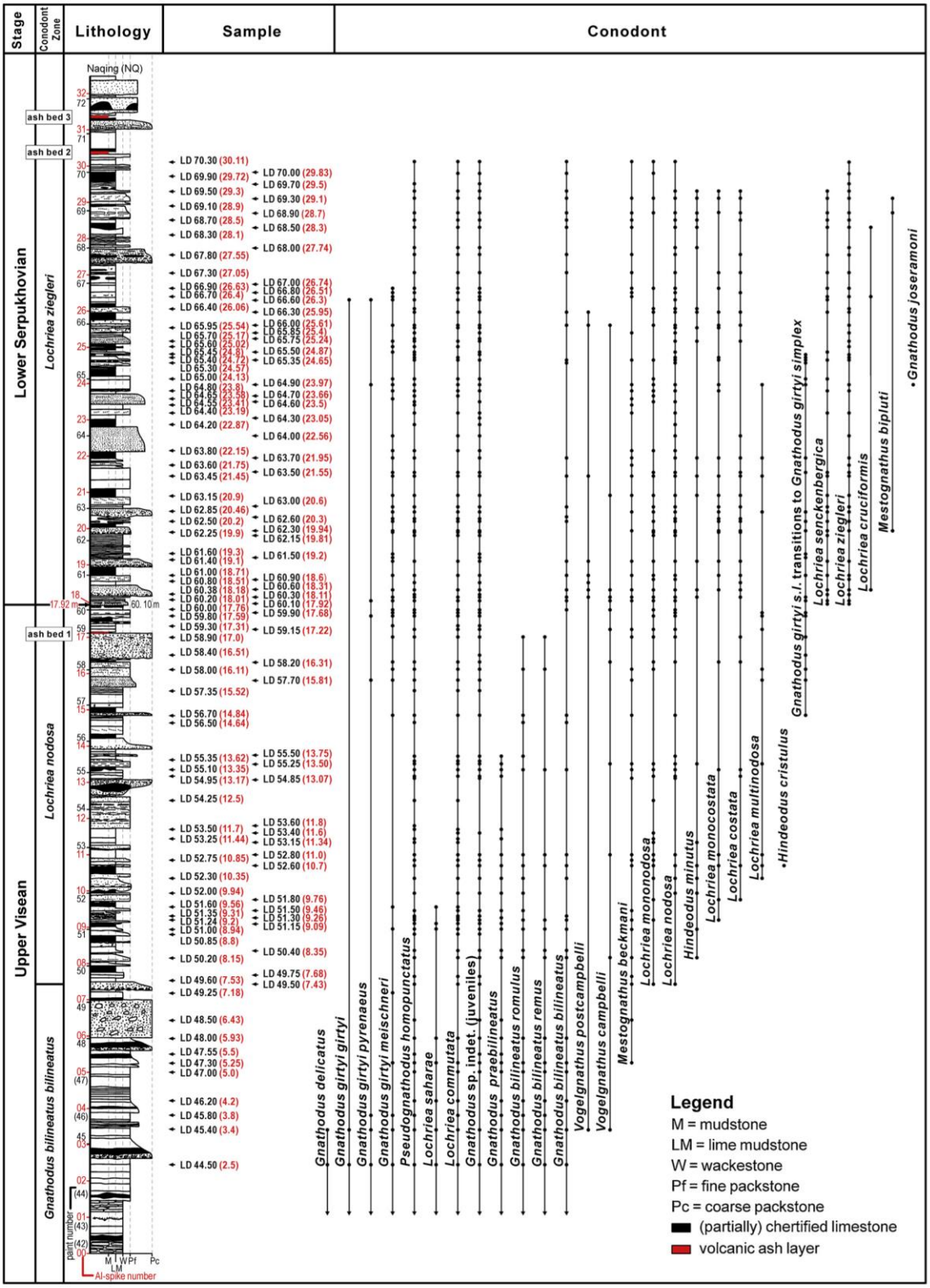

Fig. 2. Range chart of conodonts across the Visean–Serpukhovian boundary at the Naqing section.

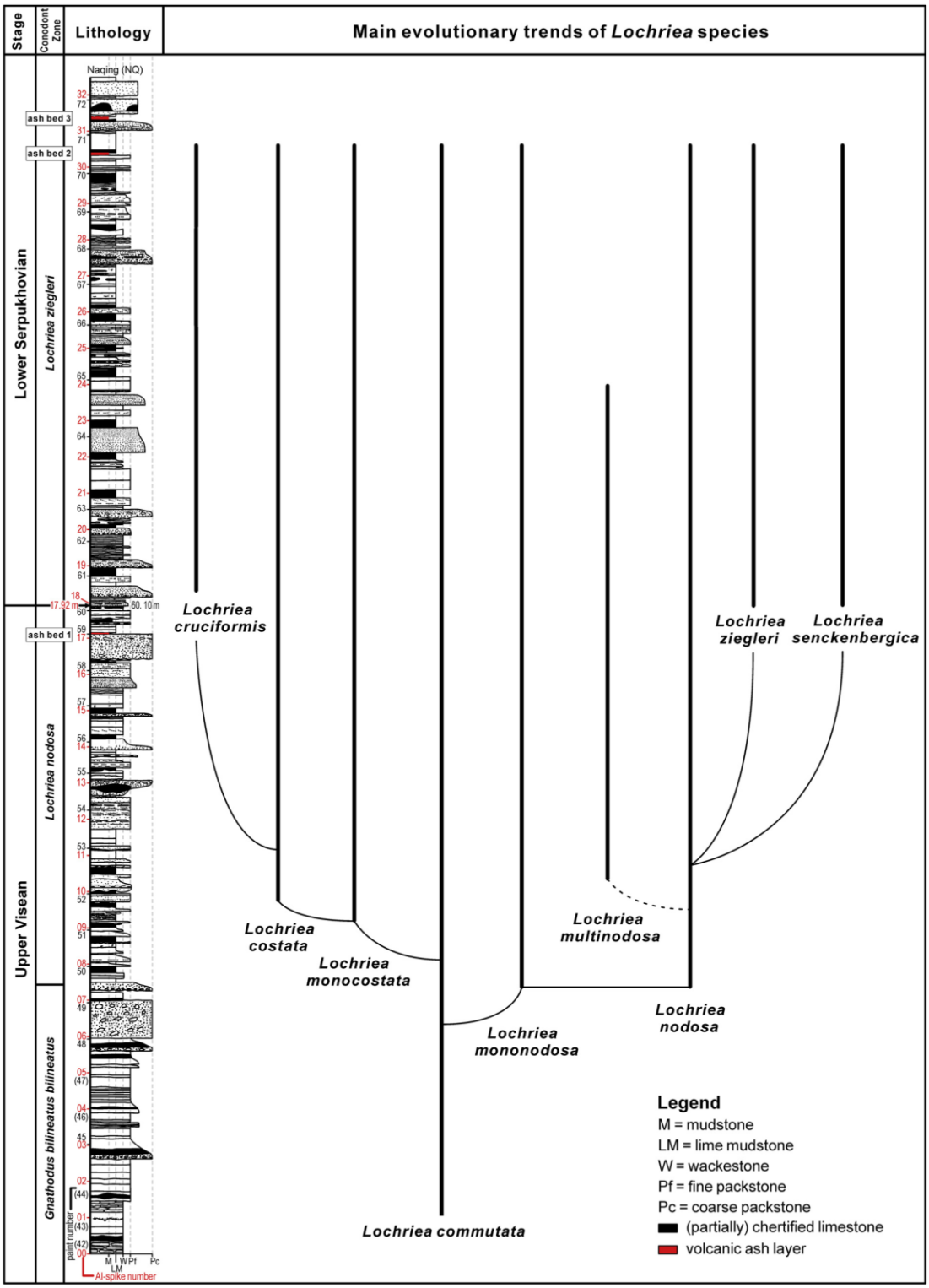

Fig. 3. Ranges of *Lochriea* species and their potential evolutionary relationships in the Visean–Serpukhovian boundary interval at the Naqing section.

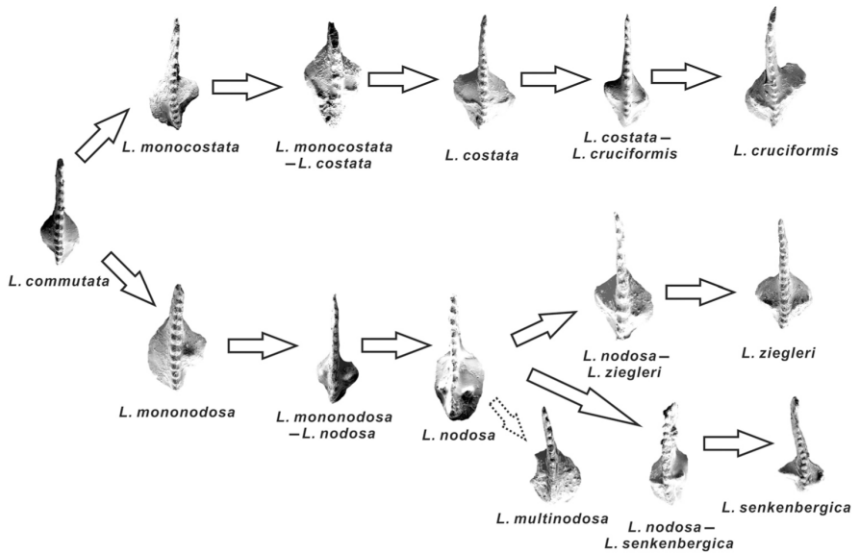

Fig. 4. Main evolutionary trends of *Lochriea* species from the Visean–Serpukhovian boundary interval at the Naqing section.

Lochriea commutata (Branson and Mehl, 1941)

Lochriea costata (Pazukhin and Nemirovskaya in Kulagina et al., 1992)

Lochriea cracoviensis (Belka, 1985)

Lochriea cruciformis (Clarke, 1960)

Lochriea monocostata (Pazukhin and Nemirovskaya in Kulagina et al., 1992)

Lochriea mononodosa (Rhodes, Austin and Druce, 1969)

Lochriea multinodosa (Wirth, 1967)

Lochriea nodosa (Bischoff, 1957)

Lochriea saharae Nemyrovska, Perret and Weyant, 2006

Lochriea senckenbergica (Nemirovskaya, Perret and Meischner, 1994)

Lochriea ziegleri (Nemirovskaya, Perret and Meischner, 1994)

Diagnosis: Platform elements of *Lochriea* consist of a subrectangular blade and carina and a low subcircular to subquadrate, slightly asymmetrical cup, positioned in most cases at the dorsal end of the element. Constituent species exhibits the change from a simple unornamented platform to a sculptured one bearing nodes or ridges. Laterally, the platform elements are rectangular in shape. The basal cavity is large and deep.

Remarks: *Lochriea* Scott differs from the closely related *Pseudognathodus* Park, 1983 by having much higher position of the platform sides and by the rectangular lateral shape of the platform.

Range: Visean–earliest Bashkirian worldwide.

Lochriea costata Pazukhin and Nemirovskaya in Kulagina et al., 1992

(Fig. 6I–P)

1969 *Gnathodus nodosus* – Rhodes et al., p. 104, pl. 19, figs. 16, 19, 20, non figs. 17, 18.
1975 *Paragnathodus nodosus* – Higgins, p. 72, pl. 7, figs. 15, 18, 19, non figs. 17, 22, 23.
1987 *Paragnathodus nodosus* – Wang et al., p. 131, pl. 1, figs. 4, 5, non fig. 3.
1992 *Paragnathodus costatus* – Pazukhin and Nemirovskaya in Kulagina et al., p. 88, pl. 29, figs. 9–12.
2009 *Lochriea costata* – Pazukhin in Nikolaeva et al., pl. 3, figs. 3, 5.
2010 *Lochriea costata* – Pazukhin et al., pl. 3, figs. 3, 5.
2014 *Lochriea costata* – Qi et al., fig. 5h.
2015 *Lochriea costata* – Barham et al., figs. 8.2, 8.4.

Diagnosis: "Platform is wide, almost symmetrical, with two large ridges on both sides of the platform (one on each side). The ridges are not fused with carina" (Pazukhin and Nemirovskaya in Kulagina et al., 1992, p. 88).

Description: P1 element with wide, rounded, subcircular, or subquadrate platform that extends inwards at the caudal side and in some specimens slightly ventralwards at the rostral side providing an asymmetrical shape of the platform. Carina consists of 7–9 denticles. Caudal and rostral parts of the platform bear ridges — one on each side. The ridges are commonly unequal; they vary in size, length and height. The ridge on the caudal side is always larger. The ridges can come close to the carina but they do not fuse with it. Sometimes the ridges consist of a row of elongated small fused nodes.

Remarks: *L. costata* is similar to *L. nodosa* and *L. cruciformis* but differs from the first by possessing ridges instead of nodes on both sides of the platform and from *L. cruciformis* by the lack of fusion of the ridges with the carina. *L. costata* probably was derived from *L. monocostata* by the appearance of a small node on the dorsal part of the platform, which later developed into a ridge. In turn, *L. costata* could give rise to *L. cruciformis* through the development of ridges fused with carina.

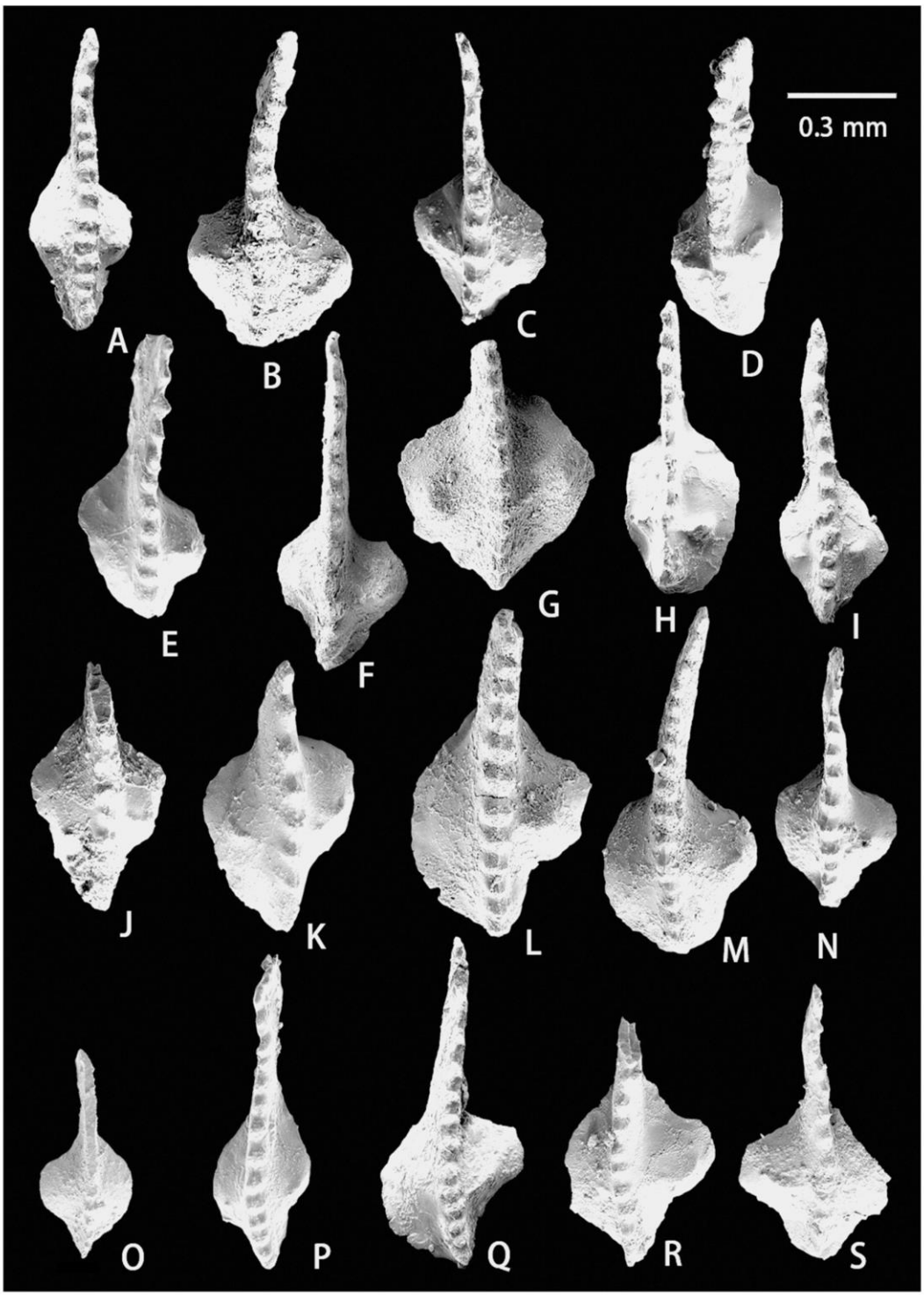

Fig. 5. Conodonts from the V–S boundary beds in the Naqing section. All illustrations in this paper are oral views of P1 elements; they are deposited in Nanjing Institute of Geology and Palaeontology, Chinese Academy of Sciences and listed with sampling horizons and catalogue numbers respectively below. (A, G–I) *Lochriea nodosa* (Bischoff, 1957); (A) NSC58.2 m, PZ161386; (G) NSC51.8 m, PZ161391; (H) NSC52.6 m, PZ161392; (I) NSC54.85 m, 155777. (B, C) Transitional elements between *Lochriea nodosa* (Bischoff, 1957) and *Lochriea ziegleri* Nemirovskaya, Perret and Meischner, 1994; (B) NSC51.8 m, PZ161387; (C) NSC59.15 m,

Range: Latest Visean–earliest Bashkirian of Europe and Asia.

Occurrence: Naqing section, 52.6 m (upper half of the Late Visean) through the earliest Bashkirian.

Lochriea cruciformis (Clarke, 1960)

(Fig. 7 D–G)

1960 *Gnathodus cruciformis* – Clarke, p. 25, pl. 4, figs. 10–12.
1967 *Gnathodus commutatus nodosus* – Wirth, fig. 9b–d.
1975 *Paragnathodus cruciformis* – Higgins, p. 71, pl. 7, fig. 10.
1983 *Paragnathodus cruciformis* – Nemirovskaya, pl. 1, fig. 11.
1993 *Paragnathodus cruciformis* – Perret, p. 288, pl. C9, figs. 12–14.
1994 *Lochriea cruciformis* – Nemirovskaya et al., pl. 1, fig. 13; pl. 2, fig. 13.
1995 *Lochriea cruciformis* – Skompski et al., pl. 2, fig. 8; pl. 3, fig. 10; pl. 4, fig. 16.
1996 *Lochriea cruciformis* – Skompski, pl. 3, figs. 6, 7.
1998 *Lochriea cruciformis* – Belka and Lehmann, pl. 4, fig. 4.
1999 *Lochriea cruciformis* – Nemyrovska, p. 74.
2002 *Lochriea cruciformis* – Pazukhin et al., pl. 1, fig. 8.
2005 *Lochriea cruciformis* – Nemyrovska and Samankassou, p. 41, pl. 8, fig. 2.
2009 *Lochriea cruciformis* – Kabanov et al., pl. 1, fig. 6 only.
2010 *Lochriea cruciformis* – Nigmadganov et al., pl. 3, figs. 2, 4.
2011 *Lochriea cruciformis* – Nemyrovska et al., pl. 2, fig. 4.
2014 *Lochriea cruciformis* – Qi et al., fig. 6c, d.
2015 *Lochriea cruciformis* – Barham et al., figs. 8.1, 8.3, 8.5.

Diagnosis: "*Gnathodus* with a short bowed blade, a sub-rectangular platform and an extremely large sub-circular escutcheon. Orally the unit is in the shape of a Celtic Cross" (Clarke, 1960, pp. 25–26). In the description of the species Clarke wrote: . . ."At each side" of the platform "stands a large node; the nodes being joined to carina by a transverse ridge, which is more prominent on the caudal half of the platform". Subsequent conodont workers slightly modified the concept of this species, and the most popular one is of Higgins (1975, p. 71): "Its oral surface bears two ridges, one on each side, which extends ventrally at a variable angle but is commonly 45°. The ridges usually consist of fused nodes. They often slope to the carina on their ventral face but are commonly almost vertical on their dorsal. They are fused to the carina in the dorsal half of the platform or about its midpoint either by a low ridge or directly by a node".

Revised diagnosis: P1 elements of *Lochriea* with an asymmetrical platform bearing two ridges or rows of nodes on each side of the platform. They are fused to the carina by a low ridge or directly by a node.

Description: P1 elements with round asymmetrical platform. Rostral part is subcircular. Caudal dorsal part extends inwards. Each side of the platform bears a large node or ridge, which is fused to the carina by a low thin ridge (Fig. 7E, G) or directly by a node. Some specimens have coarse ridges on both sides of the platform and these ridges are fused with carina (Fig. 7F). The ridges are fused to the carina in the dorsal part of the platform or about its midpoint and extend ventrally at the angle about 45–50°.

Remarks: *L. cruciformis* is close to *L. nodosa* and *L. costata* by having the platform ornamented by ridges or rows of nodes on both sides. It differs from *L. nodosa* and *L. costata* by the junction of lateral ridges or rows of nodes with the carina. This feature is most important in distinguishing *L. cruciformis* from the other coarsely ornamented species, such as *L. ziegleri*, *L. senckenbergica* and *L. multinodosa*. In our collection, there are also a number of specimens, which have either very weak difficult to see fusion of ridges to carina or a very weak connection observed only on one side of the platform. These are mostly in cases where the ornament of the platform is generally not very coarse; the ridges are thin, sometimes short. Some specimens show a transitional trend from *L. costata*. The tendency of specimens ornamented by nodes to develop the fusion with carina was not observed.

Range: Serpukhovian to earliest Bashkirian of Eurasia.

Occurrence: Naqing section, Serpukhovian to earliest Bashkirian (entry 60.60 m).

Lochriea monocostata Pazukhin and Nemirovskaya in Kulagina et al., 1992

(Fig. 5J, K, P–S)

1969 *Gnathodus mononodosus* – Rhodes et al., p. 103, pl. 19, fig. 13.
1975 *Paragnathodus mononodosus* – Higgins, pl. 7, fig. 14.
1992 *Paragnathodus monocostatus* – Pazukhin and Nemirovskaya in Kulagina et al., p. 88, pl. 29, figs. 5–8.
1994 *Lochriea monocostata* – Nemirovskaya et al., pl. 2, figs. 3, 4.
1995 *Lochriea monocostata* – Skompski et al., pl. 1, fig. 6.
2009 *Lochriea mononodosa* – Pazukhin in Nikolaeva et al., pl. 3, fig. 2.
2010 *Lochriea monocostata* – Pazukhin et al., pl. 3, fig. 2.
2014 *Lochriea monocostata* – Qi et al., fig. 5g.
2015 *Lochriea monocostata* – Barham et al., figs. 7.2, 7.6.

Diagnosis: P1 elements of *Lochriea* with a slightly asymmetrical platform and one ridge on the caudal side of the platform.

Description: P1 elements with asymmetrical platform that is oval to round in shape. Carina consists of 6–8 denticles, in some specimens it extends slightly beyond the dorsal tip of the platform. The rostral part of the platform is subcircular and flat; the caudal varies in shape from subcircular to subtriangular and extends dorsally inwards. It bears a single ridge, located near the mid-point of the platform or shifted dorsally. Upward in the

155786. (D) Transitional element between *Lochriea nodosa* (Bischoff, 1957) and *Lochriea senckenbergica* Nemirovskaya, Perret and Meischner, 1994, NSC52.6 m, PZ161388. (E, L–N) *Lochriea mononodosa* (Rhodes, Austin and Druce, 1969); (E) NSC62.5 m, PZ161389; (L) NSC49.5 m, PZ161395; (M) NSC51.8 m, PZ161396; (N) NSC60.6 m, PZ161397. (F) Transitional element between *Lochriea mononodosa* (Rhodes, Austin and Druce, 1969) and *Lochriea nodosa* (Bischoff, 1957), NSC49.5 m, PZ161390. (J, K) Transitional elements between *Lochriea monocostata* Pazukhin and Nemirovskaya in Kulagina et al., 1992 and *Lochriea costata* Pazukhin and Nemirovskaya in Kulagina et al., 1992; (J) NSC58.9 m, PZ161393; (K) NSC60.3m, PZ161394. (O) *Lochriea commutata* (Branson and Mehl, 1941), LD48.00 m, PZ161398. (P–S) *Lochriea monocostata* Pazukhin and Nemirovskaya in Kulagina et al., 1992; (P) NSC51.24 m, PZ161399; (Q) NSC52.8 m, PZ161400; (R) NSC60.6m, PZ161401; (S) NSC64.9 m, PZ161402.

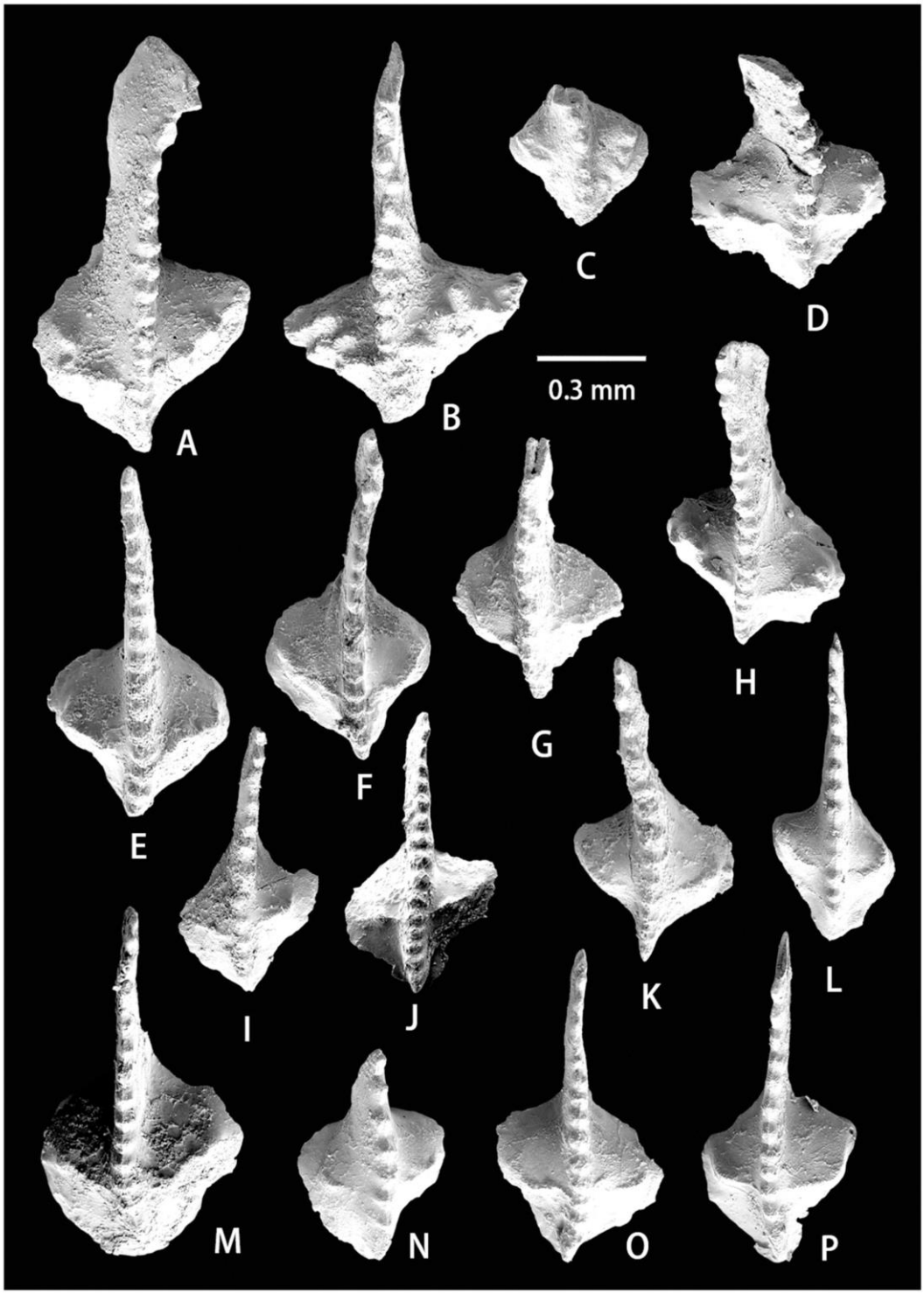

Fig. 6. Conodonts from the V–S boundary beds in the Naqing section. (A–H) *Lochriea ziegleri* Nemirovskaya, Perret and Meischner, 1994; (A) NSC63.7 m, PZ161403; (B) NSC68.9 m, 155781; (C) NSC70.3 m, PZ161404; (D) NSC63.0 m, PZ161405; (E, F) NSC60.1 m, PZ161406, PZ161407; (G) NSC60.6 m, PZ161408; (H) NSC62.5 m, 155780. (I, M–P) *Lochriea costata* Pazukhin and Nemirovskaya in Kulagina et al., 1992; (I) NSC63.0 m, PZ161409; (M) NSC51.8 m, PZ161413; (N) NSC60.3 m, PZ161414; (O) NSC60.3 m, 155775; (P) NSC60.3 m, PZ161415. (J–L) Transitional elements between *Lochriea costata* Pazukhin and Nemirovskaya in Kulagina et al., 1992 and *Lochriea ziegleri* Nemirovskaya, Perret and Meischner, 1994; (J) NSC52.6 m, PZ161410; (K) NSC60.1 m, PZ161411; (L) NSC67.8 m, PZ161412.

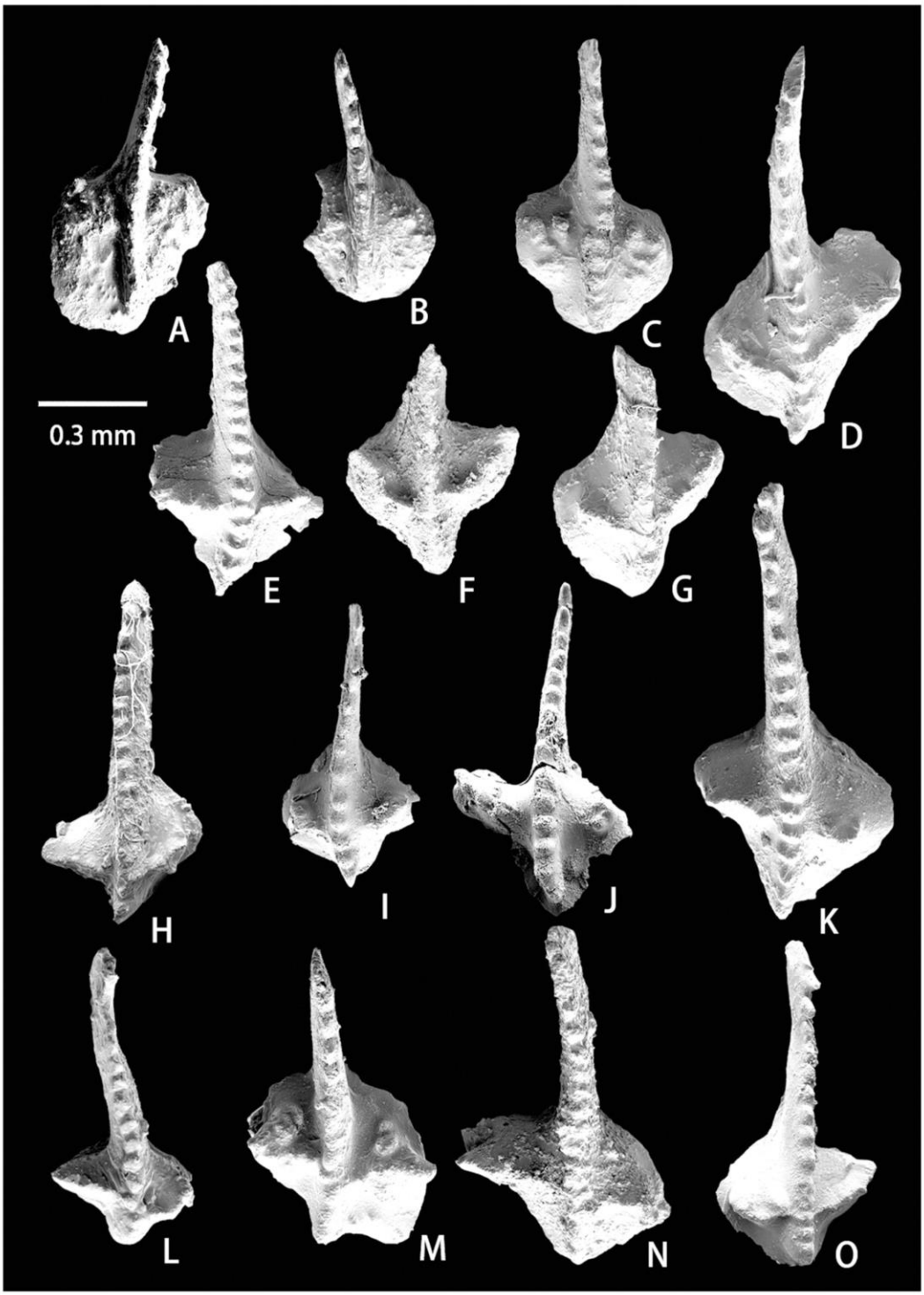

Fig. 7. Conodonts from the V–S boundary beds in the Naqing section. (A–C) *Lochriea multinodosa* (Wirth, 1967); (A) NSC52.3 m, PZ161416; (B) NSC52.8 m, PZ161417; (C) NSC63.7 m, 155776. (D–G) *Lochriea cruciformis* (Clarke, 1960); (D) NSC68.5 m, 155785; (E) NSC62.5 m, PZ161418; (F) NSC66.7 m, 155784; (G) NSC68.5 m, PZ161419. (H–J, L–O) *Lochriea senckenbergica* Nemirovskaya, Perret and Meischner, 1994; (H) NSC66.9 m, PZ161420; (I, J) NSC74.4 m, PZ161421, PZ161422; (L) NSC60.6 m, PZ161424; (M) NSC61.0 m, PZ161425; (N) NSC62.3 m, 155788; (O) NSC66.9 m, PZ161426. (K) Transitional element between *Lochriea nodosa* (Bischoff, 1957) and *Lochriea senckenbergica* Nemirovskaya, Perret and Meischner, 1994, NSC61.0 m, PZ161423.

section, it is close to the dorsal margin of the platform (60.6 m; 69.3 m). Specimens extend ventrally commonly at 45–50°. Platform ridges vary in length, height and thickness — from short and thin, to long and sometimes consisting of fused small denticles. In several specimens there is a tendency to connect to the carina (52.6 m).

Remarks: *L. monocostata* is very close to *L. mononodosa* but differs from the latter having a ridge but not a node on the caudal side of the platform. It probably gave rise to *L. costata*, which has ridges on both sides of the platform.

Range: Latest Visean–Serpukhovian of Urals and Moscow Syncline (Russia) and Western Europe (Ireland and Britain).

Occurrence: Naqing section, Late Visean (from 51.3 m) through the earliest Bashkirian.

Lochriea mononodosa (Rhodes, Austin and Druce, 1969)

(Fig. 5E, F, L–N)

1969 *Gnathodus mononodosus* – Rhodes et al., p. 103, pl. 19, figs. 14, 15 only.
1975 *Paragnathodus mononodosus* – Higgins, p. 71, pl. 7, fig. 14
1978 *Paragnathodus mononodosus* – Kozitskaya et al., pl. 13, figs. 1, 3.
1994 *Lochriea mononodosa* – Nemirovskaya et al., pl. 2, fig. 2.
1996 *Lochriea mononodosa* – Skompski, pl. 1, figs. 1, 2; pl. 3, fig. 8; pl. 4, figs. 5, 14.
2009 *Lochriea mononodosa* – Pazukhin in Nikolaeva et al., pl. 3, fig. 1.
2010 *Lochriea mononodosa* – Pazukhin et al., pl. 3, fig. 1.
2014 *Lochriea mononodosa* – Qi et al., fig. 5f.
2015 *Lochriea mononodosa* – Barham et al., figs. 7.5, 7.7.

Diagnosis: P1 element of *Lochriea* with slightly asymmetrical platform ornamented by one node on its caudal side.

Description: P1 elements with round to slightly asymmetrical platform. Rostral side of the platform is flat, caudal side bears a node, which varies in size. In Naqing there are mostly specimens with a small node located in the middle of the platform side or slightly shifted dorsally.

Remarks: *L. mononodosa* is closest to *L. monocostata*, but differs from the latter by having a node and not a ridge on the caudal side of the platform. From *L. nodosa* it differs by having one node on one side of the upper element.

Range: Late Visean–earliest Bashkirian of Eurasia.

Occurrence: Late Visean–earliest Bashkirian in the Naqing section (from 49.45 m).

Lochriea multinodosa (Wirth, 1967)

(Fig. 7A–C)

1962 *Gnathodus commutatus* var. *multinodosus* – Higgins, p. 8, pl. 2, figs. 13–16 only.
1967 *Gnathodus commutatus multinodosus* – Wirth, p. 208, pl. 19, figs. 19, 20.
1979 *Gnathodus commutatus multinodosus* – von Buchroithner, pl. 3, fig. 1.
1982 *Paragnathodus multinodosus* – Higgins and Wagner-Gentis, p. 335, pl. 34, figs. 13, 15 only.
1983 *Paragnathodus multinodosus* – Park, p. 125, pl. 4, fig. 22 only.
1993 *Paragnathodus multinodosus* – Perret, p. 291, pl. 109, figs. 19, 20, 27 only.
1994 *Lochriea multinodosa* – Nemirovskaya et al., p. 312, pl. 1, fig. 10.
1995 *Lochriea multinodosa* – Skompski et al., pl. 2, figs. 9–11.
1998 *Lochriea multinodosa* – Belka and Lehmann, pl. 3, figs. 1–4.
2005 *Lochriea multinodosa* – Nemyrovska and Samankassou, pl. 8, fig. 13.
2005 *Lochriea multinodosa* – Qi and Wang, pl. 1, fig. 11.
2013 *Lochriea multinodosa* – Ishida et al., p. 46, pl. 1, fig. 10 only.

Diagnosis: P1 elements of *Lochriea* with subcircular platform, both sides of which are covered by numerous small nodes.

Description: The platform is subcircular, slightly asymmetrical. Both sides of the platform are almost completely ornamented by numerous small nodes.

Remarks: P1 elements of *L. multinodosa* differ from those of the other species of *Lochriea* by platform sides being almost completely covered with numerous small nodes.

Range: Visean–Serpukhovian boundary interval in the Cantabrian Mountains (Spain), Pyrenees (Spain and France), South China and Japan.

Occurrence: Naqing section (52.3 m–64.8 m).

Lochriea nodosa (Bischoff, 1957)

(Figs. 5A–D, G–I, 7K)

1957 *Gnathodus commutatus nodosus* – Bischoff, p. 23, pl. 4, figs. 12, 13.
1967 *Gnathodus commutatus nodosus* – Wirth, p. 207, pl. 19, fig. 13 only.
1975 *Paragnathodus nodosus* – Higgins, p. 72, pl. 7, figs. 12, 17, 23 only.
1983 *Paragnathodus nodosus* – Park, p. 127, pl. 4, figs. 12, 17 only.
1992 *Paragnathathodus nodosus* – Pazukhin in Kulagina et al., pl. 29, fig. 13.
1994 *Lochriea nodosa* – Nemirovskaya et al., pl. 1, fig. 8.
1995 *Lochriea nodosa* – Skompski et al., pl. 1, figs. 3, 4; pl. 2, Fig. 4; pl. 3, figs. 1, 3, 6, 7, 9; pl. 4, fig. 4.
1996 *Lochriea nodosa* – Skompski, pl. 3, figs. 8, 9.
2005 *Lochriea nodosa* – Nemyrovska and Samankassou, p. 42, pl. 8, figs. 10, 15, 17.
2009 *Lochriea nodosa* – Pazukhin in Nikolaeva et al., pl. 3, fig. 4.
2014 *Lochriea nodosa* – Qi et al., fig. 5j.
2015 *Lochriea nodosa* – Barham et al., figs. 7.3, 7.4.

Diagnosis: P1 element of *Lochriea* with platform ornamented by single, large and massive elongated nodes on both sides of the platform (Bischoff, 1957).

Remarks: Meischner (1970, p. 1176) pointed out that "the earliest *L. nodosa* bear mostly very simple nodes but later the ornament is more complicated". By more complicated, he obviously meant at that time the coarser ornament of *L. ziegleri* and *L. senckenbergica*. This trend from simple nodes of the early *L. nodosa* to more complicated ornament upward in the section (closer to the V–S boundary) was recorded in the Naqing section. There are a number of transitional forms between *L. nodosa* and *L. senckenbergica* (Figs. 5 D, 7 K). More complicated ornament always starts on the caudal side of the platform.

L. nodosa differs from the close *L. costata* and *L. cruciformis* by having nodes and not ridges on the platform sides. It differs also from *L. cruciformis* by having nodes not connected to carina.

Range: Latest Visean–earliest Bashkirian of Eurasia.

Occurrence: Latest Visean through earliest Bashkirian in the Naqing section (entry 49.5 m).

Lochriea senckenbergica Nemirovskaya, Perret and Meischner, 1994

(Fig. 7H–J, L–O)

1994 *Lochriea senckenbergica* – Nemirovskaya et al., p. 313, pl. 1, fig. 5; pl. 2, figs. 7–10, 12.

1995 *Lochriea senckenbergica* – Skompski et al., pl. 2, figs. 1–3, 5, 6; pl. 3, fig. 13; pl. 4, figs. 8, 10–12.

2014 *Lochriea senckenbergica* – Qi et al., fig. 6f, g.

Diagnosis: P1 elements with "the platform ornamented with high, thick and steep bars on both sides of the ventral platform. Caudal bar much higher than the rostral one and the carina" (Nemirovskaya et al., 1994).

Remarks: *L. senckenbergica* has the coarsest ornament of the platform among the other species of *Lochriea*. It differs from the close *L. ziegleri* by its large and high bars located slightly ventral of the center of the platform. *L. ziegleri* has its coarse ornament close to the dorsal margin of the platform.

Range: Serpukhovian of Germany (Rhenish Mountains), Ireland (County Clare), northern England (Cumbria), Poland (Lublin Basin) and Ukraine (Lvov-Volhyn Basin) and Spain (Esla area, Leon and Palencia).

Occurrence: Naqing section, Sepukhovian to earliest Bashkirian (entry 60.1 m).

Lochriea ziegleri Nemirovskaya, Perret and Meischner, 1994

(Fig. 6A–H)

1962 *Gnathodus commutatus* var. *multinodosus* – Higgins, pl. 2, figs. 17, 18 only.

1967 *Gnathodus commutatus nodosus* – Wirth, pl. 19, figs. 14, 17 only.

1978 *Paragnathodus nodosus* – Kozitskaya et al., pl. 13, figs. 7, 8.

1983 *Paragnathodus* sp. 1 – Nemirovskaya, pl. 1, figs. 15, 19.

1994 *Lochriea ziegleri* – Nemirovskaya et al., p. 312, pl. 1, figs. 1–4, 6, 7, 11, 12; pl. 2, fig. 11 (see synonyms).

1995 *Lochriea ziegleri* – Skompski et al., pl. 1, figs. 5, 7–9, 11, 12; pl. 2, figs. 7, 10; pl. 3, figs. 2, 4, 5, 11, 14; pl. 4, figs. 6, 7, 9, 13, 15.

1996 *Lochriea ziegleri* – Skompski, pl. 3, figs. 1–3.

1998 *Lochriea ziegleri* – Belka and Lehmann, p. 4, figs. 6, 7.

1999 *Lochriea ziegleri* – Nemyrovska, pl. 1, fig. 6.

2005 *Lochriea ziegleri* – Nemyrovska and Samankassou, p. 45, pl. 8, figs. 11, 14, 16.

2005 *Lochriea ziegleri* – Qi and Wang, pl. 1, figs. 14, 15, 17, 18.

2008 *Lochriea ziegleri* – Kullmann et al., pl. 8, figs. 2, 6, 8.

2009 *Lochriea ziegleri* – Pazukhin in Nikolaeva et al., pl. 3, fig. 6.

2010 *Lochriea ziegleri* – Nigmadganov et al., pl. 3, fig. 3.

2011 *Lochriea ziegleri* – Nemyrovska et al., p. 161, pl. 2, figs. 3, 5, 16.

2014 *Lochriea ziegleri* – Qi et al., fig. 5l–n.

2015 *Lochriea ziegleri* – Barham et al., figs. 8.6–8.10.

Diagnosis: P1 elements are ornamented by large discrete or partly fused nodes located on ridge-like elevations (bars) or thick long ridges on both sides of the platform close to the dorsal margin.

Description: The platform is subcircular to subquadrate in shape. Ventral part of the platform is mostly subcircular while the dorsal part varies in shape. The outline is asymmetrical because of the concave dorsal-caudal margin. The oral surface of the platform is ornamented by large, partly fused or less common discrete nodes located on thick long ridges or bars close to the dorsal margin of the platform. Long ridges or bars do not join carina. They are higher and thicker commonly at the caudal part of the platform. The platform is rectangular in lateral view.

Remarks: *L. ziegleri* differs from the more simply ornamented *L. nodosa* and *L. costata* by a much coarser and prominent ornament of the platform and the dorsal location of bars or ridges in comparison to the more central position of nodes or ridges in *L. nodosa* and *L. costata*. The latter feature distinguishes *L. ziegleri* from the other coarsely ornamented *Lochriea* species such as *L. cruciformis* and *L. senckenbergica*. In addition, *L. ziegleri* differs from *L. cruciformis* by having more complicated ridges or bars not connected to the carina. *L. ziegleri* differs from *L. senckenbergica* by having lower ridges or bars decorated by partly fused nodes that are not as prominent and as high as more ventrally located bars in *L. senckenbergica*. *L. ziegleri* differs from *L. multinodosa* by differences in ornament of the platform; small nodes cover both sides of the platform of *L. multinodosa*. In our collections there are many specimens with partly or completely fused nodes on the bars.

There are many transitional forms between *L. costata* and *L. ziegleri* (Fig. 6J–L) as well as forms intermediate between *L. ziegleri* and *L. senckenbergica* (Fig. 7H–J). Some specimens show intermediate features between *L. nodosa* and *L. ziegleri* (Fig. 5B, C), such as elongated ridge-like elevations (bars) with nodes on them on one side of the platform and few discrete nodes or a row of nodes on the other side. The majority of transitional forms with ridge-like elevations on both sides of the platform and forms with nodes on at least one side of the platform need further investigation to understand their evolutionary relationships.

Range: Serpukhovian to earliest Bashkirian in Eurasia. Serpukhovian of the Rhenish Mountains (Germany). Rare in North America — only one specimen is identified.

Occurrence: Naqing section, Serpukhovian to earliest Bashkirian (entry 60.1 m).

Acknowledgements

Wen-Kun Qie (Nanjing Institute of Geology and Palaeontology, Nanjing, China) assisted with geological setting information. Ji-Tao Chen (Nanjing Institute of Geology and Palaeontology, Nanjing, China) reviewed an early version of this work. We thank Milo Barham (Curtin University of Technology, Perth, Australia) and another anonymous reviewer for their valuable comments that greatly improved the quality of this manuscript. This work was supported by National Natural Science Foundation of China (grant nos. 41630101, 41290260, 41372023), the Strategic Priority Research Program of Chinese Academy of Sciences (grant no. XDB26000000), and Ministry of Science and Technology of China (grant no. 2015FY310100).

References

Atakul-özdemir, A., Purnell, M.A., Riley, N.J., 2012. Cladistic tests of monophyly and relationships of biostratigraphically significant conodonts using

multielement skeletal data — *Lochriea homopunctatus* and the genus *Lochriea*. Palaeontology 55, 1279–1291.

Austin, R.L., Husri, S., 1974. Dinantian conodont faunas of County Clare, County Limerick and County Leitrim, An Appendix. In: Bouckaert, J., Streel, M. (Eds.), International Symposium on Belgian Micropaleontological Limits – Namur 1974. Geological Survey of Belgium, Brussels, pp. 18–69.

Barham, M., Murray, J., Sevastopulo, G.D., Williams, D.M., 2015. Conodonts of the genus *Lochriea* in Ireland and the recognition of the Visean–Serpukhovian (Carboniferous) boundary. Lethaia 48, 151–171.

Belka, Z., 1985. Lower Carboniferous conodont biostratigraphy in the northern part of the Moravia–Silesia Basin. Acta Geologica Polonica 35, 1–60.

Belka, Z., Lehmann, J., 1998. Late Visean/early Namurian conodont succession from the Esla area of the Cantabrian Mountains. Acta Geologica Polonica 48, 31–41.

Bischoff, G., 1957. Die Conodonten-Stratigraphie des rheno-herzynischen Unterkarbons mit Berücksichtigung der Wocklumeria-Stufe und der Karbon/Devon-Grenze. Abhandlungen des Hessischen Landesamtes für Bodenforschung 19, 1–64 (in German).

Blanco-Ferrera, S., Sanz-Lopez, J., Garcia-Lopez, S., Bastida, F., 2009. Visean to Serpukhovian (Carboniferous) occurrences of Lochriea species at the Vegas de Sotres section (Cantabrian Mountains, Spain). Permophiles 53, 9–10.

Branson, E.B., Mehl, M.G., 1941. New and little known Carboniferous genera. Journal of Paleontology 15, 97–106.

Chen, J.T., Montanez, I.P., Qi, Y.P., Wang, X.D., Wang, Q.L., Lin, W., 2016. Coupled sedimentary and $\delta^{13}C$ records of late Mississippian platform-to-slope successions from South China: Insight into $\delta^{13}C$ chemostratigraphy. Palaeogeography, Palaeoclimatology, Palaeoecology 448, 162–178.

Clarke, W.J., 1960. Scottish Carboniferous conodonts. Transactions of the Edinburgh Geological Society 18, 1–31.

Feng, Z.Z., Yang, Y.Q., Bao, Z.D., 1999. Lithofacies palaeogeography of the Carboniferous in South China. Journal of Palaeogeography 1, 75–86 (in Chinese).

Gibshman, N.B., 2001. Foraminiferal biostratigraphy of the Serpukhovian Stage stratotype (Zaborie quarry, Moscow Basin). Newsletter on Carboniferous Stratigraphy 19, 31–34.

Groves, J.R., Wang, Y., Qi, Y.P., Richards, B.C., Ueno, K., Wang, X.D., 2012. Foraminiferal biostratigraphy of the Visean–Serpukhovian (Mississippian) boundary interval at slope and platform sections in southern Guizhou (South China). Journal of Paleontology 86, 753–774.

Heckel, P.H., 2002. Chairman's column. Newsletter on Carboniferous Stratigraphy 20, 1–2.

Heckel, P.H., 2004. Chairman's column. Newsletter on Carboniferous Stratigraphy 22, 1–3.

Higgins, A.C., 1961. Some Namurian conodonts from North Staffordshire. Geological Magazine 98, 219–224.

Higgins, A.C., 1962. Conodonts of the Griotte Limestone of north-west Spain. Notas y Comunicaciones del Instituto Geológico y Minero de España 65, 5–22.

Higgins, A.C., 1975. Conodont zonation of the Late Visean–Early Westphalian strata of the south and central Pennines of northern England. Bulletin of Geological Survey of Great Britain 53, 1–90.

Higgins, A.C., Wagner-Gentis, C.H.T., 1982. Conodonts, goniatites and biostratigraphy of the earlier Carboniferous from the Cantabrian Mountains. Spain. Palaeontology 25, 313–350.

Ishida, K., Suzuki, S., Inada, N., 2013. Visean–Moscovian conodont biostratigraphy of the Ko-yama Limestone Group, Akiyoshi Belt, SW Japan. Natural Science Research, University of Tokushima 27, 29–52.

Kabanov, P.B., Gibshman, N.B., Barskov, I.S., Alekseev, A.S., Goreva, N.V., 2009. Zaborie section lectostratotype of Serpukhovian Stage. In: Alekseev, S., Goreva, N.N. (Eds.), Type and Reference Carboniferous Sections in the South Part of the Moscow Basin. Borissiak Paleontological Institute of Russian Academy of Sciences, August 11–12, 2009, Field Trip Guidebook, pp. 45–64.

Kaiser, S.I., 2009. The Devonian/Carboniferous boundary stratotype section (La Serre, France) revisited. Newsletters on Stratigraphy 43, 195–205.

Kozitskaya, R.I., Kossenko, Z.A., Lipnjagov, O.M., Nemirovskaya, T.I., 1978. Konodonty karbona Donetskogo baseina [Carbonifeous conodonts of the Donets Basin]. Naukova Dumka, Academy of Sciences of Ukraine, Kiev, 120 pp. (in Russian).

Kulagina, E.I., Rumyantseva, Z.S., Pazukhin, V.N., Kotchetkova, N.M., 1992. Granitsa nizhnego–srednego karbona na Yuzhnom Urale I Srednem Tyanshane [Lower/Middle Carboniferous Boundary at South Urals and Middle Tianshan]. Nauka, Moscow, 112 pp. (in Russian).

Kullmann, J., Perret, M.-F., Delvove, J.J., 2008. Late Visean–Serpukhovian goniatites and conodonts from the Central and Western Pyrenees, France. Geobios 41, 635–656 (in French).

Lane, H.R., Brenckle, P.L., 2005. Type Mississippian subdivisions and biostratigraphic succession. In: Heckel, P.H. (Ed.), Stratigraphy and Biostratigraphy of the Mississippian Subsystem (Carboniferous System) in Its Type Region, the Mississippi River Valley of Illinois, Missouri, and Iowa. I.U.G.S. Subcommission on Carboniferous Stratigraphy Guidebook for Field Conference, 8–13 September 2001, St. Louis. Illinois State Geological Survey Guidebook 34, 76–105.

Lane, H.R., Brenckle, P.L., Baesemenn, J.F., Richards, B.C., 1999. IUGS Carboniferous in the middle of the Carboniferous Arrow Canyon, Nevada, USA. Episodes 22, 272–283.

Meischner, D., 1970. Conodonten-Chronologie des deutschen Karbons. Compte Rendu VI Congrès International du Stratigraphie et Géologie du Carbonifère, Sheffield 1967, 1169–1180 (in French).

Nemirovskaya, T.I., 1983. Konodonty serpukhovskikh I nizhnebashkirskikh otlozhenij Dnieprovsko-Donetskoj vpadiny [Serpukhovian and early Bashkirian conodonts of the Dnieper-Donets Depression]. Izvestiya Akademii Nauk SSSR, Seriya Geologicheskaya 11, 59–69 (in Russian).

Nemirovskaya, T.I., Perret, M.-F., Meischner, D., 1994. *Lochriea ziegleri* and *Lochriea senckenbergica* — new conodont species from the latest Visean and Serpukhovian in Europe. Courier Forschungsinstitut Senckenberg 168, 311–317.

Nemyrovska, T.I., 1999. Bashkirian conodonts of the Donets Basin. Scripta Geologica 119, 1–115.

Nemyrovska, T.I., Samankassou, E., 2005. Late Visean/early Serpukhovian conodont succession from the Triollo section, Palencia (Cantabrian Mountains, Spain). Scripta Geologica 129, 13–89.

Nemyrovska, T.I., Perret, M.-F., Weyant, M., 2006. The early Visean (Carboniferous) conodonts from the Saoura Valley, Algeria. Acta Geologica Polonica 56, 361–370.

Nemyrovska, T.I., Wagner, R.H., Prins-Winkler, C.F., Montanez, I., 2011. Conodont faunas across the mid-Carboniferous boundary from the Barcaliente Formation at La Lastra (Palentian Zone, Cantabrian Mountains, northwest Spain); geological setting, sedimentological characters and faunal descriptions. Scripta Geologica 143, 127–183.

Nigmadganov, I.M., Nikolaeva, S.V., Konovalova, V.A., Orlov-Labkovsky, O., 2010. Integrated ammonoid, conodont and foraminiferal stratigraphy in the Paltau Section Middle Tienshan, Uzbekistan. Newsletter on Carboniferous Stratigraphy 28, 50–60.

Nikitin, S.N., 1890. Carboniferous deposits of the Moscow region and artesian waters near Moscow. Trudy Geologicheskogo Komiteta 5, 1–182 (in Russian).

Nikolaeva, S.V., Kulagina, E.I., Pazukhin, V.I., Kucheva, N.A., Stepanova, T.I., Kochetova, N.N., Gibshman, N.B., Amon, E.O., Konovalova, V.A., Zainakaeva, G.F., 2005. Advances in the understanding of the Visean–Serpukhovian boundary in the South Urals and its correlation. Newsletter on Carboniferous Stratigraphy 23, 27–30.

Nikolaeva, S.V., Kulagina, E.I., Pazukhin, V.N., Kochetova, N.N., Konovalova, V.A., 2009. Paleontology and microfacies of the Serpukhovian in the Verkhnyaya Kaidailovka section, South Urals, Russia, potential candidate for the GSSP for the Visean–Serpukhovian boundary. Newsletters on Stratigraphy 43, 165–193.

Norby, R.D., 1976. Conodont apparatuses from Chesterian (Mississippian) strata of Montana and Illinois. PhD Thesis, University of Illinois at Urbana-Champaign, 305 pp.

Paproth, E., Conil, R., Bless, M.J.M., Boonen, P., Carpentier, N., Coen, M., Delcambre, B., Deprijck, C.H., Deuzon, S., Dreesen, R., Groessens, E., Hance, L., Hennebert, M., Hibo, D., Hahn, G.R., Hislaire, O., Kasig, W., Laloux, M., Lauwers, A., Lees, A., Lys, M., de Beek, O.P., Overlau, P., Pirlet, H., Poty, E., Ramsbottom, W., Streel, M., Swennen, R., Thorez, J., Vanguestaine, M., van

Steenwinkel, M., Vieslet, J.L., 1983. Bio- and lithostratigraphic subdivisions of the Dinantian in Belgium, a review. Annales de la Societe Geologique de Belgique 106, 185–283.

Paproth, E., Feist, R., Flajs, G., 1991. Decision on the Devonian–Carboniferous boundary stratotype. Episodes 14, 331–336.

Park, S.I., 1983. Zonenfolge, Phylogenie und Taxonomie karbonischer Conodonten zwischen Tournai und Westfal (Westeuropa). PhD Thesis, Philipps-Universität Marburg, 187 pp. (in German) .

Pazukhin, V.N., Kulagina, E.I., Nikolaeva, S.V., Kochetova, N.N., Konovalova, V.A., 2002. Zonal'noe rasch-lenenie verkhnevizeiskikh I serpukhovskikh otlozheniy v razreze Verkhnyaya Kardailovka (vostochny srlon Yuzhnogo Urala) [Zonal subdivision of Upper Visean and Serpukhovian in the Verkhnyaya Kardailovka section (eastern slope of the Southern Urals)]. In: Chuvashov, B.I., Amon, E.O. (Eds.), Stratigrafiya i paleogeografiya karbona Yevrazii [Carboniferous Stratigraphy and Palaeogeography in Eurasia]. Institute of Geology and Geochemistry, Ural Branch of the Russian Academy of Sciences, Ekaterinburg, pp. 220–229 (in Russian).

Pazukhin, V.N., Kulagina, E.I., Nikolaeva, S.V., Kochetova, N.N., Konovalova, V.A., Zainakaeva, L.Z., 2009. Substantiation of the Serpukhovian Lower Boundary in the Verkhnyaya Kardailovka Section as a Candidate for GSSP. In: Puchkov, V.N., Kulagina, E.I., Nikolaeva, S.V., Kochetova, N.N. (Eds.), Carboniferous Type Sections in Russia and Potential Global Stratotypes, Proceedings of the International Field Meeting, Southern Urals Session, Ufa–Sibai, August 13–18, 2009. Design Poligraph Service, Ufa, pp. 129–141 (in Russian).

Pazukhin, V.N., Kulagina, E.I., Nikolaeva, S.V., Kochetova, N.N., Konovalova, V.A., 2010. The Serpukhovian Stage in the Verkhnyaya Kardailovka Section, South Urals. Stratigraphy and Geological Correlation 18, 269–289.

Perret, M.F., 1993. Recherches micropaléontologiques et biostratigraphiques (Conodontes-Foraminifères) dans le Carbonifère Pyrénéen. Strata 21, 1–597 (in French).

Purnell, M.A., Donoghue, P.C.J., 1998. Skeletal architecture, homologies and taphonomy of Ozarkodinid conodonts. Palaeontology 41, 57–102.

Qi, Y.P., 2008. Conodont biostratigraphy of the candidate GSSP's for the base of the Serpukhovian Stage and Moscovian Stage in the Naqing (Nashui) section, Luosu, Luodian, Guizhou, South China. PhD Thesis, Graduate School of Chinese Academy of Sciences, 157 pp. (in Chinese, with English summary).

Qi, Y.P., Wang, Z.H., 2005. Serpukhovian conodont sequence and the Visean–Serpukhovian boundary in South China. Rivista Italiana di Paleontologia e Stratigrafia 111, 3–10.

Qi, Y.P., Wang, X.D., Wang, Z.H., Lane, H.R., Richards, B.C., Ueno, K., Groves, J.R., 2009. Conodont biostratigraphy of the Naqing (Nashui) section in South China: candidate GSSPs for both the Serpukhovian and Moscovian Stages. Permophiles 53, 39–40.

Qi, Y.P., Wang, X.D., Richards, B.C., Groves, J.R., Ueno, K., Wang, Z.H., Wu, X.H., Hu, K.Y., 2010. Recent progress on conodonts and foraminifers from the candidate GSSP of the Carboniferous Visean–Serpukhovian boundary in the Naqing (Nashui) section of south China. In: Wang, X.D., Qi, Y.P., Groves, J.R., Barrick, J.E., Nemirovskaya, T.I., Ueno, K., Wang, Y. (Eds.), Carboniferous Carbonate Succession from Shallow Marine to Slope in Southern Guizhou. Field Excursion Guidebook for the SCCS Workshop on GSSPs of the Carboniferous System. Nanjing Institute of Geology and Palaeontology, Chinese Academy of Sciences, Nanjing, pp. 35–64.

Qi, Y.P., Nemyrovska, T.I., Wang, X.D., Chen, J.T., Wang, Z.H., Lane, H.R., Richards, B.C., Hu, K.Y., Wang, Q.L., 2014. Late Visean–Early Serpukhovian conodont succession at the Naqing (Nashui) section in Guizhou, south China. Geological Magazine 151, 254–268.

Rexroad, C.B., 1957. Conodonts from the Chester Series in the type area of southwestern Illinois. Illinois State Geological Survey, Report of Investigation 199, 1–43.

Rhodes, F.H.T., Austin, R.L., Druce, E.C., 1969. British Avonian (Carboniferous) conodont faunas, and their value in local and intercontinental correlation. Bulletin of the British Museum (Natural History). Geology (Supplement 5), 1–313.

Richards, B.C., Task Group, 2003. Progress report from the Task Group to establish a GSSP close to the existing Visean–Serpukhovian boundary. Newsletter on Carboniferous Stratigraphy 21, 6–10.

Richards, B.C., Task Group, 2005. The Viséan–Serpukhovian boundary: a summary of progress made on research goals established at the XV ICCP Carboniferous Workshop in Utrecht. Newsletter on Carboniferous Stratigraphy 23, 7–8.

Richards, B.C., Task Group, 2009. Report of the Joint Devonian–Carboniferous Boundary GSSP Reappraisal Task Group. Newsletter on Carboniferous Stratigraphy 27, 7–9.

Richards, B.C., Task Group, 2010. Report of the Task Group to establish a GSSP close to the existing Viséan–Serpukhovian boundary. Newsletter on Carboniferous Stratigraphy 28, 30–34.

Richards, B.C., Task Group, 2014. Report of the Task Group to establish a GSSP close to the existing Visean–Serpukhovian Boundary. Newsletter on Carboniferous Stratigraphy 31, 29–33.

Rygel, M.C., Fielding, C.R., Frank, T.D., Birgenheier, L.P., 2008. The magnitude of Late Paleozoic glacioeustatic fluctuations: a synthesis. Journal of Sedimentary Research 78, 500–511.

Scott, H.W., 1942. Conodont assemblage from the Heath Formation, Montana. Journal of Paleontology 16, 293–300.

Sevastopulo, G.D., Barham, M., 2014. Correlation of the base of the Serpukhovian Stage (Mississippian) in NW Europe. Geological Magazine 152, 244–253.

Sheng, Q.Y., 2016. Mississippian foraminifers from South China. PhD Thesis, University of Chinese Academy of Sciences, 285 pp. (in Chinese, with English summary).

Skompski, S., 1996. Stratigraphic position and facies significance of the limestone bands in the subsurface Carboniferous succession of the Lublin Upland. Acta Geologica Polonica 46, 171–268.

Skompski, S., Alekseev, A., Meischner, D., Nemirovskaya, T., Perret, M.-F., Varker, W.J., 1995. Conodont distribution across the Viséan/Namurian boundary. Courier Forschungsinstitut Senckenberg 188, 177–209.

Varker, W.J., 1993. Multielement conodont faunas from the proposed mid-Carboniferous boundary stratotype locality at Stonehead Beck Cowling, North Yorkshire, England. Annales de la Société Géologique de Belgique 116, 301–321.

von Buchroithner, M.F., 1979. Die Conodonten-Chronologie im Karbon der Pyrenaën. Mitteilungen der Österreichischen Geologischen Geselschaft 70, 75–118 (in German).

Wang, Q.L., Korn, D., Nemyrovska, T., Qi, Y.P., 2018. The Wenne river bank section — an excellent section for the Viséan–Serpukhovian boundary based on conodonts and ammonoids (Mississippian; Rhenish Mountains, Germany). Newsletters on Stratigraphy 51 (4), 427–444.

Wang, Z.H., Qi, Y.P., 2003. Report on the Upper Visean–Serpukhovian conodont zonation in South China. Newsletter on Carboniferous Stratigraphy 21, 22–24.

Wang, Z.H., Lane, H.R., Manger, W.L., 1987. Carboniferous and Early Permian conodont zonation of North and Northwest China. Courier Forschungsinstitut Senckenberg 98, 119–157.

Wirth, M., 1967. Zur Gliederung des höheren Paläozoikums (Givet–Namur) im Gebiet des Quinto Real (Westpyrenäen) mit Hilfe vn Conodonten. Neues Jahrbuch für Geologie und Paläontologie, Abhandlungen 127, 179–224 (in German).

Work, D.M., 2008. Secretary/Editor's Report 2007-2008. Newsletter on Carboniferous Stratigraphy 26, 4.

Springer Geology

Mingguo Zhai *Editor*

Precambrian Geology of China

Springer

Formation and Evolution of Archean Continental Crust of the North China Craton

Yu-Sheng Wan, Dun-Yi Liu, Chun-Yan Dong, Hang-Qian Xie, Alfred Kröner, Ming-Zhu Ma, Shou-Jie Liu, Shi-Wen Xie and Peng Ren

Abstract The North China Craton (NCC) has had a long geological history back to ca. 3.8 Ga ago. In the Anshan area, northeastern part of the craton, three distinct complexes with ages of 3.8–3.1 Ga (Baijiafen, Dongshan, and Shengousi) have been identified, along with widespread 3.1–2.5 Ga rocks of different origins and ages. In eastern Hebei Province, abundant 3.88–3.4 Ga detrital zircons were obtained from metasedimentary rocks of the Caozhuang Complex, and the oldest rock identified is a 3.4 Ga gneissic quartz diorite. The oldest zircons that may originally have been derived from the NCC are 4.1–3.9 Ga grains in Paleozoic volcano-sedimentary rocks in the northern Qinling Orogenic Belt bordering the NCC in the south. 3.0–2.8 Ga rocks occur in Anshan, eastern Hebei, eastern Shandong, and Lushan. ca. 2.7 Ga rocks of igneous origin are exposed in eight areas of the NCC, but ~2.7 Ga supracrustal rocks have so far only been identified in western Shandong. ca. 2.5 Ga intrusive and supracrustal rocks and associated regional metamorphism occur in almost all Archean areas of the NCC. Banded iron formations contain the most important ore deposit of the Archean in the NCC and mainly formed during the late Neoarchean. Ancient crustal records obtained from deep crust beneath the NCC are similar to those in the exposed areas, with the oldest ca. 3.6 Ga rock enclaves occurring in Xinyang near the southern margin of the NCC. This synthesis is based on the compilation of a large database of zircon ages as well as whole-rock Nd isotopic and Hf-in-zircon isotopic data in order to understand the formation and evolution of the early Precambrian basement of the NCC. Considering the craton as an entity, there is a continuous age record from 3.8 to 1.8 Ga, and two tectono-thermal events are most significant in the late Neoarchean to the earliest Paleoproterozoic and late Paleoproterozoic history, with age peaks at ~2.52 and ~1.85 Ga, respectively. Whole-rock Nd and Hf-in-zircon isotopic data show similar features, documenting the addition of juvenile material to the continental crust at 3.8–3.55, 3.45, 3.35–3.3, 2.9, and 2.85–2.5 Ga with the late

Y.-S. Wan (✉) · D.-Y. Liu · C.-Y. Dong · H.-Q. Xie · A. Kröner · M.-Z. Ma · S.-J. Liu
S.-W. Xie · P. Ren
Beijing SHRIMP Center, Institute of Geology, Chinese Academy of Geological Sciences,
26 Baiwanzhuang Road, Beijing 100037, China
e-mail: wanyusheng@bjshrimp.cn

M. Zhai (ed.), *Precambrian Geology of China*,
Springer Geology, DOI 10.1007/978-3-662-47885-1_2

Mesoarchean to early Neoarchean being the most important period. Crustal recycling began as early as 3.8 Ga and continued until 3.25 Ga and appears to have played a more important role than juvenile additions between 3.25 and 2.90 Ga. After outlining the general geological history of the NNC basement, we discuss several issues relating to Archean crust formation and evolution and arrive at the following major conclusions: (1) Similar to several other cratons, the late Mesoarchean to early Neoarchean was the most important period for rapid production of continental crust, and the most intensive and widespread tectono-thermal event occurred at the end of the Neoarchean. (2) In our new tectonic model, we define and outline three ancient terranes containing abundant 3.8–2.6 Ga rocks, namely the Eastern Ancient Terrane, Southern Ancient Terrane, and Central Ancient Terrane. (3) Vertical magmatic growth is seen as the main mechanism of crust formation prior to the Mesoarchean. We favor a multi-island arc model related to subduction/collision and amalgamation of different ancient terranes in the late Neoarchean. (4) The NCC may already have been a large crustal unit as a result of cratonic stabilization at the end of the late Neoarchean, probably due to magmatic underplating.

Keywords North China Craton · Archean · Magmatism · Metamorphism · Zircon dating · Nd–Hf isotopes

1 Introduction

The North China Craton (NCC) is one of the largest cratons in the eastern Eurasian continent with a total area of 300,000 km^2. It has a triangular shape and is surrounded by young orogenic belts in the north and south, and faces the Pacific Ocean in the east. The major tectonic structures are cut off by the craton boundary, and this suggests that the NCC is a fragment of a once larger craton (Li et al. 2000). It is one of a few areas on the Earth where >3.8 Ga rocks have been identified (Liu et al. 1992; Song et al. 1996; Wan et al. 2005a, 2012a). Rocks older than ca. 2.6 Ga occur widely in the craton (Fig. 1). The NCC is characterized by strong late Neoarchean tectono-thermal events (Shen et al. 2005; Wan et al. 2011a; Zhai and Santosh 2011), and this makes it different from several other cratons worldwide, providing a chance for better understanding the tectonic property of the Archean/Proterozoic boundary. Similar to other cratons, 80–90 % of the continental crust of the NCC may have formed in the Archean.

The Archean rocks are covered in many areas by Paleo- to Neoproterozoic sedimentary sequences deposited into major basins such as the Songliao basin, North China basin, and Ordos basin. Furthermore, several events since the Paleoproterozoic modified the original features of the Archean basement, including (1) Paleoproterozoic tectono-thermal events that resulted in strong reworking of Archean crust and overprinted the original geological relationships; (2) long-term

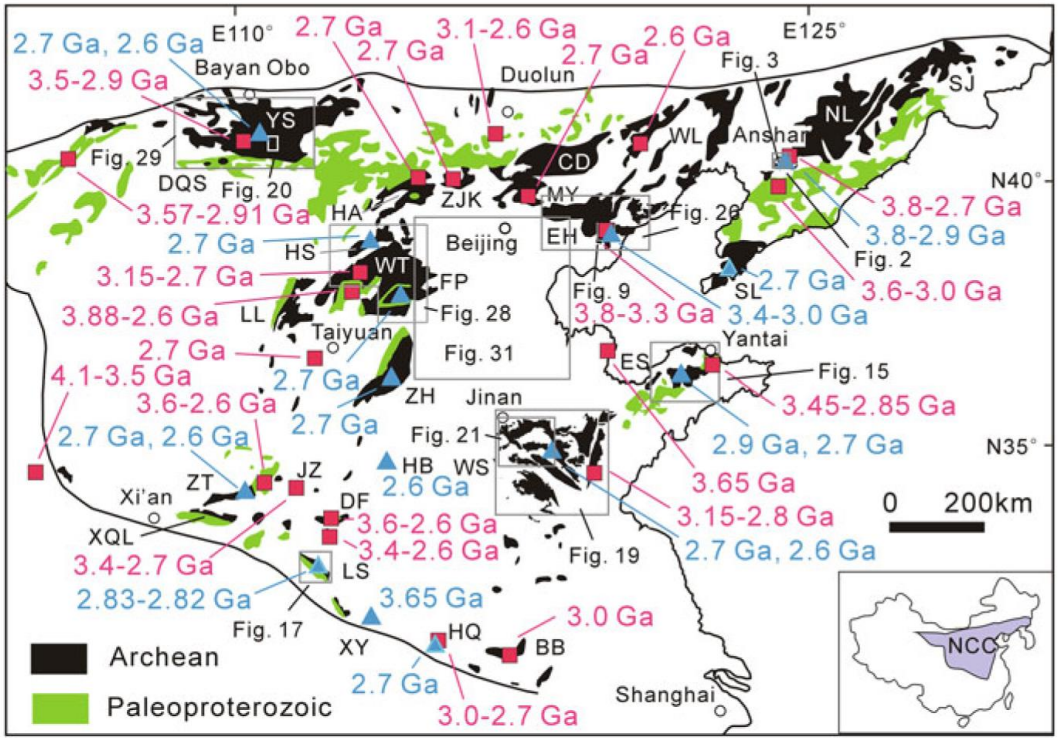

Fig. 1 Simplified sketch map showing distribution and zircon ages for the early Precambrian rocks in the North China Craton. Also shown are the locations of rocks and zircons of >2.6 Ga and Figs. 2, 3, 9, 15, 17, 19, 20, 21, 26, 28, 29, and 31. *YS* Yinshan; *HA* Huai'an; *ZJK* Zhangjiakou; *HS* Hengshan; *WT* Wutai; *FP* Fuping; *LL* Lüliang; *ZH* Zanhuang; *ZT* Zhongtiao; *JZ* Jiaozuo; *DF* Dengfeng; *XQL* Xiaoqinling; *LS* Lushan; *CD* Chengde; *MY* Miyun; *EH* eastern Hebei; *WL* western Liaoning; *SL* southern Liaoning; *NL* northern Liaoning; *SJ* southern Jilin; *WS* western Shandong; *ES* eastern Shandong; *HQ* Huoqiu; *BB* Bengbu. *Blue triangle* rock age; *red square* detrital or xenocrystic zircon age

erosion destroyed part of the Archean basement; and (3) craton destruction since the Mesozoic was mainly related to deep crustal processes but also influenced the shallow crust. All these modifications make it difficult to comprehensively understand the Archean geology of the NCC. Nevertheless, geoscientists carried out geological, petrological, geochronological, and geochemical studies in almost every Archean area of the craton. Research was also undertaken on rock samples recovered from drill cores that penetrate into basement beneath some sedimentary basins and on Archean enclaves brought up from the deep crust by young igneous rocks. In view of all these new data, the main features of the Archean basement of the NCC have become better understood although significant debates still occur as indicated by different tectonic models (e.g., Kusky and Li 2003; Wu et al. 1998; Zhai and Santosh 2011; Zhao et al. 2002, 2005; Zhao 2014).

The NCC has a long history of geological studies, and some specific case studies carried out in the last century laid important foundations for later work (e.g., Bai et al. 1986, 1996; Cao et al. 1996; Cheng et al. 1982; Li et al. 1986; Lu et al. 1996; Qian et al. 1985, 1994; Shen et al. 1990, 1992, 1994a, b, 2000; Sun et al. 1984;

Sun and Hu 1993; Wu et al. 1989, 1998; Zhang et al. 1988; Zhao et al. 1993). Since the beginning of this century, numerous papers were published on Archean rocks and their evolution, and in this chapter, we try to synthesize present knowledge by first outlining the general geological records of the Archean basement and then discussing several important issues relating to Archean crust formation and evolution.

2 Archean Geological Record

2.1 Eoarchean (>3.6 Ga)

Rocks older than 3.8 Ga have been discovered in only a few areas worldwide such as northern Canada (Bowring and Williams 1999; O'Neil et al. 2007), eastern Antarctica (Black et al. 1986), West Greenland (Kinny 1986; Nutman et al. 1996), and around Anshan city in the NNC (Liu et al. 1992; Song et al. 1996; Wan et al. 2005a, 2012a). Anshan is located southwest of the Anben (Anshan-Benxi) area where 2.5 Ga BIF-bearing supracrustal rocks (the Anshan "Group," we use the word group with quotation marks to indicate that it does not conform to modern stratigraphic terminology but constitutes a tectono-stratigraphic term) and granitoids (mainly syenogranites) occur widely (Fig. 2).

In Anshan, 3.8 Ga rocks occur within three complexes, namely the Baijiafen, Dongshan, and Shengousi complexes (Fig. 3). Baijiafen quarry was the site where 3.8 Ga rocks were first discovered (Liu et al. 1992). The complex is ~700 m long and ~50 m wide in exposure and extends in a NW–SE direction, in tectonic contact with the 3.3–3.1 Ga Chentaigou granite in the southwest and 3.36 Ga Chentaigou supracrustal rocks in the northeast (Wan et al. 2005a; Wan unpublished data). It is mainly composed of strongly mylonitized trondhjemitic gneiss of different ages with some biotite schist, gneissic monzogranite, and quartz diorite (Fig. 4). In an early study, all granitoids of the complex were considered to have formed at 3.8 Ga (Liu et al. 1992), but later studies indicated that these rocks formed at different times ranging from 3.8 to 3.1 Ga (Liu et al. 2008). The 3.8 Ga mylonitized trondhjemitic gneiss occurs in narrow layers such as sample A0518 (Fig. 5a) that is distinguished from the surrounding rocks (also trondhjemitic gneisses) by containing less biotite. The biotite schist (Fig. 5b) varies in thickness between a few centimeters and half a meter and alternates with igneous units, including trondhjemitic gneiss. There are two opinions on the origin of the schist, namely an altered mafic dike (Song et al. 1996) or a metasedimentary rock (Liu et al. 2008). The latter is based on the observation that the schist is interlayered with chert that is composed of recrystallized quartz with some banded biotite + epidote aggregates. However, at some localities, quartz veins occur together with biotite schist; therefore, the "chert" may, in fact, be a deformed quartz vein. Although it is uncertain whether the biotite schist is derived from a mafic dike or a supracrustal

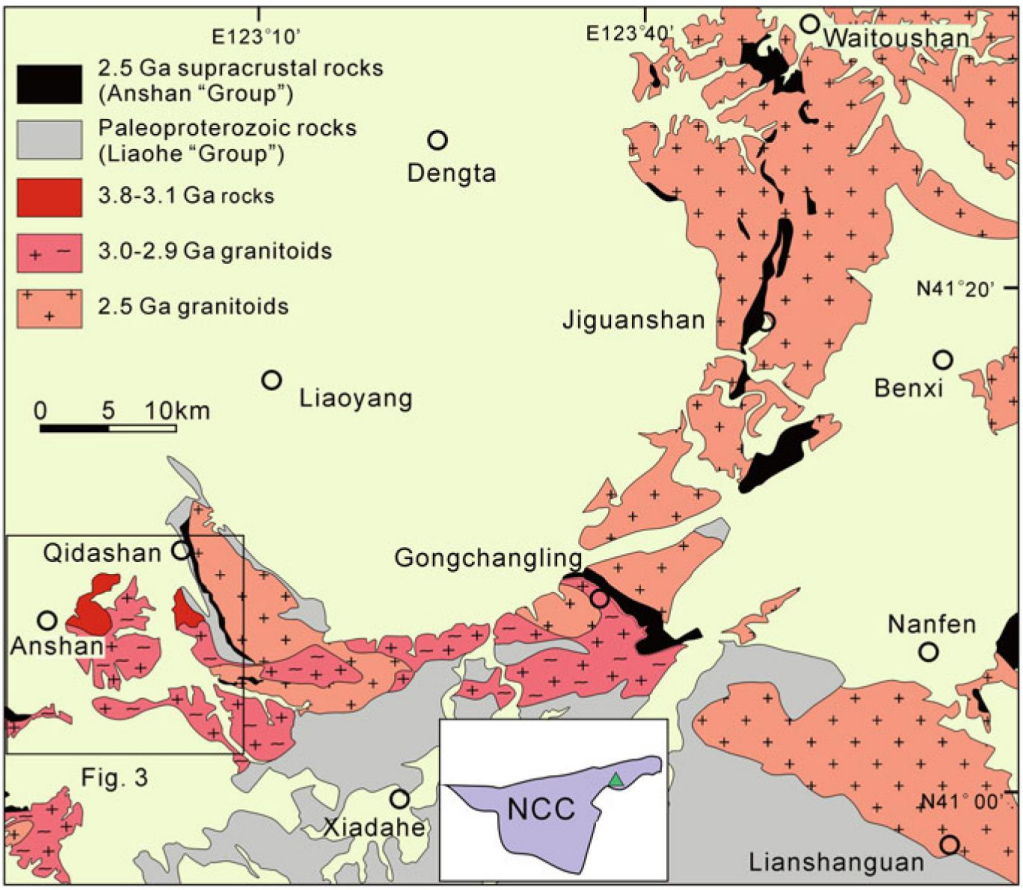

Fig. 2 Geological map of the Anben (Anshan-Benxi) area, North China Craton. Modified after LBGMRE (1975a, b, 1976); Wan (1993), and Wan et al. (2015a). *Triangle* in *inset* map shows location of Fig. 2 in the NCC

rock, it is considered to be older than 3.6 Ga because it is cut by 3.62 Ga trondhjemitic gneiss (Fig. 5b). Some younger magmatic rocks (samples A0405, A0517, A0521) contain xenocrystic zircons with ages of 3.8–3.6 Ga.

Rocks of the Dongshan Complex trend approximately WNW–ESE (Fig. 3), and the exposure is more than 10 m wide and up to 1000 m long. It occurs as a large enclave within the 3.14 Ga Lishan trondhjemite and is cut by veins derived from the Lishan trondhjemite intrusion. Different types of 3.8–3.1 Ga rocks have been identified in the complex, including banded trondhjemitic gneiss, gneissic trondhjemite, gneissic monzogranite, pegmatite, meta-ultramafic rock (komatiite?), amphibolite (metabasalts or gabbro), and meta-quartz diorite. These units are mostly structurally concordant to each other because of strong ductile deformation, and their original contact relationships are often difficult or impossible to recognize. Rocks older than 3.6 Ga were identified in three locations, including 3.81–3.68 Ga banded trondhjemitic gneisses and 3.79 Ga meta-quartz diorite. The 3.81 Ga banded trondhjemitic gneiss (sample Ch28, Fig. 5c) near a pavilion was first identified in the complex (Song et al. 1996). 3.79 Ga meta-quartz diorite (sample

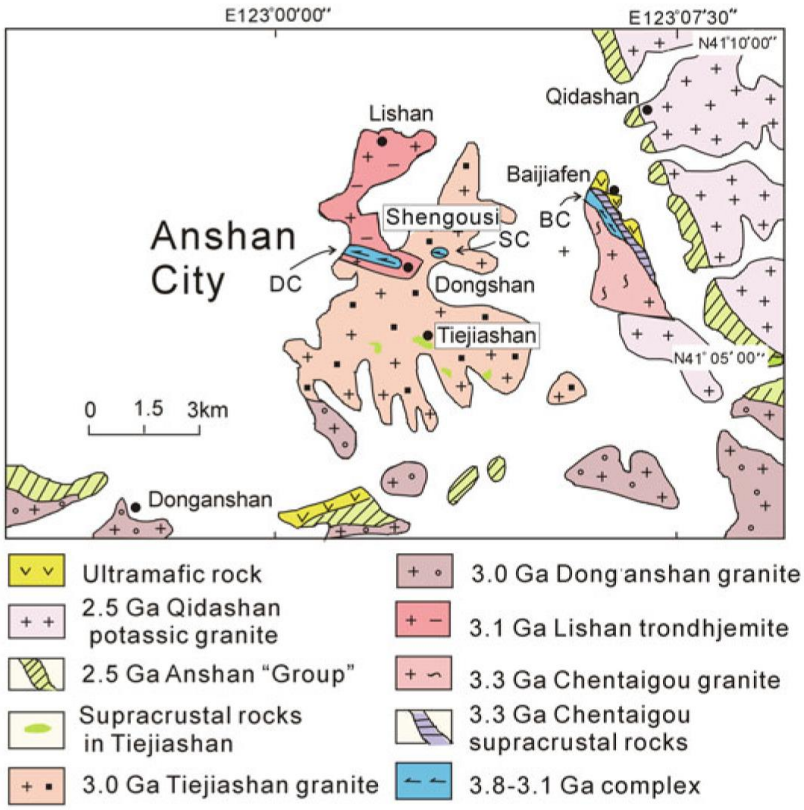

Fig. 3 Geological map of the Anshan area (Wan et al. 2012a). *BC* Baijiafen Complex; *DC* Dongshan Complex; *SC* Shengousi Complex

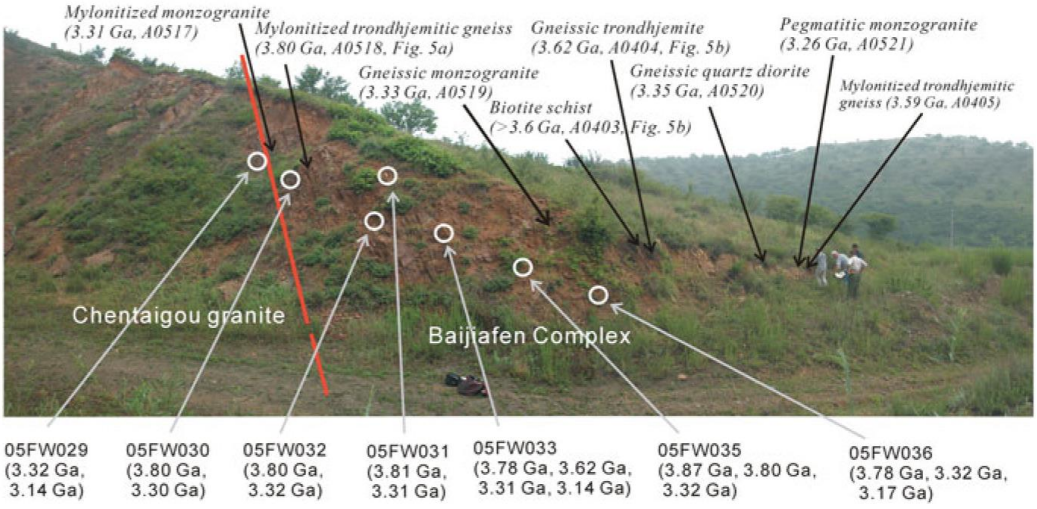

Fig. 4 Photographic mosaic showing studied section of the Baijiafen Complex with sampling sites marked (Liu et al. 2008). Samples with prefix 05FW are from Wu et al. (2008)

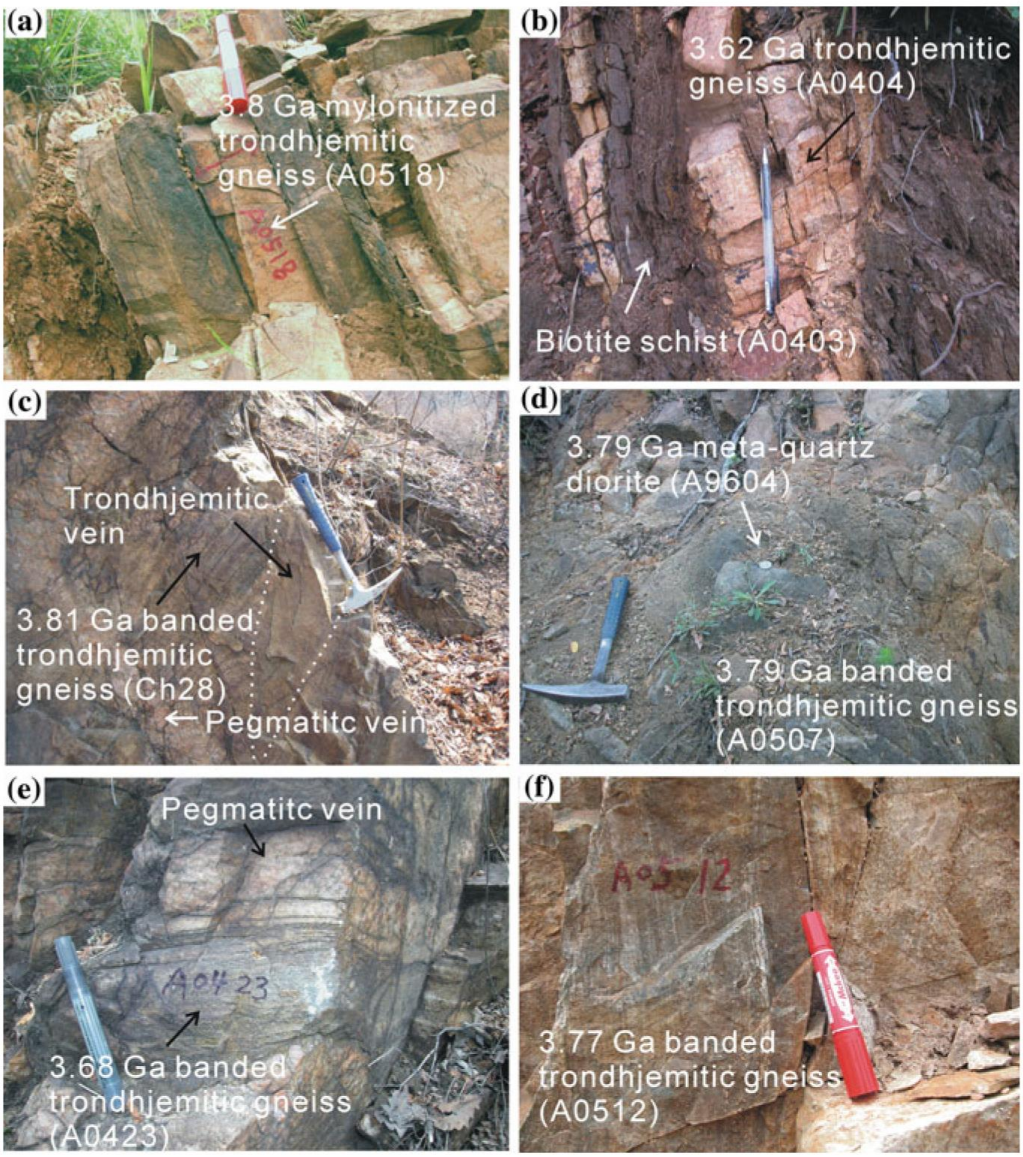

Fig. 5 Field photographs of Eoarchean rocks in the Anshan area. **a** 3.80 Ga mylonitized trondhjemitic gneiss (A0518), Baijiafen Complex; **b** biotite schist (A0403) intruded by 3.62 Ga trondhjemitic gneiss (A0404), Baijiafen Complex; **c** 3.81 Ga banded trondhjemitic gneiss (Ch28) intruded by trondhjemitic and pegmatitic veins, Dongshan Complex; **d** 3.79 Ga meta-quartz diorite (A9604) occurring in 3.79 Ga banded trondhjemitic gneiss (A0507), Dongshan Complex; **e** 3.68 Ga banded trondhjemitic gneiss (A0423) intruded by pegmatitic vein, Dongshan Complex; **f** 3.77 Ga banded trondhjemitic gneiss (A0512), Shengousi Complex

A9604) occurs as a small enclave within the 3.79 Ga banded trondhjemite (sample A0507) in an outcrop near the southeastern end of the Dongshan Complex (Fig. 5d). The identification of 3.68 Ga banded trondhjemitic gneiss (sample A0423, Fig. 5e) indicates that there are Eoarchean banded trondhjemitic gneisses of different ages in the complex although they are similar in field appearance and composition (Liu et al. 2008).

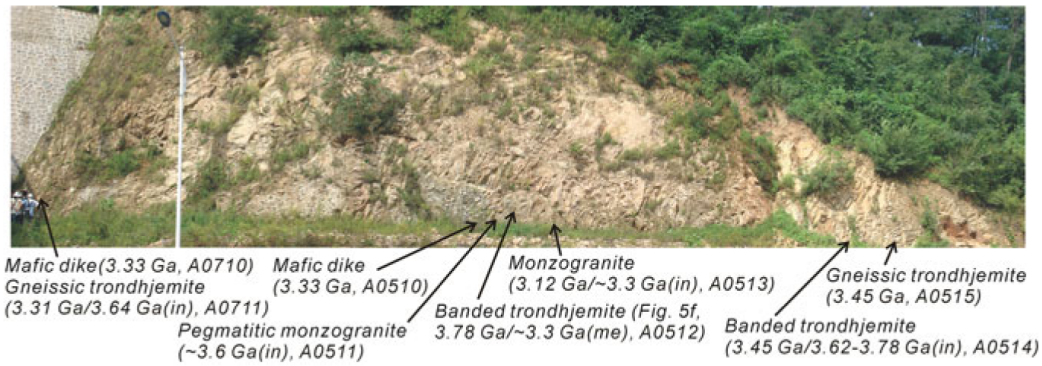

Fig. 6 Photographic mosaic showing the section of the Shengousi Complex in the Anshan area (Wan et al. 2012a)

The Shengousi Complex is located between the Dongshan and Baijiafen complexes, and its full extent is unknown due to poor exposure and is only readily apparent in a deep road cut (Wan et al. 2012a). The key locality is a ~50 m-long and up to ~10 m-high section on an elevated bench in this road cut (Fig. 6). The complex comprises polyphase migmatites, and despite a strong structural overprint through ductile deformation, there are small areas of lower strain where the relative chronologies between the different migmatite components are preserved. The youngest component on the basis of field relationships is a pegmatitic monzogranite dike. Eight samples were collected for zircon dating in this section, and these samples revealed a protracted tectono-magmatic history from 3.77 to 3.13 Ga with the oldest rocks being 3.77 Ga banded trondhjemitic gneisses (sample A0512, Fig. 5f). The complex mainly contains monzogranite and mafic metamorphic rocks besides trondhjemitic rocks of different ages (Fig. 6).

The above three complexes are similar in their geochronological record. Apart from >3.6 Ga gneisses, 3.45–3.0 Ga rocks have been identified. Many >3.6 Ga rocks notably contain younger (mainly 3.3 Ga) zircons. Some authors considered this as evidence that the trondhjemitic gneisses formed at 3.3 Ga and contained numerous 3.8 Ga zircon xenocrysts (Wu et al. 2008). However, based on field observations, zircon morphology, and cathodoluminescence (CL) images, a better explanation may be that these granitoid gneisses predominantly constitute strongly deformed igneous injection migmatites containing igneous components of several ages and/or are related to anatexis of 3.8 Ga rocks at 3.3 Ga (Liu et al. 2008; Nutman et al. 2009; Song et al. 1996; Wan et al. 2012a). There is no doubt that the 3.79 Ga quartz diorite identified in the Dongshan Complex is magmatic in origin, as indicated by its geological, petrological, and compositional features, although it also contains younger zircons (Wan et al. 2005a). Some of the <3.6 Ga rocks in the three complexes that do not show banded structures or strong deformation also contain old zircon xenocrysts (Fig. 7). All ~3.8 Ga gneisses are trondhjemitic in composition with high SiO_2 and Na_2O, and low ΣFeO (FeO + 0.9 × Fe_2O_3), MgO, CaO, and K_2O. They have very low total rare earth element (REE) contents, positive or negligible Eu anomalies, and weakly fractionated REE patterns (Fig. 8a).

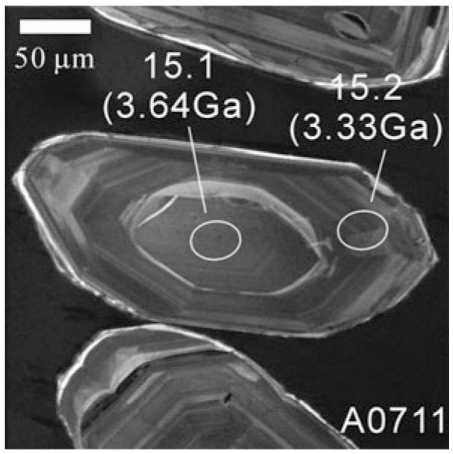

Fig. 7 3.64 Ga xenocrystic zircon core occurring in 3.33 Ga magmatic zircon from gneissic trondhjemite (A0711) in the Shengousi Complex, Anshan

Many >3.6 Ga detrital and xenocrystic zircons were also discovered in the Gongchangling and Waitoushan areas (Fig. 2) (Wan 1993; Wan et al. 2015a). This suggests that Eoarchean rocks may occur in a wider area of Anben than currently identified. The single zircon age of 4.17 Ga reported by Cui et al. (2013) from an amphibolite (metabasalt) of the 2.5 Ga Anshan "Group" in Waitoushan is questionable after rechecking the original LA-ICP-MS data (Diwu personal communication).

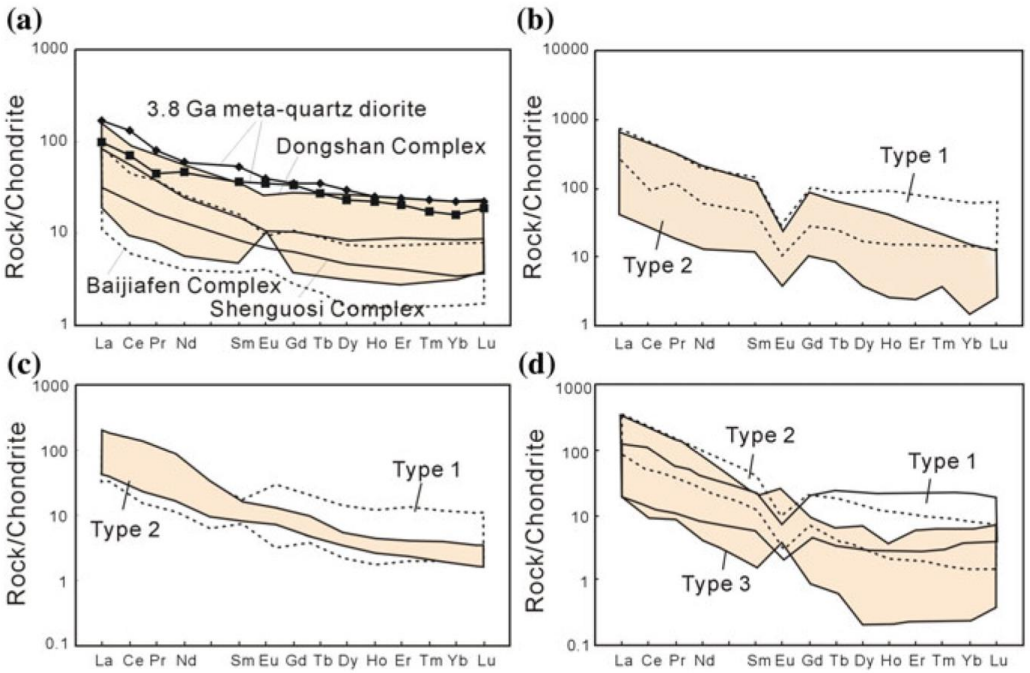

Fig. 8 Chondrite-normalized REE patterns for Archean rocks from the North China Craton. **a** 3.8 Ga trondhjemitic rocks in Anshan; **b** 3.0–2.9 Ga Tiejiashan K-rich granite in Anshan; **c** 2.75–2.7 Ga TTG rocks in the North China Craton; **d** 2.53–2.50 Ga syenogranite in the North China Craton. Data are from Jahn et al. (2008), Wan et al. (2005a, 2007, 2011b, 2012a, b, 2014a), Yang et al. (2013), and Zhu et al. (2013)

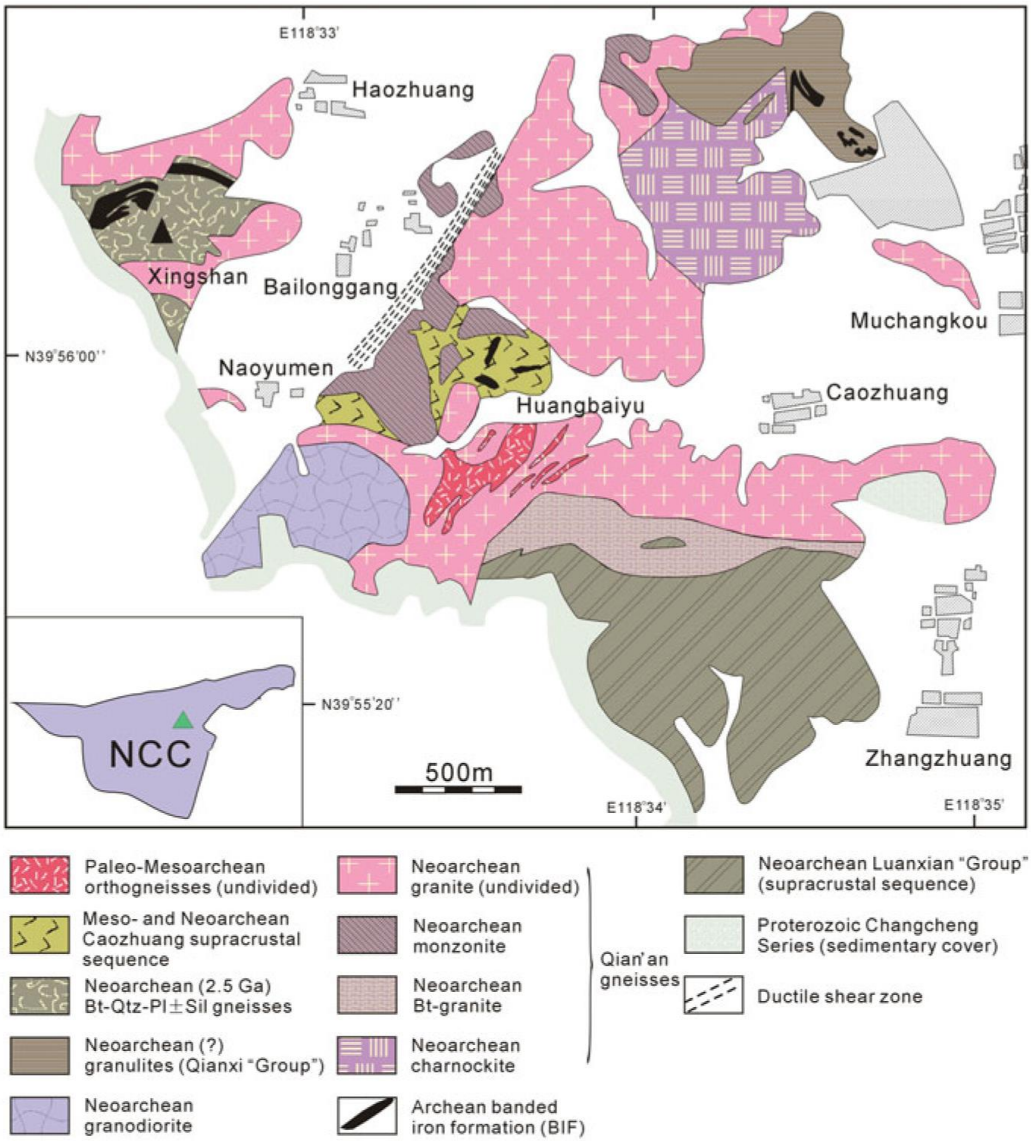

Fig. 9 Simplified geological map of the Caozhuang area, eastern Hebei. Modified after Chen (1988), Liu et al. (2013a), and Nutman et al.(2011). *Triangle* in *inset* map shows location of Fig. 9 in the NCC

Eoarchean rocks within relatively large areas in the NCC have so far only been identified in the Anben area. However, abundant Eoarchean zircons were discovered in rocks of the Caozhuang Complex, eastern Hebei Province. This complex is composed of amphibolite- to granulite-facies granitoids and a supracrustal sequence (Fig. 9). The supracrustal sequence is composed of Bt-Pl-Qtz ± Sil and Bt ± Grt gneisses, amphibolite, marble, calc-silicate, fuchsite quartzite, and banded iron formation (BIF) and was considered to have an age of 3.5 Ga on the basis of a Sm–Nd isochron age for amphibolites (Jahn et al. 1987). However, the Sm–Nd isochron was later interpreted as a mixing line (Nutman et al. 2011). The oldest rocks

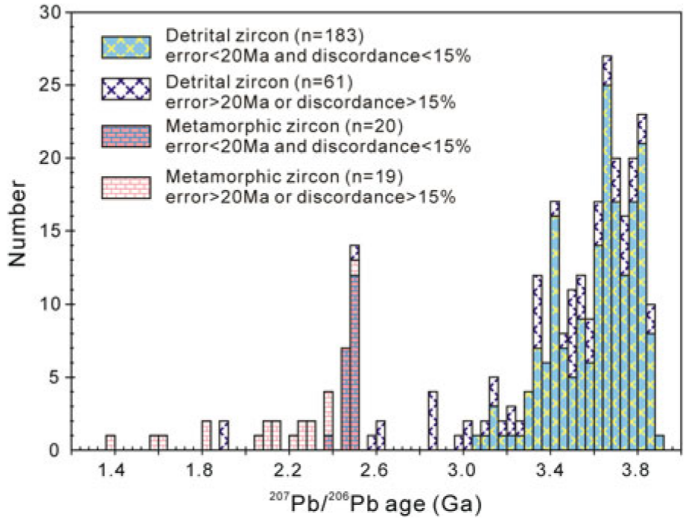

Fig. 10 Age histogram for zircons from metasedimentary rocks (including fuchsite quartzite, para-amphibolite, and metapelitic rock) in the Caozhuang area, eastern Hebei. Metamorphic zircon ages of 2.5 Ga have been identified only in para-amphibolite and metapelitic rock. Data are from Liu et al. (1992, 2013a), Nutman et al. (2011), Wilde et al. (2008), and Wu et al. (2005a)

identified in the area are 3.4–3.3 Ga granitoid gneisses (Nutman et al. 2011; Liu unpublished data). Detrital zircons with ages of 3.88–3.55 Ga were reported from the Caozhuang (fuchsite) quartzite (Liu et al. 1992; Nutman et al. 2011; Wilde et al. 2008; Wu et al. 2005a). Recently, Liu et al. (2013b) carried out SHRIMP dating on detrital zircons from para-amphibolite and Grt-Bt gneiss and obtained detrital core ages ranging from 3.8 to 3.4 Ga and metamorphic rim ages of ~2.5 Ga. Combining the detrital zircon data of the three rock types, age peaks at ~3.83, ~3.67, 3.55, and ~3.41 Ga can be recognized (Fig. 10), suggesting that detrital material was derived from crustal sources of different ages. Based on zircon morphology and inclusion studies, Nutman et al. (2014) suggested that the Caozhuang quartzite is most likely a <3.5 Ga immature sedimentary rock of local provenance. This interpretation strengthens the case for Eoarchean rocks with a substantial 3.88–3.80 Ga component occurring in eastern Hebei Province and indicates that the paragneiss protoliths of the Caozhuang Complex were deposited between 3.4 and 2.5 Ga ago (Liu et al. 2013b; Nutman et al. 2014).

Rocks and zircons older than 3.6 Ga have also been identified elsewhere in the NCC (Fig. 1), including 3.65 Ga felsic granulite enclaves in Mesozoic volcanic rocks of the Xinyang area (Zheng et al. 2004a) and ≥3.6 Ga detrital zircons in the Zhongtiao and Dengfeng areas (Liu et al. 2012a; Zhang et al. 2014a). Interesting is the discovery of three 4.1–3.9 Ga xenocrystic or detrital zircons, together with younger Archean and Paleoproterozoic grains, in Paleozoic volcano-sedimentary rocks of the northern Qinling Orogenic Belt (Diwu et al. 2010a, 2013, personal communication; Wang et al. 2007). One zircon has a 3.71 Ga overgrowth rim (Fig. 11), suggesting a tectono-thermal event at that time in the zircon source

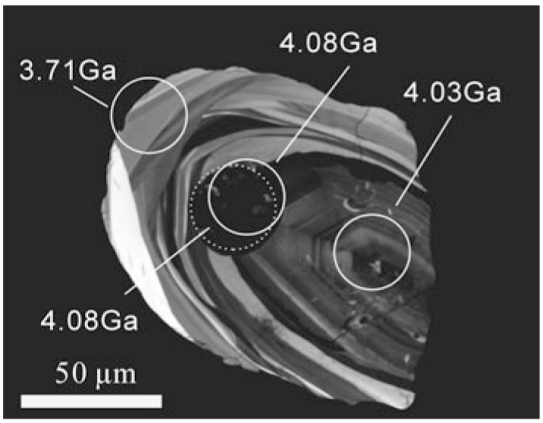

Fig. 11 Cathodoluminenscence image showing 3.71 Ga overgrowth rim on 4.08 Ga xenocrystic or detrital zircon from pyroclastic rock in the Paleozoic Caotangou Group in northern Qinling, near the North China Craton (from Diwu et al. 2010a, b). *Circle* and *dashed circles* refer to SHRIMP and LA-ICPMS dating locations, respectively

region. The volcanic rock is located near the southern margin of the NCC, and the old zircons are considered to be derived from the NCC basement (Diwu et al. 2013; Wan et al. 2009a).

2.2 Paleoarchean (3.6–3.2 Ga)

Paleoarchean rocks and components have been identified in many areas of the NCC and reflect the most important tectono-magmatic events in Anshan as indicated by their distribution and zircon age histogram (Fig. 12). The 3.36 Ga Chentaigou supracrustal rocks near Baijiafen (Fig. 3) are the oldest supracrustal rocks identified

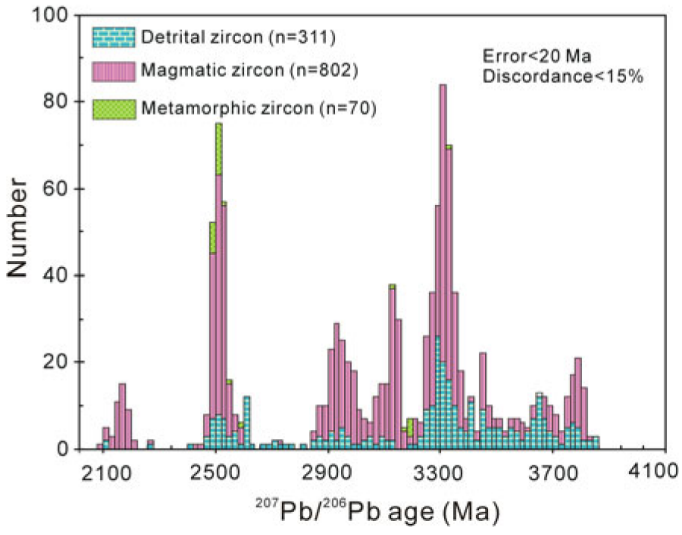

Fig. 12 Age histogram of zircons from Archean rocks in the Anben area. Data are from Liu et al. (1992, 2008), Song et al. (1996), Wan et al. (2005a, 2007, 2012a, b, d, 2015a, unpublished data), Wu et al. (2008), Yin et al. (2006), and Zhou et al. (2007, 2009)

in the NCC. Their formation age is limited by 3.36 Ga felsic metavolcanic rocks in the sequence and 3.34–3.31 Ga trondhjemitic veins intruding the sequence (Fig. 13a, b) (Song et al. 1996; Wan unpublished data). The main rock types include amphibolite, meta-ultramafic rocks, felsic metavolcanic rock, meta-calc-silicate, fuchsite quartzite, and iron-bearing chert (Fig. 13c, d). The meta-ultramafic rocks occur over a relatively large area in the northeastern exposure of the sequence, and their protolith was uncertain (volcanic or intrusive) in early studies. They are intruded by 3.31 Ga trondhjemitic veins (Fig. 13b) and are considered to belong to the sequence. They are similar to komatiites in chemical compositions with MgO contents up to 38 %, but no spinifex textures have been identified because of strong modification. The amphibolite is tholeiitic in composition, showing a flat REE pattern with no large ion lithophile element (LILE) enrichment. This is the main reason for the speculative interpretation that these supracrustal rocks formed in an arc environment (Wan et al. 1997a).

The oldest Paleoarchean rock is a 3.45 Ga trondhjemitic gneiss in the Shengousi Complex (Fig. 13e). It is considered to have interacted with Eoarchean trondhjemitic rocks nearby to form an injection migmatite that subsequently underwent strong deformation to produce a rock with layers of different ages (Wan et al. 2012a). Igneous rocks of 3.35–3.2 Ga widely occur in the Anshan area, including the Baijiafen, Dongshan, and Shengousi complexes. The rock types are metagabbro, metadiorite, meta-quartz diorite, granite, as well as trondhjemitic gneiss (Dong et al. 2013; Liu et al. 2008; Wan et al. 2001, 2012a; Zhou et al. 2007, 2009). It is common that different rocks with similar or different ages occur within a single outcrop (Fig. 13f). The Chentaigou granite was considered to be the largest pluton formed at ~3.3 Ga (Song et al. 1996). However, Wu et al. (2008) obtained ~3.3 and ~3.1 Ga zircon ages for three Chentaigou granite samples near the Baijiafen Complex and thought the latter to represent the emplacement time of the pluton. Based on geological mapping and zircon dating, Li et al. (2013) suggested that the Chentaigou granite is composed of 3.3 and 3.1 Ga granitoid rocks. Trondhjemitic rocks in the Anshan area, between 3.45 and 3.3 Ga in age, show a significant variation in REE composition from very low ΣREE contents and weakly fractionated REE patterns to high ΣREE contents and strongly fractionated REE patterns (Wan unpublished data).

In Caozhuang, eastern Hebei Province, 3.4 Ga quartz dioritic gneiss and 3.3–3.2 Ga tonalitic gneiss (Fig. 13f, g) occur as enclaves within 2.5 Ga granite (Nutman et al. 2011; Liu unpublished data). This is the second area where Paleoarchean igneous rocks were identified in the NCC. Based on the youngest detrital zircons at 3.55 Ga from a fuchsite quartzite and the oldest TTG rock at ~3.3 Ga in the area, Wan et al. (2009a) suggested that deposition of the Caozhuang Complex supracrustal rocks occurred between 3.55 and 3.3 Ga. However, the relationship between the supracrustal rocks and the ~3.3 Ga TTGs is uncertain. Based on the metamorphic zircon age of 2.5 Ga and the believable youngest detrital zircon age of 3.4 Ga of the metasedimentary rocks (Fig. 10), we can now only limit deposition to between 3.4 and 2.5 Ga. Mainly based on zircon dating, Han et al. (2014a) concluded that the supracrustal rocks in Xingshan, ~1.5 km northwest of

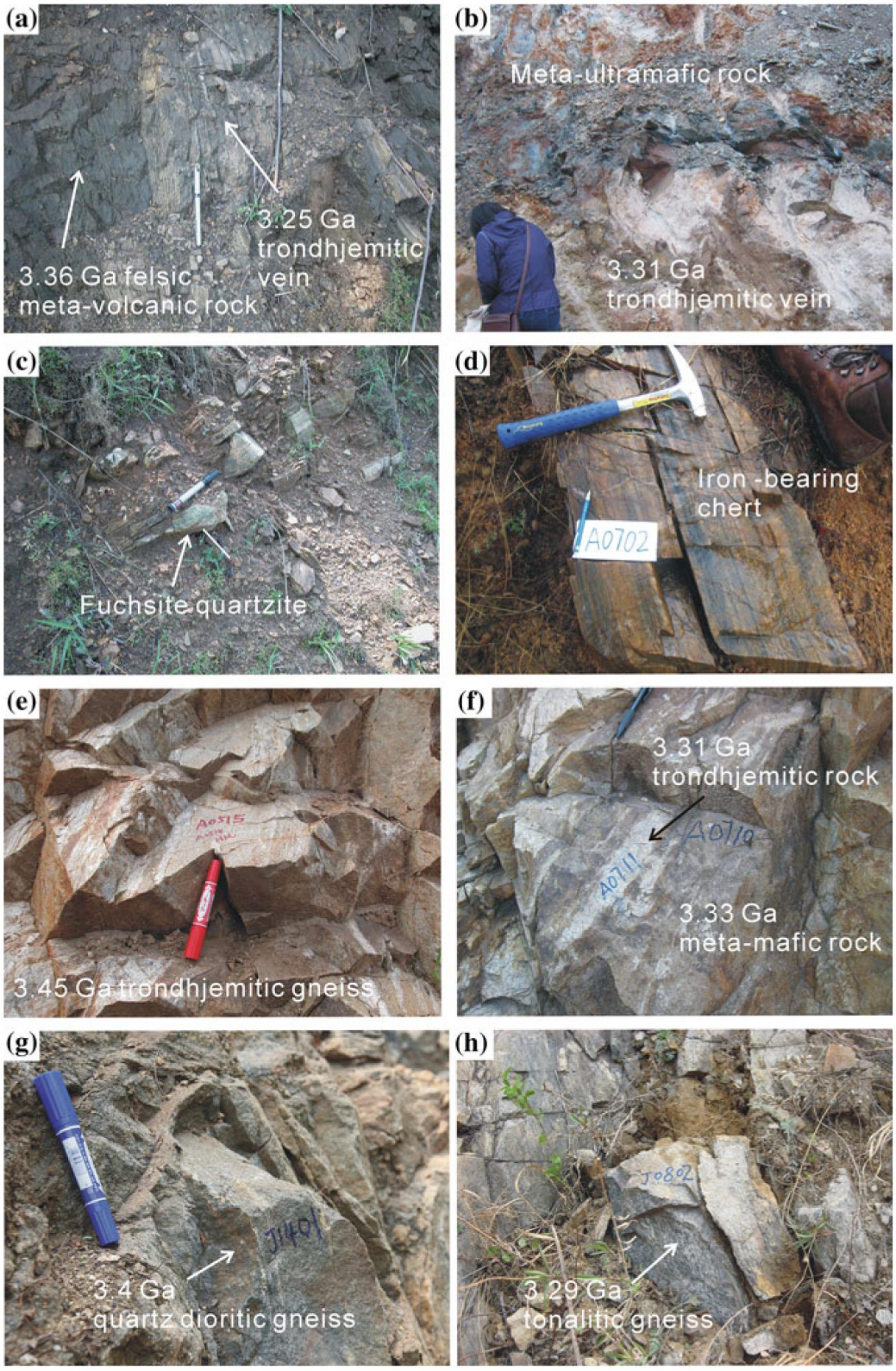
(a)
3.36 Ga felsic meta-volcanic rock
3.25 Ga trondhjemitic vein
(b)
Meta-ultramafic rock
3.31 Ga trondhjemitic vein
(c)
Fuchsite quartzite
(d)
Iron -bearing chert
A0702
(e)
3.45 Ga trondhjemitic gneiss
(f)
3.31 Ga trondhjemitic rock
A0719
A0711
3.33 Ga meta-mafic rock
(g)
3.4 Ga quartz dioritic gneiss
(h)
3.29 Ga tonalitic gneiss

◀ **Fig. 13** Field photographs of Paleoarchean rocks in the North China Craton. **a** 3.36 Ga felsic meta-volcanic rock (the Chentaigou supracrustal rocks) intruded by 3.25 Ga trondhjemitic vein, Anshan; **b** meta-ultramafic rock (the Chentaigou supracrustal rocks) intruded by 3.31 Ga trondhjemite vein, Anshan; **c** fuchsite quartzite in the Chentaigou supracrustal rocks, Anshan; **d** iron-bearing chert in the Chentaigou supracrustal rocks, Anshan; **e** 3.45 Ga trondhjemitic gneiss in the Shengousi Complex, Anshan; **f** 3.31 Ga gneissic trondhjemite and 3.33 Ga meta-mafic rock in the Shengousi Complex, Anshan; **g** 3.4 Ga gneissic quartz diorite, Huangbaiyu, eastern Hebei; **h** 3.29 Ga gneissic trondhjemite, Huangbaiyu, eastern Hebei

Huangbaiyu, that belong to the Caozhuang Complex, were deposited at 3.39 Ga. However, the dated rock contains garnet and many 3.76–3.43 Ga zircons, similar in features to the metasedimentary rocks in Huangbaiyu. Therefore, it is possible that the 3.39 Ga zircon is detrital in origin, and this age therefore only constrains the upper depositional age of the Caozhuang supracrustal rocks.

The age distribution of >3.3 Ga detrital zircons from the Caozhuang Complex is similar to that of magmatic zircons in the Anshan area (Figs. 10 and 12). However, it appears that the detrital material was derived from the surrounding area, rather than Anshan, which is too far from Caozhuang.

Paleoarchean detrital and xenocrystic zircons were identified in many areas of the NCC such as Alax, Guyang, Wutai, Jiaozue, Dengfeng, Zhongtiao, eastern Shandong, and Bengbu (Fig. 1) (Diwu et al. 2008; Gao et al. 2006; Ji 1993; Jian et al. 2012; Jin et al. 2003; Liu et al. 2012a; Shen et al. 2005; Wan et al. 2006, 2009a, c, 2010a; Wang et al. 1998; Xie et al. 2014a; Zhang et al. 2014a, b).

2.3 Mesoarchean (3.2–2.8 Ga)

Mesoarchean rocks are more widespread in the NCC than Paleoarchean rocks. In Anshan, large Mesoarchean intrusive bodies include the 3.14 Ga Lishan trondhjemite, the 3.0 Ga Dong'anshan granite, the 3.0–2.9 Ga Tiejiashan granite, and part of the 3.3–3.1 Ga Chentaigou granite (Fig. 3). The Tiejiashan granite (Fig. 14a) is the oldest and largest K-rich granite pluton in the NCC (Wan et al. 2007; Wu et al. 1998) and occupies a total area of >150 km^2 (Fig. 2). The rocks vary in their REE fractionation patterns but have high ΣREE contents and strong negative Eu anomalies (Fig. 8b). The Tiejiashan granite contains supracrustal xenoliths such as BIF and quartzite (Fig. 14b, c). There are also some mica–quartz schists (Fig. 14d) that were considered to be supracrustal enclaves (Yin et al. 2006). However, they show similar geochemical features as the Tiejiashan granite, and the so-called detrital zircons in the rocks are mainly ~3.0 Ga in age. In some thin sections, K-feldspar grains occur at different sizes in the fine-grained sericite + quartz groundmass. These features suggest that sericite resulted from strong deformation and alteration of K-feldspar during shearing. Therefore, we suggest that at least some schists are due to strong deformation and alteration of granite. Besides the large Mesoarchean granitoid bodies, many small Mesoarchean granitoid bodies or


(a)
A0432
2.91 Ga K-rich granite
(b)
BIF
(c)
A0436
(d)
K-rich granite
Mica-quartz schist
(e)
3.13 Ga augen-like granite
(f)
3.14 Ga monzogranite
3.14 Ga trondhjemite
(g)
J0604
~3.2 Ga gneissic tonalite
(h)
2.94 Ga anatectic granitoid

◀ **Fig. 14** Field photographs of Mesoarchean rocks in the North China Craton. **a** Mesoarchean Tiejiashan K-rich granite, Anshan; **b** BIF in Mesoarchean Tiejiashan K-rich granite, Anshan; **c** quartzite in Mesoarchean Tiejiashan K-rich granite, Anshan; **d** mica–quartz schist in Mesoarchean Tiejiashan K-rich granite, Anshan; **e** 3.13 Ga augen-like granitic gneiss in the Baijiafen Complex, Anshan; **f** 3.14 Ga trondhjemite and 3.14 Ga monzogranite, Dongshan Complex, Anshan; **g** ca. 3.2 Ga gneissic tonalite, Huangbaiyu, eastern Hebei; **h** 2.94 Ga anatectic granitoid, Huangbaiyu, eastern Hebei

veins also occur in the Baijiafen, Dongshan, and Shengousi complexes (Figs. 4, 6 and 14e, f).

In Caozhuang, eastern Hebei Province, Mesoarchean igneous rocks have also been discovered (Fig. 14g, h) (Nutman et al. 2011), but they only occur on a very small scale. However, Mesoarchean xenocrystic zircons are more widespread.

In eastern Shandong, 2.9 Ga rocks are widely distributed, extending from Mazhuanghe in the west to Hexikuang in the east, with some occurring in the southern portion of the area (Fig. 15). Most of the so-called Mesoarchean Tangjiazhuang "Group" consists of intrusive rather than supracrustal rocks. Only a few 2.9 Ga supracrustal rocks, named Huangyadi supracrustal rocks, occur on a small scale within 2.9 Ga igneous rocks (Jahn et al. 2008). Mesoarchean supracrustal rocks in eastern Shandong are much smaller in scale than thought before (BGMRSP 1991). At least three types of 2.9 Ga igneous rocks, namely quartz diorite, tonalite, and high-Si trondhjemite, have been identified (Jahn et al. 2008; Liu et al. 2011, 2013a; Wang et al. 2014a; Wu et al. 2014; Xie et al. 2014b). Of these, tonalite seems to be the most common, with a total area up to several tens of square km. 2.9 Ga gneissic tonalite occurs in the lower part along a ~200 m-long road cut northeast of Zhoujiagou. It is in contact with 2.9 Ga gneissic high-Si trondhjemite in the upper part; both show strong deformation with their foliations parallel to each other (Fig. 16a–c). At the Hexikuang reservoir dam, 2.9 Ga gneissic quartz diorite occurs as enclaves within 2.9 Ga gneissic tonalite, and these show a differently oriented foliation (Fig. 16d). Felsic veins in the quartz diorite are parallel to the foliation and are considered to be anatectic products. Both the gneissic quartz diorite and tonalite contain ca. 2.5 Ga metamorphic or anatectic zircon, and the gneissic tonalite around the enclave shows strong deformation and anatexis. It seems likely that the quartz diorite enclaves were rotated after leucosome formation during the ca. 2.5 Ga tectono-thermal event (Xie et al. 2014b). 2.9 Ga gneissic tonalites exhibit strong anatexis with trondhjemitic leucosomes and biotite-rich melanosomes in local outcrops (Fig. 16e). Some leucosome forms layers and lenses at different scales and is strongly or weakly deformed. Anatexis occurred syntectonically in a regime locally changing from compression to extension at the end of the Neoarchean because 2.5 Ga metamorphic or anatectic zircons have been identified.

2.8 Ga supracrustal rocks and TTGs have been identified in the Lushan area on the southern margin of the NCC (Fig. 17). These rocks are mainly composed of (garnet-bearing) amphibolite, hornblende–plagioclase gneiss, and biotite–plagioclase gneiss. Some amphibolites show a layered structure (Fig. 16f), mainly due to

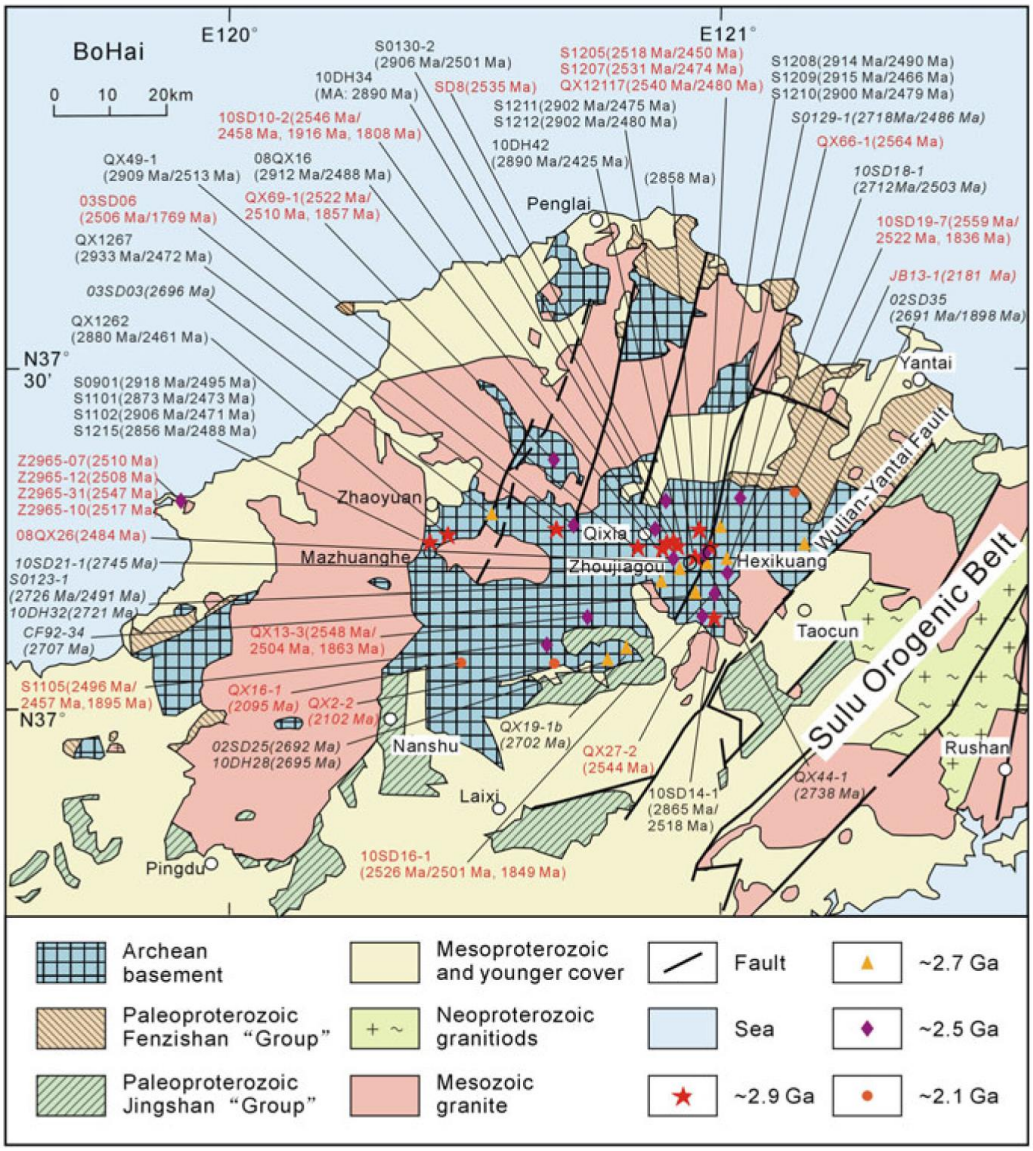

Fig. 15 Geological map of eastern Shandong. Shown also are locations of zircon dating samples, and ages in parenthesis are magmatic zircon age or magmatic zircon age/metamorphic zircon age. Data are from Jahn et al. (2008), Liu et al. (2011), Liu et al. (2011, 2013a, 2014), Liu et al. (2013b), Liu et al. (2014), Shan et al. (2015), Tang et al. (2007), Wang and Yan (1992), Wang et al. (2014a), Wu et al. (2014), Xie (2012), Xie et al. (2013, 2014b), and Zhou et al. (2008). See Fig. 1 for location of the figure in the NCC

variations in plagioclase and hornblende contents. They occur as enclaves within TTG rocks with strong deformation and local anatexis (Fig. 16g). Zircon dating of the supracrustal rocks and TTGs yielded 2.83 Ga magmatic ages and two sets of metamorphic ages at 2.79–2.77 and 2.67–2.64 Ga (Liu et al. 2009a). Huang et al. (2010) performed zircon dating on TTG-like and TTG rocks in the same area and interpreted the ages of 2.77 and 2.72 Ga as the time of crystallization of the host igneous rocks. Similar conclusions were arrived at by Diwu et al. (2010b).

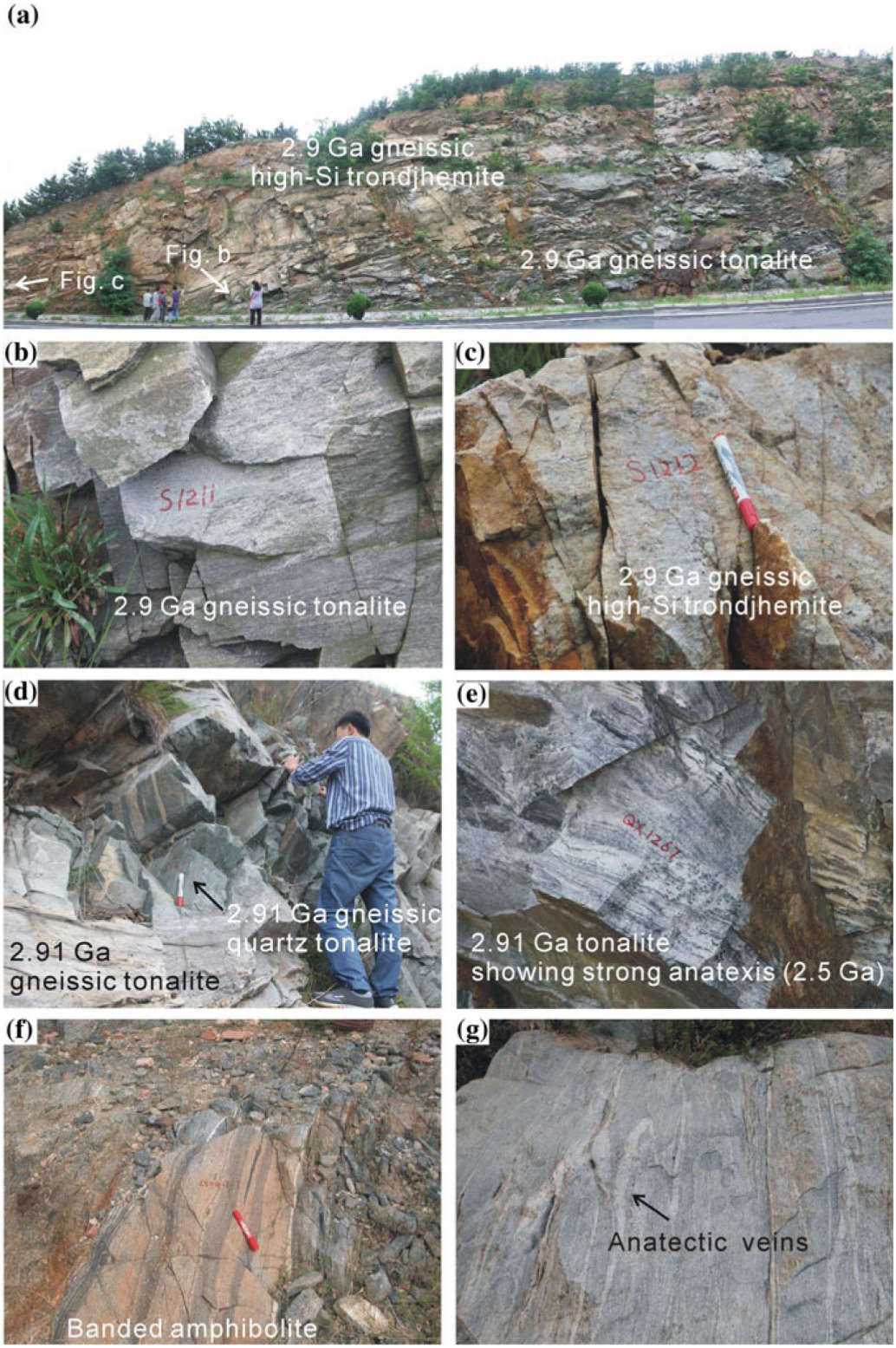
(a)
2.9 Ga gneissic high-Si trondjhemite
Fig. b
Fig. c
2.9 Ga gneissic tonalite
(b)
S1211
2.9 Ga gneissic tonalite
(c)
S1212
2.9 Ga gneissic high-Si trondjhemite
(d)
2.91 Ga gneissic quartz tonalite
2.91 Ga gneissic tonalite
(e)
QX1267
2.91 Ga tonalite showing strong anatexis (2.5 Ga)
(f)
Banded amphibolite
(g)
Anatectic veins

◀ **Fig. 16** Field photographs of Mesoarchean rocks in the North China Craton. **a** 2.9 Ga gneissic high-Si trondhjemite (*top*) in contact with gneissic tonalite (*bottom*), Qixia, eastern Shandong; **b** 2.9 Ga gneissic tonalite, local enlargement in figure a; **c** 2.9 Ga gneissic high-Si trondhjemite, local enlargement in figure a; **d** relationship between 2.91 Ga gneissic quartz diorite and 2.91 Ga gneissic tonalite, Qixia, eastern Shandong; **e** 2.91 Ga gneissic trondhjemite, Qixia, eastern Shandong; **f** 2.84 Ga amphibolites showing banded structures, Lushan, Henan; **g** anatectic veins in 2.83 Ga gneissic tonalite, Lushan, Henan

However, the dated zircons exhibit strong recrystallization and overgrowth, and it is therefore likely that these are ~2.8 Ga TTG rocks that underwent strong metamorphism in the early Neoarchean. More work is required to identify whether or not there are ~2.7 Ga rocks in the area.

Mesoarchean detrital and xenocrystic zircons were discovered all over the NCC such as Alax, Guyang, Wutai, Fuping, Dengfeng, eastern Hebei, Huoqiu, western Shandong, and eastern Shandong (Fig. 1) (Jian et al. 2012; Kröner et al. 1988; Shen et al. 2004, 2005; Wan et al. 2006, 2010a, b; Wang et al. 1998, 2014a, b, c, d, e; Zhang et al. 2014a, b).

2.4 Neoarchean (2.8–2.5 Ga)

2.4.1 Early Neoarchean (2.8–2.6 Ga)

Two magmatic events can be recognized in the Neoarchean crust formation and evolution, namely an early Neoarchean event (2.8–2.6 Ga) and a late Neoarchean event (2.6–2.5 Ga). 2.80–2.76 Ga rocks are rare, and the most important tectono-thermal event is 2.79–2.77 Ga metamorphism recorded in the Lushan area near the southern margin of the craton (Liu et al. 2009a). The identification of widespread ~2.7 Ga rocks is one of the most important discoveries made in recent years. These rocks are widespread, including western Shandong, eastern Shandong, Guyang, Fuping, Hengshan, Zanhuang, Zhongtiao, and Huoqiu (Fig. 1) (Cao et al. 1996; Dong et al. 2012a; Du et al. 2003, 2005, 2010; Guan et al. 2002; Han et al. 2012; Jahn et al. 2008; Jiang et al. 2010; Kröner et al. 2005a; Lu et al. 2008; Wan et al. 2010b, 2011b; Wang et al. 2014a, b, c, d, e; Wang et al. 2009a, b; Yang et al. 2013a, b; Zhu et al. 2013).

In eastern Shandong, the spatial distribution of 2.7 and 2.9 Ga rocks is uncertain. However, they show close spatial relationships with 2.7 Ga rocks occurring extensively in a southwest to northeast direction with a total area of >100 km^2 (Fig. 15). These Archean rocks underwent strong upper amphibolite- to granulite-facies metamorphism at the end of the Neoarchean (Jahn et al. 2008; Liu et al. 2011; Wu et al. 2014; Xie et al. 2014b). Similar to 2.9 Ga rocks, the 2.7 Ga assemblages exhibit strong deformation and anatexis with neosome material occurring in local outcrops (Fig. 18a). This makes it difficult to distinguish between

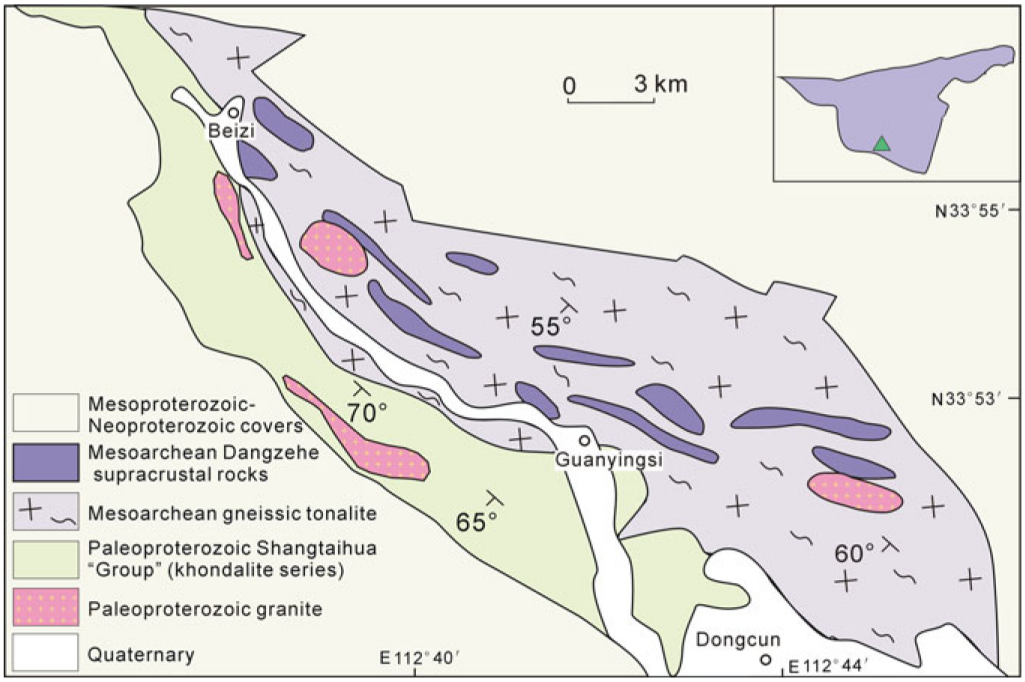

Fig. 17 Simplified geological sketch map of the Lushan area, southern margin of the North China Craton. Modified after Liu et al. (2009c). Triangle in inset map shows location of Fig. 17 in the NCC

2.9 and 2.7 Ga assemblages. At present, the only way to identify these different rocks is by zircon dating.

In western Shandong, Wan et al. (2010c, 2011b) divided the Archean basement into three belts (Fig. 19), namely a late Neoarchean belt of crustally derived granitoids in the northeast that predominantly consists of 2.53–2.49 Ga monzogranite and syenogranite (Belt A), an early Neoarchean belt in the center that is mainly composed of 2.75–2.60 Ga TTGs and supracrustal rocks (Belt B), and a late Neoarchean belt of juvenile rocks in the southwest that is dominated by granodiorite, gabbro, quartz diorite, and tonalite, with minor monzogranite and syenogranite (Belt C). Western Shandong is an area where 2.75–2.7 Ga rocks are most widely distributed in the NCC. Different types of ~2.7 Ga TTGs can be observed in contact with each other in Belt B, showing similar or different styles of deformation (Fig. 18b, c). Furthermore, western Shandong is the only area where early Neoarchean supracrustal rocks have so far been identified in the NCC. In an earlier study, the Taishan "Group," including the Yanlingguan, Liuhang, and Shancaoyu "Formations," were considered to be early Neoarchean in age (Cao et al. 1996). However, more recent studies established that only the Yanlingguan "Formation" and the lower part of the Liuhang "Formation" formed during the early Neoarchean (named the Yanlingguan-Liuhang succession). They are mainly composed of amphibolite and metamorphosed ultramafic rocks. Some of these rocks contain fine spinifex textures (Fig. 18d). Amphibolites with abundant pillow structures are abundant (Fig. 18e), and some show strong deformation (Fig. 18f, g).

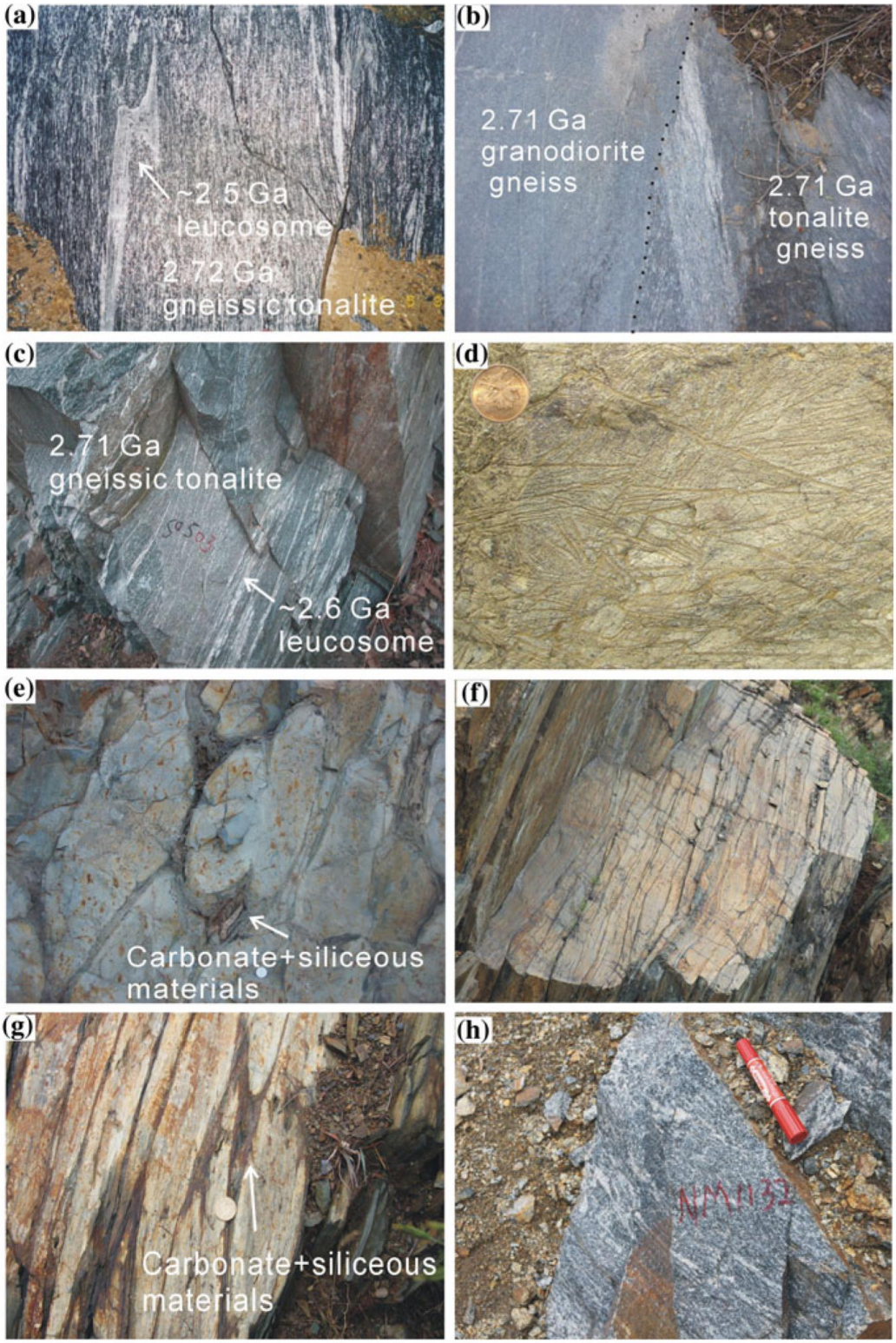
(a)
~2.5 Ga
leucosome
2.72 Ga
gneissic tonalite
(b)
2.71 Ga
granodiorite
gneiss
2.71 Ga
tonalite
gneiss
(c)
2.71 Ga
gneissic tonalite
~2.6 Ga
leucosome
(d)
(e)
Carbonate+siliceous
materials
(f)
(g)
Carbonate+siliceous
materials
(h)

◀ **Fig. 18** Field photographs of early Neoarchean rocks in the North China Craton. **a** 2.7 Ga gneissic tonalite showing anatexis, Qixia, eastern Shandong; **b** cutting relationship between 2.71 Ga gneissic tonalite and 2.71 Ga gneissic granodiorite, Taishan, western Shandong; **c** 2.71 Ga gneissic tonalite showing anatexis and deformation, Taishan, western Shandong; **d** meta-komatiite with fine spinifex structures, Sujiagou, western Shandong; **e** amphibolite with pillow lava structures, Qixingtai, western Shandong; **f** deformed pillow lava in amphibolite, Qixingtai, western Shandong; **g** carbonate + siliceous material occurring at the end of deformed pillow lava in amphibolite, Qixingtai, western Shandong; **h** 2.69 Ga gneissic tonalite showing anatexis, Xi Ulanbulang, Yinshan

Xi Wulanbulan is the only area where 2.7 Ga tonalite was identified in the Western Block of the NCC. It extends in a north–south direction over an area of >10 km^2 (Fig. 20) and shows strong metamorphism, deformation, and anatexis (Fig. 18h) with metamorphic zircons recording an age of ~2.5 Ga. These tonalities occur together with the late Neoarchean Xinghe "Group" and other TTG rocks (Dong et al. 2012a; Ma et al. 2013a, b, c).

Wan et al. (2014a) summarized the spatial distribution, rock types, geochemistry, and Nd–Hf isotopic compositions of ~2.7 Ga granitoids in the NCC. They are mainly tonalitic in composition and show large variations in SiO_2, ΣFeO, MgO, and CaO. They can be subdivided into two types in terms of REE contents (Fig. 8c). Whole-rock Nd and Hf-in-zircon isotopic compositions indicate that the strong 2.7 Ga tectono-thermal event mainly involved juvenile additions to the continental crust with recycling of older crust only in local areas.

Ca. 2.6 Ga rocks were also reported in several areas of the NCC, including western Shandong, Hebi, Zhongtiao, Guyang, and Bayan Obe (Fan et al. 2010; Jian et al. 2012; Wan et al. 2015b; Zhang et al. 2012a, b, c, d, e, f; Zheng et al. 2012; Ma unpublished data). In most of these areas, ~2.7 Ga rocks also occur. Western Shandong is the area where both 2.7 and 2.6 Ga rocks are widely distributed (Wan et al. 2015b). They mainly occur together in Belt B (Fig. 21) and include hornblendite (meta-pyroxenite), gneissic tonalite, gneissic trondhjemite, and gneissic granite (Fig. 22a–d). Geological records are almost continuous from 2.75 to 2.59 Ga (Fig. 23). Ca. 2.6 Ga metamorphism and anatexis have also been identified (Du et al. 2003, 2005; Lu et al. 2008; Ren unpublished data). This strong tectono-thermal event resulted in the formation of migmatites in Belt B (Fig. 22e–f). These are important for considering 2.6 Ga as the boundary between the middle to early Neoarchean and late Neoarchean (2.6–2.5 Ga) in western Shandong. No ~2.7 Ga metamorphism and ~2.6 Ga supracrustal rocks have been identified there, and it appears that there was a "quiet period" between 2.60 and 2.56 Ga. We speculate that this time subdivision is applicable to the entire NCC.

2.4.2 Late Neoarchean (2.6–2.5 Ga)

2.59–2.57 Ga rocks and metamorphism are rare. However, a 2.56–2.5 Ga tectono-thermal event is very strong, resulting in extensive distribution of supracrustal and intrusive rocks and metamorphism of this age all over the NCC

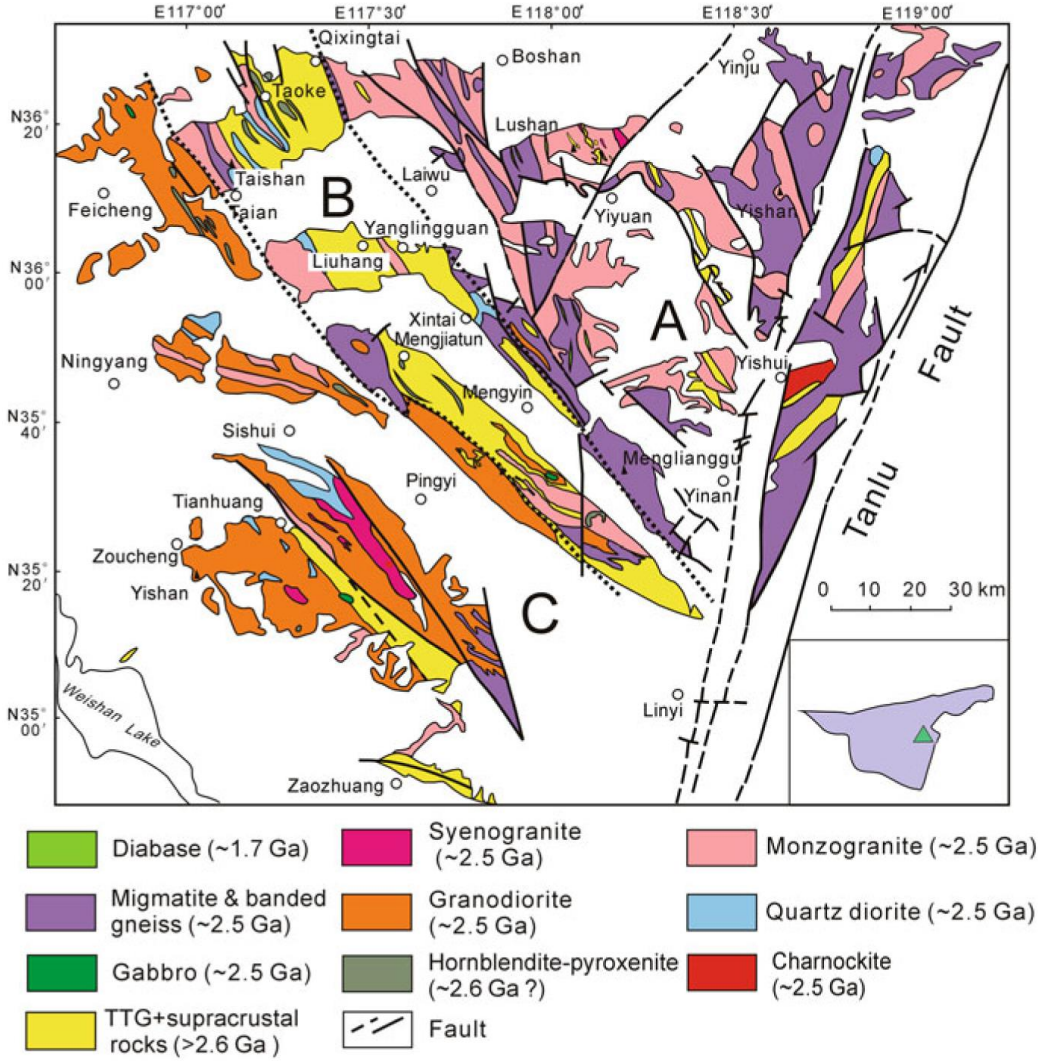

Fig. 19 Geological map of western Shandong. Modified after Wan et al. (2010c). *Belt A* A late Neoarchean crustally derived granite belt in the northeast that consists predominantly of 2.525–2.49 Ga monzogranite and syenogranite; *Belt B* An early Neoarchean belt in the center which is mainly composed of 2.75–2.60 Ga TTG and supracrustal rocks; *Belt C* A late Neoarchean belt of juvenile rocks in the southwest that is dominated by granodiorite, gabbro, quartz diorite, and tonalite, with some monzogranite and syenogranite. *Triangle* in *inset* map shows location of Fig. 19 in the NCC

(Chen 2007; Cheng et al. 2004; Cui et al. 2013, 2014; Dai et al. 2012, 2013; Dong et al. 2012b; Geng et al. 2002, 2006, 2010; Grant et al. 2009; Guo et al. 2005, 2008; Han et al. 2014a, b; He et al. 2005; Jahn et al. 1988; Jian et al. 2012; Kröner et al. 1998, 2005a, b; Li et al. 2010a, b, 2012; Liu et al. 2002, 2004a, 2007, 2009b, 2011, 2012a, 2012b; 2012c, 2014, 2011a; Lu et al. 2008; Lü et al. 2012; Ma et al. 2012, 2013a, b, c; Ma et al. 2013a, b, 2014a, b; Peng et al. 2012; Peng 2013; Peng et al. 2013; Ren et al. 2011; Shen et al. 2004, 2005, 2007; Shi et al. 2012; Song et al. 2009; Sun et al. 1991, 2010, 2014; Sun and Guan 2001; Tian et al. 2005; Wan et al.

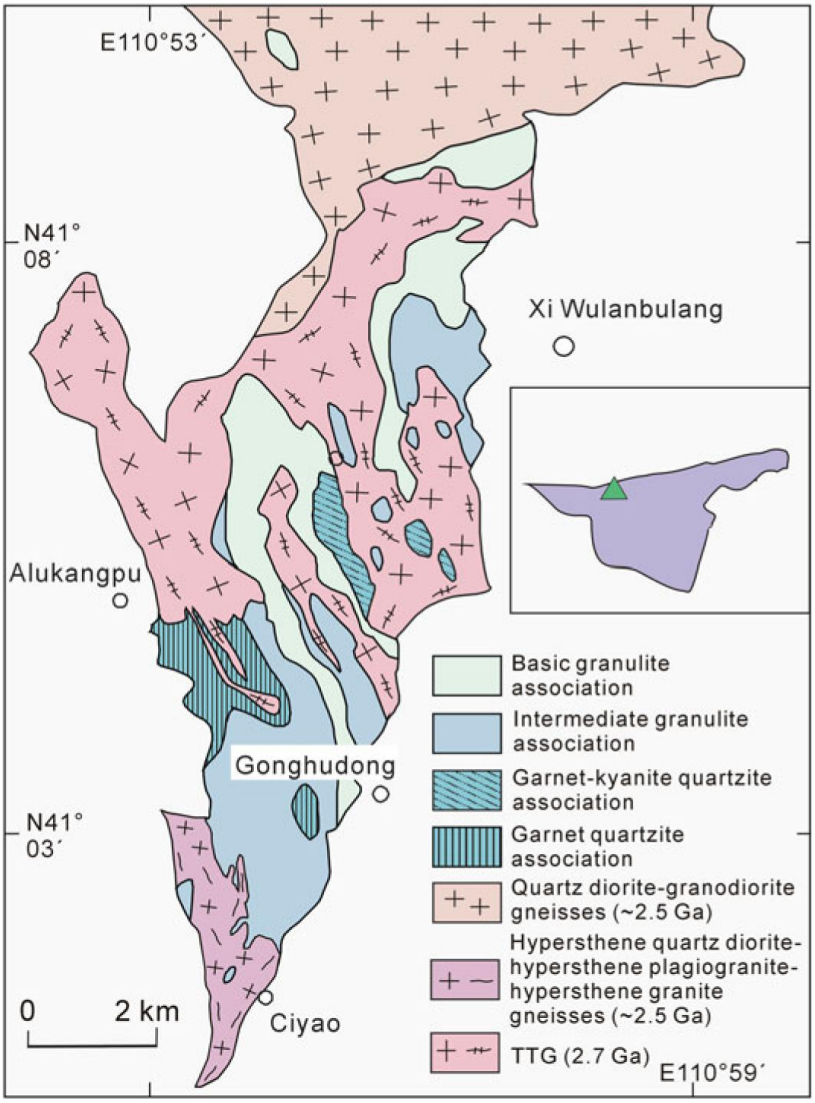

Fig. 20 Geological map of the Xi Ulanbulang area, Yinshan. Modified after Dong et al. (2012a) and Ma et al. (2013). *Triangle* in *inset* map shows location of Fig. 20 in the NCC

2005b, 2009b, c, 2010b, c, 2011a, c, 2012b, c, d, 2015a; Wang et al. 2004, 2011; Wang et al. 2014; Wang et al. 2014; Wang et al. 2010; Wang et al. 2009; Wilde et al. 2004a, 2005; Wu et al. 1998; Xiang et al. 2012; Yang et al. 2008, 2009, 2011; Yang 2013; Zhai et al. 2000, 2005; Zhang et al. 2013; Zhang et al. 2012a; Zhang et al. 2011; Zhang et al. 2014; Zhao et al. 2002, 2009; Zhao et al. 2008; Zhao et al. 2008; Zhou et al. 2009, 2011, 2014).

There are abundant Neoarchean (mainly 2.55–2.5 Ga) detrital and xenocrystic zircons in younger rocks and river sands (e.g., Diwu et al. 2012; Wan et al. 2011a). Late Neoarchean supracrustal rocks are mainly composed of mafic to felsic granulite, amphibolite, fine-grained biotite gneiss (leptinite), banded iron formation (BIF), and (fuchsite) quartzite, with the metamorphic grade ranging from

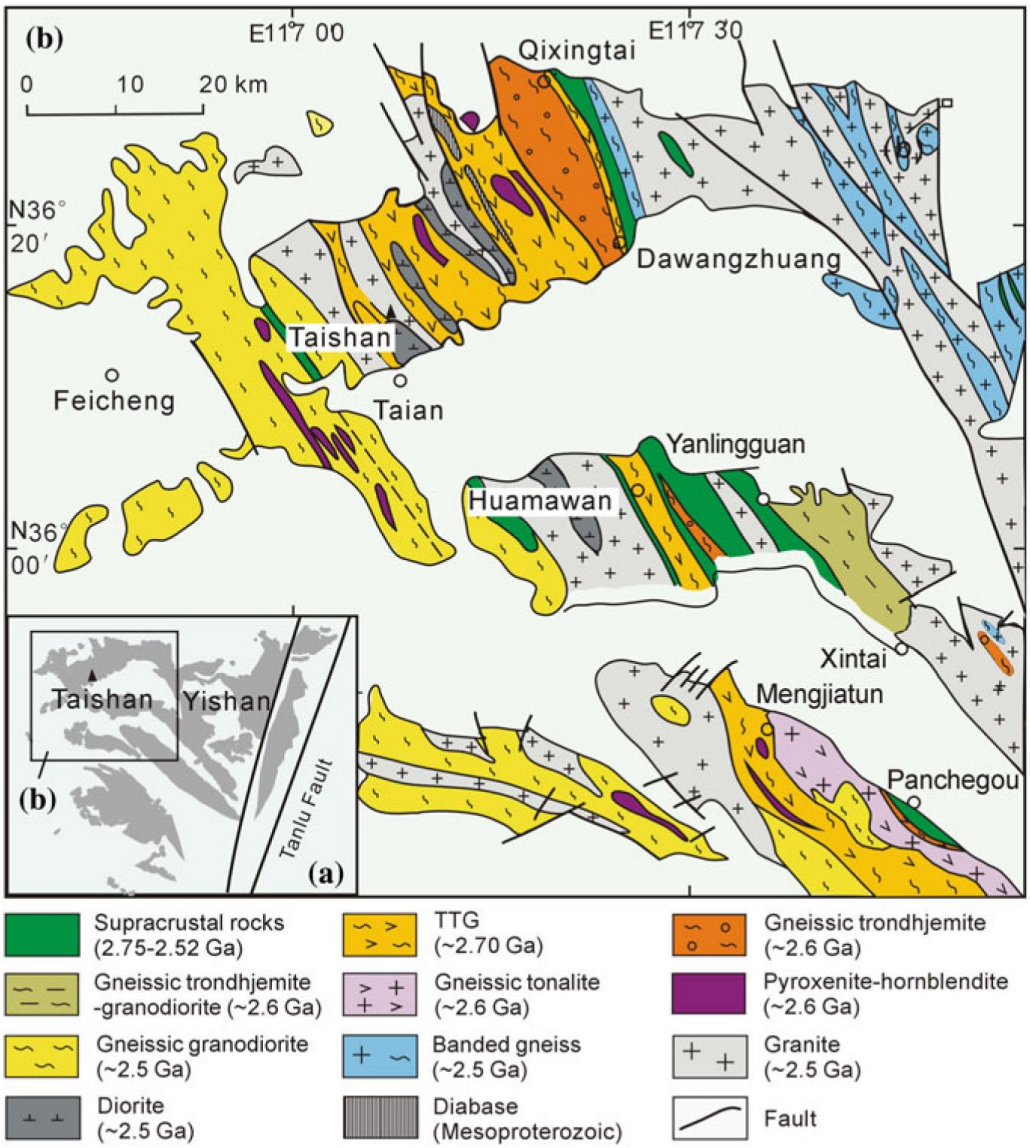

Fig. 21 Geological map of the Taishan-Mengjiatun area, western Shandong (Wan et al. 2015b)

predominantly amphibolite to granulite facies. Mafic granulite and amphibolite show light REE enrichment or flat REE patterns and are commonly rich in LILE and depleted in Nb and Ta (Wan et al. 1997b). Fine-grained biotite gneisses generally show compositional features of dacitic rocks. Late Neoarchean intrusive rocks are variable in composition, ranging from ultramafic to felsic, but TTGs and crustally derived granites constitute the main components. It is not until the late Neoarchean that granodiorites are widely distributed in the NCC. Syenogranites predominantly formed between 2.53 and 2.49 Ga and can be further subdivided into two phases with most showing massive structures and emplacement during the second phase (2.52–2.48 Ga), whereas the first phase (2.53–2.52 Ga) syenogranites show metamorphism and deformation (Wan et al. 2012b). All syenogranites share

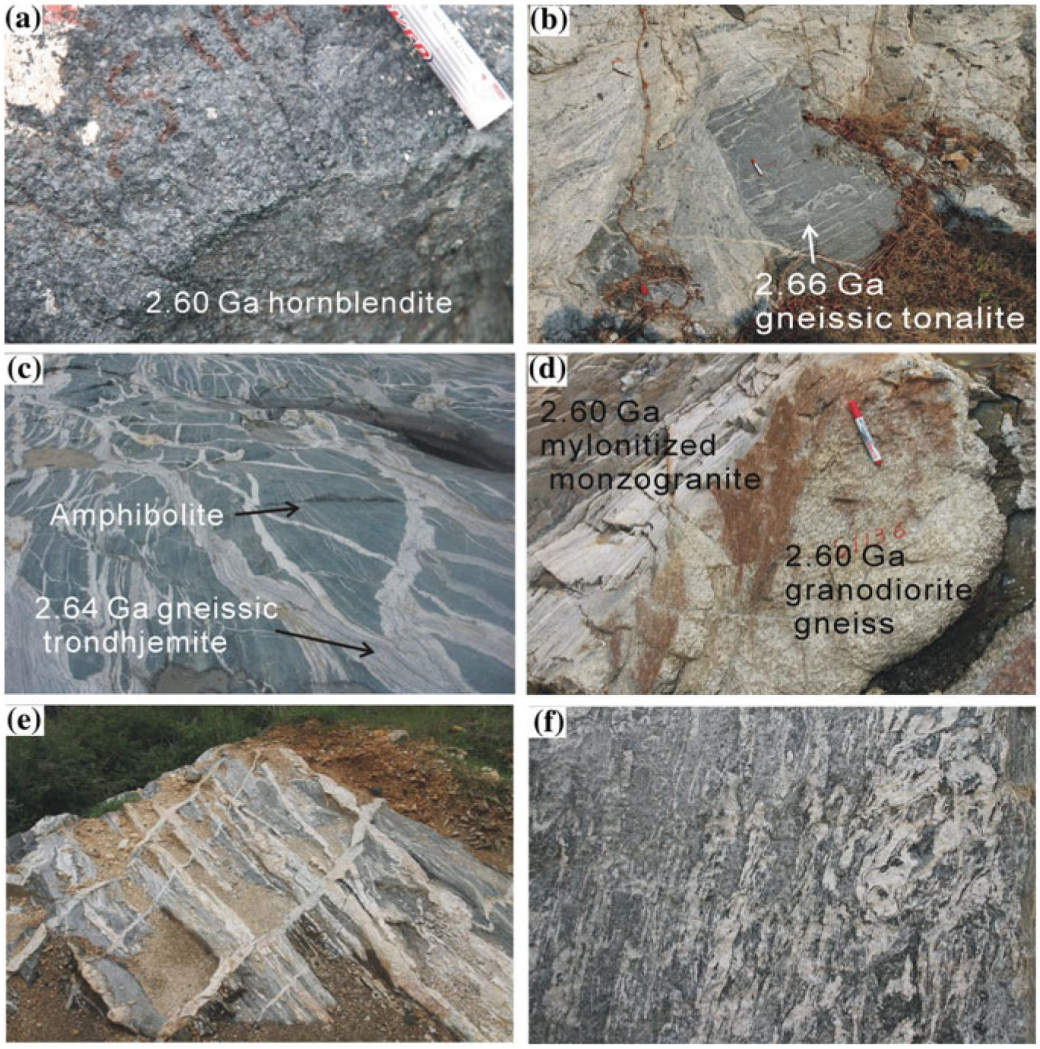

Fig. 22 Field photographs of early Neoarchean rocks in western Shandong. **a** 2.60 Ga hornblendite, southwest of Qixingtai; **b** 2.66 Ga gneissic tonalite, Yishan; **c** gneissic trondhjemite cutting amphibolite, Taishan; **d** relationship between 2.60 Ga gneissic granodiorite and 2.60 Ga mylonitized monzogranite, Xintai; **e** 2.7 Ga gneissic tonalite showing anatexis at ~2.6 Ga, Taishan; **f** 2.7 Ga gneissic tonalite showing anatexis at ~2.6 Ga, Taishan

the same major element compositions, being high in SiO_2 and low in CaO, ΣFeO, MgO, TiO_2, and P_2O_5. However, they have variable REE compositions and can be subdivided into three types (Fig. 8d). In order to better understand the late Neoarchean geological features in various parts of the NCC, several areas are described below.

(1) Western Shandong

Late Neoarchean magmatism is widespread with peak ages of 2.53–2.52 Ga (Fig. 24). A recent study indicated that the Shancaoyu "Formation" and the upper part of the Liuhang "Formation" formed during the late Neoarchean rather than in the early Neoarchean (Wan et al. 2012c). Western Shandong is the only area where

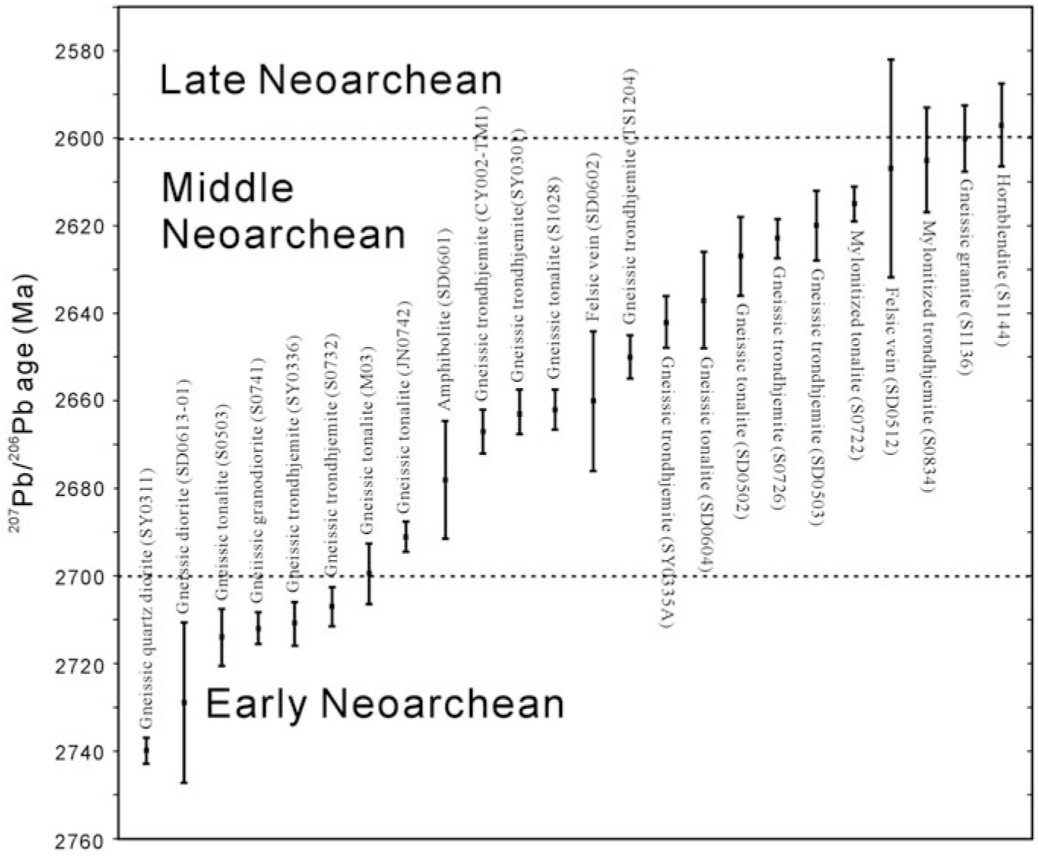

Fig. 23 Zircon age variation diagram (with *error bars*) for early to *middle Neoarchean* magmatic rocks in western Shandong. Data are from Du et al. (2003), Jiang et al. (2010), Lu et al. (2008), and Wan et al. (2011b, 2015b)

Fig. 24 Age histogram of zircons from Neoarchean rocks in western Shandong. Data are from Du et al. (2003), Jiang et al. (2010), Lu et al. (2008), Wan et al. (2010c, 2011b, 2015b), and Wan (unpublished data)

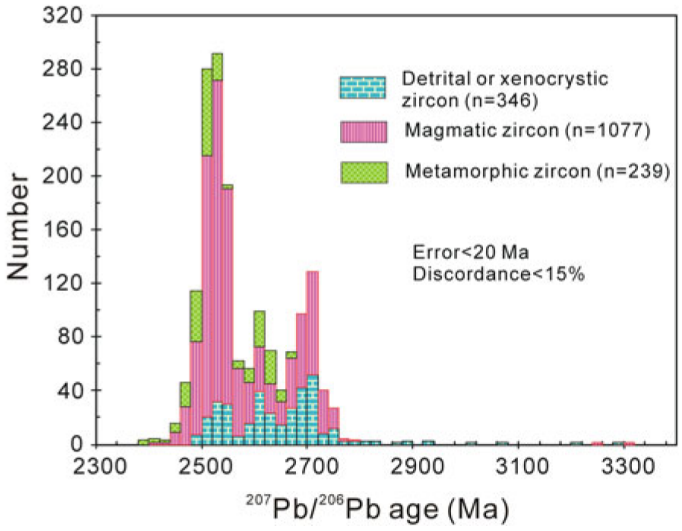

both early and late Neoarchean supracrustal rocks were identified. The late Neoarchean supracrustal rocks occur in different belts and mainly consist of meta-conglomerate, fine-grained biotite gneiss, fine-grained two-mica gneiss, mica schist, BIF, and felsic metavolcanic rocks. The metaconglomerates are interlayered with fine-grained biotite gneiss (Fig. 25a), and the conglomerate pebbles vary in size and mainly consist of TTG, monzogranite, and fine-grained felsic volcanic rocks. Some fine-grained biotite gneisses show sedimentary structures such as bedding (Fig. 25b), suggesting a clastic origin. However, in many cases, their protoliths are difficult to determine (volcanic or sedimentary) because of strong metamorphism and deformation (Fig. 25c). Mantle-derived igneous rocks in Belt C predominantly consist of gabbro, diorite, tonalite, and granodiorite. Magma mixing can be observed between different rock types (Fig. 25d, e). Different migmatite types are associated with crustally derived granites in Belt A as a result of anatexis of early supracrustal and granitoid rocks. TTGs of early and late Neoarchean ages were identified as protoliths of the anatectic rocks (Figs. 22b and 25f).

(2) Eastern Hebei

Late Neoarchean supracrustal and intrusive rocks are widespread (Fig. 26), apart from ancient crustal components documented by 3.88–3.40 Ga detrital zircons and 3.40–2.95 Ga orthogneisses in Huangbaiyu, as mentioned before. 2.55–2.53 Ga tonalites and quartz diorites are most important in the west, and 2.53–2.51 Ga granites are most important in the east, where magma mingling between granite and diorite has been also identified (Fig. 27a) (Nutman et al. 2011; Yang et al. 2008).

The Qian'an "Group" was considered to be Mesoarchean in age, but recent zircon dating indicates that most of the supracrustal rocks formed at the end of the Neoarchean (Han et al. 2014a; Zhang et al. 2011; Wan, unpublished data). Late Neoarchean supracrustal rocks commonly occur as enclaves of variable sizes in granitoids and show spatial variations in rock association, metamorphism, and deformation, with metamorphic grades varying from granulite facies in the west to lower amphibolite facies (epidote amphibolite facies) in the east and greenschist facies in local areas. These rocks have different names in different areas (Fig. 26). The Zunhua and Qian'an "Groups" and associated TTG rocks in the Zunhua-Santunying area underwent granulite-facies metamorphism and were commonly affected by amphibolite-facies retrogression. The supracrustal rocks extend in a north–south direction and are mainly composed of biotite–plagioclase gneiss, hornblende–plagioclase gneiss, two-pyroxene granulite, amphibolite, meta-ultramafic rock, and BIF. Strong metamorphism resulted in anatexis of the supracrustal rocks (Fig. 27b).

The Luanxian "Group" occurs in the Luanxian-Lulong area and is composed of fine-grained biotite gneiss, amphibolite, and BIF, whereas at Huangbaiyu, the Qian'an "Group" and Luanxian "Group" are separated by a ~2.5 Ga granite. The Dantazi and Zhuzhangzi "Groups" at Qinlong exhibit lower amphibolite-facies metamorphism. The Dantazi "Group" (or Shuangshanzi "Group") is dominated by fine-grained two-mica gneiss, garnet–mica schist, two-mica quartz schist, mafic and felsic metavolcanic rocks, and BIF. It is covered unconformably by the Zhuzhangzi "Group" (or Qinglong "Group"), commonly with >100 m of conglomerate at the

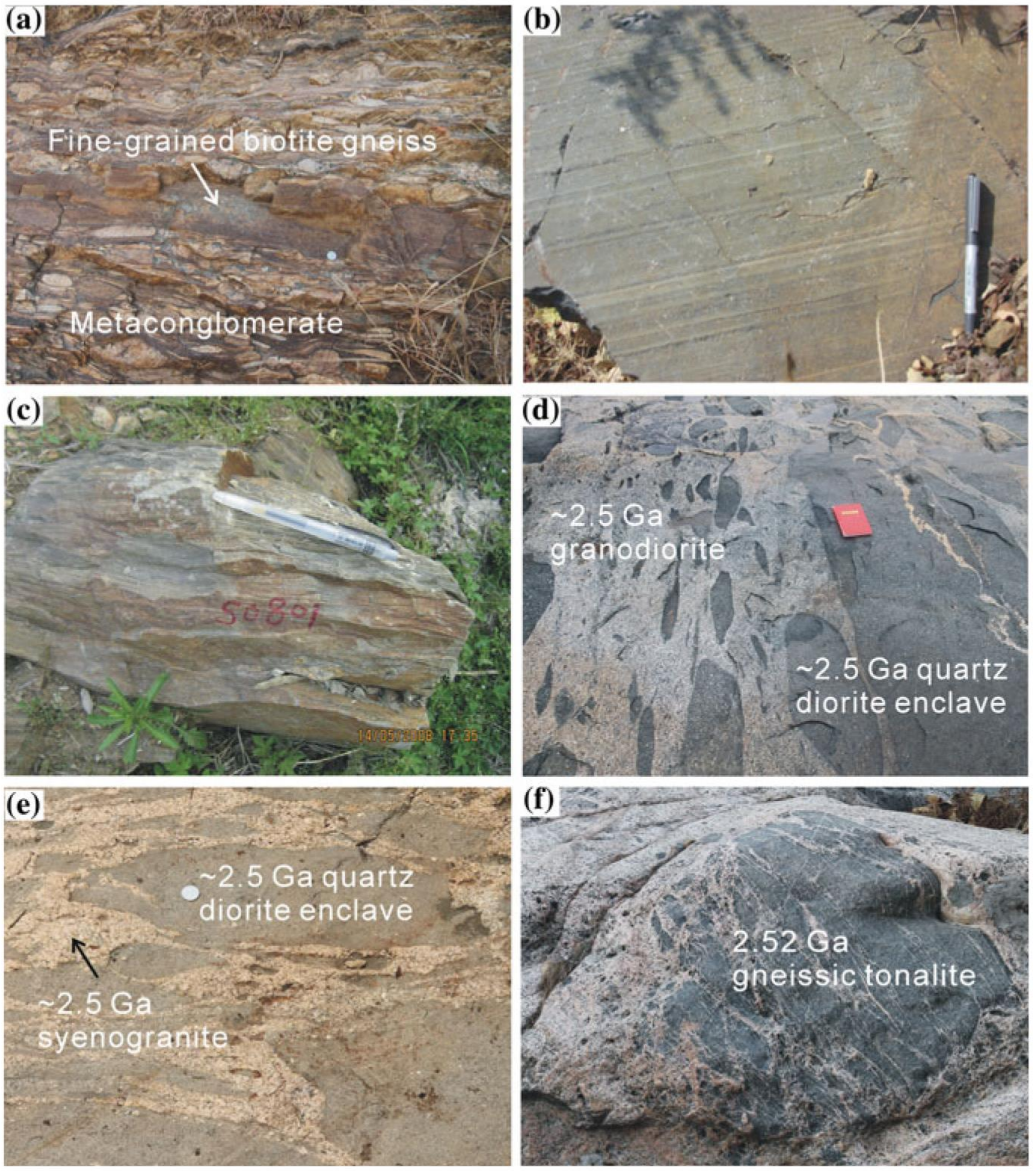

Fig. 25 Field photographs of late Neoarchean rocks in western Shandong. **a** Metaconglomerates interlayered with metasediments; pebbles are mainly TTG and felsic volcanic rocks, upper part of Liuhang "Formation," Huamawan; **b** metasedimentary rock showing bedding, Shancaoyu "Formation," Qixingtai; **c** mylonitized fine-grained biotite gneiss (S0801) of Shancaoyu "Formation," Panchegou; **d** magma mingling between ~2.5 Ga granodiorite and quartz diorite, showing large variations in proportion, southeast of Tianhuang; **e** magma mingling between ~2.5 Ga syenogranite and quartz diorite, southeast of Tianhuang; **f** 2.52 Ga gneissic tonalite showing anatexis, Yinshan

base (Fig. 27c). Furthermore, the Zhuzhangzi "Group" contains fine-grained two-mica gneiss, fine-grained biotite gneiss, mica schist, quartz schist, biotite–hornblende schist, and BIF. Ca. 2.5 Ga BIFs are well developed in eastern Hebei and contain important iron deposits. The supracrustal rocks in the Qinlong area

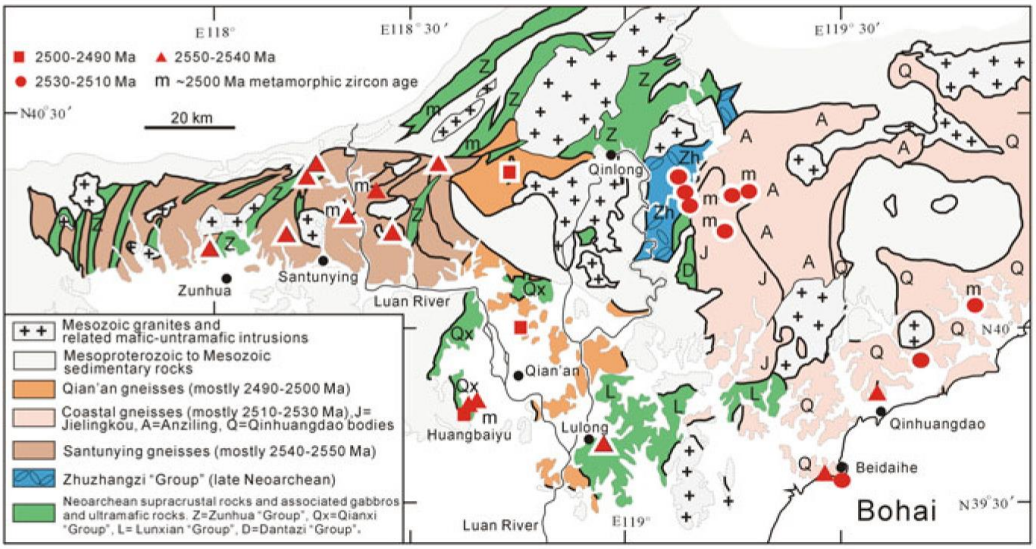

Fig. 26 Geological map of eastern Hebei, modified after Nutman et al. (2011). For location in the NCC, see Fig. 1

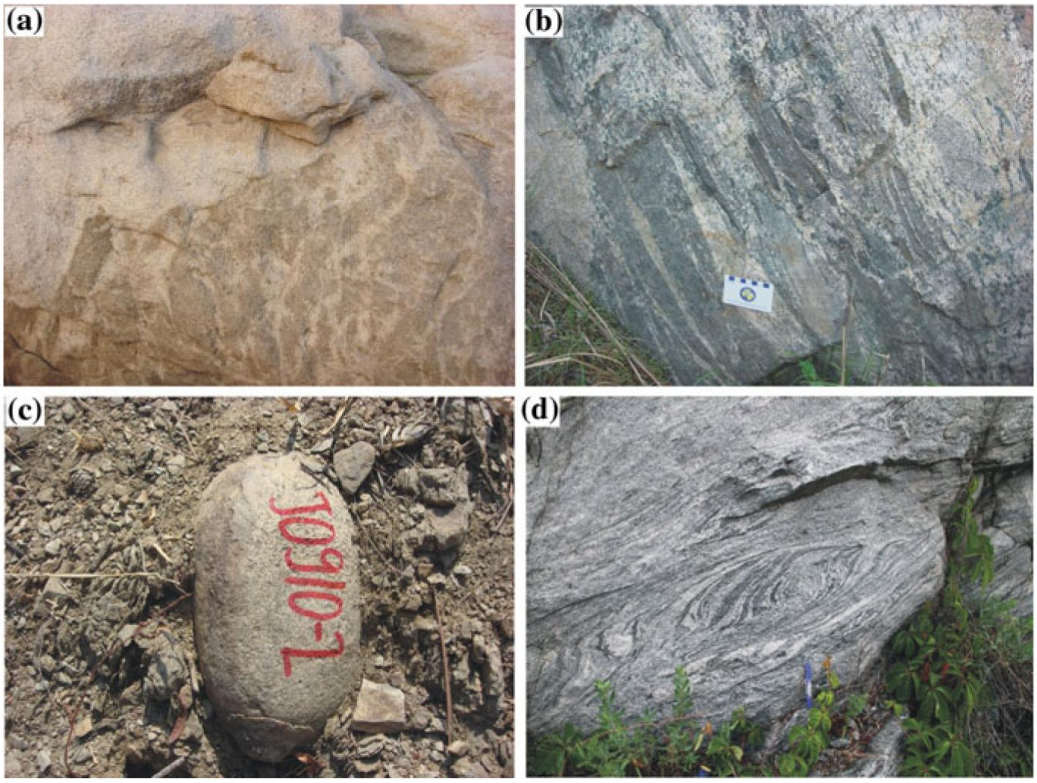

Fig. 27 Field photographs of late Neoarchean rocks in eastern Hebei. **a** Magma mingling between ~2.5 Ga granite and diorite, Beidaihe; **b** anatexis of granulite-facies gneiss (the Zunhua "Group"), north of Santunying; **c** metaconglomerate at the bottom of the Zhuzhangzi "Group," southeast of Qinlong; **d** anatexis of TTG rock, west of Anziling

commonly underwent lower amphibolite-facies metamorphism, but the TTG rocks east of Qinlong show strong anatexis and deformation (Fig. 27d). In the eastern coastal area of Hebei Province, weakly deformed 2.53–2.51 Ga granites occur together with subordinate granodiorites, diorites, and magnesian gabbros and contain slightly older Neoarchean granitoid inclusions.

Nutman et al. (2011) suggested that Neoarchean magmatism in eastern Hebei was not a single protracted event but was marked by temporally, geographically, and geochemically distinct pulses of igneous activity at 2.55–2.535, 2.53–2.52 Ga, and 2.50–2.49 Ga, respectively, with the latter accompanied by granulite-facies metamorphism.

(3) Fuping-Wutai-Hengshan

This is an important and famous exposure of Neoarchean rocks in the NCC with a long history of research. Based mainly on the work of Cheng et al. (2004), Guan et al. (2002), Han et al. (2012), Kröner et al. (2005a, 2005b, 2006), Li et al. (2010a), Liu et al. (2002), Liu et al. (2004a), Miao (2003), Qian et al. (2013), Trap et al. (2007, 2008), Wan et al. (2010a), Wang et al. (2010), Wei et al. (2014), Wilde et al. (2004a, 2004b, 2005), Wu et al. (1989, 1998), Zhang et al. (2006); Zhang et al. (2006); Zhang et al. (2007, 2009), and Zhao et al. (2011), some common features of the basement are summarized as follows (Fig. 28).

(1) The early Precambrian basement is composed of the Fuping Complex in a southeastern belt, the Wutai Complex in a central belt, and the Hengshan Complex in a northwestern belt. All of these are composed of intrusive and supracrustal rocks of different ages.
(2) Early Precambrian intrusive rocks mainly formed during the late Neoarchean (2.55–2.5 Ga), including TTGs (mainly tonalite and granodiorite) with some monzogranite and K-rich granite. 2.2–2.0 Ga intrusive rocks occur on a relatively small scale and are predominantly crustally derived granites with a few mantle-derived mafic–ultramafic rocks. Early Neoarchean (~2.7 Ga) TTGs and early Neoarchean and older detrital and xenocrystic zircons were also identified in the Fuping and Hengshan areas.
(3) No early Neoarchean or older supracrustal rocks have so far been found, but this does not mean that they do not occur in these areas. Late Neoarchean supracrustal rocks in the Wutai area are composed of mafic to felsic metavolcanic and clastic metasedimentary rocks, BIF, and minor limestone (the Wutai "Group"). In Fuping, late Neoarchean supracrustal rocks, named the Fuping "Group," are mainly composed of mafic to intermediate metavolcanic and clastic metasedimentary rocks and minor BIF and marble. Some or many biotite–plagioclase gneisses and hornblende–plagioclase gneisses of the Suojiazhuang-Yuanfang unit I of the Fuping "Group" may be strongly metamorphosed and deformed intrusive rocks (Yang, unpublished data). Late Neoarchean supracrustal rocks rarely occur as enclaves in the Hengshan Complex, including garnet-bearing biotite–plagioclase gneiss, BIF, and amphibolite. High-pressure garnet two-pyroxene granulites are derived from gabbroic dikes.

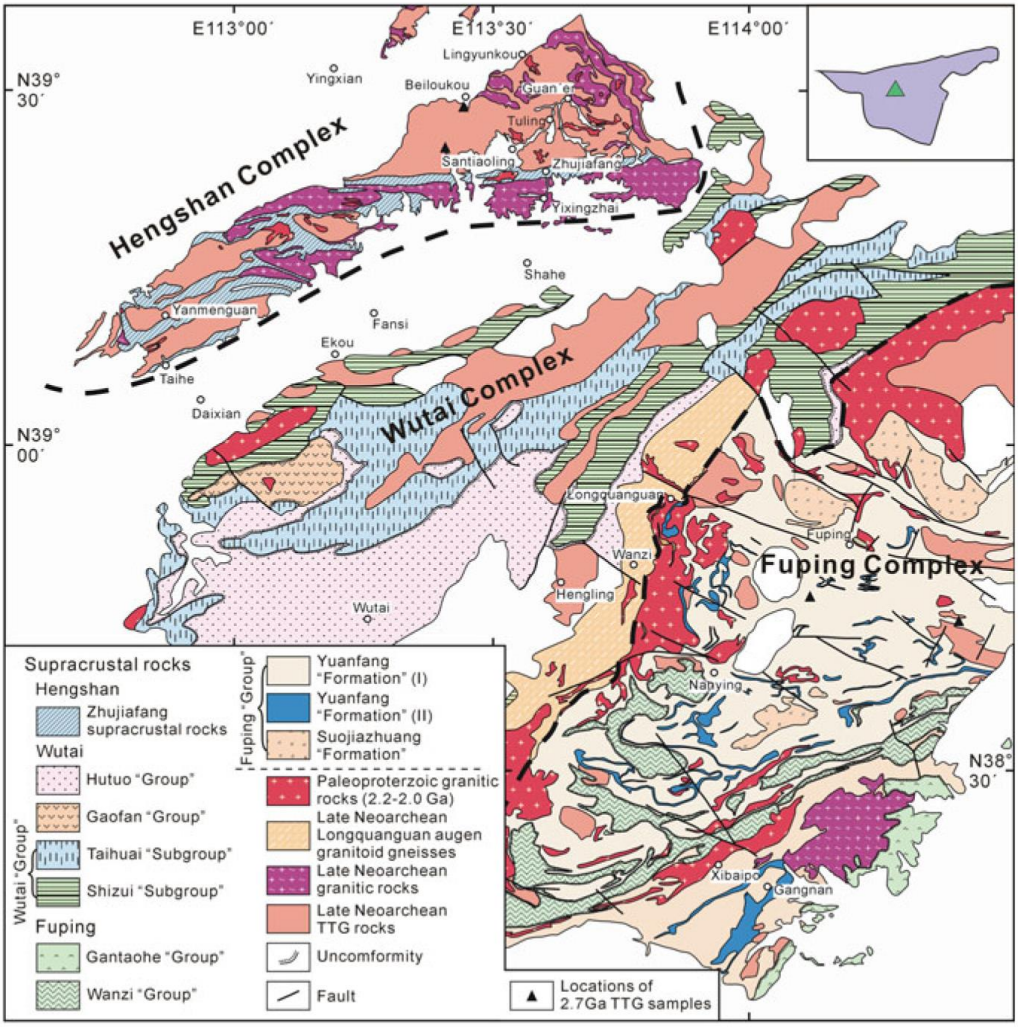

Fig. 28 Geological map of Hengshan-Wutai-Fuping, modified after Miao (2003), Cheng et al. (2004), Liu et al. (2004b), Li et al. (2010a, b), Zhao et al. (2011), and Qian et al. (2013). *Triangle* in *inset* map shows location of Fig. 28 in the NCC. The Yuanfang "Formation"(I) of the Fuping "Group" is mainly composed of anatectic biotite–plagioclase gneiss, hornblende–biotite plagioclase gneiss, and fine-grained biotite–plagioclase (two feldspar) gneiss (leptinite), and some of them may be metamorphic igneous rocks; Yuanfang "Formation"(II) of the Fuping "Group" is composed mainly of amphibolite, fine-grained garnet–biotite gneiss, fine-grained feldspar gneiss, fine-grained hornblende gneiss, banded iron formation, calc-silicate rock, and marble

(4) In Wutai, the Gaofan "Group," originally named as the Gaofan "Subgroup" of the Wutai "Group," unconformably overlies the Wutai "Group" and was deposited between 2.47 and 2.14 Ga. It should therefore be excluded from the Wutai "Group." The Hutou "Group" unconformably overlies the Gaofan "Group" and is considered to be ~2.14 Ga or younger in age. The Wanzi "Group" in the Fuping Complex was originally considered to be late Neoarchean in age, but some authors considered it to be early Paleoproterozoic (Guan et al. 2002; Li et al. 2005). It is composed of

metasedimentary rocks including marble and is similar to the khondalite sequences of the northwestern NCC in rock association and metamorphism.

(5) Whole-rock Nd and Hf-in-zircon isotopic studies indicate that the formation of all early and most late Neoarchean TTGs involved juvenile magmatic additions to the continental crust; most late Neoarchean and early Paleoproterozoic (2.2–2.0 Ga) granitoids formed by recycling of early Neoarchean or older crustal material.

(6) The Fuping Complex and the northern portion of the Hengshan Complex underwent upper amphibolite- to granulite-facies metamorphism, whereas the Shizui "Subgroup" of the Wutai "Group" and the southern portion of the Hengshan Complex underwent lower amphibolite-facies metamorphism, and the Taihuai "Subgroup" of the Wutai "Group" underwent greenschist-facies metamorphism. Metamorphic grades vary from granulite facies to greenschist facies from both sides to the center. Consequently, the late Neoarchean granitoid bodies in Wutai commonly show weaker metamorphism and deformation than their equivalents in the Fuping and Hengshan complexes.

(7) Fold axes, foliations, and lineations mainly extend in a west–east or southwest–northeast direction. Three episodes of folding and two phases of ductile thrusting and shearing have been identified (Li et al. 2010a). There are two major shear zones: One is the west–east-striking Zhujiafang shear zone separating the granulite-facies Hengshan Complex in the north from the amphibolite-facies Hengshan Complex in the south. Another is the southwest–northeast-striking Longquanguan shear zone separating the Wutai "Group" in the northeast from the Fuping Complex in the southwest.

(8) A strong late Paleoproterozoic tectono-thermal event is recorded by well-developed 1.95–1.83 Ga metamorphic zircons. This event resulted in strong metamorphism and deformation in the Fuping and Hengshan complexes and the lower part of the Wutai Complex and formation of the above two shear zones. ~2.5 Ga metamorphic zircons have also been identified in Fuping (Yang, unpublished data), but their significance is uncertain.

(4) Yinshan

Little was known about the early Precambrian basement of the Yinshan Block, but new data were acquired in recent years (Chen 2007; Dong et al. 2012a, b; Fan et al. 2010; Jian et al. 2012; Li et al. 1987; Liu et al. 2012d, 2014; Ma et al. 2013; Ma 2013a, b, 2014a, b; Mei 1991; Zhang et al. 2003; Zhang and Liu 2004; Zhang et al. 2014). The main features of the basement are summarized as follows (Figs. 29 and 30).

(1) There are 2.7 Ga tonalites and 2.6 Ga granites and older xenocrystic zircons in ~2.5 Ga granitoid rocks. The 2.7 Ga tonalite exposure is >10 km^2 in size. Zhang et al. (2014) obtained a zircon age of 2.51 Ga for a charnockite exposed near a 2.7 Ga tonalite dated by Ma et al. (2013) and interpreted this to reflect emplacement of the charnockite precursor. However, considering strong recrystallization of the zircon cores, the significance of the 2.51 Ga age is

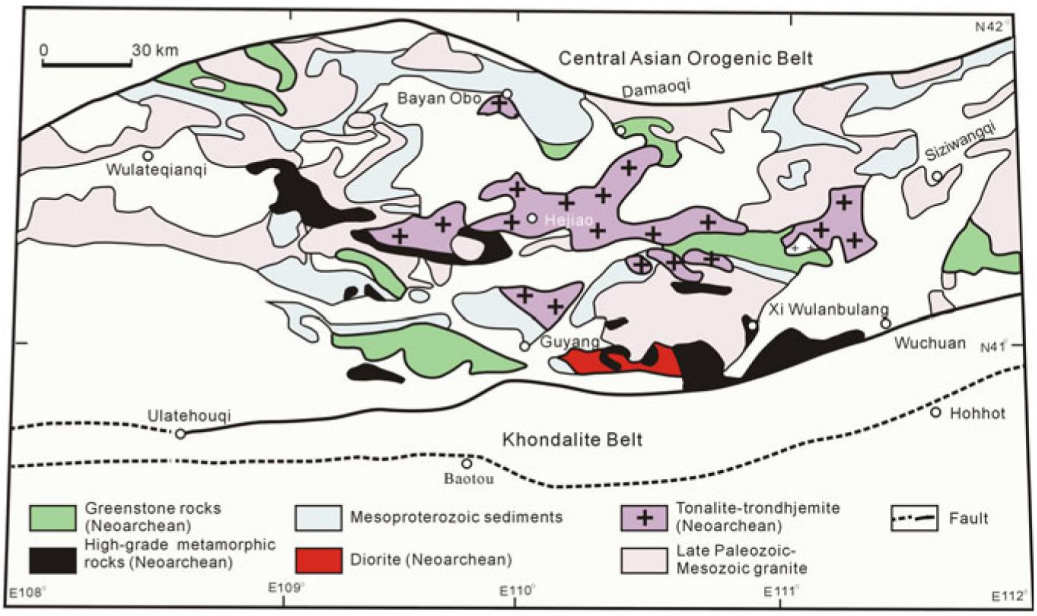

Fig. 29 Geological map of Yinshan, modified after Jian et al. (2012). For location in the NCC, see Fig. 1

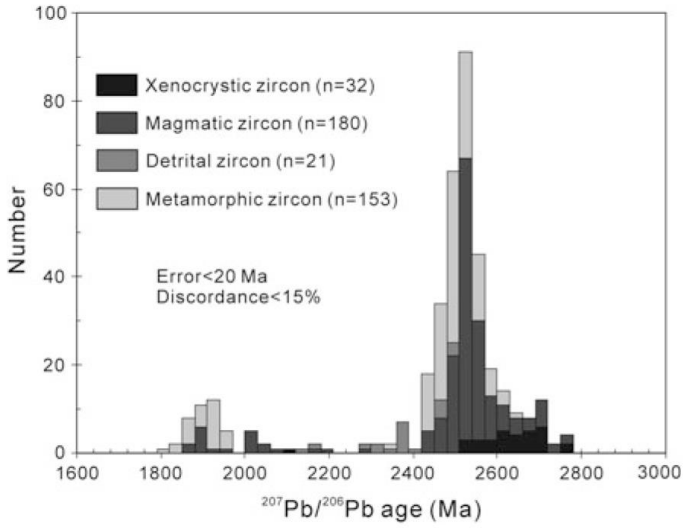

Fig. 30 Age histogram of zircons from early Precambrian rocks in Yinshan Block. Data are from Dong et al. (2012a, b), Fan et al. (2010), Jian et al. (2012), Liu et al. (2012d, 2014), Ma et al. (2013); Ma et al. (2013a, b, 2014a, b), and Zhang et al. (2014)

uncertain. We suggest that more >2.6 Ga rocks and zircons will be discovered in Yinshan as more work is carried out.

(2) 2.55–2.5 Ga magmatism was widespread and resulted in the formation of intrusive rocks composed of tonalite–trondhjemite and subordinate gabbro, diorite, granite, and syenogranite, whereas granodiorite is rare. It appears that

most tonalite–trondhjemite formed during an early phase in this event. It also seems likely that, for some rocks, strong recrystallization and Pb loss caused the magmatic zircon apparent ages to become younger than their original ages. Middle to late Paleoproterozoic (2.2–1.9 Ga) granitoid rocks were identified in local areas.

(3) Late Neoarchean supracrustal rocks include metavolcanic and volcano-sedimentary sequences including BIFs. Two types of supracrustal sequence can be recognized in terms of metamorphic grade. The high-grade metamorphic supracrustal rocks (the Xinghe "Group") consist of mafic to felsic granulite with some containing garnet, and the low-grade metamorphic supracrustal rocks (the Sheerteng "Group" or greenstone belt) consist of greenschist- to lower amphibolite-facies mafic to felsic metavolcanic rocks and minor metamorphosed ultramafic rocks, clastic metasediments, and BIF, with some mafic lavas showing relict pillows. The supracrustal and associated intrusive rocks broadly extend in an east–west direction. Some metasedimentary rocks of the high- and low-grade supracrustal sequences are Paleoproterozoic in age (Z.Y. Xu, unpublished data).

(4) Whole-rock Nd and Hf-in-zircon isotopic analyses of 2.7, 2.6, and 2.55–2.50 Ga intrusive as well as 2.55–2.50 Ga supracrustal rocks indicate that addition of significant juvenile material from the mantle occurred at 2.8–2.7 Ga, and both juvenile magmatism and crustal recycling played significant roles during magmatic events at the end of the Neoarchean.

(5) A late Neoarchean tectono-thermal event was widespread in the Yinshan Block as indicated by abundant ~2.5 Ga metamorphic zircons. Late Paleoproterozoic (1.94–1.86 Ga) metamorphic zircons were also found at several localities. These metamorphic zircons are rare in the high-grade metamorphic rocks, and this was interpreted to be due to late Paleoproterozoic metamorphism having occurred in a dominantly "dry" system caused by previous late Neoarchean high-grade metamorphism (Ma et al. 2012; Wan et al. 2011a, b, c)

3 Distribution of Zircon Ages and Isotope Geochemistry

3.1 Zircon Age Distribution

Wan et al. (2011a) compiled a total of 7586 early Precambrian zircon age data for the entire NCC and arrived at the conclusion that the most significant zircon-forming tectono-thermal events occurred in the late Neoarchean to the earliest Paleoproterozoic (2.55–2.48 Ga) and in the late Paleoproterozoic (1.95–1.80 Ga), with age peaks at ~2.52 and ~1.85 Ga, respectively. In the present study, we compiled additional zircon age data bringing the total to 15060. The geographic distribution of these data is similar to those compiled by Wan et al. (2011a).

The main differences include the following: (1) More data were obtained from the Western Block, including the basement of the Ordos basin. (2) Only data are considered where the 1σ error and discordance are less than 20 Ma and 15 %, thus excluding many results obtained by LA-ICP-MS. (3) In areas where rocks underwent strong metamorphism during the late Neoarchean and late Paleoproterozoic, such as eastern Shandong and Daqingshan, some published ages of 2.45–2.0 Ga are not included in our compilation. Although these data satisfy the above analytical conditions, they may still be geologically meaningless because of likely partial resetting of the U–Pb isotopic systems in the zircons and/or partial Pb loss during high-grade metamorphism.

Our new compilation of zircon data supports the earlier conclusions of Wan et al. (2011a) that, considering the NCC as an entity, there is a continuous age record from 3.8 to 1.8 Ga. Two tectono-thermal events are very significant in the late Neoarchean to the earliest Paleoproterozoic and late Paleoproterozoic history of the craton, reflected by age peaks at ~2.52 and ~1.85 Ga, respectively (Fig. 31a). However, the age valleys are slightly different in our new compilation at ~3.6, ~3.2, ~2.85, ~2.65, ~2.25, and 2.0 Ga. Although there is an age valley at ~2.3 Ga worldwide for zircon ages (Condie et al. 2009), rocks of this age were widely identified along the southern margin of the NCC (Diwu et al. 2007, 2014; Huang et al. 2012a b, 2013; Jiang et al. 2011; Wang et al. 2012).

As indicated by Wan et al. (2011a), the Eastern Block shows an important difference to the Western Block and the Trans-North China Orogen (TNCO) in showing abundant ages >3.0 Ga (Fig. 31b–d) because of the well-studied ancient rocks in Anshan and eastern Hebei. The discovery of many >3.3 Ga detrital zircons in the Zhongtiao, Dengfeng, and Jiaozuo areas (Diwu et al. 2008; Gao et al. 2006; Liu et al. 2012a; Yin et al. 2015) reduces the previous age difference between the TNCO and Eastern Block. Significant progress was recently made in dating of early Precambrian basement rocks in the Western Block, including the discovery of 2.7 Ga TTGs and identification of strong magmatism and metamorphism at ~2.5 Ga in the Yinshan Block (Dong et al. 2012a, b; Jian et al. 2012; Liu et al. 2014; Ma et al. 2012, 2013a, b, 2014a, b; Zhang et al. 2014). More data were also obtained from the TNCO and Eastern Block. However, these new results do not change the earlier conclusion that the Eastern Block, Western Block, and TNCO have almost identical late Neoarchean age distribution patterns with zircon ages varying from 2.55 to 2.48 Ga and a prominent age peak at ~2.52 Ga. The prominent age peak in the Western Block seems slightly shifted toward younger ages (Fig. 31d), probably due to the significant early and late Paleoproterozoic metamorphic events.

3.2 Whole-Rock Nd Isotopic Composition

Wu et al. (2005b) compiled Nd isotopic data from NCC rocks and constructed depleted mantle Nd model age histograms that indicated an important period of

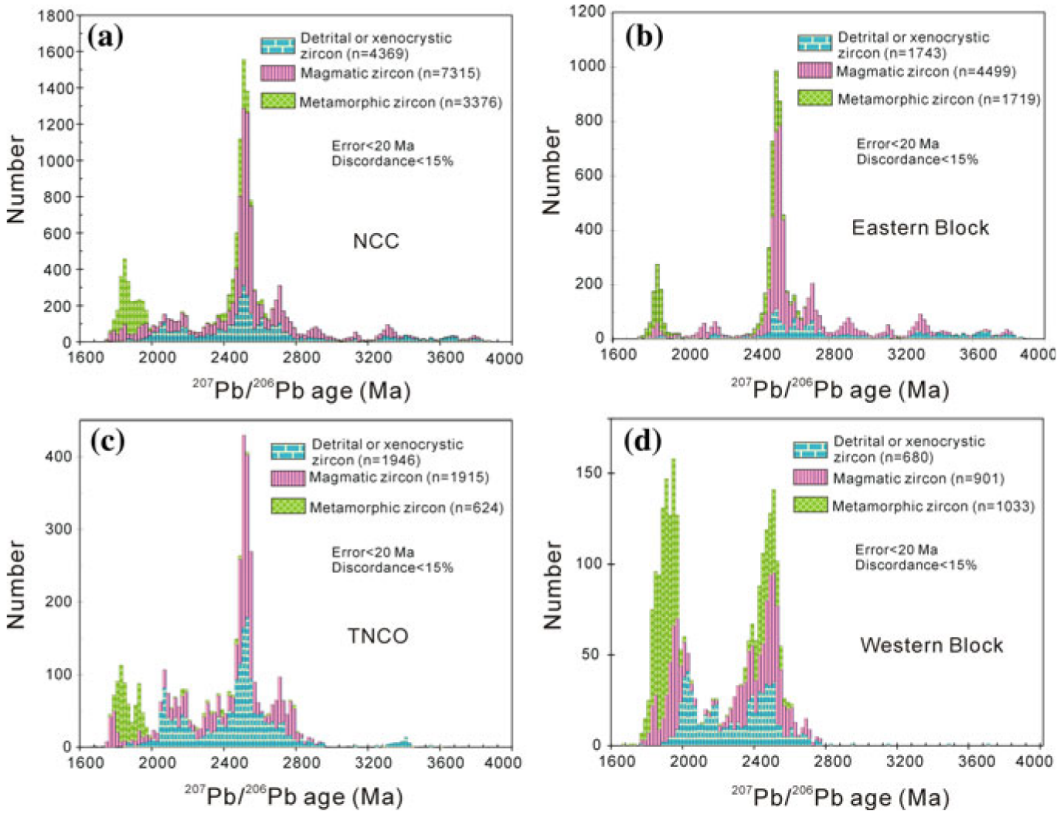

Fig. 31 Age histogram for zircons from the early Precambrian basement of the North China Craton. **a** All data for the North China Craton; **b** data for the Eastern Block; **c** data for the Trans-North China Orogen (TNCO); **d** data for the Western Block. See text for interpretation and references

crustal growth during 3.0–2.6 Ga and minor events at 3.6–3.2 and ~2.2 Ga. Many samples in their compilation were Paleoproterozoic or even younger in age. In order to better understand the Archean geological evolution, we only used data of Archean rocks in our compilation, including some 2.5–2.45 Ga samples. The total number of samples for our $\varepsilon_{Nd}(t)$ versus formation age diagram and the Nd model age histogram are 1103 and 871, respectively. The data are mainly from references published within the last twenty years (more than 70 papers, most are listed in the "References") together with our unpublished data. Similar to the zircon ages, the whole-rock Nd isotopic data show an uneven geographic distribution. Most results come from the eastern Block, and rock samples older than 2.9 Ga are mainly from Anshan, eastern Hebei, and eastern Shandong. We divided the samples into four types, namely ultramafic to intermediate rocks (including gabbro, diorite, quartz diorite, metamorphic ultramafic rocks, mafic granulite, amphibolite, greenschist, fine-grained hornblende gneiss), TTG and related rocks (e.g., metadacite, fine-grained biotite gneiss), crustally derived granites, and metasedimentary rocks. All parameters and equations used for calculation of depleted mantle Nd model ages are those of Jahn et al. (1990) and Wu et al. (2005b). The crystallization ages of most geological bodies in the NCC were determined from zircon dating.

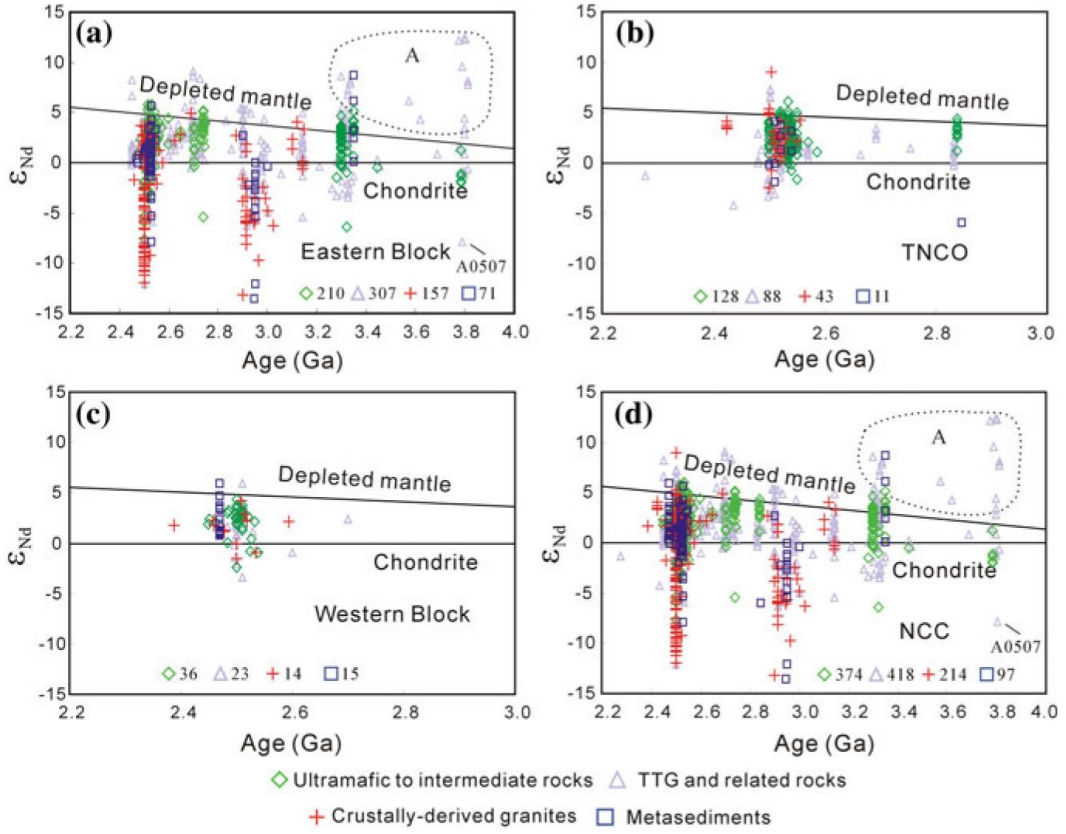

Fig. 32 $\varepsilon_{Nd}(t)$ versus formation age diagram for Archean rocks of the North China Craton. **a** Data for the Eastern Block; **b** data for the Trans-North China Orogen (TNCO); **c** data for the Western Block; **d** all data for the North China Craton. See text for interpretation and references

This made it possible to construct $\varepsilon_{Nd}(t)$ versus crystallization age diagrams for the Archean rocks (Fig. 32a–d). Some important features are as follows.

(1) Juvenile, mantle-derived material was added to the crust during several major periods, namely at 3.8, 3.35–3.3, 3.1, 2.9, 2.8, and 2.75–2.5 Ga. Crustal recycling occurred during almost every period of juvenile crustal additions. Some 3.8 Ga rocks from Anshan have negative $\varepsilon_{Nd}(t)$ values, probably suggesting that crustal recycling was already an important process in the Eoarchean. This is similar to the most ancient rocks in Canada (Acasta gneiss, Iizuka et al. 2009) and the Ancient Gneiss Complex of Swaziland, southern Africa (Kröner et al. 2014). Crustal recycling became more dominant with the evolution of continental crust as indicated by $\varepsilon_{Nd}(t)$ values becoming more negative with time.

(2) Neoarchean (2.75–2.5 Ga) rocks from the Eastern and Western blocks and TNCO show similar Nd isotopic features. However, the Eastern Block shows higher maturity in crustal evolution than the Western Block and TNCO at the end of Archean.

(3) Young, crustally derived rocks inherited the Nd isotopic features from their source material in different areas to variable degrees. In Anshan, for example, some 2.5 Ga crustally derived granites have very negative $\varepsilon_{Nd}(t)$ values due to long geological history up to 3.8 Ga. In contrast, in western Shandong, where the majority of the oldest rocks formed during 2.75–2.7 Ga as addition of juvenile material from depleted mantle source, the 2.5 Ga crustally derived granites commonly have depleted mantle Nd model ages of 2.8 2.7 Ga.

(4) Some rocks older than 3.3 Ga show very high $\varepsilon_{Nd}(t)$ values (Fig. 32a, d). Many of these are from the Anshan area and have very low Sm and Nd contents and are strongly deformed and metamorphosed. Therefore, the above positive anomalies are not considered to be original features of the rocks but are likely due to analytical uncertainty and/or more probably to post-crystallization Nd mobility during metamorphism and other late, fluid-induced geological processes. Some rock samples reported in the earlier literature from the Baijiafen Complex may not be ~3.8 Ga in age, and thus, their $\varepsilon_{Nd}(t)$ values were incorrectly calculated.

The $f_{Sm/Nd}$ values for Archean rock samples selected for the Nd model age histogram are limited to between –0.2 and –0.6 in order to reduce the uncertainties in the model age calculations caused by strong Sm/Nd fractionation during geological processes (Jahn et al. 1990; Wu et al. 2005b). In the single-stage Nd model age (depleted mantle Nd model age) histogram, the data are concentrated between 2.8 and 2.6 Ga with a model age peak at ~2.75 Ga (Fig. 33a). Different rock types show similar single-stage Nd model ages between 3.1 and 2.5 Ga. Compared with TTGs, however, ultramafic to intermediate rocks commonly have young Nd model ages. A model age valley is seen at ~3.1 Ga, and the model ages show a plateau distribution between 3.9 and 3.1 Ga. Two-stage model ages (crustal model ages) show a similar distribution but are commonly shifted toward older ages by 100–50 Ma (Fig. 33a, b).

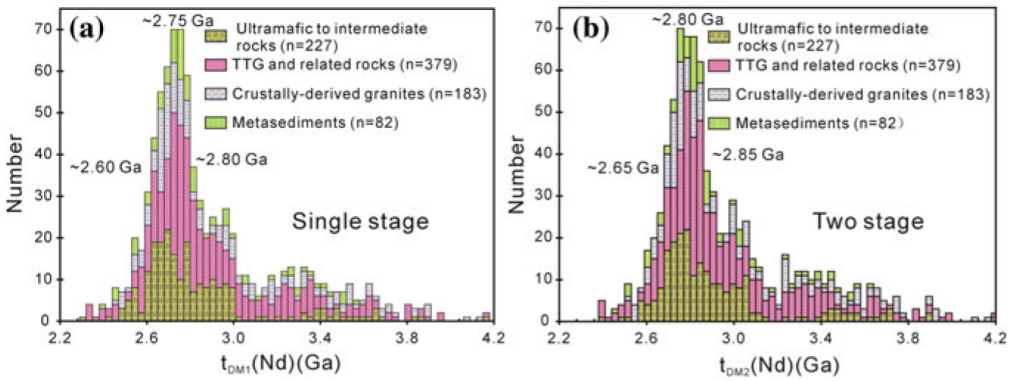

Fig. 33 Nd model age histograms for Archean rocks of the North China Craton. **a** *Single-stage* model age (depleted mantle model age); **b** *two-stage* model age (crustal model age). See text for further interpretation and references

3.3 Hf-in-Zircon Isotopic Composition

Geng et al. (2012) and Wang and Liu (2012) summarized the Hf isotopic features of zircons from early Precambrian basement rocks of the NCC and arrived at the conclusion that crust formation and growth of the craton mainly occurred during the early Neoarchean (2.8–2.7 Ga). In this paper, we used 8564 and 8736 data to compile $\varepsilon_{Hf}(t)$ versus formation age diagrams and Hf model age histograms, respectively. These data are mainly from Archean rocks of the NCC (some are 2.49–2.45 Ga in age, and some detrital zircon data are from Paleoproterozoic metasedimentary rocks). The data sources are mainly from references published within the last ten years (more than 80 papers, many listed in the "References"), together with our unpublished data, and the geographic distribution of the data is similar to those of zircon U–Pb ages with most data for >2.9 Ga rocks being from Anshan, eastern Hebei, and eastern Shandong. Zircon subdivisions are the same in Sect. 3.1. All parameters and equations used for calculation and diagram are those used by Bouvier et al. (2008), Griffin et al. (2000), and Söderlund et al. (2004).

In $\varepsilon_{Hf}(t)$ versus formation age diagrams, data points far below the depleted mantle evolution line have two possible interpretations: (1) the rock formed by melting of older crustal material; (2) zircons with apparently depleted mantle Hf isotopic compositions underwent lead loss, and therefore, their age assessment is wrong. In order to avoid such possibly erroneous data, we only used weighted mean $^{207}Pb/^{206}Pb$ ages and upper concordia intercept ages for magmatic and metamorphic zircons. We also excluded data where zircon analyses have a discordance of >40 %. For detrital zircons, individual data were only used when the 1σ error is less than 20 Ma and the discordance is less than 15 %. Considering the entire NCC, the Hf-in-zircon isotopic data show a similar distribution as the whole-rock Nd isotopic compositions, namely addition of juvenile material to the crust at 3.8–3.55, 3.45, 3.35–3.3, 2.9, and 2.8–2.5 Ga (Fig. 34a–d). Crustal recycling began as early as 3.8 Ga, lasted from 3.8 to 3.25 Ga and, between 3.25 and 2.90 Ga, played a more important role than addition of juvenile material. Ca. 2.90 Ga granitoids in Anben and eastern Shandong show different zircon Hf isotopic features, reflecting differences in their early geological histories. It seems that the original features of Hf-in-zircon isotopic compositions are better preserved than those of whole-rock Nd isotopic compositions. Compared to the whole-rock Nd isotopic data, Hf-in-zircon data reveal significant additions of juvenile material and stronger crustal recycling. This is probably due to a much larger data set and may thus more objectively reflect the Archean geological evolution of the NCC. For the Eastern Block and TNCO, whole-rock Nd isotopic data show obvious differences in the $\varepsilon_{Nd}(t)$ versus formation age diagram (Fig. 32a–b), whereas the Hf-in-zircon isotopic data are similar in the $\varepsilon_{Hf}(t)$ versus formation age diagram (Fig. 34a–b). For example, many detrital zircons from the Zhongtiao area of the TNCO have distinctly negative $\varepsilon_{Hf}(t)$ values, suggesting that >2.9 Ga rocks may occur in this area, and therefore, the TNCO shows similar isotopic features in early crustal evolution as the Eastern Block. In many cases, metamorphic zircons inherited the Hf isotopic

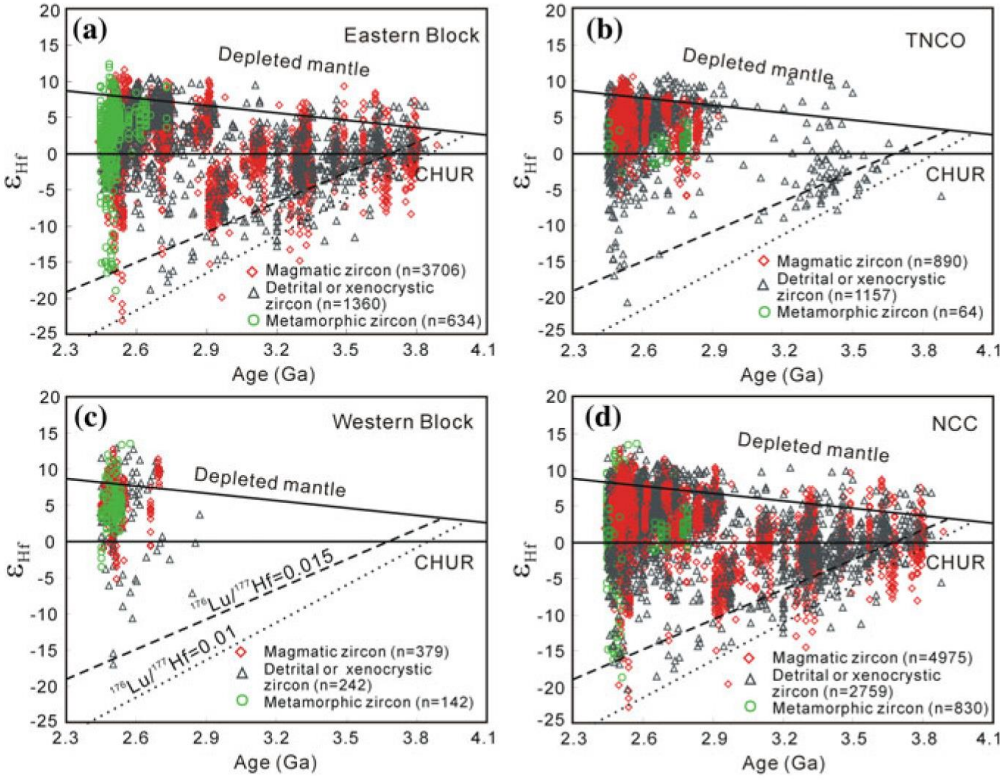

Fig. 34 $\varepsilon_{Hf}(t)$ versus formation age diagrams for zircons of Archean rocks from the North China Craton. **a** Data for the Eastern Block; **b** data for the Trans-North China Orogen (TNCO); **c** data for the Western Block; **d** all data for the North China Craton. *Dotted* and *dashed lines* represent felsic crust with $^{176}Lu/^{177}Hf$ being 0.01 and 0.015, respectively. See text for interpretation and references

features of their magmatic zircons in the same rocks unless metamorphic garnet occurs in the metamorphic rocks. It may therefore be incorrect to assign a metamorphic age to the $^{176}Hf/^{177}Hf$ ratio, but it should be the igneous age of the host rock. However, if using the igneous ages, metamorphic zircon analyses will occur in the same area as the magmatic zircons, making it more difficult to distinguish them. Considering this and presence of garnet in only a few metamorphic rocks, we still use metamorphic zircon ages in this paper. It is easily observed that metamorphic zircons are similar in their Hf isotopic features to magmatic zircons.

Zircons do not generally crystallize from magmas derived directly from mantle sources. Therefore, their single-stage Hf model ages (depleted mantle Hf model ages) are geologically meaningless, and corresponding histograms are not shown here. Two-stage Hf model ages (crustal Hf model ages) are commonly shifted by about 100–50 Ma toward old ages compared with depleted mantle Hf model ages. In the two-stage Hf model age histogram, the data are concentrated between 2.85 and 2.6 Ga with an age peak at ~2.8 Ga (Fig. 35). The age valley occurs at ~3.3 Ga. Compared with the whole-rock Nd model ages, the zircon Hf model ages show an obvious plateau distribution but with a larger age variation between 4.1 and 3.2 Ga. We point out that the continuous whole-rock Nd and zircon Hf model

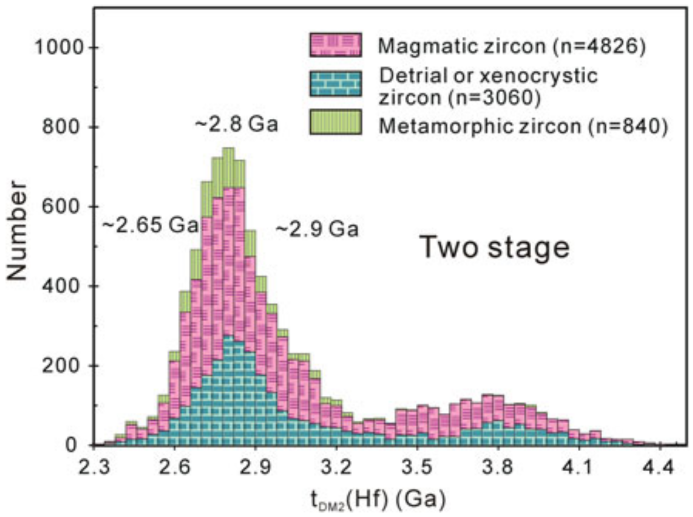

Fig. 35 *Two-stage* Hf model age (crustal Hf model age) histogram for zircons of Archean rocks from the North China Craton. Some are 2.49–2.45 Ga in age, and some detrital zircons are from Paleoproterozoic metasedimentary rocks. See text for interpretation and references

age distributions do not mean that juvenile material was continuously added to the continental crust. We rather suggest that the patterns in whole-rock $\varepsilon_{Nd}(t)$ and zircon $\varepsilon_{Hf}(t)$ versus formation age diagrams are partly a result of mixing of juvenile and recycled material.

4 Formation and Evolution of the Archean Basement of the NCC

4.1 Temporal Evolution

Rocks older than 2.8 Ga only occur in local areas such as Anshan, eastern Hebei, eastern Shandong, Lushan, and Xinyang, amounting to less than 5 % of the area of the NCC Archean basement. However, detrital and xenocrystic zircons older than 2.8 Ga occur over a wider area. Rocks >3.4 Ga consist mainly of granitoids, but ultramafic to mafic rocks of these ages are also present, but most were not dated due to lack of magmatic zircon. Almost all rocks and zircons were involved in a late Neoarchean tectono-thermal event. Rocks >2.8 Ga do not show an increasing trend in distribution with time, but this may be due to uneven reworking of old rocks during later geological processes. 2.75–2.6 Ga magmatic rocks have recently been identified in many areas, and 2.55–2.5 Ga rocks occur more widely than thought before.

Only a few >2.6 Ga supracrustal rocks have been identified, including the 3.36 Ga Chentaigou supracrustals and the 3.0–2.9 Ga Tiejiashan supracrustals in Anshan, the 2.9 Ga Huangyadi supracrustals in eastern Shandong, the 2.82 Ga

Xiataihua supracrustals in Lushan, and the 2.75–2.71 Ga Yanlingguan-Liuhang succession in western Shandong. However, 2.56–2.51 Ga supracrustal rocks occur in almost every late Neoarchean terrane, although their proportions are small (commonly <10 %). Basaltic, intermediate, and felsic volcano-sedimentary rocks are the predominant protoliths of the supracrustal sequences.

Intrusive rocks show variations in rock types with time. The 3.8–3.1 and 2.9–2.7 Ga intrusive rocks are mainly trondhjemitic and tonalitic in composition, respectively, but some gabbroic and dioritic rocks also occur. The oldest large-scale K-rich granite body is the crustally derived 3.0–2.9 Ga Tiejiashan pluton. Granodiorites only began to occur in the late Neoarchean on a large scale, together with tonalites and trondhjemites, whereas crustally derived late Neoarchean granites (mainly monzogranites and syenogranites) are widely distributed.

TTG rocks with ages between 3.45 and 3.3 Ga exhibit variable REE contents, resulting in weakly to strongly fractionated REE patterns. This is considered to be a result of cooling of the Earth (Wan et al. 2005a). However, Moyen (2011) indicated that variable REE patterns in TTGs do not have any relationships with the cooling Earth. Some late Neoarchean rock types such as syenogranite show large variations in REE and trace element compositions, suggesting that the source regions and conditions of magma formation became more complex with time.

The NCC exhibits a continuous evolution from 3.8 to 2.5 Ga, but there are age valleys at ~3.5, ~3.2, 2.85, and ~2.65 Ga. Whole-rock Nd isotopes and Hf-in-zircon isotopes indicate that both juvenile additions and crustal recycling played important roles during almost every tectono-thermal event. The Neoarchean was the most important period for the formation of continental crust in the NCC, and this will be discussed below in more detail.

Metamorphic zircons older than 2.8 Ga were rarely found, and their formation may be related to local events. The oldest (2.76 Ga) well-developed metamorphic zircons are from 2.82 Ga rocks in the Lushan area. Widespread 2.6 Ga metamorphic zircon ages were obtained from rocks in western Shandong. The most important Archean metamorphic event occurred at the end of the Neoarchean, as indicated by widespread ~2.5 Ga metamorphic zircon ages all over the craton. These may suggest that significant crustal thickening only occurred after the Mesoarchean and reached a climax at the end of the Neoarchean due to subduction/collision and/or underplating. Ca. 2.5 Ga metamorphic zircons have not been identified in some areas such as Wutai, but this may be due to the low metamorphic grade in these rocks. In Anshan, there are 3.8–2.5 Ga rocks and zircons, and in eastern Hebei, 3.88–3.4 Ga detrital zircons and 3.4–3.0 Ga and 2.5 Ga rocks have been identified. Many old zircons show overgrowth and recrystallization, suggesting that they became involved in later crustal recycling and metamorphism.

The most important Archean ore deposits in the NCC are BIFs and some massive Cu–Zn sulfide deposits. Although BIFs show large variations in formation age from the Paleoarchean to the early Paleoproterozoic, they are predominantly late Neoarchean in age (2.55–2.51 Ga) (Wan et al. 2012d; Zhang et al. 2012b). It seems that a stable depositional environment was necessary for the formation of large-scale BIF deposits. Gold deposits mainly formed in the Mesozoic, but it is

generally considered that Archean mafic–ultramafic supracrustal rocks (greenstone belts) were the main sources (Zhai 2010).

4.2 Ancient Material Records Beneath the NCC

Understanding the geological, geochemical, and geochronological processes during the early Precambrian evolution of the NCC is mainly based on studying the exposed basement as shown above. However, some progress has been made to recognize ancient material in the deep crust of the NCC. There are two ways to obtain information from this cratonic region. One is from rock samples recovered from drill holes that penetrated the basement. One such study revealed late Paleoproterozoic magmatism and metamorphism in basement rocks beneath the Songliao basin in the northeastern NCC (Pei et al. 2007), whereas another study indicated that the basement beneath the Ordos basin in the western NCC was involved in a late Paleoproterozoic tectono-thermal event (Hu et al. 2012; Wan et al. 2013).

Wan et al. (2014b) recently carried out zircon dating, Hf-in-zircon isotopic analyses, and a whole-rock geochemical study of igneous and metasedimentary rocks from basement covered by Mesoproterozoic and younger sedimentary rocks in the Central Hebei Basin (CHB). The CHB extends in a NE–SW direction and covers an area of >35,000 km^2 (Fig. 36). Based on drill core data and geophysical investigations (NCOCP 2012), the basement is composed of greenschist- to upper amphibolite-facies magmatic and supracrustal rocks that locally experienced anatexis. The bottom of the basin shows irregular elevations with the greatest depth being >5000 m. This study identified late Neoarchean magmatic and Paleoproterozoic metasedimentary rocks that were subjected to late Neoarchean to early Paleoproterozoic and late Paleoproterozoic tectono-thermal events, similar to those identified in the early Precambrian basement around the basin. Wan et al. (2014b) concluded that the basement beneath the CHB is part of the NCC. On the basis of this study, the authors suggested that early Precambrian rocks are extensive beneath the Mesoproterozoic and younger sedimentary cover all over the NCC.

Another way to reveal ancient material in the deep crust is to study rock enclaves (xenoliths) and xenocrystic zircons brought to the surface by eruption of volcanoes and/or intrusion of magmas from a deep source. Zheng et al. (2012), Zhang et al. (2012a, b), and Zhang (2014) summarized progresses made in the investigation of such rocks and zircons. Young igneous rocks containing old xenoliths and xenocrystic zircons include Paleozoic kimberlite and lamproite, Mesozoic volcanic or intrusive rocks, and Cenozoic basalts (Fig. 37). The xenoliths are considered to be derived from the lower crust and upper mantle. The lower crustal xenoliths consist of high-grade metamorphic rocks generally less than 10 cm in diameter. Many igneous rocks also contain xenocrystic zircons that were derived from lower crustal sources or were captured during magma ascent. These samples provide important information on the age and composition of the deep NCC crust.

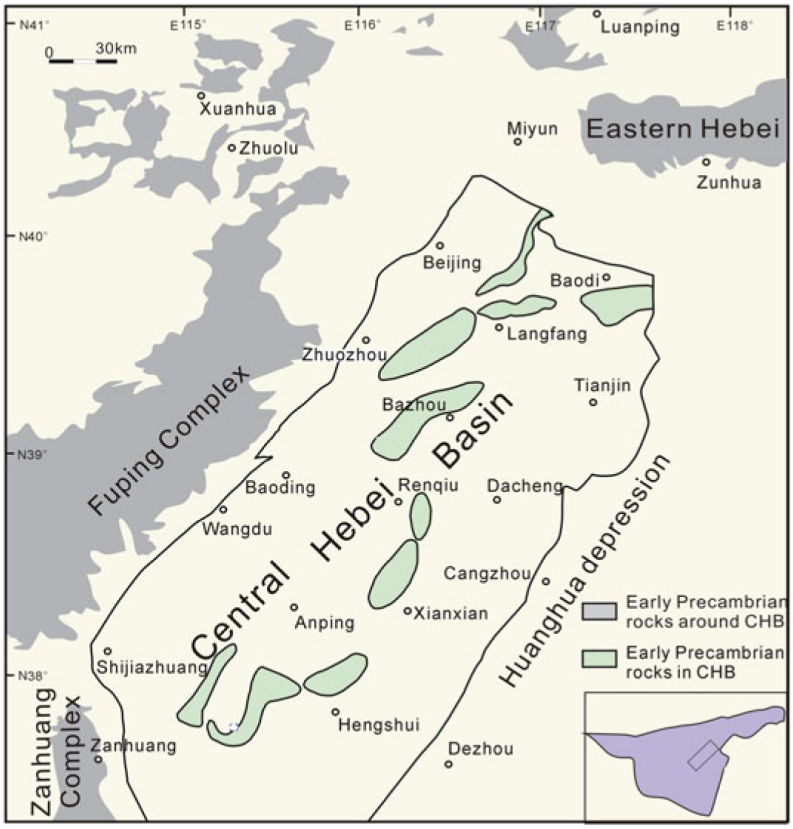

Fig. 36 Geological map of the Central Hebei Basin and surrounding areas, modified after NCOCP (2012) and Wan et al. (2014b). *Inset* shows location in the NCC

The concordia diagram with zircon age data from xenoliths shows several clusters around 2.5, 1.9–1.8, and 0.1 Ga (Fig. 38a). Some data for old zircons from xenoliths of the Xinyang volcanic rocks plot along a discordia line with an upper concordia intercept age of ~3.6 Ga. Note that there is significant lead loss in some of these zircons. Thus, a cumulative histogram compiling all data may lead to an overestimate of zircon crystallization events. Several lead loss trends can be recognized: (1) ancient lead loss in Paleoarchean zircon grains at ca. 2.5 and 1.8 Ga; (2) ancient lead loss in Neoarchean zircon grains at 1.8 Ga; and (3) lead loss in Neoarchean and Paleoproterozoic zircons during the Phanerozoic. The concordia diagram of zircon xenocrysts shows a similar age pattern, including lead loss (Fig. 38b). These features were also observed in the zircon age distribution of the exposed early Precambrian basement. However, there are no zircon grains with Paleoarchean ages, consistent with the limited occurrence of such rocks in the NCC.

All early Paleoproterozoic zircon data, including those with variable lead loss, are shown in Fig. 38c and d. The Hf-in-zircon isotopic data from the xenoliths show that the oldest age group has even more negative $\varepsilon_{Hf}(t)$ (Fig. 38c) than the Paleoarchean zircons in the Anben and Caozhuang areas, indicating that they represent recycled crust. The ~2.5 Ga zircon grains have both negative and

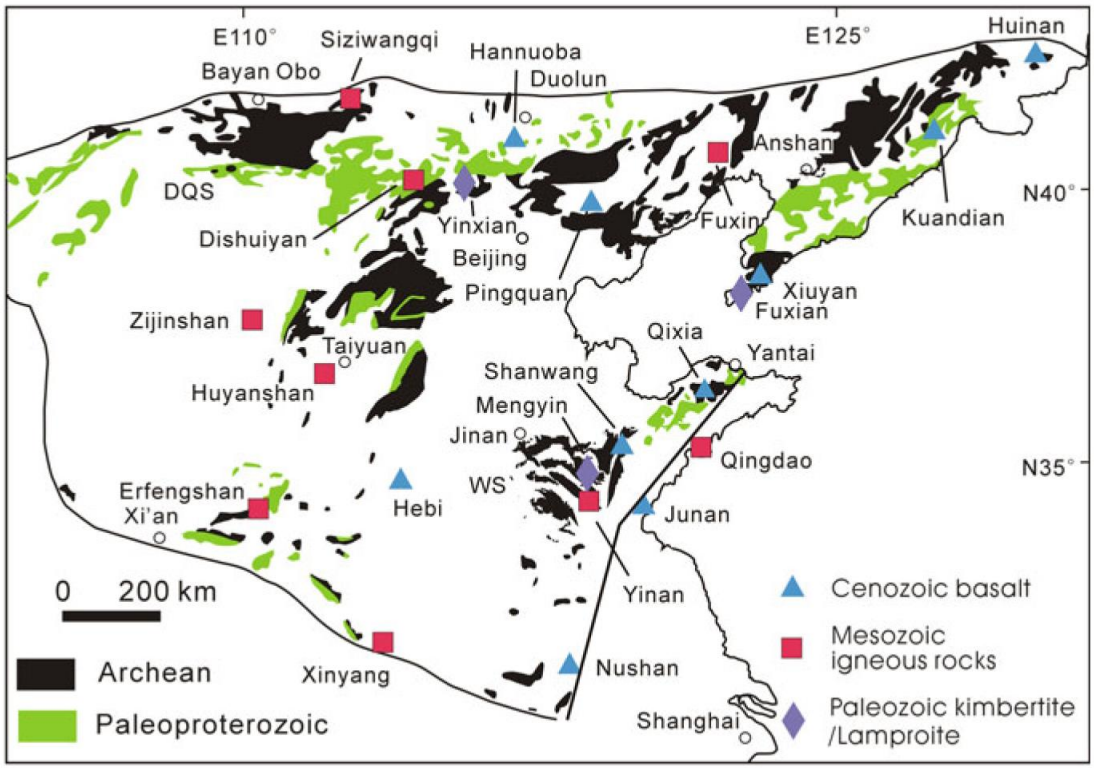

Fig. 37 Geological map showing locations of rocks containing xenoliths and xenocrystic zircons in the North China Craton and adjacent area. Paleozoic kimbertite/lamproite: Mengyin, Fuxin, and Yingxian; Mesozoic volcanic/intrusive rocks: Xinyang, Erfengshan, Yinan, Qingdao, Huyanshan, Zijinshan, Dishuiyan, Siziwangqi, and Fuxian; Cenozoic basalt: Nushan, Hebi, Junan, Shanwang, Qixia, Xiuyan, Pingquan, Hannuoba, Huinan, and Kuandian. Locations of rocks containing xenoliths and xenocrystic zircons are from HF Zhang et al. (2012a, b) and Zheng et al. (2012)

positive $\varepsilon_{Hf}(t)$, implying that juvenile material was added to the crust and recycling of older material also occurred. A similar pattern was observed in the 1.9–1.8 Ga zircons. Specifically, Phanerozoic zircon grains mainly show negative $\varepsilon_{Hf}(t)$ values, and some grains have extremely low $\varepsilon_{Hf}(t)$ of –40 and even lower. There is no doubt that some Archean material was recycled during Phanerozoic tectono-magmatic events. The Hf isotopic data of the zircon xenocryst show a similar pattern (Fig. 38d).

Both the data from xenoliths and zircon xenocrysts show similar Hf model age distributions (Fig. 38e, f) as those from basement rocks exposed on the surface. The major peak is at about 2.8 Ga, and very old model ages near the beginning of the formation of continental crust on the Earth suggest that there may be some very old material in the deep crust of the NCC.

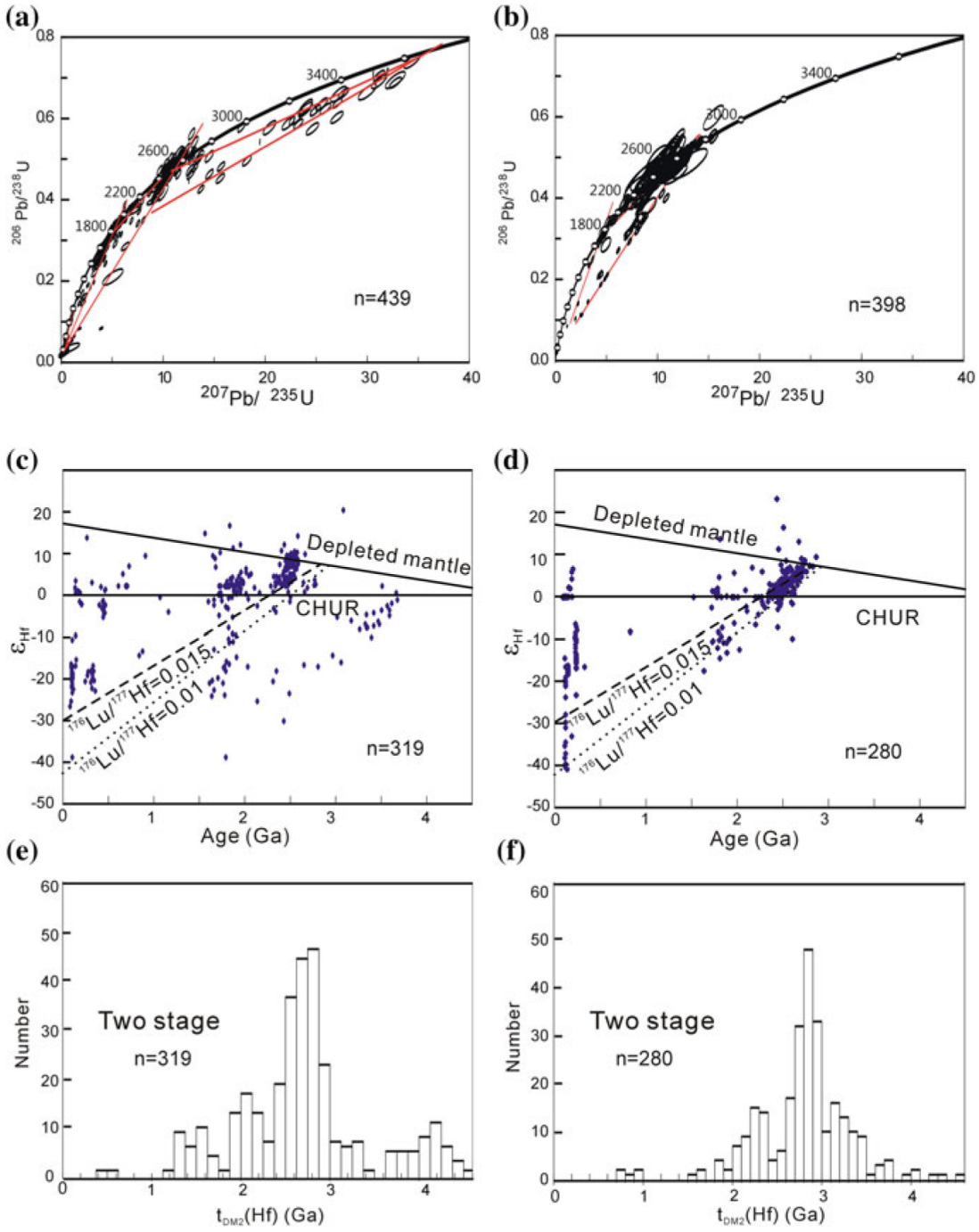

Fig. 38 Ages and Hf isotopes of zircons from deep crust in the North China Craton. **a** and **b** U–Pb concordia diagrams; **c** and **d** age versus $\varepsilon_{Hf}(t)$ diagrams; **e** and **f** Hf model age histograms. **a**, **c**, and **e** zircons from xenoliths; **b**, **d**, and **f** xenocrystic zircons. Data are from Gao et al. (2004), YS Liu et al. (2004b), Ying et al. (2011), Zhang (2012), Zhang et al. (2012a, b, c), and Zheng et al. (2004a, b, c, 2008)

4.3 Major Periods of Continent Formation

Formation of continental crust in the NCC can be traced back to the Eoarchean. Geological records earlier than Mesoarchean were most likely partly destroyed during later tectono-metamorphic processes, and it seems likely that the Neoarchean was a major period of crust formation in the NCC. This means that some crucial processes occurred in the Earth during this time, probably indicating a transformation in the global tectonic regime due to changes in the thermal state of the Earth from hot to cool. Zircon age histograms indicate that the most important tectono-thermal event occurred at ~2.5 Ga. Evidence for addition of juvenile material at ~2.5 Ga includes the following: (1) Ca. 2.5 Ga supracrustal rocks (greenstone belts), commonly with a high proportion of metabasalt, occur in almost every terrane; (2) Ca. 2.5 Ga gabbroic to dioritic rocks are widely distributed all over the NCC (Li et al. 2010b; Ma et al. 2012; Wan et al. 2010c; Wan, unpublished data); and (3) some ~2.5 Ga TTGs exhibit whole-rock Nd and Hf-in-zircon isotopic compositions similar to the depleted mantle (Diwu et al. 2012; Geng et al. 2012; Liu et al. 2009b; Wang and Liu 2012; this study). However, mafic to intermediate assemblages (including volcanic and intrusive rocks) constitute only a small portion of the granitoid–greenstone belts, and 2.5 Ga TTGs with depleted mantle model ages are relatively rare (Figs. 32d and 34d).

In western Shandong, >2.8 Ga rocks have not been identified, but voluminous ~2.5 Ga crustally derived granites show the same whole-rock Nd and Hf-in-zircon isotopic features as the 2.75–2.7 Ga rocks. Therefore, the ~2.5 Ga granitoids are considered to have been derived from 2.75–2.7 Ga sources (Wan et al. 2010c, 2011b). In areas where >2.8 Ga rocks are exposed, ~2.5 Ga granites with Nd and Hf isotopic compositions of 2.7 Ga juvenile rocks could have formed as a result of mixtures of depleted mantle-derived magmas and older crustal material. However, >2.8 Ga rocks are rare in the NCC, so this may not have been a significant process for the formation of ~2.5 Ga granitoids. On the other hand, some magmatic zircons from ~2.5 Ga gabbros, diorites, and granodiorites show Hf isotopic enrichment, similar to the Nd isotopic composition of some ~2.5 Ga amphibolites. This may be a feature of a mantle source or a result of crustal contamination of magmas derived from a depleted mantle. There are three potential sources for the ~2.5 Ga magmatic rocks with similar Nd and Hf isotopic compositions as the 2.7 Ga juvenile rocks (Wan et al. 2014a): (1) Ca. 2.7 Ga granitoids that constituted precursors for the ~2.5 Ga crustally derived granitoids; (2) Ca. 2.7 Ga mafic rocks that also constituted precursors for the ~2.5 Ga intermediate and more felsic rocks; and (3) a mantle source with ~2.7 Ga depleted mantle model ages from which some mafic rocks could have been derived. The possibility cannot be excluded that ~2.5 Ga granitoids with ~2.7 Ga depleted mantle model ages resulted from crustal recycling of ~2.5 Ga mantle-derived rocks with the same isotopic features; however, rocks formed in this way must be limited in volume. Therefore, the conclusion can be drawn that the most important period of addition of juvenile material occured in the early Neoarchean rather than in the late Neoarchean, consistent with rocks and

detrital and xenocrystic zircons of these ages occurring in many areas of the NCC. Fundamentally, therefore, the NCC is similar to many other cratons elsewhere in that tectono-thermal and crust-forming events at ~2.7 Ga are globally well developed. The main difference between the NCC and many other cratons is that a superimposed ~2.5 Ga tectono-thermal event was particularly strong in the former (Wan et al. 2010c, 2011b, 2014a, 2015b; Zhai and Santosh 2011).

4.4 Tectonic Subdivision of the NCC

The early Precambrian subdivision of the craton is mainly based on the distribution of late Neoarchean to Paleoproterozoic rocks because of insufficient data for the earlier geological evolution. The subdivision is debated in the literature, and several schemes have been proposed as summarized by Zhai and Santosh (2011) and Zhao and Zhai (2013).

Wu et al. (1998) subdivided the NCC into five blocks, namely the Jiaoliao, Qianhuai, Jinji, Yuwan, and Mongshan blocks (Fig. 39a). The Jiaoliao and Qianhuai blocks were considered to have assembled along the Jiao-Liao-Ji Belt, resulting from an east-dipping subduction zone to form a larger block at ~2.5 Ga which then collided with other blocks to result in final amalgamation of the NCC during the late Paleoproterozoic.

Zhao et al. (2001) suggested a 3-fold subdivision of the craton, namely the Eastern Block, Western Block, and Trans-North China Orogen (TNCO). Late Archean anticlockwise P-T paths for the two blocks were interpreted to have resulted from several mantle plumes, resulting in magmatic underplating and high-grade metamorphism at ~2.5 Ga, whereas the clockwise path in the TNCO was interpreted to reflect continental collision between the Eastern and Western blocks, leading to Paleoproterozoic assembly of the NCC at ~1.85 Ga. Zhao et al. (2005) later modified this model into the currently favored 6-fold subdivision of the craton (Fig. 39b), resulting from the speculative interpretation of major collisional zones within both the Eastern and Western blocks.

Li et al. (2002), Kusky and Li (2003), and Kusky et al. (2007) suggested that collision between the Eastern and Western blocks occurred in the late Neoarchean (~2.5 Ga) along the Central Orogenic Belt (COB) to form a unified NCC. The COB is similar in spatial distribution to the TNCO of Zhao et al. (2001, 2005) with differences being that the COB extends farther northeast into southern Jilin (Fig. 39c) and that the subduction polarity was west-dipping, rather than east-dipping, as suggested by Zhao et al. (2001, 2005).

Zhai and Santosh (2011) subdivided the NCC into seven microblocks, mainly based on the spatial distribution of ancient rocks and tectonic boundaries revealed by several granite–greenstone belts. These were named the Alashan (ALS), Xuhuai (XH), Xuchang (XCH), Jining (JN), Ordos (OR), Qianhuai (QH), and Jiaoliao (JL) blocks, with very different boundaries from those of other authors. They

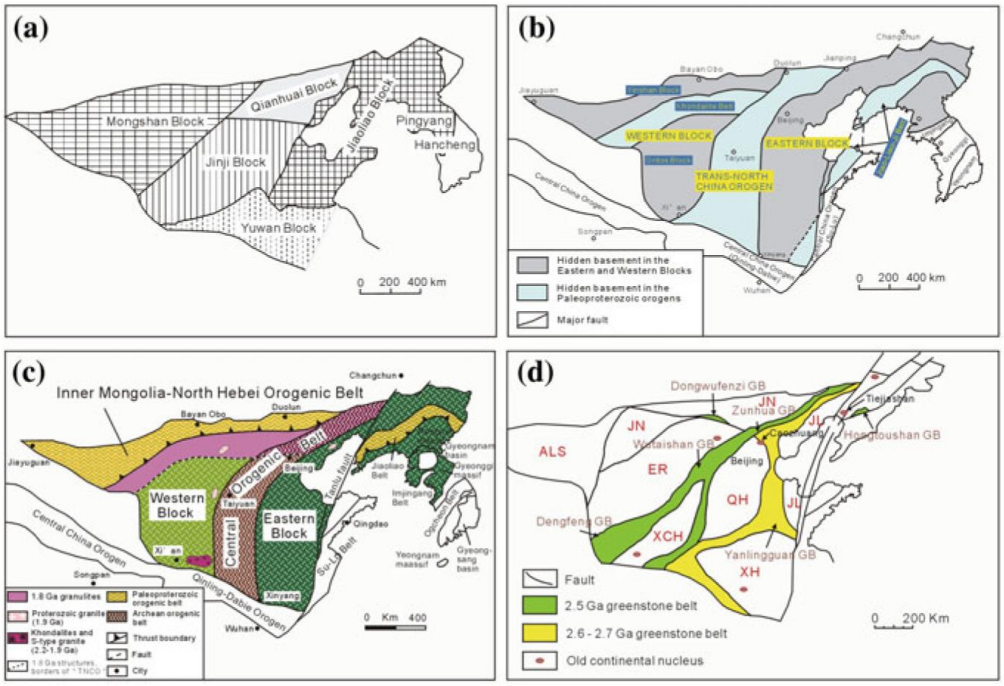

Fig. 39 Different tectonic subdivisions of the North China Craton. **a** Wu et al. (1998); **b** Zhao et al. (2005); **c** Li et al. (2002); **d** Zhai and Santosh (2011)

suggested that these microblocks were welded together along Neoarchean granite–greenstone belts at ~2.5 Ga (Fig. 39d).

In order to understand the tectonic setting of the NCC during the late Neoarchean, it is necessary to determine the spatial distribution of ancient (≥2.6 Ga) continental domains in the craton. A strong tectono-thermal event at ~2.6 Ga in western Shandong is an important reason for considering 2.6 Ga as a chronological boundary between the early and late Neoarchean. With regard to the spatial distribution of these ancient crustal domains, rocks and zircons of different origins and ages have different geodynamic interpretations. Rocks ≥2.6 Ga themselves represent ancient crust, whereas ≥2.6 Ga detrital zircons in late Neoarchean and Paleoproterozoic metasedimentary rocks suggest the existence of ancient crust in nearby areas, and ≥2.6 Ga xenocrystic zircons in young (<1.8 Ga) intrusive rocks may indicate the existence of old material in the deep crust. However, old detrital zircons in young sedimentary rocks have no significance because they may have undergone multirecycling. Figure 1 shows ≥2.6 Ga detrital and xenocrystic zircons from Paleoproterozoic or older rocks. Based on the spatial distribution of ancient rocks and zircons, three ancient terranes can be delineated, namely the Eastern Ancient Terrane, Southern Ancient Terrane, and Central Ancient Terrane (Fig. 40).

(1) Eastern Ancient Terrane

This is the best understood ancient terrane and occurs along the eastern margin of the NCC in a NE–SW direction, including Anben, eastern Hebei, eastern Shandong, and western Shandong. The oldest rocks and zircons mainly occur in

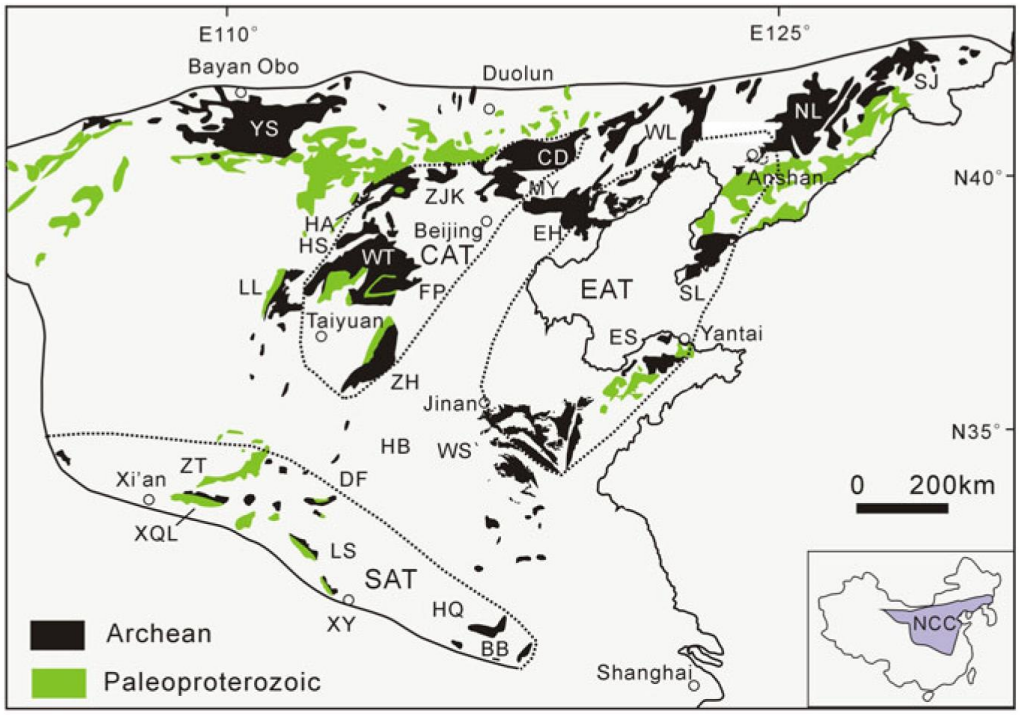

Fig. 40 Distribution of ancient (>2.6 Ga) terranes in the North China Craton. *EAT* Eastern Ancient Terrane; *SAT* Southern Ancient Terrane; *CAT* Central Ancient Terrane. Abbreviations are as in Fig. 1

this terrane. Besides the 3.8–2.9 Ga rocks in Anshan and 3.4–3.0 Ga rocks and 3.8–3.3 Ga detrital zircons in eastern Hebei, 2.9–2.6 Ga rocks were identified in eastern Shandong and western Shandong. The spatial relationships between the old rocks in the terrane may not have changed significantly since the early Neoarchean (2.6 Ga). In western Shandong, the margin of the ancient terrane is the boundary between belts B and C (Fig. 19). Although granitoids in Belt A are mainly ~2.5 Ga in age, they are derived from melting of older basement. Syenogranites and monzogranites are also widely distributed in eastern Hebei, Jinzhou, and Anben, and they constitute the largest crustally derived late Neoarchean granite belt in the NCC. It is notable that these ~2.5 Ga granitoids inherited their compositional features from older basement. As mentioned above, in Anshan, recycling of >3.0 Ga crust played a profound role in the formation of the ~2.5 Ga syenogranites, as evidenced by the presence of older xenocrystic zircons as well as whole-rock Nd and Hf-in-zircon isotopic compositions (Wan et al. 2015a). In western Shandong, on the other hand, the ~2.5 Ga crustally derived granites in Belt A have similar whole-rock Nd and Hf-in-zircon isotopic compositions as the adjacent early Neoarchean rocks (Wan et al. 2010c, 2011b).

(2) Southern Ancient Terrane

This terrane occurs along the southern margin of the NCC in a nearly E–W direction. 3.65, 2.83–2.82, 2.7, and 2.7–2.6 Ga rocks have been identified in

Xinyang, Lushan, Huoqiu, and Zhongtiao, respectively, and 3.6–2.6 Ga detrital and xenocrystic zircons were discovered in additional areas (Liu et al. 2012b). Importantly, as pointed out before, the captured or detrital 4.1–3.5 Ga zircons in Paleozoic volcano-sedimentary rocks of the northern Qinling Orogenic Belt may be derived from the southern margin of the NCC. This suggests that the Southern Ancient Terrane may have a long geological history back to 4.1 Ga ago. Widespread identification of >2.6 Ga rocks and zircons in this terrane is an important progress made in recent years.

(3) Central Ancient Terrane

This includes the Zanhuang, Fuping, Hengshan, Zhangjaikou, and Chengde areas where 2.7 Ga TTG rocks and zircons were identified, although the TTG rocks commonly occur at small scales. It is likely that more rocks and zircons older than 2.6 Ga will be discovered in this terrane, and the widespread presence of crustally derived granites in the Central Ancient Terrane is also consistent with the existence of older material in the deep crust. However, there are also many ~2.5 Ga TTG rocks in the terrane, and this makes it uncertain whether or not the Central Ancient Terrane existed prior to 2.6 Ga.

Besides the above three ancient terranes, >2.6 Ga rocks and zircons were identified in other areas of the NCC. For example, in Xi Wulanbulang, 2.7 Ga TTG rocks with a relatively wide distribution as well as older detrital and xenocrystic zircons were discovered (Jian et al. 2012; Dong et al. 2012a, 2012b; Ma et al. 2013). Ca. 2.5 Ga zircons in late Neoarchean supracrustal and intrusive rocks have the same Hf isotopic compositions as zircons from the 2.7 Ga TTG rocks, providing evidence for crustal recycling or contamination of early Neoarchean crust. Therefore, there may also be an ancient terrane in the Yinshan Block.

4.5 Tectonic Regime

Mantle plume activity resulting in magmatic underplating and plate tectonics are considered to have been the most important processes involving the formation and evolution of early continental crust (Van Kranendonk et al. 2014), but the timing of initiation of plate tectonics is debatable. Some authors suggested that present-type plate tectonics only began in the late Paleoproterozoic or later, whereas others considered that tectonic regimes similar to those of today occurred as early as the Eoarchean (e.g., Nutman et al. 2013). Therefore, there are different opinions on whether mantle plume activity (or underplating) and/or arc magmatism or both played key roles in the Neoarchean, an important period when much of the global continental crust formed (Bédard 2013; Condie and Kröner 2013; Dostal and Mueller 2013; Halla et al. 2009; Manikyamba and Kerrich 2012; Mohan et al. 2013; Wyman 2013a, b). Magmatic underplating is considered to be related to mantle plume activity or, more probably, to mantle overturn (Davies 1995; Rey et al. 2003) and may have been an important mechanism in continental growth and reworking (Frost et al. 2001; Warren and Ellis 1996). Mantle plumes generally last for only

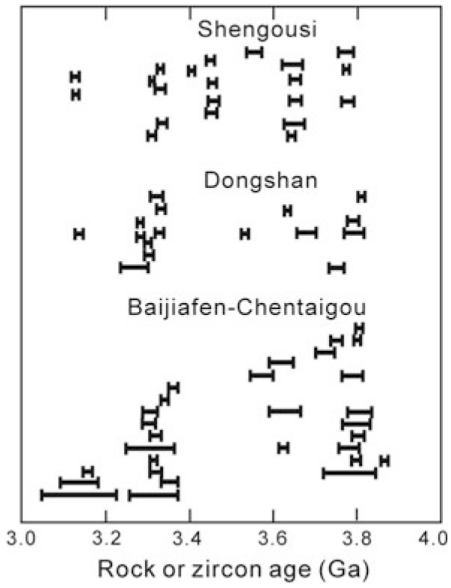

Fig. 41 Comparison of the Archean magmatic records of the Baijiafen, Dongshan, and Shengousi complexes in the Anshan area. Data are from Liu et al. (1992, 2008), Song et al. (1996), Wan et al. (2005a, b, c, 2012a), Wu et al. (2008), and Wan (unpublished data)

5–10 Ma (Abbott and Isley 2002), a much shorter time span than the late Neoarchean (2.55–2.50 Ga) igneous activity in the NCC. Mantle overturn may have led to longer magmatism.

We now have a better understanding of the early (>2.8 Ga) evolution of the NCC through detailed studies in some areas. In Anshan, magmatism almost continuously lasted for a long time from 3.8 to 2.9 Ga (Fig. 12), where multiple and complex phases of igneous activity were recorded in all three complexes (Fig. 41). The rock types include both mantle-derived and crustally derived rocks (Dong et al. 2013; Liu et al. 1992, 2008; Song et al. 1996; Wan et al. 2005a, 2007, 2012a, 2015a; Zhou et al. 2007; Zhou et al. 2009). These data suggest that long-term magmatism related to mantle activity widely occurred in Anshan and adjacent area. In eastern Hebei, detrital zircons record almost continuous ages ranging from 3.88 to 3.4 Ga, although only 3.4–3.0 Ga Paleoarchean–Mesoarchean rocks were discovered until now. We suggest that widespread magmatism due to mantle overturn activity may have been the main mechanism of continental growth and reworking before the Mesoarchean, consistent with the underplating model.

Western Shandong and eastern Shandong are areas where ~2.7 Ga rocks are most widely distributed in the NCC. Metabasalts with REE depletion and enrichment have been identified in western Shandong, and komatiites with well-preserved spinifex textures (Fig. 18d) were considered to be ~2.7 Ga in age (Polat et al. 2006a). In eastern Shandong, ~2.7 Ga TTGs formed about 200 Ma later than ~2.9 Ga TTGs, and this suggests that subduction may not have been responsible for the formation of the ~2.7 Ga rocks because a 200 Ma time span is too short for a full Wilson cycle (Jahn et al. 2008). Furthermore, the majority of TTG rocks in both western Shandong and eastern Shandong show strongly fractionated REE patterns and Nb–Ti–P depletion (Jahn et al. 2008; Wan et al. 2014a). Based on rock associations, TTG compositions, and the geological evolution, mafic magma

underplating was considered as a viable process for the formation of the supracrustal and intrusive rocks (Jahn et al. 2008; Polat et al. 2006a). The tectonic setting of ~2.7 Ga rocks in other areas is not so clear because of their small size and poor data. However, Yang et al. (2013a) favored a subduction model for the formation of ~2.7 Ga TTG rocks in the Zanhuang area.

Underplating and arc magmatism have been proposed for crustal growth in the late Neoarchean. The former model was mainly suggested from studies of the eastern NCC (Geng et al. 2006; Yang et al. 2008; Zhao et al. 1998, 1999, 2001). Zhao and Zhai (2013) summarized the main features supporting this view as follows: (1) An exceptionally large exposure of granitoid intrusions formed over a short time period (2.55–2.50 Ga) and shows no systematic age progression across a ~800-km-wide block; (2) generation of komatiitic magmas with eruption temperatures as high as ~1650 °C; (3) dominant domal structures; (4) bimodal volcanic assemblages in the greenstone sequences; (5) affinities of mafic rocks to continental tholeiitic basalts; and (6) metamorphism with anticlockwise P-T paths involving isobaric cooling. Jian et al. (2012) attributed the strong late Neoarchean (2.55–2.50 Ga) magmatism and metamorphism in the Yinshan Block to episodic mantle upwelling/melting as a result of spontaneous delamination of the lower crust and periodic delamination of melt residues during granitoid production. They considered this to have occurred in a continental environment because of the presence of >2.6 Ga rocks and zircons.

Some authors suggested a scenario of arc magmatism followed by collisional orogeny, although there are different opinions on the timing and spatial distribution of collisional belts (Kröner et al. 2005a, b; Kusky and Li 2003; Kusky et al. 2007; Li et al. 2002; Nutman et al. 2011; Polat et al. 2006b; Wan et al. 2005b, c, 2010c, 2012c; Wilde et al. 2005; Wu et al. 1998; Zhang et al. 2007, 2009; Zhao et al. 2001, 2002, 2005). The main points include the following: (1) Igneous rocks of different ages and compositions occur in different zones and spatially show an asymmetrical distribution in some areas such as western Shandong and eastern Hebei; (2) compared with TTGs, syenogranites and monzogranites commonly formed during a slightly late phase; (3) older rocks (2.56–2.525 Ga) commonly underwent stronger deformation and metamorphism than younger rocks (2.525–2.48 Ga); (4) intrusive and volcanic activities occurred during almost a same period, and the intrusive rocks were uplifted quickly to the surface to form the source for sediments in the late Neoarchean basins, suggesting an active tectonic environment; (5) there are metabasaltic rocks with depletion and enrichment features in many supracrustal belts; and (6) intrusive rocks of different compositions are commonly depleted in Nb and Ta and thus display a subduction-related chemical signature. Nutman et al. (2011) indicated that the complexity of the late Neoarchean eastern Hebei arc magmatism matches that found in long-lived arc systems that involved older continental crust, such as the Andean margin of South America (Hildreth and Moorbath 1988), the Paleoproterozoic of South Greenland (Garde et al. 2002), and the Neoarchean crustal development in southern India (Chadwick et al. 2007).

In fact, some of the above features can be intercepted by both the underplating and subduction models. More data, including geophysical surveys, are required in

order to better understand the tectonic regime in the NCC during the late Neoarchean. These include (1) the difference in the spatial distribution of Archean rocks at present and in the late Neoarchean and (2) the compositions and ages of the unexposed basement. It is difficult to explain that the above two different tectonic settings worked at the same time with underplating having occurred beneath the Eastern and Western blocks when both these blocks moved toward each other resulting in subduction/collision. On the basis of similarities in rock association, ages of formation, and geological evolution in different areas, we suggest that only one tectonic setting played an important role in the NCC during the late Neoarchean.

It is notable that globally, apart from the NCC, ~2.5 Ga rocks only occur in a few areas such as southern India (Chadwick et al. 2007; Clark et al. 2009; Dey et al. 2012; Jayananda et al. 2000; Moyen et al. 2003), Antarctica (Corvino and Henjes-Kunst 2007; Clark et al. 2012; Duclaux et al. 2008; Tsunogae et al. 2014), and northern Australia (Drüppel et al. 2009; McCready et al. 2004). The NCC underwent a much stronger tectono-thermal event at ~2.5 Ga than many other cratons characterized by ~2.7 Ga events (Condie 2000; Condie et al. 2009). It may be possible that all these continental terranes once belonged to a single block (Clark et al. 2012; Wan et al. 2011a; Zhao et al. 2003), but more work is required to identify this. If underplating was active at ~2.5 Ga, it may have modified an early Neoarchean supracontinent previously formed by a widespread and strong ~2.7 Ga tectono-thermal event. On the other hand, if arc magmatism was active at this time, the areas where ~2.5 Ga TTG rocks are well developed may represent an ancient subduction/collision belt between two large blocks of the early Neoarchean. In both cases, the different cratons may be dispersed remnants of what was once a single continent at the end of the Neoarchean, consistent with many cratons showing fragmented features (Bleeker 2003).

All late Neoarchean tectono-magmatic belts so far proposed in the NCC, such as the Liao-Ji-Lu magmatic belt (Wu et al. 1998), the Central Orogenic Belt (Li et al. 2002), and the greenstone belts (Zhai and Santosh 2011), only contain a relatively small portion of the late Neoarchean areas. Therefore, these are not consistent with the arc magmatism model. In order to overcome this problem, we propose a multi-island arc model in which the three ancient terranes, and possibly other old terranes, occurred in an oceanic domain, and amalgamation of these terranes due to subduction/collision resulted in the formation of supracrustal and intrusive rocks as well as juvenile additions and crustal recycling and finally assembled the NCC at the end of the Neoarchean. This is consistent with rocks of continental and oceanic affinities in many areas of the NCC. In the western Liaoning, Dengfeng and Huai'an areas, for example, there are supracrustal and intrusive rocks apparently derived from depleted mantle sources, but crustally derived granites and sediments have also been identified (Diwu et al. 2011; Liu et al. 2009b; Wang et al. 2011). The late Neoarchean may have been a period when plate tectonics began to play an important role in crust formation, although subduction/collision would have been different in pattern and scale from present-day processes because the Earth was hotter than now and the oceanic lithosphere was thicker, softer, and more buoyant, and continent blocks were smaller.

4.6 Craton Stabilization

Although there are different opinions on the late Neoarchean tectono-thermal event in the NCC, it is accepted by many authors, including those who favored the arc magmatism model (Nutman et al. 2011; Wan et al. 2010c, 2011b), that the latest Neoarchean event was related to an extensional tectonic setting, probably due to magmatic underplating. Most latest Neoarchean crustally derived granites have formation ages of 2.52–2.49 Ga and either are undeformed and massive or show weak deformation. They intruded into earlier, deformed rocks and are associated with undeformed, mantle-derived gabbroic and dioritic rocks of the same age. In western Shandong, for example, intrusive rocks older than 2.525 Ga commonly show strong deformation, whereas intrusive rocks younger than 2.525 Ga commonly are undeformed or only weakly deformed (Fig. 42). This suggests that the tectonic regime probably changed from compressional to extensional between 2.53 and 2.52 Ga (Wan et al. 2010c). Similar scenarios were proposed for other areas of the NCC such as Wutai and Zanhuang (Wilde et al. 2005; Yang et al. 2013a).

It is also evident that migmatites occur on large scales and are associated with crustally derived granites in many areas such as western Shandong (Fig. 19). Migmatization occurred at the same time or slightly earlier than the formation of granites. Metamorphism and associated crustally derived granites were identified all

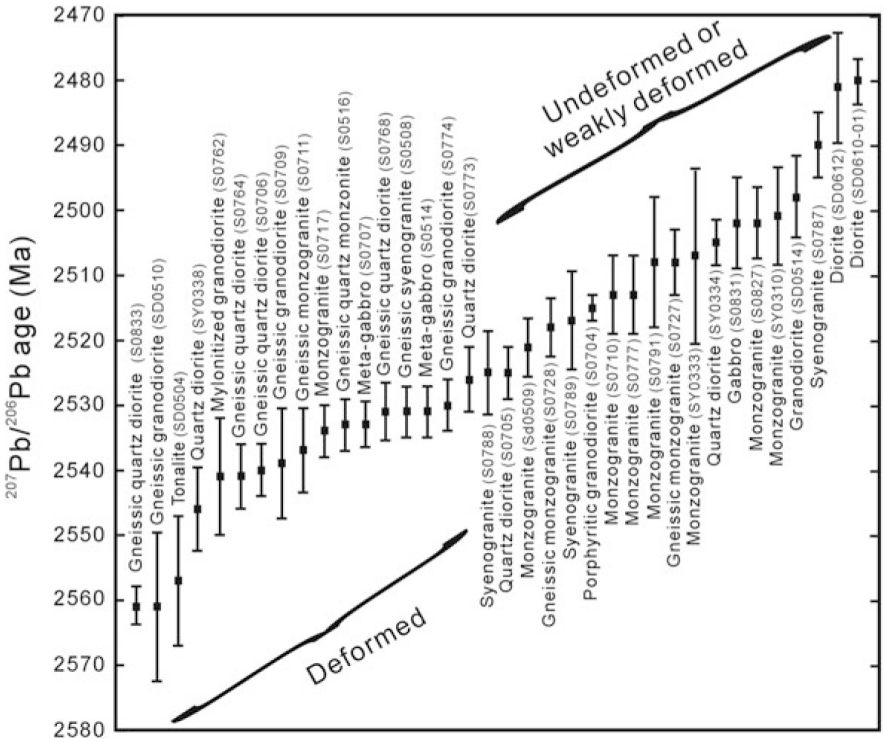

Fig. 42 Zircon age variation diagram (with *error bars*) for different types of intrusive rocks in western Shandong. Data are from Lu et al. (2008) and Wan et al. (2010c)

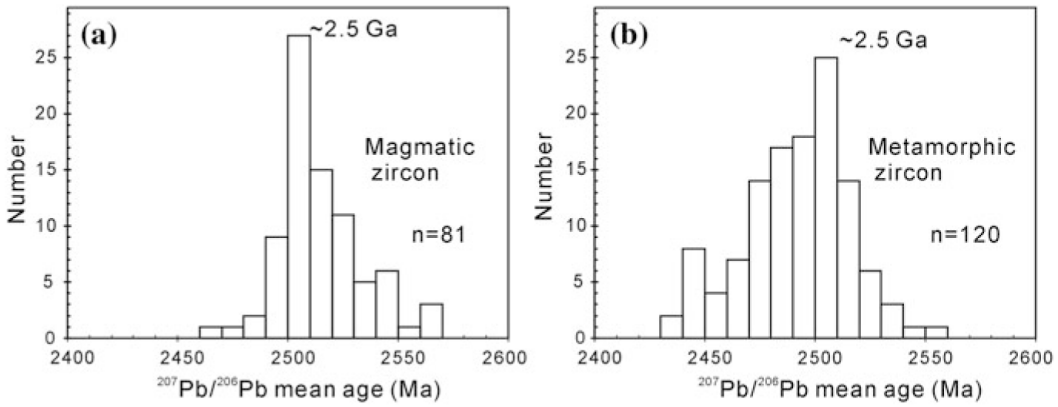

Fig. 43 Weighted mean $^{207}Pb/^{206}Pb$ age histograms for magmatic zircons from crustally derived granites (**a**) and metamorphic zircons from high-grade metamorphic rocks (**b**) in the North China Craton. See text for interpretation and references

over the NCC, including eastern Shandong, western Shandong, northern Liaoning, western Liaoning, eastern Hebei, Dengfeng, Yinshan, and Daqingshan, with metamorphic ages identical to crystallization ages of many crustally derived granites, mainly ranging from 2.53 to 2.49 Ga and 2.53 to 2.45 Ga, respectively (Fig. 43) (Bai et al. 2014; Chen et al. 2006; Cui et al. 2013; Dai et al. 2013; Deng et al. 2014; Dong et al. 2012a, b; Geng et al. 2006; Grant et al. 2009; Guan et al. 2002; Guo et al. 2013; Han et al. 2014a; Jahn et al. 2008; Jian et al. 2012; Kröner et al. 1998, 2005a; Li et al. 2009, 2010b, 2011a, b 2013a, b; Lu et al. 2008; Lü et al. 2012; Ma et al. 2013, 2013a; Nutman et al. 2011; Peng et al. 2012, 2013a, b; Ren 2010; Ren et al. 2013; Shen et al. 2004; Shi et al. 2012; Sun et al. 2010; Wan et al. 2005b, 2009c, 2010c, 2012b, d, 2015a, unpublished data; Wang et al. 2000, 2011, 2012, 2013, 2014a, b; Wilde et al. 1997, 2005; Wu et al. 2013, 2014; Xie et al. 2013, 2014b; Yang et al. 2008, 2011; Zhang et al. 2011, 2012a, 2014; Zhao et al. 2002, 2008b2009, 2011; Zhu et al. 2015). The association of undeformed, mantle-derived rocks (gabbro, diorite) of the same age (mainly 2.52–2.49 Ga) suggests that underplating may have played an important role in causing metamorphism and anatexis in the lower crust to produce crustally derived granites during extension in the NCC basement at the end of the Neoarchean. These magmas moved to higher crustal levels to form intrusive bodies at different scales, including syenogranites. The formation of large-scale granite batholiths and widespread high-grade metamorphism and anatexis are considered to have been important processes to cause cratonic stabilization of the NCC at the end of the Neoarchean, a convenient time to set 2.5 Ga as the Archean–Proterozoic boundary (Wan et al. 2012b, 2015a; Yang et al. 2011).

Metamorphic zircon ages are younger than magmatic zircon ages of crustally derived granites in some areas, down to 2.45 Ga or even later, although some may be the result of partial resetting of the U–Pb isotopic system in the zircons due to the strong late Paleoproterozoic tectono-thermal event. It is uncertain whether the

metamorphism lasted from the late Neoarchean to the earliest Paleoproterozoic (~2.45 Ga) or whether the earliest Paleoproterozoic metamorphism was a different event. In western Liaoning, metamorphism was considered to be one event and lasted from the latest Archean to early Paleoproterozoic (Kröner et al. 1998; Liu et al. 2011a). In Daqingshan, however, the earliest Paleoproterozoic Daqingshan supracrustal sequence (mainly metasediments) contains 2.45 2.40 Ga metamorphic zircons, suggesting that here the earliest Paleoproterozoic metamorphism was a separate tectono-thermal event.

Cratonic stabilization implies that the NCC was already a single tectonic unit at the end of the Neoarchean as suggested by Wan et al. (2011a), Zhai and Peng (2007), and Zhai and Santosh (2011). The Eastern and Western blocks and the TNCO share many common features, and some have been discussed before: (1) These tectonic units display almost identical late Neoarchean zircon age spectra with age peaks at ~2.52 Ga; (2) there is evidence for >2.8 Ga material, although this is more evident in the Eastern Block; (3) there are ~2.7 Ga TTGs in all three blocks; (4) there are ~2.5 Ga supracrustal rocks with similar rock associations with BIFs being typical components; (5) there was strong juvenile magma addition from mantle sources to the crust between 2.8 and 2.7 Ga; (6) there are abundant ~2.5 Ga TTGs, associated with minor gabbroic and dioritic rocks; (7) the old rocks underwent metamorphism and anatexis between 2.52 and 2.48 Ga; (8) crustally derived late Neoarchean granites occur in all three blocks and are commonly younger than the TTGs; (9) crustal recycling of ~2.7 Ga rocks at ~2.5 Ga played an more important role than juvenile addition; and (10) young sediments in different areas commonly contain late Neoarchean and late Paleoproterozoic detrital zircons.

In general, it is difficult to determine the original relationships between the different blocks just by comparing rock types and ages. Considering the limited distribution of the ~2.5 Ga tectono-thermal event worldwide, however, the obvious similarity of the Eastern and Western blocks may suggest that they formed in a similar tectonic setting, supporting the conclusion that the NNC had already been a single unit at the end of the Neoarchean.

5 Summary and Conclusions

(1) The NCC underwent a long and complex evolution from 3.8 to 2.5 Ga. Rocks older than 2.8 Ga occur only locally, with Anshan and eastern Hebei being the most important areas where >3.8 Ga rocks and crustal components have been identified.

(2) The most important tectono-thermal event in the NCC occurred at ~2.5 Ga, and this is different from many other cratons worldwide. However, whole-rock Nd and Hf-in-zircon isotopic compositions indicate that the late Mesoarchean to early Neoarchean is the most important period for rapid production of continental crust. This is similar to several other cratons.

(3) The deep crust of the NCC shows similar evidence for the presence of ancient material as the surface exposures, and the available data suggest that the most important tectono-thermal events occurred in the late Neoarchean and late Paleoproterozoic, and juvenile material was added to the crust during the late Mesoarchean to early Neoarchean.
(4) We suggest that three ancient terranes older than 2.6 Ga can be delineated in the NCC, namely the Eastern, Southern, and Central Ancient Terranes.
(5) Vertical crustal growth is considered to have been the main mechanism of continental evolution prior to the Mesoarchean, and this is mainly based on geological features in the Anshan area. It is still uncertain whether magmatic underplating or arc magmatism played a decisive role in the evolution of the NCC during the late Neoarchean. We favor a multi-island arc model related to amalgamation through subduction/collision of different ancient terranes.
(6) The NCC may have been a single tectonic unit at the end of the late Neoarchean, due to cratonic stabilization as indicated by the formation of widespread and voluminous granites and extensive high-grade metamorphism and anatexis all over the craton, probably as a result of mantle underplating.

Acknowledgements We are grateful to the members of the Beijing SHRIMP Center for zircon separation, mount making, CL imaging, dating, and other help. Chunli Guo, Kejun Hou, Liewen Xie, Yueheng Yang, Honglin Yuan, Chunrong Diwu, and Hongying Zhou assisted in Hf-in-zircon isotopic analysis, and Suohan Tang, Jinhui Wang, Chaofeng Li, Jinghui Guo, Fukun Cheng, and Hongying Zhou assisted in whole-rock Nd isotopic analysis. We also thank Vickie Bennett, Michael Brown, Bin Chen, Yuelong Chen, Kent Condie, Xiaozhong Ding, Chunrong Diwu, Lilin Du, Clark R.L. Friend, Yuansheng Geng, Yongchang Gu, Jinghui Guo, Baofu Han, Jianmin Hu, Ping Jian, Wei Jin, Huaikun Li, Huimin Li, Houmin Li, Jianghai Li, Jinyi Li, Sanzhong Li, Tingdong Li, Xianhua Li, Xuping Li, Yanhe Li, Shoufa Lin, Fulai Liu, Junlai Liu, Shuwen Liu, Xiaochun Liu, Yongshun Liu, Zhihong Liu, Songnian Lu, Changqian Ma, Peisen Miao, Zhiyao Ni, Allen Nutman, Dominic Papineau, Peng Peng, Jishun Ren, M. Santosh, Qihan Shen, Min Sun, Yong Sun, Jeff D. Vervoort, Huichu Wang, Renmin Wang, Shijin Wang, Shiyan Wang, Tao Wang, Zejiu Wang, Chunjing Wei, Ian Williams, Simon A. Wilde, Chunming Wu, Fuyan Wu, Yuanbao Wu, Qinghui Xiao, Wenliang Xu, Zhongyuan Xu, Chonghui Yang, Jinhui Yang, Zhensheng Yang, Hongfu Zhang, Lianchang Zhang, Fengqing Zhao, Minggou Zhai, Guochun Zhao, Taiping Zhao, Yue Zhao, Jianping Zheng, Jianbo Zhou, Xiaodong Zhou, Xiangkun Zhu, and others for discussions and help in this study. We particularly thank Academician Minggou Zhai for originating this book. This paper is the result of long-term work in the NCC, supported financially by the Major State Basic Research Program of the People's Republic of China (2012CB416600, 2015FY310100), the National Natural Science Foundation of China (40172044, 40672127, 41002062, 41472167, 41472169, 49473172, 49872024), and the Key Program of the Ministry of Land and Resources of China (1212010711815, 1212011120151, 12120114021301, 12120113013700, 1212011220465, 1212011120142, 1212010811033, DKD2001020-3, DKD9904011, DKD20010209, J1.3.1). We express our sincere appreciation to the distinguished geologist Academician Yuqi Cheng who is one of the most important founders of metamorphic petrology, metamorphic geology, and geochronology in China and who has made significant contributions to the geology of China.

References

Abbott DH, Isley AE (2002) The intensity, occurrence, and duration of superplume events and eras over geological time. J Geodyn 34:265–307

Bureau of Geology Mineral Resources of Shandong Province (BGMRSP) (1991) Regional geology of Shandong Province. Geological Publishing House, Beijing, pp 1–595 (in Chinese with English abstract)

Bai J et al (1986) The early Precambrian geology of Wutaishan. Tianjing Publishing press, Tianjin, pp 1–46 (in Chinese with English abstract)

Bai J, Huang X-G, Wang H-C, Guo J-J (1996) The Precambrian evolution of China, 2nd edn. Geological Publishing House, Beijing, pp 1–259 (in Chinese)

Bai X, Liu S-W, Guo R-R, Zhang L-F, Wang W (2014) Zircon U-Pb-Hf isotopes and geochemistry of Neoarchean dioritic-trondhjemitic gneisses, Eastern Hebei, North China Craton: constraints on petrogenesis and tectonic implications. Precambr Res 251:1–20

Bédard J (2013) How many arcs can dance on the head of a plume? A 'comment' on: a critical assessment of Neoarchean 'plume only' geodynamics: evidence from the Superior Province, by Derek Wyman. Precambr Res 229:189–197

Black LP, Williams IS, Compston W (1986) Four zircon ages from one rock: the history of a 3930 Ma-old granulite from Mount Sones, Enderby Land, Antarctica. Contrib Miner Petrol 94:427–437

Bleeker W (2003) The late Archean record: a puzzle in ca. 35 pieces. Lithos 71:99–134

Bowring SA, Williams IS (1999) Priscoan (4.00-4.03 Ga) orthogneisses from northwestern Canada. Contrib Miner Petrol 134:3–16

Bouvier A, Vervoort JD, Patchett PJ (2008) The Lu-Hf and Sm-Nd isotopic composition of CHUR: constraints from unequilibrated chondrites and implications for the bulk composition of terrestrial planets. Earth Planet Sci Lett 273:48–57

Cao G-Q et al (1996) Early Precambrian geology of western Shandong. Geological Publishing House, Beijing, pp 1–193 (in Chinese with English abstract)

Chadwick B, Vasudev VN, Hegde GV, Nutman AP (2007) Structure and SHRIMP U/Pb zircon ages of granites adjacent to the Chitradurga Schist Belt: implications for Neoarchean convergence in the Dharwar Craton, southern India. J Geol Soc India 69:5–24

Chen L (2007) Geochemistry and Geochronology of the Guyang Greenstone Belt. Postdoctoral Report. Institute of Geology and Geophysics, Chinese Academy of Sciences, Beijing, pp 1–40 (in Chinese)

Chen T (1988) The geology and petrological characteristics of granitic rocks in the Caozhuang-Bailonggang area, Qian'an, Hebei. Bull Inst Geol, Chin Acad Geol Sci 18:82–97 (in Chinese with English abstract)

Chen B, Liu S-W, Geng Y-S, Liu C-Q (2006) Zircon U-Pb ages, Hf isotopes and significance of the late Archean-Paleoproterozoic granitoids from the Wutai-Lüliang terrain, North China. Acta Petrologica Sinica 22:296–304

Cheng Y-Q, Sheng Q-H, Wang Z-J (1982) Preliminary study of the metamorphosed basic Volcano-Sedimentary Yanlingguan formation of the Taishan Group of Xintai, Shandong. Geological Publishing House, Beijing, pp 1–72 (in Chinese)

Cheng Y-Q, Yang C-H, Wan Y-S, Liu Z-X, Zhang X-P, Du L-L, Zhang S-G, Wu J-S, Gao J-F (2004) Early Precambrain geological characters and anatectic reconstruction of crust in the north part of middle Taihang Mountain. Geological Publishing House, Beijing, pp 1–191 (in Chinese)

Clark C, Collins AS, Timms NE, Kinny PD, Chetty TRK, Santosh M (2009) SHRIMP U-Pb age constraints on magmatism and high-grade metamorphism in the Salem Block, southern India. Gondwana Res 16:27–36

Clark C, Kinny PD, Harley SL (2012) Sedimentary provenance and age of metamorphism of the Vestfold Hills, East Antarctica: evidence for a piece of Chinese Antarctica? Precambr Res 196–197:23–45

Condie KC (2000) Episodic continental growth models: afterthoughts and extensions. Tectonophysics 322:153–162

Condie KC, Belousova E, Griffin WL, Sircombe KN (2009) Granitoid events in space and time: constraints from igneous and detrital zircon age spectra. Gondwana Res 15:228–242

Condie KC, Kröner A (2013) The building blocks of continental crust: evidence for a major change in the tectonic setting of continental growth at the end of the Archean. Gondwana Res 23:394–402

Corvino AF, Henjes-Kunst F (2007) A record of 2.5 and 1.1 billion year old crust in the Lawrence Hills, Antarctic southern Prince Charles Mountains. Terra Antartica 14:13–30

Cui M-L, Zhang L-C, Wu H-Y, Xu Y-X, Li W-J (2014) Timing and tectonic setting of the Sijiaying banded iron deposit in the eastern Hebei province, North China Craton: constraints from geochemistry and SIMS zircon U-Pb dating. J Asian Earth Sci 94:240–251

Cui P-L, Sun J-G, Sha D-M, Wang X-J, Zhang P, Gu A-L, Wang Z-Y (2013) Oldest zircon xenocryst (4.17 Ga) from the North China Craton. Int Geol Rev 55:1902–1908

Dai Y-P, Zhang L-C, Wang C-L, Liu L, Cui M-L, Zhu M-T, Xiang P (2012) Genetic type, formation age and tectonic setting of the Waitoushan banded iron formation, Benxi, Liaoning Province. Acta Petrologica Sinica 28:3574–3594 (in Chinese with English abstract)

Dai Y-P, Zhang L-C, Zhu M-T, Wang C-L, Liu L (2013) Chentaigou BIF-type iron deposit, Anshan area associated with Archean crustal growth: constraints from zircon U-Pb dating and Hf isotope. Acta Petrologica Sinica 29:2537–2550 (in Chinese with English abstract)

Davies GF (1995) Punctuated tectonic evolution of the earth. EarthPlanet Sci Lett 136:363–379

Deng H, Kusky T, Polat A, Wang J-P, Wang L, Fu J-M, Wang Z-S, Yuan Y (2014) Geochronology, mantle source composition and geodynamic constraints on the origin of Neoarchean mafic dikes in the Zanhuang Complex, Central Orogenic Belt, North China Craton. Lithos 205:359–378

Dey S, Pandey UK, Rai AK, Chaki A (2012) Geochemical and Nd isotope constraints on petrogenesis of granitoids from NW part of the eastern Dharwar craton: possible implications for late Archaean crustal accretion. J Asian Earth Sci 45:40–56

Diwu C-R, Sun Y, Lin C-L, Liu X-M, Wang H-L (2007) Zircon U-Pb ages and Hf isotopes and their geological significance of Yiyang TTG gneisses from Henan Province, China. Acta Petrologica Sinica 23:253–262 (in Chinese with English abstract)

Diwu C-R, Sun Y, Yuan H-L, Wang H-L, Zhong X-P, Liu X-M (2008) U-Pb ages and Hf isotopes for detrital zircons from quartzite in the Paleoproterozoic Songshan Group on the southwestern margin of the North China Craton. Chin Sci Bull 53:2828–2839

Diwu C-R, Sun Y, Dong Z-C, Wang H-L, Chen D-L, Chen L, Zhang H (2010a) In situ geochronology of Hadean zircon xenocryst (4.1 $\sim$ 3.9 Ga) west of the Northern Qinling Orogenic Belt. Acta Petrologica Sinica 26:1171–1174 (in Chinese with English abstract)

Diwu C-R, Sun Y, Lin C-L, Wang H-L (2010b) LA-(MC)-ICP-MS U-Pb zircon geochronology and Lu-Hf isotope compositions of the Taihua complex on the southern margin of the North China Craton. Chin Sci Bull 55:2557–2571

Diwu C-R, Sun Y, Guo A-L, Wang H-L, Liu X-M (2011) Crustal growth in the North China Craton at $\sim$2.5 Ga: evidence from in situ zircon U-Pb ages, Hf isotopes and whole-rock geochemistry of the Dengfeng Complex. Gondwana Res 20:149–170

Diwu C-R, Sun Y, Zhang H, Wang Q, Guo A-L, Fan L-G (2012) Episodic tectonothermal events of the western North China Craton and North Qinling Orogenic Belt in central China: constraints from detrital zircon U-Pb ages. J Asian Earth Sci 47:107–122

Diwu C-R, Sun Y, Wilde SA, Wang H-L, Dong Z-C, Zhang H, Wang Q (2013) New evidence for $\sim$4.45 Ga terrestrial crust from zircon xenocrysts in Ordovician ignimbrite in the North Qinling Orogenic Belt, China. Gondwana Research 23:1484–1490

Diwu C-R, Sun Y, Zhao Y, Lai S-C (2014) Early Paleoproterozoic (2.45-2.20 Ga) magmatic activity during the period of global magmatic shutdown: Implications for the crustal evolution of the southern North China Craton. Precambr Res (in press)

Dong X-J, Xu Z-Y, Liu Z-H, Sha Q (2012a) 2.7 Ga granitic gneiss in the Northern Foot of Daqingshan Mountain, Central Inner Mongolia, and its geological implications. Earth Sci 37(Suppl.):45–52 (in Chinese with English abstract)

Dong X-J, Xu Z-Y, Liu Z-H, Sha Q (2012b) Zircon U-Pb geochronology of Archean high-grade metamorphic rocks from Xi Ulanbulang area, central Inner Mongolia. Sci China Ser D-Earth Sci 55:204–212

Dong C-Y, Wan Y-S, Zhang Y-H, Yang Z-Q, Liu D-Y (2013) 3.3-3.1 Ga magmatism recorded in an outcrop of the Dongshan Complex in the Anshan area, North China Craton: evidence from geochemistry and SHRIMP zircon dating. Acta Petrologica Sinica 29:414–420 (in Chinese with English abstract)

Dostal J, Mueller WU (2013) Deciphering an Archean mantle plume: Abitibi greenstone belt, Canada. Gondwana Res 23:493–505

Drüppel K, McCready AJ, Stumpfl EF (2009) High-K granites of the Rum Jungle Complex, N-Australia: insights into the Late Archean crustal evolution of the North Australian Craton. Lithos 111:203–219

Du L-L, Zhuang YX, Yang CH, Wan Y-S, Wang X-S, Wang S-J, Zhang L-F (2003) Characters of zircons in the Mengjiatun formation in Xintai of Shandong and their chronological significance. Acta Geol Sinica 77:359–366 (in English with Chinese abstract)

Du L-L, Zhuang Y-X, Yang C-H, Wan Y-S, Wang X-S (2005) SHRIMP U-Pb zircon chronology of fine-grained amphibolite in the Mengjiatun area, western Shandong. Acta Geoscientica Sinica 26:429–434 (in English with Chinese abstract)

Du L-L, Yang C-H, Zhuang Y-X, Wei R-Z, Wan Y-S, Ren L-D, Hou K-J (2010) Hf isotopic compositions of zircons from 2.7 Ga metasedimentary rocks and biotite-plagioclase gneiss in the Mengjiatun Formation Complex, western Shandong Province. Acta Geol Sinica 84:991–1001 (in Chinese with English abstract)

Duclaux G, Rolland Y, Ruffet G, Ménot RP, Guillot S, Peucat JJ, Fanning M, Rey P, Pêcher A (2008) Superimposed Neoarchaean and Paleoproterozoic tectonics in the Terre Adélie Craton (East Antarctica): Evidence from Th-U-Pb ages on monazite and $^{40}Ar/^{39}Ar$ ages. Precambr Res 167:316–338

Gao L-Z, Zhao T, Wan Y-S, Zhao X, Ma Y-S, Yang S-Z (2006) Report on 3.4 Ga SHRIMP zircon age from the Yuntaishan Geopark in Jiaozuo, Henan Province. Acta Geologica Sinica 80:52–57

Gao S, Rudnick RL, Yuan H-L, Liu X-M, Liu Y-S, Xu W-L, Ling W-L, Ayers J, Wang X-C, Wang Q-H (2004) Recycling lower continental crust in the North China craton. Nature 432:892–897

Garde AA, Hamilton MA, Chadwick B, Grocott J, McCaffrey KJW (2002) The Ketilidian orogen of South Greenland: geochronology, tectonics, magmatism, and fore-arc accretion during Paleoproterozoic oblique convergence. Can J Earth Sci 39:765–793

Geng Y-S, Wan Y-S, Shen Q-H (2002) Early Precambrian basic volcanism and crustal growth in the North China Craton. Acta Geol Sinica 76:199–202 (in Chinese with English abstract)

Geng Y-S, Liu F-L, Yang C-H (2006) Magmatic event at the end of the Archean in eastern Hebei Province and its geological implication. Acta Geol Sinica 80:819–833

Geng Y-S, Shen Q-H, Ren L-D (2010) Late Neoarchean to Paleoproterozoic magmatic events and tectonothermal systems in the North China Craton. Acta Petrologica Sinica 26:1945–1966 (in Chinese with English abstract)

Geng Y-S, Du L-L, Ren L-D (2012) Growth and reworking of the early Precambrian continental crust in the North China Craton: constraints from zircon Hf isotopes. Gondwana Res 21:517–529

Grant ML, Wilde SA, Wu F-Y, Yang J-H (2009) The application of zircon cathodoluminescence imaging, Th-U-Pb chemistry and U-Pb ages in interpreting discrete magmatic and high-grade metamorphic events in the North China Craton at the Archean/Proterozoic boundary. Chem Geol 261:155–171

Griffin WL, Pearson NJ, Belousova E, Jackson SE, Achterbergh EV, O'Reilly SY, Shee SR (2000) The Hf isotope composition of cratonic mantle: LAM-MC-ICPMS analysis of zircon megacrysts in kimberlites. Geochimica Cosmochimica Acta 64:133–147

Guan H, Sun M, Wilde SA, Zhou X-H, Zhai M-G (2002) SHRIMP U-Pb zircon geochronology of the Fuping Complex: implications for formation and assembly of the North China Craton. Precambr Res 113:1–18

Guo J-H, Sun M, Chen F-K, Zhai M-G (2005) Sm-Nd and SHRIMP zircon geochronology of high-pressure granulites in the Sanggan area, North China Craton: timing of Paleoproterozoic continental collision. J Asian Earth Sci 24:629–642

Guo L-S, Liu S-W, Liu Y-L, Tian W, Yu S-Q, Li Q-G, Lü Y-J (2008) Zircon Hf isotopic features of TTG gneisses and formation environment of Precambrian Sushui complex in Zhongtiao mountains. Acta Petrologica Sinica 24:139–148 (in Chinese with English abstract)

Guo R-R, Liu S-W, Santosh M, Li Q-G, Bai X, Wang W (2013) Geochemistry, zircon U-Pb geochronology and Lu-Hf isotopes of metavolcanics from eastern Hebei reveal Neoarchean subduction tectonics in the North China Craton. Gondwana Res 24:664–686

Fan H-R, Yang K-F, Hu F-F, Wang K-Y, Zhai M-G (2010) Zircon geochronology of basement rocks from the Bayan Obo area, Inner Mongolia, and tectonic implications. Acta Petrologica Sinica 26:1342–1350 (in Chinese with English abstract)

Frost CD, Bell JM, Frost BR, Chamberlain KR (2001) Crustal growth by magmatic underplating: isotopic evidence from the northern Sherman batholith. Geology 29:515–518

Halla J, Hunen JV, Heilimo E, Hölttäd P (2009) Geochemical and numerical constraints on Neoarchean plate tectonics. Precambr Res 174:155–162

Han B-F, Xu Z, Ren R, Li L-L, Yang J-H, Yang Y-H (2012) Crustal growth and intracrustal recycling in the middle segment of the Trans-North China Orogen, North China Craton: a case study of the Fuping Complex. Geol Mag 149:729–742

Han C-M, Xiao W-J, Su B-X, Chen Z-L, Zhang X-H, Ao S-J, Zhang J-E, Zhang Z-Y, Wan B, Song D-F, Wang Z-M (2014a) Neoarchean Algoma-type banded iron formations from Eastern Hebei, North China Craton: SHRIMP U-Pb age, origin and tectonic setting. Precambr Res 251:212–231

Han C-M, Xiao W-J, Su B-X, Sakyi PA, Chen Z-L, Zhang X-H, Ao S-J, Zhang J, Wan B, Zhang Z-Y, Wang Z-M, Ding J (2014b) Formation age and genesis of the Gongchangling Neoarchean banded iron deposit in eastern Liaoning Province: constraints from geochemistry and SHRIMP zircon U-Pb dating. Precambr Res 254:306–322

He Y-H, Sun Y, Chen L, Li H-P, Yuan H-L, Liu X-M (2005) Zircon U-Pb chronology of Longshan complex by LA-ICP-MS and its geological significance. Acta Petrologica Sinica 21:125–134 (in Chinese with English abstract)

Hildreth W, Moorbath S (1988) Crustal contributions to arc magmatism in the Andes of Central Chile. Contrib Miner Petrol 98:455–489

Hu J-M, Liu X-S, Li Z-H, Zhao Y, Zhang S-H, Liu X-C, Qu H-J, Chen H (2012) SHRIMP U-Pb zircon dating of the Ordos Basin basement and its tectonic significance. Chin Sci Bull 58:118–127

Huang D-M, Zhang D-H, Wang S-Y, Zhang Y-X, Dong C-Y, Liu D-Y, Wan Y-S (2012a) 2.3 Gamagmatism and 1.94 Ga metamorphism in the Xiatang Area, southern margin of the North China Craton. Geol Rev 58:565–573 (in Chinese with English abstract)

Huang X-L, Niu Y-L, Xu Y-G, Yang Q-J, Zhong J-W (2010) Geochemistry of TTG and TTG-like gneisses from Lushan-Taihua complex in the southern North China Craton: implications for late Archean crustal accretion. Precambr Res 182:43–56

Huang X-L, Wilde SA, Yang QJ, Zhong JW (2012b) Geochronology and petrogenesis of gray gneisses from the Taihua Complex at Xiong'er in the southern segment of the Trans-North China Orogen: implications for tectonic transformation in the Early Paleoproterozoic. Lithos 134–135:236–252

Huang X-L, Wilde SA, Zhong J-W (2013) Episodic crustal growth in the southern segment of the Trans-North China Orogen across the Archean-Proterozoicboundary. Precambr Res 233:337–357

Iizuka T, Komiya T, Johnson SP, Kon Y, Maruyama S, Hirata T (2009) Reworking of Hadean crust in the Acasta gneisses, northwestern Canada: evidence from in-situ Lu-Hf isotope analysis of zircon. Chem Geol 259:230–239

Jahn B-M, Auvray B, Cornichet J, Bai Y-L, Shen Q-H, Liu D-Y (1987) 3.5 Ga Old amphibolites from eastern Hebei province, China: field occurrence, petrography, Sm-Nd isochron age and REE chemistry. Precambr Res 34:311–346

Jahn B-M, Auvray B, Shen Q-H, Liu D-Y, Zhang Z-Q, Dong Y-J, Ye X-J, Zhang Q-Z, Cornichet J, Mace J (1988) Archean crustal evolution in China: the Taishan Complex, and evidence for juvenile crustal addition from long-term depleted mantle. Precambr Res 38:381–403

Jahn B-M, Zhou X-H, Li JL (1990) Formation and tectonic evolution of Southeastern China and Taiwan: isotopic and geochemical constraints. Tectonophysics 183:145–160

Jahn B-M, Liu D-Y, Wan Y-S, Song B, Wu J-S (2008) Archean crustal evolution of the Jiaodong peninsula, China, as revealed by zircon SHRIMP geochronology, elemental and Nd-isotope geochemistry. Am J Sci 308:232–269

Jayananda M, Moyen FF, Martin H, Peucat JJ, Auvray B, Mahabaleswar B (2000) Late Archaean (2550-2520 Ma) juvenile magmatism in the Eastern Dharwar Craton, Southern India: constraints from geochronology Nd-Sr isotopes and whole rock geochemistry. Precambr Res 99:225–254

Ji Z-Y (1993) New data on isotope age of the Proterozoic metamorphic rocks from northern Jiaodong and its geological significance.Shandong. Geology 9:40–51 (in Chinese with English abstract)

Jian P, Kröner A, Windley BF, Zhang Q, Zhang W, Zhang L-Q (2012) Episodic mantle melting-crustal reworking in the late Neoarchean of the northwestern North China Craton: Zircon ages of magmatic and metamorphic rocks from the Yinshan Block. Precambr Res 222–223:230–254

Jiang N, Guo J-H, Zhai M-G, Zhang S-Q (2010) ~2.7 Ga crust growth in the North China craton. Precambr Res 179:37–49

Jiang Z-S, Wang G-D, Xiao L-L, Diwu C-R, Lu J-S, Wu C-M (2011) Paleoproterozoic metamorphic P-T-t path and tectonic significance of the Luoning metamorphic complex at the southern terminal of the Trans-North China Orogen, Henan Province. Acta Petrologica Sinica 27:3701–3717 (in Chinese with English abstract)

Jin K, Xu W-L, Wang Q-H, Gao S, Liu X-C (2003) Formation time and sources of the Huaiguang "Migmatitic Granodiorite" in Bengbu, Anhui Provinece: evidence from SHRIMP zircon U-Pb geochronology. Acta Geoscientia Sinica 24:331–335 (in Chinese with English abstract)

Kinny PD (1986) 3820 Ma zircons from a tonalitic Amitsoq gneiss in the Godthab district of southern West Greenland. Earth Planet Sci Lett 79:337–347

Kröner A, Compston W, Zhang G-W, Guo A-L, Todt W (1988) Age and tectonic setting of Late Archean greenstone-gneiss terrain in Henan Province, China, as revealed by single grain zircon dating. Geology 16:211–215

Kröner A, Cui W-Y, Wang S-Q (1998) Single zircon ages from high-grade rocks of the Jianping Complex, Liaoning Province, NE China. J Asian Earth Sci 16:519–532

Kröner A, Wilde SA, O'Brien PJ, Li J-H, Passchier CW, Walte NP, Liu D-Y (2005a) Field relationships, geochemistry, zircon ages and evolution of a late Archaean to Palaeoproterozoic lower crustal section in the Hengshan terrain of northern China. Acta Geologica Sinica 79: 605–629

Kröner A, Wilde SA, Li J-H, Wang K-Y (2005b) Age and evolution of a late Archean to Paleoproterozoic upper to lower crustal section in the Wutaishan/Hengshan/Fuping terrain of northern China. J Asian Earth Sci 24:577–595

Kröner A, Wilde SA, Zhao G-C, O'Brien PJ, Sun M, Liu D-Y, Wan Y-S, Liu S-W, Guo J-H (2006) Zircon geochronology and metamorphic evolution of mafic dykes in the Hengshan Complex of northern China: evidence for late Palaeoprotero-zoic extension and subsequent high-pressure metamorphism in the North ChinaCraton. Precambr Res 146:45–67

Kröner A, Hoffmann JE, Xie H, Münker C, Hegner E, Wan Y, Hofmann A, Liu D, Yang J (2014) Generation of early Archaean grey gneisses through crustal melting of older crust in the eastern Kaapvaal craton, southern Africa. Precambr Res 255:833–846

Kusky TM, Li J-H (2003) Paleoproterozoic tectonic evolution of the North China Craton. J Asian Earth Sci 22:383–397

Kusky TM, Li J-H, Santosh M (2007) The Paleoproterozoic North Hebei Orogen: North China Craton's collisional suture with the Columbia supercontinent. Gondwana Res 12:4–28

Li B, Jin W, Zhang J-H, Wang Y-F, Cai L-B, Wang Q-L (2013) Composition and structural characteristics of Archean granite in Chentaigou area of Anshan. Global Geol 32:191–199 (in Chinese with English abstract)

Li C-D, Zhang F-Q, Miao L-C, Du Y-L, Hua Y-Q, Xu Y-W, Kang S-M (2009) Zircon SHRIMP U-Pb geochronology of the Zhangsangou Formation Complex in the northeastern margin of North China Craton and its geological significance. Acta Geol Sinica 83:642–650 (in Chinese with English abstract)

Li C-J, Bao Z-W, Zhao Z-H, Qiao Y-L (2012) Zircon U-Pb age and Hf isotopic compositions of the granitic gneisses from the Sanggan complex in the Zhangjiakouk area: constraints on the early evolution of North China Craton. Acta Petrologica Sinica 28:1057–1072 (in Chinese with English abstract)

Li J-H, Qian X-L, Hou G-T, Liu S-W, Chen J (2000) Late Paleoproterozoic to early Mesoproterozoic tectonic framework and major tectono-thermal episodes of north China: new interpretation of "Luliang orogeny". Earth Sci 25:15–20 (in Chinese with English abstract)

Li J-H, Kusky TM, Huang X-N (2002) Archean podiform chromitites and mantle tectonites in ophiolitic mélange, North China Craton: a record of early oceanic mantle processes. GSA Today 12:4–11

Li J-H, Yang C-H, Du L-L, Wan Y-S, Liu Z-X (2005) SHRIMP U-Pb geochronology evidence for the formation time of the Wanzi Group at Pingshan County, Hebei Province. Geol Rev 51:201–207 (in Chinese with English abstract)

Li S-X, Ji S-K, Ma Z-H, Huo G-P, Tian Y-Q, Yang W-K (1986) Geology of metasedimentary iron deposit in Wutaishan. Jilin Science and Technology Press, Changchun, pp 1–299 (in Chinese)

Li S-X, Liu X-S, Zhang L-Q (1987) Granite-greenstone belt in Sheerteng area, Inner Mongolia, China. J Changchun Univ Geol 17:81–102 (in Chinese with English abstract)

Li S-Z, Zhao G-C, Wilde SA, Zhang J, Sun M, Zhang G-W, Dai L-M (2010a) Deformation history of the Hengshan-Wutai-Fuping Complexes: implications for the evolution of the Trans-North China Orogen. Gondwana Res 18:611–631

Li T-S, Zhai M-G, Peng P, Chen L, Guo J-H (2010b) Ca. 2.5 billion year old coeval ultramafic-mafic and syenitic dykes in Eastern Hebei: implicaitons for cratonization of the North China Craton. Precambr Res 180:143–155

Liaoning Bureau of Geology and Mineral Resources Exploration (LBGMRE) (1975a) Geological map of Liaoyang sheet (1:200000)

Liaoning Bureau of Geology and Mineral Resources Exploration (LBGMRE) (1975b) Geological map of Yingkou sheet (1:200000)

Liaoning Bureau of Geology and Mineral Resources Exploration (LBGMRE) (1976) Geological map of Shenyang sheet (1:200000)

Liu C-H, Zhao G-C, Sun M, Zhang J, Yin C-Q (2012a) U-Pb geochronology and Hf isotope geochemistry of detrital zircons from the Zhongtiao Complex: constraints on the tectonic evolution of the Trans-North China Orogen. Precambr Res 222–223:159–172

Liu D-Y, Nutman AP, Compston W, Wu J-S, Shen Q-H (1992) Remnants of 3800 Ma crust in the Chinese part of the Sino-Korean Craton. Geology 20:339–342

Liu D-Y, Wilde SA, Wan Y-S, Wu J-S, Zhou H-Y, Dong C-Y, Yin X-Y (2008) New U-Pb and Hf isotopic data confirm Anshan as the oldest preserved segment of the North China Craton. Am J Sci 308:200–231

Liu D-Y, Wilde SA, Wan Y-S, Wang S-Y, Valley JW, Kita N, Dong C-Y, Xie H-Q, Yang C-X, Zhang Y-X, Gao L-Z (2009a) Late Mesoarchean-early Neoarchean tectonothermal events at the southern margin of the North China Craton: evidence of multiple events from SHRIMP U-Pb dating and hafnium isotope analysis of zircons from metamorphosed supracrustal rocks and tonalites. Chem Geol 261:140–154

Liu F, Guo J-H, Lu X-P, Diwu C-Y (2009b) Crustal growth at ~2.5 Ga in the North China Craton: evidence from whole-rock Nd and zircon Hf isotopes in the Huai'an gneiss terrane. Chin Sci Bull 54:4704–4713

Liu J-H, Liu F-L, Liu P-H, Wang F, Ding Z-J (2011a) Polyphase magmatic and metamorphic events from early Precambrian metamorphic basement in Jiaobei area: evidence from the Zircon U-Pb dating of TTG and granitic gneisses. Acta Petrologica Sinica 27:943–960 (in Chinese with English abstract)

Liu J-H, Liu F-L, Ding Z-J, Liu P-H, Wang F (2012b) The zircon Hf isotope characteristics of ~2.5 Ga magmatic event and implication for the crustal evolution in the Jiaobei terrane, China. Acta Petrologica Sinica 28:2697–2704

Liu J-H, Liu F-L, Ding Z-J, Liu C-H, Yang H, Liu P-H, Wang F, Meng E (2013a) The growth, reworking and metamorphism of early Precambrian crust in the Jiaobei terrane, the North China Craton: constraints from U-Th-Pb and Lu-Hf isotopics ystematics, and REE concentrations of zircon from Archean granitoid gneisses. Precambr Res 224:287–303

Liu L, Zhang L-C, Dai Y-P, Wang C-L, Li Z-Q (2012) Formation age, geochemical signatures and geological significance of the Sanheming BIF-type iron deposit in the Guyang greenstone belt, Inner Mongolia: Acta Petrologica Sinica 28:3623–3637 (in Chinese with English abstract)

Liu L, Zhang L-C, Dai Y-P (2014) Formation age and genesis of the banded iron formations from the Guyang Greenstone Belt, Western North China Craton. Ore Geol Rev 63:388–404

Liu S-J, Wan Y-S, Sun H-Y, Nutman A, Xie H-Q, Dong C-Y, Ma M-Z, Du L-L, Liu D-Y, Jhan B-M (2013b) Paleo- to Eoarchean crustal materials in eastern Hebei, North China Craton: new evidence from SHRIMP U-Pb dating and in-situ Hf isotopic studies in detrital zircons of supracrustal rocks. J Asian Earth Sci 78:4–17

Liu S-W, Pan Y, Li J-H, Li G-G, Zhang J (2002) Geological and isotopic geochemical constraints on the evolution of the Fuping Complex, North China Craton. Precambr Res 117:41–56

Liu S-W, Pan Y-M, Xie Q-L, Zhang J, Li Q-G (2004a) Archean geodynamics in the Central Zone, North China Craton: constraints from geochemistry of two contrasting series of granitoids in the Fuping and Wutai complexes. Precambr Res 130:229–249

Liu S-W, Lü Y-J, Feng Y-G, Zhang C, Tian W, Yan Q-R, Liu X-M (2007) Geology and zircon U-Pb isotopic chronology of Dantazi Complex, northern Hebei Province. Geol J China Univ 13:484–497 (in Chinese with English abstract)

Liu S-W, Santosh M, Wang W, Bai X, Yang P-T (2011b) Zircon U-Pb chronology of the Jianping Complex: implications for the Precambrian crustal evolution history of the northern margin of North China Craton. Gondwana Res 20:48–63

Liu S-W, Lü Y-J, Wang W, Yang P-T, Bai X, Feng Y-G (2011c) Petrogenesis of the Neoarchean granitoid gneisses in northern Hebei Province. Acta Petrologica Sinica 27:909–921 (in Chinese with English abstract)

Liu X-C, Zhao Y, Song B, Liu J, Cui J-J (2009c) SHRIMP U-Pb zircon geochronology of high-grade rocks and charnockites from the eastern Amery Ice Shelf and southwestern Prydz Bay, East Antarctica: constraints on Late Mesoproterozoic to Cambrian tectonothermal events related to supercontinent assembly. Gondwana Res 16:342–361

Liu Y-S, Gao S, Yuan H-L, Zhou L, Liu X-M, Wang X-C, Hu Z-C, Wang L-S (2004b) U-Pb zircon ages and Nd Sr, and Pb isotopes of lower crustal xenoliths from North China Craton: insights on evolution of lower continental crust. Chem Geol 211:87–109

Lu L-Z, Xu X-C, Liu F-L (1996) Early Precambrian Khondalite series of North China. Changchun Publishing House, Changchun, pp 1–272 (in Chinese)

Lu S-N, Chen Z-H, Xiang Z-Q (2008) The world geopark of Taishan: geochronological framework of Ancient Intrusives. Geological Publishing House, Beijng, pp 1–90 (in Chinese)

Lü B, Zhai M-G, Li T-S, Peng P (2012) Zircon U-Pb ages and geochemistry of the Qinglong volcano-sedimentary rock series in Eastern Hebei: implication for ~2500 Ma intra-continental rifting in the North China Craton. Precambr Res 208–211:145–160

Ma M-Z, Wan Y-S, Santosh M, Xu Z-Y, Xie H-Q, Dong C-Y, Liu D-Y (2012) Decoding multiple tectonothermal events in zircons from single rock samples: SHRIMP zircon U-Pb data from the late Neoarchean rocks of Daqingshan, North China Craton. Gondwana Res 22:810–827

Ma M-Z, Xu Z-Y, Zhang L-C, Dong C-Y, Liu S-J, Liu D-Y, Wan Y-S (2013a) SHRIMP dating and Hf isotope analysis of zircons from the early Precambrian basement in the Xi Ulanbulang

area, Wuchuan, Inner Mongolia. Acta Petrologica Sinica 29:501–516 (in Chinese with English abstract)
Ma X-D, Fan H-R, Santosh M, Guo J-H (2013b) Geochemistry and zircon U-Pb chronology of charnockites in the Yinshan Block, North China Craton: tectonic evolution involving Neoarchaean ridge subduction. Int Geol Rev 55:1688–1704
Ma X-D, Guo J-H, Liu F, Qian Q, Fan H-R (2013c) Zircon U-Pb ages, trace elements and Nd-Hf isotopic geochemistry of Guyang sanukitoids and related rocks: implications for the Archean crustal evolution of the Yinshan Block, North China Craton. Precambr Res 230:61–78
Ma X-D, Fan H-R, Santosh M, Guo J-H (2014a) Chronology and geochemistry of Neoarchean BIF-type iron deposits in the Yinshan Block, North China Craton: implications for oceanic ridge subduction. Ore Geol Rev 63:405–417
Ma X-D, Fan H-R, Santosh M, Liu X, Guo J-H (2014b) Origin of sanukitoid and hornblendite enclaves in the Dajitu pluton from the Yinshan Block, North China Craton: product of Neoarchaean ridge subduction? Int Geol Rev. doi:10.1080/00206814.2014.929055
Manikyamba C, Kerrich R (2012) Eastern Dharwar Craton, India: Continental lithosphere growth by accretion of diverse plume and arc terranes. Geosci Front 3:225–240
McCready AJ, Stumpfl EF, Lally J, Ahmad M, Gee RD (2004) Polymetallic mineralization at the Browns deposit, Rum Jungle Mineral Field, Northern Territory, Australia. Econ Geol 99:257–277
Mei H-L (1991) P-T path of basic granulite in the Zhulagou complex, Inner Mongolia, China. Acta Petrologica et Minerlogica 10:133–142 (in Chinese with English abstract)
Miao P-S (2003) Tectonic style of the high-grade metamorphic terrain of Hengshan in the North China Craton. Tianjing Publishing press, Tianjing, pp 1–86 (in Chinese with English abstract)
Mohan MR, Piercey SJ, Kamber BS, Sarma DS (2013) Subduction related tectonic evolution of the Neoarchean eastern Dharwar Craton, southern India: new geochemical and isotopic constraints. Precambr Res 227:204–226
Moyen JF (2011) The composite Archaean grey gneisses: petrological significance, and evidence for a non-unique tectonic setting for Archaean crustal growth. Lithos 123:21–36
Moyen JF, Martin H, Jayananda M, Auvray B (2003) Late Archaean granites: a typology based on the Dharwar Craton (India). Precambr Res 127:103–123
North China Oilfield Company of PetroChina (NCOCP) (2012) Introduction on Drilling Cores Relating to Precambrian Basement in the Central Hebei Basin. Unpublished Ms, pp 1–18
Nutman AP, McGregor VR, Friend CRL, Bennett VC, Kinny PD (1996) The Itsaq Gneiss Complex of southern West Greenland: the world's most extensive record of early crustal evolution (3900-3600 Ma). Precambr Res 78:1–39
Nutman AP, Wan Y-S, Liu D-Y (2009) Integrated field geological and zircon morphology evidence for ca. 3.8 Ga rocks at Anshan: Comment on "Zircon U-Pb and Hf isotopic constraints on the Early Archean crustal evolution in Anshan of the North China Craton" by Wu et al. [Precambr Res 167 (2008) 339–362]. Precambr Res 172:357–360
Nutman AP, Wan Y-S, Du L-L, Friend CRL, Dong C-Y, Xie H-Q, Wang W, Sun H-Y, Liu D-Y (2011) Multistage late Neoarchaean crustal evolution of the North China Craton, eastern Hebei. Precambr Res 189:43–65
Nutman AP, Bennett VC, Friend CRL, Hidaka H, Yi K, Lee SR, Kamiichi T (2013) The Itsaq gneiss complex of Greenland: episodic 3900 to 3600 Ma juvenile crust formation and recycling in the 3600 to 3600 Ma Isukasian orogeny. Am J Sci 313:877–911
Nutman AP, Maciejowski R, Wan Y-S (2014) Protoliths of enigmatic Archaean gneisses established from zircon inclusion studies: case study of the Caozhuang quartzite, E. Hebei, China. Geosci Front 5:445–455
O'Neil J, Maurice C, Stevenson RK, Larocque J, Cloquet C, David J, Francis D (2007) The geology of the 3.8 Ga Nuvvuagittuq (Porpoise Cove) greenstone belt, northeastern Superior Province, Canada. In: van Kranendonk MJ, Smithies RH, Bennett VC (eds) Earth's oldest rocks, developments in Precambrian Geology, vol 15. pp 219–250
Pei F-P, Xu W-L, Yang D-B, Zhao Q-G, Liu X-M, Hu Z-C (2007) Zircon U-Pb geochronology of basement metamorphic rocks in the Songliao Basin. Chin Sci Bull 52:942–948

Peng M-S, Zhang P, Yang H-Z, Wang X-J, Qiao S-Y (2013a) Geochemical characteristics and geological significance of iron deposit in Nanfen, Liaoning. Sci Technol Rep 31:33–37 (in Chinese with English abstract)

Peng P, Li Y, Liu F, Wang F (2012) Geological relation of late Archean lithologic units in northwest Hebei, North China Craton: implication for building of early continental crust. Acta Petrologica Sinica 28:3531–3544 (in Chinese with English abstract)

Peng T-P, Wilde SA, Fan W-M, Peng B-X (2013b) Late Neoarchean potassic high Ba-Sr granites in the Taishan granite-greenstone terrane: petrogenesis and implications for continental crustal evolution. Chem Geol 344:23–41

Polat A, Li J, Fryer B, Kusky T, Gagnon J, Zhang S (2006a) Geochemical characteristics of the Neoarchean (2800-2700 Ma) Taishan greenstone belt, North China Craton: Evidence for plume-craton interaction. Chem Geol 230:60–87

Polat A, Herzberg C, Münker C, Rodgers R, Kusky T, Li J, Fryer B, Delaney J (2006b) Geochemical and petrological evidence for a suprasubduction zone origin of Neoarchean (ca. 2.5 Ga) peridotites, central osorgenic belt, North China Craton. Bull Geol Soc Am 118:771–784

Qian J-H, Wei C-J, Zhou X-W, Zhang Y-H (2013) Metamorphic P-T paths and new zircon U-Pb age data for garnet-mica schist from the Wutai Group, North China Craton. Precambr Res 233:282–296

Qian X-L, Cui W-Y, Wang S-Q, Wang G-Y (1985) Geology of Precambrian iron ores in eastern Hebei Province, China. Hebei Science and Tecnology Press, Shijiazhuang, pp 1–273 (in Chinese)

Qian X-L, Wang R-M et al. (1994) Geological evolution of the granulite terrain in north part of the North China Craton. Seismological Press, Beijing, pp 1–234 (in Chinese)

Ren K-X, Yan G-H, Cai J-H, Zou T-R, Mu B-L, Li F-T (2013) SHRIMP U-Pb zircon age and its implications of quartz syenite in Hadamengou, Inner Mongolia. Adv Geosci 3:42–47 (in Chinese with English abstract)

Ren R, Han B-F, Zhang Z-C, Li J-F, Yang Y-H, Zhang Y-B (2011) Zircon U-Pb and Hf isotopic studies of basement gneiss and overlying Meso-Neoproterozoic sedimentary rocks from the Changping area, Beijing, and their geological implications. Acta Petrologica Sinica 27:1721–1745 (in Chinese with English abstract)

Ren Y-W (2010) The study of granite-greenstone belt in Xihongshan Area, Inner Mongolia. Ms. Thesis, Jilin University, pp 1–64 (in Chinese with English abstract)

Rey PF, Philippot P, Thebaud N (2003) Contribution of mantle plumes, crustal thickening and greenstone blanketing to the 2.75-2.65 Ga global crisis. Precambr Res 127:43–60

Shan H-X, Zhai M-G, Wang F, Zhou Y-Y, Santosh M, Zhu X-Y, Zhang H-F, Wang W (2015) Zircon U-Pb ages, geochemistry, and Nd-Hf isotopes of the TTG gneisses from the Jiaobei terrane: Implications for Neoarchean crustal evolution in the North China Craton. J Asian Earth Sci (in press)

Shen B-F, Luo H, Li S-B, Li J-J, Peng X-L, Hu X-D, Mao D-B, Liang R-X (1994a) Geology and metallization of Archean Greenstone Belt in North China Plateform. Geological Publishing House, Bejing, pp 1–202 (in Chinese with English abstract)

Shen B-F, Luo H, Han G-G, Dai X-Y, Jin W-S, Hu X-D, Li S-B, Bi S-Y (1994b) Archean geolgy and metallization in northern Liaoning Province and southern Jilin Province. Geological Publishing House, Beijing, pp 1–255 (in Chinese with English abstract)

Shen Q-H, Zhang Y-F, Gao J-F, Wang P (1990) Study on Archaean metamorphic rocks in midsouthern Nei Mongol of China. In: Bulletin of Institute of Geology of Chinese Academy of Geological Scienes. Geological Publishing House, Beijing, pp 1–192 (in Chinese)

Shen Q-H, Xu H-F, Zhang Z-Q, Gao J-F, Wu J-S, Ji C-L (1992) Early Precambrain granulites of China. Geological Publishing House, Beijing, pp 1–237 (in Chinese)

Shen Q-H, Shen K, Geng Y-S, Xu H-F (2000) Compositions and geological evolution of Yishui Complex, Shandong. Geological Publishing House, Bejing, pp 1–179 (in Chinese)

Shen Q-H, Song B, Xu H-F, Geng Y-S, Shen K (2004) Emplacement and metamorphism ages of the Caiyu and Dashan igneous bodies, Yishui County, Shandong Province: zircon SHRIMP chronology. Geol Rev 50:275–284 (in Chinese with English abstract)

Shen Q-H, Geng Y-S, Song B, Wan Y-S (2005) New information from the surface outcrops and deep crust of Archean rocks of the North China and Yangtze Blocks, and Qinling-Dabie Orogenic Belt. Acta Geol Sinica 79:616–627 (in Chinese with English abstract)

Shen Q-H, Zhao Z-R, Song B, Song H-X (2007) Geology, petrochemistry and SHRIMP zircon U-Pb dating of the Mashan and Xueshan granitoids in Yishui County, Shandong Province. Geol Rev 53:180–186 (in Chinese with English abstract)

Shi Y-R, Wilde SA, Zhao X-T, Ma Y-S, Du L-L, Liu D-Y (2012) Late Neoarchean magmatic and subsequent metamorphic events in the northern North China Craton: SHRIMP zircon dating and Hf isotopes of Archean rocks from Yunmengshan Geopark, Miyun, Beijing. Gondwana Res 21:785–800

Song B, Nutman AP, Liu D-Y, Wu J-S (1996) 3800 to 2500 Ma crustal evolution in the Anshan area of Liaoning Province, northeastern China. Precambr Res 78:79–94

Song H-X, Zhao Z-R, Shen Q-H, Song B (2009) Study on petrochemistry and hafnium isotope in Yishui Complex, Shandong Province. Acta Petrologica Sinica 25:1872–1882 (in Chinese with English abstract)

Söderlund U, Patchett PJ, Vervoort JD, Isachsen CE (2004) The ^{176}Lu decay constant determined by Lu-Hf and U-Pb isotope systematics of Precambrian mafic intrusions. Earth Planet Sci Lett 219:311–324

Sun D-Z et al (1984) The early Precambrian geology of eastern Hebei. Tiangjing Science and Technology Press, Tianjing, pp 1–273 (in Chinese with English abstract)

Sun D-Z, Li H-M, Lin Y-X, Zhou H-F, Zhao F-Q, Tang M (1991) Precambrian geochronology, chronotectonic framework and model of chronocrustal structure of the Zhongtiao mountains. Acta Geol Sinica 65:216–231 (in Chinese with English abstract)

Sun D-Z, Hu H-F (1993) The tectonic framework of Precambrian in Zhongtiaoshan. Geological Publishing House, Beijing, pp 1–180 (in Chinese with English abstract)

Sun H-Y, Dong C-Y, Xie H-Q, Wang W, Ma M-Z, Liu D-Y, Nutman A, Wan Y-S (2010) The formation age of the Neoarchean Zhuzhangzi and Dantazi groups in the Qinglong area, eastern Hebei Province: evidence from SHRIMP U-Pb zircon dating. Geol Rev 56:888–898 (in Chinese with English abstract)

Sun M, Guan H (2001) Zircon U-Pb ages of the Fuping Complex and their implications: some comments on the geochronological study of the Precambrian high-grade metamorphic terranes. Acta Petrologica Sinica 17:145–156 (in Chinese with English abstract)

Sun X-H, Zhu X-Q, Tang H-S, Zhang Q, Luo T-Y (2014) Reprint of "The Gongchangling BIFs from the Anshan-Benxi area, NE China: petrological-geochemical characteristics and genesis of high-grade iron ores". Ore Geol Rev 63:374–387

Tang J, Zheng Y-F, Wu Y-B, Gong B, Liu X-M (2007) Geochronology and geochemistry of metamorphic rocks in the Jiaobei terrane: constraints on its tectonic affinity in the Sulu orogen. Precambrian Res 152:48–82

Tian W, Liu S-W, Liu C-Q, Yu S-Q, Li Q-G, Wang Y-R (2005) Zircon SHRIMP geochronology and geochemistry of TTG rocks of the Sushui Complex in the Zhongtiao area, and its geological significance. Nat Sci Prog 15:1476–1484 (in Chinese)

Trap P, Faure M, Lin W, Monié P (2007) Late Palaeoproterozoic (1900–1800 Ma) nappe stacking and polyphase deformation in the Hengshan-Wutaishan area: implication for the understanding of the Trans-North China Belt, North China Craton. Precambr Res 156:85–106

Trap P, Faure M, Lin W, Monié P, Bruguier O (2008) Contrasted tectonic styles for the Paleoproterozoic evolution of the North China Craton. Evidence for a $\sim$2.1 Ga thermal and tectonic event in the Fuping Massif. J Struct Geol 30:1109–1125

Tsunogae T, Dunkley DJ, Horie K, Endo T, Miyamoto T, Kato M (2014) Petrology and SHRIMP zircon geochronology of granulites from Vesleknausen, Lützow-Holm Complex, East Antarctica: Neoarchean magmatism and Neoproterozoic high-grade metamorphism. Geosci Front 5:167–182

Van Kranendonk MJ, Smithies RH, Griffin WL, Huston DL, Hickman AH, Champion DC, Anhaeusser CR, Pirajno F (2014) Making it thick: a volcanic plateau origin of Palaeoarchean continental lithosphere of the Pilbara and Kaapvaal cratons. In: Roberts NMW, Van

Kranendonk M, Parman S, Shirey S, Clift PD (eds) Continent formation through time, vol 389. Geological Society, London, Special Publications, pages unknown

Wan Y-S (1993) The formation and evolution of the iron-bearing rock series of the Gongchangling area, Liaoning Province. Beijing Science and Technology Publishing House, Beijing, pp 1–108 (in Chinese with English abstract)

Wan Y-S, Zhang Z-Q, Wu J-S, Song B, Liu D-Y (1997a) Geochemical and Nd isotopic characteristics of some rocks from the Paleoarchaean Chentaigou supracrustal, Anshan area, NE China. Cont Dyn 2:39–46

Wan Y-S, Geng Y-S, Wu J-S (1997b) Geochemical compositions of early Precambrian meta-basaltic rocks in the North China Craton and its adjacent area. In: Cheng Y-Q (ed) Essay collection of early Precambrian geology of the North China Platform 39–59 (in Chinese)

Wan Y-S, Song B, Liu D-Y, Li H-M, Yang C, Zhang Q-D, Yang C-H, Geng Y-S, Shen Q-H (2001) Geochronology and geochemistry of 3.8-2.5 Ga ancient rock belt in the Dongshan scenic park, Anshan area. Acta Geologica Sinica 75:363–370 (in Chinese with English abstract)

Wan Y-S, Liu D-Y, Song B, Wu J-S, Yang C-H, Zhang Z-Q, Geng Y-S (2005a) Geochemical and Nd isotopic compositions of 3.8 Ga meta-quartz dioritic and trondhjemitic rocks from the Anshan area and their geological significance. J Asian Earth Sci 24:563–575

Wan Y-S, Song B, Yang C, Wu J-S (2005b) Zircon SHRIMP U-Pb geochronology of Archaean rocks from the Fushun-Qingyuan area, Liaoning Province and its geological significance. Acta Geol Sinica 79:78–87 (in Chinese with English abstract)

Wan Y-S, Song B, Geng Y-S, Liu D-Y (2005c) Geochemical characteristics of Archaean basement in the Fushun-Qingyuan area, northern Liaoning Province and its geological significance. Geol Rev 51:128–137 (in Chinese with English abstract)

Wan Y-S, Song B, Liu D-Y, Wilde SA, Wu J-S, Shi Y-R, Yin X-Y, Zhou H-Y (2006) SHRIMP U-Pb zircon geochronology of Paleoproterozoic metasedimentary rocks in the North China Craton: evidence for a major Late Paleoproterozoic tectonothermal event. Precambr Res 149:249–271

Wan Y-S, Liu D-Y, Yin X-Y, Wu J-S, Wilde SA (2007) SHRIMP geochronology and Hf isotope composition of zircons from the Tiejiashan granite and supracrustal rocks in the Anshan area, Liaoning province. Acta Petrologica Sinica 23:241–252 (in Chinese with English abstract)

Wan Y-S, Liu D-Y, Dong C-Y, Nutman A, Wilde SA, Wang W, Xie H-Q, Yin X-Y, Zhou H-Y (2009a) The oldest rocks and zircons in China. Acta Petrologica Sinica 25:1793–1807 (in Chinese with English abstract)

Wan Y-S, Liu D-Y, Dong C-Y, Xu Z-Y, Wang Z-J, Wilde SA, Yang Y-H, Liu Z-H, Zhou H-Y (2009b) The Precambrian Khondalite Belt in the Daqingshan area, North China Craton: evidence for multiple metamorphic events in the Palaeoproterozoic. In: Reddy SM, Mazumder R, Evans DAD, Collins AS (eds) Palaeoproterozoic supercontinents and global evolution: Journal of the London Geological Society, vol 323. Special Publications, pp 73–97

Wan Y-S, Liu D-Y, Wang S-Y, Zhao X, Dong C-Y, Zhou H-Y, Yin X-Y, Yang C-X, Gao L-Z (2009c) Early Precambrian crustal evolution in the Dengfeng area: constraints from geochemistry and SHRIMP U-Pb zircon dating. Acta Geol Sinica 83:982–999 (in Chinese with English abstract)

Wan Y-S, Miao P-S, Liu D-Y, Yang C-H, Wang W, Wang H-C, Wang Z-J, Dong C-Y, Du L-L, Zhou H-Y (2010a) Formation ages and source regions of the Palaeoproterozoic Gaofan, Hutuo and Dongjiao groups in the Wutai and Dongjiao areas of the North China Craton from SHRIMP U-Pb dating of detrital zircons: resolution of debates over their stratigraphic relationships. Chin Sci Bull 55:1278–1284

Wan Y-S, Dong C-Y, Wang W, Xie H-Q, Liu D-Y (2010b) Archaean basement and a Palaeoproterozoic collision orogen in the Huoqiu area at the southeastern margin of the North China Craton: evidence from SHRIMP U-Pb zircon geochronology. Acta Geol Sinica 84:91–104

Wan Y-S, Liu D-Y, Wang S-J, Dong C-Y, Yang E-X, Wang W, Zhou H-Y, Ning Z-G, Du L-L, Yin X-Y, Xie H-Q, Ma M-Z (2010c) Juvenile magmatism and crustalrecycling at the end of the

Neoarchean in Western Shandong Province, NorthChina Craton: evidence from SHRIMP zircon dating. Am J Sci 310:1503–1552

Wan Y-S, Liu D-Y, Wang W, Song T-R, Kröner A, Dong C-Y, Zhou H-Y, Yin X-Y (2011a) Provenance of Meso- to Neoproterozoic cover sediments at the Ming Tombs, Beijing, North China Craton: An integrated study of U-Pb dating and Hf isotopic measurement of detrital zircons and whole-rock geochemistry. Gandwana Res 20:219–242

Wan Y-S, Liu D-Y, Wang S-J, Yang E-X, Wang W, Dong C-Y, Zhou H-Y, Du L-L, Yang Y-H, Diwu C-R (2011b) ~2.7 Ga juvenile crust formation in the North China Craton (Taishan-Xintai area, western Shandong Province): further evidence of an understated event from U-Pb dating and Hf isotopic composition of zircon. Precambr Res 186:169–180

Wan Y-S, Liu D-Y, Dong C-Y, Liu S-J, Wang S-J, Yang E-X (2011c) U-Th-Pb behaviorof zircons under high-grade metamorphic conditions: a case study of zircon dating of meta-diorite near Qixia, eastern Shandong. Geosci Front 2:137–146

Wan Y-S, Liu D-Y, Nutman A, Zhou H-Y, Dong C-Y, Yin X-Y, Ma M-Z (2012a) Multiple 3.8–3.1 Ga tectono-magmatic events in a newly discovered area of ancient rocks (the Shengousi Complex), Anshan, North China Craton. J Asian Earth Sci 54–55:18–30

Wan Y-S, Dong C-Y, Liu D-Y, Kröner A, Yang C-H, Wang W, Du L-L, Xie H-Q, Ma M-Z (2012b) Zircon ages and geochemistry of late Neoarchean syenogranites in the North China Craton: a review. Precambr Res 222–223:265–289

Wan Y-S, Wang S-J, Liu D-Y, Wang W, Kröner A, Dong C-Y, Yang E-X, Zhou H-Y, Xie H-Q, Ma M-Z (2012c) Redefinition of depositional ages of Neoarchean supracrustal rocks in western Shandong Province, China: SHRIMP U-Pb zircon dating. Gondwana Res 21:768–784

Wan Y-S, Dong C-Y, Xie H-Q, Wang S-J, Song M-C, Xu Z-Y, Wang S-Y, Zhou H-Y, Ma M-Z, Liu D-Y (2012d) Formation ages of early Precambrian BIFs in North China Craton: SHRIMP zircon U-Pb dating. Acta Geol Sinica 86:1447–1478 (in Chinese with English abstract)

Wan Y-S, Xie H-Q, Yang H, Wang Z-J, Liu D-Y, Kröner A, Wilde SA, Geng Y-S, Sun L-Y, Ma M-Z, Liu S-J, Dong C-Y, Du L-L (2013) Is the Ordos Block Archean or Paleoproterozoic in age? Implications for the Precambrian evolution of the North China Craton. Am J Sci 313:683–711

Wan Y-S, Xie S-W, Yang C-H, Kröner K, Ma M-Z, Dong C-Y, Du L-L, Xie H-Q, Liu D-Y (2014a) Early Neoarchean (~2.7 Ga) tectono-thermal events in the North China Craton: a synthesis. Precambr Res 247:45–63

Wan Y-S, Zhao X-Z, Wang Z-J, Liu D-Y, Kröner A, Dong C-Y, Xie H-Q, Geng Y-S, Zhang Y-H, Fan R-L, Sun H-Y (2014b) SHRIMP zircon dating and LA-ICPMS Hf analysis of early Precambrian rocks from drill holes into the basement beneath the Central Hebei Basin, North China Craton. Geosci Front 5:471–484

Wan Y-S, Ma M-Z, Dong C-Y, Xie H-Q, Xie S-W, Ren P, Liu D-Y (2015a) Widespread late Neoarchean reworking of Meso- to Paleoarchean continental crust in the Anshan-Benxi area, North China Craton, as documented by U-Pb-Nd-Hf-O isotopes. Am J Sci (in press)

Wan Y-S, Dong C-Y, Wang S-J, Kröner A, Xie H-Q, Ma M-Z, Zhou H-Y., Xie S-W, Liu D-Y (2015b) Middle Neoarchean magmatism in western Shandong, North China Craton: SHRIMP zircon dating and LA-ICP-MS Hf isotope analysis. Precambr Res (in press)

Wang A-D, Liu Y-C (2012) Neoarchean (2.5-2.8 Ga) crustal growth of the North China Craton revealed by zircon Hf isotope: a synthesis. Geosci Front 3:147–173

Wang A-D, Liu Y-C, Gu X-F, Hou Z-H, Song B (2012a) Late-Neoarchean magmatism and metamorphism at the southeastern margin of the North China Craton and their tectonic implications. Precambr Res 220–221:65–79

Wang C-L, Zhang L-C, Lan C-Y, Dai Y-P (2014a) Petrology and geochemistry of the Wangjiazhuang banded iron formation and associated supracrustal rocks from the Wutai greenstone belt in the North China Craton: implications for their origin and tectonic setting. Precambr Res 255:603–626

Wang C-Q, Cui W-Y, Kröener A, Nemchin AA (2000) Zircon isotopic ages from magnetite quartzites of the Jianping metamorphic complex, western Liaoning Province. Chin Sci Bull 45:547–551

Wang E-D, Xia J-M, Fu J-F, Jia S-S, Men Y-K (2014b) Formation mechanism of Gongchangling high-grade magnetite deposit hosted in Archean BIF, Anshan-Benxi area, Northeastern China. Ore Geol Rev 57:308–321

Wang G-D, Wang H, Chen H-X, Lu J-S, Xiao L-L, Wu C-M (2012b) U-Pb dating of zircons from metamorphic rocks of the Taihua metamorphic complex, Mt. Huashan, southern margin of the Tans-North China Orogen. Acta Geol Sinica 86:1541–1551 (in Chinese with English abstract)

Wang H-L, Chen L, Sun Y, Liu X-M, Xu X-Y, Chen J-L, Zhang H, Diwu C-R (2007) 4.1 Ga xenocrystal zircon from Ordovician volcanic rocks in western part of North Qinling Orogenic Belt. Chin Sci Bull 52:3002–3010

Wang J, Kusky T, Polat A, Wang L, Deng H, Wang S (2013a) A late Archean tectonic mélange in the Central Orogenic Belt, North China Craton. Tectonophysics 608:929–946

Wang L-G, Qiu Y-M, McNaughton NJ, Groves DI, Luo Z-K, Huang J-Z, Miao L-C, Liu Y-K (1998) Constraints on crustal evolution and gold metallogeny in the Northwestern Jiaodong Peninsula, China, from SHRIMP U-Pb zircon studies of granitoids. Ore Geol Rev 13:275–291

Wang L-M, Yan T-M (1992) The Archaean tonalites in Qixia area, Shandong. Shandong Geol 8:80–87 (in Chinese with English abstract)

Wang Q-Y, Zheng J-P, Pan Y-M, Dong Y-J, Liao F-X, Zhang Y, Zhang L, Zhao G, Tu Z-B (2014c) Archean crustal evolution in the southeastern North China Craton: new data from the Huoqiu Complex. Precambr Res 255:294–315

Wang R-M, Wan Y-S, Cheng S-H, Feng Y-G (2009a) Modern-style subduction processes in the Archean: evidence from the Shangyi Complex in North China Craton. Acta Geol Sinica 83:535–543

Wang W, Yang E-X, Wang S-J, Du L-L, Xie H-Q, Dong C-Y, Wan Y-S (2009b) Petrography of Archean metamorphic pillow basalt in Taishan Rock Group, western Shandong, and SHRIMP U-Pb dating of zircons from intruding trondhjemite. Geol Rev 5:737–744 (in Chinese with English abstract)

Wang W, Wang S-J, Liu D-Y, Li P-Y, Dong C-Y, Xie H-Q, Ma M-Z, Wan Y-S (2010a) Formation age of the Neoarchaean Jining Group (banded iron formation) in the western Shandong Province: constraints from SHRIMP zircon U-Pb dating. Acta Petrologica Sinica 26:1171–1174 (in Chinese with English abstract)

Wang W, Liu S-W, Bai X, Yang P-T, Li Q-G, Zhang L-F (2011) Geochemistry and zircon U-Pb-Hf isotopic systematics of the Neoarchean Yixian-Fuxin greenstone belt, northern margin of the North China Craton: implications for petrogenesis and tectonic setting. Gondwana Res 20:64–81

Wang W, Liu S-W, Santosh M, Bai X, Li Q-G, Yang P-T, Guo R-R (2013b) Zircon U-Pb-Hf isotopes and whole-rock geochemistry of granitoid gneisses in the Jianping gneissic terrane, Western Liaoning Province: constraints on the Neoarchean crustal evolution of the North China Craton. Precambr Res 224:184–221

Wang W, Zhai M-G, Li T-S, Santosh M, Zhao L, Wang H-Z (2014d) Archean-Paleoproterozoic crustal evolution in the eastern North China Craton: zircon U-Th-Pb and Lu-Hf evidence from the Jiaobei terrane. Precambr Res 241:146–160

Wang W, Zhai M-G, Tao Y-B, Santosh M, Lü B, Zhao L, Wang S-J (2014e) Late Neoarchean crustal evolution of the eastern North China Craton: a study on the provenance and metamorphism of paragneiss from the Western Shandong Province. Precambr Res 255:583–602

Wang Z-H, Wilde SA, Wan J-L (2010b) Tectonic setting and significance of 2.3-2.1 Ga magmatic events in the Trans-North China Orogen: new constraints from the Yanmenguan mafic-ultramafic intrusion in the Hengshan-Wutai-Fuping area. Precambr Res 178:27–42

Wang Z-J, Shen Q-H, Wan Y-S (2004) SHRIMP U-Pb zircon geochronology of the Shipaihe "metadiorite mass" from Dengfeng County, Henan Province. Acta Geoscientica Sinica 25:295–298 (in Chinese with English abstract)

Warren RG, Ellis DJ (1996) Mantle underplating, granite tectonics, and metamorphic P-T-t paths. Geology 24:663–666

Wei C-J, Qian J-H, Zhou X-W (2014) Paleoproterozoic crustal evolution of the Hengshan-Wutai-Fuping region, North China Craton. Geosci Front 5:485–497

Wilde SA, Dorsett-Bain HL, Jinglan L (1997) The identication of a Late Pan-African granulite facies event in northeastern China: SHRIMP U-Pb zircon dating of the Mashan Group at Liu Mao, Heilongjiang Province, China. In: Proceedings of the 30th international geological congress. VSP International Science Publishers, Amsterdam, pp 59–74

Wilde SA, Cawood PA, Wang K-Y, Nemchin AA, Zhao G-C (2004a) Determining Precambrian crustal evolution in China: a case-study from Wutaishan, Shanxi Province, demonstrating the application of precise SHRIMP U-Pb geochronology. J Lond Geol Soc 226:5–25

Wilde SA, Zhao G-C, Wang K-Y, Sun M (2004b) First SHRIMP U-Pb ages for Hutuo Group in Wutaishan: further evidence for Palaeoproterozoic amalgamation of North China Craton. Chin Sci Bull 49:83–90

Wilde SA, Cawood PA, Wang K-Y, Nemchin AA (2005) Granitoid evolution in the Late Archean Wutai Complex, North China Craton. J Asian Earth Sci 24:597–613

Wilde SA, Valley JW, Kita NT, Cavosie AJ, Liu D-Y (2008) SHRIMP U-Pb and CAMECA 1280 Oxygen isotope results from ancient detrital zircons in the Caozhuang Quartzite, Eastern Hebei, North China Craton: evidence for crustal reworking 3.8 Ga ago. Am J Sci 308:185–199

Wu F-Y, Yang J-H, Liu X-M, Li T-S, Xie L-W, Yang Y-H (2005a) Hf isotopes of the 3.8 Ga zircons in eastern Hebei Province, China: implications for early crustal evolution of the North China Craton. Chin Sci Bull 50:2473–2480

Wu F-Y, Zhao G-C, Wilde S-A, Sun D (2005b) Nd isotopic constraints on crustal formation in the North China Craton. J Asian Earth Sci 24:523–545

Wu F-Y, Zhang Y-B, Yang J-H, Xie L-W, Yang Y-H (2008) Zircon U-Pb and Hf isotopic constraints on the Early Archean crustal evolution in Anshan of the North China Craton. Precambr Res 167:339–362

Wu J-S, Geng Y-S, Xu H-F, Jin L-G, He S-Y, Sun S-W (1989) Metamorphic geology of the Fuping Group. Bull Inst Geol Chin Acad Geol Sci 19:1–213 (in Chinese with English abstract)

Wu J-S, Geng Y-S, Shen Q-H, Wan Y-S, Liu D-Y, Song B (1998) Archaean geology characteristics and tectonic evolution of China-Korea Paleo-continent. Geological Publishing House, Beijing., pp 1–212 (in Chinese)

Wu M-L, Zhao G-C, Sun M, Li S-Z, He Y-H, Bao Z-A (2013) Zircon U-Pb geochronology and Hf isotopes of major lithologies from the Yishui Terrane: Implications for the crustal evolution of the Eastern Block, North China Craton. Lithos 170–171:164–178

Wu M-L, Zhao G-C, Sun M, Li S-Z, Bao Z-A, Yuk TP, Eizenhöefer PR, He Y-H (2014) Zircon U-Pb geochronology and Hf isotopes of major lithologies from the Jiaodong Terrane: implications for the crustal evolution of the Eastern Block of the North China Craton. Lithos 190–191:71–84

Wyman DA (2013a) A critical assessment of Neoarchean “plume only” geodynamics: evidence from the Superior Province. Precambr Res 229:3–19

Wyman DA (2013b) A reply to “How many arcs can dance on the head of a plume?” by Jean Bédard, Precambrian Research, 2013. Precambr Res 229:198–202

Xiang P, Cui M-L, Wu H-Y, Zhang X-J, Zhang L-C (2012) Geological characteristics, ages of host rocks and its geological significance of the Zhoutaizi iron deposit in Luanping, Hebei Province. Acta Petrologica Sinica 28:3655–3669 (in Chinese with English abstract)

Xie S-W (2012) Zircon chronology and geochemical characteristics of Jiaolai basin and its basement. China University of Geosciences (Wuhan), Wuhan, pp 1–142

Xie H-Q, Wan Y-S, Wang S-J, Liu D-Y, Xie S-W, Liu S-J, Dong C-Y, Ma M-Z (2013) Geology and zircon dating of trondhjemitic gneiss and amphibolite in the Tangezhuang area, eastern Shandong. Acta Petrologica Sinica 29:619–629 (in Chinese with English abstract)

Xie S-W, Wang S-J, Xie H-Q, Liu S-J, Dong C-Y, Ma M-Z, Liu D-Y, Wan Y-S (2014a) SHRIMP U-Pb dating of detrital zircons from the Fenzishan Group in eastern Shandong, North China craton. Acta Petrologica Sinica 30:2989–2998 (in Chinese with English abstract)

Xie S-W, Xie H-Q, Wang S-J, Kröner A, Liu S-J, Zhou H-Y, Ma M-Z, Dong C-Y, Liu D-Y, Wan Y-S (2014b) Ca. 2.9 Ga granitoid magmatism in eastern Shandong, North China Craton: zircon dating, Hf-in-zircon isotopic analysis and whole-rock geochemistry. Precambr Res 255:538–562

Yang C-H, Du L-L, Ren L-D, Wan Y-S, Song H-X, Yuan Z-L, Wang S-Y (2009) SHRIMP U-Pb ages and stratigraphic comparison of Angou group, on the southern margin of North China Craton. Acta Petrologica Sinica 25:1853–1862 (in Chinese with English abstract)

Yang C-H, Du L-L, Ren L-D, Song H-X, Wan Y-S, Xie H-Q, Liu Z-X (2011) Petrogenesis and geodynamic setting of Jiandeng potassic granite at the end of the Neoarchean in Zanhuang Complex, North China Craton. Earth Sci Front 18:62–78 (in Chinese with English abstract)

Yang C-H, Du L-L, Ren L-D, Song H-X, Wan Y-S, Xie H-Q, Geng Y-S (2013a) Delineation of the ca. 2.7 Ga TTG gneisses in the Zanhuang Complex, North China Craton and its geological implications. J Asian Earth Sci 72:178–189

Yang J-H, Wu F-Y, Wilde SA, Zhao G-C (2008) Petrogenesis and geodynamics of Late Archean magmatism in eastern Hebei, eastern North China Craton: geochronological, geochemical and Nd-Hf isotopic evidence. Precambr Res 167:125–149

Yang X-Q, Li H-M, Xue C-J, Li L-X, Liu M-J, Chen J (2013b) Geochemical characteristics of two iron ores from the Waitoushan Iron deposit, Liaoning Province: constraints on ore-forming mechanism. Acta Geol Sinica 87:1580–1592 (in Chinese with English abstract)

Yin X-Y, Wan Y-S, Liu D-Y, Wilde SA, Zhou H-Y, Wu J-S (2006) Formation time of supracrustal rocks in the Tiejiashan granite in the Anshan area: evidence from detrital zircon SHRIMP dating. Acta Petrologica et Mineralogica 25:282–286

Yin X-Y, Zhou H-Y, Liu D-Y, Gao L-Z, Dong C-Y, Wan Y-S (2015) Ancient Material Records in the North China Craton: SHRIMP U-Pb Dating and LA-MC-ICPMS Hf analysis of zircons from Archean Metamorphic Rocks in the Jiaozou Area, Henan. Geol Rev 61:183–194 (in Chinese with English abstract)

Ying J-F, Zhang H-F, Tang Y-J (2011) Crust-mantle interaction in the central North China Craton during the Mesozoic: evidence from zircon U-Pb chronology, Hf isotope and geochemistry of syenitic-monzonitic intrusions from Shanxi province. Lithos 125:449–462

Zhai M-G, Bian A-G, Zhao T-P (2000) The amalgamation of the supercontinent of North China Craton at the end of Neo-Archaean and its breakup during late Palaeoproterozoic and Meso-Proterozoic. Sci China Ser D-Earth Sci 43:219–232

Zhai M-G, Guo J-H, Liu W-J (2005) Neoarchean to Paleoproterozoic continental evolution and tectonic history of the North China Craton: a review. J Asian Earth Sci 24:547–561

Zhai M-G, Peng P (2007) Paleoproterozoic events in the North China Craton. Acta Petrologica Sinica 23:2665–2682 (in Chinese with English abstract)

Zhai M-G (2010) Tectonic evolution and metallogenesis of North China Craton. Miner Deposits 29:24–36 (in Chinese with English abstract)

Zhai M-G, Santosh M (2011) The early Precambrian odyssey of the North China Craton: a synoptic overview. Gondwana Res 20:6–25

Zhang H-F (2012) Destruction of ancient lower crust through magma underplating beneath Jiaodong Peninsula, North China Craton: U-Pb and Hf isotopic evidence from granulite xenoliths. Gondwana Res 21:281–291

Zhang H-F (2014) Neoarchean recycling of ^{18}O-enriched supracrustal materials into the lower crust: zircon record from the North China Craton. Precambr Res 248:60–71

Zhang H-F, Zhai M-G, Santosh M, Diwu C-R, Li S-R (2011a) Geochronology and petrogenesis of Neoarchean potassic meta-granites from Huai'an Complex: Implications for the evolution of the North China Craton. Gondwana Res 20:82–105

Zhang H-F, Ying J-F, Santosh M, Zhao G-C (2012a) Episodic growth of Precambrian lower crust beneath the North China Craton: a synthesis. Precambr Res 222–223:255–264

Zhang H-F, Yang Y-H, Santosh M, Zhao X-M, Ying J-F, Xiao Y (2012b) Evolution of the Archean and Paleoproterozoic lower crust beneath the Trans-North China Orogen and the Western Block of the North China Craton. Gondwana Res 22:73–85

Zhang H-F, Ying J-F, Tang Y-J, Li X-H, Feng C, Santosh M (2012c) Phanerozoic reactivation of the Archean North China Craton through episodic magmatism: evidence from zircon U-Pb geochronology and Hf isotopes from the Liaodong Peninsula. Gondwana Res 19:446–459

Zhang H-F, Wang J-L, Zhou D-W, Yang Y-H, Zhang G-W, Santosh M, Yu H, Zhang J (2014a) Hadean to Neoarchean episodic crustal growth: Detrital zircon records in Paleoproterozoic quartzites from the southern North China Craton. Precambr Res 254:245–257

Zhang J, Zhao G-C, Sun M, Wilde SA, Li S-Z, Liu S-W (2006a) High-pressure mafic granulites in the Trans-North China Orogen: tectonic significance and age. Gondwana Res 9:349–362

Zhang J, Zhao G-C, Li S-Z, Sun M, Liu S-W, Wilde SA, Kröner A, Yin C-Q (2007) Deformation history of the Hengshan Complex: implications for the tectonic evolution of the Trans-North China Orogen. J Struct Geol 29:933–949

Zhang J, Zhao G-C, Li S-Z, Sun M, Wilde SA, Liu S-W, Yin C-Q (2009) Deformational history of the Fuping Complex and new U-Th-Pb geochronological constraints: implications for the tectonic evolution of the Trans-North China Orogen. J Struct Geol 31:177–193

Zhang J, Zhang H-F, Lu X-X (2013) Zircon U-Pb age and Lu-Hf isotope constraints on Precambrian evolution of continental crust in the Songshan area, the south-central North China Craton. Precambr Res 226:1–20

Zhang J-J, Zhao L, Liu S-W (2006b) Structures of syn-deformational granites in the Longquanguan shear zone and their monazite electronic microprobe dating. Acta Geol Sinica 80:864–874 (in Chinese with English abstract)

Zhang L-C, Zhai M-G, Zhang X-J, Xiang P, Dai Y-P, Wang C-L, Franco P (2012d) Formation age and tectonic setting of the Shirengou Neoarchean Banded iron deposit in eastern Hebei Province: constrains from geochemistry and SIMS zircon U-Pb dating. Precambr Res 222–223:325–388

Zhang L-C, Zhai M-G, Wan Y-S, Guo J-H, Dai Y-P, Wang C-L, Liu L (2012e) Study of the Precambrian BIF-iron deposits in the North China Craton: progreese and problems. Acta Petrologica Sinica 28:3431–3445 (in Chinese with English abstract)

Zhang Q-S, Yang Z-S, Wang Y-J (1988) Early crust and mineral deposits of Liaodong Peninsula. China Geological Publishing House, Beijing, pp 1–451 (in Chinese with English abstract)

Zhang R-Y, Zhang C-L, Diwu C-R, Sun Y (2012f) Zircon U-Pb geochronology, geochemistry and its geological implications for the Precambrian granitoids in Zhongtiao Mountain, Shanxi Province. Acta Petrologica Sinica 28:3559–3573 (in Chinese with English abstract)

Zhang X-J, Zhang L-C, Xiang P, Wan B, Francon P (2011) Zircon U-Pb age, Hf isotopes and geochemistry of Shuichang Algoma-type banded iron-formation, North China Craton on the ore-forming age and techonic setting. Gondwana Res 20:137–148

Zhang X-H, Yuan L-L, Xue F-H, Zhai M-G (2014b) Neoarchean metagabbro and charnockite in the Yinshan block, western North China Craton: petrogenesis and tectonic implications. Precambr Res 255:563–582

Zhang Y-Q, Wang T, Jia H-Y, Zhang Z-X (2003) U-Pb ages of zircons from the Xiulanbulang hypersthene-plagioclase granulite in the north Daqing Mountains, Central Inner Mongolia. Geol China 30:394–399 (in Chinese with English abstract)

Zhang Y-Q, Liu Y-J (2004) Zircon U-Pb age of the quartz diorite in North Daqing Mountains, central Inner Mongolia. Geol Miner Resour South China 4:22–27 (in Chinese with English abstract)

Zhao G-C (2014) Precambrian evolution of the North China Craton. Elsevier, Amsterdam, pp 1–194

Zhao G-C, Wilde SA, Cawood PA, Lu L-Z (1998) Thermal evolution of Archean basement rocks from the eastern part of the North China carton and its bearing on tectonic setting. Int Geol Rev 40:706–721

Zhao G-C, Wilde SA, Cawood PA, Lu L-Z (1999) Thermal evolution of two types of mafic granulites from the North China craton: implications for both mantle plume and collisional tectonics. Geol Mag 136:223–240

Zhao G-C, Wilde SA, Cawood PA, Sun M (2001) Archean blocks and their boundaries in the North China Craton: lithological, geochemical, structural and P-T path constrains and tectonic evolution. Precambr Res 107:45–73

Zhao G-C, Wilde SA, Cawood PA, Sun M (2002) SHRIMP U-Pb zircon ages of the Fuping complex: implications for Late Archean to Paleoproterozoic accretion and assembly of the North China Craton. Am J Sci 302:191–226

Zhao G-C, Sun M, Wilde SA (2003) Correlations between the Eastern Block of the North China Craton and the South Indian Block of the Indian Shield: an Archaean to Palaeoproterozoic link. Precambr Res 122:201–233

Zhao G-C, Sun M, Wilde SA, Li S-Z (2005) Late Archean to Paleoproterozoic evolution of the North China Craton: key issues revisited. Precambr Res 136:177–202

Zhao G-C, Wilde SA, Sun M, Guo J-H, Kröner A, Li S-Z, Li X-P, Zhang J (2008a) SHRIMP U-Pb zircon geochronology of the Huai'an Complex: constraints on late Archean to Paleoproterozoic magmatic and metamorphic events in the Trans-North China Orogen. Am J Sci 308:270–303

Zhao G-C, Zhai M-G (2013) Lithotectonic elements of Precambrian basement in the North China Craton: review and tectonic implications. Gondwana Res 23:1207–1240

Zhao R-F, Guo J-H, Peng P, Liu F (2011) 2.1 Ga crustal remelting event in Hengshan Complex: evidence fom U-Pb dating and Hf-Nd isotopic study on potassic granites. Acta Petrologica Sinica 27:1607–1623 (in Chinese with English abstract)

Zhao, Z.-P., et al., 1993. Precambrian crustal evolution of the Sino-Korean Paraplatform. Beijing: Science Press: 1–444 (in Chinese)

Zhao Z-R, Song H-X, Shen Q-H, Song B (2008b) Geological and geochemical char acter istics and SHRIMP U-Pb zircon dating of the Yinglingshan granite and its xenoliths in Yishui County, Shandong, China. Geol Bull China 27:1551–1558 (in Chinese with English abstract)

Zhao Z-R, Song H-X, Shen Q-H, Song B (2009) The petrogeochemiscal characters and SHRIMP U-Pb zircon ages of the meta-mafic rocks from the Yushui Complex, in Yishui County, Shandong Province. Geol Rev 55:286–299 (in Chinese with English abstract)

Zheng J-P, Griffin WL, O'Reilly SY, Lu F-X, Wang C-Y, Zhang M, Wang F-Z, Li H-M (2004a) 3.6 Ga lower crust in central China: new evidence on the assembly of the NCC. Geology 32:229–232

Zheng J-P, Griffin WL, O'Reilly SY, Lu F-X, Yu C-M, Zhang M, Li H-M (2004b) U-Pb and Hf-isotope analysis of zircons in mafic xenoliths from Fuxian kimberlites: evolution of the lower crust beneath the North China craton. Contrib Miner Petrol 148:79–103

Zheng J-P, Lu F-X, Yu S-M, Tang H-Y (2004c) An in situ Zircon Hf isotopic U-Pb age and trace element study of banded granulite xenolith from Hannuoba basalt: tracking the early evolution of the lower crust in the North China Craton. Chin Sci Bull 49:3277–3285

Zheng J-P, Griffin WL, O'Reilly SY, Hu B-Q, Zhang M, Tang H-Y, Su Y-P, Zhang Z-H, Pearson N, Wang F-Z, Lu F-X (2008) Continental collision and accretion recorded in the deep lithosphere of central China. Earth Planet Sci Lett 269:496–506

Zheng J-P, Griffin WL, Ma Q, O'Reilly SY, Xiong Q, Tang H-Y, Zhao J-H, Yu C-M, Su Y-P (2012) Accretion and reworking beneath the North China Craton. Lithos 149:61–78

Zhou H-Y, Liu D-Y, Wan Y-S, Wilde SA, Wu J-S (2007) 3.3 Ga magmatic events in the Anshan area: new SHRIMP age and geochemical constraints. Acta Petrologica et Mineralogica 26:123–129 (in Chinese with English abstract)

Zhou H-Y, Liu D-Y, Wan Y-S, Dong C-Y (2009a) 3.3-3.1 Ga magmatism in the Dongshan Complex, Anshan: evidence from SHRIMP U-Pb zircon dating. Geol Bull China 27:2122–2126 (in Chinese with English abstract)

Zhou J-B, Wilde SA, Zhao G-C, Zheng C-Q, Jin W, Zhang X-Z, Cheng H (2008) SHRIMP U-Pb zircon dating of the Neoproterozoic Penglai Group and Archean gneisses from the Jiaobei Terrane, North China, and their tectonic implications. Precambr Res 160:323–340

Zhou Y-Y, Zhao T-P, Xue L-W, Wang S-Y, Gao J-F (2009b) Petrological, geochemical and chronological constraints for the origin and geological significance of Neoarchean TTG gneiss in the Songshan area, North China Craton. Acta Petrologica Sinica 25:331–347 (in Chinese with English abstract)

Zhou Y-Y, Zhao T-P, Wang C-Y, Hu G-H (2011) Geochronology and geochemistry of 2.5 to 2.4 Ga granitic plutons from the southern margin of the North China Craton: implications for a tectonic transition from arc to post-collisional setting. Gondwana Res 20:171–183

Zhou Y-Y, Zhao T-P, Zhai M-G, Gao J-F, Sun Q-Y (2014) Petrogenesis of the Archean tonalite-trondhjemite-granodiorite (TTG) and granites in the Lushan area, southern margin of

the North China Craton: implication for crustal accretion and transformation. Precambr Res 255:514–537

Zhu M-T, Zhang L-C, Dai Y-P, Wang C-L (2015) In situ zircon U-Pb dating and O isotopes of the Neoarchean Hongtoushan VMS Cu-Zn deposit in the North China Craton: implication for the ore genesis. Ore Geol Rev 67:354–367

Zhu X-Y, Zhai M-G, Chen F-K, Lü B, Wang W, Peng P, Hu B (2013) ∼2. 7 Gacrustal growth in the North China Craton: evidence from zircon U-Pb ages and Hf isotopes of the Sushui Complex in the Zhongtiao terrane. J Geol 121:239–254

http://www.springer.com/978-3-662-47884-4

Precambrian Geology of China

Zhai, M. (Ed.)
2015, VIII, 390 p. 156 illus., 119 illus. in color., Hardcover
ISBN: 978-3-662-47884-4

[American Journal of Science, Vol. 315, September, 2015, P. 620–670, DOI 10.2475/07.2015.02]

WIDESPREAD LATE NEOARCHEAN REWORKING OF MESO- TO PALEOARCHEAN CONTINENTAL CRUST IN THE ANSHAN-BENXI AREA, NORTH CHINA CRATON, AS DOCUMENTED BY U-Pb-Nd-Hf-O ISOTOPES

YUSHENG WAN*,**,†, MINGZHU MA*, CHUNYAN DONG*, HANGQIANG XIE*, SHIWEN XIE*, PENG REN*, and DUNYI LIU*

ABSTRACT. We present an integrated study of zircon U-Pb dating and O-Hf isotopic analyses combined with whole-rock geochemistry and Nd isotopic systematics on widespread late Neoarchean syenogranites (Qidashan Pluton) and other granitoids (granodiorite, quartz monzonite, monzogranite) in the Anshan-Benxi area, eastern North China Craton. All these rocks were emplaced at *ca.* 2.5 Ga according to SHRIMP zircon U-Pb dating and other indirect methods. The syenogranites are characterized by high SiO_2 and K_2O/Na_2O and low CaO, FeOt, MgO, TiO_2 and P_2O_5. However, they differ in trace element and REE compositions and can be roughly subdivided into two types. Type 1 syenogranite has strongly negative Eu anomalies and Ba depletion, with large variations of LREE to HREE differentiation; type 2 syenogranite has no negative Eu anomaly and Ba depletion. Other granitoids are also rich in K_2O and show similar trace element and REE compositional features as the type 2 syenogranite. Most syenogranite samples have whole-rock $\varepsilon_{Nd(t)}$ values of –10.5 to –2.7 and $t_{DM(Nd)}$ ages of 2.96 to 3.90 Ga, whereas the other granitoids have $\varepsilon_{Nd(t)}$ values of –5.2 to –2.2 and $t_{DM(Nd)}$ ages of 2.95 to 3.19 Ga. Magmatic zircon from the syenogranites has $\varepsilon_{Hf(t)}$ values and Hf crustal model ages ranging mainly from –11.0 to +4.4 and 2.70 to 3.46 Ga, respectively; those from other granitoids have $\varepsilon_{Hf(t)}$ values and Hf crustal model ages of –16.0 to +2.4 and 2.81 to 3.72 Ga, respectively. All these rocks contain Meso- to Paleoarchean xenocrystic zircon grains with $\varepsilon_{Hf(t)}$ values and Hf crustal model ages ranging from –14.3 to +8.3 and 2.79 to 3.93 Ga, respectively. Decoupling of whole-rock Nd and Hf-in-zircon isotopes occurs in some samples. Most low-U magmatic zircon (U<200 ppm) from all granitoids has $\delta^{18}O$ values in the range of +4 to +7.2 permil, whereas high-U magmatic zircon (U≥200 ppm) shows a larger variation with the lowest $\delta^{18}O$ value being 1.6. The xenocrystic zircon grains have $\delta^{18}O$ values in the normal range of Archean magmatic zircon. Combined with previous studies, we conclude that the 2.5 Ga granitoids formed by recycling of mature, old continental crust, including metasedimentary sources, probably in an extensional tectonic environment.

Keywords: Neoarchean, syenogranite, Anshan-Benxi, zircon dating, Nd-Hf-O isotopes

INTRODUCTION

Archean granitoids wordwide consist mainly of tonalite-trondhjemite-granodiorite (TTG) (Moyen, 2011; Moyen and Martin, 2012; LaFlamme and others, 2014). Large bodies of pre-Neoarchean potassic granites are relatively rare and occur only in a few areas such as the 2.9 to 3.0 Ga Tiejiashan granite in the Anshan-Benxi area, eastern North China Craton (NCC) (Wu and others, 1998; Wan and others, 1998, 2007), the 3.1 Ga Mpuluzi-Piggs Peak Batholith in eastern South Africa and Swaziland, eastern Kaapvaal Craton (Kamo and Davis, 1994), and the 3.3 Ga Carbana-Mondana granites in the East Pilbara Craton, western Australia (Bagas and others, 2002). Early Neo-

* Beijing SHRIMP Center, Institute of Geology, Chinese Academy of Geological Sciences, Beijing 100037, China
** State Key Laboratory for Continental Tectonics and Dynamics, Institute of Geology, Chinese Academy of Geological Sciences, Beijing 100037, China
† Corresponding author: wanyusheng@bjshrimp.cn

archean (2.6–2.7 Ga) potassic granites also occur locally such as in southeastern Greenland, Wyoming, the Superior Province and southern India (Nutman and Rosing, 1994; Frost and others, 1998; Whalen and others, 2004; Jayananda and others, 2006). It is only until the late Neoarchean that potassic granites became more voluminous and widespread such as in the NCC, Northern Australia, southern India, southwestern Greenland, the Kaapvaal craton, and Antarctica (Moyen and others, 2003; Nutman and others, 2007; Condie and others, 2009; Drüppel and others, 2009; Dey and others, 2012; Wan and others, 2012a). It is evident that potassic granites are more extensively developed after the Archean, and their occurrence is considered to reflect increased maturity of the continental crust and may be related to the process of craton stabilization (Frost and others, 1998; Moyen and others, 2003; Drüppel and others, 2009; Wan and others, 2012a).

The NCC is characterized by widespread late Neoarchean tectono-thermal events producing a variety of granitoids (Wan and others, 2011a; Zhai and Santosh, 2011; Zhao and Cawood, 2012; Zhao and other, 2012; Zhao and Zhai, 2013), but ≥2.6 Ga rocks and zircon grains occur widely, with >3.8 Ga rocks and zircon grains having been identified locally (Liu and others, 1992, 2007, 2008; Song and others, 1996; Wan and others, 2009a, 2012b, 2014a, 2014b, 2015; Wu and others, 2014a, 2014b). Based on published geological and geochronological data, Wan and others (2015) identified three ancient terranes (>2.6 Ga), namely the Eastern Ancient Terrane, Southern Ancient Terrane and Central Ancient Terrane (fig. 1). There may also be an ancient terrane in the Yinshan Block, northwestern NCC. These terranes define a foundation for the late Neoarchean tectonic evolution of the NCC.

The Anshan-Benxi area is located in the northern part of the Eastern Ancient Terrane (fig. 1), where the late Neoarchean Qidashan (or Qidashan-Gongchangling) Pluton has extensive outcrops with a total area of >2000 km^2 (fig. 2). It is composed mainly of syenogranite with some K-rich granite that according to divisions by Wan and others (2012a) are (1) syenogranite, a rock high in K_2O (commonly >4 %) and with a K_2O/Na_2O ratio of >1.3; and (2) K-rich granite, a rock high in K_2O but not necessarily high in K_2O/Na_2O. It is the largest late Neoarchean syenogranite pluton in the NCC. In order to reveal the petrogenesis of these rocks and to provide evidence for widespread Meso- to Paleoarchean components in the Eastern Ancient Terrane, we carried out an integrated study of U-Pb zircon dating and O-Hf isotopic analysis, combined with whole-rock chemistry and Nd isotopic systematics on the Qidashan Pluton and other late Neoarchean granitoids (granodiorite, quartz monzonite, monzogranite) in the area.

GEOLOGICAL BACKGROUND

In the western area of Anshan-Benxi, near the city of Anshan (fig. 2), three 3.0 to 3.8 Ga predominantly granitoid complexes (Baijiafen, Dongshan and Shengousi) as well as 2.5 to 3.3 Ga intrusive rocks have been identified (Liu and others, 1992, 2007, 2008; Wan, 1993; Song and others, 1996; Wu and others, 1998, 2008; Wan and others, 1998, 2002, 2005, 2007, 2012b). These three complexes are composed mainly of >3.3 Ga trondhjemitic rocks with low ΣREE contents and low $(La/Yb)_n$ ratios, besides minor 3.8 Ga meta-quartz diorites and 3.3 Ga meta-gabbroic rocks. The 2.5 to 3.3 Ga granitoids are voluminous and extensive, including the 2.5 Ga Qidashan (syenogranite) Pluton, 3.0 Ga Dong'anshan (granite) Pluton, 2.9 to 3.0 Ga Tiejiashan (K-rich granite) Pluton, 3.1 Ga Lishan (trondhjemite) Pluton and the Chentaigou (granite) Pluton.

The Qidashan Pluton occurs widely in the Anshan-Benxi area (fig. 2). It appears reddish or gray when fresh and yellow-reddish when weathered and commonly is massive, unfoliated and weakly gneissic in appearance (figs. 3A–3D). In previous studies, identification of the rocks of the Qidashan Pluton was mainly based on field

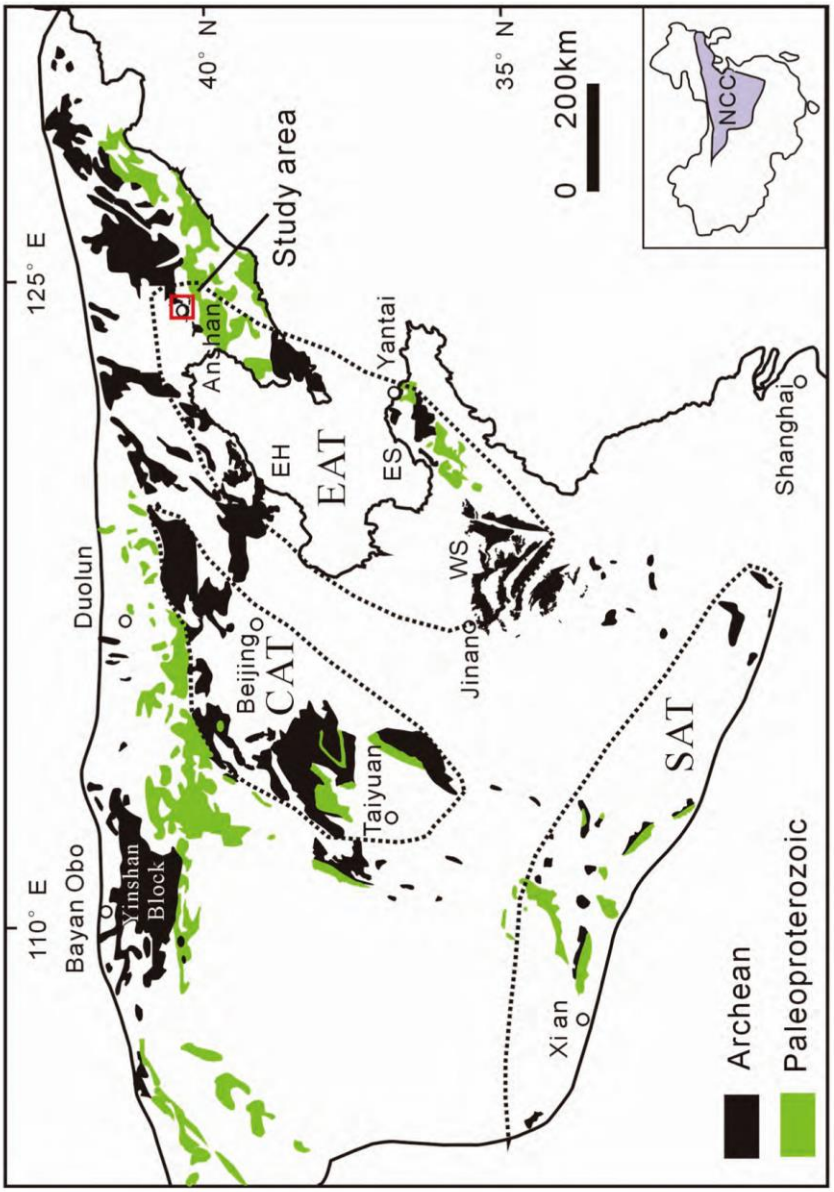

Fig. 1. Distribution of ancient (>2.6 Ga) terranes in the North China Craton (Wan and others, 2015). EH: eastern Hebei; ES: eastern Shandong; WS: western Shandong; EAT: Eastern Ancient Terrane; SAT: Southern Ancient Terrane; CAT: Central Ancient Terrane.

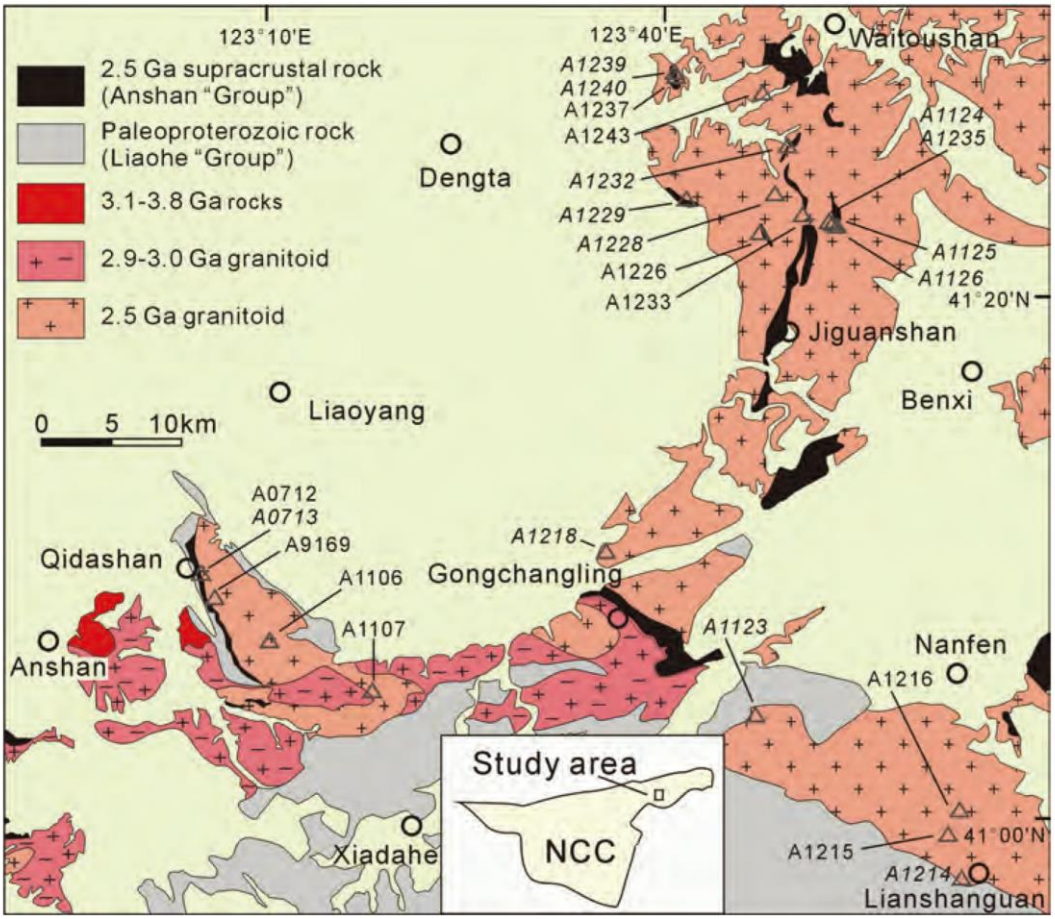

Fig. 2. Geological map of the Anshan-Benxi area, North China Craton, modified after LBGMRE (1975a, 1975b, 1976), Wan (1993) and Wan and others (2012a). Also shown are sample locations of this study, with SHRIMP zircon ages samples in italic numbers.

relationships and limited chemical data from the Anshan area and environs. SHRIMP U-Pb zircon dating was performed on only one sample (A0713 in fig. 2, see Wan and others, 2012a). The 2.9 to 3.0 Ga Tiejiashan Pluton is lower in K_2O/Na_2O ratios than the Qidashan Pluton and is classified as K-rich granite. Although the Tiejiashan Pluton is somewhat different in major element composition from the Qidashan Pluton, both are similar in their REE patterns and trace element composition, commonly showing strong negative Eu anomalies, depletion in Ba, Nb, Ti and P, and low $\varepsilon_{Nd(t)}$ values (Wan and others, 1998, 2002; Wu and others, 1998). Earlier studies suggested that the Tiejiashan Pluton occurs only in the Anshan area but new data indicate that it extends eastwards to Gongchangling (fig. 2) (Dong C. Y., unpublished data), where all granites were previously believed to belong to the Qidashan variety (Wan and others, 1998; Wu and others, 1998). Besides the widespread Qidashan Pluton there occur other types of granitoids such as granodiorite, quartz monzonite and monzogranite. These only occur locally and commonly distinctly show deformation with some exhibiting a layered structure (figs. 3E and 3F).

The 2.5 Ga Anshan "Group" (we place the word "group" in parentheses to show that the term was traditionally used to include supracrustal rocks and does not conform to modern stratigraphic terminology) occurs in a "sea" of Qidashan Pluton

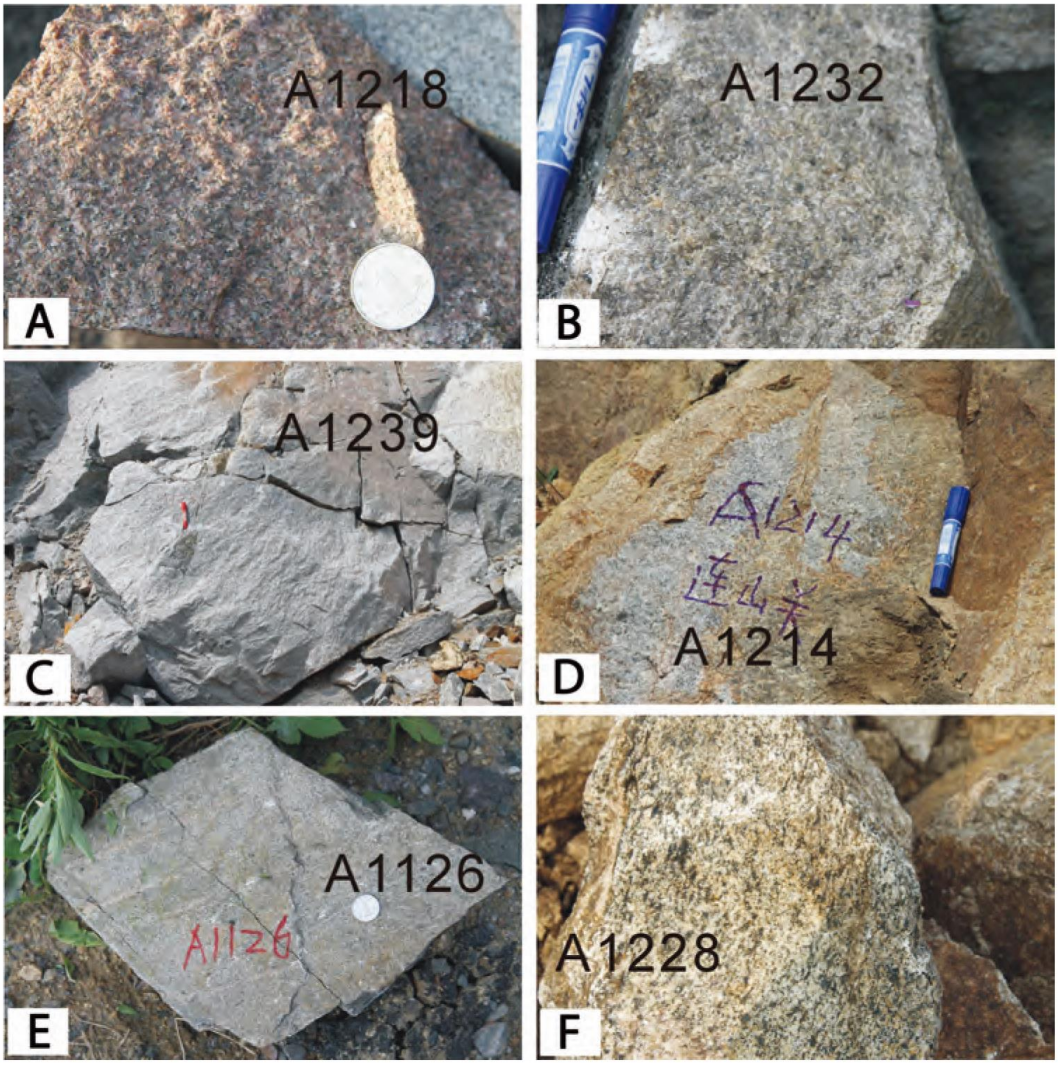

Fig. 3. Field photographs of late Neoarchean magmatic rocks in the Anshan-Benxi area, North China Craton. (A) Massive syenogranite north of Gongchangling (A1218); (B) gneissic syenogranite (A1232) south of Waitoushan; (C) weakly deformed syenogranite (A1239) southwest of Waitoushan; (D) weakly deformed syenogranite (A1214) Lianshanguan; (E) banded granodiorite (A1126) north of Jiguanshan; (F) gneissic monzogranite (A1228) north of Jiguanshan; (G) supracrustal rock of the Anshan "Group" showing anatexis, Waitoushan; (H) granitoid showing anatexis, Waitoushan. (I) 2.5 Ga syenogranite intruding the BIF-bearing Anshan "Group", Qidashan; (J) BIF-bearing Anshan "Group" intruded by a syenogranite vein derived from 2.5 Ga Qidahsan granite, south of Waitoushan.

plutonic rocks, with a total exposed area less than 10 percent (fig. 2). The Anshan "Group" mainly comprises amphibolites, fine-grained gneisses (leptynites), quartzites, phyllites and schists of volcano-sedimentary origin (Zhai and others, 1990; Wan, 1993). The Anshan "Group" underwent greenschist- to amphibolite-facies metamorphism in the southwest of Anshan-Benxi, but higher-grade metamorphism in the northeast of Anshan-Benxi, with anatexis occurring locally. In some outcrops leucosome-rich strips and lenses in anatectic supracrustal rocks and granitoids show weak deformation (figs. 3G and 3H). The occurrence of major BIF within the supracrustal succession makes the Anshan-Benxi area one of the most important iron deposit regions in China. The supracrustal rocks are cut by bodies of 2.5 Ga syenogranite (figs. 3I and 3J) that defines a youngest age limit for their deposition.

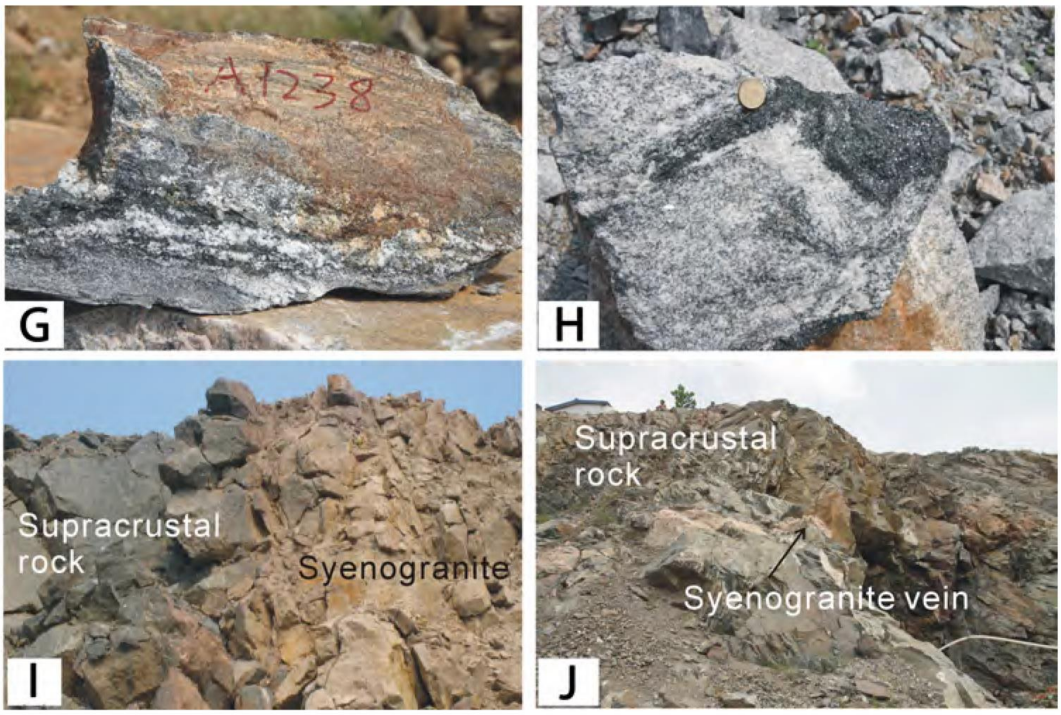

Fig. 3. (continued)

The *ca.* 2.18 Ga Liaohe "Group" crops out extensively in the southeastern part of the Anshan-Benxi area and is composed mainly of clastic sedimentary rocks, high-Mg carbonates, and basic to acid volcano-sedimentary rocks, which underwent greenschist- to amphibolite-facies metamorphism during late Paleoproterozoic time (1.83–1.95 Ga) (Luo and others, 2004, 2008; Wan and others, 2006; Li and Zhao, 2007; Liu and others, 2012). These rocks also occur in the Anshan area (fig. 2), suggesting that the Anshan-Benxi area was also affected by the late Paleoproterozoic tectono-thermal event. This is supported by hydrothermal zircon from a chlorite-garnet rock in Gongchangling (fig. 2) recording an age of *ca.* 1.85 Ga (Li and others, 2014).

The syenogranites of the Qidashan Pluton are composed mainly of quartz, K-feldspar and plagioclase, with some muscovite and biotite. Some syenogranites show none or only weak deformation and preserve original magmatic textures (fig. 4A), whereas others display foliation defined by oriented quartz, muscovite and biotite aggregates (figs. 4B, 4C and 4D). K-feldspar is mainly microcline with some orthoclase (figs. 4A–4D). Some K-feldspar occurs as patches in altered plagioclase (fig. 4E) or as phenocrysts containing euhedral or subhedral plagioclase grains (figs. 4D and 4F). Plagioclase commonly shows polysynthetic twinning and is often altered to epidote and sericite (figs. 4A–4D). Quartz shows undulose extinction or/and occurs as oriented aggregates and also occurs as veinlets cutting feldspar grains (fig. 4G). Biotite and muscovite flakes are scattered between quartz and feldspar, and some form oriented aggregates (figs. 4C and 4D). Reddish-brown biotite flakes with needle-shaped titanite inclusions occur in some samples (fig. 4H) that are different from the yellow-green magmatic biotite in most samples. These are interpreted as residual minerals following anatexis (for example, Wan and others, 2009b). The petrographic features indicate that (1) the syenogranites seem to have formed at variable but relatively low temperatures; (2) at least some syenogranites contain residual minerals inherited from their source region; (3) the syenogranites are variably deformed.

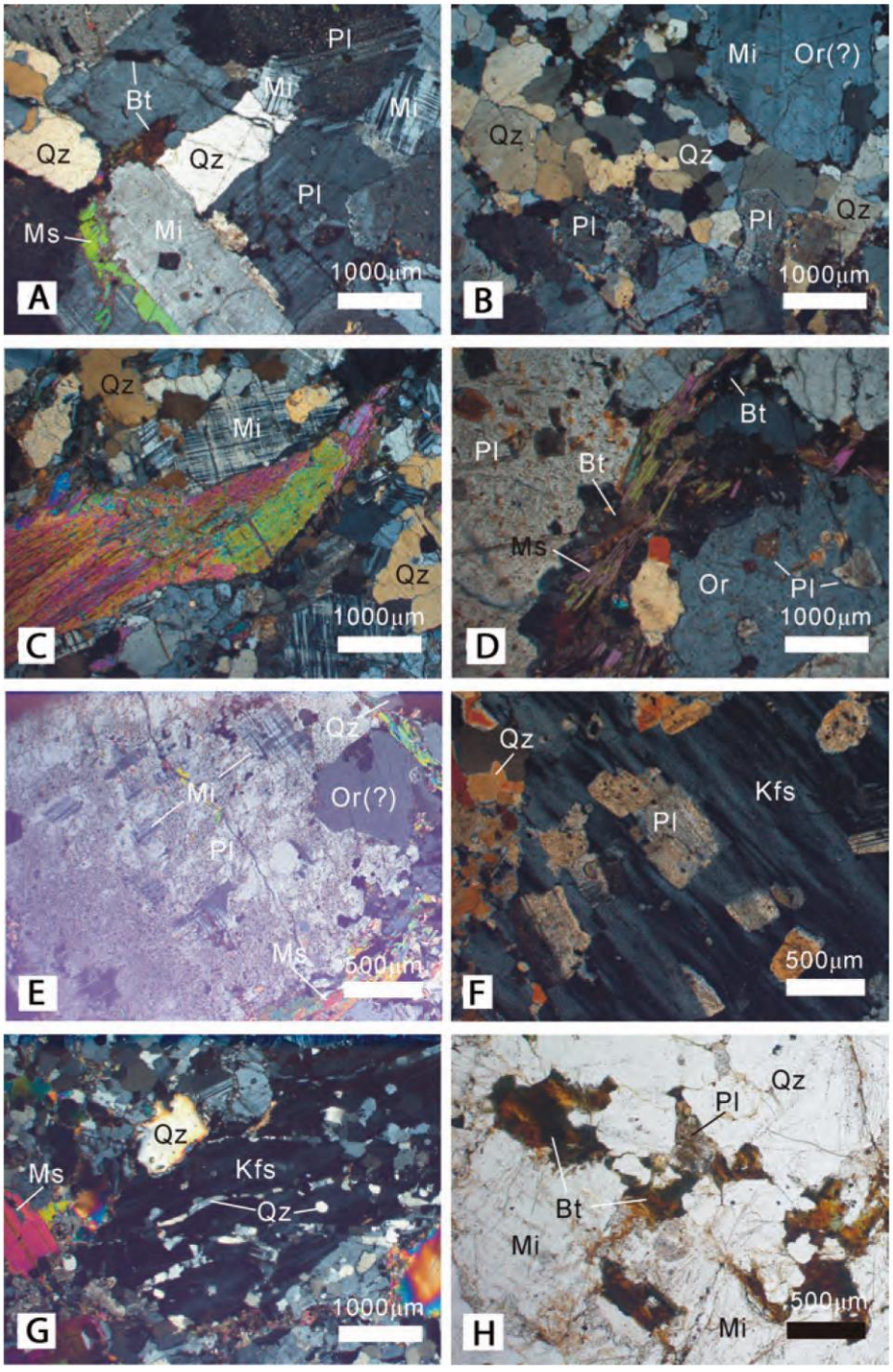

Fig. 4. Photographs of late Neoarchean magmatic rocks in the Anshan-Benxi area, North China Craton. (A) Massive syenogranite (A1218): all minerals show weak deformation; (B) gneissic syenogranite (A1107): quartz grains occur as aggregates, a K-feldspar phenocryst shows a Carlsbad twin with the left and right portions being microcline and orthoclase, respectively; (C) gneissic syenogranite (A1233): muscovite flakes show deformation; (D) gneissic syenogranite (A1216): biotite and muscovite occur as aggregates; (E) gneissic syenogranite (A0712): microcline occurs as patchs in altereted plagioclase; (F) gneissic syenogranite (A1123): a K-feldspar phenocryst contains euhedral plagioclase; (G) gneissic syenogranite (A0713): quartz veinlets cut K-feldspar phenocryst and other minerals; (H) gneissic syenogranite (A1229) containing reddish-brown biotite flakes with needle-shaped titanite inclusions. Pl: Plagioclase; Kfs: K-feldspar; Mi: Microcline; Or: Orthoclase; Bt: Biotite; Ms: Muscovite; Qz: Quartz.

The gneissic granodiorites are composed of plagioclase, quartz, K-feldspar and minor biotite. Plagioclase commonly shows polysynthetic twinning and is frequently altered to epidote and sericite. K-feldspar occurs as microcline and orthoclase. Foliation is indicated by oriented quartz aggregates. The gneissic quartz monzonite mainly consists of plagioclase, K-feldspar and quartz. Almost all plagioclase is sericiticized. K-feldsapr is mainly microcline with some containing plagioclase stripes. Quartz shows undulose extinction and is locally oriented as aggregates. The gneissic monzogranite is similar to the deformed syenogranite in many aspects but contains less K-feldspar and quartz.

ZIRCON U-Pb DATING

Sample locations are shown in figure 2, and SHRIMP analytical data are listed in table 1, in which Th and U contents and Th/U ratios are given, so they are listed only when necessary in the following text.

Massive Syenogranite (A1218)

The magmatic zircon grains are stubby or elongate in shape and commonly show blurred oscillatory zoning in cathodoluminescence (CL) images (grains 3, 8 and 10 in fig. 5A). Some zircons have cores with narrow magmatic rims showing recrystallization (grains 1 and 6 in fig. 5A). Twelve analyses were made on 12 zircon grains. The zircon cores with $^{207}Pb/^{206}Pb$ ages >3.0 Ga (4 analyses) (fig. 6A), are likely to be xenocrystic in origin (inherited or captured) because the syenogranite is homogeneous and massive. Analysis 4.1X has a high Th content (4079 ppm) and Th/U ratio (4.59), probably due to the analytical spot being on a Th-rich mineral inclusion. No precise age could be obtained for the magmatic zircon because of strong lead loss shown by all analyses (fig. 6A) due to high U contents (8 analyses, 875–11556 ppm). The intrusive age of the syenogranite is estimated to be *ca.* 2500 Ma, in line with the other syenogranites in the Anshan-Benxi area as shown below.

Gneissic Syenogranite (A1123)

The magmatic zircon is stubby and prismatic in habit and shows oscillatory zoning in CL images (fig. 5B). Eight grains were analyzed, and all except spot 4.1MA, plot indistinguishable from concordia, yielding a weighted mean $^{207}Pb/^{206}Pb$ age of 2512 ± 29 Ma (MSWD = 0.65) (fig. 6B) that is interpreted to reflect the time of intrusion of the host syenogranite. One xenocrystic zircon shows an irregular shape (grain 7 in fig. 5B) and has a near-concordant age of 3452 Ma (7.1X in fig. 6B).

Weakly Deformed Syenogranite (A1214)

The magmatic zircon is stubby or elongate in shape and shows oscillatory zoning with narrow light or gray rims in CL images (fig. 5C). Fourteen analyses show variable lead loss with 5 analyses on or near concordia providing a weighted mean $^{207}Pb/^{206}Pb$ age of 2489 ± 20 Ma (MSWD = 1.04) (fig. 6C). This is considered to be the formation age of the syenogranite.

Gneissic Syenogranite (A1125)

The zircon grains are of stubby or elongate habit and show oscillatory zoning in CL images, commonly with strong recrystallization (fig. 5D). It is notable that some grains have core-rim structures, and there are light CL domains between the core and rim and the rims are generally too narrow for SHRIMP dating. A total of sixteen analyses on the xenocrystic cores were performed, with some spots yielding low Th/U ratios (<0.1) due to recrystallization. The core analyses show strong lead loss (fig. 6D) and large variations in their $^{207}Pb/^{206}Pb$ ratios with the oldest minimum age being

TABLE 1

SHRIMP U-Pb data for zircon from late Neoarchean magmatic rocks in the Anshan-Benxi area, North China Craton

Spot	$^{206}Pb_c$ (%)	U (ppm)	Th (ppm)	Th/U	$^{206}Pb^*$ (ppm)	$^{207}Pb^*/^{206}Pb^*$	± %	$^{207}Pb^*/^{235}U$	± %	$^{206}Pb^*/^{238}U$	± %	err corr	$^{206}Pb/^{238}U$ Age (MA)		$^{207}Pb/^{206}Pb$ Age (MA)		Discordance (%)
Massive syenogranite (A1218)																	
1.1X	0.23	192	69	0.37	72	0.3200	3.40	19.28	3.6	0.4364	1.2	0.34	2335	± 24	3572	± 52	35
2.1MA	0.15	875	61	0.07	140	0.1042	0.69	2.68	1.3	0.1865	1.1	0.84	1102	± 11	1700	± 13	35
3.1MA	1.07	3738	3332	0.92	155	0.0823	1.20	0.54	1.6	0.0478	1.0	0.64	301	± 3	1253	± 24	76
4.1X	5.06	918	4079	4.59	68	0.2513	1.70	2.85	2.1	0.0821	1.2	0.57	509	± 6	3193	± 27	84
5.1X	0.31	310	160	0.54	96	0.2775	0.50	13.70	1.2	0.3580	1.1	0.92	1973	± 19	3349	± 8	41
6.1X	0.75	446	238	0.55	88	0.2463	4.00	7.71	4.2	0.2270	1.2	0.28	1319	± 14	3161	± 64	58
7.1MA	3.35	2359	451	0.20	114	0.1788	1.40	1.34	1.7	0.0544	1.1	0.62	341	± 4	2642	± 23	87
8.1MA	3.12	2977	1346	0.47	153	0.1223	1.90	0.98	2.2	0.0579	1.1	0.49	363	± 4	1990	± 34	82
10.1MA	4.57	11556	2172	0.19	242	0.0808	3.30	0.26	3.4	0.0232	1.1	0.31	148	± 2	1217	± 64	88
11.1MA	1.29	1939	1027	0.55	121	0.1049	1.20	1.04	1.6	0.0718	1.0	0.65	447	± 5	1712	± 22	74
12.1MA	1.42	1614	601	0.39	117	0.0847	2.10	0.97	2.3	0.0833	1.1	0.45	516	± 5	1308	± 40	61
13.1MA	2.20	1226	1047	0.88	117	0.1133	1.90	1.70	2.2	0.1085	1.1	0.49	664	± 7	1852	± 35	64
Gneissic syenogranite (A1123)																	
1.1MA	1.64	64	74	1.19	27	0.1663	5.00	10.99	5.5	0.4790	2.3	0.43	2524	± 49	2521	± 83	0
2.1MA	0.95	45	52	1.20	18	0.1715	3.10	11.11	4.0	0.4700	2.6	0.65	2483	± 55	2572	± 51	3
3.1MA	0.35	170	167	1.02	67	0.1628	1.70	10.24	2.2	0.4562	1.3	0.63	2423	± 27	2485	± 28	2
4.1MA	0.26	72	61	0.89	25	0.1708	2.40	9.37	3.2	0.3979	2.1	0.66	2159	± 38	2565	± 40	16
5.1MA	0.19	58	58	1.03	23	0.1667	2.40	10.74	3.3	0.4670	2.2	0.68	2471	± 46	2525	± 40	2
6.1MA	0.48	82	64	0.81	34	0.1653	2.00	11.06	2.7	0.4851	1.8	0.67	2550	± 38	2511	± 33	-2
7.1X	0.09	330	100	0.31	206	0.2965	0.88	29.59	1.4	0.7237	1.1	0.79	3510	± 30	3452	± 14	-2
7.2X	0.49	432	137	0.33	219	0.2896	0.85	23.40	1.2	0.5860	0.9	0.73	2973	± 22	3415	± 13	13
8.1MA	0.56	77	73	0.98	32	0.1613	2.80	10.58	3.5	0.4760	2.1	0.60	2510	± 44	2469	± 47	-2
9.1MA	0.73	87	76	0.90	36	0.1685	2.30	11.03	3.0	0.4747	1.9	0.64	2504	± 40	2543	± 39	2
Weakly deformed syenogranite (A1214)																	
1.1MA	1.07	94	73	0.80	40	0.1611	1.30	10.78	1.9	0.4854	1.3	0.71	2551	± 28	2468	± 22	-3
2.1MA	0.38	62	83	1.38	25	0.1611	1.20	10.53	2.1	0.4742	1.7	0.81	2502	± 36	2467	± 21	-1
3.1MA	0.20	187	73	0.40	56	0.1470	0.94	7.05	1.5	0.3476	1.2	0.79	1923	± 20	2312	± 16	17
4.1MA	0.49	44	45	1.06	18	0.1634	1.60	10.85	2.4	0.4819	1.8	0.75	2536	± 38	2491	± 26	-2
5.1MA	0.23	66	70	1.09	25	0.1628	2.50	9.95	2.9	0.4434	1.5	0.52	2366	± 30	2485	± 42	5
6.1MA	0.62	44	39	0.92	16	0.1637	2.10	9.24	4.2	0.4090	3.7	0.87	2211	± 69	2495	± 35	11
8.1MA	0.30	43	52	1.26	16	0.1676	1.50	10.16	2.3	0.4395	1.7	0.76	2348	± 34	2534	± 25	7
9.1MA	0.45	34	24	0.75	11	0.1524	1.90	8.20	3.5	0.3900	2.9	0.83	2123	± 52	2373	± 33	11

TABLE 1
(Continued)

Spot	$^{206}Pb_c$ (%)	U (ppm)	Th (ppm)	Th/U	$^{206}Pb^*$ (ppm)	$^{207}Pb^*/^{206}Pb^*$	± %	$^{207}Pb^*/^{235}U$	± %	$^{206}Pb^*/^{238}U$	± %	err corr	$^{206}Pb/^{238}U$ Age (MA)		$^{207}Pb/^{206}Pb$ Age (MA)		Discordance (%)
Weakly deformed syenogranite (A1214)																	
10.1MA	0.18	139	72	0.53	49	0.1574	0.85	8.98	1.5	0.4138	1.2	0.82	2232	± 23	2428	± 14	8
11.1MA	0.25	70	44	0.65	28	0.1649	1.10	10.76	1.8	0.4735	1.4	0.79	2499	± 29	2507	± 18	0
12.1MA	0.57	33	33	1.01	13	0.1664	1.80	10.66	2.5	0.4646	1.8	0.71	2460	± 37	2521	± 30	2
13.1MA	1.58	259	90	0.36	55	0.1248	2.90	4.16	3.1	0.2415	1.0	0.32	1395	± 12	2027	± 51	31
14.1MA	6.63	299	54	0.19	50	0.1133	4.90	2.81	5.0	0.1798	1.3	0.26	1066	± 13	1854	± 87	43
15.1MA	0.26	45	52	1.18	19	0.1635	1.40	10.74	2.0	0.4764	1.4	0.73	2512	± 30	2492	± 23	-1
Gneissic syenogranite (A1125)																	
1.1X	3.71	1368	449	0.34	238	0.2024	2.40	5.45	2.6	0.1953	1.0	0.38	1150	± 10	2846	± 39	60
2.1X	1.08	198	219	1.14	95	0.2932	1.20	22.29	1.7	0.5512	1.3	0.73	2830	± 29	3435	± 19	18
3.1X	0.16	725	608	0.87	209	0.1913	0.80	8.84	1.1	0.3350	0.7	0.67	1863	± 12	2753	± 13	32
3.2MA	0.26	1535	736	0.50	263	0.1517	0.85	4.16	1.1	0.1987	0.6	0.59	1168	± 7	2365	± 15	51
4.1X	2.76	432	348	0.83	201	0.3142	1.30	22.77	1.6	0.5255	1.1	0.64	2722	± 23	3542	± 19	23
5.1X	1.04	2322	530	0.24	457	0.2151	0.75	6.73	0.9	0.2268	0.5	0.55	1318	± 6	2944	± 12	55
5.2X	3.04	1569	157	0.10	355	0.2065	1.40	7.27	2.4	0.2553	1.9	0.80	1466	± 25	2879	± 23	49
6.1X	2.87	1221	78	0.07	257	0.2389	1.30	7.84	1.4	0.2380	0.7	0.49	1377	± 9	3112	± 20	56
7.1X	0.24	1979	203	0.11	290	0.1938	0.93	4.55	1.1	0.1703	0.5	0.50	1014	± 5	2774	± 15	63
7.2X	0.33	1991	595	0.31	394	0.2375	0.84	7.52	1.0	0.2297	0.6	0.60	1333	± 8	3103	± 13	57
8.1MA	2.59	2479	364	0.15	150	0.1713	2.20	1.62	2.4	0.0688	0.7	0.31	429	± 3	2570	± 38	83
9.1X	0.28	1145	696	0.63	241	0.2202	0.69	7.43	1.0	0.2446	0.7	0.69	1411	± 8	2982	± 11	53
10.1X	0.98	598	274	0.47	249	0.2831	0.98	18.70	1.3	0.4791	0.9	0.68	2524	± 19	3380	± 15	25
11.1X	0.44	1221	71	0.06	273	0.2400	0.65	8.59	0.9	0.2595	0.6	0.65	1487	± 8	3120	± 10	52
12.1X	1.55	550	88	0.16	211	0.2463	1.00	14.94	2.3	0.4399	2.0	0.89	2350	± 39	3161	± 17	26
13.1X	0.65	757	51	0.07	176	0.2145	1.00	7.96	2.2	0.2690	2.0	0.89	1536	± 27	2940	± 17	48
14.1X	0.91	767	165	0.22	202	0.1568	1.30	6.55	2.4	0.3030	2.0	0.83	1706	± 30	2421	± 23	30
15.1X	3.64	749	172	0.24	192	0.2325	1.70	9.21	2.7	0.2872	2.1	0.77	1628	± 30	3070	± 28	47
Gneissic syenogranite (A1229)																	
1.1MA	1.05	397	333	0.87	83	0.1552	0.93	5.16	1.6	0.2413	1.3	0.81	1393	± 16	2403	± 16	42
2.1MA	0.58	196	698	3.68	61	0.1610	0.83	7.97	1.4	0.3593	1.1	0.81	1979	± 20	2466	± 14	20
3.1MA	0.60	729	493	0.70	115	0.1469	0.63	3.70	1.2	0.1825	1.0	0.85	1080	± 10	2310	± 11	53
4.1MA	0.84	90	77	0.88	35	0.1643	1.20	10.08	1.8	0.4451	1.3	0.73	2373	± 26	2500	± 20	5
5.1MA	0.74	166	401	2.49	56	0.1619	0.91	8.60	1.5	0.3853	1.2	0.79	2101	± 21	2476	± 15	15
6.1MA	1.89	133	224	1.73	33	0.1706	1.60	6.70	2.0	0.2847	1.2	0.62	1615	± 18	2564	± 26	37

TABLE 1
(Continued)

Spot	$^{206}Pb_c$ (%)	U (ppm)	Th (ppm)	Th/U	$^{206}Pb^*$ (ppm)	$^{207}Pb^*/^{206}Pb^*$	± %	$^{207}Pb^*/^{235}U$	± %	$^{206}Pb^*/^{238}U$	± %	err corr	$^{206}Pb/^{238}U$ Age (MA)		$^{207}Pb/^{206}Pb$ Age (MA)		Discordance (%)
Gneissic syenogranite (A1229)																	
7.1MA	0.33	238	191	0.83	79	0.1628	0.64	8.66	1.3	0.3856	1.1	0.87	2102	± 20	2485	± 11	15
8.1MA	0.53	81	68	0.87	33	0.1626	1.10	10.60	1.7	0.4728	1.3	0.77	2496	± 28	2482	± 18	-1
9.1MA	0.27	183	68	0.39	69	0.1642	0.68	9.90	2.0	0.4373	1.9	0.94	2339	± 37	2499	± 11	6
9.2MA	0.24	302	141	0.48	87	0.1530	0.71	7.04	0.9	0.3338	0.6	0.66	1857	± 10	2379	± 12	22
10.1MA	6.13	278	495	1.84	79	0.1593	2.40	6.76	2.4	0.3071	0.8	0.35	1726	± 12	2452	± 38	30
11.1MA	0.38	118	221	1.94	45	0.1638	0.88	10.03	2.1	0.4441	1.9	0.91	2369	± 38	2495	± 15	5
12.1MA	0.15	314	183	0.60	119	0.1673	0.50	10.20	0.8	0.4420	0.6	0.77	2360	± 12	2531	± 9	7
13.1MA	0.12	152	102	0.69	60	0.1691	0.65	10.73	1.1	0.4603	0.8	0.79	2441	± 17	2549	± 11	4
14.1MA	0.18	108	289	2.75	39	0.1636	0.86	9.32	1.3	0.4134	10.0	0.76	2230	± 19	2493	± 14	11
15.1MA	1.80	243	424	1.81	74	0.1595	1.20	7.66	1.4	0.3480	0.8	0.54	1925	± 13	2451	± 20	21
Gneissic syenogranite (A1232)																	
1.1X	0.17	1420	1333	0.97	442	0.2228	0.34	11.11	1.4	0.3616	1.4	0.97	1990	± 23	3001	± 6	34
1.2MA+X	0.18	2652	370	0.14	1020	0.1883	0.63	11.63	0.7	0.4482	0.4	0.50	2387	± 7	2727	± 10	12
2.1X	0.03	674	121	0.19	316	0.2931	0.19	22.02	1.2	0.5449	1.2	0.99	2804	± 27	3434	± 3	18
3.1X	0.29	222	155	0.72	112	0.2826	0.36	22.83	1.3	0.5859	1.3	0.96	2973	± 31	3377	± 6	12
3.2MA	0.24	1244	170	0.14	164	0.1733	0.92	3.65	1.0	0.1529	0.4	0.42	917	± 4	2590	± 15	65
4.1X	1.43	1068	998	0.97	207	0.1987	1.80	6.09	2.9	0.2223	2.3	0.78	1294	± 27	2816	± 30	54
4.2MA	0.72	2124	309	0.15	217	0.1332	3.50	2.17	3.5	0.1180	0.5	0.13	719	± 3	2141	± 61	66
5.1X	0.05	664	719	1.12	329	0.2952	0.91	23.45	1.5	0.5761	1.2	0.80	2933	± 29	3445	± 14	15
6.1X	0.07	340	454	1.38	174	0.2973	0.25	24.43	1.3	0.5960	1.2	0.98	3014	± 30	3456	± 4	13
7.1X	1.45	1111	474	0.44	259	0.2265	0.65	8.35	1.4	0.2675	1.2	0.88	1528	± 17	3027	± 10	50
7.1X	0.22	518	481	0.96	219	0.2827	0.24	19.16	1.2	0.4917	1.2	0.98	2578	± 26	3378	± 4	24
8.1X	0.10	298	130	0.45	138	0.2874	0.64	21.36	1.4	0.5390	1.3	0.89	2779	± 28	3404	± 10	18
9.1X	0.48	1064	218	0.21	279	0.2364	1.10	9.89	1.6	0.3034	1.2	0.76	1708	± 18	3096	± 17	45
10.1MA	0.12	930	168	0.19	152	0.1513	3.60	3.96	3.8	0.1898	1.2	0.32	1120	± 12	2361	± 61	53
11.1X	0.39	705	456	0.67	141	0.2438	0.35	7.80	1.3	0.2319	1.2	0.96	1345	± 15	3145	± 6	57
12.1X	0.09	219	99	0.47	122	0.2974	0.36	26.52	0.7	0.6469	0.6	0.87	3216	± 16	3457	± 6	7
13.1X	0.08	264	192	0.75	165	0.2974	0.54	29.81	1.0	0.7270	0.8	0.83	3522	± 21	3457	± 8	-2
14.1MA	0.39	935	53	0.06	130	0.1704	3.80	3.80	3.8	0.1616	0.4	0.11	966	± 4	2562	± 63	62
11.1X	0.39	705	456	0.67	141	0.2438	0.35	7.80	1.3	0.2319	1.2	0.96	1345	± 15	3145	± 6	57
12.1X	0.09	219	99	0.47	122	0.2974	0.36	26.52	0.7	0.6469	0.6	0.87	3216	± 16	3457	± 6	7
13.1X	0.08	264	192	0.75	165	0.2974	0.54	29.81	1.0	0.7270	0.8	0.83	3522	± 21	3457	± 8	-2

TABLE 1
(Continued)

Spot	$^{206}Pb_c$ (%)	U (ppm)	Th (ppm)	Th/U	$^{206}Pb^*$ (ppm)	$^{207}Pb^*/^{206}Pb^*$	± %	$^{207}Pb^*/^{235}U$	± %	$^{206}Pb^*/^{238}U$	± %	err corr	$^{206}Pb/^{238}U$ Age (MA)		$^{207}Pb/^{206}Pb$ Age (MA)		Discordance (%)
Gneissic syenogranite (A1232)																	
14.1MA	0.39	935	53	0.06	130	0.1704	3.80	3.80	3.8	0.1616	0.4	0.11	966	± 4	2562	± 63	62
15.1X	0.06	458	176	0.40	148	0.2587	0.49	13.45	0.9	0.3771	0.7	0.82	2063	± 13	3239	± 8	36
16.1X	0.15	762	304	0.41	142	0.1925	0.61	5.75	0.8	0.2167	0.5	0.63	1264	± 6	2764	± 10	54
17.1MA	1.13	1771	189	0.11	176	0.1382	1.10	2.18	1.2	0.1144	0.5	0.38	699	± 3	2204	± 20	68
18.1MA	0.41	436	244	0.58	66	0.1600	1.10	3.86	1.4	0.1751	0.8	0.59	1040	± 8	2455	± 19	58
19.1X	0.31	823	169	0.21	184	0.1936	0.69	6.92	0.9	0.2593	0.6	0.67	1486	± 8	2773	± 11	46
20.1X	0.04	293	154	0.54	88	0.2593	0.61	12.47	1.0	0.3487	0.8	0.78	1928	± 13	3243	± 10	41
21.1X	0.35	323	84	0.27	169	0.2927	0.48	24.57	1.0	0.6087	0.9	0.88	3065	± 22	3432	± 8	11
22.1X	0.51	686	693	1.04	275	0.2630	0.47	16.83	0.7	0.4642	0.5	0.74	2458	± 11	3265	± 7	25
23.1X	0.16	443	413	0.96	197	0.2828	0.43	20.17	0.9	0.5173	0.8	0.88	2688	± 17	3378	± 7	20
Weakly deformed syenogranite (A1239)																	
1.1MA	0.44	19	44	2.35	8	0.1668	1.60	11.06	2.9	0.4810	2.4	0.84	2532	± 50	2526	± 26	0
2.1MA	2.08	86	94	1.12	15	0.1485	3.00	4.06	3.4	0.1984	1.7	0.48	1167	± 18	2328	± 51	50
3.1MA	0.55	54	104	1.96	21	0.1627	1.30	10.12	2.1	0.4512	1.6	0.78	2401	± 33	2484	± 22	3
4.1MA	1.19	25	59	2.49	11	0.1648	2.20	11.10	3.0	0.4885	2.0	0.68	2564	± 43	2506	± 37	-2
5.1MA	1.46	23	48	2.14	10	0.1656	2.60	10.91	3.4	0.4780	2.1	0.63	2519	± 45	2513	± 44	0
6.1MA	0.24	27	56	2.11	11	0.1644	2.10	10.95	2.9	0.4830	2.0	0.69	2540	± 43	2501	± 36	-2
7.1MA	0.24	46	99	2.23	18	0.1661	1.20	10.30	2.1	0.4496	1.7	0.82	2394	± 34	2519	± 20	5
8.1MA	0.37	32	67	2.19	13	0.1692	1.80	10.88	2.6	0.4665	1.9	0.72	2468	± 39	2550	± 30	3
9.1MA	0.18	75	99	1.36	24	0.1607	1.10	8.34	1.9	0.3763	1.5	0.81	2059	± 27	2463	± 19	16
10.1MA	0.27	110	141	1.33	26	0.1518	1.00	5.66	1.8	0.2701	1.4	0.81	1541	± 20	2367	± 18	35
11.1MA	0.35	63	188	3.08	25	0.1645	1.30	10.20	2.1	0.4498	1.6	0.78	2394	± 33	2502	± 22	4
12.1MA	0.56	513	86	0.17	82	0.1327	0.72	3.38	1.4	0.1846	1.3	0.87	1092	± 13	2135	± 13	49
Weakly deformed Syenogranite (A1240)																	
1.1X	2.91	771	243	0.33	166	0.2227	0.98	7.46	2.0	0.2430	1.7	0.87	1402	± 22	3000	± 16	53
1.2MA	8.77	2501	186	0.08	179	0.0997	4.90	1.04	5.0	0.0758	1.3	0.26	471	± 6	1619	± 90	71
2.1MA	2.76	4037	433	0.11	233	0.0849	2.30	0.77	2.6	0.0654	1.2	0.46	409	± 5	1312	± 45	69
2.2X	0.21	572	171	0.31	207	0.3533	0.39	20.51	0.7	0.4212	0.6	0.82	2266	± 11	3721	± 6	39
3.1MA	1.11	561	363	0.67	309	0.1604	0.62	14.03	1.4	0.6342	1.2	0.89	3166	± 31	2460	± 10	-29
4.1MA	1.51	1054	388	0.38	158	0.1232	10.00	2.93	1.7	0.1724	1.4	0.81	1025	± 13	2003	± 18	49
5.1MA	15.13	3095	1033	0.34	161	0.1260	12.00	0.90	12.0	0.0515	1.7	0.14	324	± 6	2050	± 210	84
6.1X	0.29	356	91	0.26	98	0.2242	0.52	9.83	0.8	0.3180	0.5	0.72	1780	± 8	3011	± 8	41

TABLE 1
(Continued)

Spot	$^{206}Pb_c$ (%)	U (ppm)	Th (ppm)	Th/U	$^{206}Pb^*$ (ppm)	$^{207}Pb^*/^{206}Pb^*$	± %	$^{207}Pb^*/^{235}U$	± %	$^{206}Pb^*/^{238}U$	± %	err corr	$^{206}Pb/^{238}U$ Age (MA)		$^{207}Pb/^{206}Pb$ Age (MA)		Discordance (%)
Weakly deformed Syenogranite (A1240)																	
7.1MA+X	0.30	355	250	0.73	116	0.1754	0.94	9.16	1.2	0.3789	0.7	0.61	2071	± 13	2609	± 16	21
8.1X	0.15	244	136	0.58	98	0.2762	0.60	17.87	1.2	0.4693	1.0	0.86	2481	± 21	3341	± 9	26
9.1X	0.50	414	278	0.69	46	0.3013	0.90	5.39	1.2	0.1298	0.7	0.62	787	± 5	3477	± 14	77
10.1MA	0.50	1050	291	0.29	128	0.1627	0.84	3.16	1.0	0.1408	0.5	0.49	849	± 4	2484	± 14	66
11.1MA	0.14	647	350	0.56	109	0.1404	0.75	3.80	10.0	0.1965	0.7	0.66	1157	± 7	2232	± 13	48
12.1MA	0.94	865	767	0.92	133	0.1583	2.00	3.88	2.1	0.1777	0.6	0.29	1054	± 6	2437	± 34	57
13.1X	0.24	777	242	0.32	166	0.2259	0.58	7.71	0.9	0.2475	0.6	0.74	1426	± 8	3023	± 9	53
14.1X	0.21	525	169	0.33	150	0.2505	0.54	11.46	0.8	0.3318	0.6	0.75	1847	± 10	3188	± 9	42
15.1MA	1.91	2002	87	0.04	262	0.1245	1.20	2.56	1.3	0.1492	0.5	0.36	896	± 4	2022	± 22	56
16.1MA	0.95	2156	130	0.06	172	0.1131	1.50	1.44	1.6	0.0922	0.4	0.26	569	± 2	1850	± 28	69
17.1MA	0.76	2436	112	0.05	218	0.1107	1.20	1.58	1.3	0.1035	0.4	0.34	635	± 3	1810	± 22	65
18.1MA	0.23	1648	154	0.10	189	0.1033	0.85	1.90	1.0	0.1330	0.5	0.51	805	± 4	1684	± 16	52
Banded granodiorite (A1126)																	
1.1X	1.03	111	95	0.88	69	0.3100	1.30	30.38	2.8	0.7110	2.5	0.89	3463	± 67	3521	± 19	2
1.2MA	0.36	256	128	0.52	103	0.1657	1.10	10.67	2.4	0.4676	2.1	0.89	2473	± 43	2515	± 18	2
1.3MA	0.28	325	124	0.40	107	0.1587	1.50	8.37	2.7	0.3830	2.2	0.82	2090	± 39	2442	± 26	14
2.1MA	0.53	209	114	0.56	85	0.1669	1.20	10.80	2.4	0.4700	2.1	0.87	2484	± 44	2527	± 20	2
3.1MA	0.66	427	248	0.60	141	0.1598	1.00	8.39	2.5	0.3817	2.3	0.91	2084	± 40	2454	± 17	15
4.1X	0.63	98	90	0.95	62	0.3037	1.10	30.25	2.8	0.7250	2.6	0.92	3515	± 70	3489	± 17	-1
4.2MA	0.37	374	202	0.56	128	0.1647	0.92	9.02	2.2	0.3976	2.0	0.91	2158	± 37	2505	± 15	14
5.1X	0.38	186	83	0.46	115	0.3040	0.76	29.97	2.3	0.7170	2.2	0.94	3483	± 58	3491	± 12	0
6.1MA	0.18	448	288	0.67	156	0.1648	0.80	9.18	2.1	0.4041	2.0	0.93	2188	± 37	2506	± 13	13
7.1X	8.40	73	47	0.67	35	0.1640	6.90	11.16	7.6	0.5070	3.2	0.42	2643	± 66	2502	± 120	-4
8.1X	0.27	206	106	0.53	137	0.3581	0.74	38.04	2.3	0.7720	2.2	0.95	3687	± 62	3742	± 11	2
9.1X	1.03	55	10	0.19	24	0.1769	3.80	12.24	5.0	0.5030	3.1	0.63	2628	± 67	2624	± 64	0
10.1MA	0.27	368	241	0.68	147	0.1656	0.87	10.55	2.2	0.4624	2.0	0.92	2450	± 41	2514	± 15	3
11.1MA	0.79	397	293	0.76	131	0.1656	1.10	8.67	2.4	0.3807	2.1	0.87	2080	± 36	2514	± 19	17
12.1X	0.13	534	392	0.76	292	0.3077	0.45	26.96	2.0	0.6360	2.0	0.97	3173	± 49	3509	± 7	10
13.1X	0.28	125	80	0.67	83	0.3674	1.10	38.90	2.8	0.7700	2.6	0.92	3680	± 72	3781	± 17	3
14.1X	0.07	464	28	0.06	285	0.3277	0.50	32.29	2.1	0.7150	2.0	0.97	3476	± 54	3607	± 8	4
15.1X	0.33	1150	707	0.64	321	0.2463	0.65	10.96	2.1	0.3233	2.0	0.95	1806	± 31	3161	± 10	43
16.1X	0.87	590	246	0.43	138	0.2963	1.10	10.93	2.3	0.2689	2.1	0.89	1535	± 28	3451	± 16	56

TABLE 1
(Continued)

Spot	$^{206}Pb_c$ (%)	U (ppm)	Th (ppm)	Th/U	$^{206}Pb^*$ (ppm)	$^{207}Pb^*/^{206}Pb^*$	± %	$^{207}Pb^*/^{235}U$	± %	$^{206}Pb^*/^{238}U$	± %	err corr	$^{206}Pb/^{238}U$ Age (MA)		$^{207}Pb/^{206}Pb$ Age (MA)		Discordance (%)
Gneissic quartz monzonite (A1124)																	
1.1X	0.23	171	41	0.25	109	0.3084	0.75	31.43	2.3	0.7390	2.2	0.95	3568	± 60	3513	± 12	-2
1.2X	0.89	81	40	0.51	50	0.3167	1.70	31.10	3.4	0.7110	2.9	0.87	3463	± 78	3554	± 26	3
2.1MA	0.30	569	235	0.43	149	0.1563	1.00	6.57	2.2	0.3049	2.0	0.89	1715	± 29	2416	± 17	29
3.1MA	0.40	358	215	0.62	133	0.1641	0.97	9.74	2.2	0.4307	2.0	0.90	2309	± 39	2498	± 16	8
4.1X	1.97	357	160	0.46	224	0.3371	1.00	32.94	2.5	0.7090	2.3	0.92	3456	±61	3648	±15	5
5.1MA	0.52	411	172	0.43	136	0.1639	0.98	8.64	2.2	0.3824	2.0	0.90	2088	±36	2496	±17	16
5.2X	0.61	456	303	0.69	187	0.3186	1.20	20.90	2.3	0.4756	2.0	0.87	2508	± 42	3563	± 18	30
6.1X	0.23	698	33	0.05	391	0.2881	0.55	25.79	2.1	0.6490	2.0	0.96	3226	± 50	3407	± 9	5
7.1MA	1.71	613	562	0.95	138	0.1526	2.70	5.42	3.4	0.2574	2.1	0.61	1477	± 27	2375	± 45	38
8.1MA	1.25	379	222	0.60	144	0.1659	1.70	10.01	2.7	0.4378	2.1	0.79	2341	± 42	2517	± 28	7
9.1X	0.20	165	107	0.67	110	0.3351	0.72	35.91	2.3	0.7770	2.2	0.95	3706	± 62	3641	± 11	-2
10.1X	7.75	335	70	0.21	198	0.3200	4.00	28.00	4.8	0.6360	2.5	0.53	3171	± 63	3569	± 62	11
11.1X	0.84	52	20	0.39	35	0.3266	1.80	34.20	3.5	0.7590	3.0	0.86	3641	± 85	3601	± 27	-1
11.2MA	10.09	1046	623	0.62	223	0.1638	4.80	5.04	5.2	0.2233	2.1	0.41	1299	± 25	2496	± 80	48
12.1X	0.66	212	113	0.55	127	0.3175	1.20	30.37	2.5	0.6940	2.2	0.87	3397	± 57	3558	± 19	5
13.1X	0.40	161	36	0.23	100	0.3019	0.91	29.80	4.4	0.7160	4.3	0.98	3483	± 120	3480	± 14	0
14.1MA	0.21	528	435	0.85	206	0.1656	0.78	10.35	2.1	0.4536	1.9	0.93	2411	± 39	2513	± 13	4
15.1MA	2.08	472	385	0.84	154	0.1582	2.70	8.11	3.4	0.3720	2.1	0.61	2039	± 37	2437	± 46	16
16.1X	4.49	534	265	0.51	195	0.1804	3.50	10.10	4.1	0.4062	2.2	0.53	2197	± 41	2657	± 58	17
17.1X	11.52	197	103	0.54	86	0.1790	8.20	11.11	8.7	0.4490	2.9	0.33	2391	± 58	2647	± 140	10
18.1X	3.61	188	168	0.93	92	0.1929	2.80	14.59	3.7	0.5490	2.4	0.66	2820	± 55	2767	± 45	-2
19.1X	3.68	121	59	0.50	84	0.3567	1.60	38.60	3.1	0.7840	2.6	0.85	3733	± 74	3736	± 25	0
Gneissic quartz monzonite (A1235)																	
1.1MA	0.10	417	288	0.71	130	0.1624	0.60	8.13	3.3	0.3630	3.2	0.98	1997	± 55	2481	± 10	20
2.1X	0.10	502	177	0.36	176	0.2673	0.41	15.04	3.2	0.4080	3.2	0.99	2207	± 60	3290	± 6	33
2.2MA	7.68	432	209	0.50	138	0.1745	3.60	8.12	4.6	0.3340	3.3	0.71	1860	± 54	2617	± 54	29
3.1MA	1.85	1001	468	0.48	171	0.1405	1.50	3.76	3.5	0.1939	3.2	0.91	1142	± 34	2237	± 25	49
4.1MA	12.31	1329	143	0.11	161	0.1780	8.10	2.94	8.6	0.1180	3.8	0.44	719	± 25	2658	± 130	73
4.2X	1.69	131	117	0.93	54	0.1860	1.90	11.96	3.9	0.4650	3.5	0.88	2463	± 71	2711	± 30	9
6.1MA	0.06	251	296	1.22	102	0.1644	0.80	10.75	3.4	0.4740	3.3	0.97	2501	± 68	2502	± 13	0
7.1X	0.05	348	195	0.58	157	0.2821	1.40	20.45	3.5	0.5260	3.2	0.92	2724	± 71	3375	± 21	19
8.1MA	0.97	520	454	0.90	108	0.1511	1.00	4.99	3.4	0.2394	3.2	0.95	1384	± 40	2360	± 17	41

TABLE 1
(Continued)

Spot	$^{206}Pb_c$ (%)	U (ppm)	Th (ppm)	Th/U	$^{206}Pb^*$ (ppm)	$^{207}Pb^*/^{206}Pb^*$	± %	$^{207}Pb^*/^{235}U$	± %	$^{206}Pb^*/^{238}U$	± %	err corr	$^{206}Pb/^{238}U$ Age (MA)		$^{207}Pb/^{206}Pb$ Age (MA)		Discordance (%)
Gneissic quartz monzonite (A1235)																	
9.1MA	4.06	280	237	0.87	92	0.1645	2.80	8.25	4.2	0.3620	3.3	0.78	1992	± 57	2511	± 45	21
10.1X	0.33	128	122	0.99	85	0.3108	0.62	33.20	3.4	0.7740	3.3	0.98	3696	± 93	3525	± 10	-5
11.1X	26.28	2119	200	0.10	212	0.2000	11.00	2.11	10.0	0.0742	4.2	0.42	461	± 20	2880	± 150	84
12.1MA	4.11	1412	92	0.07	153	0.1131	2.90	1.88	4.2	0.1198	3.2	0.77	729	± 22	1862	± 48	61
13.1MA	1.73	450	372	0.85	108	0.1623	1.70	6.13	4.3	0.2730	4.0	0.93	1557	± 56	2484	± 28	37
13.2MA	2.16	630	271	0.44	141	0.1568	1.40	5.50	3.4	0.2536	3.2	0.93	1457	± 42	2426	± 22	40
14.1MA	0.41	528	415	0.81	129	0.1598	0.75	6.22	3.3	0.2823	3.2	0.97	1603	± 46	2454	± 13	35
15.1X	0.03	378	256	0.70	222	0.3279	0.36	30.90	3.2	0.6830	3.2	0.99	3357	± 84	3607	± 6	7
16.1X	0.08	65	36	0.58	35	0.2836	0.78	24.54	3.5	0.6280	3.4	0.97	3140	± 84	3383	± 12	7
17.1MA	1.03	372	272	0.76	116	0.1599	1.20	7.92	3.4	0.3590	3.2	0.94	1976	± 55	2457	± 20	20
18.1MA	1.28	588	613	1.08	104	0.1561	1.20	4.38	3.4	0.2032	3.2	0.94	1192	± 35	2417	± 19	51
19.1MA	0.17	622	297	0.49	166	0.1590	0.67	6.80	3.3	0.3100	3.2	0.98	1741	± 49	2445	± 11	29
20.1MA	1.72	552	306	0.57	129	0.1726	1.40	6.35	3.5	0.2663	3.2	0.93	1522	± 44	2587	± 22	41
21.1MA	6.30	613	630	1.06	147	0.1760	6.60	6.23	7.3	0.2552	3.4	0.47	1465	± 45	2624	± 110	44
22.1MA	0.12	351	177	0.52	99	0.1629	0.69	7.38	3.3	0.3290	3.2	0.98	1832	± 51	2487	± 12	26
23.1MA	0.69	674	817	1.25	129	0.1514	0.93	4.62	3.3	0.2212	3.2	0.96	1288	± 37	2364	± 16	45
24.1MA	3.96	533	1578	3.06	115	0.1630	7.10	5.39	7.8	0.2380	3.6	0.46	1377	± 43	2500	± 120	45
25.1MA	0.03	407	286	0.73	140	0.1637	0.52	9.03	3.2	0.4000	3.2	0.99	2169	± 59	2494	± 9	13
26.1MA	0.08	364	211	0.60	127	0.1629	0.61	9.10	3.3	0.4050	3.2	0.98	2192	± 60	2487	± 10	12
27.1MA	0.29	389	401	1.07	95	0.1603	0.79	6.27	3.3	0.2837	3.2	0.97	1610	± 46	2460	± 13	35
28.1MA	0.03	464	387	0.86	136	0.1588	0.54	7.46	3.3	0.3410	3.2	0.99	1889	± 53	2443	± 9	23
Gneissic monzogranite (A1228)																	
1.1MA	0.16	58	68	1.21	24	0.1651	1.10	11.03	1.9	0.4847	1.6	0.83	2548	± 34	2508	± 18	-2
2.1MA	0.69	169	59	0.36	68	0.1647	0.90	10.49	1.5	0.4618	1.2	0.80	2447	± 25	2504	± 15	2
3.1MA	0.72	46	37	0.84	19	0.1654	1.50	10.97	2.3	0.4812	1.7	0.75	2533	± 35	2511	± 25	-1
4.1MA	0.35	35	36	1.08	14	0.1640	1.80	10.84	2.5	0.4793	1.7	0.70	2524	± 36	2497	± 30	-1
5.1MA	0.30	125	73	0.60	48	0.1661	1.00	10.16	1.6	0.4439	1.2	0.77	2368	± 24	2519	± 17	6
6.1MA	0.14	353	300	0.88	111	0.1632	0.56	8.21	1.2	0.3646	1.1	0.89	2004	± 19	2489	± 9	19
7.1MA	0.60	43	30	0.72	18	0.1644	1.80	10.64	2.7	0.4696	2.0	0.75	2482	± 42	2501	± 30	1
8.1MA	0.34	69	33	0.49	28	0.1628	1.10	10.42	2.6	0.4640	2.4	0.90	2458	± 48	2485	± 19	1
9.1MA	0.07	352	301	0.88	142	0.1674	0.41	10.86	1.1	0.4705	1.1	0.93	2486	± 22	2532	± 7	2

Table 1
(Continued)

Spot	$^{206}Pb_c$ (%)	U (ppm)	Th (ppm)	Th/U	$^{206}Pb^*$ (ppm)	$^{207}Pb^*/^{206}Pb^*$	± %	$^{207}Pb^*/^{235}U$	± %	$^{206}Pb^*/^{238}U$	± %	err corr	$^{206}Pb/^{238}U$ Age (MA)		$^{207}Pb/^{206}Pb$ Age (MA)		Discordance (%)
Gneissic monzogranite (A1228)																	
10.1MA	0.18	221	193	0.90	81	0.1646	0.59	9.72	1.3	0.4286	1.1	0.88	2299	± 22	2503	± 10	8
11.1MA	0.43	33	29	0.90	13	0.1631	1.80	10.59	2.8	0.4710	2.2	0.78	2487	± 45	2488	± 30	0
12.1MA	0.37	223	127	0.59	87	0.1635	0.62	10.20	1.0	0.4523	0.8	0.77	2405	± 15	2492	± 10	3
13.1MA	0.21	42	42	1.05	18	0.1634	1.30	11.02	1.9	0.4894	1.4	0.73	2568	± 29	2491	± 21	-3
14.1MA	0.02	65	81	1.28	27	0.1664	0.93	11.14	1.5	0.4855	1.1	0.77	2551	± 24	2522	± 16	-1
15.1MA	0.39	31	30	1.01	13	0.1638	1.90	10.75	2.5	0.4761	1.7	0.66	2510	± 34	2495	± 32	-1
16.1MA	0.22	39	42	1.11	16	0.1650	1.50	10.35	2.0	0.4547	1.4	0.69	2416	± 28	2508	± 25	4
17.1MA	-0.08	55	47	0.88	23	0.1682	1.00	11.11	1.6	0.4791	1.2	0.77	2524	± 25	2540	± 17	1
18.1MA	0.00	71	62	0.89	29	0.1680	0.87	10.75	1.5	0.4642	1.2	0.82	2458	± 25	2538	± 15	3
19.1MA	0.09	179	55	0.32	70	0.1631	0.65	10.21	1.0	0.4539	0.8	0.78	2413	± 16	2488	± 11	3
20.1MA	0.09	174	211	1.25	73	0.1641	0.90	10.99	1.2	0.4859	0.7	0.63	2553	± 15	2498	± 15	-2

Note: 1) Common lead corrected using measured ^{204}Pb; 2) $^{206}Pb^*$ is radiogenic lead; 3) Discordance(%) is defined as [(1– ($^{206}Pb/^{238}U$)age)/($^{207}Pb/^{206}Pb$)age]×100; 4) MA=magmatic zircon; X=xenocrystal zircon.

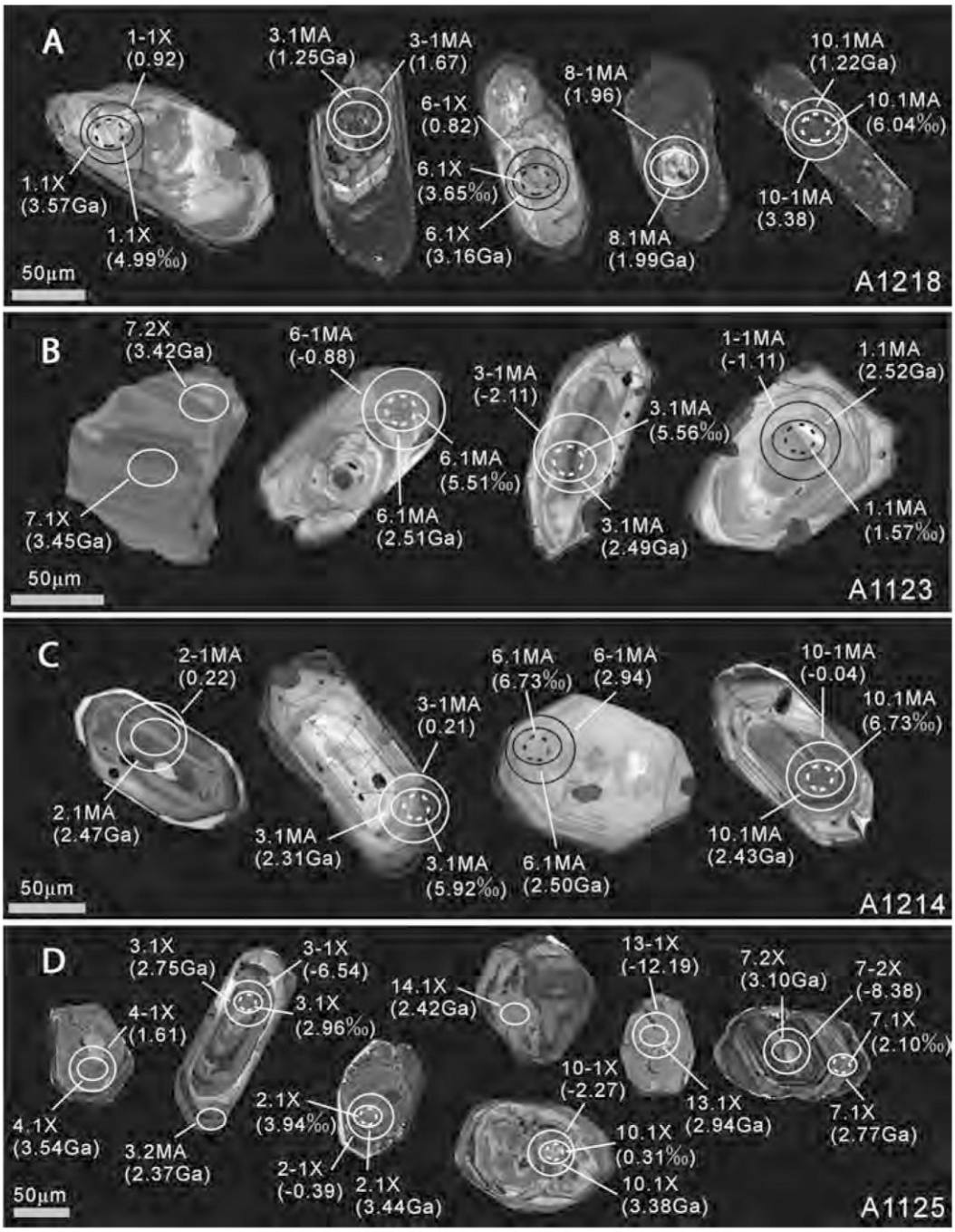

Fig. 5. Zircon cathodoluminescence images from late Neoarchean magmatic rocks in the Anshan-Benxi area, North China Craton. (A)-(H) Syenogranite (A1218, A1123, A1214, A1125, A1229, A1232, A1239, A1240); (I) banded granodiorite (A1126); (J) gneissic quartz monzonite (A1124); (K) gneissic quartz monzonite (A1235); (L) gneissic monzogranite (A1228).

3435 Ma. Only two analyses (spots 3.2MA, 8.1MA) were made on magmatic rims, and these show even more severe lead loss than the cores. We estimate that the magmatic zircon has a formation age of *ca.* 2.5 Ga.

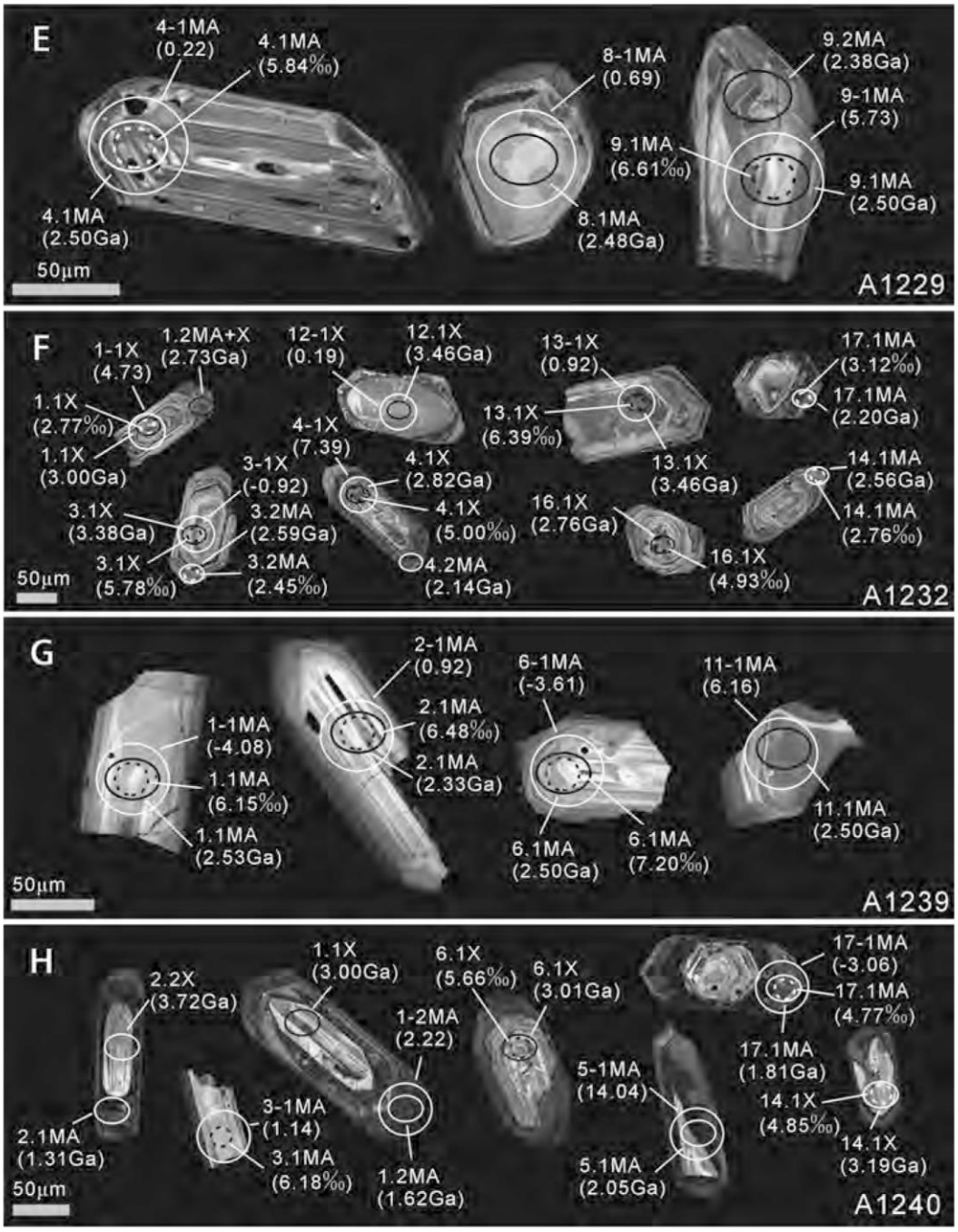

Fig. 5. (continued)

Gneissic Syenogranite (A1229)

The magmatic zircon grains are elongate or stubby in habit and show oscillatory zoning in CL images with some showing recrystallization and dark rims (fig. 5E). Fifteen analyses on 15 magmatic zircon exhibit lead loss to variable degrees, but the analyses define a discordia line with an upper concordia intercept age of 2502 ± 30 Ma (MSWD = 2.5) (fig. 6E). This is interpreted as the formation age of the syenogranite.

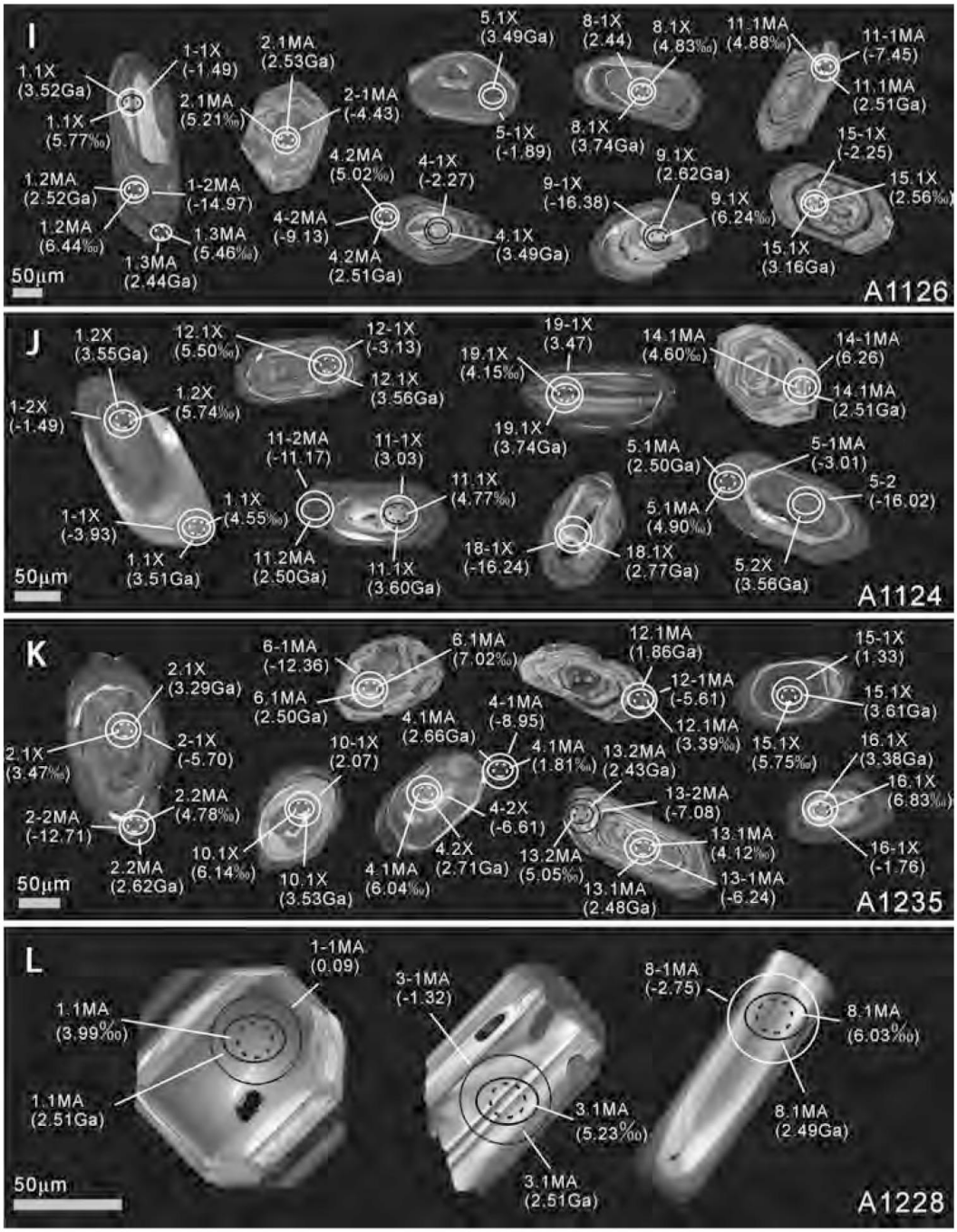

Fig. 5. (continued)

Gneissic Syenogranite (A1232)

The zircon is of stubby or elongate habit, and some grains show core-rim structures, with cores exhibiting oval or irregular shapes and narrow magmatic rims exhibiting prismatic terminations (grains 12, 16 and 17 in fig. 5F). Others have no such clear core-rim structures, and the cores and rims show the same zoning (grains 1, 3 and 4 in fig. 5F). Twenty one analyses on xenocrystic cores show lead loss to variable

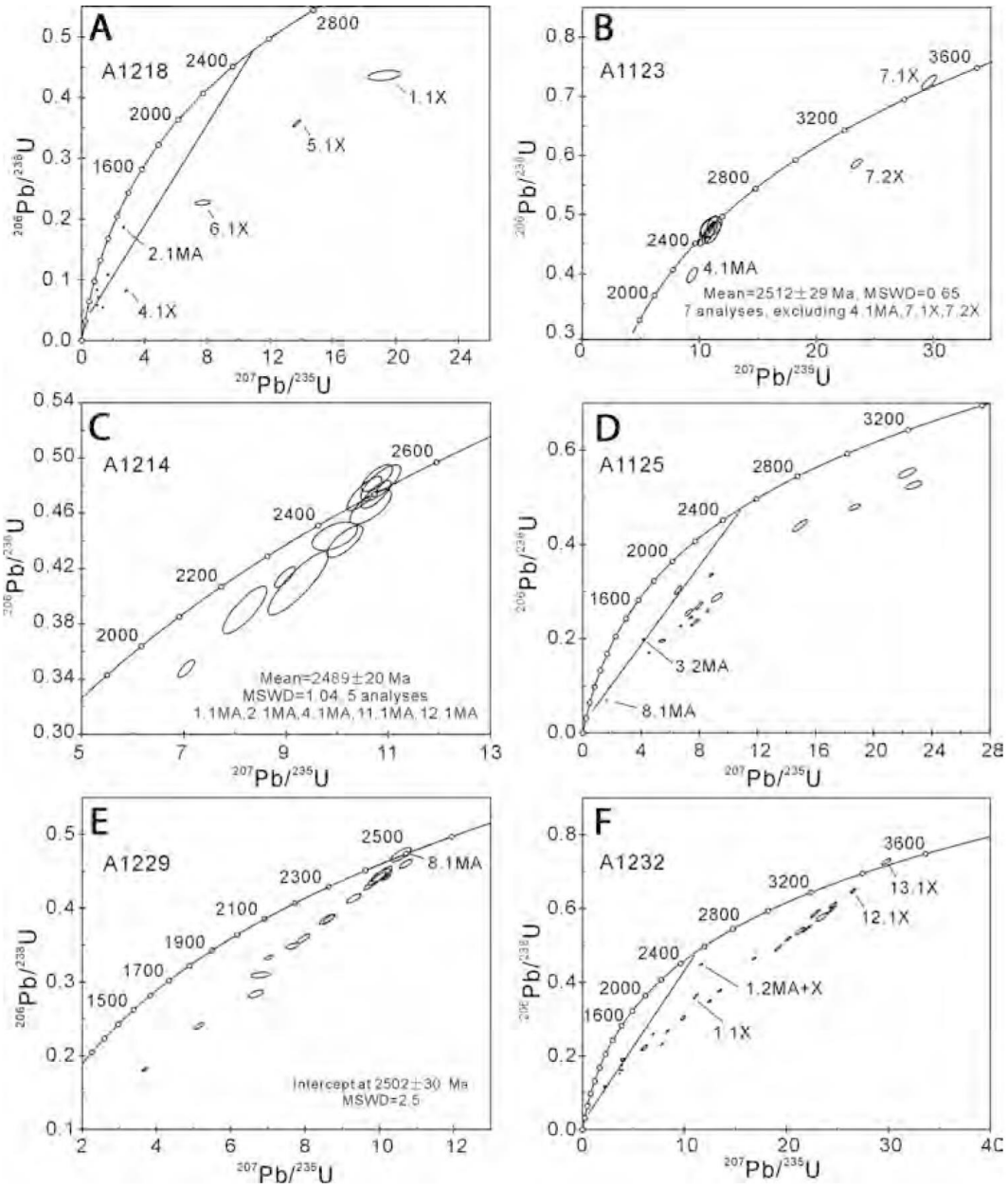

Fig. 6. Concordia diagrams showing SHRIMP analytical data of zircons from late Neoarchean magmatic rocks in the Anshan-Benxi area, North China Craton. (A)-(H) Syenogranite (A1218, A1123, A1214, A1125, A1229, A1232, A1239, A1240); (I) banded granodiorite (A1126); (J) gneissic quartz monzonite (A1124); (K) gneissic quartz monzonite (A1235); (L) gneissic monzogranite (A1228).

degrees, but all analyses define a linear array in the concordia diagram with an upper intercept age of *ca.* 3.45 Ga (fig. 6F). All five analyses on magmatic rims show higher U contents (930–2126 ppm), lower Th/U ratios (0.06–0.19) and stronger lead loss than the cores and roughly plot on the same discordia line as those of the cores (fig. 6F). However, the cores are xenocrysts for the following reasons: (1) the internal structures are different from the magmatic rims; (2) the syenogranite intruded into nearby *ca.* 2.5 Ga BIF-bearing supracrustal rocks (the Anshan "Group"); (3) analysis 1.2MA+X is near-concordant and has a $^{207}Pb/^{206}Pb$ age of 2727 ± 10 Ma (fig. 6F). We suggest that

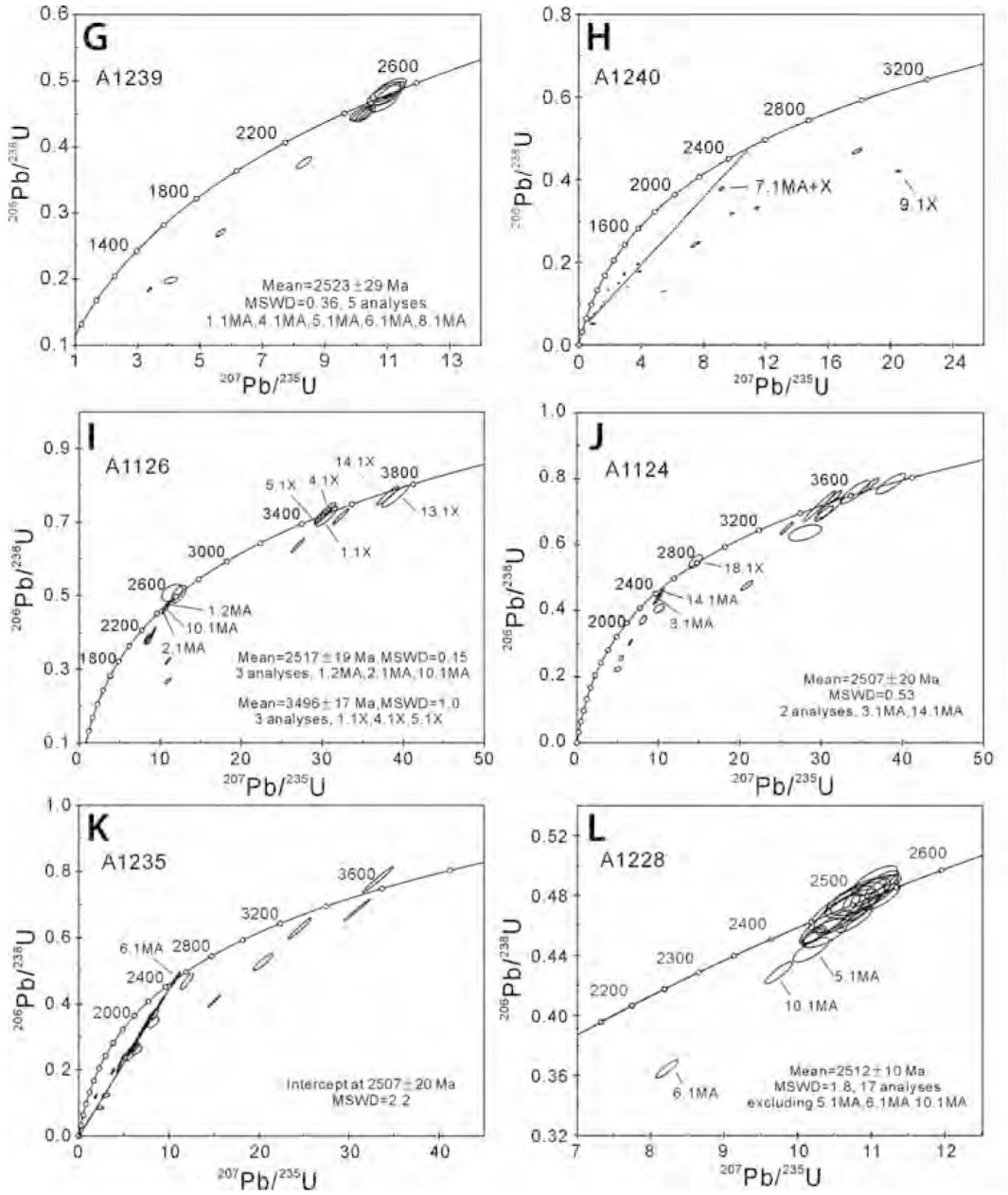

Fig. 6. (continued)

the magmatic rims have a mean $^{207}Pb/^{206}Pb$ age of *ca.* 2.5 Ga and the older age of analysis 1.2MA+X is due to the analytical spot being partly placed on part of a core during analysis (grain 1 in fig. 5F).

Weakly Deformed Syenogranite (A1239)

The zircon is elongate in shape and shows oscillatory or banded zoning (fig. 5G). Twelve analyses on magmatic zircon were performed, and the zircon with high U contents shows lead loss to variable degrees. Five analyses on or near concordia yielded a weighted mean $^{207}Pb/^{206}Pb$ age of 2523 ± 29 Ma (MSWD = 0.36) (fig. 6C), which is considered to reflect the time of intrusion of the syenogranite.

Weakly Deformed Syenogranite (A1240)

The zircon grains show similar features in shape and internal structure as those from sample A1232, but commonly have wider magmatic rims (fig. 5H). Nineteen analyses were carried out on 17 zircon grains, and those on magmatic rims show strong lead loss but the analyses are aligned and roughly define a discordia line (fig. 6H). Analysis 7.1MA+X has a Th/U ratio of 0.73 and is relatively close to concordia with a minimum $^{207}Pb/^{206}Pb$ age of 2609 ± 16 Ma. The reason for the slightly older age is likely the same as for analysis 1.2MA+X of syenogranite sample A1232 mentioned above. We consider that the syenogranite was formed at *ca.* 2.5 Ga. Seven analyses on xenocrystic domains also show strong lead loss, and the oldest minimum $^{207}Pb/^{206}Pb$ age is 3477 ± 14 Ma (analysis 9.1X).

Banded Granodiorite (A1126)

The zircon grains are stubby or elongate in shape and show oscillatory zoning with some containing xenocrystic cores (grains 1, 4, 8, 9 and 15 in fig. 5I). Some cores have light gray rims in CL images, which may have formed as a result of fluid alteration. Eight analyses on magmatic domains show variable lead loss, and three analyses close to concordia with small errors yielded a weighted mean $^{207}Pb/^{206}Pb$ age of 2517 ± 19 Ma (MSWD = 0.15) (fig. 6I) that we interpret as the emplacement age of the granodiorite. Eleven analyses on cores yielded large variations of U contents and Th/U ratios and those on or close to concordia have $^{207}Pb/^{206}Pb$ ages ranging from 3489 to 3781 Ma, with three analyses plotting on concordia yielded a weighted mean $^{207}Pb/^{206}Pb$ age of 3496 ± 17 Ma (MSWD = 1.0).

Gneissic Quartz Monzonite (A1124)

The zircon grains are similar in shape, internal structure in CL images (fig. 5J), and analytical data (fig. 6J) to those from sample A1126. Seven analyses on magmatic domains were performed, and two analyses close to concordia yielded a weighted mean $^{207}Pb/^{206}Pb$ age of 2507 ± 20 Ma (MSWD = 0.53). Thirteen analyses on xenocrystic cores have $^{207}Pb/^{206}Pb$ ages of 3407 to 3736 Ma, with the exception of analysis 18.1X that has a minimum $^{207}Pb/^{206}Pb$ age of 2767 Ma but with a large error.

Gneissic Quartz Monzonite (A1235)

The zircon grains show similar features to those from sample A1126 (fig. 5K). Twenty four analyses on magmatic zircons commonly show severe lead loss, and some grains yielding low Th/U ratios (<0.1) may be the result of growth during metamorphism or anatexis. Most analyses define a linear array in the concordia diagram with an upper intercept age of 2507 ± 20 Ma (MSWD = 2.2) (fig. 6K). Seven analyses on xenocrystic cores provided $^{207}Pb/^{206}Pb$ ages between 2711 and 3607 Ma.

Gneissic Monzogranite (A1228)

The magmatic zircon is stubby or elongate in habit and shows banded or oscillatory zoning in CL images (fig. 5L). Seventeen of twenty analyses yielded a weighted mean $^{207}Pb/^{206}Pb$ age of 2512 ± 10 Ma (MSWD = 1.8) (fig. 6L).

GEOCHEMISTRY

Whole-Rock Chemical Composition

Most of the studied 2.5 Ga magmatic rocks are syenogranite, besides a few granodiorites, quartz monzonites, monzogranites and K-rich granites, consistent with syenogranite being the main type of ~2.5 Ga granitoids in the Anshan-Benxi area. The syenogranites are high in SiO_2 (commonly 70–75 %) and low in CaO, FeOt (total Fe as FeO), MgO, TiO_2 and P_2O_5 (table 2), and plot in the granite field in an An-Ab-Or

TABLE 2

Element compositions of late Neoarchean magmatic rocks in the Anshan-Benxi area, North China Craton

No.	1	2	3	4	5	6	7
Sample no.	A0712	A0713	A9169	A1106	A1107	A1218	A1123
Rock type	Gneissic syenogranite	Gneissic syenogranite	Syenogranite	Massive syenogranite	Gneissic syenogranite	Massive syenogranite	Gneissic syenogranite
Sample location	Qidashan	Qidashan	Southeast of Qidashan	Southeast of Qidashan	North of Shangdahe	North of Gongchangling	Southeast of Gongchangling
Longitude and latitude	N41°09'15" E123°06'35"	N41°09'15" E123°06'35"		N41°06'48" E123°10'11"	N41°04'55" E123°15'17"	N41°10'10" E123°27'03"	N41°03'58" E123°34'34"
Age		2503±10 Ma					2512±29 Ma
SiO_2	75.06	73.61	74.48	73.63	74.33	73.05	76.84
TiO_2	0.07	0.18	0.16	0.28	0.15	0.14	0.16
Al_2O_3	13.58	13.74	13.87	13.91	13.42	13.83	11.85
Fe_2O_3	0.60	1.21	1.01	1.02	0.55	0.68	0.13
FeO	0.65	0.48	0.55	0.75	1.31	1.06	1.28
MnO	0.04	0.04	0.04	0.05	0.06	0.04	0.04
MgO	0.48	0.30	0.27	0.34	0.35	0.58	0.38
CaO	0.51	0.40	0.31	0.21	0.39	0.27	0.19
Na_2O	3.46	2.92	3.17	2.90	3.22	3.11	2.71
K_2O	4.72	5.51	5.08	5.74	5.11	5.98	5.22
P_2O_5	0.06	0.12	0.11	0.10	0.04	0.06	0.07
H_2O^+	0.70	0.66	0.90	0.80	0.80	0.72	0.46
$LOL+CO_2$	1.08	1.09		0.10	0.12	0.09	0.10
Total	101.01	100.26	99.95	99.83	99.85	99.61	99.43
K_2O/Na_2O	1.36	1.89	1.60	1.98	1.59	1.92	1.93
Cr	22	11		7	10	7	17
Ni				4	5	3	5
Sc	4	3		3	3	3	3
Rb	321	327	319	235	184	269	257
Ba	312	318	503	468	522	372	461
Sr	97	94	53	75	38	43	43
Nb	28.8	20.4		16.5	24.3	19.1	23.9
Ta	2.9	2.2		0.7	0.8	3.2	2.6
Hf	2.1	4.3		8.3	5.1	6.3	4.8
Zr	76	154	121	256	175	157	152
Y	29	19	24	22	28	30	35
Th	18.6	33.0	42.0	59.8	26.4	61.5	51.8
U	25.3	6.9	12.0	4.1	3.7	20.7	3.6
La	20.40	18.50	37.33	102.00	23.20	67.10	62.90
Ce	37.70	31.50	74.87	176.00	63.30	118.00	115.00
Pr	3.83	4.11	7.16	18.60	4.28	12.80	11.90
Nd	12.70	13.70	27.41	61.50	14.40	42.30	39.00
Sm	2.82	2.94	5.64	9.89	2.97	9.07	7.41
Eu	0.38	0.26	0.52	0.68	0.20	0.57	0.36
Gd	3.35	3.08	3.41	6.82	3.32	7.92	5.64
Tb	0.64	0.51	0.65	0.95	0.64	1.22	0.97
Dy	4.25	3.13	4.43	4.53	4.10	6.62	5.42
Ho	0.90	0.61	0.83	0.77	0.95	1.21	1.11
Er	2.87	1.85	2.34	2.22	2.98	3.29	3.53
Tm	0.49	0.27	0.30	0.22	0.40	0.41	0.44
Yb	3.54	1.72	1.95	1.45	2.58	2.53	3.04
Lu	0.51	0.25	0.34	0.21	0.36	0.38	0.41
ΣREE	94.4	82.4	167.2	385.8	123.7	273.4	257.1
$(La/Yb)_n$	3.8	7.1	12.6	46.3	5.9	17.5	13.6
Eu/Eu*	0.38	0.26	0.34	0.24	0.20	0.20	0.17
Ba/Ba*	0.12	0.10	0.14	0.11	0.23	0.08	0.12

TABLE 2
(Continued)

No.	8	9	10	11	12	13	14
Sample no.	A1216	A1214	A1226	A1233	A1125	A1229	A1232
Rock type	Gneissic syenogranite	Weakly deformed syenogranite	Massive syenogranite	Gneissic syenogranite	Gneissic syenogranite	Gneissic syenogranite	Gneissic syenogranite
Sample location	Northwest of Lianshanguan	West of Lianshanguan	North of Jiguanshan	North of Jiguanshan	North of Jiguanshan	Southeast of Dengta	East of Dengta
Longitude and latitude	N41°00'11" E123°44'51"	N40°57'41" E123°44'57"	N41°22'24" E123°34'56"	N41°23'07" E123°36'55"	N41°22'50" E123°38'27"	N41°23'41" E123°31'03"	N41°25'50" E123°36'11"
Age		2489±20 Ma				2500±24 Ma	
SiO_2	72.76	72.25	74.65	81.49	75.60	71.46	74.21
TiO_2	0.17	0.27	0.10	0.11	0.01	0.36	0.15
Al_2O_3	14.22	13.81	13.40	9.52	13.10	14.02	13.62
Fe_2O_3	0.87	0.76	0.59	0.13	0.10	0.83	0.44
FeO	0.77	1.65	0.88	0.92	0.52	1.80	1.10
MnO	0.04	0.04	0.06	0.05	0.05	0.06	0.05
MgO	0.37	0.47	0.36	0.31	0.13	0.85	0.34
CaO	0.37	0.60	0.88	0.63	0.21	1.08	0.59
Na_2O	3.17	3.55	3.17	2.08	3.38	2.59	3.64
K_2O	5.63	4.85	5.15	3.71	5.91	5.11	4.79
P_2O_5	0.05	0.12	0.03	0.04	0.03	0.13	0.05
H_2O^+	0.80	0.88	0.70	0.54	0.38	0.94	0.60
LOL+CO_2	0.09	0.17	0.09	0.09	0.12	0.09	0.09
Total	99.31	99.42	100.06	99.62	99.54	99.32	99.67
K_2O/Na_2O	1.78	1.37	1.62	1.78	1.75	1.97	1.32
Cr	7	18	21	24	8	20	8
Ni	3	8	8	11	4	11	6
Sc	2	4	3	2	1	6	3
Rb	206	238	195	94	105	177	157
Ba	600	944	307	1015	568	1049	369
Sr	61	77	122	188	80	209	63
Nb	10.0	21.2	7.7	2.1	0.8	12.6	11.0
Ta	0.7	2.1	2.1	0.3	0.2	1.1	1.5
Hf	5.4	8.0	3.6	2.1	1.4	9.7	4.8
Zr	149	267	82	63	35	371	138
Y	22	33	27	4	3	25	26
Th	49.3	38.2	20.0	12.0	5.8	49.7	27.2
U	5.5	22.4	8.6	1.3	1.1	4.0	3.1
La	69.90	70.40	21.40	25.30	11.30	103.00	30.00
Ce	128.00	131.00	40.30	37.30	17.00	181.00	64.50
Pr	12.50	13.60	4.64	4.02	1.74	20.60	5.58
Nd	41.20	45.50	16.20	13.60	5.78	65.70	18.50
Sm	8.13	7.57	3.52	1.92	0.90	10.30	3.78
Eu	0.54	0.69	0.50	0.66	0.20	1.23	0.42
Gd	6.40	6.38	3.62	1.51	0.67	7.51	3.87
Tb	0.91	0.97	0.60	0.18	0.11	1.02	0.71
Dy	4.89	6.15	4.30	0.97	0.55	5.57	4.56
Ho	0.89	1.27	0.98	0.16	0.08	1.00	1.02
Er	2.22	3.79	3.15	0.45	0.26	2.77	3.06
Tm	0.26	0.56	0.50	0.05	0.03	0.38	0.48
Yb	1.56	3.62	3.59	0.31	0.25	2.22	2.85
Lu	0.23	0.54	0.56	0.06	0.05	0.33	0.45
ΣREE	277.6	292.0	103.9	86.5	38.9	402.6	139.8
$(La/Yb)_n$	29.5	12.8	3.9	53.8	29.8	30.6	6.9
Eu/Eu*	0.22	0.30	0.43	1.15	0.76	0.41	0.34
Ba/Ba*	0.17	0.30	0.16	0.95	0.70	0.31	0.17

diagram (fig. 7). These rocks show large variations in ΣREE and $(La/Yb)_n$ ratios, and most have negative Eu anomalies. Based on REE patterns, two types of syenogranite can be recognized. Type 1 is enriched in LILE and depleted in Ba, Nb, Ta, P, Ti, Sc and

TABLE 2

(Continued)

No.	15	16	17	18	19	20	21
Sample no.	A1237	A1239	A1240	A1243	Q-030	Q-040	Q-041
Rock type	Weakly deformed syenogranite	Weakly deformed syenogranite	Weakly deformed syenogranite	Weakly deformed syenogranite	Syenogranite	Syenogranite	Syenogranite
Sample location	Northeast of Dengta	Northeast of Dengta	Northeast of Dengta	East of Dengta	Anshan-Benxi	Anshan-Benxi	Anshan-Benxi
Longitude and latitude	N41°28'23" E123°30'36"	N41°28'31" E123°30'30"	N41°28'29" E123°30'30"	N41°27'41" E123°34'55"			
Age		2523±29 Ma					
SiO_2	75.16	70.69	74.78	72.27	73.65	69.13	74.50
TiO_2	0.07	0.28	0.05	0.13	0.12	0.20	0.13
Al_2O_3	13.14	14.45	13.55	14.57	13.75	15.79	14.12
Fe_2O_3	0.41	0.34	0.21	0.78	1.33	2.23	1.69
FeO	0.48	2.48	0.66	0.70	0.29	0.13	0.13
MnO	0.04	0.05	0.04	0.04	0.08	0.05	0.05
MgO	0.16	0.66	0.28	0.34	0.15	0.31	0.22
CaO	0.12	1.21	0.43	1.19	0.67	0.60	0.38
Na_2O	3.70	3.47	3.47	2.96	3.14	3.22	3.63
K_2O	5.55	4.98	5.33	5.74	5.30	6.32	4.81
P_2O_5	0.03	0.07	0.04	0.02	0.09	0.10	0.08
H_2O^+	0.42	0.64	0.54	0.58	0.63	0.87	0.56
LOL+CO_2	0.09	0.09	0.09	0.09			
Total	99.37	99.41	99.47	99.41	99.20	98.95	100.30
K_2O/Na_2O	1.50	1.44	1.54	1.94	1.69	1.96	1.33
Cr	7	14	6	52			
Ni	3	6	3	16			
Sc	1	4	1	2			
Rb	109	172	133	119			
Ba	670	552	598	2189			
Sr	70	101	121	372			
Nb	5.1	15.2	3.0	3.3			
Ta	0.7	1.3	0.4	0.5			
Hf	5.1	10.6	2.9	4.6			
Zr	136	355	77	148			
Y	16	74	6	3			
Th	36.1	87.2	18.6	6.2			
U	4.7	52.8	2.5	1.1			
La	53.10	110.00	23.60	17.10	34.40	36.47	48.89
Ce	82.20	213.00	47.80	27.50	63.57	87.25	76.81
Pr	9.95	21.70	4.61	2.54	7.08	7.20	8.50
Nd	34.90	73.80	15.40	8.50	30.59	30.69	33.09
Sm	6.38	14.80	2.77	1.28	5.52	5.29	5.71
Eu	0.81	0.86	0.79	1.22	0.33	0.41	0.46
Gd	5.62	14.00	2.21	0.87	4.94	4.98	4.96
Tb	0.71	2.29	0.31	0.12	0.82	0.91	0.96
Dy	3.60	14.80	1.49	0.61	4.95	5.35	6.49
Ho	0.68	2.82	0.26	0.12	0.84	0.95	1.23
Er	1.73	7.71	0.62	0.36	2.37	2.68	3.78
Tm	0.23	1.03	0.09	0.05	0.34	0.39	0.53
Yb	1.35	5.77	0.45	0.42	1.97	2.32	3.22
Lu	0.22	0.90	0.07	0.07	0.27	0.31	0.40
ΣREE	201.5	483.5	100.5	60.8	158.0	185.2	195.0
$(La/Yb)_n$	25.9	12.6	34.5	26.8	11.5	10.4	10.0
Eu/Eu*	0.41	0.18	0.95	3.37	0.19	0.24	0.26
Ba/Ba*	0.29	0.11	0.37	2.42			

Cr and shows strong negative Eu anomalies, but displays large variations in LREE to HREE differentiation, with average $(La/Yb)_n$ being 5.5, 11.9 and 30.3, respectively (table 2; figs. 8A–8F). Type 2 syenogranite has no obvious negative Eu anomalies and

TABLE 2
(Continued)

No.	22	23	24	25	26
Sample no.	A1215	A1126	A1124	A1235	A1228
Rock type	Gneissic K-rich granite	Banded granodiorite	Gneissic quartz monzonite	Gneissic quartz monzonite	Gneissic monzogranite
Sample location	Northwest of Lianshanguan	North of Jiguanshan	North of Jiguanshan	North of Jiguanshan	North of Jiguanshan
Longitude and latitude	N40°59'17" E123°44'12"	N41°22'43" E123°38'42"	N41°22'54" E123°38'15"	N41°22'53" E123°38'15"	N41°23'56" E123°35'33"
Age		2517±19 Ma	2507±20 Ma	2507±20 Ma	2512±10 Ma
SiO_2	74.47	66.28	68.41	69.36	67.27
TiO_2	0.13	0.40	0.33	0.32	0.54
Al_2O_3	13.97	14.52	14.83	14.85	14.50
Fe_2O_3	0.29	2.50	1.48	0.96	1.95
FeO	0.54	2.03	1.87	2.19	2.01
MnO	0.04	0.08	0.11	0.07	0.08
MgO	0.21	2.32	1.41	1.61	1.31
CaO	0.77	3.66	2.60	2.31	2.16
Na_2O	4.23	3.50	2.56	2.28	3.46
K_2O	4.23	3.04	4.52	4.18	4.87
P_2O_5	0.01	0.15	0.13	0.13	0.31
H_2O^+	0.42	0.86	0.90	1.10	0.76
LOL+CO_2	0.09	0.10	0.19	0.24	0.09
Total	99.40	99.44	99.34	99.60	99.31
K_2O/Na_2O	1.00	0.87	1.77	1.83	1.41
Cr	7	73	44	50	37
Ni	4	38	21	26	17
Sc	1	10	6	5	9
Rb	133	103	171	169	180
Ba	1863	929	1142	1211	1226
Sr	166	485	308	278	356
Nb	7.5	6.0	6.5	6.1	15.6
Ta	1.1	0.7	0.7	0.6	1.9
Hf	2.0	4.3	5.1	4.1	7.2
Zr	49	160	195	143	270
Y	3	14	11	7	20
Th	25.4	15.8	20.3	14.7	15.2
U	2.2	3.0	2.8	1.6	3.4
La	40.90	42.10	52.60	65.30	68.20
Ce	73.90	66.90	86.60	97.30	165.00
Pr	6.76	7.41	8.86	10.10	13.60
Nd	21.30	26.10	30.50	33.30	45.70
Sm	3.13	4.51	4.87	4.27	7.26
Eu	0.69	1.21	1.02	1.15	1.29
Gd	1.95	3.34	2.88	2.83	5.41
Tb	0.18	0.49	0.41	0.30	0.74
Dy	0.78	2.42	2.11	1.54	4.67
Ho	0.15	0.45	0.36	0.29	0.91
Er	0.37	1.31	1.03	0.79	2.70
Tm	0.06	0.20	0.12	0.10	0.40
Yb	0.35	1.20	0.85	0.63	2.84
Lu	0.06	0.17	0.12	0.09	0.44
ΣREE	150.6	157.8	192.3	218.0	319.2
$(La/Yb)_n$	77.0	23.1	40.8	68.3	15.8
Eu/Eu^*	0.80	0.92	0.77	0.96	0.61
Ba/Ba^*	0.96	0.71	0.61	0.77	0.74

Note: 1) Major element in %, trace and REE elements in ppm; 2) Nos. 1-3 and 19-21 are from Wan and others (2012) and Wu and others (1998), respectively. Rest is from this study.

Ba depletion (figs. 8G and 8H). The K-rich granite shows similar geochemical features as the type 2 syenogranite (table 2, figs. 7, 8I and 8J), except for a lower K_2O/Na_2O ratio. The granodiorite and quartz monzonite are also similar in their REE patterns

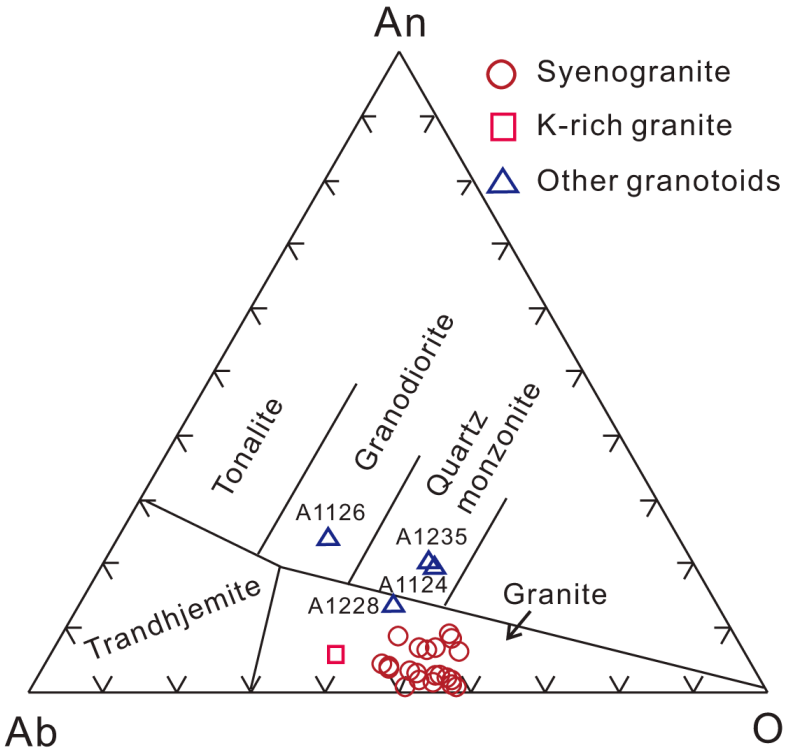

Fig. 7. Modal An–Ab–Or diagram for late Neoarchean magmatic rocks in the Anshan-Benxi area, North China Craton. See notes in table 2 for data sources.

and trace element distribution to but are higher in ΣREE contents than type 2 syenogranite (table 2, figs. 8K and 8L). Compared with type 1 syenogranite, the monzogranite has a weak negative Eu anomaly and Ba depletion (figs. 8K and 8L).

Whole-Rock Nd Isotopic Compositions

Nd isotope data of the 2.5 Ga rocks are listed in table 3 and shown in figure 9. Twenty one syenogranite samples of the Qidashan Pluton have $\varepsilon_{Nd(t)}$ values of –10.5 to –2.7. Correspondingly, they have old Nd depleted mantle model ages ranging from 2.96 to 3.90 Ga with the exception of samples A1214 and 1226 which have $\varepsilon_{Nd(t)}$ values of +3.6 to +3.7 and Nd depleted mantle model ages of 2.55 to 2.58 Ga. Compared with the syenogranites, the other granitoids have high $\varepsilon_{Nd(t)}$ values (–2.2 to –6.1) and young model ages of 2.95 to 3.19 Ga.

Zircon Hf Isotopic Composition

Hf-in-zircon isotope data from the dated 2.5 Ga rocks are listed in table A1 in the Appendix and shown in figures 10A and 10B. Thirty-nine analyses on magmatic zircon from the syenogranites of the Qidashan Pluton yielded $\varepsilon_{Hf(t)}$ values and crustal model ages ($t_{cc(Hf)}$) ranging from –11.0 to +4.4 and 2.70 to 3.46 Ga, respectively, with the exception of analysis 1-1MA for sample A0713 which has a higher $\varepsilon_{Hf(t)}$ value of +7.6 and younger model age of 2.54 Ga. Magmatic zircon from the other granitoids commonly has lower $\varepsilon_{Hf(t)}$ values and older crustal model ages and ranges from –16.0 to +2.4 and 2.81 to 3.72 Ga, respectively (47 analyses). However, xenocrystic zircon from all these rocks are similar in Hf isotope composition. Fourteen analyses on

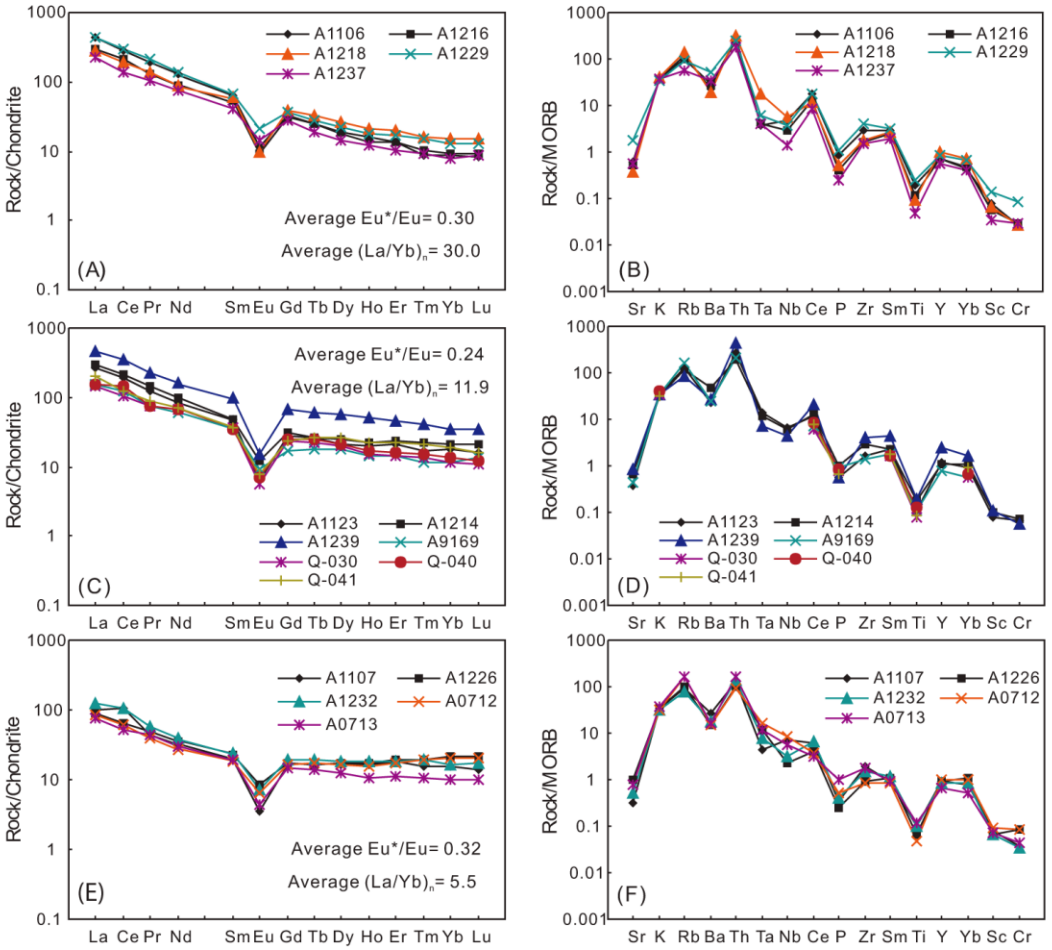

Fig. 8. REE and trace element distribution patterns for late Neoarchean magmatic rocks in the Anshan-Benxi area, North China Craton. (A)-(F) type 1 syenogranite showing variations in LREE to HREE differentiation; (G) and (H) type 2 syenogranite; (I) and (J) K-rich granite; (K) and (L) other granitoids. See notes in table 2 for data sources. REE-normalizing values after Masuda (1975) and rock/MORB values after Pearce (1983).

xenocrystic zircon from the syenogranites have $\varepsilon_{Hf(t)}$ values of –12.2 to +8.3 and model ages of 3.06 to 3.88 Ga, and xenocrystic zircon from the other granitoids has $\varepsilon_{Hf(t)}$ values and Hf model ages of –14.0 to +5.0 and 2.79 to 3.93 Ga, respectively (25 analyses).

O-in-Zircon Isotopic Compositions

O-in-zircon isotopic data from the 2.5 Ga granitoids of this study and previously published values are listed in table A2 in the Appendix and are shown in figures 11A to 11D. Most low-U magmatic zircon (U<200 ppm) from the syenogranites of the Qidashan Pluton have $\delta^{18}O$ values in the range of +5.1 to +7.2 permil, typical of unaltered, juvenile crustal Archean zircon (Valley and others, 2005). Five zircon analyses from sample A0713 have $\delta^{18}O$ values up to +10.9 permil (Wan and others, 2013). Analysis A1123-1.1MA has a very low $\delta^{18}O$ value of +1.6 permil, but the analyzed zircon domain contains high common lead (table 1). Therefore, we suspect that the low $\delta^{18}O$ value is due to the analytical spot being partly placed on fluid-bearing mineral inclusion(s) or low $\delta^{18}O$ metamict areas. Most high-U magmatic zircons (U>200 ppm)

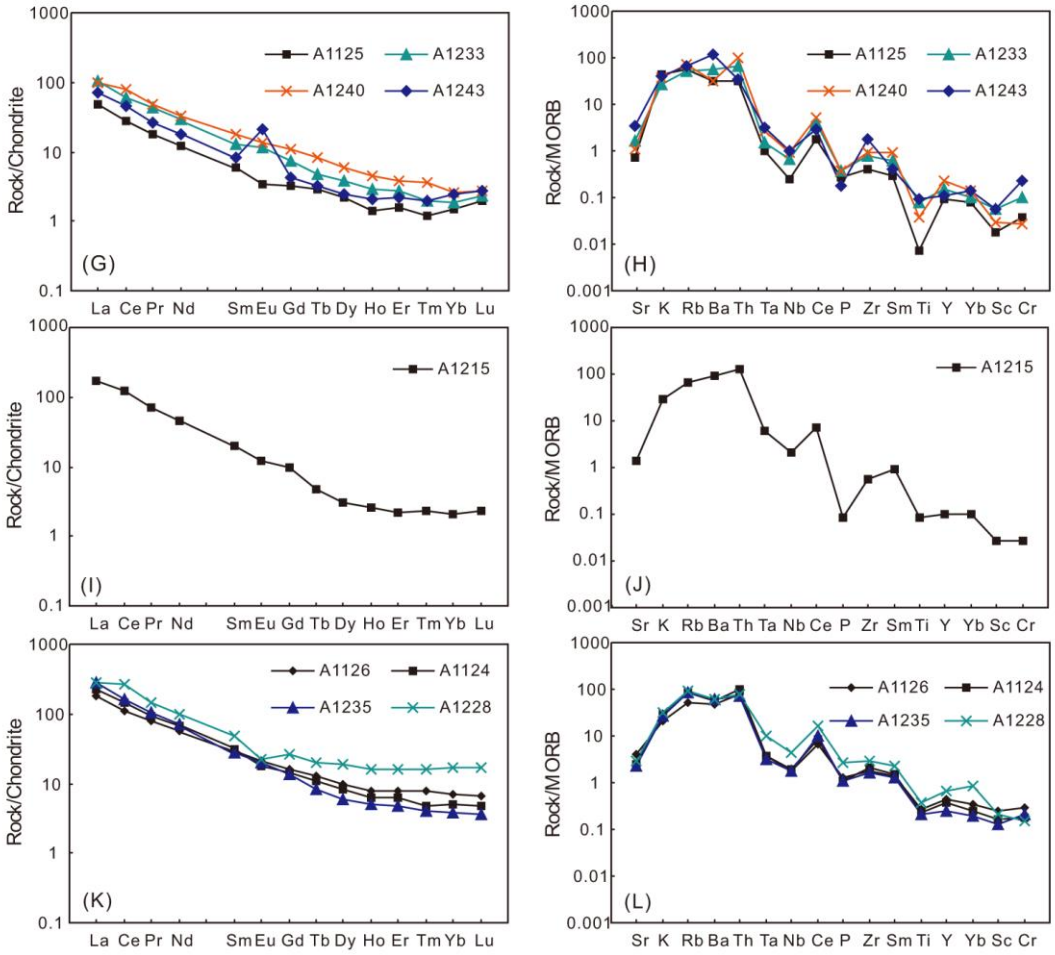

Fig. 8. (continued)

have similar $\delta^{18}O$ values to those with low U contents, ranging from +4.5 to +6.9 permil (figs. 11A and 11B), with the exception of three analyses on high-U magmatic zircons from sample A1232 yielding very low $\delta^{18}O$ values of +2.5 to +3.1 permil, again possibly due to metamictization. Low-U magmatic zircon from other granitoids has similar $\delta^{18}O$ values to that from the syenogranites of the Qidashan Pluton, ranging from +4.0 to +6.9 permil (figs. 11C and 11D). Compared with the syenogranites, however, high-U magmatic zircon from these rocks has low $\delta^{18}O$ values (between +1.8 and +7.0‰) (figs. 11C and 11D).

Low- and high-U xenocrystic zircons from the Qidashan Pluton have $\delta^{18}O$ values ranging from +3.9 to +5.0 permil and +0.3 to +6.6 permil, respectively (figs. 11A and 11B); Low- and high-U xenocrystic zircons from other granitoids have $\delta^{18}O$ values ranging from +3.0 to +6.8 permil and +1.8 to +6.2 permil, respectively (figs. 11C and 11D). The O isotope values of many high-U xenocrystic zircons plot in the field of Archean magmatic zircon as defined by Valley and others (2005).

DISCUSSION

Formation Ages

We obtained magmatic zircon ages of *ca.* 2.5 Ga for samples A0713, A1123, A1124, A1126, A1214, A1228, A1229, A1235 and A1239. Some ages have very big errors mainly

TABLE 3

Whole-rock Nd isotopic compositions of late Neoarchean magmatic rocks in the Anshan-Benxi area, North China Craton

No.	Sample no.	Rock type	Age (Ma)	Sm (ppm)	Nd (ppm)	$\frac{^{147}Sm}{^{144}Nd}$	$\frac{^{143}Nd}{^{144}Nd}$	2σ	$f_{Sm/Nd}$	$\varepsilon_{Nd(0)}$	$\varepsilon_{Nd(t)}$	$t_{DM(Nd)}$ (Ga)
1	A1106	Massive syenogranite	2500	9.03	56.34	0.0970	0.510781	5	-0.51	-36.2	-4.2	3.07
2	A1123	Gneissic syenogranite	2512±29	6.28	33.31	0.1140	0.510863	8	-0.42	-34.6	-8.0	3.47
3	A1107	Gneissic syenogranite	2500	3.21	14.69	0.1321	0.511040	11	-0.33	-31.2	-10.5	3.90
4	A1125	Gneissic syenogranite	2500	1.28	7.16	0.1079	0.510886	7	-0.45	-34.2	-5.7	3.24
5	A1214	Weakly deformed syenogranite	2489±20	7.10	42.35	0.1014	0.511260	6	-0.48	-26.9	3.7	2.55
6	A1216	Gneissic syenogranite	2500	6.88	37.54	0.1109	0.510807	12	-0.44	-35.7	-8.4	3.45
7	A1218	Massive syenogranite	2500	7.75	37.51	0.1251	0.511083	5	-0.36	-30.3	-7.5	3.53
8	A1226	Massive syenogranite	2500	3.90	21.21	0.1112	0.511409	10	-0.43	-24.0	3.6	2.58
9	A1229	Gneissic syenogranite	2502±30	9.71	64.23	0.0914	0.510732	9	-0.54	-37.2	-3.4	2.99
10	A1232	Gneissic syenogranite	2500	4.21	21.06	0.1210	0.510878	5	-0.38	-34.3	-10.3	3.70
11	A1233	Gneissic syenogranite	2500	1.37	9.48	0.0873	0.510646	5	-0.56	-38.9	-3.8	3.00
12	A1237	Weakly deformed syenogranite	2500	6.16	32.34	0.1151	0.511031	10	-0.41	-31.3	-5.3	3.25
13	A1239	Weakly deformed syenogranite	2523±29	13.45	67.25	0.1210	0.511113	5	-0.38	-29.7	-5.3	3.32
14	A1240	Weakly deformed syenogranite	2500	2.45	13.26	0.1119	0.511007	5	-0.43	-31.8	-4.7	3.19
15	A1243	Weakly deformed syenogranite	2500	1.06	6.85	0.0936	0.510804	10	-0.52	-35.8	-2.7	2.96
16	A-7	Syenogranite	2500	2.36	17.73	0.0805	0.510252	7	-0.59	-46.5	-9.2	3.29
17	A-44	Syenogranite	2500	4.02	19.37	0.1257	0.510995	8	-0.36	-32.0	-9.3	3.70
18	A-125	Syenogranite	2500	3.45	19.69	0.1060	0.510676	9	-0.46	-38.3	-9.2	3.47
19	A-126	Syenogranite	2500	7.48	39.03	0.1158	0.510865	5	-0.41	-34.6	-8.6	3.53
20	A9169	Syenogranite	2500	5.81	29.11	0.1208	0.511152	5	-0.39	-29.0	-4.6	3.25
21	G9502	Syenogranite	2500	2.13	9.22	0.1396	0.511369	13	-0.29	-24.8	-6.4	3.63
22	A1126	Banded granodiorite	2517±19	3.62	21.17	0.1035	0.510827	5	-0.47	-35.3	-5.2	3.19
23	A1124	Gneissic quartz monzonite	2507±20	4.12	27.13	0.0919	0.510727	7	-0.53	-37.3	-3.5	3.01
24	A1215	Gneissic K-rich granite	2500	2.62	17.61	0.0899	0.510576	7	-0.54	-40.2	-6.1	3.15
25	A1228	Gneissic monzogranite	2512±10	5.50	34.16	0.0974	0.510883	13	-0.50	-34.2	-2.2	2.95
26	A1228E	Gneissic monzogranite	2512±10	6.44	33.67	0.1157	0.51118	8	-0.41	-28.4	-2.3	3.04
27	A1235	Gneissic quartz monzonite	2507±20	3.68	28.34	0.0786	0.510504	6	-0.60	-41.6	-3.7	2.97

Note: 1) Ages are estimated excepting those with errors; 2) Nos. 16-19 and 20-21 are from Qiao and others (1990) and Wan and others (2012), respectively. Rest is from this study.

due to high common lead contents and lead loss from zircons with high U and Th contents. No magmatic zircon ages have been obtained for samples A1106, A1218, A1226, A1237, A1240 and A1243. However, none or weak deformation can be used as a fingerprint to ensure their emplacement at the end of the Neoarchean, because many dated syenogranites are ~2.5 Ga in age and no Paleoproterozoic magmatism has been identified in the area. Some deformed rocks may also be late Neoarchean. Syenogranites represented by samples A0712 and A1232 show deformation, but they were intruded into 2.52 to 2.55 Ga BIF-bearing supracrustal rocks (the Anshan "Group"), so they must be younger than 2.52 Ga. The syenogranites of the 2.5 Ga Qidashan Pluton and the K-rich granites of the 2.9 to 3.0 Ga Tiejiashan Pluton are similar in their trace element compositions with both showing strong negative Eu anomalies (Wan and others, 1998, 2002; Wu and others, 1998; this study). The deformed Qidashan Pluton is also easy to confuse with the Tiejiashan Pluton in the field, especially when weathered. However, the Qidashan Pluton commonly exhibits higher K_2O/Na_2O ratios than the Tiejiashan Pluton. Therefore, we contend that major element compositions can be used as a fingerprint to estimate the formation age for the remaining samples, such as A1107, A1125 and A1233 of this study and Q-030, Q-040 and Q-041 from the literature (Qiao and others, 1990). Based on the present study and previous work, the Qidashan Pluton is composed mainly of syenogranite with some K-rich granite. Besides this, there are a few other *ca.* 2.5 Ga granitoids such as granodiorite, quartz monzonite and monzogranite.

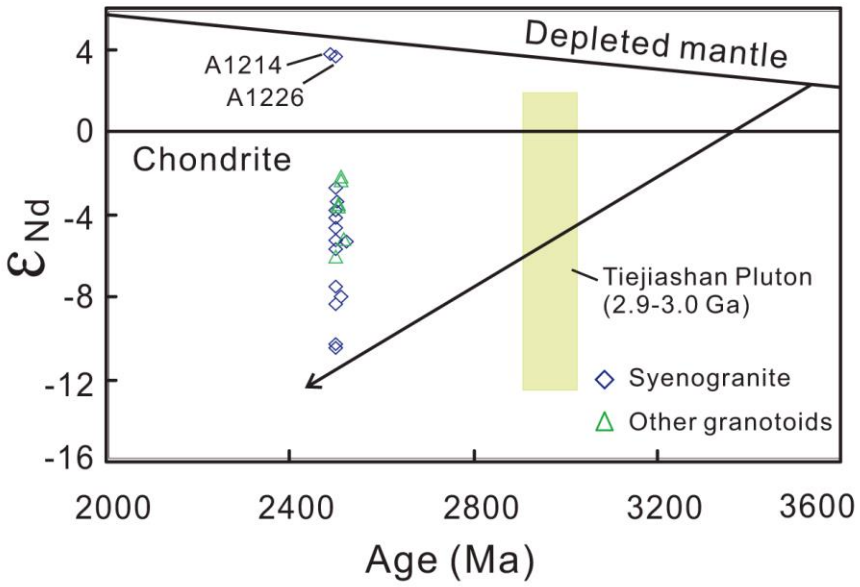

Fig. 9. Age vs. whole-rock $\varepsilon_{Nd(t)}$ diagram for late Neoarchean magmatic rocks in the Anshan-Benxi area, North China Craton. See notes in table 3 for data sources. Data of the Tiejiashan Pluton are from Dong C.Y. (unpublished data).

Relationships Between Zircon U Content, Discordance, $\delta^{18}O$ and $\delta^{16}O^1H$

For zircon from other granitoids (quartz monzonite and monzogranite) U content, discordance, $\delta^{18}O$ and $\delta^{16}O^1H$ show linear variations (figs. 12A–12F). High-U content causes radiation damage in zircon but does not necessarily result in strong lead loss (Geisler and others, 2002). Therefore, the positive variation between U content and discordance suggests that the zircon underwent post-crystallization alteration (Silver and Deutsch, 1963; Pidgeon and others, 1966; Black, 1987) during which

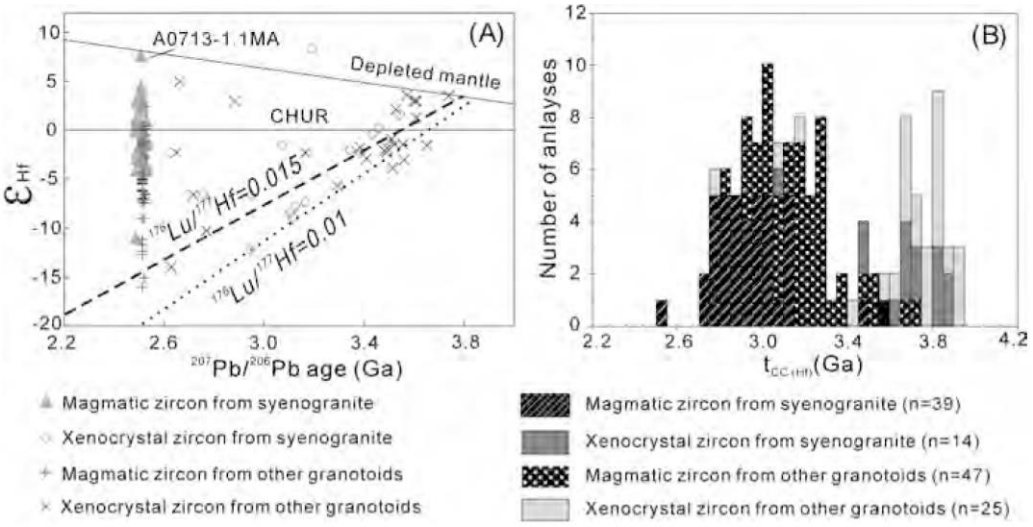

Fig. 10. Hf-in-zircon isotopic compositions for late Neoarchean magmatic rocks in the Anshan-Benxi area, North China Craton. (A) Zircon age vs. $\varepsilon_{Hf(t)}$ diagram; (B) zircon crustal model age histogram. Dotted and dashed lines represent felsic crust with $^{176}Lu/^{177}Hf$ being 0.01 and 0.015, respectively.

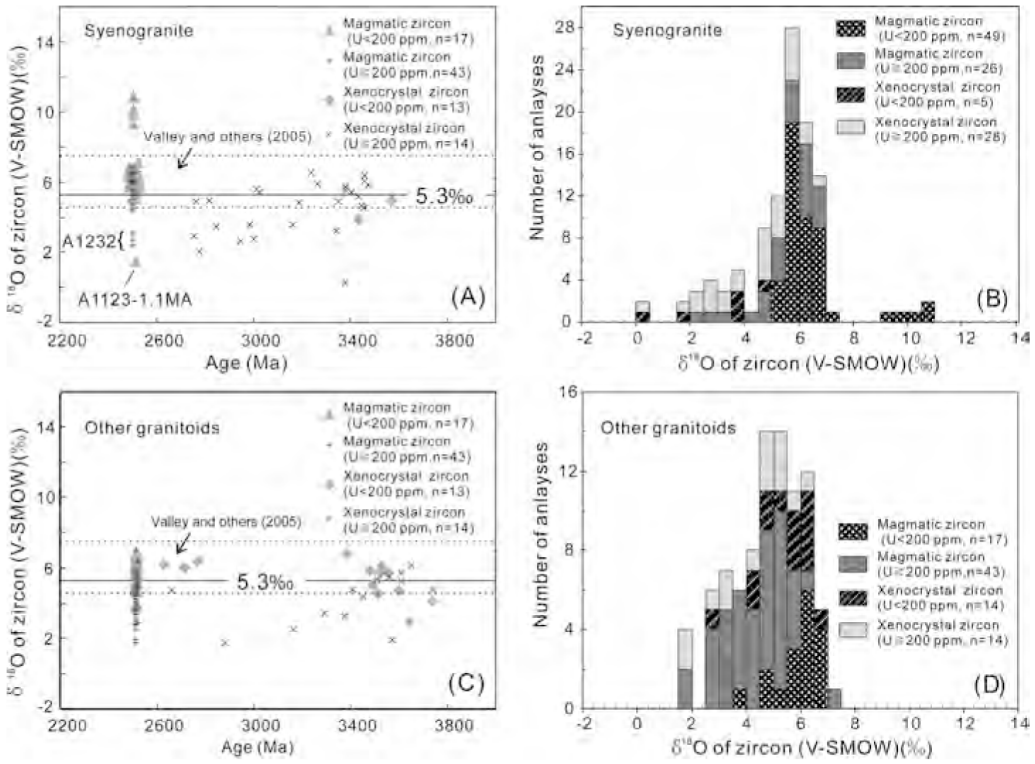

Fig. 11. O-in-zircon isotopic compositions for zircon analyses from late Neoarchean magmatic rocks in the Anshan-Benxi area, North China Craton. (A) and (B) Syenogranite; (C) and (D) other granitoids.

process fluid-bearing mineral(s) formed in the damaged areas within the zircon (Geisler and others, 2007) as indicated by positive relationships between U content, discordance and $\delta^{16}O^{1}H$ (figs. 12A, 12B and 12C). Water is low in $\delta^{18}O$ and this may be the reason why $\delta^{18}O$ shows negative relationships with U content, discordance and $\delta^{16}O^{1}H$ (figs. 12D, 12E and 12F). This further supports the conclusion that strong radiogenic Pb loss from zircon can be used as an indicator that the zircon $\delta^{18}O$ is likely to be of secondary origin (Booth and others, 2005; Valley and others, 2005; Wan and others, 2013). It may be concluded that radiation damage does not necessarily result in decreasing $\delta^{18}O$ values in high-U zircon if the zircon has not undergone post-crystallization alteration.

For zircon from syenogranites of the Qidashan Pluton, U content and discordance roughly show a positive correlation (fig. 12A), suggesting that damaged zircon underwent late alteration. Being different from zircons from other granitoids, however, U content and discordance show only weak correlations with $\delta^{18}O$ and $\delta^{16}O^{1}H$ (figs. 12B–12F). This may indicate that additional factors must be considered. Some zircon grains have $\delta^{18}O$ values in the normal Archean range (+4.6 to +7.5‰) but show strong lead loss. This means that their O isotopic compositions cannot be assumed to be primary, and the zircon might have had higher $\delta^{18}O$ values (fig. 12E).

Origin of the Magmatic Rocks

The Qidashan Pluton is composed mainly of syenogranite, with some K-rich granite, characterized by high SiO_2 and K_2O and low CaO, FeOt and MgO. All samples plot in the peraluminuous field in an A/CNK-A/NK diagram (fig. 13), although they are also rich in alkaline compositions (K_2O+Na_2O). They are low in Sr and high in Y

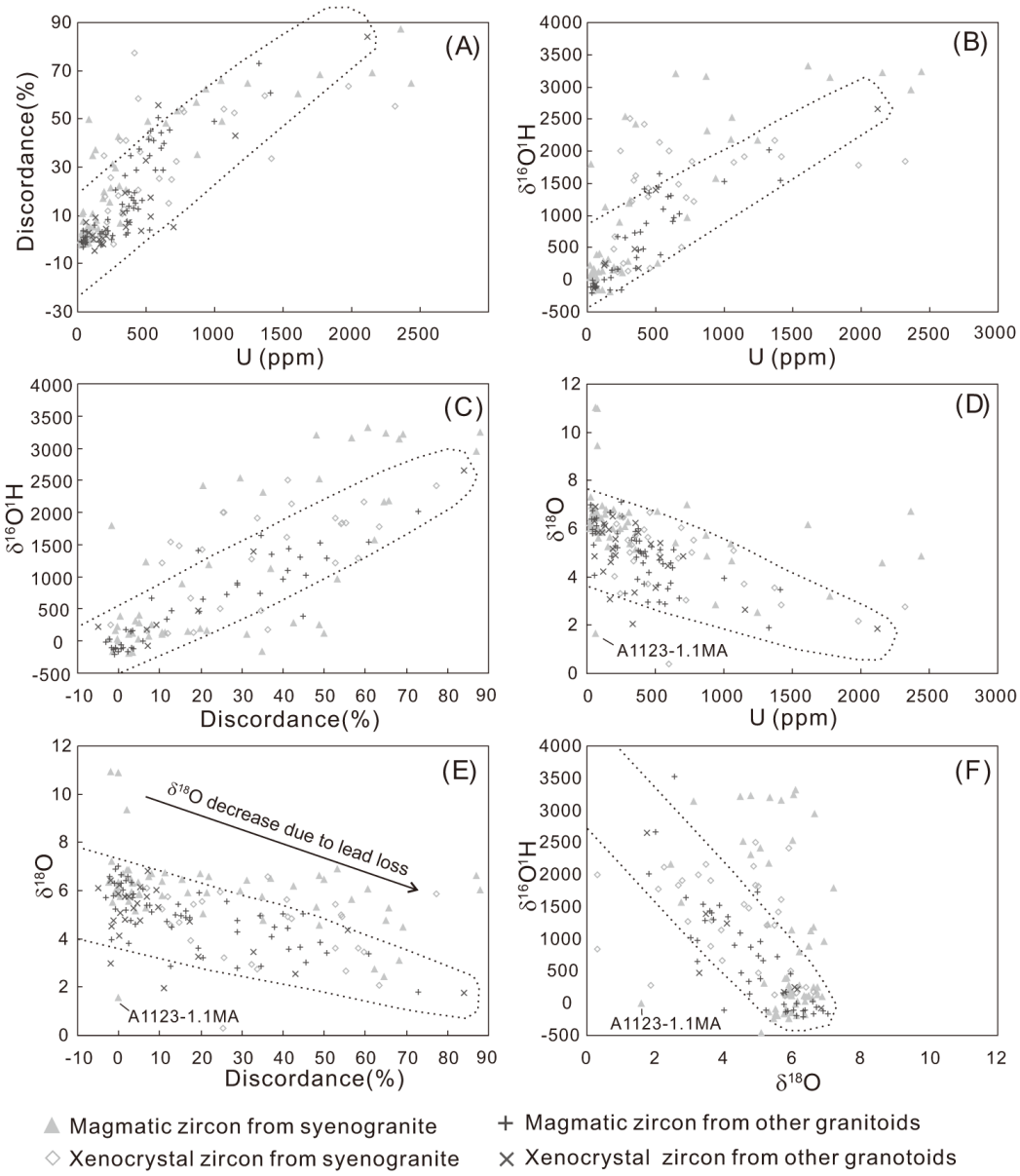

Fig. 12. Relationships between U content, discordance, $\delta^{18}O$ and $\delta^{16}O^1H$ in zircon from late Neoarchean magmatic rocks in the Anshan-Benxi area, North China Craton. (A) U vs, discordance; (B) U vs. $\delta^{16}O^1H$; (C) discordance vs. $\delta^{16}O^1H$; (D) U vs. $\delta^{18}O$; (E) discordance vs. $\delta^{18}O$; (F) $\delta^{18}O$ vs. $\delta^{18}O^1H$. An analysis with U >10000 ppm is not shown.

and Yb and plot below the potassic granitoid area in a Y-Sr/Y diagram and in or below the potassic granitoid field in a Yb-La/Yb diagram (figs. 14A and 14B). Most of the rocks are similar in displaying negative Eu anomalies and Ba, Nb, Ta, P and Ti depletion, but show large variations in ΣREE contents and $(La/Yb)_n$ ratios. The latter probably reflects the features of their source regions and cannot be explained only by magma crystallization and melt-crystal mixture. The $\varepsilon_{Nd(t)}$ values show a large variation but commonly are lower than zero, and many have whole-rock $t_{DM(Nd)}$ model ages up to 3.5 Ga. Most magmatic zircons have $\varepsilon_{Hf(t)}$ values lower than +5, with a few having Hf crustal model ages up to 3.5 Ga. As mentioned above, strong lead loss causes

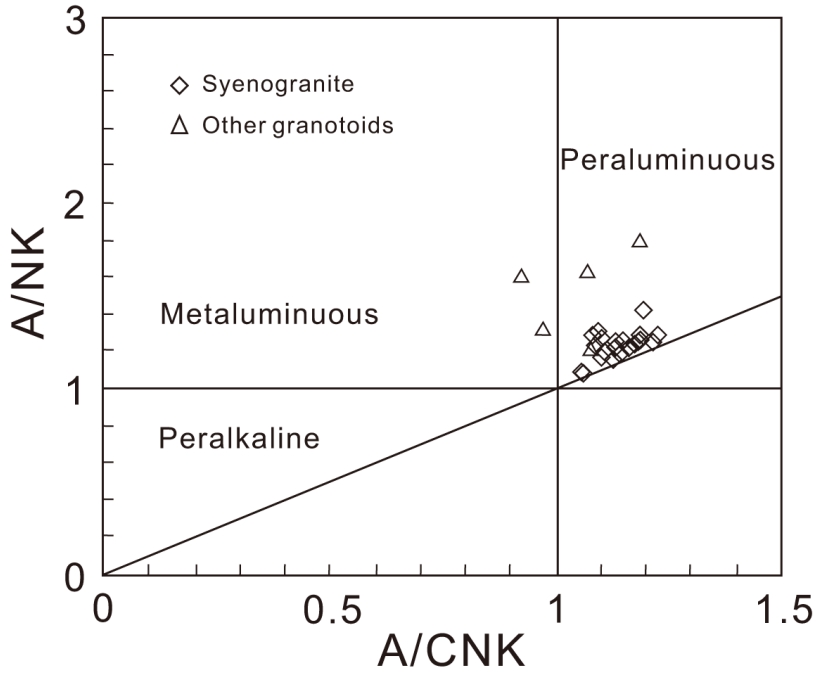

Fig. 13. A/CNK-A/NK diagram for late Neoarchean magmatic rocks in the Anshan-Benxi area, North China Craton.

decreasing $\delta^{18}O$ values in damaged zircon, therefore, "primary" (undamaged) magmatic zircon of the syenogranites should display a large $\delta^{18}O$ variation although only a few of magmatic zircon grains have $\delta^{18}O$ values higher than 7.5 permil. We speculate that at least some magmatic zircon grains originally had higher $\delta^{18}O$ values. All these features reveal that the 2.5 Ga syenogranites of the Qidashan Pluton are derived from old continental crust, including mature metasedimentary material with long crustal residence times. The conclusion that recycling of older crust played an important role in the petrogenesis of the syenogranites is supported by numerous old xenocrystic

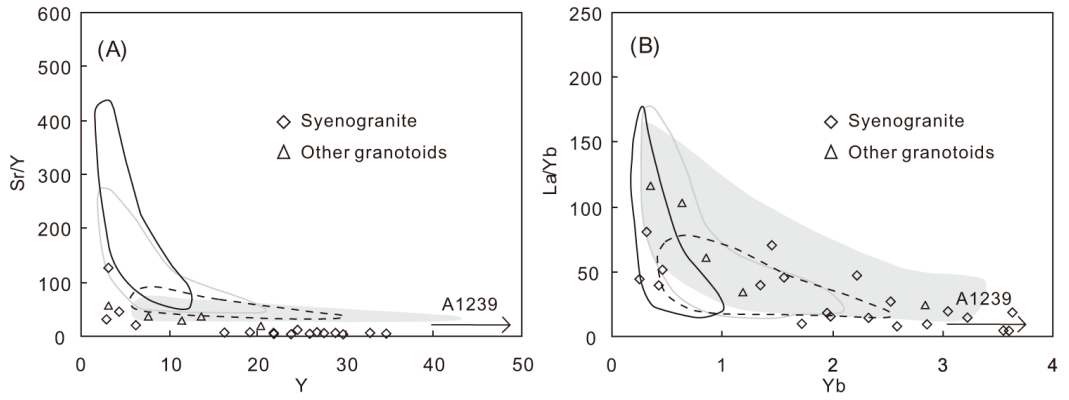

Fig. 14. Y-Sr/Y (A) and Yb-La/Yb (B) diagrams (Moyen, 2011) for late Neoarchean magmatic rocks in the Anshan-Benxi area, North China Craton. Shaded area: potassic granitoid; black line: high-pressure TTG; gray line: medium-pressure TTG; dotted line: low-pressure TTG. Sample A1239 has high Y and Yb contents (74 and 5.77 ppm) and plots outside the figures.

zircon cores and restitic biotite in some syenogranite samples. Widespread syenogranites with low whole-rock $\varepsilon_{Nd(t)}$ and magmatic zircon $\varepsilon_{Hf(t)}$ are consistent with a long crustal history up to 3.8 Ga in the Anshan-Benxi area. However, some syenogranite samples have $\varepsilon_{Nd(t)} > 0$ (fig. 9) and the magmatic zircons of some syenogranite samples (mainly A0713) have $\varepsilon_{Hf(t)} > 0$ (fig. 10A) although it is the same as many other syenogranites of type 1 in element composition and field appearance. It is uncertain whether this indicates juvenile addition from mantle source or recycling of early Neoarchean continental material. *Ca.* 2.7 Ga detrital zircon grains were discovered in the Anshan-Benxi area (Wan, 1993) although rocks of this age have not been identified.

Although there are abundant >3.4 Ga xenocrystic zircon cores, the syenogranites cannot have been derived exclusively from the >3.4 Ga rocks that have been identified in the Anshan-Benxi area. These are trondhjemitic in composition with very low REE contents (Wu and others, 1998; Wan and others, 2012b). However, contamination with >3.4 Ga rocks may have played a significant role in the formation of some syenogranites. The Qidashan Pluton is similar in geochemical compositions to the 2.9 to 3.0 Ga Tiejiashan Pluton which also shows strong negative Eu anomalies and Ba depletion with low whole-rock $\varepsilon_{Nd(t)}$ and zircon $\varepsilon_{Hf(t)}$ values (fig. 9). This may suggest that the Tiejiashan Pluton is an important candidate for the source region of the Qidashan Pluton. A conclusion can be drawn that there must be >3.4 Ga source rocks with relatively high K_2O/Na_2O ratios and REE contents in the Anshan-Benxi area from which the 2.9 to 3.0 Ga K-rich granites (the Tiejiashan Pluton) and 2.5 Ga syenogranites (the Qidashan Pluton) are derived, although these have not yet been identified.

Granodiorite, quartz monzonite and monzogranite occur locally in the Anshan-Benxi area and formed at the same time as the syenogranites of the Qidashan Pluton. The granodiorite and quartz monzonite are similar to type 2 syenogranite in showing high LREE/HREE ratios. The monzogranite is similar to type 1 syenogranite in its REE pattern but has weaker negative Eu and Ba anomalies. All these granotoid rocks have whole-rock $\varepsilon_{Nd(t)}$ and magmatic zircon $\varepsilon_{Hf(t)}$ values commonly < 0, and the undamaged magmatic zircon has $\delta^{18}O$ values within the normal range of Archean magmatic zircon (Valley and others, 2005). Combined with abundant xenocrystic zircon cores, we suggest that they may be products of mantle-crust interaction or melting of more mafic igneous rocks, similar to the high-K intermediate to felsic granites in the Rum Jungle Complex, Northern Australia (Drüppel and others, 2009), but older crust with long crustal residence times must play an important role in their fomation. Their geochemical differences from the syenogranites of the Qidashan Pluton indicate large compositional variations in the source region and /or magmatic processes during late Neoarchean magmatism in the Anshan-Benxi area. In any case, identification of abundant 3.3 to 3.8 Ga xenocrystic zircon cores in Waitoushan-Jiguanshan indicates that there is more than one area where Paleoarchean magmatism occurred in the Anshan-Benxi area, and 3.8 Ga rocks may be discovered in Waitoushan-Jiguanshan when more work is carried out.

It is notable that some granitoids show decoupling of whole-rock Nd and Hf-in-zircon isotopic compositions. For example, syenogranite (A1226), granodiorite (A1126) and quartz monzonite (A1124) samples have whole-rock $\varepsilon_{Nd(t)}$ and magmatic zircon $\varepsilon_{Hf(t)}$ values of +3.6/–5.2/–3.5 and –15.0 to –4.4/–15.0 to –4.4/–16.0 to –2.7 and $t_{DM(Nd)}$ and $t_{DM2(Hf)}$ model ages of 2.6/3.2/3.0 Ga and 3.2 to 3.7 Ga/3.2 to 3.7 Ga/3.1 to 3.7 Ga, respectively. This decoupling may suggest contamination of the original magmas by crustal material containing old zircon. In these rocks, some magmatic zircons are formed around old xenocrysts, but show oscillatory zoning and have high Th/U ratios (0.40–0.95) and are thus different from anatectic zircon which commonly

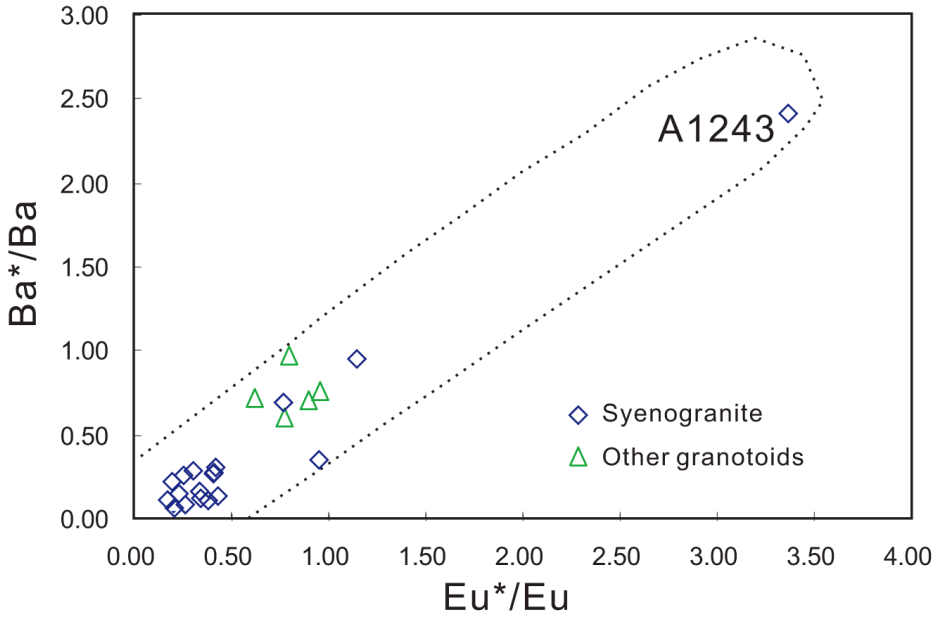

Fig. 15. Eu*/Eu vs. Ba*/Ba diagram for late Neoarchean magmatic rocks in the Anshan-Benxi area. See notes in table 2 for data sources. Eu*/Eu = 2×(Eu/0.0866)/((Sm/0.23)+(Gd/0.311)), Ba*/Ba = 2×(Ba/20)/((Rb/2)+(Th/0.2)). Normalization values for Sm, Eu and Gd after Masuda (1975) and for Rb, Ba and Th after Pearce (1983).

shows diffuse oscillatory zoning and low Th/U ratios (<0.3, mostly <0.1) (for example, Wan and others, 2009b). This suggests that at least some magmatic zircons were formed after contamination with old crustal material when the magmas ascended to higher crustal levels. The magmatic zircon probably formed by dissolution-reprecipitation of xenocrystic cores during magmatism and inherited the Hf isotopic composition from the old cores to variable degrees. This is similar to the formation of metamorphic overgrowth rims with Hf isotopic features inherited from zircon cores that have been identified as a result of dissolution-reprecipitation in previous studies (Dong and others, 2009; Xie and others, 2014). In the magmatic process, on the other hand, the whole-rock Nd isotopic compositions in the magmas did not noticeably change if the addition of old crustal material was not obvious, thus the contaminated magmas had Nd isotopic compositions being similar to original magmas. In this case, whole-rock Nd isotopes may record more reliably the crustal residence time of the source material from which the granitoids were derived. The magmas could not completely dissolve xenocrystic zircon grains, this may be due to the fact that their temperatures were relatively low when contamination occurred.

Considering all the rocks of this study, the Eu and Ba anomalies show a positive correlation (fig. 15). Type 1 syenogranite has low Eu*/Eu and Ba*/Ba values, most type 2 syenogranite and other granitoids have medium Eu*/Eu and Ba*/Ba values, whereas sample A1243 of type 2 syenogranite has very high Eu*/Eu and Ba*/Ba values. Although plagioclase fractionation decreases the Eu*/Eu values of magmatic rocks, the large Eu*/Eu and Ba*/Ba variations, even in syenogranites that are similar in major element composition, seem to mainly reflect differences in their source region. Many of the Late Neoarchean syenogranites from other areas of the NCC also show the same feature (Wan and others, 2012a). Rocks with low Eu*/Eu and Ba*/Ba values were most likely derived from a mature crustal source region.

Implication for the Archean Evolution of the NCC

The late Neoarchean tectonic evolution of the NCC is debated in the literature. Two main models are arc magmatism followed by collisional orogeny (Wu and others, 1998; Kröner and others, 2005; Wilde and others, 2005; Wan and others, 2010; Liu and others, 2011; Nutman and others, 2011; Peng and others, 2013; Wang and others, 2013) and magmatic underplating caused by mantle plumes (Zhao and others, 1998, 1999a, 2001; Geng and others, 2006; Yang and others, 2008; Wu and others, 2012, 2013a, 2013b). There were different opinions on the early phase (mainly 2.52–2.55 Ga) of the late Neorchean tectonic event (arc magmatism or underplating), but most authors suggested that the NCC was in an extensional tectonic setting at the end of the Neoarchean (mainly 2.50–2.52 Ga), probably resulting from the underplating of mantle derived magmas (Zhao and others, 1999b; Geng and others, 2006; Yang and others, 2008; Wan and others, 2010, 2012b; Nutman and others, 2011).

Wan (1993) suggested a scenario of back-arc basin evolution to interpret the formation of late Neoarchean supracrustal rocks (the Anshan "Group") in the Anshan-Benxi area. All *ca.* 2.5 Ga magmatic rocks identified in this study are potassic granitoids from granodiorite to syenogranite, which excludes an island-arc setting where Na-rich tonalite and trondhjemite should be formed. Furthermore, strong intracrustal recycling of continental crust and intrusion of crustally-derived granites into the supracrustal rocks indicate that the back-arc basin did not extend over a large region although the supracrustal rocks contain abundant MORB-like metabasalts (Zhai and others, 1990; Wan, 1993; Cui and others, 2013). A relatively stable environment may have been an important reason for the formation of a thick BIF deposit in the area during the late Neoarchean.

Some features relating to metamorphism, deformation, anatexis and the formation of the Qidashan syenogranites can be summarized as follows: 1) Many of the syenogranites show a massive texture with some showing gneissic structures; 2) some of these structures seem to be magmatic flow banding and are not related to deformation, but more work is required to confirm this; 3) undeformed syenogranite veins derived from the Qidashan pluton cut the Anshan "Group" rocks and older granitoids in different directions; 4) metamorphism and anatexis occurred at the same time or slightly earlier than formation of the syenogranites, and leucosome-rich material in anatectic supracrustal rocks and granitoids shows strong or weak deformation. These features indicate that the syenogranites formed syntectonically in a tectonic regime changing from compression to extension. Furthermore, geochemical studies indicate that the widespread syenogranites were generated through reworking (partial melting) of older crust. This reworking must have occurred in the upper and/or the middle crust rather than in the lower crust where melting would result in calc-alkaline TTG rocks, therefore requiring extra heat from mantle. The latter should be related to underplating due to upwelling of buoyant asthenosphere, consistent with the extensional setting. It is noted that the type 2 syenogranites without negative Eu*/Eu and Ba*/Ba anomalies and other granitoids mainly occur in the Waitoushan area. Some of these are considered to be products of mantle-crust interaction or melting of more mafic igneous rocks in the lower crust. Together with higher grade metamorphism, we speculate that magmatism occurred in the low crust and was strongly influenced by mantle material in the northeast of Anshan-Benxi compared with the southwest of Anshan-Benxi. Large-scale intracrustal recycling of old continental material signifies cratonic stability. More work is required to identify mantle-derived rocks (gabbro, diorite) of the same age to provide evidence for magmatic underplating.

Crustally-derived granites in rift settings commonly have low $\delta^{18}O$ values because their source has been affected by meteoric water with low $\delta^{18}O$ that has moved down along extensional structures (for example, Zheng and others, 2007). However, this has

not occurred in the ~2.5 Ga granitoids of the Anshan-Benxi area, probably indicating that reworking of old crust occurred during an early phase of extension.

As indicated in the introduction, at least three ancient terranes can be identified in the NCC. It is considered that the three ancient terranes, and possibly other old terranes, occurred in an oceanic domain, and amalgamation of these terranes due to subduction/collision resulted in the formation of supracrustal and intrusive rocks as well as juvenile additions and crustal recycling and finally assembled the NCC at the end of the Neoarchean (Wan and others, 2015). The Eastern Ancient Terrane includes Anshan-Benxi, eastern Hebei, eastern Shandong and western Shandong where ≥2.6 Ga rocks and zircon grains have been identified and 2.5 Ga crustally-derived granites formed by recycling of ≥2.6 Ga continental material (Liu and others, 1992, 2007, 2008; Cao, 1996; Song and others, 1996; Wan and others, 1998, 2002, 2005, 2007, 2011b, 2012a, 2012b, 2014a, 2014b, 2015; Jahn and others, 2008; Lu and others, 2008; Jiang and others, 2010; Liu and others, 2013, 2014a, 2014b; Wang and others, 2014; Wu and others, 2014a, 2014b). In this study, we provide new evidence for widespread Meso- to Paleoarchean components in the Anshan-Benxi area, an important portion of the Eastern Ancient Terrane. *Ca.* 2.5 Ga crustally-derived granites inherited the compositional features from the older basement. This is consistent with a long geological evolution back to 3.8 Ga revealed in early work (Wan and others, 2012b; references wherein). Apart from zircon dating, Nd-Hf-O isotope tracing is an effective method to identify old continental material. In cases where the old crust has been completely overprinted by intracrustal recycling, isotope tracing is the sole method to determine its previous presence, if xenocrystic zircon grains cannot be discovered.

CONCLUSIONS

1) 2.5 Ga magmatic rocks occur extensively in the Anshan-Benxi area and are mainly composed of syenogranite with some other granitoids such as granodiorite, quartz monzonite, monzogranite and K-rich granite. Two types of syenogranite can be recognized in terms of REE patterns although they are similar in major element composition and age of crystallization.

2) U contents, discordance, $\delta^{18}O$ and $\delta^{16}O^{1}H$ show linear variations in zircon grains from the granogranite, quartz monzonite and monzogranite, as a result of high U contents causing radiation damage and late alteration in zircon. Zircon from the syenogranite shows more complex relationships. We conclude that some zircon grains with strong lead loss originally had higher $\delta^{18}O$ values although they plot in the normal $\delta^{18}O$ range of Archean magmatic zircon.

3) The 2.5 Ga granitoid rocks formed by recycling of mature, old continental crust, probably in an extensional tectonic environment. Some syenogranites of the Qidashan Pluton may have been derived from metasedimentary precursors. However, their geochemical differences indicate large variations in the source region.

4) The Eastern Ancient Terrane (>2.6 Ga) of the NCC is composed of pre-late Neoarchean basement with different crustal residence times. Anshan-Benxi is an important area where a long geological evolution back to 3.8 Ga was identified by Nd-Hf-O isotope tracing and zircon dating.

ACKNOWLEDGMENTS

We are grateful to Chun Yang, Weilin Gan, Qingmin Du, Liqing Zhou and Ning Li for mount making and zircon CL imaging, Yuhai Zhang, Jianhui Liu and Tiao Long for SHRIMP zircon dating and O isotopic analysis, Chunli Ge and Kejun Hou for zircon Hf isotope analysis, and Suohan Tang and Jinhui Wang for whole-rock Nd isotopic analysis. We thank A. Kröner for discussion in the study and improving English writing. We are grateful to Allen Nutman and Gouchun Zhao for their valuable comments.

This research was financially supported by the Major State Basic Research Program of the People's Republic of China (2012CB416600, 2015FY310100), the Key Program of the Ministry of Land and Resources of China (12120114021301, 1212010811033, 12120115070301, and 12120113013700), and the National Natural Science Foundation of China (41472169, 40672127).

APPENDIX

ANALYTICAL TECHNIQUES

Whole-rock chemical analyses were conducted at the National Research Center of Geoanalysis, Chinese Academy of Geological Sciences (CAGS), Beijing. Major and trace elements were determined by XRF and ICP-MS respectively. Uncertainties depend upon the concentration in the samples, but generally for XRF and ICP-MS are estimated at *ca.* 3 to 5 percent and *ca.* 3 to 8 percent, respectively. When the rock sample contains large phenocryst feldspars, a large sample was used in order to get a truly representative sample. Whole-rock Sm and Nd isotopic compositions were determined by isotope dilution at the Key Laboratory of Isotope Geology, Ministry of Land and Resources of China, Beijing. Details of the procedures were described by Zhang and Ye (1987).

SHRIMP zircon dating was carried out at the Beijing SHRIMP Center, Institute of Geology, CAGS. The analytical procedures were similar to those described by Williams (1998). Five scans through the mass stations were made for each analysis. The intensity of the primary ion beam was 3 to 4 nA, and beam size was ~30 μm, and each site was rastered for 120 to 200 s prior to analysis to reduce or remove common Pb. International zircon standards M257 (U = 840 ppm, Nasdala and others, 2008) and TEMORA 2 ($^{206}Pb/^{238}U$ age = 417 Ma; Black and others, 2004) were mounted together with the unknowns and used for calibration of U abundances and $^{206}Pb/^{238}U$ ratios, respectively. The TEMORA 2 to unknown ratio was 1:3–4. Data processing and age assessment was carried out using the SQUID and ISOPLOT programs (Ludwig, 2001, 2003), and the measured ^{204}Pb was used for common lead correction. $^{207}Pb/^{206}Pb$ ratios were used to determine the age of all samples. The uncertainties for individual analyses are quoted at the 1 sigma level, whereas uncertainties on weighted mean ages are quoted at the 95 percent confidence level.

In-situ O and OH isotopic compositions were measured on previously SHRIMP-dated zircon spots. The analytical procedures and conditions were described by Ickert and others (2008) and Wan and others (2013). The intensity of the Cs^+ primary ion beam was ~3 nA. Spot diameter was ~30 μm, and each site was rastered for 120 to 200 s prior to analysis. The reference material used for calibration of instrumental mass fractionation was TEMORA 2 zircon ($\delta^{18}O$ = 8.20‰; Black and others, 2004), mounted together with the unknowns. The standard was analyzed 2 to 4 times at the start of each analytical session, then after every 3 unknown analyses. The uncertainties for individual analyses are quoted at the 1 sigma level. $\delta^{18}O(V\text{-}SMOW) = (((^{18}O/^{16}O)_{sample}/(^{18}O/^{16}O)_{v\text{-}smow}-1)\times1000$, $\delta^{16}OH^1H(ref) = (((^{16}OH^1H/^{16}O)_{sample}/(^{16}OH^1H/^{16}O)_{ref}-1)\times1000$, where $(^{18}O/^{16}O)_{v\text{-}smow}$ (= 0.0020052) is $(^{18}O/^{16}O)$ of Standard Mean Ocean Water, whereas $(^{16}OH^1H/^{16}O)_{ref}$ (= 0.0020) is an artificial value.

Hf-in-zircon analyses were carried out on the similar internal domains and close to the original pit for SHRIMP U-Pb and O analysis, using a Newwave UP213 laser-ablation microprobe, attached to a Neptune multicollector ICP-MS at the Institute of Mineral Resources, CAGS, Beijing. Instrumental conditions and data acquisition were described in Hou and others (2007). $^{176}Yb/^{172}Yb$=0.5887 was used and the β_{Yb} value obtained from the sample itself is applied for the Yb correction (Wu and others, 2006). For high $^{176}Yb/^{177}Hf$ zircon, it is more difficult to accurately corrcct the Hf isotopic composition, since the interference of ^{176}Yb on ^{176}Hf is significant (Wu and others, 2006). In this study, only the data with $^{176}Yb/^{177}Hf<0.08$ are used. Zircon standard 91500 yielded a $^{176}Hf/^{177}Hf$ average of 0.282296 (n = 19), being close to the $^{176}Hf/^{177}Hf$ value of standard 91500 (0.282306, Woodhead and others, 2004). All Lu–Hf isotopic results are reported at 95 percent confidence limits. The calculation of Hf model ages was based on a depleted-mantle source with a present-day $^{176}Hf/^{177}Hf$ = 0.28325 and $^{176}Lu/^{177}Hf$ = 0.0384, using a ^{176}Lu decay constant of 1.865×10^{-11} $year^{-1}$ (Nowell and others, 1998; Vervoort and Blichert, 1999; Scherer and others, 2001) and assuming that the evolution of the Hf isotopic composition of the depleted mantle with time was linear. Calculation of Hf crustal model ages ($t_{cc(Hf)}$) is based on the assumption of a mean $^{176}Lu/^{177}Hf$ ratio of 0.01 for the average continental crust (Kröner and others, 2014), rather than 0.015 as recommended by Griffin and others (2002). The calculation of $\varepsilon_{Hf(t)}$ values was based on zircon ages and the chondritic values ($^{176}Hf/^{177}Hf$ = 0.282785, $^{176}Lu/^{177}Hf$ = 0.0336, Bouvier and others, 2008).

TABLE A1

In-situ Hf isotopic compositions of zircon from late Neoarchean magmatic rocks in the Anshan-Benxi area, North China Craton

Hf spot	$^{176}Yb/^{177}Hf$	$^{176}Lu/^{177}Hf$	$^{176}Hf/^{177}Hf$	2σ	Age (Ma)	$\varepsilon_{Hf(0)}$	$\varepsilon_{Hf(t)}$	2σ	$t_{DM(Hf)}$ (Ga)	2σ	$t_{CC(Hf)}$ (Ga)	2σ	$f_{Lu/Hf}$
Gneissic syenogranite (A0713)													
1-1MA	0.038681	0.000833	0.281436	0.000031	2503	-47.2	7.6	1.1	2.53	0.09	2.54	0.14	-0.97
2-1MA	0.040450	0.000835	0.281333	0.000023	2503	-50.9	3.9	0.8	2.67	0.06	2.72	0.10	-0.97
3-1MA	0.042968	0.000934	0.281318	0.000022	2503	-51.4	3.2	0.8	2.70	0.06	2.76	0.10	-0.97
4-1MA	0.045227	0.001013	0.281356	0.000021	2503	-50.1	4.4	0.8	2.65	0.06	2.70	0.09	-0.97
5-1MA	0.035870	0.000750	0.281285	0.000023	2503	-52.6	2.3	0.8	2.73	0.06	2.80	0.10	-0.98
6-1MA	0.040341	0.000840	0.281286	0.000021	2503	-52.5	2.2	0.7	2.73	0.06	2.81	0.09	-0.97
7-1MA	0.037371	0.000775	0.281287	0.000021	2503	-52.5	2.4	0.8	2.73	0.06	2.80	0.09	-0.98
8-1MA	0.040943	0.000907	0.281322	0.000024	2503	-51.3	3.4	0.9	2.69	0.07	2.75	0.11	-0.97
9-1MA	0.062758	0.001522	0.281346	0.000023	2503	-50.4	3.2	0.8	2.70	0.06	2.76	0.10	-0.95
10-1MA	0.033685	0.000753	0.281301	0.000021	2503	-52.0	2.9	0.7	2.71	0.06	2.77	0.09	-0.98
11-1MA	0.063543	0.001558	0.281314	0.000025	2503	-51.6	2.0	0.9	2.75	0.07	2.82	0.11	-0.95
Gneissic syenogranite (A1123)													
1-1MA	0.045875	0.000839	0.281187	0.000030	2512	-56.1	-1.1	1.1	2.87	0.08	2.98	0.13	-0.97
2-1MA	0.023585	0.000425	0.281138	0.000022	2512	-57.8	-2.1	0.8	2.90	0.06	3.03	0.10	-0.99
3-1MA	0.055928	0.000974	0.281165	0.000019	2512	-56.8	-2.1	0.7	2.91	0.05	3.03	0.08	-0.97
4-1MA	0.039553	0.000702	0.281196	0.000021	2512	-55.8	-0.6	0.7	2.85	0.06	2.95	0.09	-0.98
5-1MA	0.033623	0.000601	0.281207	0.000019	2512	-55.3	0.0	0.7	2.82	0.05	2.92	0.08	-0.98
6-1MA	0.032202	0.000668	0.281185	0.000020	2512	-56.1	-0.9	0.7	2.86	0.05	2.97	0.09	-0.98
9-1MA	0.030641	0.000590	0.281166	0.000021	2512	-56.8	-1.4	0.7	2.87	0.06	3.00	0.09	-0.98
Weakly deformed syenogranite (A1214)													
1-1MA	0.076562	0.001452	0.281270	0.000027	2489	-53.1	0.3	1.0	2.80	0.07	2.89	0.12	-0.96
2-1MA	0.031544	0.000712	0.281233	0.000021	2489	-54.4	0.2	0.7	2.80	0.06	2.90	0.09	-0.98
4-1MA	0.062637	0.001028	0.281278	0.000017	2489	-52.8	1.3	0.6	2.76	0.05	2.81	0.07	-0.97
5-1MA	0.047878	0.000806	0.281246	0.000017	2489	-54.0	0.5	0.6	2.78	0.05	2.88	0.07	-0.98
6-1MA	0.049540	0.000871	0.281317	0.000019	2489	-51.5	2.9	0.7	2.69	0.05	2.76	0.08	-0.97
7-1MA	0.046535	0.000968	0.281176	0.000019	2489	-56.4	-2.2	0.7	2.89	0.05	3.02	0.08	-0.97
8-1MA	0.056715	0.001078	0.281239	0.000021	2489	-54.2	-0.2	0.8	2.81	0.06	2.95	0.09	-0.97
9-1MA	0.039326	0.000697	0.281250	0.000014	2489	-53.8	0.9	0.5	2.77	0.04	2.86	0.06	-0.98
10-1MA	0.058037	0.001102	0.281244	0.000019	2489	-54.0	0.0	0.7	2.81	0.05	2.91	0.08	-0.97
11-1MA	0.059945	0.001296	0.281172	0.000023	2489	-56.6	-2.9	0.8	2.92	0.06	3.05	0.10	-0.96
12-1MA	0.054069	0.000953	0.281263	0.000019	2489	-53.4	0.9	0.7	2.77	0.05	2.86	0.08	-0.97
Gneissic syenogranite (A1125)													
2-1X	0.073439	0.001350	0.280652	0.000022	3435	-75.0	-0.4	0.8	3.63	0.06	3.69	0.09	-0.96
3-1X	0.077369	0.001484	0.280915	0.000024	2753	-65.7	-6.5	0.8	3.29	0.07	3.45	0.10	-0.96
4-1X	0.077922	0.001431	0.280645	0.000019	3542	-75.2	1.6	0.7	3.65	0.05	3.68	0.08	-0.96
5-1X	0.076030	0.001494	0.280794	0.000019	2944	-70.0	-6.6	0.7	3.46	0.05	3.61	0.08	-0.96
6-1X	0.038640	0.000806	0.280583	0.000014	3112	-77.4	-8.9	0.5	3.68	0.04	3.86	0.06	-0.98
7-2X	0.073812	0.001413	0.280641	0.000020	3103	-75.4	-8.4	0.7	3.66	0.05	3.82	0.09	-0.96
10-1X	0.024678	0.000491	0.280578	0.000020	3380	-77.6	-2.3	0.7	3.65	0.05	3.74	0.09	-0.99
11-1X	0.044109	0.001092	0.280627	0.000014	3120	-75.8	-7.8	0.5	3.64	0.04	3.81	0.07	-0.97
12-1X	0.049619	0.000975	0.280604	0.000021	3161	-76.7	-7.4	0.7	3.66	0.06	3.82	0.09	-0.97
13-1X	0.032449	0.000676	0.280594	0.000017	2940	-77.0	-12.2	0.6	3.65	0.05	3.88	0.07	-0.98
15-1X	0.071071	0.001317	0.280848	0.000020	3070	-68.1	-1.6	0.7	3.67	0.05	3.46	0.08	-0.96
Gneissic syenogranite (A1229)													
4-1MA	0.046336	0.000776	0.281229	0.000020	2500	-54.6	0.2	0.7	2.81	0.05	2.90	0.09	-0.98
Gneissic syenogranite (A1232)													
12-1X	0.072908	0.001203	0.280644	0.000022	3457	-75.3	0.2	0.8	3.63	0.06	3.68	0.09	-0.96
Weakly deformed syenogranite (A1239)													
1-1MA	0.076379	0.001125	0.281110	0.000024	2523	-58.8	-4.1	0.9	2.99	0.07	3.14	0.11	-0.97
2-1MA	0.061109	0.001064	0.281248	0.000030	2523	-53.9	0.9	1.1	2.80	0.08	2.89	0.13	-0.97
3-1MA	0.040334	0.000626	0.281159	0.000020	2523	-57.0	-1.5	0.7	2.89	0.06	3.01	0.09	-0.98
4-1MA	0.079082	0.001411	0.281139	0.000025	2523	-57.8	-3.6	0.9	2.98	0.07	3.11	0.11	-0.96
5-1MA	0.056740	0.000889	0.281100	0.000022	2523	-59.1	-4.0	0.8	2.99	0.06	3.14	0.10	-0.97
6-1MA	0.069323	0.001208	0.281128	0.000023	2523	-58.2	-3.6	0.8	2.98	0.06	3.11	0.10	-0.96
12-1MA	0.067686	0.001199	0.281198	0.000020	2523	-55.7	-1.1	0.7	2.88	0.05	2.99	0.09	-0.96

TABLE A1

(Continued)

Hf spot	$^{176}Yb/^{177}Hf$	$^{176}Lu/^{177}Hf$	$^{176}Hf/^{177}Hf$	2σ	Age (Ma)	$\varepsilon_{Hf}(0)$	$\varepsilon_{Hf(t)}$	2σ	$t_{DM(Hf)}$ (Ga)	2σ	$t_{CC(Hf)}$ (Ga)	2σ	$f_{Lu/Hf}$
Weakly deformed syenogranite (A1240)													
3-1MA	0.058510	0.001182	0.281136	0.000032	2484	-57.9	-4.1	1.1	2.96	0.09	3.11	0.14	-0.96
8-1X	0.050081	0.000836	0.280634	0.000027	3341	-75.6	-2.0	1.0	3.61	0.07	3.70	0.11	-0.97
10-1MA	0.071095	0.001189	0.280942	0.000024	2484	-64.7	-11.0	0.8	3.23	0.06	3.46	0.10	-0.96
14-1X	0.079864	0.001403	0.281056	0.000024	3188	-60.7	8.3	0.9	3.09	0.07	3.06	0.10	-0.96
Banded granodiorite (A1126)													
1-1X	0.057488	0.001022	0.280544	0.000022	3521	-78.8	-1.5	0.8	3.75	0.06	3.82	0.10	-0.97
1-2MA	0.039909	0.000738	0.280789	0.000028	2517	-70.1	-15.0	1.0	3.39	0.08	3.68	0.12	-0.98
2-1MA	0.033108	0.000668	0.281082	0.000023	2517	-59.8	-4.4	0.8	3.00	0.06	3.15	0.10	-0.98
3-1MA	0.039296	0.000776	0.281030	0.000020	2517	-61.6	-6.5	0.7	3.07	0.05	3.25	0.09	-0.98
4-1X	0.044803	0.000846	0.280531	0.000017	3489	-79.3	-2.3	0.6	3.75	0.05	3.83	0.07	-0.97
4-2MA	0.015561	0.000356	0.280935	0.000016	2517	-65.0	-9.1	0.6	3.17	0.04	3.39	0.07	-0.99
5-1X	0.059806	0.001180	0.280563	0.000017	3491	-78.1	-1.9	0.6	3.74	0.05	3.81	0.07	-0.96
6-1MA	0.033037	0.000704	0.281007	0.000017	2517	-62.4	-7.2	0.6	3.10	0.05	3.29	0.08	-0.98
9-1X	0.034486	0.000679	0.280747	0.000017	2624	-71.6	-14.0	0.6	3.45	0.05	3.71	0.07	-0.98
10-1MA	0.024883	0.000528	0.281005	0.000019	2517	-62.5	-6.9	0.7	3.09	0.05	3.28	0.08	-0.98
11-1MA	0.030273	0.000746	0.281001	0.000016	2517	-62.6	-7.5	0.6	3.11	0.04	3.30	0.07	-0.98
12-1X	0.072189	0.001228	0.280583	0.000017	3509	-77.4	-0.9	0.6	3.72	0.05	3.78	0.07	-0.96
14-1X	0.059735	0.001111	0.280617	0.000022	3607	-76.2	2.9	0.8	3.66	0.06	3.67	0.09	-0.97
15-1X	0.079369	0.001517	0.280783	0.000018	3161	-70.3	-2.3	0.6	3.47	0.05	3.56	0.08	-0.95
Gneissic quartz monzongranite (A1124)													
1-1X	0.034177	0.000635	0.280454	0.000017	3513	-82.0	-3.9	0.6	3.83	0.05	3.93	0.07	-0.98
1-2X	0.025912	0.000481	0.280486	0.000019	3554	-80.9	-1.5	0.7	3.77	0.05	3.85	0.08	-0.99
2-1MA	0.026781	0.000493	0.280876	0.000020	2507	-67.0	-11.7	0.7	3.26	0.05	3.51	0.09	-0.99
3-1MA	0.055341	0.001083	0.281158	0.000020	2507	-57.1	-2.7	0.7	2.92	0.05	3.05	0.09	-0.97
4-1X	0.035316	0.000696	0.280436	0.000019	3648	-82.6	-1.6	0.7	3.86	0.05	3.93	0.08	-0.98
5-1MA	0.041040	0.000818	0.280770	0.000019	2507	-70.8	-16.0	0.7	3.43	0.05	3.72	0.08	-0.98
6-1X	0.038296	0.000794	0.280561	0.000019	3407	-78.2	-2.9	0.7	3.70	0.05	3.80	0.08	-0.98
7-1MA	0.067398	0.001354	0.281141	0.000021	2507	-57.7	-3.7	0.8	2.97	0.06	3.11	0.09	-0.96
8-1MA	0.041816	0.000825	0.281012	0.000018	2507	-62.3	-7.4	0.6	3.10	0.05	3.29	0.08	-0.98
10-1X	0.048905	0.000968	0.280651	0.000020	3569	-75.0	3.6	0.7	3.60	0.05	3.61	0.08	-0.97
11-1X	0.067965	0.001306	0.280639	0.000022	3601	-75.4	3.0	0.8	3.65	0.06	3.66	0.09	-0.96
11-2MA	0.037666	0.000783	0.280904	0.000018	2507	-66.0	-11.2	0.6	3.24	0.05	3.48	0.08	-0.98
12-1X	0.044893	0.000920	0.280467	0.000018	3558	-81.5	-3.1	0.6	3.84	0.05	3.93	0.08	-0.97
13-1X	0.041224	0.000873	0.280543	0.000018	3480	-78.8	-2.1	0.7	3.74	0.05	3.82	0.08	-0.97
14-1MA	0.028320	0.000636	0.281036	0.000016	2507	-61.4	-6.3	0.6	3.06	0.04	3.23	0.07	-0.98
15-1MA	0.033338	0.000757	0.281011	0.000016	2507	-62.3	-7.4	0.6	3.10	0.04	3.29	0.07	-0.98
16-1X	0.067937	0.001344	0.281294	0.000020	2657	-52.3	5.0	0.7	2.76	0.05	2.79	0.09	-0.96
17-1X	0.025540	0.000537	0.281051	0.000021	2647	-60.8	-2.3	0.7	3.03	0.06	3.15	0.09	-0.98
18-1X	0.028983	0.000523	0.280750	0.000022	2767	-71.5	-10.3	0.8	3.43	0.06	3.65	0.09	-0.98
19-1X	0.019264	0.000409	0.280500	0.000021	3736	-80.3	3.5	0.8	3.75	0.06	3.75	0.09	-0.99
Gneissic quartz monzongranite (A1235)													
1-1MA	0.041537	0.000949	0.281172	0.000020	2507	-56.6	-1.9	0.7	2.90	0.05	3.02	0.09	-0.97
2-1X	0.048106	0.001032	0.280574	0.000015	3290	-77.7	-5.7	0.6	3.71	0.04	3.84	0.07	-0.97
2-2MA	0.017043	0.000464	0.280846	0.000015	2507	-68.1	-12.7	0.5	3.30	0.04	3.56	0.06	-0.99
3-1MA	0.035217	0.000851	0.281051	0.000017	2507	-60.9	-6.1	0.6	3.05	0.05	3.23	0.08	-0.97
4-1MA	0.020877	0.000592	0.280958	0.000017	2507	-64.2	-9.0	0.6	3.16	0.05	3.37	0.07	-0.98
4-2X	0.033752	0.000747	0.280902	0.000016	2711	-66.1	-6.6	0.6	3.24	0.04	3.42	0.07	-0.98
6-1MA	0.005467	0.000116	0.280839	0.000015	2507	-68.4	-12.4	0.5	3.28	0.04	3.54	0.06	-1.00
8-1MA	0.047955	0.001215	0.281248	0.000019	2507	-53.9	0.3	0.7	2.81	0.05	2.91	0.08	-0.96
9-1MA	0.043593	0.001100	0.281187	0.000018	2507	-56.0	-1.7	0.7	2.89	0.05	3.00	0.08	-0.97
10-1X	0.038846	0.000944	0.280636	0.000018	3525	-75.5	2.1	0.6	3.62	0.05	3.65	0.08	-0.97
11-1X	0.025171	0.000886	0.281067	0.000016	2880	-60.3	2.9	0.6	3.03	0.05	3.08	0.07	-0.97
12-1MA	0.022523	0.000673	0.281055	0.000013	2507	-60.7	-5.6	0.5	3.03	0.04	3.20	0.06	-0.98
13-1MA	0.041232	0.001066	0.281057	0.000017	2507	-60.7	-6.2	0.6	3.06	0.05	3.23	0.07	-0.97
13-2MA	0.019706	0.000617	0.281012	0.000014	2507	-62.3	-7.1	0.5	3.09	0.04	3.28	0.06	-0.98
14-1MA	0.041190	0.001096	0.281207	0.000018	2507	-55.4	-1.0	0.7	2.86	0.05	2.97	0.08	-0.97

TABLE A1

(Continued)

Hf spot	$^{176}Yb/^{177}Hf$	$^{176}Lu/^{177}Hf$	$^{176}Hf/^{177}Hf$	2σ	Age (Ma)	$\varepsilon_{Hf}(0)$	$\varepsilon_{Hf(t)}$	2σ	$t_{DM(H)}$ (Ga)	2σ	$t_{C(H)}$ (Ga)	2σ	$f_{Lu/Hf}$
Gneissic quartz monzongranite (A1235)													
15-1X	0.047874	0.001289	0.280586	0.000016	3607	-77.3	1.3	0.6	3.72	0.04	3.75	0.07	-0.96
16-1X	0.029779	0.000755	0.280607	0.000017	3383	-76.6	-1.8	0.6	3.64	0.05	3.72	0.07	-0.98
17-1MA	0.025293	0.000715	0.281078	0.000014	2507	-59.9	-4.9	0.5	3.00	0.04	3.17	0.06	-0.98
18-1MA	0.037604	0.001091	0.281146	0.000015	2507	-57.5	-3.1	0.5	2.94	0.04	3.08	0.06	-0.97
19-1MA	0.026878	0.000782	0.281066	0.000013	2507	-60.3	-5.4	0.5	3.03	0.04	3.19	0.06	-0.98
20-1MA	0.021166	0.000638	0.281065	0.000013	2507	-60.4	-5.2	0.5	3.02	0.04	3.18	0.06	-0.98
21-1MA	0.025865	0.000924	0.281072	0.000017	2507	-60.1	-5.5	0.6	3.03	0.05	3.20	0.08	-0.97
22-1MA	0.032555	0.000963	0.281191	0.000014	2507	-55.9	-1.3	0.5	2.87	0.04	3.00	0.06	-0.97
23-1MA	0.028450	0.000870	0.281083	0.000016	2507	-59.7	-5.0	0.6	3.01	0.04	3.17	0.07	-0.97
24-1MA	0.046760	0.001404	0.281096	0.000015	2507	-59.3	-5.4	0.5	3.04	0.04	3.19	0.06	-0.96
25-1MA	0.020576	0.000661	0.281066	0.000014	2507	-60.3	-5.2	0.5	3.02	0.04	3.18	0.06	-0.98
26-1MA	0.024471	0.000676	0.281006	0.000013	2507	-62.5	-7.4	0.5	3.10	0.04	3.29	0.06	-0.98
28-1MA	0.029630	0.000811	0.281097	0.000016	2507	-59.2	-4.4	0.6	2.99	0.04	3.14	0.07	-0.98
32-1MA	0.025973	0.001023	0.281153	0.000030	2507	-57.2	-2.7	1.1	2.93	0.08	3.06	0.13	-0.97
35-1MA	0.025325	0.000734	0.281173	0.000015	2507	-56.5	-1.5	0.5	2.88	0.04	3.00	0.06	-0.98
Gneissic monzogranite (A1228)													
2-1MA	0.034781	0.000583	0.281203	0.000018	2519	-55.5	0.1	0.6	2.83	0.05	2.93	0.08	-0.98
3-1MA	0.033433	0.000691	0.281169	0.000021	2519	-56.7	-1.3	0.7	2.88	0.06	3.00	0.09	-0.98
4-1MA	0.056412	0.000899	0.281284	0.000022	2519	-52.6	2.4	0.8	2.74	0.06	2.81	0.09	-0.97
5-1MA	0.076417	0.001458	0.281231	0.000030	2519	-54.5	-0.5	1.1	2.85	0.08	2.95	0.13	-0.96
7-1MA	0.046506	0.000750	0.281209	0.000023	2519	-55.3	0.0	0.8	2.83	0.06	2.93	0.10	-0.98
8-1MA	0.060116	0.001374	0.281162	0.000028	2519	-56.9	-2.8	1.0	2.94	0.08	3.07	0.12	-0.96
9-1MA	0.057757	0.000925	0.281033	0.000018	2519	-61.5	-6.6	0.6	3.08	0.05	3.26	0.08	-0.97
11-1MA	0.045263	0.000744	0.281222	0.000022	2519	-54.8	0.4	0.8	2.81	0.06	2.91	0.09	-0.98

Note: MA = magmatic zircon; X = xenocrystal zircon.

TABLE A2

In-situ O isotopic compositions of zircon from late Neoarchean magmatic rocks in the Anshan-Benxi area, North China Craton

Sample no.	Analysis no. of SHRIMP dating	Age of zircon (Ma)	Discordance (%)	U (ppm)	Th/U	Age type	$\delta^{18}O$ (V-SMOW) (‰)	95% ±	$\Delta^{16}O^{1}H$ (ref) (‰)	95% ±
Gneissic syenogranite (A0713)										
1.1MA	1.1MA	2503	3	66	0.82	WMA	6.5	0.4		
2.1MA	2.1MA	2503	0	101	1.06	WMA	6.4	0.6		
3.1MA	4.1MA	2503	-2	60	1.00	WMA	11.0	0.6		
4.1MA	5.1MA	2503	1	65	0.68	WMA	6.7	0.6		
5.1MA	6.1MA	2503	2	78	0.87	WMA	9.4	0.5		
6.1MA	7.1MA	2503	0	74	0.69	WMA	10.9	0.7		
7.1MA	9.1MA	2503	0	84	0.94	WMA	5.9	0.3		
8.1MA	11.1MA	2503	2	112	1.08	WMA	6.9	0.8		
9.1MA		2503		Gray		EA	5.8	0.5		
10.1MA		2503		Gray		EA	10.2	0.6		
11.1MA		2503		Gray		EA	9.9	0.5		
Massive syenogranite (A1218)										
1.1X	1.1X	3572	35	192	0.37	Pb/Pb age	5.0	0.2	477	57
2.1MA	2.1MA	2500	35	875	0.07	EA	4.8	0.1	2316	27
5.1X	5.1X	3349	41	310	0.54	Pb/Pb age	4.9	0.1	2504	20
6.1X	6.1X	3161	58	446	0.55	Pb/Pb age	3.7	0.1	1288	25
7.1MA	7.1MA	2500	87	2359	0.20	EA	6.6	0.1	2955	16
10.1MA	10.1MA	2500	88	11556	0.19	EA	6.0	0.1	3238	1
12.1MA	12.1MA	2500	61	1614	0.39	EA	6.1	0.1	3324	2
Gneissic syenogranite (A1123)										
1.1MA	1.1MA	2512	0	64	1.19	WMA	1.6	0.2	6	36
2.1MA	2.1MA	2512	3	45	1.20	WMA	6.4	0.1	-179	28
3.1MA	3.1MA	2512	2	170	1.02	WMA	5.6	0.1	-196	43
6.1MA	6.1MA	2512	-2	82	0.81	WMA	5.5	0.1	-154	33
10.1MA		2512		Gray		WMA	6.1	0.1	-187	21
11.1MA		2512		Dark		EA	5.5	0.1	-91	37
12.1MA		2512		Dark		EA	6.1	0.1	-15	42
13.1MA		2512		Light gray		EA	5.4	0.1	-235	45
14.1MA		2512		Dark gray		EA	6.0	0.1	1150	43
15.1MA		2512		Gray		EA	5.3	0.1	-130	24
16.1MA		2512		Gray		EA	5.8	0.1	-151	16
17.1MA		2512		Gray		EA	5.1	0.2	-463	87
19.1MA		2512		Gray		EA	5.9	0.1	-238	46
20.1MA		2512		Gray		EA	6.0	0.1	-145	45
21.1MA		2512		Light gray		EA	5.5	0.1	-191	42
22.1MA		2512		Gray		EA	5.8	0.1	-82	34
Weakly deformed syenogranite (A1214)										
3.1MA	3.1MA	2489	17	187	0.40	WMA	5.9	0.1	156	15
5.1MA	5.1MA	2489	5	66	1.09	WMA	6.4	0.2	36	43
6.1MA	6.1MA	2489	11	44	0.92	WMA	6.7	0.1	135	20
7.1MA		2489		Gray		EA	5.9	0.2	186	44
8.1MA	8.1MA	2489	7	43	1.26	WMA	6.6	0.1	78	28
9.1MA	9.1MA	2489	11	34	0.75	WMA	6.4	0.2	108	28
10.1MA	10.1MA	2489	8	139	0.53	WMA	6.7	0.2	251	22
11.1MA	11.1MA	2489	0	70	0.65	WMA	5.8	0.1	394	27
12.1MA	12.1MA	2489	2	33	1.01	WMA	6.9	0.1	111	16
13.1MA	13.1MA	2489	31	259	0.36	WMA	6.4	0.1	109	16
14.1MA	14.1MA	2489	43	299	0.19	WMA	6.2	0.2	281	60
15.1MA	15.1MA	2489	-1	45	1.18	WMA	6.0	0.1	171	21
Gneissic syenogranite (A1125)										
1.1X	1.1X	2846	60	1368	0.34	Pb/Pb age	3.5	0.1	2157	28
2.1X	2.1X	3435	18	198	1.14	Pb/Pb age	3.9	0.1	668	117
3.1X	3.1X	2753	32	725	0.87	Pb/Pb age	3.0	0.2	1276	45
5.1X	5.1X	2944	55	2322	0.24	Pb/Pb age	2.7	0.1	1843	23
7.1X	7.1X	2774	63	1979	0.11	Pb/Pb age	2.1	0.1	1774	45
9.1X	9.1X	2982	53	1145	0.63	Pb/Pb age	3.6	0.2	1911	40
10.1X	10.1X	3380	25	598	0.47	Pb/Pb age	0.3	0.1	2000	28
15.1X	15.1X	3070	49	749	0.24	Pb/Pb age	2.3	0.1	2120	16
16.1X				Dark gray			0.3	0.1	845	77
17.1X				Dark			1.9	0.3	285	166
18.1X				Gray			3.6	0.1	885	40
19.1X				Gray			3.9	0.1	1146	65

TABLE A2
(Continued)

Sample no.	Analysis no. of SHRIMP dating	Age of zircon (Ma)	Discordance (%)	U (ppm)	Th/U	Age type	$\delta^{18}O$ (V-SMOW) (‰)	95% ±	$\Delta^{18}O^{1}H$ (ref) (‰)	95% ±
Gneissic syenogranite (A1229)										
2.1MA	2.1MA	2500	20	196	3.68	UIA	6.7	0.1	189	22
3.1MA	3.1MA	2500	53	729	0.70	UIA	6.9	0.2	966	46
4.1MA	4.1MA	2500	5	90	0.88	UIA	5.8	0.2	398	37
6.1MA	6.1MA	2500	37	133	1.73	UIA	6.5	0.1	1121	21
7.1MA	7.1MA	2500	15	238	0.83	UIA	6.5	0.1	885	43
9.1MA	9.1MA	2500	22	302	0.48	UIA	6.6	0.1	1194	29
10.1MA	10.1MA	2500	30	278	1.84	UIA	6.0	0.2	2534	47
11.1MA	11.1MA	2500	5	118	1.94	UIA	5.9	0.1	292	15
12.1MA	12.1MA	2500	7	314	0.60	UIA	5.3	0.2	1236	46
13.1MA	13.1MA	2500	4	152	0.69	UIA	5.2	0.1	311	24
14.1MA	14.1MA	2500	11	108	2.75	UIA	5.8	0.2	131	54
15.1MA	15.1MA	2500	21	243	1.81	UIA	5.9	0.2	165	55
Gneissic syenogranite (A1232)										
1.1X	1.1X	3001	34	1420	0.97	Pb/Pb age	2.8	0.1	1908	23
3.1X	3.1X	3377	12	222	0.72	Pb/Pb age	5.8	0.1	124	37
3.2MA	3.2MA	2500	65	1244	0.14	EA	2.5	0.2	2172	20
4.1X	4.1X	2816	54	1068	0.97	Pb/Pb age	5.0	0.1	1819	29
5.1X	5.1X	3445	15	664	1.12	Pb/Pb age	4.7	0.1	1477	20
6.1X	6.1X	3456	13	340	1.38	Pb/Pb age	4.6	0.1	1548	35
8.1X	8.1X	3404	18	298	0.45	Pb/Pb age	5.5	0.1	134	13
12.1X	12.1X	3457	7	219	0.47	Pb/Pb age	6.1	0.2	164	37
13.1X	13.1X	3457	-2	264	0.75	Pb/Pb age	6.4	0.2	250	43
14.1MA	14.1MA	2500	62	935	0.06	EA	2.8	0.2	1567	67
15.1X	15.1X	3239	36	458	0.40	Pb/Pb age	6.6	0.2	176	53
16.1X	16.1X	2764	54	762	0.41	Pb/Pb age	4.9	0.1	1833	17
17.1MA	17.1MA	2500	68	1771	0.11	EA	3.1	0.2	3148	15
21.1X	21.1X	3432	11	323	0.27	Pb/Pb age	5.2	0.1	1218	24
22.1X	22.1X	3265	25	686	1.04	Pb/Pb age	5.9	0.2	507	46
23.1X	23.1X	3378	20	443	0.96	Pb/Pb age	5.6	0.1	1423	13
Weakly deformed syenogranite (A1239)										
1.1MA	1.1MA	2523	0	19	2.35	WMA	6.2	0.2	26	54
2.1MA	2.1MA	2523	50	86	1.12	WMA	6.5	0.2	119	66
3.1MA	3.1MA	2523	3	54	1.96	WMA	6.3	0.1	122	32
4.1MA	4.1MA	2523	-2	25	2.49	WMA	6.4	0.2	29	32
5.1MA	5.1MA	2523	0	23	2.14	WMA	5.9	0.1	222	18
6.1MA	6.1MA	2523	-2	27	2.11	WMA	7.2	0.1	1795	35
8.1MA	8.1MA	2523	3	32	2.19	WMA	6.0	0.1	119	15
10.1MA	10.1MA	2523	35	110	1.33	WMA	5.7	0.5	-161	100
12.1MA	12.1MA	2523	49	513	0.17	WMA	6.6	0.1	248	25
Weakly deformed syenogranite(A1240)										
3.1MA	3.1MA	2484	-29	561	0.67	UIA	6.5	0.1	800	42
4.1MA	4.1MA	2484	49	1054	0.38	UIA	4.6	0.1	2521	20
6.1X	6.1X	3011	41	356	0.26	Pb/Pb age	5.7	0.2	1611	42
7.1MA+X	7.1MA	2484	21	355	0.73	UIA	5.1	0.1	2411	20
8.1X	8.1X	3341	26	244	0.58	Pb/Pb age	3.2	0.4	2006	74
9.1X	9.1X	3477	77	414	0.69	Pb/Pb age	5.9	0.2	2414	26
10.1MA	10.1MA	2484	66	1050	0.29	UIA	5.3	0.1	2178	34
11.1MA	11.1MA	2484	48	647	0.56	UIA	5.3	0.1	3199	1
12.1MA	12.1MA	2484	57	865	0.92	UIA	5.7	0.1	3149	16
13.1X	13.1X	3023	53	777	0.32	Pb/Pb age	5.5	0.2	1214	53
14.1X	14.1X	3188	42	525	0.33	Pb/Pb age	4.9	0.1	2137	31
16.1MA	16.1MA	2484	69	2156	0.06	UIA	4.5	0.2	3213	8
17.1MA	17.1MA	2484	65	2436	0.05	UIA	4.8	0.2	3223	4
Banded granodiorite (A1126)										
1.1X	1.1X	3521	2	111	0.88	Pb/Pb age	5.8	0.1		
1.2MA	1.2MA	2517	2	256	0.52	WMA	6.4	0.1		
1.3MA	1.3MA	2517	14	325	0.40	WMA	5.5	0.1		
2.1MA	2.1MA	2517	2	209	0.56	WMA	5.2	0.1		
3.1MA	3.1MA	2517	15	427	0.60	WMA	5.0	0.2		
4.2MA	4.2MA	2517	14	374	0.56	WMA	5.0	0.1		
5.1X	5.1X	3491	0	186	0.46	Pb/Pb age	5.1	0.1		
6.1MA	6.1MA	2517	13	448	0.67	WMA	2.9	0.2		
8.1X	8.1X	3742	2	206	0.53	Pb/Pb age	4.8	0.1		

TABLE A2
(Continued)

Sample no.	Analysis no. of SHRIMP dating	Age of zircon (Ma)	Discordance (%)	U (ppm)	Th/U	Age type	$\delta^{18}O$ (V-SMOW) (‰)	95% ±	$\Delta^{16}O^{1}H$ (ref) (‰)	95% ±
Banded granodiorite (A1126)										
9.1X	9.1X	2624	0	55	0.19	Pb/Pb age	6.2	0.1		
10.1MA	10.1MA	2517	3	368	0.68	WMA	3.9	0.1		
11.1MA	11.1MA	2517	17	397	0.76	WMA	4.9	0.1		
12.1X	12.1X	3509	10	534	0.76	Pb/Pb age	5.3	0.1		
14.1X	14.1X	3607	4	464	0.06	Pb/Pb age	5.3	0.1		
15.1X	15.1X	3161	43	1150	0.64	Pb/Pb age	2.6	0.1		
16.1X	16.1X	3451	56	590	0.43	Pb/Pb age	4.4	0.1		
Gneissic quartz monzonite (A1124)										
1.1X	1.1X	3513	-2	171	0.25	Pb/Pb age	4.6	0.1		
1.2X	1.2X	3554	3	81	0.51	Pb/Pb age	5.7	0.1		
2.1MA	2.1MA	2507	29	569	0.43	WMA	2.8	0.1		
3.1MA	3.1MA	2507	8	358	0.62	WMA	5.4	0.1		
4.1X	4.1X	3648	5	357	0.46	Pb/Pb age	6.2	0.1		
5.1MA	5.1MA	2507	16	411	0.43	WMA	4.9	0.2		
6.1X	6.1X	3407	5	698	0.05	Pb/Pb age	4.8	0.1		
7.1MA	7.1MA	2507	38	613	0.95	WMA	4.5	0.2		
8.1MA	8.1MA	2507	7	379	0.60	WMA	5.4	0.1		
9.1X	9.1X	3641	-2	165	0.67	Pb/Pb age	3.0	0.1		
10.1X	10.1X	3569	11	335	0.21	Pb/Pb age	2.0	0.2		
11.1X	11.1X	3601	-1	52	0.39	Pb/Pb age	4.8	0.1		
12.1X	12.1X	3558	5	212	0.55	Pb/Pb age	5.5	0.1		
13.1X	13.1X	3480	0	161	0.23	Pb/Pb age	5.9	0.1		
14.1MA	14.1MA	2507	4	528	0.85	WMA	4.6	0.1		
15.1MA	15.1MA	2507	16	472	0.84	WMA	5.3	0.1		
16.1X	16.1X	2657	17	534	0.51	Pb/Pb age	4.8	0.1		
17.1X	18.1X	2767	-2	188	0.93	Pb/Pb age	6.4	0.1		
19.1X	19.1X	3736	0	121	0.50	Pb/Pb age	4.2	0.1		
Gneissic quartz monzonite (A1235)										
1.1MA	1.1MA	2507	20	417	0.71	UIA	3.7	0.1	1408	13
2.1X	2.1X	3290	33	502	0.36	Pb/Pb age	3.5	0.1	1392	10
2.2MA	2.2MA	2507	29	432	0.50	UIA	4.8	0.1	877	37
3.1MA	3.1MA	2507	49	1001	0.48	UIA	3.9	0.1	1528	20
4.1MA	4.1MA	2507	73	1329	0.11	UIA	1.8	0.1	2021	33
4.2X	4.2X	2711	9	131	0.93	Pb/Pb age	6.0	0.1	251	62
5.1X				Gray			4.1	0.1	1251	37
6.1MA	6.1MA	2507	0	251	1.22	UIA	7.0	0.2	-162	203
7.1X	7.1X	3375	19	348	0.58	Pb/Pb age	3.3	0.1	471	10
8.1MA	8.1MA	2507	41	520	0.90	UIA	3.6	0.1	1434	22
9.1MA	9.1MA	2507	21	280	0.87	UIA	3.2	0.1	648	89
10.1X	10.1X	3525	-5	128	0.99	Pb/Pb age	6.1	0.1	232	60
11.1X	11.1X	2880	84	2119	0.10	Pb/Pb age	1.8	0.1	2653	29
12.1MA	12.1MA	2507	61	1412	0.07	UIA	3.4	0.1	1537	38
13.1MA	13.1MA	2507	37	450	0.85	UIA	4.1	0.1	1356	11
13.2MA	13.2MA	2507	40	630	0.44	UIA	5.1	0.1	961	10
14.1MA	14.1MA	2507	35	528	0.81	UIA	2.9	0.1	1652	19
15.1X	15.1X	3607	7	378	0.70	Pb/Pb age	5.8	0.1	187	46
16.1X	16.1X	3383	7	65	0.58	Pb/Pb age	6.8	0.1	-74	63
17.1MA	17.1MA	2507	20	372	0.76	UIA	5.9	0.1	459	25
18.1MA	18.1MA	2507	51	588	1.08	UIA	3.4	0.2	1296	22
19.1MA	19.1MA	2507	29	622	0.49	UIA	4.3	0.1	901	40
19.2MA		2507		Gray		EA	5.0	0.1	1728	10
20.1MA	20.1MA	2507	41	552	0.57	UIA	4.5	0.2	1096	48
21.1MA	21.1MA	2507	44	613	1.06	UIA	3.7	0.1	1299	25
22.1MA	22.1MA	2507	26	351	0.52	UIA	5.6	0.1	731	42
23.1MA	23.1MA	2507	45	674	1.25	UIA	3.0	0.1	1027	27
24.1MA	24.1MA	2507	45	533	3.06	UIA	5.1	0.1	395	22
25.1MA	25.1MA	2507	13	407	0.73	UIA	4.5	0.1	474	68
26.1MA	26.1MA	2507	12	364	0.60	UIA	4.7	0.1	339	31
27.1MA	27.1MA	2507	35	389	1.07	UIA	5.0	0.1	742	21
32.1MA		2507		Dark		EA	2.0	0.1	2668	34
35.1MA		2507		Dark		EA	3.2	0.2	973	128
36.1MA		2507		Dark		EA	2.6	0.1	3533	16

TABLE A2

(Continued)

Sample no.	Analysis no. of SHRIMP dating	Age of zircon (Ma)	Discordance (%)	U (ppm)	Th U	Age type	$\delta^{18}O$ (V-SMOW) (‰)	95% ±	$\delta^{16}OH$ (ref) (‰)	95% ±
Gneissic monzongranite (A1228)										
1.1MA	1.1MA	2512	-2	58	1.21	WMA	4.0	0.1	-97	42
2.1MA	2.1MA	2512	2	169	0.36	WMA	6.6	0.2	-162	55
3.1MA	3.1MA	2512	-1	46	0.84	WMA	5.2	0.3	-98	47
4.1MA	4.1MA	2512	-1	35	1.08	WMA	6.3	0.2	-210	78
5.1MA	5.1MA	2512	6	125	0.60	WMA	6.1	0.1	10	40
7.1MA	7.1MA	2512	1	43	0.72	WMA	6.7	0.2	-62	22
8.1MA	8.1MA	2512	1	69	0.49	WMA	6.0	0.2	-103	63
9.1MA	9.1MA	2512	2	352	0.88	WMA	5.8	0.1	184	36
10.1MA	10.1MA	2512	8	221	0.90	WMA	5.2	0.2	670	50
12.1MA	12.1MA	2512	3	223	0.59	WMA	5.7	0.1	167	25
13.1MA	13.1MA	2512	-3	42	1.05	WMA	5.7	0.2	-13	38
14.1MA	14.1MA	2512	-1	65	1.28	WMA	5.8	0.1	-123	56
15.1MA	15.1MA	2512	-1	31	1.01	WMA	6.9	0.1	-120	28
16.1MA	16.1MA	2512	4	39	1.11	WMA	5.9	0.1	-113	22
17.1MA	17.1MA	2512	1	55	0.88	WMA	6.3	0.1	-118	15
18.1MA	18.1MA	2512	3	71	0.89	WMA	6.4	0.1	-107	13
19.1MA	19.1MA	2512	3	179	0.32	WMA	4.8	0.1	156	41
20.1MA	20.1MA	2512	-2	174	1.25	WMA	6.6	0.1	28	15
21.1MA		2512		Gray		EA	6.1	0.1	-188	38

Note: 1) $\delta^{18}O(V\text{-}SMOW) = (({}^{18}O/{}^{16}O)sample/({}^{18}O/{}^{16}O)v\text{-}smow-1)\times1000$, $({}^{18}O/{}^{16}O)v\text{-}smow = 0.0020052$;$\delta^{16}OH^{1}H(ref) = (({}^{16}OH^{1}H/{}^{16}O)sample/({}^{16}OH^{1}H/{}^{16}O)ref -1)\times1000$, $({}^{16}OH^{1}H/{}^{16}O)ref = 0.0020$) MA = magmatic zircon; X = xenocrystal zircon; WMA = weighted mean $^{207}Pb/^{206}Pb$ age; UIA = upper intercept age; Pb/Pb age = $^{207}Pb/^{206}Pb$ age; EA = estimated age; 3) Sample A0713 is from Wan and others (2013), rest are from this study.

REFERENCES

Bagas, L., Smithies, R. H., and Champion, D. C., 2002, Geochemistry of the Corunna Downs granitoid complex, east Pilbara granite–greenstone terrane, western Australia: Geological Survey of Western Australia, 2001–02 Annual Review, p. 61–69.

Black, L. P., 1987, Recent Pb loss in zircon: A natural or laboratory induced phenomenon: Chemical Geology, v. 65, n. 1, p. 25–33, http://dx.doi.org/10.1016/0168-9622(87)90059-5

Black, L. P., Kamo, S. L., Allen, C. M., Davis, D. W., Aleinikoff, J. N., Valley, J. W., Mundil, R., Campbell, I. H., Korsch, R. J., Williams, I. S., and Foudoulis, C., 2004, Improved $^{206}Pb/^{238}U$ microprobe geochronology by the monitoring of a trace-element-related matrix effect; SHRIMP, ID-TIMS, ELA-ICP-MS and oxygen isotope documentation for a series of zircon standards: Chemical Geology, v. 205, n. 1–2, p. 115–140, http://dx.doi.org/10.1016/j.chemgeo.2004.01.003

Booth, A. L., Kolodny, Y., Chamberlain, C. P., Mcwilliams, M., Schmitt, A. K., and Wooden, J., 2005, Oxygen isotopic composition and U–Pb discordance in zircon: Geochimica et Cosmochimica Acta, v. 69, n. 20, p. 4895–4905, http://dx.doi.org/10.1016/j.gca.2005.05.013

Bouvier, A., Vervoort, J. D., and Patchett, P. J., 2008, The Lu–Hf and Sm–Nd isotopic composition of CHUR: Constraints from unequilibrated chondrites and implications for the bulk composition of terrestrial planets: Earth and Planetary Science Letters, v. 273, p. 48–57, http://dx.doi.org/10.1016/j.epsl.2008.06.010

Cao, G. Q., 1996, Early Precambrian Geology of western Shandong: Beijing, Geological Publishing House, p. 1–193 (in Chinese with English abstract).

Condie, K. C., Belousova, E., Griffin, W. L., and Sircombe, K. N., 2009, Granitoid events in space and time: Constraints from igneous and detrital zircon age spectra: Gondwana Research, v. 15, n. 3–4, p. 228–242, http://dx.doi.org/10.1016/j.gr.2008.06.001

Cui, P. L., Sun, J. G., Sha, D. M., Wang, X. J., Zhang, P., Gu, A. L., and Wang, Z. Y., 2013, Oldest zircon xenocryst (4.17 Ga) from the North China Craton: International Geology Review, v. 55, n. 15, p. 1902–1908 (in Chinese with English abstract), http://dx.doi.org/10.1080/00206814.2013.805925

Dey, S., Pandey, U. K., Rai, A. K., and Chaki, A., 2012, Geochemical and Nd isotope constraints on petrogenesis of granitoids from NW part of the eastern Dharwar craton: Possible implications for late Archaean crustal accretion: Journal of Asian Earth Sciences, v. 45, p. 40–56, http://dx.doi.org/10.1016/j.jseaes.2011.09.013

Dong, C. Y., Liu, D. Y., Wan, Y. S., Xu, Z. Y., Wang, W., and Xie, H. Q., 2009, Hf Isotope Composition and REE pattern of zircons from early Precambrian metamorphic rocks in the Daqing Mountains, Inner Mongolia: Geological Review, v. 55, p. 509–520 (in Chinese with English abstract).

Drüppel, K., McCready, A. J., and Stumpfl, E. F., 2009, High-K granites of the Rum Jungle Complex,

N-Australia: Insights into the Late Archean crustal evolution of the North Australian Craton: Lithos, v. 111, n. 3–4, p. 203–219, http://dx.doi.org/10.1016/j.lithos.2009.04.007

Frost, C. D., Frost, B. R., Chamberlain, K. R., and Hulsebosch, T. P., 1998, The Late Archean history of the Wyoming province as recorded by granitic magmatism in the Wind River Range, Wyoming: Precambrian Research, v. 89, n. 3–4, p. 145–173, http://dx.doi.org/10.1016/S0301-9268(97)00082-X

Geisler, T., Pidgeon, R. T., van Bronswijk, W., and Kurtz, R., 2002, Transport of uranium, thorium, and lead in metamict zircon under low temperature hydrothermal conditions: Chemical Geology, v. 191, n. 1–3, p. 141–154, http://dx.doi.org/10.1016/S0009-2541(02)00153-5

Geisler, T., Schaltegger, U., and Tomaschk, F., 2007, Re-equilibration of zircon in aqueous fluids and melts: Elements, v. 3, n. 1, p. 43–50, http://dx.doi.org/10.2113/gselements.3.1.43

Geng, Y. S., Liu, F. L., and Yang, C. H., 2006, Magmatic event at the end of the Archean in Eastern Hebei province and its geological implication: Acta Geologica Sinica, v. 80, n. 6, p. 819–833 (in Chinese with English abstract), http://dx.doi.org/10.1111/j.1755-6724.2006.tb00305.x

Griffin, W. L., Wang, X., Jackson, S. E., Pearson, N. J., O'Reilly, S. Y., Xu, X., and Zhou, X., 2002, Zircon chemistry and magma mixing, SE China: *In-situ* analysis of Hf isotopes, Tonglu and Pingtan igneous complexes: Lithos, v. 61, p. 237–269, http://dx.doi.org/10.1016/S0024-4937(02)00082-8

Hou, K. J., Li, Y. H., Zou, T. R., Shi, Y. R., and Xie, G. Q., 2007, Laser ablation MC-ICP-MS technique for Hf isotope microanalysis of zircon and its geological applications: Acta Petrologica Sinica, v. 23, n. 10, p. 2595–2604 (in Chinese with English abstract).

Ickert, R. B., Hiess, J., Williams, I. S., Holden, P., Ireland, T. R., Lanc, P., Schram, N., Foster, J. J., and Clement, S. W., 2008, Determining high precision, *in situ*, oxygen isotope ratios with a SHRIMP II: Analyses of MPI-DING silicate-glass reference materials and zircon from contrasting granites: Chemical Geology, v. 257, n. 1–2, p. 114–128, http://dx.doi.org/10.1016/j.chemgeo.2008.08.024

Jahn, B. M., Liu, D. Y., Wan, Y. S., Song, B., and Wu, J. S., 2008, Archean crustal evolution of the Jiaodong peninsula, China, as revealed by zircon SHRIMP geochronology, elemental and Nd-isotope geochemistry: American Journal of Science, v. 308, n. 3, p. 232–269, http://dx.doi.org/10.2475/03.2008.03

Jayananda, M., Chardon, D., Peucat, J. J., and Capdevila, R., 2006, 2.61 Ga potassic granites and crustal reworking in the western Dharwar craton, southern India: Tectonic, geochronologic and geochemical constraints: Precambrian Research, v. 150, n. 1–2, p. 1–26, http://dx.doi.org/10.1016/j.precamres.2006.05.004

Jiang, N., Guo, J. H., Zhai, M. G., and Zhang, S. Q., 2010, ~2.7 Ga crust growth in the North China craton: Precambrian Research, v. 179, n. 1–4, p. 37–49, http://dx.doi.org/10.1016/j.precamres.2010.02.010

Kamo, S. L., and Davis, D. W., 1994, Reassessment of Archean crustal development in the Barberton Mountain Land South Africa, based on U–Pb dating: Tectonics, v. 13, n. 1, p. 167–192, http://dx.doi.org/10.1029/93TC02254

Kröner, A., Wilde, S. A., Li, J. H., and Wang, K. Y., 2005, Age and evolution of a late Archean to Paleoproterozoic upper to lower crustal section in the Wutaishan/Hengshan/Fuping terrain of northern China: Journal of Asian Earth Sciences, v. 24, n. 5, p. 577–595. http://dx.doi.org/10.1016/j.jseaes.2004.01.001

Kröner, A., Kovach, V., Belousova, E., Hegner, E., Armstrong, R., Dolgopolova, A., Seltmann, R., Alexeiev, D. V., Hoffmann, J. E., Wong, J., Sun, M., Cai, K., Wang, T., Tong, Y., Wilde, S. A., Degtyarev, K. E., and Rytsk, E., 2014, Reassessment of continental growth during the accretionary history of the Central Asian Orogenic Belt: Gondwana Research, v. 25, n. 1, p. 103–125, http://dx.doi.org/10.1016/j.gr.2012.12.023

LaFlamme, C., McFarlane, C. R. M., and Corrigan, D., 2014, U-Pb, Lu-Hf and REE in zircon from 3.2 to 2.6 Ga Archean gneisses of the Repulse Bay block, Melville Peninsula, Nunavu: Precambrian Research, v. 252, p. 223–239, http://dx.doi.org/10.1016/j.precamres.2014.07.012

Liaoning Bureau of Geology and Mineral Resources Exploration (LBGMRE), 1975a, Geological map of Liaoyang sheet (1:200000).

Liaoning Bureau of Geology and Mineral Resources Exploration (LBGMRE), 1975b, Geological map of Yingkou sheet (1:200000).

Liaoning Bureau of Geology and Mineral Resources Exploration (LBGMRE), 1976, Geological map of Shenyang sheet (1:200000).

Li, H. M., Liu, M. J., Li, L. X., Yang, X. Q., Yao, L. D., Chen, J., and Yao, T., 2014, SHRIMP U-Pb geochronology of zircons from the garnet-rich altered rocks in the mining area II of the Gongchangling iron deposit: Constraints on the ages of the high-grade iron deposit: Acta Petrologica Sinica, v. 30, n. 5, p. 1205–1217 (in Chinese with English abstract).

Li, S. Z., and Zhao, G. C., 2007, SHRIMP U-Pb zircon geochronology of the Liaoji granitoids: constraints on the evolution of the Paleoproterozoic Jiao-Liao-Ji belt in the Eastern Block of the North China Craton: Precambrian Research, v. 158, n. 1–2, p. 1–16, http://dx.doi.org/10.1016/j.precamres.2007.04.001

Liu, D. Y., Nutman, A. P., Compston, W., Wu, J. S., and Shen, Q. H., 1992, Remnants of ≥3800 Ma crust in the Chinese part of the Sino–Korean Craton: Geology, v. 20, n. 4, p. 339–342, http://dx.doi.org/10.1130/0091-7613(1992)020<0339:ROMCIT>2.3.CO;2

Liu, D. Y., Wan, Y. S., Wu, J. S., Wilde, S. A., Zhou, H. Y., Dong, C. Y., and Yin, X. Y., 2007, Eoarchean rocks and zircons in the North China Craton, *in* Van Kranendonk, M. J., Smithies, R. H., and Bennett, V., editors, Earth's Oldest Rocks: Developments in Precambrian Geology, v. 15, p. 251–273, http://dx.doi.org/10.1016/S0166-2635(07)15035-0

Liu, D. Y., Wilde, S. A., Wan, Y. S., Wu, J. S., Zhou, H. Y., Dong, C. Y., and Yin, X. Y., 2008, New U–Pb and Hf isotopic data confirm Anshan as the oldest preserved segment of the North China Craton: American Journal of Science, v. 308, n. 3, p. 200–231, http://dx.doi.org/10.2475/03.2008.02

Liu, F. L., Liu, P. H., Wang, F., Liu, J. H., Meng, E., Cai, J., and Shi, J. R., 2014a, U-Pb dating of zircons from granitic leucosomes in migmatites of the Jiaobei Terrane, southwestern Jiao-Liao-Ji Belt, North China

Craton: Constraints on the timing and nature of partial melting: Precambrian Research, v. 245, p. 80–99, http://dx.doi.org/10.1016/j.precamres.2014.01.001

Liu, J. D., Xiao, R. G., Zhang, Y. F., Fan, M. H., Wang, S. Z., Jia, Y. G., Wang, G., and Liu, Z. X., 2012, Zircon SHRIMP U-Pb dating of the tourmalinites from boron–bearing series of borate deposits in Eastern Liaoning and its geological implications: Acta Geologica Sinica, v. 86, p. 118–130 (in Chinese with English abstract), http://dx.doi.org/10.1111/j.1755-6724.2012.00616.x

Liu, J. H., Liu, F. L., Ding, Z. J., Liu, C. H., Yang, H., Liu, P. H., Wang, F., and Meng, E., 2013, The growth, reworking and metamorphism of early Precambrian crust in the Jiaobei terrane, the North China Craton: Constraints from U-Th-Pb and Lu-Hf isotopic systematics, and REE concentrations of zircon from Archean granitoid gneisses: Precambrian Research, v. 224, p. 287–303, http://dx.doi.org/10.1016/j.precamres.2012.10.003

Liu, S. J., Wan, Y. S., Sun, H. Y., Nutman, A. P., Xie, H. Q., Dong, C. Y., Ma, M. Z., Du, L. L., Liu, D. Y., and Jahn, B., 2014b, Paleo- to Eoarchean crustal evolution in eastern Hebei, North China Craton: New evidence from SHRIMP U-Pb dating and *in-situ* Hf isotopic study of detrital zircons from paragneises: Journal of Asian Earth Sciences, v. 78, p. 4–17, http://dx.doi.org/10.1016/j.jseaes.2013.07.041

Liu, S. W., Santosh, M., Wang, W., Bai, X., and Yang, P. T., 2011, Zircon U-Pb chronology of Jianping Complex: Implications for the Precambrian crustal evolution history of the northern margin of the North China Craton: Gondwana Research, v. 20, n. 1, p. 48–63, http://dx.doi.org/10.1016/j.gr.2011.01.003

Lu, S. N., Chen, Z. H., and Xiang, Z. Q., 2008, The World Geopark of Taishan: Geochronological Framework of Ancient Intrusives: Beijing, Geological Publishing House, 90 p. (in Chinese).

Luo, Y., Sun, M., Zhao, G. C., Li, S. Z., Xu, P., Ye, K., and Xia, X. P., 2004, LA-ICP-MS U-Pb zircon ages of the Liaohe Group in the Eastern Block of the North China Craton: constraints on the evolution of the Jiao-Liao-Ji Belt: Precambrian Research, v. 134, n. 3–4, p. 349–371, http://dx.doi.org/10.1016/j.precamres.2004.07.002

Luo, Y., Sun, M., Zhao, G. C., Li, S. Z., Ayers, J. C., Xia, X. P., and Zhang, J. H., 2008, A comparison of U-Pb and Hf isotopic compositions of detrital zircons from the North and South Liaohe Group: Constraints on the evolution of the Jiao-Liao-Ji Belt, North China Craton: Precambrian Research, v. 163, p. 279–306, http://dx.doi.org/10.1016/j.precamres.2008.01.002

Ludwig, K. R., 2001, Squid 1.02: a User's Manual: Berkeley, California, Berkeley Geochronology Centre Special Publication.

——— 2003, ISOPLOT 3.00: A Geochronological Toolkit for Microsoft Excel: Berkeley, California, Berkeley Geochronology Center.

Masuda, A., 1975, Abundances of monoisotopic REE, consistent with the Leedey chondrite values: Geochemical Journal, v. 9, n. 3, p. 183–184, http://dx.doi.org/10.2343/geochemj.9.183

Moyen, J. F., 2011, The composite Archaean grey gneisses: Petrological significance, and evidence for a non-unique tectonic setting for Archaean crustal growth: Lithos, v. 123, n. 1–4, p. 21–36, http://dx.doi.org/10.1016/j.lithos.2010.09.015

Moyen, J. F., and Martin, H., 2012, Forty years of TTG research: Lithos, v. 148, p. 312–336, http://dx.doi.org/10.1016/j.lithos.2012.06.010

Moyen, J. F., Martin, H., Jayananda, M., and Auvray, B., 2003, Late Archaean granites: a typology based on the Dharwar Craton (India): Precambrian Research, v. 127, n. 1–3, p. 103–123, http://dx.doi.org/10.1016/S0301-9268(03)00183-9

Nasdala, L., Hofmeister, W., Norberg, N., Martinson, J. M., Corfu, F., Dörr, W., Kamo, S. L., Kennedy, A. K., Kronz, A., Reiners, P. W., Frei, D., Kosler, J., Wan, Y. S., Götze, J., Häger, T., Kröner, A., and Valley, J. W., 2008, Zircon M257 – a Homogeneous Natural Reference Material for the Ion Microprobe U-Pb Analysis of Zircon: Geostandards and Geoanalytical Research, v. 32, n. 3, p. 247–265, http://dx.doi.org/10.1111/j.1751-908X.2008.00914.x

Nowell, G. M., Kempton, P. D., Noble, S. R., Fitton, J. G., Saunders, A. D., Mahoney, J. J., and Taylor, R. N., 1998, High precision Hf isotope measurements of MORB and OIB by thermal ionisation mass spectrometry: insights into the depleted mantle: Chemical Geology, v. 149, n. 3–4, p. 211–233, http://dx.doi.org/10.1016/S0009-2541(98)00036-9

Nutman, A. P., and Rosing, M., 1994, SHRIMP U–Pb zircon geochronology of the late Archaean Ruinæsset syenite, Skjoldungen alkaline province, South-East Greenland: Geochimica et Cosmochimica Acta, v. 58, n. 16, p. 3515–3518, http://dx.doi.org/10.1016/0016-7037(94)90102-3

Nutman, A. P., Christiansen, Q., and Friend, C. R. L., 2007, 2635 Ma amphibolite facies gold mineralisation near a terrane boundary (suture?) on Storø Nuuk region, southern West Greenland: Precambrian Research, v. 159, n. 1–2, p. 19–32, http://dx.doi.org/10.1016/j.precamres.2007.04.007

Nutman, A. P., Wan, Y. S., Du, L. L., Friend, C. R. L., Dong, C. Y., Xie, H. Q., Wang, W., Sun, H. Y., and Liu, D. Y., 2011, Multistage late Neoarchaean crustal evolution of the North China Craton, eastern Hebei: Precambrian Research, v. 189, n. 1–2, p. 43–65, http://dx.doi.org/10.1016/j.precamres.2011.04.005

Pearce, J. A., 1983, The role of sub-continental lithosphere in magma genesis at active continental margins, *in* Hawkesworth, C. J., and Norry, M. J., editors, Continental Basalts and Mantle Xenoliths: Cambridge, Shiva Publishing Limited, p. 230–249.

Peng, T., Wilde, S. A., Fan, W., and Peng, B., 2013, Neoarchean siliceous high-Mg basalt (SHMB) from the Taishan granite-greenstone terrane, Eastern North China Craton: Petrogenesis and tectonic implications: Precambrian Research, v. 228, p. 233–249, http://dx.doi.org/10.1016/j.precamres.2013.01.017

Pidgeon, R. T., O'Neil, J. R., and Silver, L. T., 1966, Uranium and lead isotopic stability in a metamict zircon under experimental hydrothermal conditions: Science, v. 154, n. 3756, p. 1538–1540, http://dx.doi.org/10.1126/science.154.3756.1538

Qiao, G. S., Zhai, M. G., and Yan, Y. H., 1990, Geochronological study of Archaean rocks in Anshan Liaoning province: Scientia Geologica Sinica, v. 2, p. 158–165 (in Chinese with English abstract).

Scherer, E., Munker, C., and Mezger, K., 2001, Calibration of the Lutetium Hafnium clock: Science, v. 293, n. 5530, p. 683–687, http://dx.doi.org/10.1126/science.1061372

Silver, L. T., and Deutsch, S., 1963, Uranium–lead isotopic variations in zircon: A case study: The Journal of Geology, v. 71, n. 6, p. 721–758, http://dx.doi.org/10.1086/626951

Song, B., Nutman, A. P., Liu, D. Y., and Wu, J. S., 1996, 3800 to 2500 Ma crustal evolution in the Anshan area of Liaoning Province, northeastern China: Precambrian Research, v. 78, n. 1–3, p. 79–94, http://dx.doi.org/10.1016/0301-9268(95)00070-4

Valley, J. W., Lackey, J. S., Cavosie, A. J., Clechenko, C. C., Spicuzza, M. J., Basei, M. A. S., Bindeman, I. N., Ferreira, V. P., Sial, A. N., King, E. M., Peck, W. H., Sinha, A. K., and Wei, C. S., 2005, 4.4 billion years of crustal maturation: oxygen isotope ratios of magmatic zircon: Contributions to Mineralogy and Petrology, v. 150, n. 6, p. 561–580, http://dx.doi.org/10.1007/s00410-005-0025-8

Vervoort, J. D., and Blichert-Toft, J., 1999, Evolution of the depleted mantle: Hf isotope evidence from juvenile rocks through time: Geochimica et Cosmochimica Acta, v. 63, n. 3–4, p. 533–556, http://dx.doi.org/10.1016/S0016-7037(98)00274-9

Wan, Y. S., 1993, The formation and evolution of the iron-bearing rock series of the Gongchangling area, Liaoning Province: Beijing, Beijing Science and Technology Publishing House, p. 1–108 (in Chinese with English abstract).

Wan, Y. S., Liu, D. Y., Wu, J. S., Zhang, Z. Q., and Song, B., 1998, The origin of Mesoarchaean granitic rocks from Anshan-Benxi area: constraints of geochemistry and Nd isotope: Acta Petrologica Sinica, v. 14, n. 3, p. 278–288 (in Chinese with English abstract).

Wan, Y. S., Geng, Y. S., Shen, Q. H., Liu, D. Y., Tang, S. H., and Wang, J. H., 2002, Geochemical characteristics of supracrustal enclaves in Mesoarchaean Tiejiashan granite of the Anshan area and its geological significance: Scientia Geologica Sinica, v. 37, n. 2, p. 143–151 (in Chinese with English abstract).

Wan, Y. S., Liu, D. Y., Song, B., Wu, J. S., Yang, C. H., Zhang, Z. Q., and Geng, Y. S., 2005, Geochemical and Nd isotopic compositions of 3.8 Ga meta-quartz dioritic and trondhjemitic rocks from the Anshan area and their geological significance: Journal of Asian Earth Sciences, v. 24, n. 5, p. 563–575, http://dx.doi.org/10.1016/j.jseaes.2004.02.009

Wan, Y. S., Song, B., Liu, D. Y., Wilde, S. A., Wu, J. S., Shi, Y. R., Yin, X. Y., and Zhou, H. Y., 2006, SHRIMP U–Pb zircon geochronology of Paleoproterozoic metasedimentary rocks in the North China Craton: Evidence for a major Late Paleoproterozoic tectonothermal event: Precambrian Research, v. 149, n. 3–4, p. 249–271, http://dx.doi.org/10.1016/j.precamres.2006.06.006

Wan, Y. S., Liu, D. Y., Yin, X. Y., Wilde, S. A., Xie, L. W., Yang, Y. H., Zhou, H. Y., and Wu, J. S., 2007, SHRIMP geochronology and Hf isotope composition of zircons from the Tiejiashan granites and supracrustal rocks in the Anshan area, Liaoning Province: Acta Petrologica Sinica, v. 23, n. 2, p. 241–252 (in Chinese with English abstract).

Wan, Y. S., Liu, D. Y., Dong, C. Y., Nutman, A., Wilde, S. A., Wang, W., Zuo, Z., Yin, X. Y., and Zhou, H. Y., 2009a, The oldest rocks and zircons in China: Acta Petrologica Sinica, v. 25, n. 8, p. 1793–1807 (in Chinese with English abstract).

Wan, Y. S., Liu, D. Y., Dong, C. Y., Xu, Z. Y., Wang, Z. J., Wilde, S. A., Yang, Y. H., Liu, Z. H., and Zhou, H. Y., 2009b, The Precambrian Khondalite Belt in the Daqingshan area, North China Craton: evidence for multiple metamorphic events in the Palaeoproterozoic, *in* Reddy, S. M., Mazumder, R., Evans, D. A. D., and Collins, A. S., editors, Palaeoproterozoic Supercontinents and Global Evolution: Journal of the Geological Society, London, Special Publications, v. 323, p. 73–97, http://dx.doi.org/10.1144/SP323.4

Wan, Y. S., Liu, D. Y., Wang, S. J., Dong, C. Y., Yang, E. X., Wang, W., Zhou, H. Y., Ning, Z., Du, L. L., Yin, X. Y., Xie, H. Q., and Ma, M. Z., 2010, Juvenile magmatism and crustal recycling at the end of Neoarchean in western Shandong province, North China Craton: Evidence from SHRIMP zircon dating: American Journal of Science, v. 310, n. 10, p. 1503–1552, http://dx.doi.org/10.2475/10.2010.11

Wan, Y. S., Liu, D. Y., Wang, W., Song, T. R., Kröner, A., Dong, C. Y., Zhou, H. Y., and Yin, X. Y., 2011a, Provenance of Meso- to Neoproterozoic cover sediments at the Ming Tombs, Beijing, North China Craton: An integrated study of U-Pb dating and Hf isotopic measurement of detrital zircons and whole-rock geochemistry: Gondwana Research, v. 20, n. 1, p. 219–242, http://dx.doi.org/10.1016/j.gr.2011.02.009

Wan, Y. S., Liu, D. Y., Wang, S. J., Yang, E. X., Wang, W., Dong, C. Y., Zhou, H. Y., Du, L. L., Yang, Y. H., and Diwu, C. R., 2011b, ~2.7 Ga juvenile crust formation in the North China Craton (Taishan-Xintai area, western Shandong Province): Further evidence of an understated event from U-Pb dating and Hf isotopic composition of zircon: Precambrian Research, v. 186, n. 1–4, p. 169–180, http://dx.doi.org/10.1016/j.precamres.2011.01.015

Wan, Y. S., Dong, C. Y., Liu, Y. D., Kröner, A., Yang, C. H., Wang, W., Du, L. L., Xie, H. Q., and Ma, M. Z., 2012a, Zircon ages and geochemistry of late Neoarchean syenogranites in the North China Craton: A review: Precambrian Research, p. 222–223, p. 265–289, http://dx.doi.org/10.1016/j.precamres.2011.05.001

Wan, Y. S., Liu, D. Y., Nutman, A., Zhou, H. Y., Dong, C. Y., Yin, X. Y., and Ma, M. Z., 2012b, Multiple 3.8–3.1 Ga tectono-magmatic events in a newly discovered area of ancient rocks (the Shengousi Complex), Anshan, North China Craton: Journal of Asian Earth Sciences, v. 54–55, p. 18–30, http://dx.doi.org/10.1016/j.jseaes.2012.03.007

Wan, Y. S., Zhang, Y. H., Williams, I. S., Liu, D. Y., Dong, C. Y., Fan, R. L., Shi, Y. R., and Ma, M. Z., 2013, Extreme zircon O isotopic compositions from 3.8 to 2.5 Ga magmatic rocks from the Anshan area, North China Craton: Chemical Geology, v. 352, p. 108–124, http://dx.doi.org/10.1016/j.chemgeo.2013.06.009

Wan, Y. S., Xie, S. W., Yang, C. H., Kröner, A., Ma, M. Z., Dong, C. Y., Du, L. L., Xie, H. Q., and Liu, D. Y.,

2014a, Early Neoarchean (~2.7 Ga) tectono-thermal events in the North China Craton: A synthesis: Precambrian Research, v. 247, p. 45–63, http://dx.doi.org/10.1016/j.precamres.2014.03.019

Wan, Y. S., Dong, C. Y., Wang, S. J., Kröner, A., Xie, H. Q., Ma, M. Z., Zhou, H. Y., Xie, S. W., and Liu, D. Y., 2014b, Middle Neoarchean magmatism in western Shandong, North China Craton: SHRIMP zircon dating and LA-ICP-MS Hf isotope analysis: Precambrian Research, v. 255, Part 3, p. 865–884, http://dx.doi.org/10.1016/j.precamres.2014.07.016

Wan, Y. S., Liu, D. Y., Dong, C. Y., Xie, H. Q., Kröner, A., Ma, M. Z., Liu, S. J., Xie, S. W., and Ren, P., 2015, Formation and evolution of Archean continental crust of the North China Craton, *in* Zhai, M. G., editor, Precambrain Geology of China: Berlin, Germany Springer.

Wang, W., Yang, E., Zhai, M., Wang, S., Santosh, M., Du, L., Xie, H., Lv, B., and Wan, Y., 2013, Geochemistry of ~2.7 Ga basalts from Taishan area: Constraints on the evolution of early Neoarchean granite-greenstone belt in western Shandong Province, China: Precambrian Research, v. 224, p. 94–109, http://dx.doi.org/10.1016/j.precamres.2012.09.009

Wang, W., Zhai, M. G., Li, T. S., Santosh, M., Zhao, L., and Wang, H. Z., 2014, Archean-Paleoproterozoic crustal evolution in the eastern North China Craton: Zircon U-Th-Pb and Lu-Hf evidence from the Jiaobei terrane: Precambrian Research, v. 241, p. 146–160, http://dx.doi.org/10.1016/j.precamres.2013.11.011

Whalen, J. B., Percival, J. A., McNicoll, V. J., and Longstaffe, F. J., 2004, Geochemical and isotopic (Nd–O) evidence bearing on the origin of late- to post-orogenic high-K granitoid rocks in the Western Superior Province: implications for late Archean tectonomagmatic processes: Precambrian Research, v. 132, n. 3, p. 303–326, http://dx.doi.org/10.1016/j.precamres.2003.11.007

Wilde, S. A., Cawood, P. A., Wang, K. Y., and Nemchin, A. A., 2005, Granitoid evolution in the Late Archean Wutai Complex North China Craton: Journal of Asian Earth Sciences, v. 24, n. 5, p. 597–613, http://dx.doi.org/10.1016/j.jseaes.2003.11.006

Williams, I. S., 1998, U–Th–Pb geochronology by ion microprobe, *in* Mckibben, M. A., Shanks, W. C., III, and Ridley, W. I., editors, Applications of Microanalytical Techniques to Understanding Mineralizing Processes: Reviews in Economic Geology, v. 7, p. 1–35.

Woodhead, J., Hergt, J., Shelley, M., Eggins, S., and Kemp, R., 2004, Zircon Hf isotope analysis with an excimer laser, depth profiling, ablation of complex geometries, and concomitant age estimation: Chemical Geology, v. 209, n. 1–2, p. 121–135, http://dx.doi.org/10.1016/j.chemgeo.2004.04.026

Wu, F. Y., Yang, Y. H., Xie, L. W., Yang, J. H., and Xu, P., 2006, Hf isotopic compositions of the standard zircons and baddeleyites used in U-Pb geochronology: Chemical Geology, v. 234, n. 1–2, p. 105–126, http://dx.doi.org/10.1016/j.chemgeo.2006.05.003

Wu, F. Y., Zhang, Y. B., Yang, J. H., Xie, L. W., and Yang, Y. H., 2008, Zircon U–Pb and Hf isotopic constraints on the Early Archean crustal evolution in Anshan of the North China Craton: Precambrian Research, v. 167, n. 3–4, p. 339–362, http://dx.doi.org/10.1016/j.precamres.2008.10.002

Wu, J. S., Geng, Y. S., Shen, Q. H., Wan, Y. S., Liu, D. Y., and Song, B., 1998, Archaean geology characteristics and tectonic evolution of China-Korea Paleo-continent: Beijing, Geological Publishing House, 212 p (in Chinese).

Wu, K. K., Zhao, G. C., Sun, M., Yin, C. Q., He, Y. H., and Tam, P. Y., 2013a, Metamorphism of the Northern Liaoning Complex: Implications for the tectonic evolution of Neoarchean basement of the Eastern Block, North China Craton: Geoscience Frontiers, v. 4, n. 3, p. 305–320, http://dx.doi.org/10.1016/j.gsf.2012.11.005

Wu, M. L., Zhao, G. C., Sun, M., Yin, C. Q., Li, S. Z., and Tam, P. Y., 2012, Petrology and *P-T* path of the Yishui mafic granulites: Implications for tectonothermal evolution of the Western Shandong Complex in the Eastern Block of the North China Craton: Precambrian Research, v. 222–223, p. 312–324, http://dx.doi.org/10.1016/j.precamres.2011.08.008

Wu, M. L., Zhao, G. C., Sun, M., Li, S. Z., He, Y. H., and Bao, Z. A., 2013b, Zircon U-Pb geochronology and Hf isotopes of major lithologies from the Yishui terrane: Implications for the crustal evolution of the Eastern Block, North China Craton: Lithos, v. 170–171, p. 164–178, http://dx.doi.org/10.1016/j.lithos.2013.03.005

Wu, M. L., Zhao, G. C., Sun, M., Bao, Z. A., Tam, P. Y., and He, Y. H., 2014a, Tectonic affinity and reworking of the Archean Jiaodong Terrane in the Eastern Block of the North China Craton: Evidence from LA-ICP-MS U-Pb zircon ages: Geological Magazine, v. 151, n. 2, p. 365–371, http://dx.doi.org/10.1017/S0016756813000721

Wu, M. L., Zhao, G. C., Sun, M., Li, S. Z., Bao, Z., Tam, P. Y., Eizenhöefer, P. R., and He, Y. H., 2014b, Zircon U-Pb geochronology and Hf isotopes of major lithologies from the Jiaodong Terrane: Implications for the crustal evolution of the Eastern Block of the North China Craton: Lithos, v. 190–191, p. 71–84, http://dx.doi.org/10.1016/j.lithos.2013.12.004

Xie, S. W., Xie, H. Q., Wang, S. J., Kröner, A., Liu, S. J., Zhou, H. Y., Ma, M. Z., Dong, C. Y., Liu, D. Y., and Wan, Y. S., 2014, *Ca.* 2.9 Ga magmatism in eastern Shandong, North China Craton: Zircon U-Pb dating, and Hf-in-zircon isotopic analysis and whole-rock geochemistry: Precambrian Research, v. 255, Part 2, p. 538–562, http://dx.doi.org/10.1016/j.precamres.2014.09.006

Yang, J. H., Wu, F. Y., Wilde, S. A., and Zhao, G. C., 2008, Petrogenesis and geodynamics of Late Archean magmatism in eastern Hebei, eastern North China Craton: Geochronological, geochemical and Nd–Hf isotopic evidence: Precambrian Research, v. 167, n. 1–2, p. 125–149, http://dx.doi.org/10.1016/j.precamres.2008.07.004

Zhai, M. G., and Santosh, M., 2011, The early Precambrian odyssey of the North China Craton: A synoptic overview: Gondwana Research, v. 20, n. 1, p. 6–25, http://dx.doi.org/10.1016/j.gr.2011.02.005

Zhai, M. G., Windley, B. F., and Sills, J. D., 1990, Archaean Gneisses, Amphibolites and Banded Iron-Formations from the Anshan Area of Liaoning Province, NE China: Their geochemistry, metamor-

phism and petrogenesis: Precambrian Research, v. 46, n. 3, p. 195–216, http://dx.doi.org/10.1016/0301-9268(90)90002-8

Zhang, Z. Q., and Ye, X. J., 1987, Mass-spectrometric isotope dilution analysis of REE and precise measurement of $^{143}Nd/^{144}Nd$ ratios: Chinese Academy of Geological Sciences, Bulletin of the Institute of Geology, v. 1, p. 108–128 (in Chinese with English abstract).

Zhao, G. C., and Cawood, P. A., 2012, Precambrian Geology of China: Precambrian Research, v. 222–223, p. 13–54, http://dx.doi.org/10.1016/j.precamres.2012.09.017

Zhao, G. C., and Zhai, M. G., 2013, Lithotectonic elements of Precambrian basement in the North China Craton: Review and tectonic implications: Gondwana Research, v. 23, n. 4, p. 1207–1240, http://dx.doi.org/10.1016/j.gr.2012.08.016

Zhao, G. C., Wilde, S. A., Cawood, P. A., and Lu, L. Z., 1998, Thermal evolution of Archean basement rocks from the eastern part of the North China carton and its bearing on tectonic setting: International Geological Review, v. 40, n. 8, p. 706–721, http://dx.doi.org/10.1080/00206819809465233

Zhao, G. C., Wilde, S. A., Cawood, P. A., and Lu, L. Z., 1999a, Tectonothermal history of the basement rocks in the western zone of the North China Craton and its tectonic implications: Tectonophysics, v. 310, n. 1–4, p. 37–53, http://dx.doi.org/10.1016/S0040-1951(99)00152-3

Zhao, G. C., Wilde, S. A., Cawood, P. A., and Lu, L. Z., 1999b, Thermal evolution of two textural types of mafic granulites from the North China craton: evidence for both mantle plume and collisional tectonics: Geological Magazine, v. 136, n. 3, p. 223–240, http://dx.doi.org/10.1017/S001675689900254X

Zhao, G. C., Wilde, S. A., Cawood, P. A., and Sun, M., 2001, Archean blocks and their boundaries in the North China Craton: lithological geochemical, structural and *P–T* path constraints and tectonic evolution: Precambrian Research, v. 107, n. 1–2, p. 45–73, http://dx.doi.org/10.1016/S0301-9268(00)00154-6

Zhao, G. C., Cawood, P. A., Li, S., Wilde, S. A., Sun, M., Zhang, J., He, Y. H., and Yin, C. Q., 2012, Amalgamation of the North China Craton: Key issues and discussion: Precambrian Research, v. 222–223, p. 55–76, http://dx.doi.org/10.1016/j.precamres.2012.09.016

Zheng, Y. F., Zhang, S. B., Zhao, Z. F., Wu, Y. B., Li, X. H., Li, Z. X., and Wu, F. Y., 2007, Contrasting zircon Hf and O isotopes in the two episodes of Neoproterozoic granitoids in South China: Implications for growth and reworking of continental crust: Lithos, v. 96, n. 1–2, p. 127–150, http://dx.doi.org/10.1016/j.lithos.2006.10.003

China Geology 3 (2018) 450−452

China Geology

Journal homepage: http://chinageology.cgs.cn

Research Advances

Land submerged to carbonate platform by conodonts: paleoenvironment reconstruction of the western Gangdese in Tibet during Triassic

Zhan-sheng Ji[a], Jian-xin Yao[b], Gui-chun Wu[b,*], Qian Sun[b], Qiu-yuan Shi[b], Hao Li[b], Ji-fu He[b], Shao-wen Zhang[b]

[a] *Chinese Academy of Geological Science, CAGS, Beijing* 100037, *China*
[b] *Institute of Geology, CAGS, Beijing* 100037, *China*

1. Objectives

The western Gangdese in Tibet during Triassic was previously considered to be a part of the Gangdese Oldland (Zhao ZZ et al., 2001; Fig. 1). If the Gangdese Oldland did exist, it means no prospect of petroleum exploration of the Triassic strata in western Gangdese area. Fortunately, the recent biostratigraphic progresses don't support the existence of the Gangdese Oldland. This paper aims to briefly introduce the new paleogeographic interpretation and the reason that the western Gangdese in the Triassic was marine instead of terrigenous on the basis of the recent conodont data.

2. Methods

The logic link of denying such a vast land as the Gangdese Oldland by discovering such tiny fossils as conodonts is based on the following geological principles. The first is the paleogeographic principle that the existence of an ancient land is interpreted by the absence of strata. The second is the sedimentologic principle that limestone or dolomite containing marine fossils were accumulated in an environment of carbonate platform or slope. The third is the stratigraphic principle that the existence of a certain-age strata is determined by the existence of its index fossils.

Conodonts, the index fossils for the marine strata from Middle Cambrian up to Late Triassic, played a critical role in the denying of the Gangdese Oldland. The conception of the Gangdese Oldland was established on the stratigraphic cognition that the Triassic strata did not deposit. If the above stratigraphic understanding is true, there is no chance to find Triassic conodonts. On the contrary, if Triassic conodonts were discovered, it suggests the existence of the Triassic marine strata. If the Triassic marine strata are found anywhere in the scope of the Gangdese Oldland, the conception of the Gangdese Oldland will be proved to be incorrect. Furthermore, the paleoenvironment of the related area of the Gangdese Oldland should be reinterpreted by the lithologic facies of the strata yielding Triassic conodonts.

3. Results

The conception of the Gangdese Oldland was first questioned by the discovery of the typical Late Triassic Norian conodont *Epigondolella* specimens in the so-called Middle Permian Xiala Formation at the Dibu Co section which is located in the middle west of the Gangdese Oldland by Ji ZS et al. in 2006. The above conodont data suggest the existence of the Late Triassic Norian carbonate sediments over there. The carbonate sediments suggest its environment probably was carbonate platform or slope, but never land as thought before. It is the first evidence to collapse the conception of the Gangdese Oldland. More conodont samples were collected and checked in the so-called Middle Permian Xiala Formation limestone nearby the Dibu Co section to verify its reliability. Inspiringly, not only Late Triassic conodonts are found repeatedly but also abundant Early and Middle Triassic conodonts were found (Fig. 2). *Neogondolella carinata* zone, *Neospathodus triangularis - N. homeri* zone, *Chiosella timorensis* zone, *Paragondolella inclinata - P. polygnathiformis* zone and *Epigondolella* zone, ranging from the Early Triassic to Late Triassic, could be recognized in ascending order.

In a similar way, the Early and Middle Triassic conodonts indicate that the existence of the Lower and Middle Triassic carbonate sediments and furtherly means its environment in

* Corresponding author: *E-mail address*: jizhansheng@vip.sina.com (Zhan-sheng Ji).

doi:10.31035/cg2018053

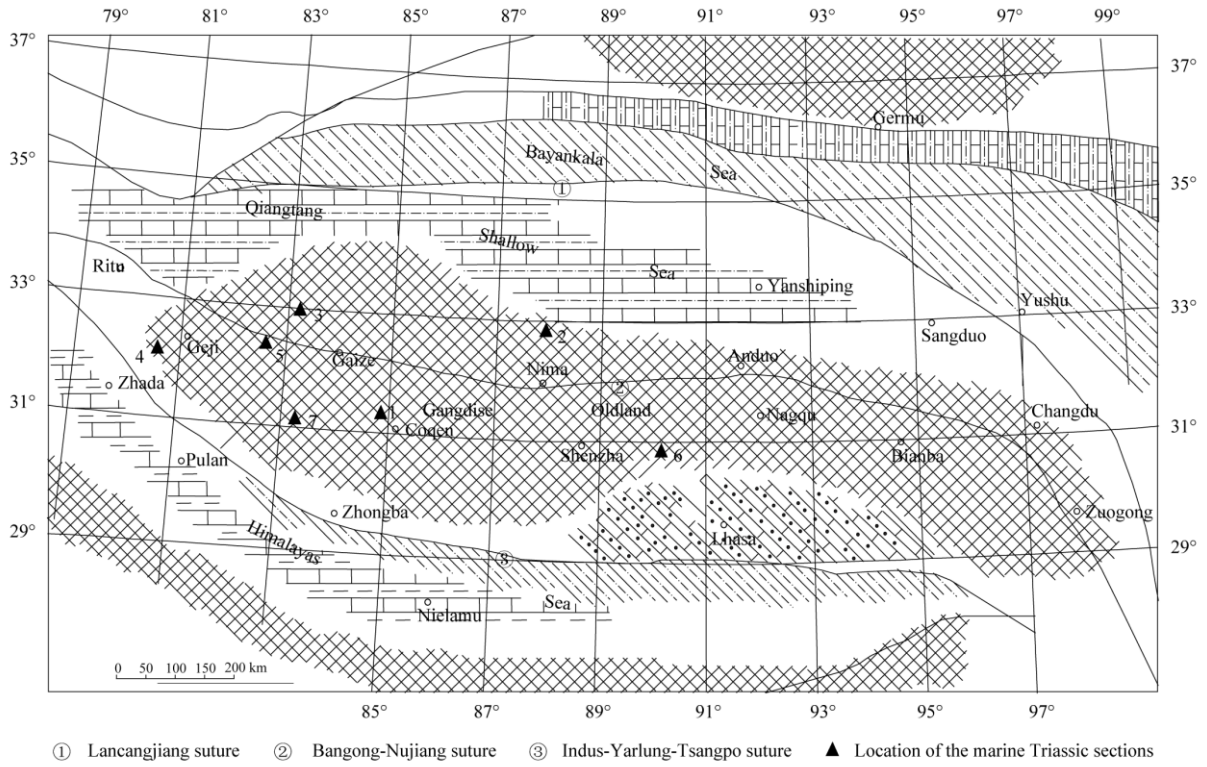

Fig. 1. Sections producing Triassic conodonts in the"Gangdese land"(after Zhao ZZ et al., 2001 and references therein).

this area was probably carbonate platform or slope in the Early and Middle Triassic too.

Judging from one site of the Dibu Co area, the authors deduced that there was a vast carbonate platform or slope in the scope of the so-called Gangdese Oldland from Early Triassic to Late Triassic Norian. If this deduction is correct, more locations of the Triassic carbonate sediments could be found in the Gangdese Oldland elsewhere. Checking conodonts in the so-called Middle Permian Xiala formation elsewhere was inspired by the study of the Dibu Co section.

Then more conodont investigations were carried out in other locations to testify the existences of Triassic marine deposition. Inspiring and expectant results were obtained in the following works. Early Triassic conodonts were found at the Langjiu section of the Shiquanhe area in the westmost Gangdese Oldland by Ji ZS et al. in 2007. Late Triassic conodonts were found at the Yawa section by Ji ZS et al. in 2010. Early Triassic conodonts were found at the Wenbudangsang section in the northwest Gangdese Oldland by Wu GC et al. in 2014. Early Triassic conodonts were found both at the Namtso section by Wu GC et al. in 2017 and at the Renduo section by Wu GC et al. in 2018.

In addition, Early Triassic conodonts were discovered at the Mopanshan section and the Zishisang section in the Southern Qiangtang. The Southern Qiangtang has been considered to be the northward extending part of the Gangdese Oldland during Early and Middle Triassic. The Early Triassic conodonts were found in samples taken from the so-called Permian limestone by the geologists of the Guizou Institute of Geological Survey and Jilin Institute of Geological Survey respectively. These data indicate that the marine Triassic deposition spread widely in the so-called Gangdese Oldland.

4. Conclusions

The newly-discovered conodonts reveal the existence of Triassic carbonate in several outcrops in the western Gangdese region and the southern Qiangtang region. The conception of the Gangdese Oldland should be eliminated for the investigation of conodonts which are typical marine microfossils. These scattered outcrops nowadays suggest the existence of a vast and continuous carbonate platform or slope environment during the Triassic.

For a more detailed discussion and mentioned references in this paper, refer to the summary papers (Ji ZS et al., 2008, 2018).

Acknowledgment

This study was supported by National Natural Science Foundation of China (41472030), Basic Research Project of Ministry of Science and Technology of China

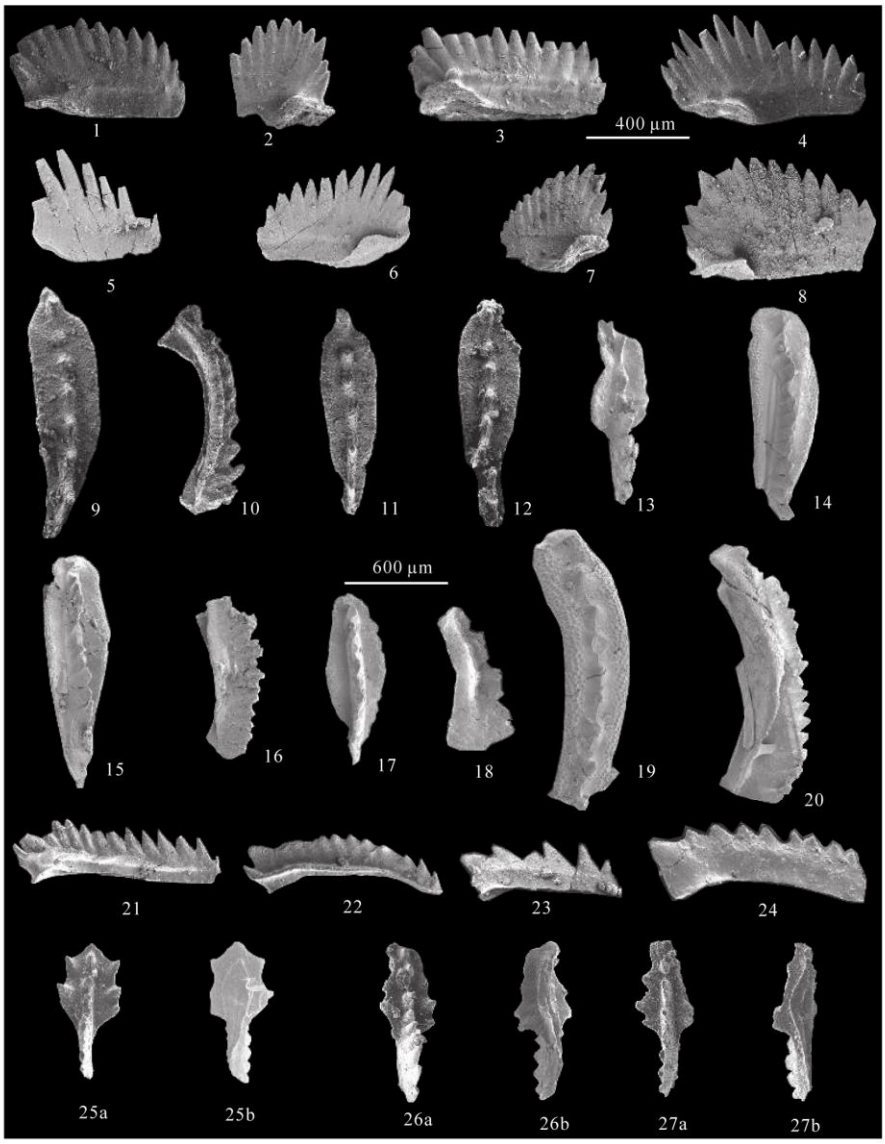

Fig. 2. Typical conodont specimens found at the Dibucuo section, Coqen County, Tibet. 1−*Neospathodus homeri* (Bender); 2−*Neospathodus triangularis* (Bender); 3−*Chiosella timorensis* (Nogami); 4−*Neospathodus conservativus* Muller; 5−*Neospathodus dieneri* Sweet; 6−*Neospathodus cristagalli* (Huckriede); 7, 8−*Neospathodus waageni* Sweet; 9–12−*Neogondolella carinata* (Clark); 13−*Budurovignathus* sp.; 14, 15−*Neogondolella* cf. *szaboi* (Kovacs); 16, 17−*Paragondolella inclinata* (Mosher); 18−*Paragondolella polygnathiformis* (Budurov and Stefanov); 19−*Gladigondolella tethydis* (Huckriede); 20−transitional form from *Paragondolella inclinata* to *Paragondolella polygnathiformis*; 21, 22−*Neogondolella bulgarica* (Budurov and Stefanov); 23−*Paragondolella inclinata* (Mosher); 24−*Cratognathodus* sp.; 25a, 25b−*Epigondolella* cf. *englandi*; 26a, 26b−*Epigondolella* sp.; 27a, 27b−the evolved *Epigongdolella serruta* Orchard. Scale bar is 400 μm for figures 1−8 and 600 μm for figures 9−30.

(2015FY310100), China Geological Survey (DD20160120-02, DD20160120-04 and DD20160126), and Central Public-interest Scientific Institution Basal Research Fund (J1607).

References

Ji ZS, Yao JX, Wu GC. 2008. Upper Paleozoic-Lower Mesozoic in the Coqên Basin, Tibet, China: a potential petroleum-bearing sedimentary sequence. Geological Bulletin of China, 27(1), 36–63 (in Chinese with English abstract).

Ji ZS, Wu GC, Yao JX, Sun Q, Shi QY, He JF, Li H, Liu ZY, Guo AC, Hou ZS, Li DZ. 2018. Suggestions on the strategic selection of petroleum target areas and the tactic breakthrough of the oil and gas exploration in the Tibetan Plateau. Acta Geoscientica Sinica, 39(4), 387–400 (in Chinese with English abstract).

Zhao ZZ, Li YT, Ye HF, Zhang YW. 2001. Tectonic characteristics and basin evolution of Qinghai-Tibet Plateau. Beijing: Science Press (in Chinese).